Recognition of Base Mismatches in DNA by Chrysenequinone Diimine Intercalators of Rhodium (III)

Thesis by
Brian Anthony Jackson

Submitted in Partial Fulfillment of
the Requirements for the Degree of
Doctor of Philosophy

California Institute of Technology
Pasadena, California

1999
(submitted April 22, 1999)

© 1999

Brian Anthony Jackson

All Rights Reserved

ACKNOWLEDGEMENTS:

At the very beginning, I would like to acknowledge my research advisor, Jacqueline Barton. In my time in her research group I have learned a great deal, about chemistry, about research, and about what it means to be a scientist. During my time exploring DNA in 133 Noyes, she gave me the freedom to follow my own hunches and discover some very exciting chemistry. Even while granting me that freedom, however, she was also there to provide needed suggestions and scientific pushes at crucial times during the course of the project. Her unflagging enthusiasm for her science will be the defining characteristic of my time here that I will take with me as I carry my scientific education into my next life in Washington, DC.

On a less personal level, I would also like to acknowledge the many sources of funding that provided the resources for this work. If there is anything I learned during my time as a graduate student, it is that scientific progress is a very expensive commodity. Without the personal funding provided to me by the NSF, the Parsons Foundation, and Caltech, and the research support from the NIH and other sources, none of the work included in this thesis would have been possible.

More important than the lesson that "science is expensive," however, in my time at Caltech I have also learned that science, when it is at its best, is a team sport. Without the very talented group of scientific colleagues with whom I have had the privilege to work, the story told in this lengthy manuscript would not exist.

I do not believe that I can fully express the debt that I feel to my fellow graduate student, now doctor, Brian Hudson. Scientifically, Brian was part of almost every

stage of this project from kicking around designs for metal complexes to troubleshooting the many steps which came afterwards. The many ideas which bounced back and forth as we sat around the group, between complaining about the cold while walking to the Caltech swimming pool, and while standing on line for movies, were both an important and highly enjoyable part of my scientific education. Without his direct efforts at teaching me NMR spectroscopy, I would still be staring at the magnet hoping I wouldn't break it. Even more important than his contributions to my work, however, were Brian's contributions to my life. He is a true friend and I will always believe that one of the best things to come from my time at Caltech was the chance to get to know him. During most of my career here, BPH was the sounding board and steady anchor which kept me moored though difficult times.

I would also like to express special thanks to Hansruedi Mürner. At the point when he arrived from Switzerland, I had been mired in synthesis difficulties for several months and my project, in the absence of sufficient quantities of metal complex, was going nowhere. The synthetic work described in the second chapter of this thesis obliterated that roadblock in a matter of weeks. Without Hansruedi's collaboration, however, that work would have never been possible. I consider myself very lucky to both have had the opportunity to work along side such a talented inorganic chemist and also to call him my friend.

During my time in the Barton group, I have noticed the pattern that most graduate students, during their last gasping run to finish up, latch on to one person to provide help and support. For me, that "clean-up" advisor was Dr. Scott Rajski. In addition to bringing his considerable organic and biochemical knowledge to bear on several problems that arose for me scientifically during my last year and a half, Scott served as a supportive voice constantly reminding me that I could indeed finish my thesis,

however long it was, and would survive grad school. Providing this support took up a considerable amount of his time during a period of his career when time was the most valuable thing in the world. I cannot begin to thank him for both his constant supply of good advice and for his friendship.

Throughout my entire tenure here, however, one group member has proven to be both an important ally and a dear friend. I cannot begin to appreciate the magnitude of the contribution that Maureen Renta has made to my graduate career. On the most basic level, without Mo's help I would likely still be either standing in front of a copy machine randomly pressing buttons or wandering aimlessly around campus in an attempt to find the right office for some task or another. But far beyond all the help that she provides which is at least related to her job here, I must thank Mo for all the personal support she has given me through my graduate career. Acting as a sounding board for my complaining and frustration, a co-conspirator in BPH and my Puckish scheming, and a participant during times of celebration, Mo has always been there when she was needed. Her wit, humor, and level-headed advice helped me through many frustrating scientific and interpersonal situations.

I would also like to acknowledge all of the members of what became the *ad hoc* task force directed at the quantitative determination of site specific binding constants of transition metal complexes to DNA. The collaboration with Curt Hastings, Brian Hudson, Tim Johann, and my father, Craig Jackson, as we all puzzled over some very confusing data, was one of the highlights of my graduate career. I would also like to thank my wife, Anduin Touw, and Bryan Hathorn of the Marcus Group for mathematical consultation on this project.

A large number of individuals also made more defined contributions to my work. I would like to acknowledge Pratt Bhattacharya for performing some NMR experiments for me as my graduate career was drawing to a close. I would also like to recognize the contribution of Elizabeth Boon, Chris Treadway, Bob Houser, Shana Kelley, and Prof. Mike Hill to electrochemical experiments on the molecules described in this work. I would also like to thank the Goddard Group for kindly giving me access to their computational resources and Prof. John Roberts for allowing the use of his slide-making facilities.

Beyond individual scientific experiments, there is a large group of people who I would like to recognize for their personal contributions to my time at Caltech. Working for more than two years now in the shadow of the huge pile of dirty glassware on my lab bench and stacks of papers on my desk, Kim Copeland has, none the less, preserved her good humor and been a good friend. Her constant manner and almost maternal disapproval of me swearing and cursing when experiments or life didn't go as I planned have been an important counterbalance to my far more incendiary approach to research. I would also like to acknowledge both Kim and Melanie Sanford for finding interest enough in my project to take up similar ones for their own. During my earlier years, the desks surrounding me were occupied by Ai Ching Lim, Yonshu Jenkins, and Sabine Coates. In addition to Ai Ching teaching me everything I know about running gels and working with DNA, all three of these talented scientists and great human beings were early mentors during a period when my research work was not going well. Pete Dandliker, Tim Johann, and Bob Terbrueggen also gave me important advice about what was required to succeed as a grad student.

Although I have attempted to remember, through a period of five years which seems both to have gone by in an instant and lasted for a lifetime, all the members of the Barton Group which have contributed to my project, I know that this is an impossible task. As a result, I would like to express a general "thank you" to the group as a whole. These talented individuals, including individuals who worked on these kinds of molecules before my tenure here, form the scientific foundation upon which this work is placed. For the members of the group who traveled this path with me, I would like express thanks for their tolerance and help.

I would also like to thank the many members of the Caltech staff who contributed scientifically and professionally to many of my activities during my time here. Without the efforts of a great many people, often on very short notice, portions of the work described in this thesis and the written document itself would not exist. Larry Henling in the crystallography facility solved the crystal structure of $[Rh(bpy)_2(chrysi)]Cl_3$ and provided me visual access to answer a couple of puzzling questions about the compounds that were central to my scientific efforts. Dana Roth in the chemistry library managed to find information I was certain didn't exist and saved me many months of work in the laboratory. The talents of Tom Dunn were also critical in solving several computer and instrumentation problems which might have otherwise consumed huge amounts of time as I made ineffective attempts to fix them myself. I must also thank the members of the Biopolymer Synthesis facility in the Beckman Institute – they produced a large number of oligonucleotides very quickly when the pace of experiments outpaced my ability to make and purify DNA for myself. All the members of the graphic arts department and photo lab deserve a special thank you for all the hard work over the last few years; I would particularly like to thank Richard Gomez for not telling me I was crazy every time I brought in a huge photo order that I needed the next day. I would also like to thank the members

of Caltech's student health center – particularly Alice Sogomonian – for all their help during a very stressful part of my life and for enduring my particular brand of hypochondria.

I would also like to acknowledge the role of my family – without the background and strength that their love provided I would have been ill prepared for the trials inherent in scientific work. In addition, the many hours of conversation with my father through these long years provided not only another, fresh mind to consider my data, but also the perspective of someone who had a great deal more experience in the scientific game regarding my work and my experiences at Caltech in the Barton Group.

Lastly, and most importantly, I must thank over and over again, my wonderful wife and collaborator in life, Anduin Touw. Without her support through what have been, in many ways, the most difficult years of my life to date, I would not be in a position to be composing this manuscript. Her tolerance through these years where we saw each other far less than we might have wished is matched only the infinite amount of emotional energy and love she provided to sustain me through an excruciatingly long period of questioning and self doubt. Words cannot fully capture the magnitude of my gratitude and love. It would indeed now be a worthy goal to spend the rest of my life making her happy.

℘

ABSTRACT:

The ability to recognize base mismatches in DNA is of interest both for application to the molecular diagnosis of genetic mutations and for the design of chemotherapeutic agents for diseases associated with failure of cellular mismatch repair. The design and synthesis of a family of transition metal complexes containing the novel chrysenequinone diimine (chrysi) intercalating ligand is described. This sterically bulky intercalating ligand was designed to preferentially bind to the destabilized regions of DNA introduced by most base mismatches. One such compound, bis 2,2'-bipyridine chrysenequinone diimine rhodium(III) ($[Rh(bpy)_2(chrysi)]^{3+}$), has been shown to be a broadly specific mismatch recognition agent which binds and, upon photo-activation, cleaves DNA at or near 82% of the 128 possible three base pair DNA sequences containing a central mismatched base. The cleavage of DNA at individual sites has been shown to be broadly correlated with the helix destabilization caused by the mismatch although it is clear that many factors can affect both the binding affinity and efficiency of its photocleavage chemistry from site to site.

$[Rh(bpy)_2(chrysi)]^{3+}$ has also been demonstrated to be exquisitely specific. Binding constants at some mismatch sites were found to be as high as $2 \times 10^7\ M^{-1}$ compared to an association constant of $4 \times 10^4\ M^{-1}$ to B-form DNA. This level of specificity was sufficient to allow discrimination of a single base mismatch in a 2725 base pair plasmid heteroduplex. The study of these compounds also led to the discovery that some mono-quinone diimine complexes of rhodium(III) can *photocatalytically* cleave DNA when irradiated with visible light. Such a property could be advantageous in the design of photodynamic therapy agents based on these compounds. Preliminary

experiments and progress towards the elucidation of the mechanism of this photocatalytic cleavage is also described.

In addition to the application of chrysi complexes to mismatch recognition, novel methods for the synthesis of these compounds based on the condensation of aromatic quinones with ammine ligands on rhodium(III) are also reported. Methodology for the quantitative measurement of thermodynamic binding constants for molecules which bind and cleave nucleic acids are also discussed.

TABLE OF CONTENTS:

CHAPTER 1: BACKGROUND AND INTRODUCTION.....1

1.1: INTRODUCTION.....2

1.1.1: DEOXYRIBONUCLEIC ACID: INFORMATIONAL MOLECULE.....2
1.1.2: WHY MISMATCH RECOGNITION?.....8

1.2: CHARACTERISTICS OF BASE MISMATCHES.....12

1.2.1: MISMATCH STRUCTURE AND DYNAMICS.....12
1.2.2: THERMODYNAMIC CONSEQUENCES OF MISMATCH INCORPORATION.....17
1.2.3: THE NATURE OF MISMATCH SITES IN DNA.....18

1.3: PROTEIN MECHANISMS OF BASE MISMATCH RECOGNITION.....20

1.4: RECOGNITION OF BASE MISMATCHES IN THE LABORATORY.....23

1.4.1: HYBRIDIZATION METHODS.....24
1.4.2: KINETIC DESTABILIZATION METHODS.....25
1.4.3: BIOTECHNOLOGICAL METHODS.....27
1.4.4: A CONTINUING NEED FOR NOVEL METHODS.....28

1.5: MOLECULAR RECOGNITION.....29

1.5.1: THERMODYNAMICS – DRIVING FORCES FOR MOLECULAR RECOGNITION.....30
1.5.1.1: Enthalpic Contributions to Binding.....30
1.5.1.2: Entropic Contributions to Binding.....33
1.5.2: SPECIFICITY IN BINDING EVENTS.....35

1.6: MOLECULAR RECOGNITION OF DNA.....36

1.6.1: INSIGHTS GAINED FROM PROTEIN RECOGNITION OF DNA.....37
1.6.2: SMALL MOLECULES FOR DNA RECOGNITION.....43
1.6.3: OCTAHEDRAL METALLOINTERCALATORS FOR DNA RECOGNITION.....48
1.6.3.1: Characteristics of Metallointercalators for Molecular Recognition.....49
1.6.3.2: Mechanisms of DNA Recognition by Metallointercalators.....51

1.7: CONCLUSIONS: THE DESIGN OF SMALL MOLECULES FOR MISMATCH RECOGNITION.....67

1.8: LITERATURE CITED **69**

CHAPTER 2: SYNTHESIS AND CHARACTERIZATION OF QUINONE DIIMINE COMPLEXES OF RHODIUM(III) **81**

2.1: INTRODUCTION **82**

2.2: Experimental Methods *84*

2.2.1: INSTRUMENTATION AND MATERIALS 84

2.2.2: SYNTHETIC METHODS 85

2.2.2.1: Addition of One Aromatic Quinone to $Rh(L)_2(NH_3)_2$ *85*

2.2.2.2: Addition of Two Aromatic Quinones to $Rh(L)(NH_3)_4$ *93*

2.2.2.3: Use of Condensation Chemistry as an Intermediate Synthetic Step *108*

2.2.2.4: Ligand Synthesis *115*

2.2.3: CHARACTERIZATION METHODS 115

2.2.3.1: Measurement of pH Dependent Optical Changes *115*

2.2.3.2: Crystallographic Studies of $[Rh(bpy)_2(chrysi)]Cl_3$ *116*

2.2.3.3: pH Titration of $[Rh(d_8\text{-}bpy)_2(chrysi)]Cl_3$ by 1D-^{1}H NMR Spectroscopy *118*

2.3: RESULTS AND DISCUSSION **118**

2.3.1: CONDENSATION CHEMISTRY FOR THE SYNTHESIS OF QUINONE DIIMINE COMPLEXES 118

2.3.1.1: Addition of One Aromatic Quinone to $Rh(L)_2(NH_3)_2$ *118*

2.3.1.2: Addition of Two Aromatic Quinones to $Rh(L)(NH_3)_4$ *126*

2.2.2.3: Use of Condensation Chemistry as an Intermediate Synthetic Step *130*

2.2.2.4: Broader Issues: Ammine Condensation Based Synthesis of Rhodium(III) Complexes *130*

2.3.2: PROPERTIES OF CHRYSENEQUINONE DIIMINE COMPLEXES OF RHODIUM(III): A NEW FAMILY OF DNA INTERCALATING METAL COMPLEXES 132

2.3.2.1: Spectroscopic Properties of Chrysenequinone Diimine Complexes *132*

2.3.2.2: pK_a Measurement by Spectroscopic Titration *133*

2.3.2.3: Crystallographic Characterization of $[Rh(bpy)_2(chrysi)]Cl_3$ *166*

2.3.2.4: pH Titration of $[Rh(d_8\text{-}bpy)_2(chrysi)]Cl_3$ by 1D-^{1}H NMR Spectroscopy *179*

2.3.2.5: Chrysenequinone Diimine Ligands: A Consistent Picture *188*

2.4: LITERATURE CITED **189**

CHAPTER 3: RECOGNITION OF BASE MISMATCHES IN DNA BY CHRYSENEQUINONE DIIMINE COMPLEXES OF RHODIUM(III) **192**

3.1: INTRODUCTION **193**

3.2: EXPERIMENTAL METHODS **202**

3.2.1: INSTRUMENTATION AND MATERIALS 202
3.2.2: SPECTROPHOTOMETRIC TITRATION OF THE BINDING OF Δ-$[Rh(bpy)_2(chrysi)]^{3+}$ TO B-DNA 203
3.2.3: EXAMINATION OF THE INTERACTION OF Δ-$[Rh(bpy)_2(chrysi)]^{3+}$ AND CC MISMATCH CONTAINING DNA BY NMR 204
3.2.4: COMPARISON OF DNA PHOTOCLEAVAGE BY RH(PHI) AND RH(CHRYSI) COMPLEXES 205
3.2.5: DNA PHOTOCLEAVAGE PATTERN AND POST-TREATMENT DEPENDENCE OF VARIOUS RH(CHRYSI) COMPLEXES 206
3.2.6: RECOGNITION OF ALL BASE MISMATCHES IN A SINGLE SEQUENCE CONTEXT BY $[Rh(bpy)_2(chrysi)]^{3+}$ 207

3.3: RESULTS AND DISCUSSION **208**

3.3.1: PROBING THE INTERACTION OF CHRYSENEQUINONE DIIMINE COMPLEXES WITH B-FORM DNA SPECTROPHOTOMETRICALLY 208
3.3.2: NMR EXAMINATION OF THE BINDING OF Δ-$[Rh(bpy)_2(chrysi)]^{3+}$ TO MISMATCH CONTAINING DNA 210
3.3.3: DNA PHOTOCLEAVAGE BY CHRYSENEQUINONE DIIMINE COMPLEXES OF RHODIUM(III) 229
3.3.3.1: Comparison of DNA Photocleavage by Chrysenequinone Diimine and Phenanthrenequinone Diimine Complexes *229*
3.3.3.2: DNA Photocleavage by Chrysenequinone Diimine Containing Complexes is Observed Primarily Near the Site of Destabilization in DNA *234*
3.3.3.3: Recognition of Multiple Mismatches in a Single Sequence Context by $[Rh(bpy)_2(chrysi)]^{3+}$ *246*
3.3.4: QUALITATIVE RELATIONSHIP BETWEEN THERMODYNAMIC DESTABILIZATION AND MISMATCH RECOGNITION 252

3.4: CONCLUSIONS **259**

3.5: LITERATURE CITED 260

CHAPTER 4: $[Rh(bpy)_2(chrysi)]^{3+}$ – CHARACTERIZATION OF THE BREADTH AND SPECIFICITY OF MISMATCH RECOGNITION BY A CHRYSENEQUINONE DIIMINE COMPLEX 262

4.1: INTRODUCTION 263

4.2: EXPERIMENTAL METHODS 264

4.2.1: INSTRUMENTATION AND MATERIALS 264
4.2.2: SEQUENCE CONTEXT DEPENDENCE OF MISMATCH RECOGNITION 265
4.3.3: MEASUREMENT OF THE BINDING CONSTANT OF Δ-$[Rh(bpy)_2(chrysi)]^{3+}$ AT MISMATCH SITES 266
4.2.4: MEASUREMENT OF THE BINDING CONSTANT OF Δ-$[Rh(bpy)_2(chrysi)]^{3+}$ TO B-DNA BY DIRECT PHOTOCLEAVAGE TITRATION 267
4.3.5: MEASUREMENT OF THE BINDING CONSTANT OF Δ-$[Rh(bpy)_2(chrysi)]^{3+}$ TO B-DNA BY PHOTOCLEAVAGE COMPETITION TITRATION 268
4.3.6: SPECIFIC CLEAVAGE OF A PLASMID DNA AT A SINGLE BASE MISMATCH 269
4.3.6.1: Plasmid Construction 269
4.3.6.2: Recognition of a CC Mispair on a Plasmid Heteroduplex 270
4.3.6.3: Determination of the Δ-$[Rh(bpy)_2(chrysi)]^{3+}$ Cleavage Site in $pVYA_{C/G}$ Heteroduplexes at High Resolution 271

4.3: RESULTS AND DISCUSSION 272

4.3.1: BROAD SPECIFICITY 272
4.3.1.1: DNA Base Mismatch Recognition in Variable Sequence Contexts 272
4.3.1.2: A Closer Examination of Recognition of Mismatch Recognition by $[Rh(bpy)_2(chrysi)]^{3+}$ – Implications for a Recognition Model 295
4.3.2: HIGH SELECTIVITY 303
4.3.2.1: Measurement of Binding Constants of Δ-$[Rh(bpy)_2(chrysi)]^{3+}$ to Mismatch Sites 303
4.3.2.2: Measurement of Δ-$[Rh(bpy)_2(chrysi)]^{3+}$ Binding Constants to B-DNA by Photocleavage Titrations 308
4.3.2.3: Discrimination of a Single Mismatch in a Plasmid DNA 318

4.4: CONCLUSIONS 329

4.4.1: Mismatch Discrimination and Recognition Design 329
4.4.2: Mismatch Structure and Metal Complex Binding 332
4.4.3: Speculation on Strand Selectivity of Photocleavage 332
4.4.4: General Lessons from Mismatch Recognition by Steric Exclusion 334

4.5: LITERATURE CITED 335

CHAPTER 5: CHARACTERIZATION OF ASPECTS OF THE PHOTOCHEMISTRY OF CHRYSENEQUINONE DIIMINE COMPLEXES OF RHODIUM(III) 338

5.1: INTRODUCTION 339

5.2: EXPERIMENTAL METHODS 341

5.2.1: Instrumentation and Materials 341
5.2.2: Wavelength Dependence of Photocatalytic DNA Cleavage 342
5.2.2.1: Photocleavage Saturation Experiments with $[Rh(bpy)_2(chrysi)]^{3+}$ 342
5.2.2.2: Photocleavage Saturation Experiments with $[Rh(phen)_2(phi)]^{3+}$ on Mismatch-Containing DNA 343
5.2.2.3: Photocleavage Saturation Experiments with $[Rh(phen)_2(phi)]^{3+}$ and $[Rh(bpy)_2(chrysi)]^{3+}$ on Properly Paired DNA 343
5.2.3: Estimation of the Maximal Extent of Photocatalytic Cleavage of DNA by $[Rh(bpy)_2(chrysi)]^{3+}$ 344
5.2.4: Wavelength Dependence of the Photoaquation of $[Rh(bpy)_2(chrysi)]^{3+}$ in the Presence of DNA 345
5.2.5: Characterization of $[Rh(bpy)_2(chrysi)]^{3+}$ Photochemistry in the Presence and Absence of DNA by Analytical HPLC 345
5.2.6: Photocleavage of DNA by $[Rh(bpy)_2(chrysi)]^{3+}$ using "Non-Traditional" Light Sources 346
5.2.7: Oxygen Dependence of $[Rh(bpy)_2(chrysi)]^{3+}$ Photoreaction with DNA 347
5.2.8: Products of $[Rh(bpy)_2(chrysi)]^{3+}$ Photoreaction with DNA 348
5.2.8.1: Free Base Release 348
5.2.8.2: Nucleoside Analysis 349
5.2.9: Electrochemical Characterization of $[Rh(bpy)_2(chrysi)](PF_6)_3$ 350

5.3: RESULTS 351

5.3.1: PHOTOCLEAVAGE SATURATION EXPERIMENTS USING $[RH(BPY)_2(CHRYSI)]^{3+}$ 351
5.3.2: PHOTOCATALYTIC DNA CLEAVAGE BY $[RH(PHEN)_2(PHI)]^{3+}$ 360
5.3.3: PHOTOAQUATION OF CHRYSENEQUINONE DIIMINE COMPLEXES UPON IRRADIATION WHEN BOUND TO DNA 363
5.3.4: ANALYSIS OF THE PHOTO-INDUCED REACTION BETWEEN $[RH(BPY)_2(CHRYSI)]^{3+}$ AND DNA BY ANALYTICAL HPLC 374
5.3.4.1: Irradiation of the Metal Complex Alone *374*
5.3.4.2: Irradiation of the Metal Complex with DNA *382*
5.3.5: CLEAVAGE OF DNA WITH FLUORESCENT ROOMLIGHT AND SUNLIGHT IRRADIATION 399
5.3.6: OTHER PHOTOCHEMICAL BEHAVIORS OF INTEREST 406
5.3.6.1: Changes in Cleavage Specificity with Changes in Irradiation Wavelength *406*
5.3.6.2: Oxygen Dependence of DNA Photocleavage *407*
5.3.7: CHARACTERIZATION OF DNA PHOTOCLEAVAGE PRODUCTS 414
5.3.7.1: Free Base Release *414*
5.3.7.2: Nucleoside Analysis *418*

5.4: DISCUSSION 423

5.4.1: PHOTOCATALYTIC DNA CLEAVAGE BY $[RH(BPY)_2(CHRYSI)]^{3+}$ AND $[RH(PHEN)_2(PHI)]^{3+}$ 423
5.4.2: DIFFERENCES IN PHOTOCHEMISTRY BETWEEN MONO- AND BIS-QUINONE DIIMINE COMPLEXES OF RHODIUM(III) 435
5.4.3: SPECULATION ON THE POSSIBLE MECHANISM OF PHOTOCATALYSIS 437

5.5: CONCLUSIONS 444

5.6: LITERATURE CITED 445

CHAPTER 6: CONCLUSIONS AND PERSPECTIVES 447

APPENDIX 1: CRYSTALLOGRAPHIC CHARACTERIZATION OF $[RH(BPY)_2(CHRYSI)]CL_3 \cdot 3CH_3CN \cdot 2H_2O$ 450

APPENDIX 2: DETERMINATION OF SITE-SPECIFIC BINDING CONSTANTS OF MOLECULES THAT BIND TO AND CLEAVE NUCLEIC ACIDS 487

A2.1: INTRODUCTION **488**

A2.2: COMPUTATIONAL METHODS **490**

A2.2.1: SIMULATION OF LIGAND BINDING AT ONE HIGH-AFFINITY BINDING SITE IN THE PRESENCE OF MULTIPLE LOW-AFFINITY SITES 490

A2.2.2: SIMULATION OF LIGAND PARTITIONING BETWEEN TWO HIGH-AFFINITY BINDING SITES IN THE PRESENCE OF MULTIPLE LOW-AFFINITY SITES 495

A2.3: EXPERIMENTAL METHODS **498**

A2.3.1: GENERAL PROCEDURES 498

A2.3.2: DIRECT MEASUREMENT OF SINGLE SEQUENCE-SPECIFIC ASSOCIATION CONSTANTS 498

A2.3.3: MEASUREMENT OF THE AVERAGE NON-SPECIFIC ASSOCIATION CONSTANT OF A DNA BINDING LIGAND 499

A2.3.4: MEASUREMENT OF TWO SEQUENCE SPECIFIC ASSOCIATION CONSTANTS RELATIVE TO ONE ANOTHER 500

A2.3.5: MEASUREMENT OF THE OBSERVED CLEAVAGE EFFICIENCY FOR A DNA CLEAVING LIGAND 501

A2.4: RESULTS AND DISCUSSION **501**

A2.4.1: SIMULATION OF LIGAND BINDING AT ONE HIGH-AFFINITY BINDING SITE IN THE PRESENCE OF MULTIPLE LOW-AFFINITY SITES 501

A2.4.2: SIMULATION OF NON-SPECIFIC LIGAND BINDING AT MULTIPLE LOW-AFFINITY SITES 513

A2.4.3: SIMULATION OF LIGAND PARTITIONING BETWEEN TWO HIGH-AFFINITY BINDING SITES IN THE PRESENCE OF MULTIPLE LOW-AFFINITY SITES 515

A2.4.4: MEASUREMENT OF SINGLE SEQUENCE-SPECIFIC ASSOCIATION CONSTANTS OF 1-Δ-RH(MGP)$_2$(PHI)$^{5+}$ 519

A2.4.5: RELATIVE ASSOCIATION CONSTANT MEASUREMENTS FOR 1-Δ-[RH(MGP)$_2$(PHI)]$^{5+}$ 528

A2.4.6: MEASUREMENT OF THE OBSERVED PHOTOCLEAVAGE EFFICIENCY, γ, OF 1-Δ-[RH(MGP)$_2$(PHI)]$^{5+}$ 528

A2.4.7: MEASUREMENT OF THE NON-SPECIFIC ASSOCIATION CONSTANT OF 1-Δ-[RH(MGP)$_2$(PHI)]$^{5+}$ 531

A2.5: CONCLUSIONS **536**

A2.6: LITERATURE CITED **537**

LIST OF FIGURES:

CHAPTER 1:

FIGURE 1.1. STRUCTURAL FEATURES OF DNA. 4

FIGURE 1.2. THE EIGHT POSSIBLE BASE MISMATCHES IN DNA. 6

FIGURE 1.3. MUTATION DETECTION BY DNA MISMATCH RECOGNITION. 10

FIGURE 1.4. CRYSTAL STRUCTURES OF MISMATCH CONTAINING DNA OLIGONUCLEOTIDES 13

FIGURE 1.5. FUNCTIONALITIES IN THE MAJOR AND MINOR GROOVES OF DNA 45

FIGURE 1.6. ENANTIOMERIC PREFERENCES FOR THE BINDING OF OCTAHEDRAL METAL COMPLEXES TO DNA 53

FIGURE 1.7. STRUCTURES OF THE OCTAHEDRAL COMPLEXES $[Rh(phen)_2(phi)]^{3+}$, $[Rh(phi)_2(bpy)]^{3+}$, AND $[Rh(DPB)_2(phi)]^{3+}$ 55

FIGURE 1.8. STRUCTURES OF THE OCTAHEDRAL COMPLEXES $[Rh(NH_3)_4(phi)]^{3+}$, $[Rh(en)_2(phi)]^{3+}$, AND $[Rh(cyclen)(phi)]^{3+}$ 58

FIGURE 1.9. SCHEMATIC OF THE HYDROGEN BONDING AND VAN DER WAALS INTERACTIONS CONFERRING SPECIFICITY ON THE TWO ENANTIOMERS OF $[Rh(en)_2(phi)]^{3+}$ 60

FIGURE 1.10. STRUCTURE OF Δ–α–$[Rh[(R,R)\text{-}Me_2trien]phi]^{3+}$ AND MODELS OF ITS INTERACTION WITH THE 5'-TGCA-3' SITE IN DNA 62

FIGURE 1.11. THE ENANTIOMERS OF $[Rh(MGP)_2(phi)]^{5+}$ 65

CHAPTER 2:

FIGURE 2.1. STEPWISE SYNTHESIS OF $[Rh(phen)_2(phi)]^{3+}$ BY CONDENSATION OF PHENANTHRENEQUINONE WITH COORDINATED AMMINE LIGANDS 86

FIGURE 2.2. ABSORPTION SPECTRA OF $[Rh(bpy)_2(chrysi)]^{3+}$ AND $[Rh(phen)_2(chrysi)]^{3+}$ IN DEIONIZED WATER 94

FIGURE 2.3. PROTON NMR SPECTRA OF $[Rh(bpy)_2(chrysi)]^{3+}$ AND $[Rh(D_8\text{-}bpy)_2(chrysi)]^{3+}$ IN D_4-MEOH 96

FIGURE 2.4. STEPWISE SYNTHESIS OF $[Rh(phi)_2(phen)]^{3+}$ BY CONDENSATION OF PHENANTHRENEQUINONE WITH COORDINATED AMMINE LIGANDS 98

FIGURE 2.5. *IN SITU* SYNTHESIS OF THE COMPLEX ION $[Rh(phi)(chrysi)(phen)]^{3+}$ BY STEPWISE CONDENSATION OF PHENANTHRENEQUINONE AND CHRYSENEQUINONE WITH COORDINATED AMMINE LIGANDS 101

FIGURE 2.6. ABSORPTION SPECTRA OF THE COMPLEX IONS $[Rh(phen)(phi)(chrysi)]^{3+}$ AND $[Rh(chrysi)_2(phen)]^{3+}$ IN DEIONIZED WATER 106

FIGURE 2.7. STEPWISE SYNTHESIS OF TRIS-HETEROLEPTIC COMPLEXES OF RHODIUM(III) UTILIZING BOTH *O*-QUINONE CONDENSATION WITH COORDINATED AMMINE LIGANDS AND FINAL COORDINATION OF AN ADDITIONAL CHELATING LIGAND 109

FIGURE 2.8. ABSORPTION SPECTRA OF THE COMPLEX IONS $[Rh(phen)(chrysi)(bpy')]^{3+}$ AND $[Rh(phen)(phi)(bpy')]^{3+}$ IN DEIONIZED WATER 112

FIGURE 2.9. GENERAL SYNTHETIC SCHEME FOR THE PREPARATION OF RHODIUM COMPLEXES CONTAINING QUINONE DIIMINE LIGANDS BY THE CONDENSATION OF AROMATIC QUINONES WITH COORDINATED AMMINES 119

FIGURE 2.10. REVERSE PHASE HPLC TRACES SHOWING THE CLEAN CONVERSION OF $[Rh(phen)_2(NH_3)_2]^{3+}$ AND 9,10-PHENANTHRENEQUINONE ($T_{RET} \approx 26$ MIN) TO $[Rh(phen)_2(phi)]^{3+}$ AS A FUNCTION OF THE TIME OF REACTION 122

FIGURE 2.11. ACIDIFIED ALIQUOTS OF THE REACTION BETWEEN $[Rh(bpy)_2(NH_3)_2]^{3+}$ AND 5,6-CHRYSENEQUINONE 124

FIGURE 2.12. REVERSE PHASE HPLC TRACES SHOWING THE REACTION OF $[Rh(phen)(NH_3)_4]^{3+}$ AND 9,10-PHENANTHRENEQUINONE AS A FUNCTION OF THE TIME OF REACTION 127

FIGURE 2.13. (A) COMPARISON OF THE ABSORPTION SPECTRA OF $[Rh(phen)_2(chrysi)]^{3+}$ AND $[Rh(phen)_2(phi)]^{3+}$ IN 100 MM TRIS PH 8.0. (B) COMPARISON OF THE ABSORPTION SPECTRA OF $[Rh(chrysi)_2(phen)]^{3+}$ AND $[Rh(phi)_2(phen)]^{3+}$ IN 100 MM TRIS PH 8.0 134

FIGURE 2.14. ABSORPTION SPECTRA OF 5,6-CHRYSENEQUINONE AND 5,6-CHRYSENEDIAMMINE IN MEOH 137

FIGURE 2.15. COMPARISON OF THE ABSORPTION SPECTRA OF $[Rh(bpy)_2(phi)]^{3+}$ AND $[Rh(bpy)_2(chrysi)]^{3+}$ AT BOTH PH 2.5 AND PH 9.3 139

FIGURE 2.16. SPECTRAL CHANGES WHICH OCCUR UPON TITRATION OF A SOLUTION OF $[Rh(phen)_2(phi)]^{3+}$ BETWEEN PH 2.5 AND PH 10.5 142

FIGURE 2.17. SPECTRAL CHANGES WHICH OCCUR UPON TITRATION OF A SOLUTION OF $[Rh(bpy)_2(phi)]^{3+}$ BETWEEN PH 2.5 AND PH 10.5 144

FIGURE 2.18. SPECTRAL CHANGES WHICH OCCUR UPON TITRATION OF A SOLUTION OF $[Rh(phi)_2(phen)]^{3+}$ BETWEEN PH 2.5 AND PH 10 146

FIGURE 2.19. SPECTRAL CHANGES WHICH OCCUR UPON TITRATION OF A SOLUTION OF $[Rh(phen)_2(chrysi)]^{3+}$ BETWEEN PH 2.5 AND PH 10.5 148

FIGURE 2.20. SPECTRAL CHANGES WHICH OCCUR UPON TITRATION OF A SOLUTION OF $[Rh(bpy)_2(chrysi)]^{3+}$ BETWEEN PH 2.5 AND PH 10.5 150

FIGURE 2.21. SPECTRAL CHANGES WHICH OCCUR UPON TITRATION OF A SOLUTION OF $[Rh(chrysi)_2(phen)]^{3+}$ BETWEEN PH 2.5 AND PH 10 152

FIGURE 2.22. SPECTROPHOTOMETRIC TITRATION CURVE FOR $[Rh(phen)_2(phi)]^{3+}$ BETWEEN PH 2.5 AND PH 10.5 154

FIGURE 2.23. SPECTROPHOTOMETRIC TITRATION CURVE FOR $[Rh(bpy)_2(phi)]^{3+}$ BETWEEN PH 2.5 AND PH 10.5 156

FIGURE 2.24. SPECTROPHOTOMETRIC TITRATION CURVE FOR $[Rh(phi)_2(phen)]^{3+}$ BETWEEN PH 2.5 AND PH 10 158

FIGURE 2.25. SPECTROPHOTOMETRIC TITRATION CURVE FOR $[Rh(phen)_2(chrysi)]^{3+}$ BETWEEN PH 2.5 AND PH 10.5 160

FIGURE 2.26. SPECTROPHOTOMETRIC TITRATION CURVE FOR $[Rh(bpy)_2(chrysi)]^{3+}$ BETWEEN pH 2.5 AND pH 10.5 162

FIGURE 2.27. SPECTROPHOTOMETRIC TITRATION CURVE FOR $[Rh(chrysi)_2(phen)]^{3+}$ BETWEEN pH 2.5 AND pH 10 164

FIGURE 2.28. ORTEP PLOT OF $[Rh(bpy)_2(chrysi)]^{3+}$ FROM THE X-RAY STRUCTURE OF $[Rh(bpy)_2(chrysi)]Cl_3 \bullet 3CH_3CN \bullet 2H_2O$ 167

FIGURE 2.29. MULTIPLE VIEWS OF THE CRYSTAL STRUCTURE OF $[Rh(bpy)_2(chrysi)]^{3+}$ FROM VARIED ANGLES 170

FIGURE 2.30. COMPARISON OF A MOLECULAR MODEL (A) OF $[Rh(bpy)_2(chrysi)]^{3+}$ WHOSE CHRYSENEQUINONE DIIMINE LIGAND HAS BEEN FORCED INTO PLANARITY WITH THE CRYSTAL STRUCTURE (B) OF THE SAME MOLECULE 172

FIGURE 2.31. COMPARISON OF THE PREVIOUSLY REPORTED CRYSTAL STRUCTURE OF $[Rh(Me_2trien)phi]^{3+}$ WITH THE STRUCTURE OF $[Rh(bpy)_2(chrysi)]^{3+}$ 174

FIGURE 2.32. HYDROGEN BONDING NETWORK IN THE CRYSTAL OF $[Rh(bpy)_2(chrysi)]Cl_3$ INVOLVING THE METAL COMPLEX IMMINO PROTONS, TWO CHLORIDE COUNTER-IONS AND TWO ORDERED WATER MOLECULES 177

FIGURE 2.33. SIDE VIEW OF FOUR MOLECULES FROM THE CRYSTAL STRUCTURE OF $[Rh(bpy)_2(chrysi)]Cl_3$ 180

FIGURE 2.34. TOP VIEW OF FOUR MOLECULES FROM THE CRYSTAL STRUCTURE OF $[Rh(bpy)_2(chrysi)]Cl_3$ 182

FIGURE 2.35. (A) LABELED $[Rh(bpy)_2(chrysi)]^{3+}$ FOR INTERPRETATION OF NMR TITRATION RESULTS. (B) RESULTS OF A 1-D 500 MHZ ^1H NMR pH TITRATION OF $[Rh(D_8\text{-}bpy)_2(chrysi)]Cl_3$ IN 90/10 H_2O/D_2O USING WATERGATE GRADIENT SOLVENT SUPPRESSION 184

CHAPTER 3:

FIGURE 3.1. THE CHRYSENEQUINONE DIIMINE (CHRYSI) INTERCALATING LIGAND..... 196

FIGURE 3.2. ABSTRACTED METAL COMPLEX AND BINDING SITE OF Δ–α–[RH[(*R,R*)-ME$_2$TRIEN]PHI]$^{3+}$ 198

FIGURE 3.3. COMPARISON OF THE WIDTHS OF THE CHRYSENEQUINONE DIIMINE AND PHENANTHRENEQUINONE DIIMINE INTERCALATORS..... 200

FIGURE 3.4. ABSORBANCE TITRATION OF Δ-[RH(BPY)$_2$(CHRYSI)]CL$_3$ WITH CALF THYMUS DNA..... 211

FIGURE 3.5. BINDING CURVE OF Δ-[RH(BPY)$_2$(CHRYSI)]CL$_3$ FOR CALF THYMUS DNA 213

FIGURE 3.6. FITTED BINDING CURVE OF Δ-[RH(BPY)$_2$(CHRYSI)]CL$_3$ FOR CALF THYMUS DNA..... 215

FIGURE 3.7. 1D NMR TITRATION OF A CC MISMATCH CONTAINING HAIRPIN OLIGONUCLEOTIDE WITH Δ-[RH(BPY)$_2$(CHRYSI)]CL$_3$ 218

FIGURE 3.8. 2D NOESY SPECTRUM OF A CC MISMATCH CONTAINING HAIRPIN OLIGONUCLEOTIDE IN THE ABSENCE OF RHODIUM COMPLEX 220

FIGURE 3.9. 2D NOESY SPECTRUM OF A CC MISMATCH CONTAINING HAIRPIN OLIGONUCLEOTIDE BOUND BY Δ-[RH(BPY)$_2$(CHRYSI)]CL$_3$ 222

FIGURE 3.10. 1D PROTON NMR SPECTRUM OF Δ-[RH(BPY)$_2$(CHRYSI)]CL$_3$ IN 25 MM PHOSPHATE BUFFER, PH 7.0 225

FIGURE 3.11. EXCISED SECTION OF THE 2D NOESY SPECTRA OF THE FREE AND METAL BOUND CC MISMATCH CONTAINING HAIRPIN OLIGONUCLEOTIDE..... 227

FIGURE 3.12. DNA PHOTOCLEAVAGE BY [RH(BPY)$_2$(CHRYSI)]$^{3+}$ AND [RH(BPY)$_2$(PHI)]$^{3+}$ ON DNA SAMPLES WITH AND WITHOUT A CC BASE MISMATCH 230

FIGURE 3.13. WAVELENGTH AND PIPERIDINE POST-TREATMENT DEPENDENCE OF DNA PHOTOCLEAVAGE BY Δ-[RH(PHEN)$_2$(CHRYSI)]$^{3+}$ AND Δ-[RH(CHRYSI)$_2$(PHEN)]$^{3+}$ 235

FIGURE 3.14. WAVELENGTH AND PIPERIDINE POST-TREATMENT DEPENDENCE OF DNA PHOTOCLEAVAGE BY Δ-$[Rh(phen)_2(chrysi)]^{3+}$ AND Δ-$[Rh(chrysi)_2(phen)]^{3+}$ 237

FIGURE 3.15. WAVELENGTH AND PIPERIDINE POST-TREATMENT DEPENDENCE OF DNA PHOTOCLEAVAGE BY Δ-$[Rh(bpy)_2(chrysi)]^{3+}$ 239

FIGURE 3.16. PIPERIDINE SENSITIVE GUANINE DAMAGE INDUCED BY IRRADIATION OF $[Rh(chrysi)_2(phen)]^{3+}$ BOUND TO DNA WITH 365 NM LIGHT 244

FIGURE 3.17. MISMATCH SPECIFIC DNA PHOTOCLEAVAGE BY THE ENANTIOMERS OF $[Rh(bpy)_2(chrysi)]^{3+}$ ON DOUBLE STRANDED OLIGONUCLEOTIDES WITH 313 NM LIGHT 247

FIGURE 3.18. MISMATCH SPECIFIC DNA PHOTOCLEAVAGE BY THE ENANTIOMERS OF $[Rh(bpy)_2(chrysi)]^{3+}$ ON A FAMILY OF HAIRPIN OLIGONUCLEOTIDES WITH 365 NM LIGHT 249

FIGURE 3.19. PLOT OF PHOTOCLEAVAGE AT THE MISMATCH SITE VERSUS MISMATCH INDUCED THERMODYNAMIC DESTABILIZATION IN THE 5'-C*X*T-3' SEQUENCE CONTEXT 254

FIGURE 3.20. PLOT OF PHOTOCLEAVAGE AT THE MISMATCH SITE VERSUS MISMATCH INDUCED THERMODYNAMIC DESTABILIZATION IN THE 5'-T*X*C-3' SEQUENCE CONTEXT 256

CHAPTER 4:

FIGURE 4.1. DNA PHOTOCLEAVAGE OF DNA HAIRPINS CONTAINING ALL BASE MISMATCHES IN ALL SINGLE BASE SEQUENCE CONTEXTS BY Δ AND Λ-$[Rh(bpy)_2(chrysi)]^{3+}$ AT 313 NM 274

FIGURE 4.2. COMPARISON OF DNA PHOTOCLEAVAGE BY Δ-$[Rh(bpy)_2(chrysi)]^{3+}$ ON DNA HAIRPINS CONTAINING ALL BASE MISMATCHES IN ALL SINGLE BASE SEQUENCE CONTEXTS AT 313 NM AND 440 NM 283

FIGURE 4.3. QUANTITATED 313 NM PHOTOCLEAVAGE BY Δ-$[Rh(bpy)_2(chrysi)]^{3+}$ ON DNA HAIRPINS CONTAINING CC, TT, CT, AND AC BASE MISMATCHES.....297

FIGURE 4.4. QUANTITATED 313 NM PHOTOCLEAVAGE BY Δ-$[Rh(bpy)_2(chrysi)]^{3+}$ ON DNA HAIRPINS CONTAINING AA, GT, GA, AND GG BASE MISMATCHES.....299

FIGURE 4.5. BINDING ISOTHERM FOR Δ-$[Rh(bpy)_2(chrysi)]^{3+}$ TARGETED TO A CC MISMATCH-CONTAINING OLIGONUCLEOTIDE.....304

FIGURE 4.6. BINDING ISOTHERM FOR Δ-$[Rh(bpy)_2(chrysi)]^{3+}$ TARGETED TO A NON-SPECIFIC HAIRPIN OLIGONUCLEOTIDE.....310

FIGURE 4.7. TITRATION OF SPECIFIC BINDING AND PHOTOCLEAVAGE BY Δ-$[Rh(bpy)_2(chrysi)]^{3+}$ AT THE CC MISMATCH SITE 5'-C*C*T-3' WITH INCREASING AMOUNTS OF ADDED CARRIER DNA.....313

FIGURE 4.8. GRAPHICAL RESULTS OF THE TITRATION OF Δ-$[Rh(bpy)_2(chrysi)]^{3+}$ BOUND TO THE CC MISMATCH HAIRPIN WITH UNLABELED CARRIER OLIGONUCLEOTIDE.....316

FIGURE 4.9. SCHEMATIC OF THE APPLICATION OF PLASMIDS $pVYA_C$ AND $pVYA_G$ FOR THE CONSTRUCTION OF A 2725 BASE PAIR HETERODUPLEX CONTAINING ONE MISMATCH.....320

FIGURE 4.10. CLEAVAGE OF A 2725 BASE PAIR PLASMID HETERODUPLEX AT A SINGLE MISMATCH SITE BY $[Rh(bpy)_2(chrysi)]^{3+}$.....322

FIGURE 4.11. EXPERIMENTAL PROCEDURE FOR THE DETERMINATION OF THE SITE OF THE $pVYA_C$/$pVYA_G$ HETERODUPLEX PHOTOCLEAVAGE AT HIGH RESOLUTION.....325

FIGURE 4.12. IDENTIFICATION OF THE SITE OF PLASMID CLEAVAGE BY $[Rh(bpy)_2(chrysi)]^{3+}$ IN THE $pVYA_C$/$pVYA_G$ HETERODUPLEX AT HIGH RESOLUTION.....327

CHAPTER 5:

FIGURE 5.1. PHOTOCLEAVAGE BY Δ-$[RH(BPY)_2(CHRYSI)]^{3+}$ AT A CC MISMATCH AS A FUNCTION OF IRRADIATION WAVELENGTH AND PHOTOLYSIS TIME.....352

FIGURE 5.2. PHOTOCLEAVAGE BY Δ-$[RH(BPY)_2(CHRYSI)]^{3+}$ AT THE CC/CC MISMATCH IRRADIATED AT 525 NM FOR EXTENDED TIME 358

FIGURE 5.3. PHOTOCLEAVAGE BY Δ-$[RH(PHEN)_2(PHI)]^{3+}$ AT A CC MISMATCH AS A FUNCTION OF IRRADIATION WAVELENGTH AND PHOTOLYSIS TIME.....361

FIGURE 5.4. EXAMINATION OF THE SPECTROSCOPIC CHANGES WHICH OCCUR IN Δ-$[RH(BPY)_2(CHRYSI)]^{3+}$ BOUND TO DNA OVER THE COURSE OF IRRADIATION AT VARIED WAVELENGTHS 364

FIGURE 5.5. HPLC ANALYSIS OF THE PHOTOLYSIS PRODUCTS OF $[RH(BPY)_2(CHRYSI)]^{3+}$ IRRADIATED AT 313 NM.....375

FIGURE 5.6. HPLC ANALYSIS OF THE PHOTOLYSIS PRODUCTS OF $[RH(BPY)_2(CHRYSI)]^{3+}$ IRRADIATED AT 400 NM.....378

FIGURE 5.7. ABSORPTION SPECTRA OF $[RH(BPY)_2(CHRYSI)]^{3+}$ AND ITS PRIMARY PHOTOCHEMICAL BREAKDOWN PRODUCT WHEN IRRADIATED AT 400 NM IN BUFFERED AQUEOUS SOLUTION.....380

FIGURE 5.8. HPLC ANALYSIS OF THE PHOTOLYSIS PRODUCTS OF $[RH(BPY)_2(CHRYSI)]^{3+}$ IRRADIATED AT 500 NM.....383

FIGURE 5.9. HPLC ANALYSIS OF THE PHOTOLYSIS PRODUCTS OF $[RH(BPY)_2(CHRYSI)]^{3+}$ IRRADIATED AT 313 NM IN THE PRESENCE OF CC MISMATCH-CONTAINING DNA 386

FIGURE 5.10. HPLC ANALYSIS OF THE DNA PHOTOLYSIS PRODUCTS PRODUCED BY $[RH(BPY)_2(CHRYSI)]^{3+}$ IRRADIATED AT 313 NM IN THE PRESENCE OF CC MISMATCH-CONTAINING DNA 388

FIGURE 5.11. COMPARISON OF 260 NM AND 313 NM CHROMATOGRAMS OF $[RH(BPY)_2(CHRYSI)]^{3+}$ IRRADIATED FOR 30 MIN AT 313 NM IN THE PRESENCE OF CC MISMATCH-CONTAINING DNA 390

FIGURE 5.12. ABSORPTION SPECTRUM OF THE MAJOR PHOTOLYSIS PRODUCT OF $[Rh(bpy)_2(chrysi)]^{3+}$ IRRADIATED FOR 30 MIN AT 313 NM IN THE PRESENCE OF CC MISMATCH-CONTAINING DNA DISPLAYING BOTH 260 NM AND 313 NM ABSORBANCE 392

FIGURE 5.13. HPLC ANALYSIS OF THE PHOTOLYSIS PRODUCTS OF $[Rh(bpy)_2(chrysi)]^{3+}$ IRRADIATED AT 400 NM IN THE PRESENCE OF CC MISMATCH-CONTAINING DNA 395

FIGURE 5.14. HPLC ANALYSIS OF THE DNA PHOTOLYSIS PRODUCTS PRODUCED BY $[Rh(bpy)_2(chrysi)]^{3+}$ IRRADIATED AT 400 NM IN THE PRESENCE OF CC MISMATCH-CONTAINING DNA 397

FIGURE 5.15. COMPARISON OF 260 NM AND 313 NM CHROMATOGRAMS OF $[Rh(bpy)_2(chrysi)]^{3+}$ IRRADIATED FOR 120 MIN AT 400 NM IN THE PRESENCE OF CC MISMATCH-CONTAINING DNA 400

FIGURE 5.16. HPLC ANALYSIS OF THE DNA PHOTOLYSIS PRODUCTS PRODUCED BY $[Rh(bpy)_2(chrysi)]^{3+}$ IRRADIATED AT 500 NM IN THE PRESENCE OF CC MISMATCH-CONTAINING DNA 402

FIGURE 5.17. HPLC ANALYSIS OF THE PHOTOLYSIS PRODUCTS OF $[Rh(bpy)_2(chrysi)]^{3+}$ IRRADIATED AT 500 NM IN THE PRESENCE OF CC MISMATCH-CONTAINING DNA 404

FIGURE 5.18. APPEARANCE OF DIRECT CYTOSINE-SPECIFIC STRAND CLEAVAGE AS A RESULT OF SHIFTING IRRADIATION WAVELENGTH FROM 313 NM TO 440 NM 408

FIGURE 5.19. DEPENDENCE OF THE DIRECT AND PIPERIDINE INDUCED PHOTOCLEAVAGE OF DNA BY $[Rh(bpy)_2(chrysi)]^{3+}$ AT 313 NM, 440 NM, AND 525 NM ON OXYGEN 411

FIGURE 5.20. FREE BASE RELEASE FROM CALF THYMUS DNA AFTER PHOTOLYSIS WITH $[Rh(bpy)_2(chrysi)]^{3+}$ AT 313 NM, 440 NM, AND 540 NM 416

FIGURE 5.21. COMPARISON OF THE SPECTRAL CHARACTERISTICS OF THYMINE PRODUCTS RELEASED FROM CALF THYMUS DNA AFTER PHOTOLYSIS WITH $[Rh(bpy)_2(chrysi)]^{3+}$ AT 313 NM AND 525 NM 419

FIGURE 5.22. VARIED THYMINE-LIKE PRODUCTS OBSERVED AFTER PHOTOLYSIS OF $[Rh(bpy)_2(chrysi)]^{3+}$ WITH THE CC MISMATCH-CONTAINING HAIRPIN CC/TT AT 525 NM FOR 2 HOURS 421

FIGURE 5.23. HPLC CHROMATOGRAM OF A REPRESENTATIVE IRRADIATION SAMPLE DIGESTED TO ITS INDIVIDUAL NUCLEOSIDE COMPONENTS 424

FIGURE 5.24. COMPARISON OF THE NUCLEOSIDE DIGESTS OF DNA PHOTOCLEAVAGE OF THE CC MISMATCH-CONTAINING HAIRPIN CC/GG BY $[Rh(bpy)_2(chrysi)]^{3+}$ 426

FIGURE 5.25. ABSORPTION SPECTRUM OF PUTATIVE MODIFIED NUCLEOSIDE PHOTO-PRODUCT 428

FIGURE 5.26. SATURATION PHOTOCLEAVAGE OF DNA BY Δ-$[Rh(bpy)_2(chrysi)]^{3+}$ AT THE CC/CC MISMATCH AT VARIED WAVELENGTHS AS COMPARED TO THE METAL-DNA STOICHIOMETRY AND THE ABSORPTION SPECTRUM OF THE COMPLEX BOUND TO DNA 431

FIGURE 5.27. COMPARISON OF THE MAXIMAL CLEAVAGE OF DNA OBSERVED AFTER PHOTOLYSIS WITH $[Rh(bpy)_2(chrysi)]^{3+}$ AT VARIABLE WAVELENGTH – NORMALIZED AND CORRECTED FOR LAMP POWER 433

FIGURE 5.28. CYCLIC VOLTAMMOGRAM OF $[Rh(bpy)_2(chrysi)](PF_6)_3$ 442

APPENDIX 2:

FIGURE A2.1. DIAGRAMS OF SITE POSITIONING FOR SIMULATION OF LIGAND BINDING AT ONE OR TWO HIGH-AFFINITY SITES SURROUNDED BY OTHER LOW-AFFINITY SITES ON A SINGLE DNA POLYMER 491

FIGURE A2.2. SIMULATION OF LIGAND BINDING AT ONE HIGH-AFFINITY BINDING SITE IN THE PRESENCE OF MULTIPLE LOW-AFFINITY SITES 503

FIGURE A2.3. SIMULATION OF LIGAND BINDING AND STRAND CLEAVAGE AT ONE HIGH-AFFINITY BINDING SITE IN THE PRESENCE OF MULTIPLE LOW-AFFINITY SITES 505

FIGURE A2.4. SIMULATION OF LIGAND BINDING AND STRAND CLEAVAGE AT ONE HIGH-AFFINITY BINDING SITE IN THE PRESENCE OF MULTIPLE LOW-AFFINITY SITES 507

FIGURE A2.5. SIMULATION OF LIGAND BINDING AND STRAND CLEAVAGE AT ONE HIGH-AFFINITY BINDING SITE IN THE PRESENCE OF MULTIPLE LOW-AFFINITY SITES 511

FIGURE A2.6. SIMULATION OF NON-SPECIFIC LIGAND BINDING AND STRAND CLEAVAGE AT MULTIPLE LOW-AFFINITY SITES ON A DNA POLYMER.....516

FIGURE A2.7. SIMULATION OF LIGAND PARTITIONING BETWEEN TWO HIGH-AFFINITY BINDING SITES IN THE PRESENCE OF MULTIPLE LOW-AFFINITY SITES 520

FIGURE A2.8. SIMULATION OF LIGAND PARTITIONING BETWEEN TWO HIGH-AFFINITY BINDING SITES IN THE PRESENCE OF MULTIPLE LOW-AFFINITY SITES 522

FIGURE A2.9. QUANTITATIVE PHOTOCLEAVAGE TITRATION FOR 1-Δ-$[Rh(MGP)_2(phi)]^{5+}$ AT 5'-CATCTG-3' AND 5'-TATCTA-3'.....524

FIGURE A2.10. BINDING ISOTHERMS DERIVIED FROM PHOTOCLEAVAGE TITRATION OF 1-Δ-$[Rh(MGP)_2(phi)]^{5+}$ AT 5'-CATCTG-3' AND 5'-TATCTA-3' 526

FIGURE A2.11. DNA PHOTOCLEAVAGE OF 1-Δ $Rh(MGP)_2(phi)^{5+}$ ON AN OLIGONUCLEOTIDE CONTAINING BOTH 5'-CATCTG-3' AND 5'-TATCTA-3' RECOGNITION SITES 529

FIGURE A2.12. DETERMININATION OF THE PHOTOCLEAVAGE EFFICIENCY FOR $Rh(MGP)_2(phi)^{5+}$ AT 5'-CATCTG-3' AND 5'-TATCTA-3' BINDING SITES 532

FIGURE A2.13. QUANTITATIVE PHOTOCLEAVAGE TITRATION AND BINDING ISOTHERM FOR 1-Δ $Rh(MGP)_2(phi)^{5+}$ ON A HAIRPIN OLIGONUCLEOTIDE CONTAINING NO HIGH AFFINITY BINDING SITES 534

LIST OF TABLES:

CHAPTER 2:

TABLE 2.1. CRYSTAL DATA AND STRUCTURAL ANALYSIS RESULTS FOR $[Rh(bpy)_2(chrysi)]Cl_3$ 117

TABLE 2.2. pK_A VALUES FOR PHI AND CHRYSI COMPLEXES OF RH(III) DETERMINED BY SPECTROPHOTOMETRIC TITRATION 141

CHAPTER 4:

TABLE 4.1. AVERAGE FREE ENERGY CHANGE AS A RESULT OF MISMATCH INCORPORATION – ALL SEQUENCE CONTEXTS 295

TABLE 4.2. THERMODYNAMIC BINDING CONSTANTS OF Δ-$[Rh(bpy)_2(chrysi)]^{3+}$ AT VARIED MISMATCH SITES 306

TABLE 4.3. COMPARISON OF SPECIFICITY OF $[Rh(bpy)_2(chrysi)]^{3+}$ AND NATURAL MISMATCH RECOGNITION PROTEINS 330

APPENDIX 1:

TABLE A1.1. CRYSTAL AND INTENSITY COLLECTION DATA FOR BIS 2,2'-BIPYIDYL CHRYSENEQUINONE DIIMINE RHODIUM(III) CHLORIDE $\cdot 3CH_3CN \cdot 2H_2O$ 451

TABLE A1.2. FINAL HEAVY ATOM PARAMETERS FOR BIS 2,2'-BIPYIDYL CHRYSENEQUINONE DIIMINE RHODIUM(III) CHLORIDE $\cdot 3CH_3CN \cdot 2H_2O$ 452

TABLE A1.3. DISTANCES AND ANGLES FOR BIS 2,2'-BIPYIDYL CHRYSENEQUINONE DIIMINE RHODIUM(III) CHLORIDE $\cdot 3CH_3CN \cdot 2H_2O$ 455

Table A1.4. Final Refined Hydrogen Parameters (less four half atoms) for Bis 2,2'-bipyidyl chrysenequinone diimine rhodium(III) chloride $\cdot 3CH_3CN \cdot 2H_2O$ 459

Table A1.5. Anisotropic Displacement Parameters for Bis 2,2'-bipyidyl chrysenequinone diimine rhodium(III) chloride $\cdot 3CH_3CN \cdot 2H_2O$ 460

Table A1.6. Distances and Angles Involving Hydrogen Bonding for Bis 2,2'-bipyidyl chrysenequinone diimine rhodium(III) chloride $\cdot 3CH_3CN \cdot 2H_2O$ 462

Table A1.7. Observed and Calculated Structure Factors for Bis 2,2'-bipyidyl chrysenequinone diimine rhodium(III) chloride $\cdot 3CH_3CN \cdot 2H_2O$ 463

Chapter 1:

Background and Introduction

1.1: INTRODUCTION

1.1.1: Deoxyribonucleic Acid: Informational Molecule

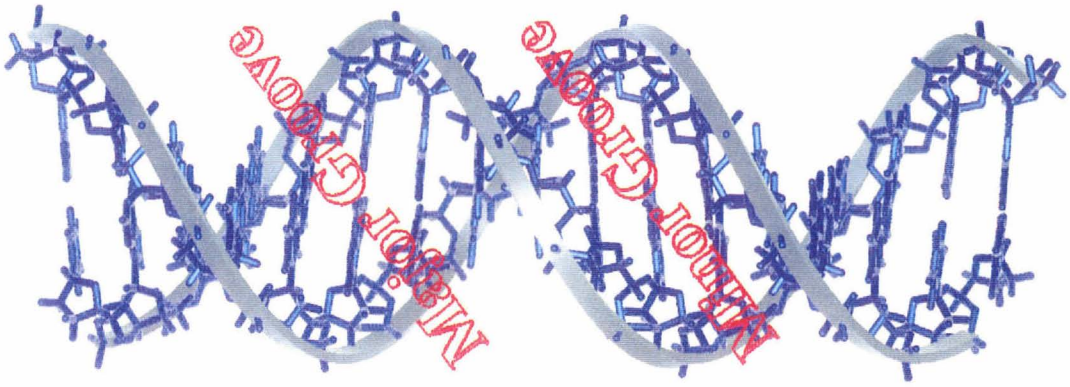
Deoxyribonucleic acid, or DNA, exists in every living thing as the storehouse of genetic information. This information, which describes all the pieces and processes required for assembling organisms as simple as a virus or as complex as a human being, is encoded as long polymeric molecules packaged within the cell's nucleus. Since the structure of DNA was reported by Watson and Crick almost half a century ago, it has become clear that both the molecule's informational content and the mechanisms for accessing and copying that information are intimately dependant on its exact chemical structure. This realization has not only revolutionized the study of DNA as a chemical entity but provided an entirely new perspective for examining its roles in cellular processes.

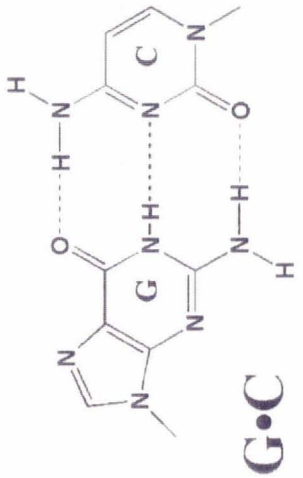
The information stored in the linear ticker-tape of DNA is encoded in a four letter alphabet of aromatic heterocyclic bases. These four bases, adenine (A), guanine (G), cytosine (C), and thymine (T), are linked together by deoxyribose sugar-phosphate units to form DNA polymers. In addition to the covalent connections between bases in a linear DNA strand, the bases themselves can also interact non-covalently with each other to form stable, hydrogen bonded base pairs. The chemical functionalities found on the bases themselves define the most stable base combinations as adenine-thymine (AT) and guanine-cytosine (CG) pairs. These pairings are termed "standard" or "Watson-Crick" base pairs and are those almost universally found in naturally occurring DNA samples. It is this association of AT and CG base pairs that allows two polymeric DNA strands of appropriate sequence to associate with one another as a DNA duplex. Such a duplex, because of the geometrical constraints of the sugar phosphate linkages and the interaction of the bases, twists to form the

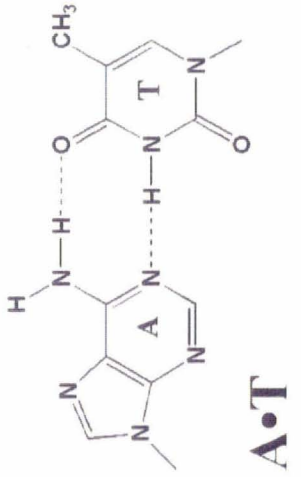
widely recognized double helical structure of DNA. These general structural features of DNA are summarized in Figure 1.1.

The specific pairing of the bases and the formation of a double helix from two complementary copies of the cell's genetic blueprint organizes the otherwise disordered single strands into a more regular and manageable helix and keeps the functionalities of the DNA bases from floating free in solution. In addition, the specific hydrogen bonding of the base pairs provides a ready mechanism of copying the molecule as a double helix can "unzip" and new strands can be made by assembling the component bases on the complementary templates. This process of copying the DNA, which is performed during cellular reproduction, is particularly critical; during this copying process, the most basic goal of the cell is the fidelity of information transfer. If a large number of mistakes were introduced into the DNA at each copying step, the resulting numerous defects and failures in the cellular machinery would almost certainly overwhelm even a large multi-celled creature and cause death. It is not possible, however, to design a system where copying fidelity is perfect at all times. As a human cell, for example, copies its 3×10^8 base pairs of DNA during cell division, it is inevitable that a certain number of errors will be made. It has been estimated that DNA polymerases, the enzymes which perform replication, make one error for every 10^4 to10^5 bases incorporated into a growing polymer.[1] These errors cause bases to be incorporated which do not form the regular base pairings and helical structure shown in Figure 1.1. These incorrectly paired structures are termed *base mismatches* and can involve any combination of the four DNA bases (Figure 1.2). In addition, base mismatches can also be generated when the DNA of a cell undergoes chemical damage resulting in base adducts or other products that are not compatible with DNA replication. At these sites, where the chemical functionality of the DNA template has been modified or lost, incorrect bases

Figure 1.1. Structural Features of DNA. The heterocyclic bases of DNA are connected to one another by a sugar phosphate backbone (left). The phosphate groups which are part of this backbone are each negatively charged making a DNA polymer polyanionic. The bases of DNA can form base pairs (middle) as a result of the interaction of hydrogen bonding groups on the periphery of their aromatic rings. These base paring interactions allow DNA to assemble into a duplex structure (right) which forms a regular double helix with two grooves of varied shape around its external surface. These grooves are termed the major and minor grooves to reflect their markedly different sizes.







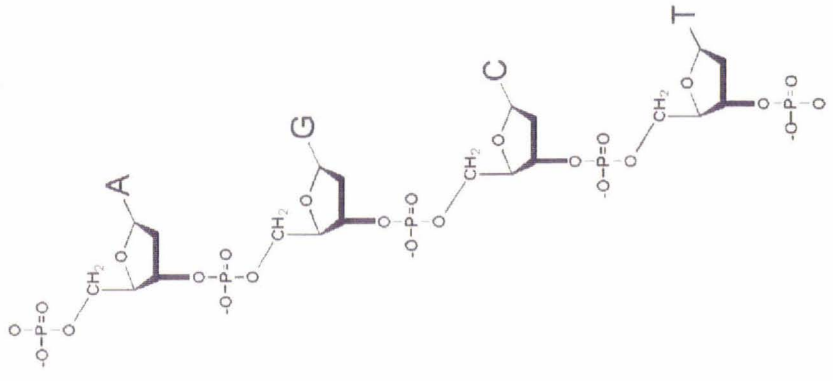
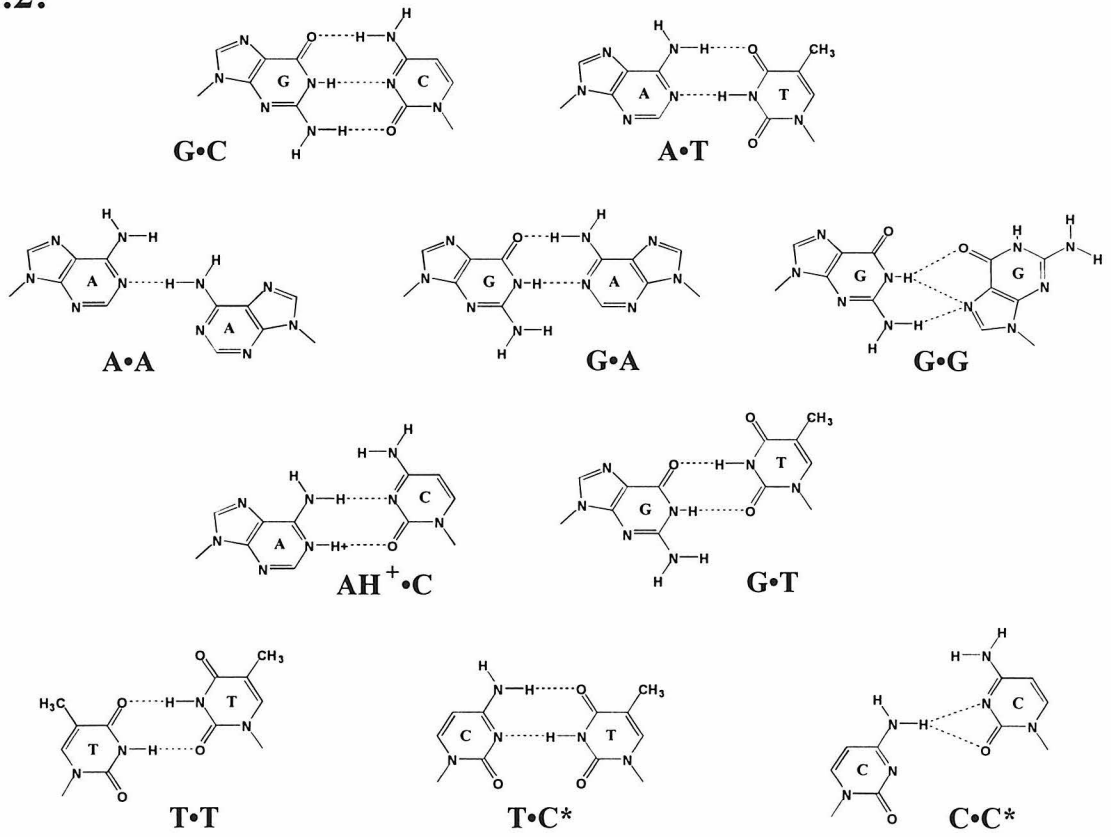


Figure 1.1:

Figure 1.2. The Eight Possible Base Mismatches in DNA.

Figure 1.2:



can be incorporated. All DNA mismatches, whatever their source, pose a serious threat to a living thing. If they are allowed to persist, the errors will cause changes to the genetic material that will not only affect an individual organism but will be passed on to all of its progeny. As a result, complex repair systems exist in most cells to correct these mistakes and prevent mutation of the genetic information.

1.1.2: Why Mismatch Recognition?

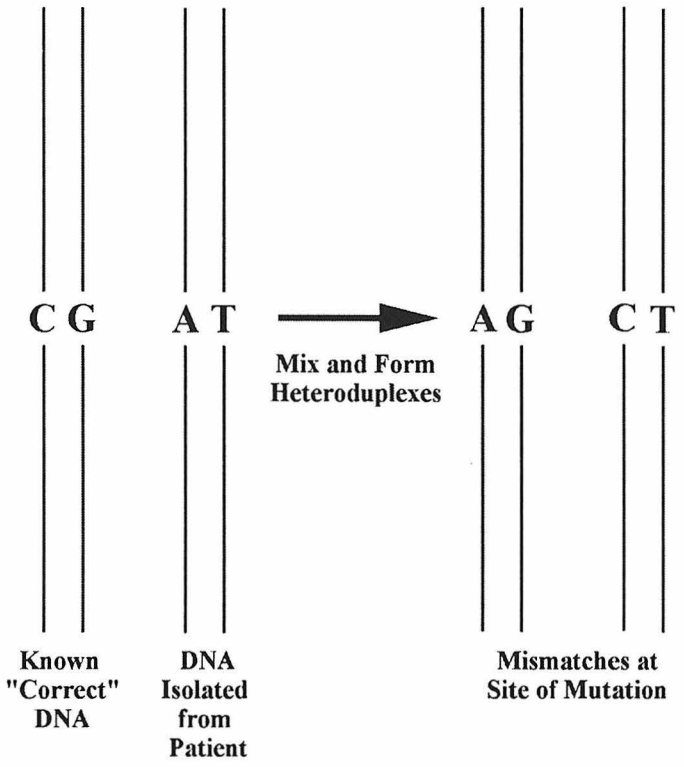
Like the DNA polymerase systems, however, the cellular mismatch recognition machinery is not always effective in removing mispairs and preventing changes in the cell's genetic information. Although they repair over 99% of mismatches which occur in DNA, the remaining few which slip through could be highly detrimental to the health of the organism.[2] In addition, it has also been shown that the mismatch repair systems are more likely to correct some mismatches than others. In *E.Coli*, for example, the hierarchy of mismatch repair is as follows: AC, GG, GT > AA ≈ TT > AG, CC, CT.[3,4] Since such failures of biological mismatch recognition can have particularly serious consequences on the health of human beings, there is considerable scientific interest in examining both the ways that biological systems identify and repair mismatches and in the construction of methods to accomplish the same tasks in the laboratory. As more and more research is done into the origins of different diseases, an ever increasing number of disorders are being identified that have genetic components to their pathogenesis. Mutations have been identified which are both the direct cause of disease, as in the case of sickle cell anemia, or that are associated with a predisposition to more complex diseases like cancer. With this ever increasing list of known genes and mutations associated with serious conditions, there is a need for easy and accurate tests to be used at the patient level to make diagnoses and medical decisions.

Although the most accurate way to make a genetic diagnosis would be to isolate DNA from a patient and completely sequence the genes of interest, this is not a cost effective or rapid enough method for commonplace usage. As a result, there is a great deal of interest in the development of better ways to quickly scan a sample of isolated nucleic acid to determine if specific mutations are present. One way of approaching this goal hinges on the ability to identify the positions of mismatched bases in an otherwise Watson-Crick paired duplex. If a sample of DNA isolated from a patient was combined and allowed to form a double helix with a copy of a gene that was known to be correct, at any position where the patient's DNA was different – sites of mutation – a base mismatch would be formed in the resulting duplex. A general scheme depicting this case is included in Figure 1.3. Because of the great commercial demand for such systems, the central objective of most research toward *in vitro* DNA mismatch detection systems has been for applications in diagnostic testing; a more extensive discussion of these systems and the strategies applied to recognize mismatches is included in later sections.

Although molecular diagnosis of genetic disease is a powerful inducement for research into mismatch recognition systems, there are additional reasons why the ability to locate single mismatches in DNA could be useful. Foremost among these is the fact that complete failure of mismatch repair systems has been associated with certain forms of cancer including hereditary nonpolyposis colorectal cancer.[5,6] Since affected tumors lack any mechanism to correct mispairs, they accumulate mismatches in their DNA. As a result, one could envision using a mismatch-specific drug molecule as a method to preferentially target cancerous tissue over nearby non-diseased cells. This prospect is of added importance as such mismatch repair deficient cancers are often resistant to many chemotherapeutic agents.[7] As will be

Figure 1.3. Mutation Detection by DNA Mismatch Recognition. In order to identify mutations in gene from an isolated genomic DNA sample, the nucleic acid is mixed with a known sample of the correct sequence gene. The strands of both are separated under denaturing conditions and allowed to recombine. Since the strands will recombine statistically, half of the resulting duplexes will be combinations of the isolated and control DNA. Any place these two differ in sequence, a DNA mismatch will occur. If methods are available to identify the presence and position of these mismatches, mutations in the unknown sample can be completely characterized.

Figure 1.3:


C G
A T
A G
C T
Mix and Form Heteroduplexes
Known "Correct" DNA
DNA Isolated from Patient
Mismatches at Site of Mutation

discussed more completely in later sections, the design of such mismatch-specific drugs is a related, but distinct, scientific challenge from the design of *in vitro* mismatch recognition systems.

1.2: Characteristics of Base Mismatches

1.2.1: Mismatch Structure and Dynamics

Because of their central role as intermediates in the process of mutagenesis, DNA mismatches have been extensively studied. These examinations, in addition to being driven by an interest in the characteristics of these "mistakes" in the nucleic acid themselves, have also focused on trying to determine the ways that the cellular mismatch repair systems might distinguish the presence of single mispairings against a large background of properly paired DNA. The earliest technique which was used to obtain high resolution information about the effect of base mismatches on DNA structure was X-ray crystallography. The first such structure, of an eight base pair duplex containing two GT mismatches was reported in 1985.[8] Since then structures have been reported for AC,[9] GA,[10-13] and GG[14] mismatches. These structural characterizations in the solid state (Figure 1.4) indicated that, although small changes occurred in the structure of DNA, even mismatch containing oligonucleotides adopted a generally regular structure essentially the same as properly paired DNA.* The structural differences which did exist in the crystal structures, however, led to the hypothesis that recognition of mismatches was based on deviation in the relative symmetry of the base pairs and their width (from C-1' to C-1' of the nucleosides) as

---

* The criticism has been made of crystallographic models of mismatch containing DNA oligonucleotides that more stable conformations of the nucleic acid may preferentially crystallize thereby making the crystallographic results non-representative of the structure which exists in solution.[15]

Figure 1.4. Crystal Structures of Mismatch Containing DNA Oligonucleotides. Note that while differences in structure do exist between mismatch containing and the regular structure of canonical B-form DNA, they are not that great. Structures adapted from coordinates found in references 14,16, and 17.

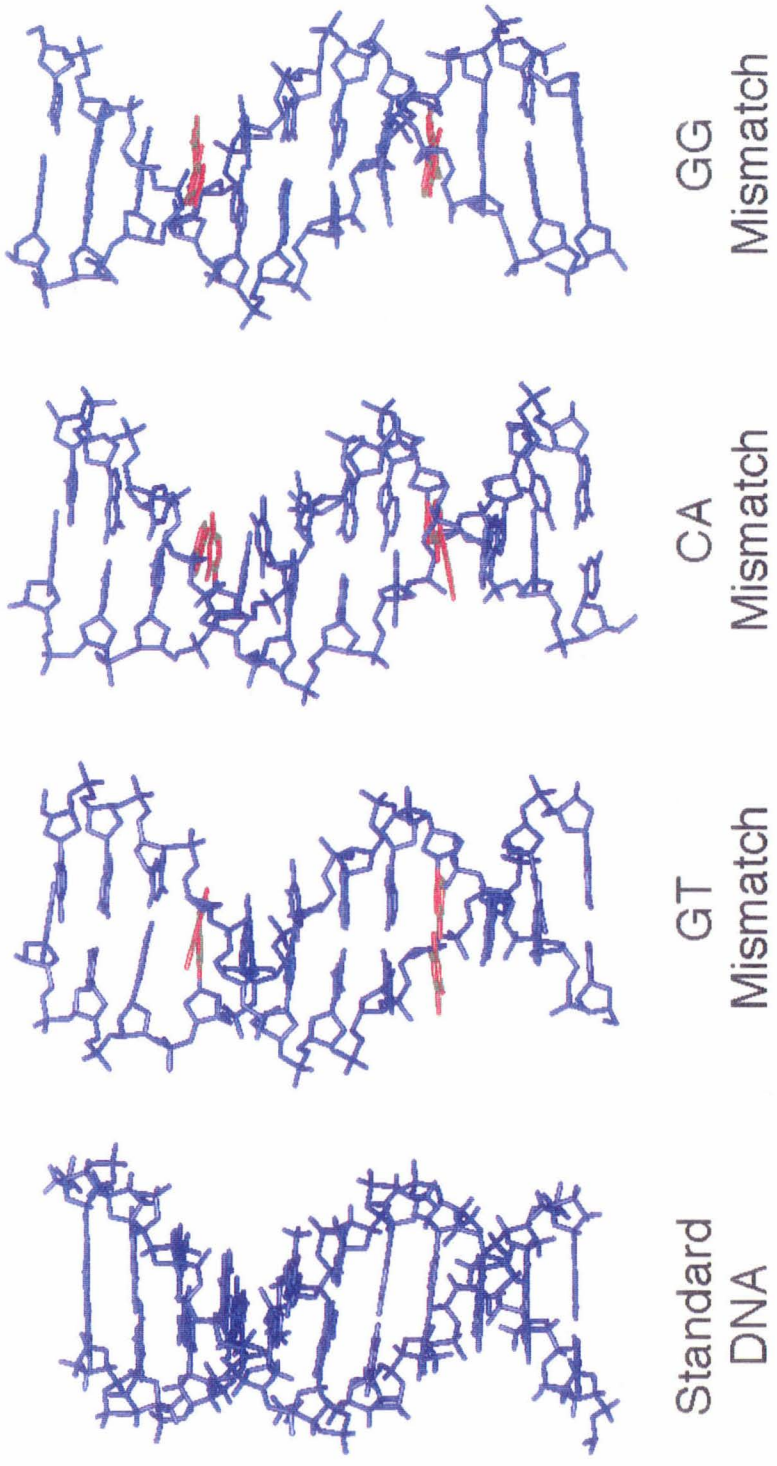


Figure 1.4:

compared to standard base pairs.[18,19] This hypothesis was proposed in light of the fact that the GA mispair, which was the most symmetrical and similar in width to a proper GC or AT, is the least efficiently repaired base mismatch. Since this hypothesis was based on only four data points, however, it was viewed with some caution.[15]

The desire to study base mismatch sites in solution led to the application of NMR techniques to mismatch structural characterization. The earliest of these studies characterized the conformational flexibility which results from the presence of mispairings by examining the increased imino proton hydrogen exchange kinetics of base pairs near mismatch sites.[20] Other studies observed the formation of mismatch containing duplexes with one-dimensional proton NMR to determine thermodynamic parameters.[21] As multi-dimensional NMR techniques became more routine and advances in DNA synthesis made concentrated NMR samples accessible, more sophisticated experiments could be performed. These techniques initially made it possible to ask questions about the base pairing and conformations of the mismatched base pairs and to determine how far mismatch induced perturbations propagated through the helical structure.[22] As techniques progressed further, the determination of solution structures of mismatch containing duplexes became more common. Using these techniques, structural models of AG,[23-27] GG,[28,29] CA,[25,30] AA,[31] TT,[31] and GT [32,33] mismatches were constructed. The overall structures determined by NMR spectroscopy agree with the qualitative conclusion reached by X-ray crystallography: the incorporation of a base mismatch does not result in large changes in the overall conformation of a B-form DNA helix.

Beyond simply structural concerns, however, the capabilities of NMR spectroscopy have also made it possible to determine the kinetics of exchange between various

conformations of the DNA at a mismatch site. Studies specifically directed to determining the conformational flexibility, base pair opening, and exchange kinetics at mismatches have been performed on the GT,[20,34] GG,[28,29,35] GA,[20,23,26] AC,[20] TC,[20] AA,[31] and TT[31] base pairs. These studies have shown that for some mismatches, such as GG, interconversion between conformations is fast enough to remain in the intermediate exchange regime down to 1°C.[29] In another study, the exchange rate between conformations of the GG mismatch was estimated to be approx. 10^4 s^{-1} at 303 K.[35] The GT mismatch has also been shown to be significantly more likely to adopt an open, extra-helical geometry than correctly paired DNA.[34] In contrast, the GA mismatch has been shown to have a conformational exchange rate on the order of only 100 s^{-1} at 303 K.[35] This is comparable to the rates of opening for Watson-Crick base pairs whose lifetimes are in the millisecond regime at room temperature.[34] As alluded to in the previous section, the GA mismatch is repaired much less efficiently than the GG or GT suggesting the hypothesis that this conformational exchange may be a recognition element for protein mediated mismatch recognition and repair.

Throughout the recent structural studies performed on mismatch containing DNA, an appreciation has developed of the fact that the base sequence which exists around a mismatch site can have a significant effect on how the mismatch effects the properties of the DNA helix. It has been known for some time that the sequence context around a mismatch can have an effect on the repair efficiency by biological recognition systems. It was determined, for example, that the repair efficiency of any given mismatch improved with increasing GC content of the surrounding base context; this effect extended as far as 10 base pairs to either side of the mismatch site.[2] More recently, it has been demonstrated that the repair efficiency of the G:T mismatch-specific thymine DNA-glycosylase is also dependent on the sequence context around

the mispaired site.[36] Taking this analysis one step further, it has been demonstrated that the probability of base pair substitution at sites in the chloroplast genome, which must proceed through a mismatched intermediate, is dependent on the bases surrounding the mutation site.[37] As more structural information has become available about mismatches in different sequence contexts, hypotheses about these context-dependent effects have been proposed. The NMR structure of the GG mismatch, for example, has been determined in two different sequence contexts, purine-G-purine[23] and pyrimidine-G-purine.[29] In the two structures resulting from these studies, the GG mispairs adopted very different conformations; in one structure, both of the guanine bases were in the *anti* conformation[29] while in the other, one base had rotated about its glycosidic bond to the *syn* configuration.[23] Other more qualitative studies have shown by NMR that the sequence context around a mismatch site can induce changes in the base pairing and geometry of the mismatch site. Such studies have shown that significant variation as a result of sequence context changes occurs at all the mismatches which were studied – the AA,[38] CC,[38] GG,[38] TT,[38] GA,[39] AC,[22] and GT.[32] Although less directly relevant to the work discussed here, studies have also shown that the conformations of sites where two GA mispairs occur next to one another (tandem GA mismatches), the overall structure is strongly dependent on the flanking sequences around the site.[40,41] As a result, it has become clear that not only the mismatch itself, but also the base pairs surrounding it, can have a significant effect on the structure adopted by a mismatch-containing DNA duplex.

1.2.2: Thermodynamic Consequences of Mismatch Incorporation

Although significant effort have been devoted to the elucidation of the structures of mismatch sites in DNA, it has also been known for some time that geometrical

changes are not the only consequences of mismatch incorporation into DNA. In addition to their structural effects on the regularity of the double helix and their kinetic destabilization – the increased tendency of mismatched bases to undergo conformational changes or base pair opening – most mismatches also destabilize the DNA duplex thermodynamically. This destabilization, resulting from the reduced ability of mismatches to hydrogen bond and the disruptions they cause to adjacent base pairs, is most readily observed in the lower temperature at which the strands of most mismatch containing duplexes separate from one another compared to properly paired nucleic acid samples. Exhaustive measurements on these helix melting (T_m) temperatures have made quantitative measurements of the exact thermodynamic consequences of mismatch incorporation into DNA helices accessible.[32,38,39,42,43] Like the structural consequences of mismatch incorporation, the thermodynamic effects of base mismatches are also highly dependent on the sequence contexts surrounding the mispair site. The greatest amount of helix destabilization observed for any mismatch site is associated with the CC mismatch in a 5'-A***C***T-3'* sequence context; this mismatch destabilizes the helix by 2.72 kcal/mol.[44] At the other end of the spectrum, certain mismatches, notably GG and GA, can stabilize the helix as a result of their incorporation. The greatest stabilization effect (-2.58 kcal/mol) is generated by the GG mismatch in a 5'-G***G***C-3' sequence context.[44] In total, approximately 80% of mismatch sites are destabilizing to the structure of the helix to some extent.[44]

1.2.3: The Nature of Mismatch Sites in DNA

The structural and thermodynamic characteristics of DNA mismatch sites explored in

---

* This notation indicates the sequence on one strand of the DNA where the CC mismatch includes the bold-italic C. It is surrounded on either side by AT and TA base pairs.

the preceding sections, although separated for the purposes of discussion, should not be viewed in isolation from one another. The two sets of properties are, in fact, interrelated with one another in a causal manner. To draw one parallel, since it is the specific hydrogen bonding and stacking interactions between bases which provide the binding affinity between two DNA strands, the disruption of these interactions at mismatch sites leads to the thermodynamic destabilization of the DNA helix. On the other hand, it is the strong stabilization which exists in a properly paired double helix which constrains the conformational motion of base pairs and preserves the stable, stacked base stack within the helix. As a result, the thermodynamic destabilization at mismatch sites could be viewed as the "cause" of the conformational flexibility which exists for mismatched bases and the base pairs near them. Mismatch sites in DNA should therefore be viewed from both these perspectives.

Unlike the stable molecular structure of properly paired DNA, the structure of the helix is much more variable and transitory at mismatch sites. The mismatches are more likely to be extra-helical with their aromatic bases extending into solution rather than being held in the core of the helix. Mismatched bases are much more likely to exist in an equilibrium mixture of multiple conformations than correctly paired Watson-Crick DNA. As a result, the structure of mismatch containing DNA is likely to be open and disordered. As shown by NMR and numerous other techniques, that disruption is both dependent on and likely to involve the bases to either side of the mismatch site. It is this disorder – or the absence of a kinetically and thermodynamically stable helical geometry at the mismatch – that must become the molecular recognition element for DNA base mismatch discrimination.

1.3: Protein Mechanisms of Base Mismatch Recognition

Because of their central roles in replication fidelity and the protection of the integrity of the genome, the mechanisms utilized by mismatch recognition (MMR) proteins is of significant interest. In addition to the basic scientific interest in understanding mismatch repair, the study of MMR proteins is also motivated by the thought that mechanisms used by these systems might be applicable to the design of *in vitro* mismatch recognition systems. Because of the similarities in their molecular recognition tasks and the complementary nature of the studies that have been done on them, it is also relevant to consider the recognition of sites of chemical damage in DNA as well. While an exhaustive review of what is known about these systems is beyond the scope of this work, some comments on the current hypotheses about protein recognition mechanisms are relevant.

Contrary to the frequent assumption in structural biology that specific binding must hinge on the binding of complementary, static *structures* to one another,[45] the current consensus in the field is that recognition of many lesions in DNA hinges on the kinetic and thermodynamic destabilization which they cause to the double helix.[46] Certain sites of damage, like most mismatches, have been shown to seriously disrupt the stability of duplex DNA. Like the mismatches discussed above, the disruptions can be very severe and cases have been demonstrated where the thermodynamically preferred conformation of a mismatched base may even be extra-helical.[47] These damaged or mismatched bases which may relatively readily "flip out" from the DNA base stack can be contrasted with properly paired or undamaged DNA that is more kinetically stable. If one envisioned an enzyme whose active site required that a base be extra-helical for tight binding, this preferential base opening at mismatch or

damage sites could be used as the basis for recognition. In properly paired DNA, there would exist a significant energetic penalty for the enzyme to "invade the DNA helix" and displace a base; at mismatched sites, this price would have "already been partially paid" as a result of the helix destabilization and so the enzyme would preferentially bind to these sites by capturing the already disrupted structures.[46]

This general model for recognition is supported by the crystallographic observation of base-flipped DNA substrates in the G:T/U mismatch-specific DNA glycosylase,[48] the uracil-DNA glycosylase,[49] the *HhaI* methyltransferase,[50], T4 Endo V bound to a pyrimidine dimer,[51] and the *HaeIII* methyltransferase.[52] In the case of T4 Endo V, the bound conformation of the DNA in the enzyme is significantly kinked; such a kink was not observed in solution studies of the pyrimidine dimer and, although it could be protein induced, it is possible that this also result from damage induced conformational flexibility and is preferentially captured by the enzyme.[51] Other studies have shown that a strong preference for the binding of helix destabilizing lesions by mammalian nucleotide excision repair proteins suggesting a thermodynamic probing of the helix.[53] AlkA, another damage specific enzyme, has an aromatic-rich active site cleft which is consistent with binding of DNA substrates in an extra-helical conformation.[46] Studies with AlkA have shown that, in addition to excising damaged bases, it can also cut out normal bases from properly paired DNA; the relative rates of excision of destabilized damage sites versus properly paired DNA is consistent with the enzyme capturing any base which is extra-helical and excising it with its preference for damage sites generated either by preferential reactivity with damaged bases[54] or by their greater propensity to be extruded from the helix.

It should not be assumed, however, that the concept of protein recognition of kinetically destabilized sites in DNA adequately characterizes the behavior of all DNA damage and mismatch recognition proteins. The comparison between two similar proteins, the mismatch-specific uracil DNA-glycosylase (MUG) and the more general uracil DNA-glycosylase (UDG) emphasizes this point.[48] Both enzymes perform the same task – excising uracil from DNA – and both gain access to their substrate by applying a base-flipping mechanism to bind the target base in an extra-helical conformation. In the UDG case, the recognition behavior of the enzyme is almost perfectly explained by the kinds of kinetic destabilization models described in the previous paragraphs. It binds most tightly to uracil in single stranded DNA where there is no energetic penalty for "extruding the base" from a non-existent helix. In double stranded DNA, its binding energy is directly related to the cost paid to disrupt base pairing binding uracil in GU mismatches better than that in AU base pairs. This enzyme has been characterized as "essentially [a] single-strand specific DNA repair enzyme that [is] also capable of processing uracil within double stranded DNA."[48] MUG, on the other hand, has a strict requirement for double stranded DNA and gains significant stabilization from interactions with the non-substrate strand of the DNA and gains little binding energy from interactions with the extra-helical uracil. As a result, rather than preferentially recognizing an extra-helical base, MUG plays a much more active role in "extruding" the target base out of the DNA.[48]

In addition to crystallographic models of the uracil excision enzymes, other facts call into question how sufficient helix destabilization and conformational flexibility are to fully explain recognition of aberrant sites in DNA by repair enzymes. Some crystal structures have also implicated more "traditional" structural recognition mechanisms for the recognition of base damage sites. For example, in the structure of T4 Endo V

bound to a pyrimidine dimer site discussed above, there are contacts to the deformed phosphate backbone generated by the damage site which are clearly recognizing structural characteristics of the DNA geometry.[51] In addition, lesions and mismatches exist that are readily repaired by the cellular machinery even though they do not significantly disturb base pairing or DNA structure or thermodynamically destabilize the DNA helix. Examples cited in the literature include guanine methylated at the N-7, uracil, 8-oxoguanine,[46] and several mismatches discussed in the earlier sections. Either these lesions have conformational exchange behaviors which are, as of yet, unappreciated or other mechanisms exist to recognize these sites. Particularly in these cases of lesions which are thought to be non-destabilizing but are still recognized, there is significant uncertainty about how active a role damage and mismatch recognition enzymes play in extruding their target bases from the DNA helix.[46] As a result, although the characteristics of thermodynamic destabilization, conformational flexibility and helical distortion which were identified in the structural studies of mismatch containing oligonucleotides likely play an important role in the recognition of mismatch and damage containing nucleic acids, these factors are not sufficient to completely explain recognition behavior. That such characteristics have been applied by natural systems does suggest, however, that similar recognition mechanisms might be applied in designed mismatch recognition systems.

1.4: Recognition of Base Mismatches in the Laboratory

The problem of mismatch recognition in the laboratory has been approached from many different directions over the last several years.[55,56] These methods have been focused on the development of technologies for the detection of mismatches in isolated samples for clinical and diagnostic application. Because of their clinical goals, all laboratory methods have as their standard 100% sensitivity and accuracy.

The standard of such accuracy in mutation detection is, of course, direct DNA sequencing of an individual gene isolated from a patient; such complete determination would provide its entire nucleotide sequence and allow assessment of any deviations which might exist between that sequence and the known sequence of the correct gene. Direct sequencing, however, is much too time consuming and expensive for application as a widely used diagnostic tool.[56] As a result, development efforts in the mutation detection field have focused on more rapid and cost effective strategies. Central among these is the use of mismatch detection techniques to allow scanning of a combination between a known copy of a gene and an isolated DNA sample to identify sites of sequence difference (Figure 1.3 above). These detection techniques, taking advantage of some of the differences in properties between mismatch containing and properly paired DNA, have taken many different forms with different strengths and weaknesses.[57,58] The various methods, however, can be broadly divided into classes which depend on hybridization differences, kinetic accessibility differences, and biotechnological application of natural mismatch recognition systems.

1.4.1: Hybridization Methods

Most techniques which have been devised for the detection of base mismatches *in vitro* focus on the different hybridization properties of properly paired versus mismatch containing DNA. As a result, these procedures generally take advantage of the reduced melting temperature (T_m) and decreased stability of mismatch containing duplexes compared to their properly paired counterparts.

The most basic methods for hybridization-based mismatch detection combine a known probe oligonucleotide with the DNA of interest in solution and apply a

detection technique to assess the level of interaction. The most common methods applied to this task utilize routine blotting techniques with probes labeled either radioactively or with enzymes,[59-62] In addition, such direct hybridizations have been detected using electochemical sensors[63] and spectroscopically by various fluorescence techniques.[64-67] More recently, the direct measurement of hybridization of oligonucleotides in solution has been performed by surface plasmon resonance; this technique focuses on kinetic discrimination between the association of matched and mismatched oligonucleotides.[68-71] A large number of electrophoretic techniques have also been applied to distinguishing mismatch containing DNA duplexes from one another.[72] They include various non-denaturing conformational analyses, the use of denaturing gradients in either 1D, 2D or capillary electrophoresis gels,[73-76] band shift methods,[77] and even the covalent attachment of probe oligonucleotides to acrylamide matrices to examine differential mobility shifts.[78] Most recently, a great deal of research has been directed toward immobilizing probe oligonucleotides on solid supports.[79-81] These assays, some of which are based on hybridization alone and some which include various modifications to conditions to improve selectivity, have the promise of making the parallel testing of many DNA sequences on a single "DNA-chip" accessible.[82-90]

1.4.2: Kinetic Destabilization Methods

In addition to methods based on the thermodynamic effects of mismatches on hybridization, there are a small number of detection techniques which exploit kinetic destabilization at mismatch sites. These procedures all take advantage of the greater accessibility of mismatched bases to solvent and, as a result, exogenous chemical reactants to discriminate them from properly paired DNA. Although electrochemical detection techniques using chemical oxidants have been used to detect reactions with

mismatched guanine bases,[91] the more general procedures use chemical reactants which can react with bases involved in all the possible mismatch sites. The most common chemical mismatch detection system involves the use of hydroxylamine to react with mismatched C bases and osmium tetroxide (or potassium permanganate) to react with mismatched T bases; the modifications generated by these reagents are subsequently converted to strand breaks by post treatment with hot piperidine.[92,93] Depending on the selection of probe strands, reaction with C and T is sufficient to detect the presence of all possible mutations. Modifications of these methods have produced chemical cleavage systems able to detect mutations in DNA linked to a solid phase support.[94,95] These chemical cleavage techniques have also been applied to fluorescently labeled DNA polymers (the so-called fluorescence assisted mismatch analysis or FAMA technique) making it possible to perform these experiments without radioactive isotope labels.[96-100] It is important to note that some mismatches, depending on their sequence contexts, are unreactive to these chemical modification reagents.[101]

A second chemical modification system which is used to detect mismatches, but is not based on DNA cleavage chemistry, uses the reagent 1-cyclohexyl-3-{2-[4-(methyl)morpholinyl]ethyl}carbodiimide. This compound is a sterically bulky reagent which reacts with imino functionalities on mispaired guanine or thymine bases in DNA.[93] The reaction of the carbodiimide reagent with a duplex of interest can be monitored by the reduction in mobility of the duplex on a polyacrylamide gel.[102] More specific site information from this technique requires the use of molecular biological techniques; these methods either take advantage of the inhibition of DNA polymerase by the adduct to identify the mismatch site[103] or visualize the lesion directly using immunomicroscopy with an adduct specific antibody.[104]

1.4.3: Biotechnological Methods

Rather than simply using molecular biological methods as a mode of detection of chemical adducts, many mismatch detection methods exist which are based solely on the recognition abilities of natural protein systems. The most straightforward of these biotechnological detection systems rely on the ability of DNA polymerase enzymes to discriminate the base pairing on their primer strand. When a mismatch is placed in the appropriate position, the enzyme will not initiate DNA synthesis. These systems, utilizing either mass spectral detection[105] or more common molecular biology detection methods,[106-109] allow the detection of known mutations at single sites in genes.

More general "scanning" method of mismatch detection which can detect the presence of unknown mutations or mismatches at multiple sites in genes have also been constructed. RNAse A, an hydrolytic enzyme which cleaves at mismatched sites in RNA:RNA duplexes or RNA:DNA hybrid duplexes, has been used to screen RNA copies of genes heteroduplexed with known DNA versions of the correct nucleic acid sequence.[110,111] Other enzymes, like endonuclease VII, have been shown to cut DNA duplexes at most mismatch sites and have been used as probes in cleavage-based detection systems.[112-115] Other mismatch recognition proteins, like MutY and MutS, have been used in the construction of either cleavage based assays or mismatch biosensors.[116-124] Although these methods have been successful for constructions of many different mismatch recognition systems, is important to note that they are limited by the substrate preferences of their component proteins. In addition, in the design of diagnostic tests which may be used routinely for a large fraction of the general population, reliance on fragile protein reagents is never ideal.

1.4.4: A Continuing Need for Novel Methods

Although many of the systems discussed above do represent significant advances in the identification of base mismatch sites in DNA, no mismatch recognition method has yet been devised which fulfills all of the desires of the medical or scientific communities. As the number of diseases with a genetic component to their cause continues to grow and the complexity of the known deleterious mutations increases, better techniques for molecular diagnosis at the genetic level are becoming increasingly important. The methods described in the previous sections, which often depend on harsh chemical treatments or complex protein/DNA systems, are not as selective, easy, inexpensive, or reliable as would be desirable for a frequently used diagnostic technique. If such genetic diagnosis truly does become commonplace, both highly precise and highly user friendly diagnosis techniques will be in ever-increasing demand. Beyond concerns of mismatch or mutation identification in the medical laboratory setting, however, currently known techniques for mismatch "recognition" are not amenable to the design of mismatch-specific chemotherapeutic agents. In order to construct such a drug molecule, selectivity for base mismatches cannot be based on protein recognition or DNA hybridization. Furthermore, the harsh chemical cleavage methods which "recognize" the presence of a mismatch by reacting preferentially with exposed base functionalities are also not applicable to treatments of living organisms. Instead, recognition of the base mismatch must be approached from the traditional perspective of true *molecular recognition* – where recognition is now defined as preferential binding at a desired site. By approaching the problem in this way, small molecules might be designed which could reasonably be expected to preserve their specificity in the complex milieu of the cell and, as a result, exert a mismatch-specific effect on a biological system. Before discussing this specific task, it is relevant to briefly introduce some of the considerations

involved in the design of molecular recognition agents and DNA targeted molecules in particular.

1.5: Molecular Recognition

When the greasy surfaces of detergent molecules associate in solution to form micelles or anions and cations combine to form an insoluble, aggregated precipitate, molecules are binding to one another. When that binding becomes specific, like the ordered combination of many viral envelope proteins to form a single icosahedral capsid, then it is molecular recognition. The blanket term molecular recognition covers a huge number of chemical and biological behaviors. It is non-covalent in nature but it can lead to covalent attachment and reaction. The hallmark of molecular recognition is its specificity; it is the specific binding of one – one kind of functionality, one molecular geometry, or one molecule alone – to the exclusion of all other possible interactions.

At the upper end of its size range, where huge proteins and protein assemblies are the reactants, molecular recognition is what makes life possible. The simple principles of specific binding control the arrangement of proteins that give an organism structure, deliver molecules through the bloodstream or through selective channels in the cell membrane, and regulate and target the thousands of chemical reactions occurring in all the body's organs and organelles. Without exquisite specificity, an organism could not effectively use the information stored in its DNA, could not segregate proteins to the cellular areas where they perform their necessary functions, and could never evaluate its environment or receive messages from cellular neighbors that allow it to adapt and change to best ensure survival. Indeed, when reduced to the most simplistic level, molecular recognition is life.

1.5.1: Thermodynamics – Driving Forces for Molecular Recognition

The study of molecular recognition is, almost without exception, the study of spontaneous binding of one molecule to another. Put another way, it is the study of processes whose free energy, ΔG, is negative. As a result, the examination of molecular recognition events can be broken down to the contributions that they make to the free energy. In a more quantitative language, each part of a molecular recognition event, whether favorable or unfavorable to the reaction of interest, can be assigned to one of the terms in the Gibbs relation, $\Delta G=\Delta H-T\Delta S$, where ΔH is the change in enthaphy, the heat released or absorbed by the binding reaction, and ΔS is the change in entropy, the order or disorder generated by the association. When approaching the study of a specific molecular recognition system, one must dissect out the energetic contributions that make specific binding possible; conversely, if the experimental goal is the design of a recognition agent for a set task, some ensemble of interactions and circumstances must be assembled that will provide a negative free energy and spontaneous molecular association.

1.5.1.1: Enthalpic Contributions to Binding

Hydrogen Bonds: Hydrogen bonds are one of the most widely observed and most completely understood elements of molecular binding events. The association of a hydrogen atom, covalently attached to an electronegative heteroatom, with another heteroatom, generates a short range, localized, and directional non-covalent bond. The energies involved in individual hydrogen bonds has been estimated by theorists to be between 3 and 19 kcals/mol depending on the atoms and charges involved in the bonding.[125] These values can be compared to a value of 4.8 kcal/mol for the dimerization enthalpy of two water molecules in a vacuum.[126,127] Rather than occurring in a vacuum, however, most molecular recognition events, especially those

between biological molecules, occur in water. As a result, the influence of the solvent on the bond energetics is of primary importance when assessing the contribution of a hydrogen bond to a molecular binding event.

Since water molecules are very adept at forming hydrogen bonds with materials in aqueous solution, virtually all possible hydrogen bond donors and acceptors on a molecule will be occupied by solvent before a binding event takes place. As a result, the net energetic contribution of a hydrogen bond to the free energy of molecular association is really the energy involved in the exchange reaction where hydrogen bonds between the solute and solvent molecules are broken and are replaced with hydrogen bonds in the complex and among the released solvent molecules. If the same number of hydrogen bonds are formed in the complex as existed between the solvent and the unbound molecules,* the net energetic contribution of hydrogen bonding will be very small since a bond must be broken for every bond that is made.[128] This simplification depends, of course, on the assumption that the bond strengths between the two associating molecules are not larger than those between solute and solvent or among solvent molecules.

This influence of the solvent on hydrogen bonding reduces their contribution significantly from the 5 kcal/mol free energy value cited above. Most estimates put the value of simple hydrogen bonds closer to 0.5 to 1.8 kcal/mol.[128] This reduction to a single number, however, should not be over-interpreted since differences in individual molecular recognition systems can cause large changes in the energy provided by individual hydrogen bonding interactions. Furthermore, reducing the energy of a hydrogen bond to a single ΔG contribution does not fully characterize

---

* Assuming that there are no geometrical constraints on binding or hydrogen bond formation.

how the competing energetics of solvent interactions, hydrogen bonding as part of the biomolecule association, and the various entropic components of these changes combine. These questions constitute an important current area of research and some controversy in the literature.[129-132]

Hydrophobic Interactions: Hydrophobic, or lipophillic, interactions are the surface/surface associations of greasy functionalities on a molecule. As a general category they also include van der Waals interactions between individual groups. Hydrophobic interactions are thought to be mainly entropy driven by the release of "perturbed" water molecules structured around the surfaces but likely have enthalpic contributions from dispersion forces between the surfaces as well. Such interactions are quite short range decaying with an r^6 dependence on distance and are estimated to contribute approximately 20 to 50 cal/(mol $Å^2$) of surface area involved.

Electrostatic Interactions: Electrostatics, or the interaction between oppositely charged groups, provide a relatively strong, longer range interaction between molecules. Such interactions decay with the square of the distance unlike the r^6 dependence of van der Waals interactions and they provide high selectivity for appropriately charged groups.* Basic physical calculations estimate that the interaction energy of two opposite single point charges is on the order of 1 to 2 kcal/mol at reasonable interaction distances.[133] This does not take into account screening by solvent and counter-ions or the possible entropic gain by release of the solvent molecules solvating the charged groups.

---

* That is, a positive charge is very selective for a negative charge and will exclude other positive charges very effectively.

1.5.1.2: Entropic Contributions to Binding

Although the previous section above set out to isolate only the enthalpic contributions to macromolecular binding events, the fact that discussion occasionally moved to entropy emphasizes the difficulty which arises in separating individual energetic contributions to binding. Upon initial examination, it might be assumed that the entropic contributions to binding would be much more straightforward; on the most basic level, it seems obvious that the primary entropic effect on macromolecular binding would be negative. The binding of two molecules to form a single molecular complex must result in a decrease in disorder as two independent molecules join together to form a single complex. In reality, entropic changes can also make very significant positive contributions to binding events as well. As was alluded to in the discussion of hydrophobic interactions above, the association of two large molecules can result in the release of many solvent molecules that would otherwise be ordered at the their binding surfaces. The release of these solvent molecules to "bulk" solvent can provide an entropic contribution to the free energy of binding.

For the purposes of designing molecular recognition agents, however, the primary entropic consideration is how the loss of disorder will hinder the formation of a desired molecular complex. The entropy loss during a binding event is customarily divided into two parts: ΔS_{T+R}, the translational and rotational entropy of the molecules, and ΔS_r, the loss in entropy as a result of restriction of the internal rotations within the molecule. If two very flexible biomolecules did in fact bind to a completely *rigid* unit, the entropy price would be extremely large – on the order of 12-15 kcal/mol for the loss of translational and rotational entropy alone.[130,134] The second value, ΔS_r, similar to the additive contributions to binding of hydrogen bonds and hydrophobic contacts, is the sum of all the internal rotors that are more hindered

in the complex than when the molecules are free in solution. The cost of restricting a rotor is in the range of 0.4 to 0.9 kcal/mol; the cost of freezing a rotor is higher at 1.2 to 1.4 kcal/mol.* Although these entropic costs could add up to a considerable contribution unfavorable to binding, the association of flexible bio-molecules seldom involves these maximal decreases in entropy. Since much of the inherent flexibility is retained in the complexes, only part of the possible total entropy loss is realized.[130,134]

This last point, however, emphasizes a significant linguistic distinction that exists in the molecular recognition literature – the two very different uses of the phrase "tight binding." The first usage, and the case discussed above, is the notion of tightness of binding as formation of a rigid complex with restricted motion of the ligand and macromolecule. The second use of tight binding is to describe a binding reaction where there is a large negative free energy, ΔG, of interaction. The two uses, in addition to being very different, are actually orthogonal. The more rigid the resulting molecular complex, the higher the entropy price that must be paid upon binding, and the lower the overall free energy of binding.[135] For the purposes of designing molecular recognition agents, one is usually interested in designing ligands that bind with large negative ΔG's of binding. The other definition, however, also has applicability to important molecular recognition events. It has been suggested that the large entropic cost paid for fixing flexible molecules into rigid complexes is used by nature as a mechanism for regulating the overall free energy of bio-recognition events.[136]

---

* These costs are for restricting rotation about an ethylene type carbon-carbon bond. The hydrogen atoms of a methyl group are considered freely rotating even in a molecular complex.

1.5.2: Specificity in Binding Events

While the energetic contributions discussed above address the reasons why two molecules might bind to one another, they do not directly consider the second important characteristic of molecular recognition, specificity. Although understanding the energetic contributions that give a biological association its binding energy is important, a comprehensive knowledge of the sources of specificity in binding reactions is even more critical. Without understanding how nature controls the formation of a desired complex over all possible competing association reactions, it is difficult both to fully understand the biological system and to design methods to modify its function or treat undesirable behaviors. At the most basic level, the specificity of a particular molecular recognition event can be described by comparing the association constant of the desired recognition reaction to the competing association constants for other binding events. In the case of a DNA binding protein, for example, the specificity would be the ratio between the binding constant at the wild type recognition sequence and the protein's binding constant at other, similar DNA sequences. In the case of a designed recognition event, the experimental goal is to maximize this ratio by both maximizing the association constant at the desired site and by discouraging binding at non-desired sites as much as possible.

In the design of specific molecular recognition agents, the stabilizing interactions discussed in the previous section are the first and most important mechanism to modulate the association constant at a molecule's binding sites. Placement of hydrogen bonds, charge-charge interactions, complementary hydrophobic surfaces and similar attractive functionalities can serve both to facilitate binding and to help prevent the dissociation of a molecule bound at a site on a biopolymer. Other, non-

desired sites which lack appropriately placed interacting functionalities and, as a result, would lack their contribution to the binding constant. The extent that single changes in functionality can contribute to specificity is somewhat limited, however. It has been estimated that an unpaired hydrogen bond, for example, increases the dissociation constant by only a factor of 2 to 20 although multiple unpaired bonds can amplify that effect.[128] Charges provide a high degree of specificity for the identity of the charge given the strong repulsion between like charged functionalities. The relatively long range of charged interactions, however, may provide more flexibility than is desired in the molecular complex.[137] A more effective, if somewhat limited, mechanism to produce specificity is steric interactions between a binding molecule and undesired binding sites. At the most simple level, a large molecule cannot enter a cleft on an enzyme designed to accept only small molecules and will therefore generate a high degree of specificity.[137] This principle can be generalized to the placement of groups to clash with features of undesired ligand binding sites, although the less serious the clash, the less discrimination will be provided. This method of specificity generation, rather than promoting or stabilizing complex formation at the desired site, reduces the association constant at undesired sites. In all cases, the methods used to design a specific molecular recognition agent must be carefully matched to the intended target of the binding molecule. In order to properly position stabilizing interactions or appropriately place groups to clash with undesired binding sites, structural information is required for both the desired and undesired binding sites.

1.6: Molecular Recognition of DNA

Although there are many challenges in the field of molecular recognition design, as discussed in the earlier sections, the specific goal of this work is the molecular

recognition of sites of base mismatches in DNA. Independent of the particular design goal, however, the molecular recognition of DNA is a particularly difficult scientific problem. Because of the large amount of information required to assemble complex organisms like human beings, the genomes of all higher animals and plants are very large. As a result, for a given molecular recognition agent to affect a single site within such a large amount of DNA, it must specifically bind to its target sequence even in the presence of a very large excess of competing undesired sites. Although such a recognition process requires an astonishing level of specificity, it is not an insurmountable challenge. As complex organisms with larger and larger genomes have evolved, nature has solved this problem in many ways to allow the successful management and use of large amounts of genetic information. As a result, before turning to the specific task of designing mismatch specific DNA binding agents, it is valuable to take a broader view of what is known about DNA recognition. Since the design of small molecule recognition systems has been so extensively informed by the study of these natural DNA recognition, it is most reasonable to begin the discussion with proteins.

1.6.1: Insights Gained from Protein Recognition of DNA

Proteins that bind and react with DNA must perform precise molecular recognition tasks to fulfill their roles in the biology of the cell. Such proteins, which vary from bacterial restriction endonucleases to human gene repression systems that ensure that skin cell genes are not expressed in lung tissue, must identify their correct binding sites from a huge background of structurally very similar nucleic acid. By using ensembles of the hydrogen bonding, charge-charge, and hydrophobic interactions discussed in the preceding sections, they achieve levels of specificity only aspired to by systems designed by chemists and biologists. These proteins, of course, have the

advantage of years of selective evolution that has perfected them for their required activities; if they were not exquisitely specific, the wrong genes could be regulated or a rogue restriction enzyme might begin cutting up its own bacterium's genome ensuring that such an organism would not have the opportunity to reproduce. In fact, the consequences of changes or breakdowns in the molecular recognition properties of DNA binding proteins are of direct concern to most of the human population. As discussed on the first sections on DNA mismatches, some of the genes involved with the development of human cancer have been identified as DNA binding proteins which, as a result of errors and mutations, are no longer correctly completing their specific tasks.

Because of their many important roles, a great deal of study has been devoted to DNA binding proteins and the mechanisms they use to bind and recognize their target sites on the nucleic acid. As discussed in more general terms in the preceding section, the binding affinity of proteins for their nucleic acid sites is controlled by an ensemble of enthalpic and entropic contributions. However, with the widespread use of protein crystallography and its molecular level view of chemical interactions, it has become clear that these simple electrostatic and steric interactions can combine to produce activities that seem greater than the sum of their individual parts. In many of the transcription factors and other proteins whose structures are now available, the recognition of a segment of DNA hinges not only on individual protein-DNA contacts but also the coupling of conformational changes in the DNA and the protein to provide enhanced binding affinity or specificity. These more complex and manifold binding pathways make it possible for a protein system to use relatively simplistic attractive forces to perform very subtle and complex recognition tasks. While a detailed review of all the details of DNA-protein recognition is beyond the scope of

this work and is available elsewhere,[138-140] a few points most relevant to the design of artificial molecular recognition systems will be highlighted.

DNA binding proteins must locate and bind their target sites very quickly. After a DNA binding protein is transcribed, it must return to the nucleus and locate its binding site in the genome. Although this is of less concern for organisms with small genomes, if a protein molecule had to find its place in the three billion base pairs in a human cell by random binding and dissociation the time scale involved would be prohibitively long. In an analogous fashion, in restriction enzyme systems, a bacterial enzyme must quickly bind and cleave invading viral DNA before it has a chance to either take over the cell or persist in the cytoplasm long enough to be protected by the modification enzymes that protect the bacterium's own DNA. As a result, a binding protein cannot rely on random diffusion to locate a single site against the large background of undesired sites. The mechanism that has evolved to accelerate the binding of specific binding proteins is called linear diffusion and takes advantage of the polymeric structure of DNA.

The behavior, which has been best characterized in the restriction enzyme systems,[139] relies on non-specific/low affinity binding of the nucleic acid by the DNA binding protein. The binding protein binds weakly to DNA utilizing electrostatic interactions between the anionic phosphate backbone and the protein. These binding events are very rapid with rate constants on the order of 10^7 to 10^8 M^{-1} s^{-1}. Furthermore, these non-specific complexes have been hypothesized to be very "loosely" bound as large numbers of water molecules are sequestered in the complex suggesting a layer of solvent exists between the protein and the DNA. Once the binding protein has formed a non-specific complex with DNA it remains associated and searches along the polymer for its specific binding site. As a result, the molecule is diffusing along

a single line eliminating the larger time required to diffuse randomly through three dimensions. The restriction enzyme *EcoRI*, for example, scans the DNA at a rate of 7×10^6 bp s^{-1}; this is approximately two orders of magnitude faster than the three-dimensional diffusion rate in solution.[141] The weak electrostatic nature of these non-specific complexes between enzyme and DNA provides a geometry were the DNA can move easily through the recognition/active site of the protein. During a single binding event the enzyme scans thousands of base pairs of DNA and, under optimal conditions, no specific binding site is overlooked. "Star sites," which are similar in sequence to the preferred binding site, cause pauses in the diffusion process roughly proportional to the affinity of the enzyme for those sites. When the protein does find a preferred site, the non-specific complex collapses to a more intimate specific association with the release of water and interaction of specific functional groups on the DNA and protein.[139]

DNA binding proteins bind with very high affinities. In order to participate in facilitated diffusion, DNA binding proteins must have a significant non-specific affinity for DNA. Most such proteins have association constants in the range of 10^5 to 10^6 M^{-1} for random sequence DNA. When bound to their specific sites, however, these affinities increase markedly into the nanomolar and picomolar regimes. Such high binding affinities are generated by the same factors that produce non-specific binding like electrostatic and hydrophobic interactions combined with interactions specific to the protein's preferred binding site. The specific interactions generally involve only a subset of the 20 amino acids: most frequently arginine, lysine, histidine, asparagine, and glutamine. These specific interactions between amino acids and base functionalities are termed *direct readout* of the DNA base sequence. It is important to note, however, that the specific interactions between individual amino acids and DNA are highly dependent on a large number of less-specific

contacts and the overall fold of the protein itself to produce the required binding geometries and alignment. In contrast to the individual interactions involved in direct readout, DNA binding proteins also use *indirect readout* mechanisms to recognize their target site and increase binding affinity. These indirect readout mechanisms include the recognition of the specific shape or exploitation of other characteristics of a specific DNA base sequence. Such indirect readout mechanisms can greatly increase the effectiveness of individual protein-DNA interactions and greatly increase the specificity of the molecular recognition process.[138,140,142]

DNA binding proteins bind their target sites with a high degree of specificity over non-target DNA. Although the level of binding affinity that proteins have for their DNA target sites is impressive, it is their level of specificity for their cognate sites over non-cognate DNA that is truly remarkable. Some of the most dramatic examples of this specificity in DNA protein recognition are found among the restriction endonucleases; it has been observed that single base changes in the enzyme binding site can lead to a million fold drop in activity.[143] It should be emphasized, however, that these endonuclease systems gain specificity both from differential binding and also differential levels of catalysis at cognate versus non-cognate sites. Extrapolating from the binding numbers included in the previous paragraphs, specificity values of between 10^3 and 10^5 would seem more general applicable and only slightly less impressive.

The major source of such high specificity is the intimate relationship that exists between the interacting surface of the DNA binding protein and the surface presented by its target binding site. Over the course of evolutionary history, functionalities and protein contacts have appeared to maximize the complementarity between these surfaces. Such tight fit leads to the maximal energetic benefit for each

thermodynamically stabilizing interaction available at the binding site. In addition, many proteins have also evolved interactions in their binding pockets that are non-complementary or clashing with undesired binding sites. While such interactions may provide no net stabilization or even an unfavorable contribution to the free energy of binding at the target site, they can markedly increase the protein's specificity as it searches for the least destabilizing site.[142]

DNA binding proteins also take advantage of indirect readout mechanisms to increase binding specificity. By taking advantage of unique structures in the binding site sequence, a protein can use shape to exclude undesired sites that might be otherwise very similar in sequence. In an extreme example, for DNA sequences that are flexible, bendable, or untwistable, proteins can use these characteristics to generate high levels of specificity between sites that might differ in only a single base pair. If a protein binding site will only accommodate a bent or unwound segment of DNA, any sequence which cannot adopt such a conformation will be immediately excluded. In addition to taking advantage of characteristics of its nucleic acid target, protein centered mechanisms also exist to increase binding specificity. For example, many proteins use dimerization of two similar (or identical) subunits and the recognition of palindromic sequences to broaden their recognition footprint on the nucleic acid and increase specificity. Such behavior serves to double the width of the recognition site with the minimum amount of protein structural changes.

The strategies "discovered" by proteins to accomplish their demanding molecular recognition tasks have proven to be an important resource as chemists have attempted to design novel binding agents for specific purposes. The specific interactions between amino acid functionalities and groups on DNA bases have provided an important starting point for molecular design. Furthermore, protein mechanisms like

indirect readout and selection of DNA sites of non-traditional geometry have also opened up entire new avenues for small molecule synthesis and application. Most importantly, DNA binding proteins have served as a standard of specificity and binding affinity against which all human efforts are measured. As such, they serve as a motivating force for synthetic and medicinal chemists because, in spite of the amazing advances that have been made in the recognition of DNA by small molecules, none of these systems have yet fully captured all the advantages of their much larger, biological archetypes.

1.6.2: Small Molecules for DNA Recognition

Because of the potential to produce compounds that could control cellular functions at the level of genetic information transfer, a great deal of research has been devoted to the design of small molecule agents that bind to DNA. These design efforts have been informed by the many lessons learned from protein recognition systems about direct and indirect readout of the characteristics of base sequences. Such molecules have proven to not only be useful from a laboratory standpoint as model systems to explore and understand DNA recognition but also from a medical standpoint as many of these small DNA binding agents have found uses as chemotherapeutic agents or antibiotics. Since a comprehensive discussion of the many families and variations of low molecular weight DNA binding agents would be extremely lengthy, the subsequent discussion will simply highlight some of the characteristics of these compounds relevant to the primary topic of this work.

Examining the body of small molecules known to interact sequence specifically with DNA, one can draw several broad generalizations. Most compounds which have either been designed to interact with a given base sequence or have been isolated from nature, like proteins, assemble their recognition and binding affinity from an

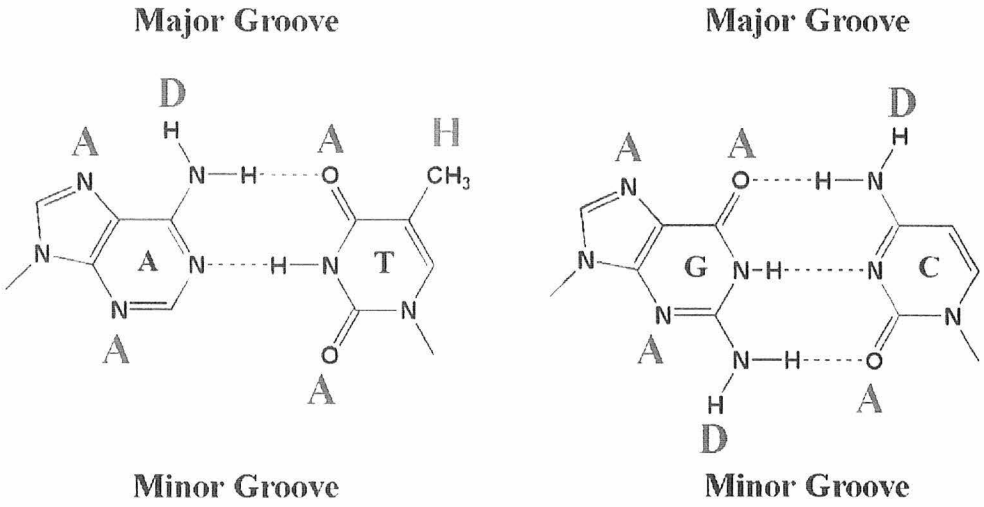
ensemble of non-covalent attractive interactions. The individual types of interactions are identical to those found in proteins – hydrogen bonds, hydrophobic contacts, electrostatic interactions – but, lacking the many thousand molecular weight protein backbone, small molecules must build more of these interactions into a much more compact space. In addition, since most small molecules do not interact with DNA in the same ways as proteins, these interactions have had to be applied somewhat differently to solve similar molecular recognition problems.

The primary difference between most small molecules and the proteins they seek to emulate is the location on the nucleic acid where binding occurs. Most small molecules which bind non-covalently to DNA do so in the minor groove of the helix (See Figure 1.1 above).[144] This preference is thought to result from the better van der Waals contacts which can occur with the walls of the deep and narrow minor groove and from better charge neutralization.[145] The larger proteins generally bind in the wider major groove of the DNA which allows more easy access by the protein helices or arms containing the recognition functionalities. In addition to its larger size, the major groove also presents a richer surface of functionality for molecular recognition. As shown in Figure 1.5, the major groove of DNA presents a large number of hydrogen bonding donors and acceptors in addition to the hydrophobic contacts with the methyl group of thymine. In contrast, the minor groove has many fewer possible contact functionalities; this more limited variety and number of interactions makes it even more challenging to perform recognition tasks in the minor groove.

The restricted array of functionality in the minor groove has not proven to be an obstacle to the design of small molecule recognition agents, however. The challenge of distinguishing the DNA base pairs with fewer possible contact points has simply

Figure 1.5. Functionalities in the Major and Minor Grooves of DNA. The major groove of DNA is far richer than the minor groove in potential interaction positions for DNA recognition. In this diagram, hydrogen bond donors are indicated with the blue D, hydrogen bond acceptors with the red A, and hydrophobic van der Waals contact points with the green H.

Figure 1.5:


Major Groove
Major Groove
D
H
A
A
H
N
H
O
CH3
N
A
N
N
H
N
T
N
A
O
A
Minor Groove
D
H
A
A
O
H
N
N
G
N
H
N
C
N
A
N
H
O
H
A
D
Minor Groove

resulted in the application of multiple recognition strategies to get around the limitations of the nucleic acid.[146] For example, large families of compounds based on the naturally occurring molecules distamycin and netropsin have been synthesized which lay into the floor of the minor groove and read out the DNA base pairs using hydrogen bonding donors and acceptors. Such compounds were readily isolated which could distinguish base pairs containing guanine and cytosine from those containing adenine and thymine. Additionally, the functionality available in the minor groove also made it straightforward to distinguish a GC base pair from a CG pair.[147] Because of the symmetry of their profile from the minor groove, however, distinguishing an AT base pair from a TA pair proved very difficult. The recent solution to this problem required combining hydrogen bonding interactions with indirect shape selection to discern the different geometries of the two base pairs.[148]

In addition to frequently binding in the minor groove, many small molecules also utilize a binding mode to interact with nucleic acids that is only occasionally observed in protein systems. This particular mode is *intercalation* or the insertion of an aromatic group on the binding molecule into the aromatic stack of DNA bases that make up the core of the double helix (see Figure 1.1 above). These intercalating groups vary widely in their substitution pattern but they are usually either heterocycles or heavily substituted ring systems. The process of intercalation requires significant deformation of the DNA structure – including increasing the separation between two adjacent base pairs and alteration in the winding of the helix – but the energetic costs of these changes are offset by the stabilization of the drug molecule inside the base stack.[149] This stabilization is thought to arise from general hydrophobic interactions, removing the aromatic heterocycle from solvent, and from dipole-dipole interactions between the intercalator and the adjacent base pairs.[150] Examples of such intercalators which bind from the minor groove of DNA include

various anthracycline based antibiotics and the actinomycin anti-tumor drugs.[146,151] This later class of drugs contains both an intercalator and appended peptide functionalities which participate in direct readout interactions in the minor groove.

The design of small molecule agents for the recognition of DNA has been an active and prolific field of research for many years. Although the levels of specificity and affinity achieved by DNA binding proteins are still the standard for what researchers in this field hope to achieve, the ways that small molecule systems diverge from their macromolecular counterparts have proven to be scientifically useful in their own right. The predominance of small molecule binding from the minor groove has led to a much deeper understanding of recognition mechanisms since strategies had to be developed to approach DNA recognition from "that side of the helix." In addition, the propensity of small molecules to bind to DNA by intercalation has also opened up entire fields which might not have been as readily discovered if these molecules had behaved more similarly to proteins. In a further divergence from the properties of DNA binding proteins, this discussion will now turn to a set of molecules removed by another discipline – inorganic chemistry – which makes properties and functionalities available that would be very unusual in "purely" biological systems.

1.6.3: Octahedral Metallointercalators for DNA Recognition

Octahedral metallointercalators are an important class of small molecule binding agents that have proven to be very useful probes for many characteristics of nucleic acids. In addition, the novel properties made available by the metal ion which serves as the central core of these complexes have made it possible to apply them to a breadth of problems that purely organic compounds could never approach. Such applications have included acting as luminescent probes for DNA,[152-155] as probes for geometrical variation in DNA structure,[156-159] and as agents to study DNA

mediated electron transfer.[160-168] In addition, this class of metal complexes has been used to inhibit the interactions of DNA binding proteins[169] and as delivery systems for appended peptides for recognition of and reaction with DNA.[170,171] Most relevant to the current work, however, is the many applications that transition metal complex have found in the design of novel DNA recognition agents. As such, these inorganic compounds have provided the opportunity to combine the lessons learned from both small molecule and biological studies of DNA molecular recognition.[172,173]

1.6.3.1: Characteristics of Metallointercalators for Molecular Recognition

Although many metal ions have served as the core of octahedral complexes designed to interact with DNA, the transition metal of interest for the design of molecular recognition agents is rhodium(III). Since it is a low spin d^6 metal ion, complexes of Rh(III) are substitutionally inert and rigidly octahedral. As a result, these rhodium complexes provide the opportunity to examine the interaction of a coordinatively saturated molecule interacting non-covalently with DNA. In addition, the inertness and rigid geometry of the central metal ion allow the construction of complexes of known geometry and the placement of functionalities at defined positions in space relative to the core of the complex. The positive charge conferred on the complex by the central (+3) metal ion is also critical for these compounds to serve as effective DNA recognition agents. Since DNA is a polyanion with a net (-2) charge for each base pair unit, the presence of a positive charge on a DNA binding molecule will generate a significant amount of non-specific electrostatic attraction between the small molecule and its DNA target. This is similar to most DNA binding proteins which tend to be quite basic to provide just this type of general electrostatic binding.

Like the small molecule DNA intercalators discussed in the previous section, judicious choice of the ligands placed around the central rhodium ion make it possible for these metal complexes to bind to DNA by intercalation. It has been known for some time that planar inorganic complexes can intercalate into DNA similar to flat organic molecules.[174,175] The intercalation of one such planar metal complex into a dinucleotide was even characterized crystallographically.[176] The intercalative binding of ligands on octahedral metal complexes has been established by numerous NMR studies[177-182] and, most recently, by X-ray crystallography.[183] By expanding these metal complexes from planar compounds into the three-dimensional coordination system of octahedral complexes, it has been possible to use the intercalation of a single ligand as a platform on which to build other DNA recognition functionalities. In this manner, the binding affinity provided by intercalative binding of one of the ligands of the complex has been applied to the delivery of functionalities placed on the other ligands in the coordination sphere. In addition to providing the intercalative binding mode required for high affinity binding, rhodium compounds containing a particular class of DNA intercalating ligands, aromatic quinone diimine ligands, also possess photochemical properties which are very convenient for the design of DNA recognition agents. Upon irradiation with ultraviolet light, phenanthrenequinone diimine (phi) complexes of rhodium(III) have been shown to induce photooxidative strand cleavage localized at their site of binding. This DNA photocleavage results from a ligand to metal charge transfer and subsequent abstraction of a hydrogen atom from the adjacent sugar in the DNA backbone.[184] This strand cleavage at the sites of metal complex binding can be used in combination with high resolution gel electrophoresis techniques and chemical sequencing methods to determine sites of metal complex binding on long, end-labeled DNA duplexes.

Beyond their convenient photochemical behavior, octahedral metallointercalators have also proven to have unique binding properties that also make them ideal for the design of DNA recognition agents. Unlike most small molecules, these compounds have been shown to bind to DNA from the major groove side of the DNA helix. This binding location has been demonstrated both by determination of the NMR solution structure of a Rh intercalator-DNA complex[185] and also by X-ray crystallography.[183] This major groove orientation, in contrast to other small molecule systems, provides this family of metallointercalators with access to the richer array of functional groups in the major groove for site specific DNA recognition. In addition, this makes these molecules a better laboratory to explore the recognition tasks performed by DNA binding proteins since their major groove localization makes the lessons learned from the natural systems more relevant to design.

1.6.3.2: Mechanisms of DNA Recognition by Metallointercalators

Because of the constellation of properties that make octahedral metallointercalators of rhodium(III) ideal for the design of DNA recognition agents, a large family of complexes have been constructed to recognize DNA based on a wide variety of characteristics. As discussed in the sections above, the mechanisms applied to these recognition tasks can be broadly divided into shape-selective, indirect readout of DNA geometry and direct readout of the functionalities on specific DNA base sequences.

Shape Selection: A large number of metallointercalators have been prepared which recognize the characteristics of DNA based on shape selectivity and geometrical complementarity. One of the most basic examples of shape selection, which is

operative in all cases of octahedral metallointercalators, is the chiral preferences which exist in the binding of different metal complex enantiomers with DNA. Because of their structure, metal complexes are prepared as mixtures of two enantiomers, labeled delta (Δ) and lambda (Λ), based on the disposition of the chelating ligands about the metal complex. Because of the right-handed, chiral structure of the DNA double helix, the different spatial placement of the ligands in these two different enantiomers results in significantly different binding characteristics. This difference is demonstrated in Figure 1.6. The delta complex, because the disposition of its ligands matches the chirality of the DNA helix, binds deeply into the major groove of the DNA; the lambda enantiomer, on the other hand, clashes sterically with the sugar-phosphate backbone and cannot interact with the nucleic acid as well.

Less dramatic uses of these mechanisms of shape selection have produced compounds that bind preferentially at sites where the DNA major groove is open to accommodate sterically bulky, aromatic ancillary ligands. The primary example of this mechanism of recognition is the complex $[Rh(phen)_2(phi)]^{3+}$. The specificity of the complex, which preferentially photocleaves at 5'-pyrimidine-***pyrimidine***-purine-3'sites.[186] This sequence preference is due to steric clashes between phenanthroline ring hydrogen atoms and base functionalities at other sites. Complexes with ancillary ligands which are pulled back from the DNA, like $[Rh(phi)_2(bpy)]^{3+}$, do not show this sequence preference.[186] The structures of both compounds are included in Figure 1.7. The most extreme example of shape selectivity in nucleic acid binding is the complex $[Rh(DPB)_2(phi)]^{3+}$, where DPB refers to the large 4,4'-diphenyl-2,2'-dipyridine ligand (Figure 1.7).[187] In addition to binding preferentially between the C and T bases of a 5'-pyrimidine-pyrimidine-purine-3' sequence, this large hydrophobic molecule dimerizes on DNA to extend its recognition to eight base pairs. In the

Figure 1.6. Enantiomeric Preferences for the Binding of Octahedral Metal Complexes to DNA. Note that the delta enantiomer of the metal complex (left) is complementary in shape to the right-handed DNA helix and can bind deeply into the major groove. The lambda enantiomer, on the other hand, clashes sterically with the DNA backbone.

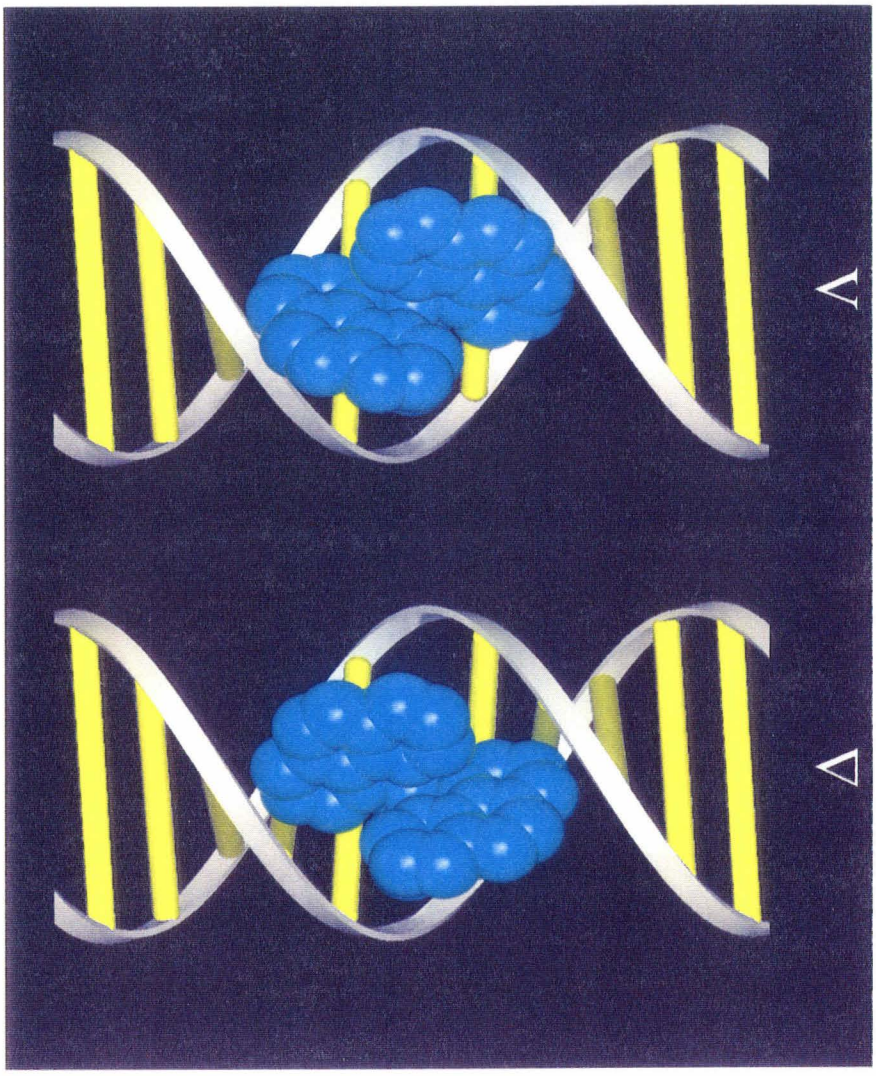
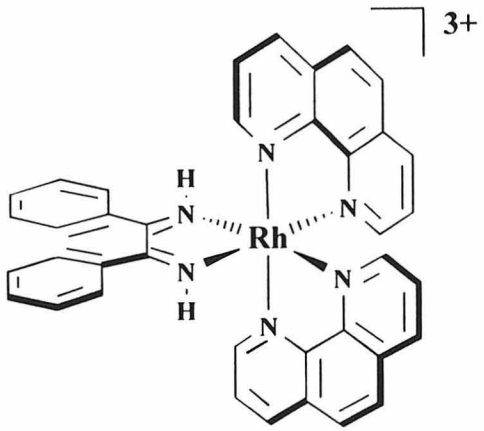


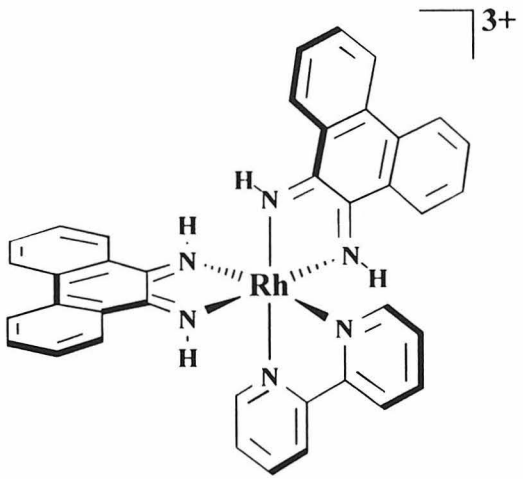
Figure 1.6:

Figure 1.7. Structures of the Octahedral Complexes $[Rh(phen)_2(phi)]^{3+}$, $[Rh(phi)_2(bpy)]^{3+}$, and $[Rh(DPB)_2(phi)]^{3+}$.

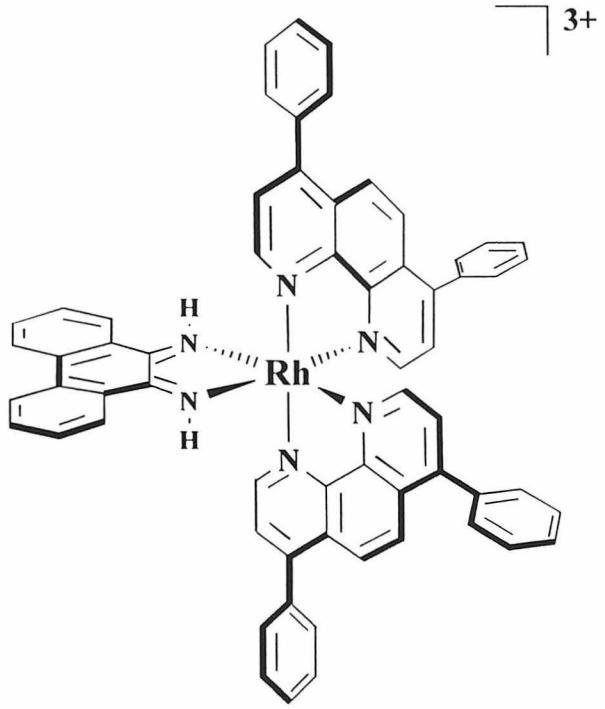
Figure 1.7:



$[Rh(phen)_2(phi)]^{3+}$



$[Rh(phi)_2(bpy)]^{3+}$



$[Rh(DPB)_2(phi)]^{3+}$

sequence 5'-CT**C**TAGAG-3' cleavage is observed at the highlighted C on both strands of the palindromic sequence. In addition, $[Rh(DPB)_2(phi)]^{3+}$ also shows the strongest enantiomeric preference for binding as the Λ enantiomer does not bind even at concentrations 1000 fold above the levels were the Δ shows specific binding behavior.[187]

Direct Readout of DNA: In addition to shape selective recognition, octahedral metallointercalators have also been designed which take advantage of the many possible direct readout interactions available in the major groove of DNA. Examples of this type of complexes, which have taken advantage of hydrogen bonding and van der Waals/hydrophobic interactions, have been made which recognize a variety of two and four base pair sites. Several of these complexes, based on aliphatic ligands of various kinds, are included in Figure 1.8.[188] The specificity of these compounds is determined either by hydrogen bond donation of axial amine groups with nitrogen or oxygen atoms on guanine bases or by van der Waals interactions between methylene or methyl units on the ligand and the methyl group of thymine.[189] Because these simple compounds are so small, their recognition properties are determined by only one of these two types of interactions. As shown in Figure 1.9, the binding *interactions* of the two enantiomers of $[Rh(en)_2(phi)]^{3+}$, where en is the ethylene diamine ligand, are enantiospecific; in the Δ case it is hydrogen bonding contacts with guanine that determine specificity, while in the Λ enantiomer van der Waals contacts come into play.[189] To combine both these mechanims of direct readout of DNA in a single molecule, a slightly larger compound, Δ–α–[Rh[(*R,R*)-Me_2trien]phi]$^{3+}$, was constructed.[190] Combining both axial amines for hydrogen bonding with pendant methyl groups for van der Waals contacts (Figure 1.10), this molecule allowed the expansion of the recognition site of the complex to the four base pair 5'-TGCA-3' sequence. Recent characterization by both NMR[185] and

Figure 1.8. Structures of the Octahedral Complexes $[Rh(NH_3)_4(phi)]^{3+}$, $[Rh(en)_2(phi)]^{3+}$, and $[Rh(cyclen)(phi)]^{3+}$.

Figure 1.8:

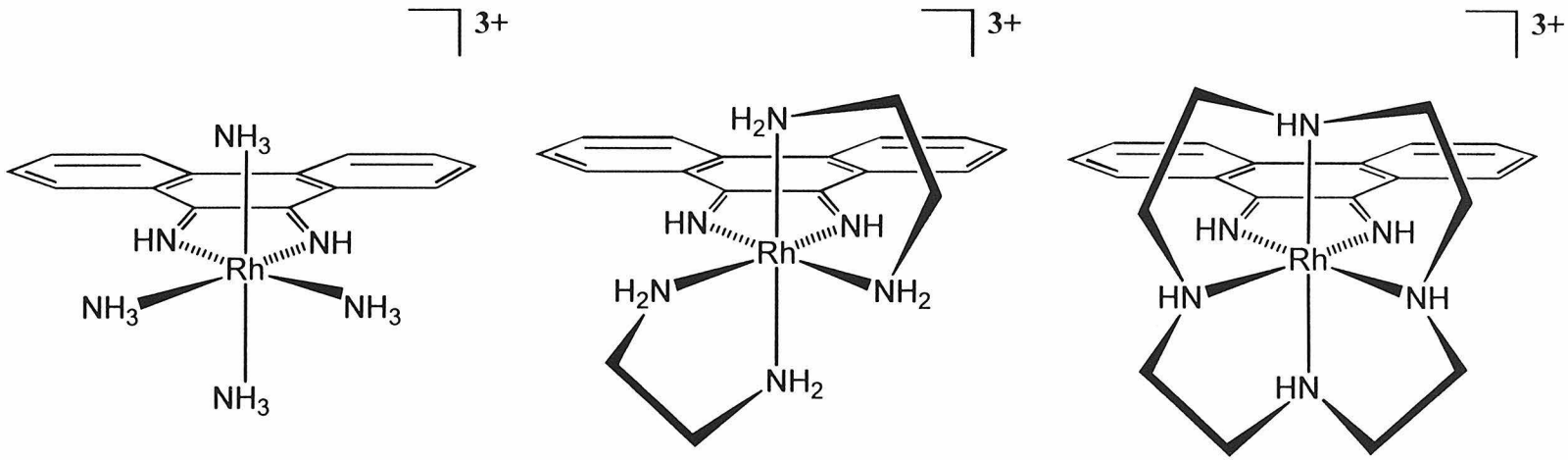
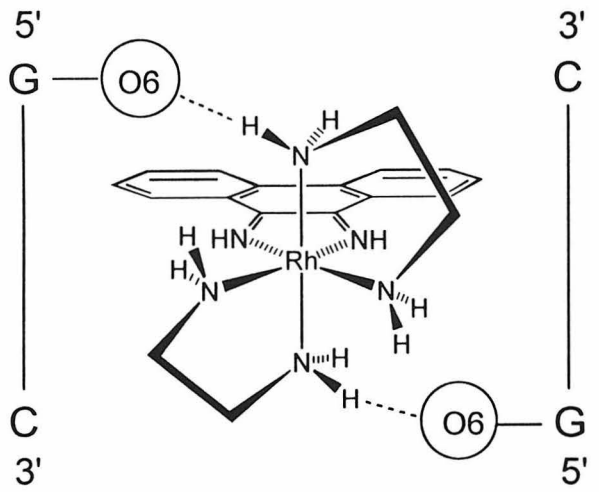
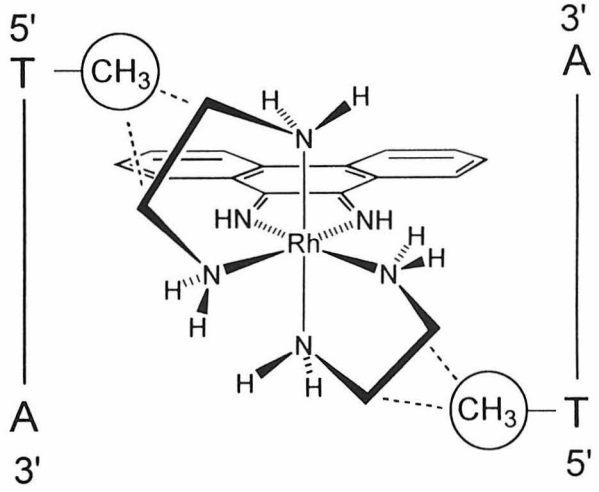

3+
NH3
HN
NH
Rh
NH3
NH3
NH3
3+
H2N
HN
NH
Rh
H2N
NH2
NH2
3+
HN
HN
NH
Rh
HN
NH
HN

Figure 1.9. Schematic of the Hydrogen Bonding and van der Waals Interactions Conferring Specificity on the Two Enantiomers of $[Rh(en)_2(phi)]^{3+}$.

Figure 1.9:



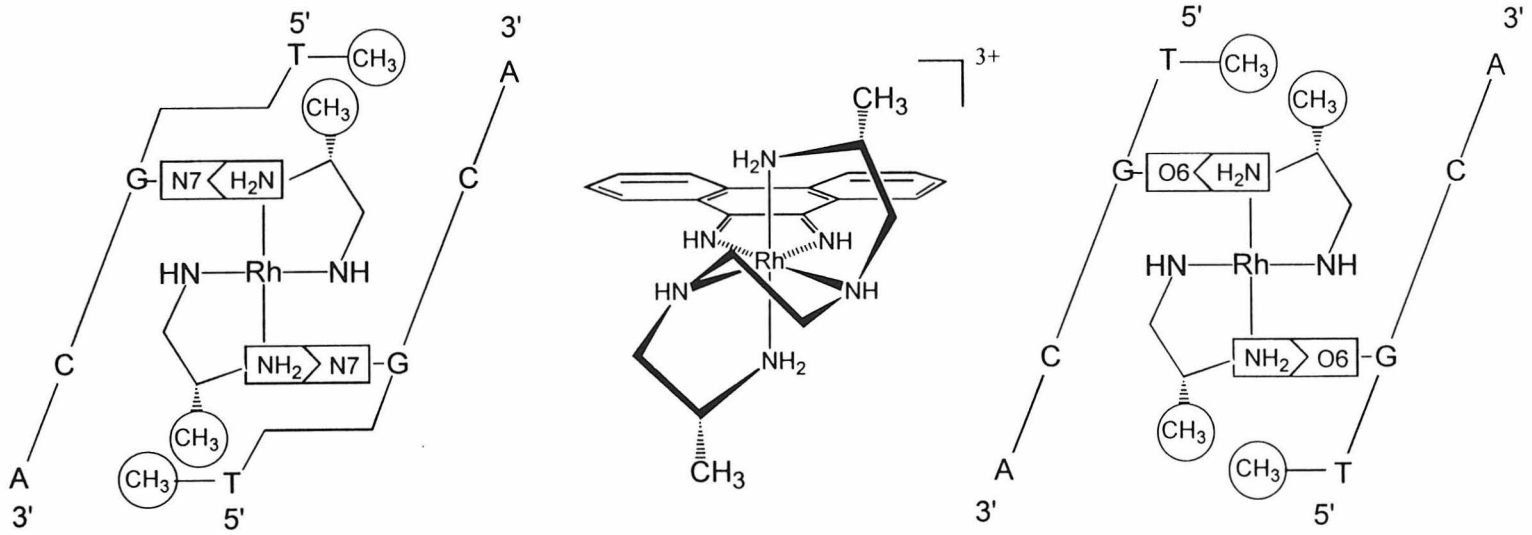
Δ–[Rh(en)$_2$phi]$^{3+}$



Λ–[Rh(en)$_2$phi]$^{3+}$

Figure 1.10. Structure of Δ–α–[Rh[(*R*,*R*)-Me_2trien]phi]$^{3+}$ and Models of its Interaction with the 5'-TGCA-3' site in DNA. This complex (center) was designed to combine both hydrogen bonding and van der Waals interactions to specifically target its intended binding site. Structural characterization by both NMR (left) and X-ray crystallography (right) support recognition via the designed interactions.

Figure 1.10:



Solution Structure

Crystal Structure

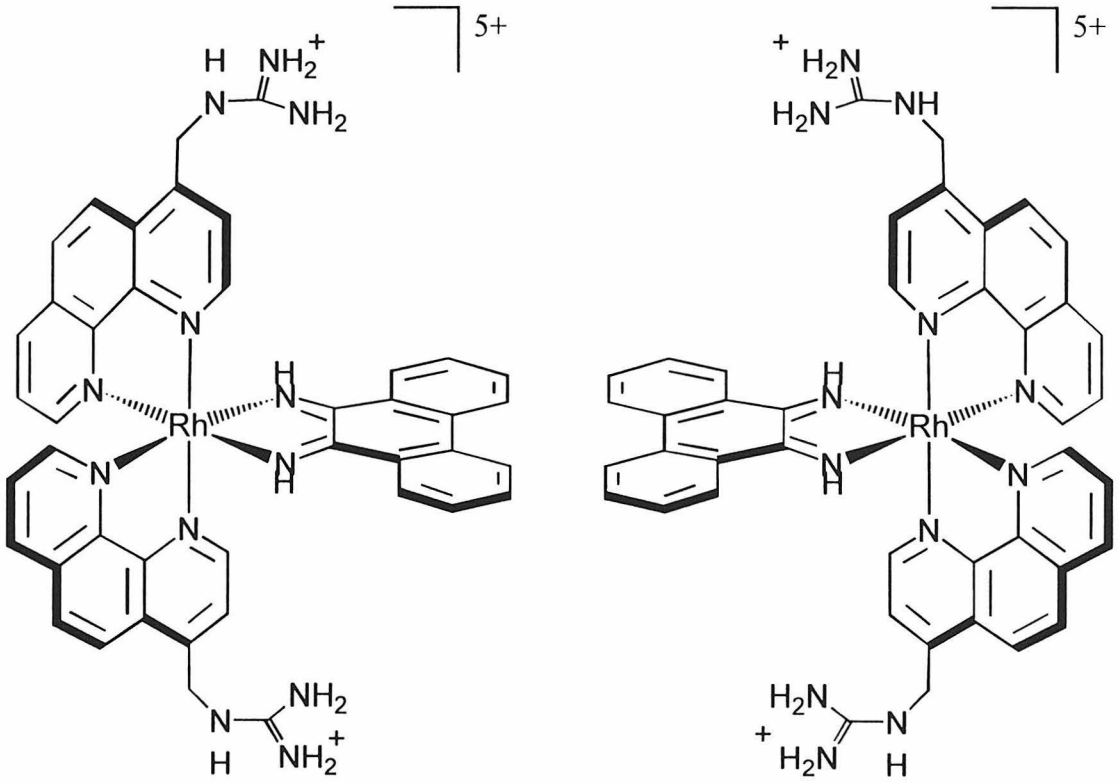
X-ray crystallography[183] (Figure 1.10) have shown that the metal complex functionalities participate in the intended contacts with the DNA bases.

Combining Shape-Selection with Direct Readout: One metal complex which uses a combination of shape selective and direct readout mechanisms of DNA recognition has also been constructed. This compound, 1-$[Rh(MGP)_2(phi)]^{3+}$, combines the ligand core of $[Rh(phen)_2(phi)]^{3+}$ with axial pendant guanidinium groups (Figure 1.11). These groups are analogous to the side chain of the amino acid arginine which have been shown to hydrogen bond to both the N7 and O6 of guanine in DNA-protein crystal structures. As a result, the metal complex was intended to recognize a hybrid site with a central shape selective portion, which should target the 5'pyrimidine-pyrimidine-purine-3' sequence like $[Rh(phen)_2(phi)]^{3+}$, and the additional direct-readout of guanine groups by the pendant guanidinium functionalities. The consensus sequence for the Δ enantiomer of the complex was determined to be 5'-CA***T***CTG-3' with photocleavage at the indicated thymine base.[191,192] Although the site does have the predicted guanine bases on its periphery, the central bases differ from the expected 5'-pyrimidine-pyrimidine-purine-3' sequence. Molecular modeling,[191,192] and subsequent NMR results,[193] have shown that the molecule must tilt significantly in its binding site to make the designed guanine contacts and that only a single contact can be made at a given time. These requirements likely explain the sequence deviation in the core of the recognition site.

Even more surprising than the behavior of the Δ enantiomer of the complex, 1-Λ-$[Rh(MGP)_2(phi)]^{3+}$ displays an even more dramatic combination of shape selective and direct readout mechanisms of DNA recognition. Instead of behaving like most Λ enantiomers of aromatic ligand complexes whose chirality is incompatible with the right-handed helicity of DNA (Figure 1.6), 1-Λ-$[Rh(MGP)_2(phi)]^{3+}$ bound to the site

Figure 1.11. The Enantiomers of $[Rh(MGP)_2(phi)]^{5+}$.

Figure 1.11:



Λ Δ

5'-CA***TA***TG-3' with high affinity and photocleaved the DNA at the central two bases.[191] It was later determined by molecular modeling[191] and verified by NMR[193] that the DNA, when bound to the metal complex, is unwound by approximately 70° over the six base pairs of the binding site. This not only explained the preference for the Λ enantiomer, since the local chirality of the DNA helix breaks down as it unwinds to a ladder conformation, but also the symmetry observed in the photocleavage pattern. This unwinding also made it possible for 1-Λ-$[Rh(MGP)_2(phi)]^{3+}$ to contact both peripheral guanine residues simultaneously unlike in the Δ case.[191,192] It has been established by other researchers that TA rich sequences in DNA unwind more readily than mixed sequence DNA.[194-197] This inherent "twistability" is the shape that the central phenanthroline ligands recognize; in the absence of a sequence which unwinds readily, the steric conflict of the Λ metal complex with the DNA backbone would dominate and the complex could not bind. As a result, like the DNA-protein cases discussed above, the deformability of the central sequence combines with the hydrogen bonding interactions at the edge of the site to produce a DNA-metallointercalator complex with very high specificity over other non-cognate sequences.

1.7: Conclusions: The Design of Small Molecules for Mismatch Recognition

At the most basic level, octahedral metallointercalators have proven to be incredibly versatile compounds for the design of novel molecular recognition agents for DNA. The binding affinity provided by the intercalative interaction efficiently delivers these compounds to the major groove of DNA where shape selective interactions, direct sequence readout, or combinations thereof can modulate the specificity of the complex for specific base sequences. In addition, the nature of inorganic compounds

has made compounds and reactivities available that do not exist in purely organic materials. The photoreactivity of the complexes, their relative ease of modification, their rigid octahedral shape and their high positive charge are all properties that are unique and conferred by these compounds unique place between the fields of inorganic and biological chemistry. As a result, like the construction of molecules which read out DNA was built on a deep literature in the DNA-protein field, the efforts described here to design small molecules which recognize base mismatches in DNA will be grounded in the extensive experience with these versatile recognition agents.

The recognition of base mismatches in DNA, however, is a challenging problem and one which is qualitatively different than any which has been performed with these complexes before. Since base mismatches can involve any of the DNA bases, all the strategies for direct-readout based interactions are not applicable to this particular challenge. In addition, as was discussed in the earlier sections of this chapter, the primary distinguishing characteristic of base mismatches is their destabilizing effect on the structure of the DNA helix. Although the work described in the following chapters demonstrates that this trait *can* be applied to the construction of specific molecular recognition agents, it is clear that the traditional design strategy applied to previous problems – the modification of the ancillary ligands of a metal complex coupled with the sequence neutral binding affinity of intercalation – will not apply.

The approach to this molecular recognition problem required the design and synthesis of a novel class of rhodium(III) compounds containing the chrysenequinone diimine (chrysi) intercalating ligand. The preparation of these compounds necessitated the development of new synthetic methods; these studies also resulted in superior synthetic routes to many previously characterized rhodium(III) aromatic quinone

diimine complexes. Compounds containing the chrysi ligand also proved to have intriguing properties independent of any possible interactions with nucleic acids. This work is the subject of the second chapter of this thesis. The application of chrysenequinone diimine intercalators to the problem of mismatch recognition is considered in the third and fourth chapters. This central portion of the thesis shows that, not only do these compounds bind to many different mismatches in DNA with high affinity, but they do it with a level specificity which allows the detection of single mismatches in long, biologically isolated samples of nucleic acids. The final chapter of the work describes experiments which further characterize the photoreactivity of rhodium(III) chrysi complexes with DNA. The properties described therein, which include the observation that the complex cleaves DNA photocatalytically, provide an added level of interest in these compounds and their possible technological applicability.

1.8: Literature Cited

1) Lehninger, A. L.; Nelson, D. L.; Cox, M. M. *Principles of Biochemistry*; Worth Publishers: New York, NY, 1993.

2) Radman, M.; Wagner, R. *Ann. Rev. Genet.* **1986**, *20*, 523.

3) Kramer, B.; Kramer, W.; Fritz, H. J. *Cell* **1984**, *38*, 879.

4) Dohet, C.; Wagner, R.; Radman, M. *Proc. Natl. Acad. Sci. USA* **1985**, *82*, 503.

5) Kolodner, R. D. *TIBS* **1995**, *20*, 397.

6) Modrich, P. *Science* **1994**, *266*, 1959.

7) Fink, D.; Aebi, S.; Howell, S. B. *Clin. Can. Res.* **1998**, *4*, 1.

8) Brown, T.; Kennard, O.; Kneale, G.; Rabinovich, D. *Nature* **1985**, *315*, 604.

9) Hunter, W. N.; Brown, T.; Anand, N. N.; Kennard, O. *Nature* **1986**, *320*, 552.

10) Brown, T.; Hunter, W. N.; Kneale, G.; Kennard, O. *Proc. Natl. Acad. Sci. USA* **1986**, *83*, 2404.

11) Brown, T.; Leonard, G. A.; Booth, E. D.; Chambers, J. *J. Mol. Biol.* **1989**, *207*, 455.

12) Leonard, G. A.; Booth, E. D.; Brown, T. *Nucleic Acids Res.* **1990**, *18*, 5617.

13) Privé, G. G.; Heinemann, U.; Chandrasegaran, S.; Kan, L. S.; Kopka, M. L.; Dickerson, R. E. *Science* **1987**, *238*, 498.

14) Skelly, J. V.; Edwards, K. J.; Jenkins, T. C.; Neidle, S. *Proc. Natl. Acad. Sci. USA* **1993**, *90*, 804.

15) Kennard, O.; Salisbury, S. A. *J. Biol. Chem.* **1993**, *268*, 10701.

16) Hunter, W. N.; Brown, T.; Kneale, G.; Anand, N. N.; Rabinovich, D.; Kennard, O. *J. Biol. Chem.* **1987**, *262*, 9962.

17) Hunter, W. N.; Brown, T.; Kennard, O. *Nucleic Acids Res.* **1987**, *15*, 6589.

18) Hunter, W. N.; Brown, T.; Annad, N. N.; Kennard, O. *Nature* **1986**, *320*, 552.

19) Brown, T. *Aldrichimica Acta* **1995**, *28*, 15.

20) Patel, D. J.; Kozlowski, S. A.; Ikuta, S.; Itakura, K. *Fed. Proc.* **1984**, *43*, 2663.

21) Salisbury, S. A.; Anand, N. N. *J. Chem. Soc. Chem. Commun.* **1985**, 985.

22) Gao, X.; Patel, D. J. *J. Biol. Chem.* **1987**, *262*, 16973.

23) Lane, A. N.; Jenkins, T. C.; Brown, D. J. S.; Brown, T. *Biochem. J.* **1991**, *279*, 269.

24) Carbonnaux, C.; van der Marel, G. A.; van Boom, J. H.; Guschlbauer, W.; Fazakerley, G. V. *Biochemistry* **1991**, *30*, 5449.

25) Cognet, J. A. H.; Boulard, Y.; Fazakerley, G. V. *J. Mol. Biol.* **1995**, *246*, 209.

26) Kuwata, K.; Liu, H.; Schleich, T.; James, T. L. *J. Mag. Res.* **1997**, *128*, 70.

27) Gao, X.; Patel, D. J. *J. Am. Chem. Soc.* **1988**, *110*, 5178.

28) Borden, K. L. B.; Jenkins, T. C.; Skelly, J. V.; Brown, T.; Lane, A. N. *Biochemistry* **1992**, *31*, 5411.

29) Faibis, V.; Cognet, J. A. H.; Boulard, Y.; Sowers, L. C.; Fazakerley, G. V. *Biochemistry* **1996**, *35*, 14452.

30) Boulard, Y.; Cognet, J. A. H.; Gabarro-Arpa, J.; Le Bret, M.; Sowers, L. C.; Fazakerley, G. V. *Nucleic Acids Res.* **1992**, *20*, 1933.

31) Gervais, V.; Cognet, J. A. H.; Le Bret, M.; Sowers, L. C.; Fazakerley, G. V. *Eur. J. Biochem.* **1995**, *228*, 279.

32) Allawi, H. T.; SantaLucia, Jr., J. *Biochemistry* **1997**, *36*, 10581.

33) Allawi, H. T.; SantaLucia, Jr., J. *Nucleic Acids Res.* **1998**, *26*, 4925.

34) Moe, J. G.; Russu, I. M. *Biochemistry* **1992**, *31*, 8421.

35) Lane, A. N.; Peck, B. *Eur. J. Biochem.* **1995**, *230*, 1073.

36) SibghatUllah; Gallinari, P.; Xu, Y. Z.; Goodman, M. F.; Bloom, L. B.; Jiricny, J.; Day, R. S. *Biochemistry* **1996**, *35*, 12926.

37) Morton, B. R.; Oberholzer, V. M.; Clegg, M. T. *J. Mol. Evol.* **1997**, *45*, 227.

38) Peyret, N.; Seneviratne, P. A.; Allawi, H. T.; SantaLucia, Jr., J. *Biochemistry* **1999**, *38*, 3468.

39) Allawi, H. T.; SantaLucia, Jr., J. *Biochemistry* **1998**, *37*, 2170.

40) Li, Y.; Agrawal, S. *Biochemistry* **1995**, *34*, 10056.

41) Cheng, J.-W.; Chou, S.-H.; Reid, B. R. *J. Mol. Biol.* **1992**, *228*, 1037.

42) Allawi, H. T.; SantaLucia, Jr., J. *Nucleic Acids. Res.* **1998**, *26*, 2694.

43) Allawi, H. T.; SantaLucia, Jr., J. *Biochemistry* **1998**, *37*, 9435.

44) SantaLucia Jr., J., Personal Communication.

45) Pilch, D. S.; Plum, G. E.; Breslauer, K. J. *Curr. Op. Struct. Biol.* **1995**, *5*, 334.

46) Verdine, G. L.; Bruner, S. D. *Chem. Biol.* **1997**, *4*, 329.

47) Morden, K. M.; Gunn, B. M.; Maskos, K. *Biochemistry* **1990**, *29*, 8835.

48) Barrett, T. E.; Savva, R.; Panayotou, G.; Barlow, T.; Brown, T.; Jiricny, J.; Pearl, L. H. *Cell* **1998**, *92*, 117.

49) Slupphaug, G.; Mol, C. D.; Kavli, B.; Arvai, A. S.; Krokan, H. E.; Tainer, J. A. *Nature* **1996**, *384*, 87.

50) Klimasauskas, S.; Kumar, S.; Roberts, R. J.; Cheng, X. *Cell* **1994**, *76*, 357.

51) Vassylyev, D. G.; Kashiwagi, T.; Mikami, Y.; Ariyoshi, M.; Iwai, S.; Ohtsuka, E.; Morikawa, K. *Cell* **1995**, *83*, 773.

52) Reinisch, K. M.; Chen, L.; Verdine, G. L.; Lipscomb, W. N. *Cell* **1995**, *82*, 143.

53) Gunz, D.; Hess, M. T.; Naegeli, H. *J. Biol. Chem.* **1996**, *271*, 25089.

54) Berdal, K. G.; Johansen, R. F.; Seeberg, E. *EMBO Journal* **1998**, *17*, 363.

55) Ferrari, M.; Carrera, P.; Cremonesi, L. *Pure Appl. Chem.* **1996**, *68*, 1913.

56) Eng, C.; Vijg, J. *Nature Biotech.* **1997**, *15*, 422.

57) Schwaab, R.; Oldenburg, J.; Lalloz, M. R.; Schwaab, U.; Pemberton, S.; Hanfland, P.; Brackmann, H. H.; Tuddenham, E. G.; Michaelides, K. *Hum. Genet.* **1997**, *101*, 323.

58) Cotton, R. G. *Clin. Chem. Lab. Med.* **1998**, *36*, 519.

59) Iitia, A.; Mikola, M.; Gregersen, N.; Hurskainen, P.; Lovgren, T. *Biotechniques* **1994**, *17*, 566.

60) Wu, D. Y.; Nozari, G.; Schold, M.; Conner, B. J.; Wallace, R. B. *DNA* **1989**, *8*, 135.

61) Kynclova, E.; Hartig, A.; Schalkhammer, T. *J. Mol. Recognit.* **1995**, *8*, 139.

62) Vary, C. P.; Carmody, M.; LeBlanc, R.; Hayes, T.; Rundell, C.; Keilson, L. *Genet. Anal.* **1996**, *13*, 59.

63) Palecek, E.; Fojta, M.; Tomschik, M.; Wang, J. *Biosens. Bioelecton.* **1998**, *13*, 621.

64) Healey, B. G.; Matson, R. S.; Walt, D. R. *Anal. Biochem.* **1997**, *251*, 270.

65) Hakala, H.; Virta, P.; Salo, H.; Lonnberg, H. *Nucleic Acids Res.* **1998**, *26*, 5581.

66) Tsuruoka, M.; Yano, K.; Ikebukuro, K.; McNiven, S.; Takeuchi, T.; Karube, I. *Anal. Let.* **1996**, *29*, 1741.

67) Nelson, N. C.; Hammond, P. W.; Matsuda, E.; Goud, A. A.; Becker, M. *Nucleic Acids Res.* **1996**, *24*, 4998.

68) Gotoh, M.; Hasegawa, Y.; Shinohara, Y.; Shimizu, M.; Tosu, M. *DNA Res.* **1995**, *2*, 285.

69) Nilsson, P.; Persson, B.; Larsson, A.; Uhlen, M.; Nygren, P. A. *J. Mol. Recognit.* **1997**, *10*, 7.

70) Persson, B.; Stenhag, K.; Nilsson, P.; Larsson, A.; Uhlen, M.; Nygren, P. *Anal. Biochem.* **1997**, *246*, 34.

71) Nilsson, P.; Larsson, A.; Lundeberg, J.; Uhlen, M.; Nygren, P. A. *Biotechniques* **1999**, *26*, 308.

72) Ganguly, A.; Prockop, D. J. *Electrophoresis* **1995**, *16*, 1830.

73) Muniappan, B. P.; Thilly, W. G. *Genet. Anal.* **1999**, *14*, 221.

74) Laprise, S. L.; Mak, E. K.; Killoran, K. A.; Layman, L. C.; Gray, M. R. *Hum. Mutat.* **1998**, *12*, 393.

75) Cremonesi, L.; Carrera, P.; Cardillo, E.; Fumagalli, A.; Lucchiari, S.; Ferrari, M.; Righetti, S. C.; Righetti, P. G.; Gelfi, C. *Clin. Chem. Lab. Med.* **1998**, *36*, 959.

76) Van Orsouw, N. J.; Vijg, J. *Genet. Anal.* **1999**, *14*, 205.

77) Chen, M.; Laszlo, A.; Roti, J. L. R.; Hunt, C. R. *Anal. Biochem.* **1996**, *239*, 61.

78) Kenney, M.; Ray, S.; Boles, T. C. *Biotechniques* **1998**, *25*, 516.

79) Balaguer, P.; Terouanne, B.; Allibert, P.; Cros, P.; Boussioux, A. M.; Mandrand, B.; Nicolas, J. C. *Mol. Cell Probes* **1993**, *7*, 155.

80) Saiki, R. K.; Walsh, P. S.; Levenson, C. H.; Erlich, H. A. *Proc. Natl. Acad. Sci. USA* **1989**, *86*, 6230.

81) Zhang, Y.; Coyne, M. Y.; Will, S. G.; Levenson, C. H.; Kawasaki, E. S. *Nucleic Acids Res.* **1991**, *19*, 3929.

82) Sosnowski, R. G.; Tu, E.; Butler, W. F.; O'Connell, J. P.; Heller, M. J. *Proc. Natl. Acad. Sci. USA* **1997**, *94*, 1119.

83) Hacia, J. G. *Nat. Genet.* **1999**, *21*, 42.

84) Hacia, J. G.; Brody, L. C.; Chee, M. S.; Fodor, S. P.; Collins, F. S. *Nat. Genet.* **1996**, *14*, 441.

85) Bains, W. *Genet. Anal. Tech. Appl.* **1994**, *11*, 49.

86) Cronin, M. T.; Fucini, R. V.; Kim, S. M.; Masino, R. S.; Wespi, R. M.; Miyada, C. G. *Hum. Mutat.* **1996**, *7*, 244.

87) Pease, A. C.; Solas, S.; Sullivan, E. J.; Cronin, M. T.; Holmes, C. P.; Fodor, S. P. *Proc. Natl. Acad. Sci. USA* **1994**, *91*, 5022.

88) Drobyshev, A.; Mologina, N.; Shik, V.; Pobedimskaya, D.; Yershov, G.; Mirzabekov, A. *Gene* **1997**, *188*, 45.

89) Guo, Z.; Guilfoyle, R. A.; Theil, A. J.; Wang, R.; Smith, L. M. *Nucleic Acids Res.* **1994**, *22*, 5456.

90) Sapolsky, R. J.; Hsie, L.; Berno, A.; Ghandour, G.; Mittmann, M.; Fan, J. B. *Genet. Anal.* **1999**, *14*, 187.

91) Johnston, D. H.; Glasgow, K. C.; Thorp, H. H. *J. Am. Chem. Soc.* **1995**, *117*, 8933.

92) Ellis, T. P.; Humphrey, K. E.; Smith, M. J.; Cotton, R. G. *Hum. Mutat.* **1998**, *11*, 345.

93) Ahmed, F. E. *Environ. Cardino. & Ecotox. Revs.* **1998**, *C16*, 47.

94) Hansen, L. L.; Justesen, J.; Kruse, T. A. *Hum. Mutat.* **1996**, *7*, 256.

95) Rowley, G.; Saad, S.; Giannelli, F.; Green, P. M. *Genomics* **1995**, *30*, 574.

96) Germain, D.; Biasotto, M.; Tosi, M.; Meo, T.; Kahn, A.; Poenaru, L. *Hum. Genet.* **1996**, *98*, 719.

97) Ren, J.; Ulvik, A.; Refsum, H.; Ueland, P. M. *Clin. Chem.* **1998**, *44*, 2108.

98) Germain, D. P.; Puech, J. P.; Caillaud, C.; Kahn, A.; Poenaru, L. *Am. J. Hum. Genet.* **1998**, *63*, 415.

99) Harris, I. I.; Green, P. M.; Bentley, D. R.; Giannelli, F. *PCR Methods Appl.* **1994**, *3*, 268.

100) Verpy, E.; Biasotto, M.; Meo, T.; Tosi, M. *Proc. Natl. Acad. Sci. USA* **1994**, *91*, 1873.

101) Cotton, R. G. H.; Dahl, H.-H. M.; Forrest, S.; Howells, D. W.; Ramus, S. J.; Bishop, R. E.; Dianzani, I.; Saleeba, J. A.; Palombo, E.; Anderson, M. J.; Milner, C. M.; Campbell, R. D. *DNA Cell Biol.* **1993**, *12*, 945.

102) Novack, D. F.; Casna, N. J.; Fischer, S. C.; Ford, J. P. *Proc. Natl. Acad. Sci. USA* **1986**, *83*, 586.

103) Ganguly, A.; Prockop, D. J. *Nucleic Acids Res.* **1993**, *18*, 3933.

104) Ganguly, A.; Rooney, J. E.; Hosomi, S.; Zeiger, A. R.; Prockop, D. J. *Genomics* **1989**, *4*, 530.

105) Higgins, G. S.; Little, D. P.; Koster, H. *Biotechniques* **1997**, *23*, 710.

106) Syvanen, A. C. *Hum. Mutat.* **1999**, *13*, 1.

107) Bi, W.; Stambrook, P. J. *Nucleic Acids Res.* **1997**, *25*, 2949.

108) Newton, C. R.; Graham, A.; Heptinstall, L. E.; Powell, S. J.; Summers, C.; Kalsheker, N.; Smith, J. C.; Markham, A. F. *Nucleic Acids Res.* **1989**, *17*, 2503.

109) Hu, Y. W.; Balaskas, E.; Kessler, G.; Issid, C.; Scully, L. J.; Murphy, D. G.; Rinfret, A.; Giulivi, A.; Scalia, V.; Gill, P. *Nucleic Acids Res.* **1998**, *26*, 5013.

110) Rzhetsky, A.; Dopazo, J.; Snyder, E.; Dangler, C. A.; Ayala, F. J. *Genetics* **1996**, *144*, 1975.

111) Kaufman, D. L.; Ramesh, V.; McClatchey, A. I.; Menkes, J. H.; Tobin, A. J. *Genomics* **1990**, *8*, 656.

112) Taylor, G. R.; Deeble, J. *Genet. Anal.* **1999**, *14*, 181.

113) Golz, S.; Birkenkamp-Demtroder, K.; Kemper, B. *Nucleic Acids Res.* **1998**, *26*, 1132.

114) Babon, J. J.; Youil, R.; Cotton, R. G. *Nucleic Acids Res.* **1995**, *23*, 5082.

115) Del Tito, J., B.J.; Poff III, H. E.; Novotny, M. A.; Cartledge, D. M.; Walker II, R. I.; Earl, C. D.; Bailey, A. L. *Clin. Chem.* **1998**, *44*, 731.

116) Geschwind, D. H.; Rhee, R.; Nelson, S. F. *Gen. Anal. Biomol. Eng.* **1996**, *13*, 105.

117) Xu, J.-F.; Yang, Q.-P.; Chen, J. Y.-J.; van Baalen, M. R.; Hsu, I.-C. *Carcinogenesis* **1996**, *17*, 321.

118) Smith, J.; Modrich, P. *Proc. Natl. Acad. Sci. USA.* **1996**, *93*, 4374.

119) Babic, I.; Andrew, S. E.; Jirik, F. R. *Mutat. Res.* **1996**, *372*, 87.

120) Wagner, R.; Debbie, P.; Radman, M. *Nucleic Acids Res.* **1995**, *23*, 3944.

121) Hsu, I. C.; Yang, Q.; Kahng, M. W.; Xu, J. F. *Carcinogenesis* **1994**, *15*, 1657.

122) Gotoh, M.; Hasebe, M.; Ohira, T.; Hasegawa, Y.; Shinohara, Y.; Sota, H.; Nakao, J.; Tosu, M. *Genet. Anal.* **1997**, *14*, 47.

123) Maulik, G.; Botchway, S.; Chakrabarti, S.; Tetradis, S.; Price, B.; Makrigiorgos, G. M. *Nucleic Acids Res.* **1999**, *27*, 1316.

124) Parsons, B. L.; Heflich, R. H. *Mutat. Res.* **1997**, *374*, 277.

125) Weiner, S. J.; Kollman, P. A.; Case, D. A.; Singh, U. C.; Ghio, C.; Alagona, G.; Profeta, S.; Weiner, P. *J. Am. Chem. Soc.* **1984**, *108*, 765.

126) Chalasinski, G.; Szczesniak, M. M. *Chem. Rev.* **1994**, *94*, 1723.

127) Kim, K. S.; Mhin, B. J.; Choi, U. S.; Lee, K. *J. Chem. Phys.* **1992**, *97*, 6649.

128) Fersht, A. R. *TIBS* **1987**, *12*, 301.

129) Böhm, H.-J.; Klebe, G. *Angew. Chem. Int. Ed. Engl.* **1996**, *35*, 2588.

130) Searle, M. S.; Williams, D. H. *J. Am. Chem. Soc.* **1992**, *114*, 10690.

131) Lemieux, R. U. *Acc. Chem. Res.* **1996**, *29*, 373.

132) Chervenak, M. C.; Toone, E. J. *J. Am. Chem. Soc.* **1994**, *116*, 10533.

133) Eisenberg, D.; Crothers, D. *Physical Chemistry with Applications to the Life Sciences*; Benjamin/Cummings Publishing Company, Inc.: Menlo Park, CA, 1979.

134) Williams, D. H.; Searle, M. S.; Groves, P.; Mackay, J. P.; Westwell, M. S.; Beauregard, D. A.; Cristofaro, M. F. *Pure Appl. Chem.* **1994**, *66*, 1975.

135) Jencks, W. P. *What Everyone Wanted to Know About Tight Binding and Enzyme Cataysis, but Never Thought of Asking*; Jencks, W. P., Ed.; Springer-Verlag: Berlin, 1980; Vol. 32, 3.

136) Jencks, W. P. *On the Economics of Binding Energies*; Jencks, W. P., Ed.; Springer-Verlag: Berlin, 1986, 59.

137) Katchalski-Katzir, E. *Design and Synthesis of Organic Molecules Based on Molecular Recognition*; Katchalski-Katzir, E., Ed.; Springer-Verlag: Berlin, 1986, 1.

138) Terbrueggen, R. *Exploring the Direct and Indirect Readout of DNA with Phenanthrenequinone Diimine Complexes of Rhodium(III)*. Ph.D. Thesis, Division of Chemistry, California Institute of Technology, 1995.

139) Pingoud, A.; Jeltsch, A. *Eur. J. Biochem.* **1997**, *246*, 1.

140) Kodadek, T. *The Molecular Basis of Sequence-Specific DNA-Protein Interactions*; Kodadek, T., Ed.; Marcel Dekker, Inc.: New York, NY, 1992, 195.

141) Ehbrecht, H.-J.; Pingoud, A.; Urbanke, C.; Maass, G.; Gualerzi, C. *J. Biol. Chem.* **1985**, *260*, 6160.

142) Härd, T.; Lundbäck, T. *Biophys. Chem.* **1996**, *62*, 121.

143) Aggarwal, A. K. *Curr. Opin. Struc. Bio.* **1995**, *5*, 11.

144) Pindur, U.; Fischer, G. *Cur. Med. Chem.* **1996**, *3*, 379.

145) Zimmer, C.; Wahnert, U. *Prog. Biophys. Mol. Biol.* **1986**, *47*, 31.

146) Krugh, T. R. *Cur. Opin. Struc. Biol.* **1994**, *4*, 351.

147) Bailly, C.; Chaires, J. B. *Bioconjugate Chem.* **1998**, *9*, 513.

148) Keilkopf, C. L.; White, S.; Szewczyk, J. W.; Turner, J. M.; Baird, E. E.; Dervan, P. B.; Rees, D. C. *Science* **1998**, *282*, 111.

149) Faddejeva, M. D.; Belyaeva, T. N. *Tsitologiya* **1991**, *33*, 3.

150) Sartoris, J.; Schneider, H. J. *J. Chem. Soc. Perkin Trans. 2* **1997**, 2319.

151) Ralph, R. K.; Marshall, B.; Darkin, S. *Trends Bio. Sci.* **1983**, *8*, 212.

152) Murphy, C. J.; Barton, J. K. *Meth. Enzymol.* **1993**, *226*, 576.

153) Friedman, A. E.; Chambron, J. C.; Sauvage, J. P.; Turro, N. J.; Barton, J. K. *J. Am. Chem. Soc.* **1990**, *112*, 4960.

154) Stoeffler, H. D.; Thornton, N. B.; Temkin, S. L.; Schanze, K. S. *J. Am. Chem. Soc.* **1995**, *117*, 7119.

155) Yam, V. W.-W.; Lo, K. K.-W.; Cheung, K. K.; Kong, R. Y.-C. *J. Chem. Soc. Chem. Commun.* **1995**, 1191.

156) Chow, C. S.; Barton, J. K. *Meth. Enzymol.* **1992**, *212*, 219.

157) Chow, C. S.; Behlen, L. S.; Uhlenbeck, O. C.; Barton, J. K. *Biochemistry* **1992**, *31*, 972.

158) Chow, C. S.; Hartmann, K. M.; Rawlings, S. L.; Huber, P. W.; Barton, J. K. *Biochemistry* **1992**, *31*, 3534.

159) Lim, A. C.; Barton, J. K. *Biochemistry* **1993**, *32*, 11029.

160) Dandliker, P. J.; Holmlin, R. E.; Barton, J. K. *Science* **1997**, *275*, 1465.

161) Murphy, C. J.; Arkin, M. R.; Ghatlia, N. D.; Bossmann, S.; Turro, N. J.; Barton, J. K. *Proc. Natl. Acad. Sci. USA* **1994**, *91*, 5315.

162) Murphy, C. J.; Arkin, M. R.; Jenkins, Y.; Ghatlia, N. D.; Bossmann, S. H.; Turro, N. J.; Barton, J. K. *Science* **1993**, *262*, 1025.

163) Arkin, M. R.; Jenkins, Y.; Murphy, C. J.; Turro, N. J.; Barton, J. K. *Adv. Chem. Ser.* **1995**, *246*, 449.

164) Arkin, M. R.; Stemp, E. D. A.; Turro, C.; Turro, N. J.; Barton, J. K. *J. Am. Chem. Soc.* **1996**, *118*, 2267.

165) Hall, D. B.; Holmlin, R. E.; Barton, J. K. *Nature* **1996**, *382*, 731.

166) Hall, D. B.; Barton, J. K. *J. Am. Chem. Soc.* **1997**, *119*, 5045.

167) Arkin, M. R.; Stemp, E. D. A.; Pulver, S. C.; Barton, J. K. *Chem. Biol.* **1997**, *4*, 389.

168) Núñez, M. E.; Hall, D.B.; Barton, J. K. *Chem. Biol.* 1999, 6, 85.

169) Johann, T. W. *Sequence-Specific Inhibition of DNA Polymerase by Phenanthrene Quinone Diimine Complexes of Rhodium(III)*. Ph.D. Thesis, Division of Chemistry, California Institute of Technology, 1997.

170) Fitzsimons, M. P.; Barton, J. K. *J. Am. Chem. Soc.* **1997**, *119*, 3379.

171) Sardesi, N. Y.; Barton, J. K. *J. Biol. Inorg. Chem.* **1997**, *2*, 762.

172) Dupureur, C. M.; Barton, J. K. in *Comprehensive Supramolecular Chemistry*. Lehn, J.-M., ed.; Pergamon Press: Tarrytown, NY, 1996; Vol. 5, 295.

173) Johann, T. W.; Barton, J. K. *Phil. Trans. Royal Soc. A.* **1996**, *354*, 299.

174) Jennette, K. W.; Lippard, S. J.; Vassiliades, G. A.; Bauer, W. R. *Proc. Natl. Acad. Sci. USA* **1974**, *71*, 3839.

175) Bond, P. J.; Langridge, R.; Jennette, K. W.; Lippard, S. J. *Proc. Natl. Acad. Sci. USA* **1975**, *72*, 4825.

176) Wang, A. H.-J.; Nathans, J.; van der Marel, G.; van Boom, J. H.; Rich, A. *Nature* **1978**, *276*, 471.

177) Greguric, I.; Aldrich-Wright, J. R.; Collins, J. G. *J. Am. Chem. Soc.* **1997**, *119*, 3621.

178) Collins, J. G.; Shields, T. P.; Barton, J. K. *J. Am. Chem. Soc.* **1994**, *116*, 9840.

179) David, S. S.; Barton, J. K. *J. Am. Chem. Soc.* **1993**, *115*, 2984.

180) Dupureur, C. M.; Barton, J. K. *J. Am. Chem. Soc.* **1994**, *116*, 10286.

181) Dupureur, C. M.; Barton, J. K. *Inorg. Chem.* **1997**, *36*, 33.

182) Shields, T. P.; Barton, J. K. *Biochemistry* **1995**, *34*, 15049.

183) Keilkopf, C. L.; Erkkila, K. E.; Hudson, B. P.; Barton, J. K.; Rees, D. C. *Manuscript in Preparation.*

184) Sitlani, A.; Long, E. C.; Pyle, A. M.; Barton, J. K. *J. Am. Chem. Soc.* **1992**, *114*, 2303.

185) Hudson, B. P.; Barton, J. K. *J. Am. Chem. Soc.* **1998**, *120*, 6877.

186) Pyle, A. M.; Long, E. C.; Barton, J. K. *J. Am. Chem. Soc.* **1989**, *111*, 4520.

187) Sitlani, A.; Dupurer, C. M.; Barton, J. K. *J. Am. Chem. Soc.* **1993**, *115*, 12589.

188) Krotz, A. H.; Kuo, L. Y.; Barton, J. K. *Inorg. Chem.* **1993**, *32*, 5963.

189) Krotz, A. H.; Kuo, L. Y.; Shields, T. P.; Barton, J. K. *J. Am. Chem. Soc.* **1993**, *115*, 3877.

190) Krotz, A. H.; Hudson, B. P.; Barton, J. K. *J. Am. Chem. Soc.* **1993**, *115*, 12577.

191) Terbrueggan, R. H.; Barton, J. K. *Biochemistry* **1995**, *34*, 8227.

192) Terbrueggen, R. H.; Johann, T. W.; Barton, J. K. *Inorg. Chem.* **1998**, *37*, 6874.

193) Franklin, S. J.; Barton, J. K. *Biochemistry* **1998**, *46*, 16093.

194) Kim, Y. C.; Geiger, J. H.; Hahn, S.; Sigler, P. B. *Nature* **1993**, *365*, 512.

195) Kim, J. L.; Nikolov, D. B.; Burley, S. K. *Nature* **1993**, *365*, 520.

196) Otwinowski, Z.; Schevitz, R. W.; Zhang, R. G.; Lawson, C. L.; Joachimiak, A.; Marmorstein, R. Q.; Luisi, B. F.; Sigler, P. B. *Nature* **1988**, *335*, 321.

197) Somers, W. S.; Phillips, S. E. V. *Nature* **1992**, *359*, 387.

Chapter 2:

Synthesis and Characterization of Quinone-Diimine Complexes of Rhodium(III)*

* This chapter is adapted in part from Mürner, H., Jackson, B.A., and Barton, J.K. *Inorg. Chem.* **1998**, *37*, 3007.

2.1: INTRODUCTION

In the field of bioinorganic chemistry, the interaction of small metal complexes with DNA has long been of interest. Depending on the metal ion and specific ligands used in the construction of such complexes, their modes of reactivity with nucleic acids can be tuned over a wide range. Such reactive pathways can include everything from the formation of covalent bonds with DNA functionalities, complex-stimulated generation of reactive species which cleave the polymer, or direct reaction of the complexes with DNA by various oxidative mechanisms.[1-7] Of particular interest have been the family of phenanthrenequinone diimine (phi) complexes of rhodium(III) which have been shown, upon photoactivation, to promote strand cleavage by hydrogen atom abstraction from a DNA sugar at their binding site.[8-12] These compounds have been shown to be versatile frameworks for the design of DNA binding agents, not only because of their convenient photochemical reactivity, but also because the octahedral geometry and kinetic inertness of the Rh(III) center provides a stable and rigid framework to place chemical functionalities in defined positions in three-dimensional space. Furthermore, the phi ligand binds to DNA by intercalating its planar aromatic surface into the base stack; this interaction provides a high level of sequence neutral binding affinity for the nucleic acid. These properties have allowed the construction of a family of many different DNA binding molecules whose binding affinity is provided by phi intercalation and whose specificity or other reactive functionality is defined by the character of their ancillary ligands.[13-16] Recently, phi compounds of rhodium(III) have also been shown to produce oxidative damage to nucleobases mediated by long range hole transfer through the DNA base stack.[17]

The synthesis of phi compounds of rhodium(III) has traditionally been performed by the reaction of 9,10-diaminophenanthrene with an appropriate metal complex intermediate. This ligand addition step is followed by air oxidation to the diimine functionality from the coordinated diamine.[18-20] Alternatively, tris-phi compounds have been prepared by the *in situ* deprotection of bis(trimethylsilyl)phenanthrene-quinone diimine for direct coordination of the diimine ligand.[21] These methods, however, have distinct disadvantages that makes the development of novel synthetic routes to these molecules desirable. The yields of the reactions are moderate to low making the addition of the diimine intercalator a stumbling block to the large scale synthesis of these compounds. Such reduced yields are likely a result of the harsh synthetic conditions involved in the diamine coordination; the reaction is typically run at reflux in a high boiling solvent over an extended period of time. Such harsh conditions are also likely to be incompatible with "fragile" functional groups that might be desirable for DNA recognition. It is also critical that oxygen free conditions be preserved during the coordination reaction to avoid degradation of the diamine ligand. It is important to note that this synthetic methodology also depends on the availability of appropriate aromatic amine starting materials; this requirement could limit the preparation of complexes with novel intercalating ligands.

The synthetic strategy adopted as an alternative to the direct coordination of aromatic diamines is based on formation of the diimine ligand by a condensation reaction at the metal center. In this route, rhodium ammine complexes react with *o*-quinones to form the coordinated, planar aromatic ligand in a single step. This general condensation between amines and aldehydes or ketones has been applied to many synthetic problems in organic chemistry. In the inorganic field, these reactions have been used to prepare ligands for subsequent coordination to metal centers.[22,23] Similar condensations have also been performed at the periphery of the ligand sphere

of metal complexes to extend ligands or assemble extended, multi-metal center super-molecules.[23-27] The concept of condensation of *coordinated* ammine ligands with either exogenous or covalently linked carbonyls has its roots in the work of Sargeson and co-workers.[28-32] Such a condensation was observed in the rearrangement of the pyruvatopentaamminecobalt(III) complex to form a coordinated immine.[33] These reactions, which are run at ambient temperatures in a basic solution open to the atmosphere, had the potential to provide a higher yielding, more versatile synthetic strategy for the preparation of diimine intercalating ligands. In fact, this strategy not only provided a superior method for the synthesis of phi intercalators, but also a route to other diimine and mixed ligand complexes of rhodium(III).

2.2: Experimental Methods

2.2.1: Instrumentation and Materials

The reagents used in this study were obtained from the following suppliers: $RhCl_3$, Pressure Chemical, Pittsburgh, PA, or Aldrich, Milwaukee, WI, and chrysene, Acros Organics, Princeton, NJ. All other reagents and ligands were obtained from various commercial sources and used as received without further purification. 4-(4-carboxybutyl)-4'-methyl-2,2'-bypyridine (bpy') was a generous gift of R. Houser in the Barton research group. The d_8-bypyridine used was provided by P. Belser and A. von Zelewsky. NMR spectra were recorded on a GE-300 MHz NMR or an AMX 500 MHz NMR. Mass Spectrometry was either performed at the University of California, Riverside, the University of Colorado, Fort Collins, or various on campus Caltech facilities. Absorption spectra were recorded on a Beckman DU 7400 spectrophotometer. Circular dichroism spectra were recorded on a Jasco J-500A spectropolarimeter. Atomic absorption measurements were made on a Varian AA-875 atomic absorption spectrometer. HPLC experiments were performed on a HP

1050 high pressure liquid chromatography system equipped with both an auto sampler and diode array detector. Analytical HPLC chromatography (monitored at 270 nm) was performed on a Varian Microsorb-MV C_{18} column using linear gradients of deionized water and acetonitrile, both containing 0.1% trifluoroacetic acid. Condensation reactions were also monitored by TLC (silica gel, acetonitrile/water/*n*-butanol/KNO_3, 4:1:1:0.1 M).

2.2.2: Synthetic Methods

The synthesis of all compounds produced to date using the condensation methodology is described. In addition to novel routes to previously reported rhodium phi compounds, these methods have also made several new compounds synthetically accessible. It is important to note, however, that the materials reported here represent only a small fraction of the many possible compounds made available by these synthetic procedures.

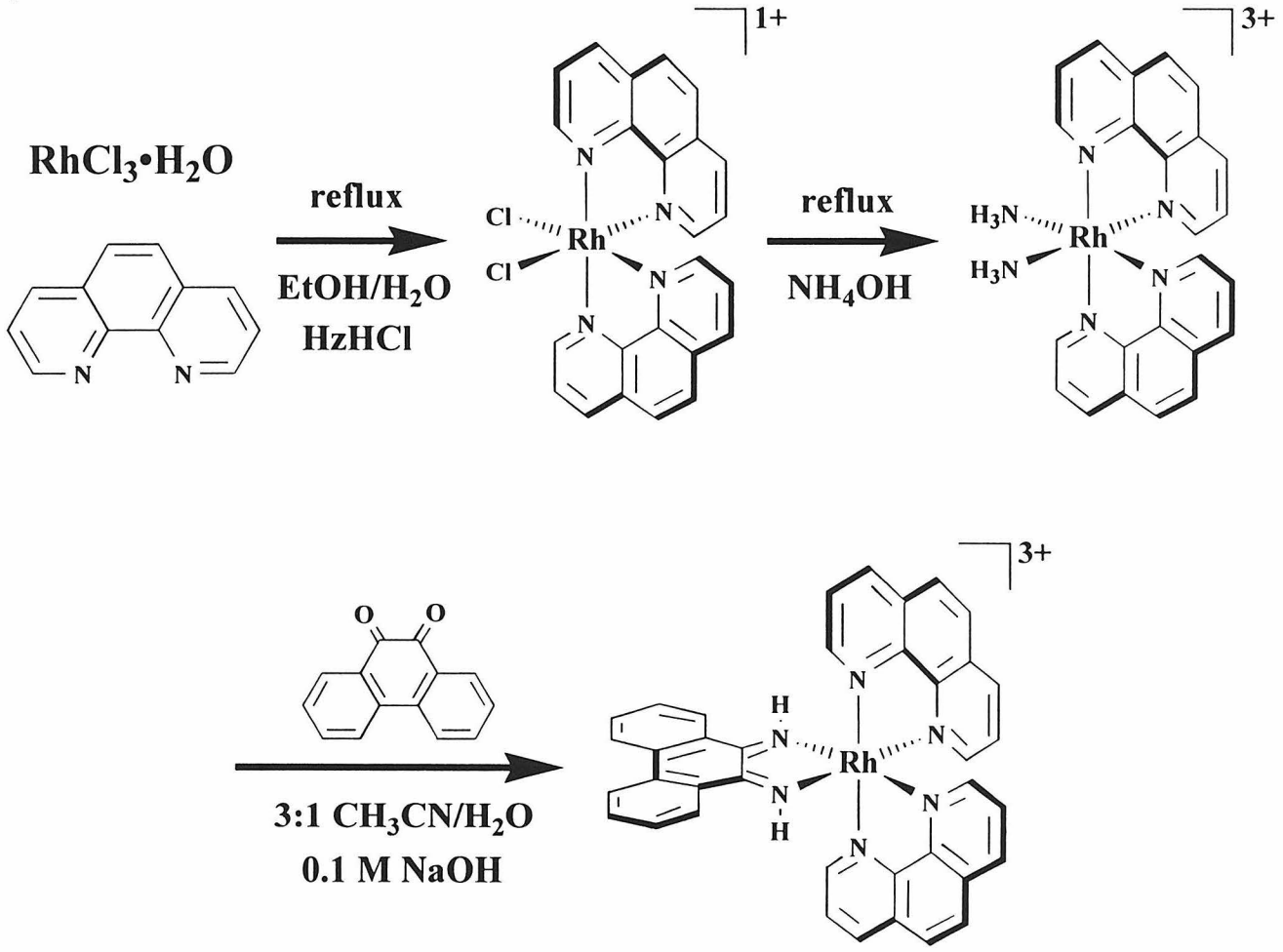
2.2.2.1: Addition of One Aromatic Quinone to $Rh(L)_2(NH_3)_2$

The general synthetic scheme for the preparation of $[Rh(phen)_2(phi)]^{3+}$ based on the condensation of phenanthrenequinone with two coordinated ammine ligands is included as Figure 2.1; this synthesis serves as a specific example of the more general synthesis of compounds of the formula $[Rh(L)_2(\text{quinone diimine L})]^{3+}$. Variants of this general scheme are applied to the preparation of the specific compounds discussed below.

$[Rh(phen)_2Cl_2]Cl$: $[Rh(phen)_2Cl_2]Cl$ was prepared by the method of Gillard and co-workers with minor modifications.[34] Rhodium(III) Chloride Hydrate (1.0 g, 4.4×10^{-3} mols) was dissolved in water (50 mL) in a 100 mL round-bottomed flask. 1,10-

Figure 2.1. Stepwise Synthesis of $[Rh(phen)_2(phi)]^{3+}$ by Condensation of Phenanthrenequinone with Coordinated Ammine Ligands. The synthesis of similar $[Rh(L)_2(quinone\text{-}diimine\ L)]^{3+}$ compounds is performed by analogous procedures.

Figure 2.1:


RhCl3•H2O
reflux
EtOH/H2O
HzHCl
1+
Cl
Cl
Rh
N
reflux
NH4OH
3+
H3N
H3N
O
O
3:1 CH3CN/H2O
0.1 M NaOH
H
N

phenanthroline (1.72 g) was added and the reaction was refluxed until all materials had dissolved and formed a yellow solution. The reaction was filtered hot through a medium frit and the filtrate was chilled to promote crystallization. The resulting yellow crystals (0.54 g, 22% yield)* were collected by filtration and dried under vacuum.[34]

^{1}H NMR, d_6-dmso: 10.02 ppm (d, 2H); 9.30 ppm (d, 2H); 8.91 ppm (d, 2H); 8.54 ppm (m, 5H); 8.44 ppm (d, 2H); 8.08 ppm (d, 2H); 7.77 ppm (q, 2H)

$[Rh(bpy)_2Cl_2]Cl$: $[Rh(bpy)_2Cl_2]Cl$ was prepared by the method of Gillard and co-workers with minor modifications.[34] Rhodium(III) Chloride Hydrate (0.6426 g, 2.8 x 10^{-3} mols) was combined with hydrazine monohydrochloride (50.3 mg) in a 50 mL round-bottomed flask and dissolved in deionized water (12.5 mL). A solution of 2,2'-bipyridyl (0.7918 g) in ethanol (18.75 mL) was added and the reaction was degassed gently by repeated applications of vacuum and back-filling with $Ar_{(g)}$. The reaction was brought to reflux and heated until all materials had dissolved and formed a yellow-orange solution. The reaction was filtered hot through a medium frit and the filtrate was chilled overnight to promote crystallization. The resulting yellow crystals (0.85 g, 59.4% yield) were collected by filtration and dried under vacuum.[34]

^{1}H NMR, d_6-dmso: 9.71 ppm (d, 2H); 9.01 ppm (d, 2H); 8.90 ppm (d, 2H); 8.63 ppm (t, 2H); 8.33 ppm (t, 2H); 8.17 ppm (t, 2H); 7.82 ppm (d, 2H); 7.59 ppm (t, 2H)

FAB-MS: 485.96 observed, 484.98 expected.

---

* It should be noted that more substantial yields are obtainable for this intermediate preparation. More typical, but unrecorded, yields were traditionally comparable to the analogous bpy procedure discussed below.

$[Rh(L)_2(NH_3)_2](OTf \text{ or } Cl)_3$: The diammine complexes of both the bisphenanthroline and bisbipyridine complexes were prepared by the method of Gidney and co-workers with minor modifications.[35] $[Rh(L)_2Cl_2]Cl$ (L = bpy or phen) was either used as prepared or first converted to the triflate complex by stirring overnight in neat triflic acid under an inert atmosphere. The conversion to the triflate requires subsequent precipitation in cold ether and results in a significant loss of material. A solid sample of one of the rhodium complexes (50 – 500 mg) was customarily refluxed in concentrated ammonium hydroxide (28-30%, 20 - 50 mL) for 15 min. Over the course of heating, the insoluble, singly charged complex is converted to the more soluble, triply charged diammino complex and goes into solution. There is also a corresponding color change from the yellow of the starting material to a much lighter, almost clear solution. After heating, the solution is allowed to cool and the product is isolated by either evaporation (yielding the chloride or triflate salts) or by precipitation with excess PF_6. Recoveries are best by evaporation and range from 80 to 100% depending on mechanical losses.[35]

Characterization for bipyridine compound:

^1H NMR, d_6-acetone (PF_6 salt): 9.45 ppm (d, 2H); 9.05 ppm (d, 2H); 8.89 ppm (d, 2H); 8.79 ppm (split t, 2H); 8.45 ppm (split t, 2H); 8.30 ppm (split t, 2H); 8.05 ppm (d, 2H); 7.74 ppm (split t, 2H); 5.06 ppm (broad s, 6H).

ESI-MS: 449.0 observed, 449.3 expected.

Characterization for phenanthroline compound:

^1H NMR, d_6-acetone (PF_6 salt): 9.93 ppm (d, 2H); 9.42 ppm (d, 2H); 8.99 ppm (d, 2H); 8.64 ppm (m, 4H); 8.51 ppm (d, 2H); 8.32 ppm (d, 2H); 7.87 ppm (dd, 2H); 5.18 ppm (broad s, 6H).

ESI-MS: 495 (M^+, also $M+PF_6$) observed, 497.1 expected.

$[Rh(phen)_2(phi)]Cl_3$: $[Rh(phen)_2(NH_3)_2]Cl_3$ (50 mg,) and 9,10-phenanthrenequinone (17.1 mg,) was dissolved in 32 mL of MeCN/water 3:1, 0.1 M in NaOH. This mixture was stirred for approx. 18 hr at ambient temperature. After neutralization with concentrated hydrochloric acid and addition of 500 mL of water, the reaction mixture was loaded onto a Sephadex SP-C25 ion exchange column equilibrated in 0.05 M $MgCl_2$. The product was purified by elution with a gradient of 0.05M - 0.5 M $MgCl_2$ and the orange product bands were collected. The fractions were concentrated on a Waters Sep-Pak 5g C_{18} cartridge and washed with copious amounts of water. The metal complex was eluted from the cartridge with a minimum volume of 0.1% TFA in MeCN/water 1:1 and lyophilized to dryness. The reaction yielded an orange powder (55.3 mg, 86%).[36]

^1H NMR, d_4-methanol: 9.21 ppm (2d, 4H); 8.98 ppm (d, 2H); 8.46 ppm (m, 8H); 8.27 ppm (split d, 2H); 8.11 ppm (d, 2H); 7.88 ppm (m, 4H); 7.57 ppm (t, 2H).

ESI-MS: 669.1 observed (M^+, also $M-2H^+$, $M-H^+$), 669.1 expected.

$[Rh(phen)_2(chrysi)]Cl_3$: $[Rh(phen)_2(NH_3)_2]Cl_3$ (50 mg,) and 5,6-chrysenequinone (21.5 mg,) was dissolved in 32 mL of MeCN/water 3:1, 0.1 M in NaOH. This mixture was stirred for approx. 18 hr at room temperature. After neutralization with concentrated hydrochloric acid and addition of 500 mL of water, the reaction mixture was loaded onto a Sephadex SP-C25 ion exchange column equilibrated in 0.05 M $MgCl_2$. The product was purified by elution with a gradient of 0.05M - 0.5 M $MgCl_2$ and the orange product bands were collected. The fractions were concentrated on a Waters Sep-Pak 5g C_{18} cartridge and washed with copious amounts

of water. The metal complex was eluted from the cartridge with a minimum volume of 0.1% TFA in MeCN/water 1:1 and lyophilized to dryness. The reaction yielded an orange powder (52.9 mg, 77%.)[36]

^{1}H NMR, d_4-methanol: 9.33 ppm (d, 1H); 9.27 ppm (d, 1H); 9.20 ppm (split d, 2H); 8.99 ppm (m, 2H); 8.46 ppm (m, 7H); 8.29 ppm (m, 4H); 8.14 ppm (d, 1H); 8.04 ppm (2D, 2H); 7.89 ppm (m, 3H); 7.60 ppm (m, 3H).

ESI-MS: 719.1 observed (M^+, also $M-2H^+$, $M-H^+$), 719.1 expected.

UV-Vis: λ_{max}: 268 nm, 303 nm (shoulder), 388 nm. (Figure 2.2)

Enantiomer Separation: The enantiomers of $[Rh(phen)_2(chrysi)]Cl_3$ were separated using on a Sephadex SP-C25 ion exchange column with a chiral mobile phase. The complex (55 mg) was loaded on the top of a 60-90 cm high, 2-3 cm diameter column equilibrated in 0.15 M filtered antimonial tartrate.[37] The column was eluted with additional tartrate solution over a period of three days during which the complex resolved into two clear bands. The column was allowed to run dry, the resin ejected and the bands were physically cut from the column. The complex was eluted from the Sephadex resin in 1 M magnesium chloride solution, isolated on a Waters Sep-Pak 5g C_{18} cartridge, and lyophillized as described previously.

$[Rh(bpy)_2(phi)]Cl_3$: $[Rh(bpy)_2(NH_3)_2]Cl_3$ (68.3 mg, 0.77 mmol) and 9,10-phenanthrenequinone (20.1 mg, 0.97 mmol) were dissolved with rapid stirring in 15 mL of methanol under atmospheric conditions. Aqueous sodium hydroxide (5 mL, 0.4 M) was added and the reaction closed with a ground glass stopper to prevent evaporation. After four hr, the reaction was stopped by addition of stoichiometric hydrochloric acid. The mixture was diluted, purified by ion exchange

chromatography as described above and isolated on a reverse phase cartridge. The product was isolated by lyophillization yielding an orange powder.[36] Although no specific yield was measured, all spectroscopic characterization corresponded with previously reported measurements.[11]

$[Rh(bpy)_2(chrysi)]Cl_3$: $[Rh(bpy)_2(NH_3)_2](PF_6)_3$ (195.5 mg, 0.22 mmol) and 5,6-chrysenequinone (56.8 mg, 0.22 mmol) were dissolved with rapid stirring in 15 mL of acetonitrile under atmospheric conditions. Aqueous sodium hydroxide (5 mL, 0.4 M) was added and the reaction closed with a ground glass stopper to prevent evaporation. After three hours, the reaction was stopped by addition of stoichiometric hydrochloric acid. The mixture was diluted, purified by ion exchange chromatography as described above and isolated on a reverse phase cartridge. The product was isolated by lyophillization yielding a brown powder (28 mg, 83 %).[36]

^{1}H NMR, d_4-methanol: 8.94 ppm (t, 2H); 8.86 ppm (t, 2H); 8.80 ppm (d, 1H); 8.77 ppm (d, 1H); 8.56 ppm (split t, 2H); 8.44 ppm (m, 5H); 8.40 ppm (d, 1H); 8.15 ppm (m, 1H); 8.03 ppm (m, 1H); 7.95 ppm (m, 3H); 7.86 ppm (d, 1H); 7.81 ppm (d, 1H); 7.64 ppm (m, 5H)

^{13}C-NMR, d_4-methanol: 183.3, 177.3, 175.4, 157.4, 157.2, 157.2, 153.8, 153.2, 152.1, 144.6, 144.5, 143.9, 143.8, 139.7, 138.8, 138.4, 136.2, 135.7, 132.3, 132.2, 132.0, 131.8, 130.9, 130.77, 130.6, 130.2, 129.4, 127.7, 127.6, 127.3, 126.9, 126.8, 123.9, 122.9, 120.8, 118.6, 116.3, 114.1

FAB-MS: 671 observed (M^+, also $M-2H^+$, $M-H^+$), 671.1 expected.

UV-Vis: λ_{max}: 302 nm, 315 nm, 384 nm. (ε_{271}: 63,800 $M^{-1}cm^{-1}$, ε_{302}: 66,100 $M^{-1}cm^{-1}$, ε_{316}: 52,600 $M^{-1}cm^{-1}$ (pH isosbestic points) determined by atomic absorption spectroscopy) (Figure 2.2)

Because of the complexity of the aromatic region arising from the asymmetry of the chrysenequinone diimine intercalating ligand, an additional synthesis of this molecule was performed with d_8-bipyridine. The corresponding proton NMR spectrum of this compound allowed a view of the chrysi intercalator protons in the absence of the overlapping bipyridine protons. These spectra are included in Figure 2.3.

Enantiomer Separation: The enantiomers of $[Rh(bpy)_2(chrysi)]Cl_3$ were separated using a Sephadex SP-C25 ion exchange column and 0.15 M antimonial tartrate as described above for the phenanthroline analogue.[37]

CD: (Δ enantiomer, H_2O): 233 nm ($\Delta\varepsilon$: 34 l $M^{-1}cm^{-1}$), 264 nm ($\Delta\varepsilon$: 26 l $M^{-1}cm^{-1}$), 286 nm ($\Delta\varepsilon$: -12 l $M^{-1}cm^{-1}$), 308 nm ($\Delta\varepsilon$: -42 l $M^{-1}cm^{-1}$), 318 nm ($\Delta\varepsilon$: -100 l $M^{-1}cm^{-1}$), 341 nm ($\Delta\varepsilon$: 6 l $M^{-1}cm^{-1}$).

2.2.2.2: Addition of Two Aromatic Quinones to $Rh(L)(NH_3)_4$

When quinone condensation is performed on a mono-chelate tetrammine rhodium(III) starting material rather than the simpler diammine case, further synthetic options are made available. The preparation of compounds of the formula $[Rh(L)_1(\text{quinone diimine L})_2]^{3+}$ is generally analogous to the chemistry described above with the exception that the possibility exists for introducing two different quinones to form a tris-heteroleptic metal complex. The general reaction process for the simpler, single quinone case is included in Figure 2.4. The more complex case for the in situ

Figure 2.2. Absorption Spectra of the Complex Ions $[Rh(bpy)_2(chrysi)]^{3+}$ and $[Rh(phen)_2(chrysi)]^{3+}$ in Deionized Water (pH ≈ 5).

Figure 2.2:

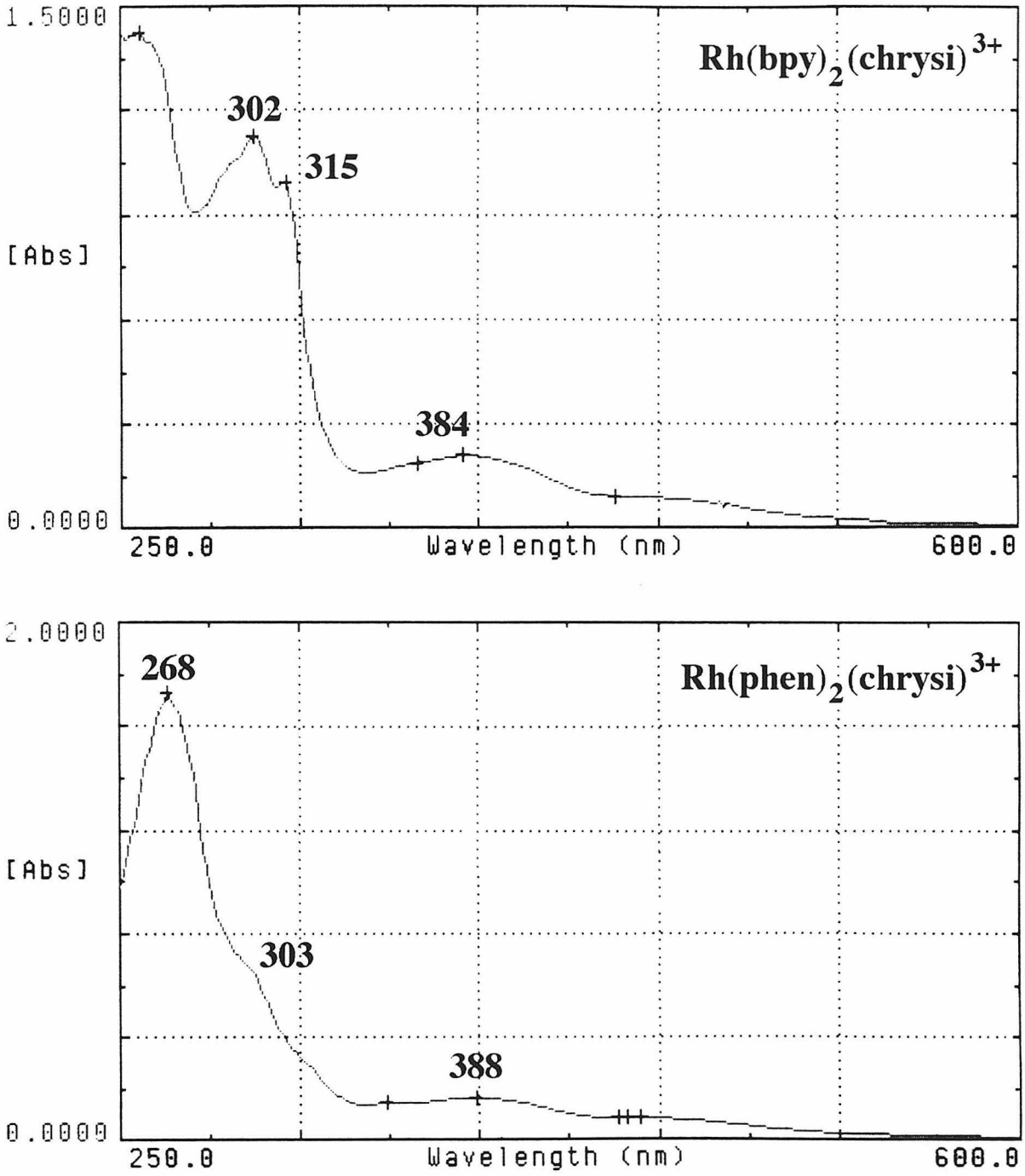

1.5000
[Abs]
0.0000
250.0
Wavelength (nm)
600.0
Rh(bpy)2(chrysi)3+
302
315
384
2.0000
[Abs]
0.0000
250.0
Wavelength (nm)
600.0
Rh(phen)2(chrysi)3+
268
303
388

Figure 2.3. Proton NMR Spectra of the Complex Ions $[Rh(bpy)_2(chrysi)]^{3+}$ and $[Rh(d_8\text{-}bpy)_2(chrysi)]^{3+}$ in d_4-MeOH for the Purposes of Distinguishing the Chrysenequinone Diimine Resonances from the Overlapping Bipyridine Peaks.

Figure 2.3:

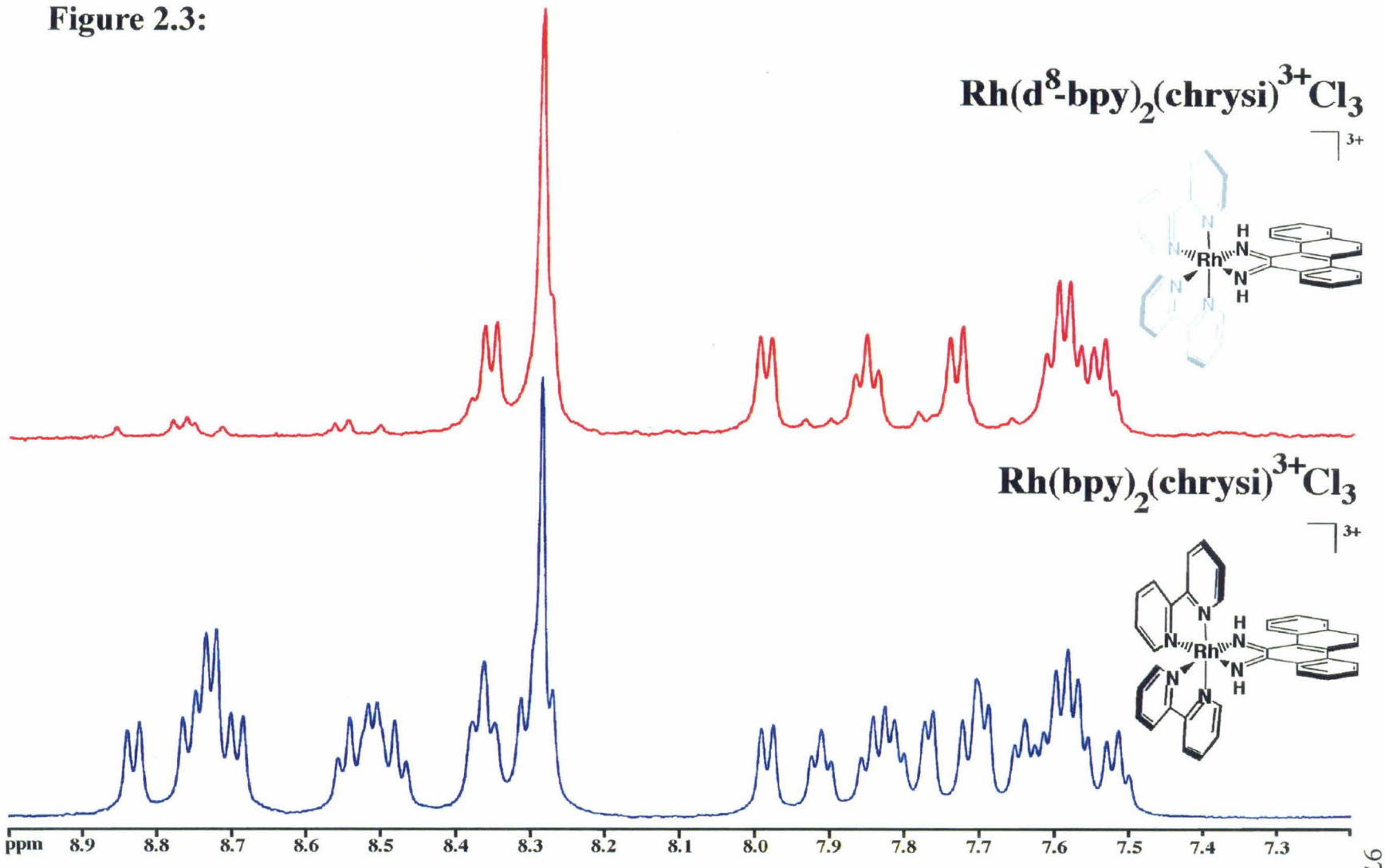
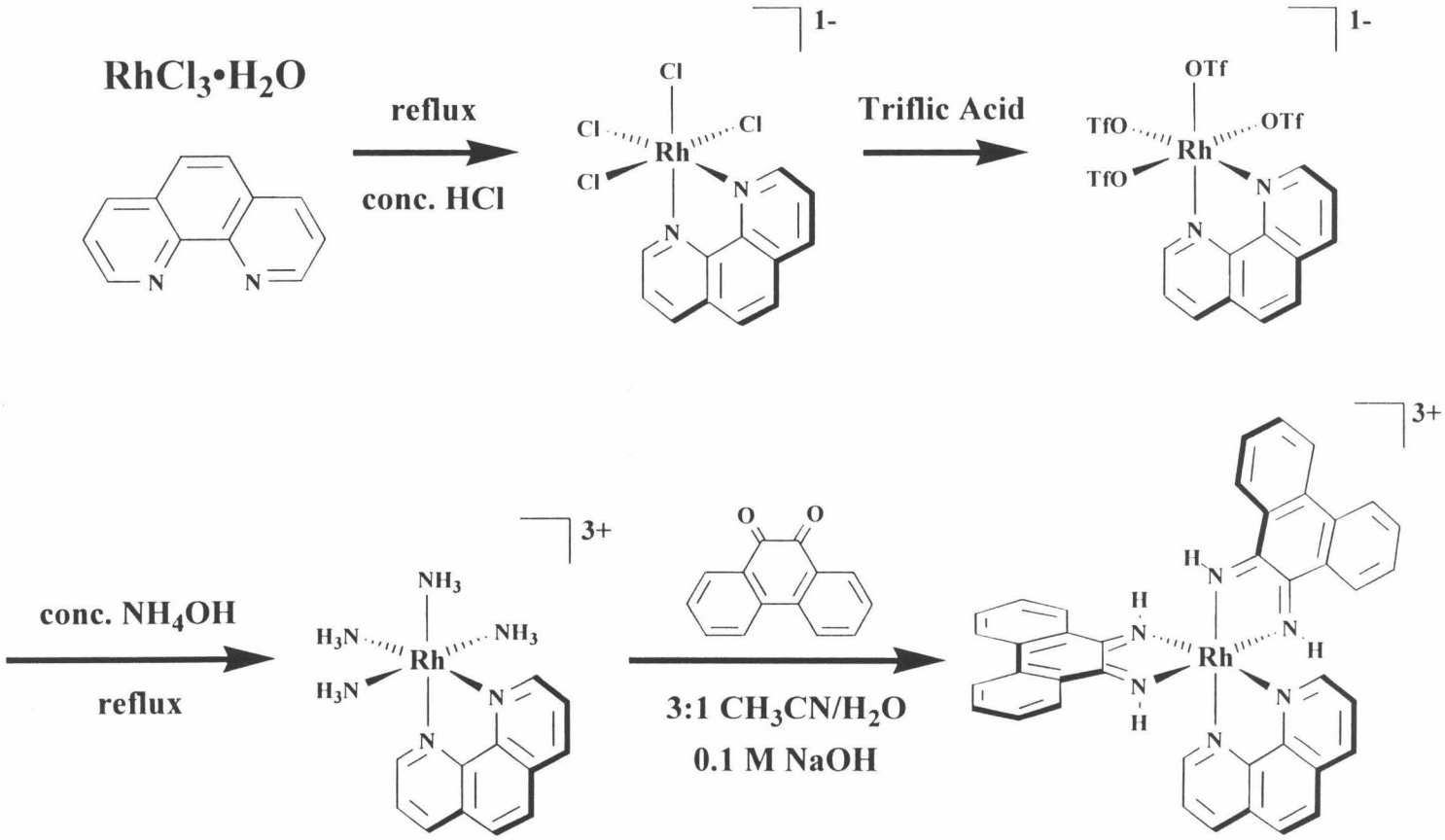

Rh(d8-bpy)2(chrysi)3+Cl3
3+
Rh(bpy)2(chrysi)3+Cl3
3+
ppm 8.9 8.8 8.7 8.6 8.5 8.4 8.3 8.2 8.1 8.0 7.9 7.8 7.7 7.6 7.5 7.4 7.3

Figure 2.4. Stepwise Synthesis of the Complex Ion $[Rh(phi)_2(phen)]^{3+}$ by Condensation of Phenanthrenequinone with Coordinated Ammine Ligands. The synthesis of analogous $[Rh(quinone\text{-}diimine\ L)_2(L)]^{3+}$ compounds is performed by the same procedure.

Figure 2.4:


RhCl3•H2O
reflux
conc. HCl
1-
Triflic Acid
1-
conc. NH4OH
reflux
3+
3:1 CH3CN/H2O
0.1 M NaOH
3+

preparation of three ligand diimine compounds is included as Figure 2.5. The variants of this general scheme applied to the preparation of specific compounds are included below.

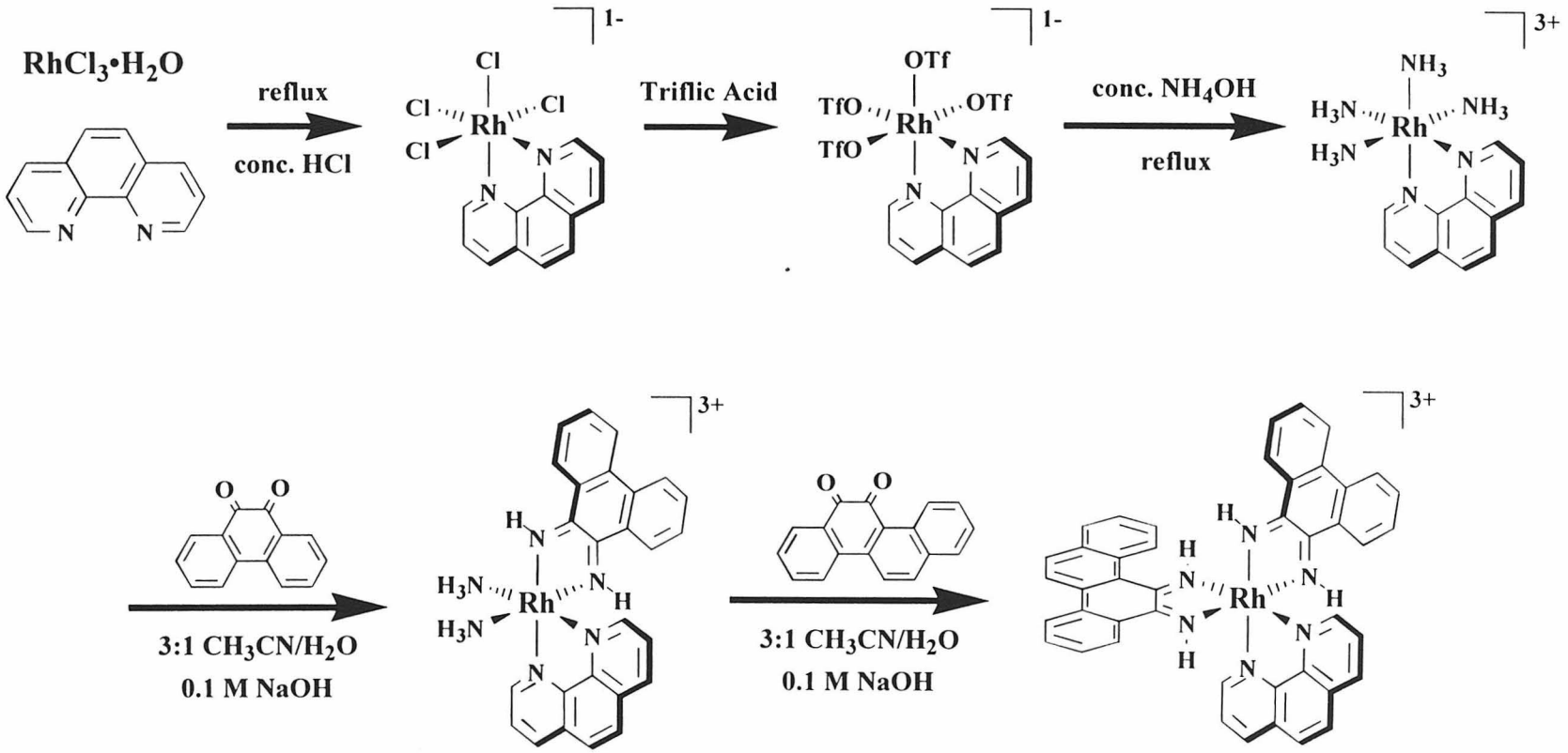
$[Rh(phen)Cl_4](H_3O^+)^-$: The phenanthrolinium salt of $[Rh(phen)Cl_4]^{1-}$ was made according to the method of Broomhead and co-workers with minor modifications.[38] Rhodium chloride hydrate (0.6 g), was added to concentrated hydrochloric acid (20 mL) in a 500 mL round-bottomed flask. The solid was completely dissolved by refluxing the mixture for 3 hr in an oil bath. Phenanthroline hydrate (1 g), was added and the solution heated for an additional 20 min during which boiling distilled water (300 mL) was added. The resulting mixture (product crystals began to form during heating) was chilled at 4°C overnight to promote more complete crystallization. The product (orange crystals, 0.9318 g, 58%) was collected by suction filtration.[38] The phenanthrolinium salt was converted to a hydronium salt according to the method of McKenzie and co-workers.[39] The isolated phenanthrolinium crystals were added to fresh concentrated hydrochloric acid (60 mL in a 100 mL round-bottomed flask) and dissolved by refluxing the mixture for 5 hr. The resulting solution was chilled at 4 °C overnight yielding the product (orange needles, 0.6637 g, 97%) which was collected by suction filtration.[39]

^{1}H NMR, d_6-dmso: 9.90 ppm (d, 2H); 8.83 ppm (d, 2H); 8.28 ppm (s, 2H); 8.16 ppm (split t, 2H).

$[Rh(phen)(OTf)_4](H_3O^+)$: The hydronium salt of $[Rh(phen)Cl_4]^{1-}$ (0.6637 g) was added to neat triflic acid (25 g, 99+% pure) and $Ar_{(g)}$ was bubbled through the solution overnight. The product was precipitated by adding the reaction mixture to a large volume (300 mL) of diethyl ether chilled on dry ice. The resulting brownish

Figure 2.5. *In Situ* Synthesis of the Complex Ion $[Rh(phi)(chrysi)(phen)]^{3+}$ by Stepwise Condensation of Phenanthrenequinone and Chrysenequinone with Coordinated Ammine Ligands.

Figure 2.5:


RhCl3•H2O
reflux
conc. HCl
1-
Triflic Acid
1-
conc. NH4OH
reflux
3+
3:1 CH3CN/H2O
0.1 M NaOH
3+
3:1 CH3CN/H2O
0.1 M NaOH
3+

chalky powder was collected by suction filtration and washed with additional ether. It was dried under vacuum yielding a beige powder (0.6972 g, 52%).[40]

[Rh(phen)(NH_3)$_4$](OTf)$_3$: The powdered triflate salt, [Rh(phen)(OTf)$_4$](H_3O^+) (0.6972 g), was added to concentrated ammonium hydroxide (28-30%, 30 mL) in a round-bottomed flask. The reaction was placed in an oil bath and refluxed for 15 min. The resulting solution was evaporated to dryness yielding a quantitative recovery of the tetra-ammine product (beige powder).

^{1}H NMR, d_6-dmso: 9.24 ppm (d, 2H); 9.03 ppm (d, 2H); 8.39 ppm (s, 2H); 8.27 ppm (m, 2H); 5.05 ppm (broad s, 6H); 4.04 ppm (broad s, 6H)

ESI-MS: 350.1 observed (M-H^+, also M-2H^+, M-3H^+), 351.1 expected.

[Rh(phen)(phi)$_2$]Cl$_3$: [Rh(phen)(NH_3)$_4$](OTf)$_3$ (51.3 mg, 6.43 x 10^{-5} mols) was combined with phenanthrenequinone (26.8 mg, 1.29 x 10^{-4} mols) in a round-bottomed flask equipped with a stirbar. Acetonitrile (24 mL), deionized water (5 mL) and sodium hydroxide (3 mL, 1.06 M) were added and the reaction was stirred for 46 hr at room temperature. The reaction was stopped by addition of stoichiometric hydrochloric acid. The reaction mixture was anion exchanged to chloride counter ions using Sephadex QAE A-25 resin equilibrated in magnesium chloride. It was then purified using Sephadex CM C-25 resin eluted with increasing concentrations (0.05 M – 0.5 M) of magnesium chloride solution. The orange product band was collected, desalted using a Sep-Pak 5g C_{18} cartridge, and lyophilized to dryness. The reaction yielded an orange powder (27.9 mg, 54%).[36]

^{1}H NMR, d_6-dmso: 13.95 ppm (s, 2H); 13.63 ppm (s, 2H); 9.12 ppm (d, 2H); 9.06 ppm (d, 2H); 8.69 ppm (d, 2H); 8.49 ppm (m, 8H); 8.23 ppm

(t, 2H); 7.90 ppm (t, 2H); 7.84 ppm (t, 2H); 7.69 ppm (t, 2H); 7.58 ppm (t, 2H).

ESI-MS: 695.1 observed (M^+, also $M\text{-}H^+$, $M\text{-}2H^+$), 695.1 expected.

$[Rh(phen)(chrysi)_2]Cl_3$: $[Rh(phen)(NH_3)_4](OTf)_3$ (39.1 mg, 0.049 mmol) was combined with 5,6-chrysenequinone (57.6 mg, excess) in acetonitrile (15 mL) and sodium hydroxide (5 mL, 0.4 M). The reaction was stopped after 24 hr by neutralization with hydrochloric acid. The mixture was then loaded onto a Sephadex CM-C25 cation exchange column equilibrated in 50/50 acetonitrile/water. The column was eluted with a gradient of 0.05M - 0.5 M $MgCl_2$ in 50/50 acetonitrile/water. The dark brown product band was separated from several orange side products, collected, and the fractions concentrated on a Sep-Pak 5g C_{18} cartridge and washed with copious amounts of water. The metal complex was eluted from the cartridge with a minimum volume of 0.1% TFA in MeCN/water 1:1 and lyophillized to dryness yielding a brown-black powder (21.0 mg, 48%).

^1H NMR, D_2O, TFA: 8.92 ppm (d, 2H); 8.72 ppm (d, 1H); 8.33 ppm (m, 11H); 8.04 ppm (d, 2H); 7.98 ppm (t, 2H); 7.78 ppm (m, 6H); 7.55 ppm (t, 2H); 7.46 ppm (t, 2H).

^1H NMR, d_6-dmso, TFA: 14.39 ppm (s, immino); 13.02 ppm (s, immino); 9.22 ppm (d, 1H); 9.14 ppm (d, 1H); 8.71 ppm (d, 1H); 8.51 ppm (m, 7H); 8.42 ppm (d?, 3H); 8.26 ppm (t, 2H); 8.13 ppm (d, 2H); 7.82 ppm (m, 4H); 7.68 ppm (m, 4H); 7.46 ppm (s, 1H); 7.29 ppm (s, 1H); 7.12 ppm (s, 1H).

ESI-MS: 796.5 observed ($M+H^+$, also, M^+, $M\text{-}H^+$, $M\text{-}2H^+$), 795.2 expected.

UV-Vis: λ_{max}: 266 nm, 390 nm. (Figure 2.6)

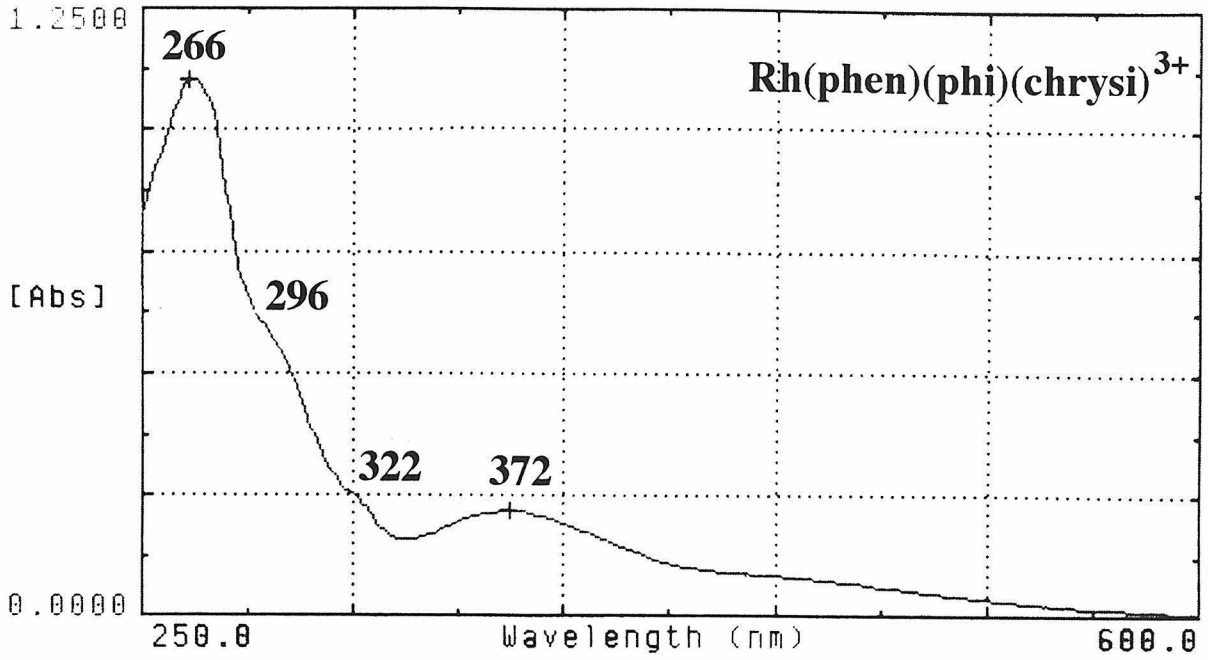
Enantiomer Separation: The enantiomers of $[Rh(chrysi)_2(phen)]Cl_3$ were separated using on a Sephadex CM-C25 ion exchange column with an antimonial tartrate mobile phase. Unlike previous separations, the bis-chrysi compound did not move on the column using only 0.15 M aqueous tartrate. As a result, the column was eluted with 10% acetonitrile/water containing 0.135 M of the chiral salt. This solution was first prepared and filtered as aqueous 0.15 M tartrate and then diluted with the organic co-solvent. This system proved sufficient to separate the two isomers of the complex over a period of eight days. Although there would be expected to be multiple geometric isomers of the complex due to the asymmetry of the chrysi ligand, no additional separation was observed.[37]

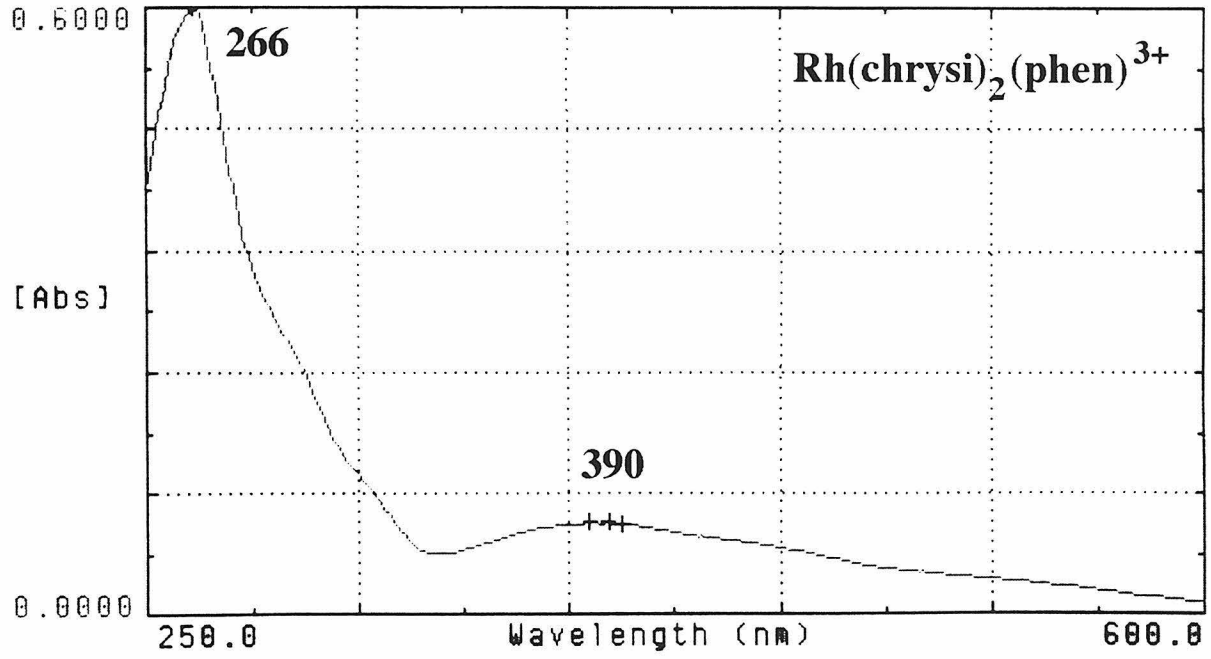
$[Rh(phen)(chrysi)(phi)]Cl_3$: $[Rh(phen)(NH_3)_4]$ $(OTf)_3$ (17 mg, 0.021 mmol) was combined with 9,10-phenanthrenequinone (5.4 mg, 0.026 mmol) in acetonitrile (9.6 mL), water (2.0 mL) and sodium hydroxide (1.2 mL, 1.06 M). After 60 min. of stirring at ambient temperature, 5,6-chrysenequinone (9.9 mg, 0.039 mmol) was added. The reaction was stopped after 20 hr by neutralization with hydrochloric acid. The product was purified on a Sephadex SP-C25 cation exchange column eluting with a gradient of 0.05M - 0.5 M $MgCl_2$. The red product band was collected, the fractions concentrated on a Waters Sep-Pak 5g C_{18} cartridge and washed with copious amounts of water. The metal complex was eluted from the cartridge with a minimum volume of 0.1% TFA in MeCN/water 1:1 and lyophillized to dryness yielding a red-orange powder (14 mg, 75%).[36]

^1H NMR, D_2O, TFA: 8.72 ppm (m, 3H); 8.85 ppm (d, 1H); 8.36 ppm (m, 9H); 8.08 ppm (m, 5H); 7.80 ppm (m, 3H); 7.56 ppm (m, 5H).

Figure 2.6. Absorption Spectra of the Complex Ions $[Rh(phen)(phi)(chrysi)]^{3+}$ and $[Rh(chrysi)_2(phen)]^{3+}$ in Deionized Water (pH ≈ 5).

Figure 2.6:


1.2500
266
Rh(phen)(phi)(chrysi)3+
[Abs]
296
322
372
0.0000
250.0
Wavelength (nm)
600.0


0.6000
266
Rh(chrysi)2(phen)3+
[Abs]
390
0.0000
250.0
Wavelength (nm)
600.0

ESI-MS: 745.3 observed (M^+, also $M\text{-}H^+$, $M\text{-}2H^+$), 745.2 expected.

UV-Vis: λ_{max}: 266 nm, 296 nm (shoulder), 322 nm (shoulder), 372 nm (Figure 2.6)

2.2.2.3: Use of Condensation Chemistry as an Intermediate Synthetic Step

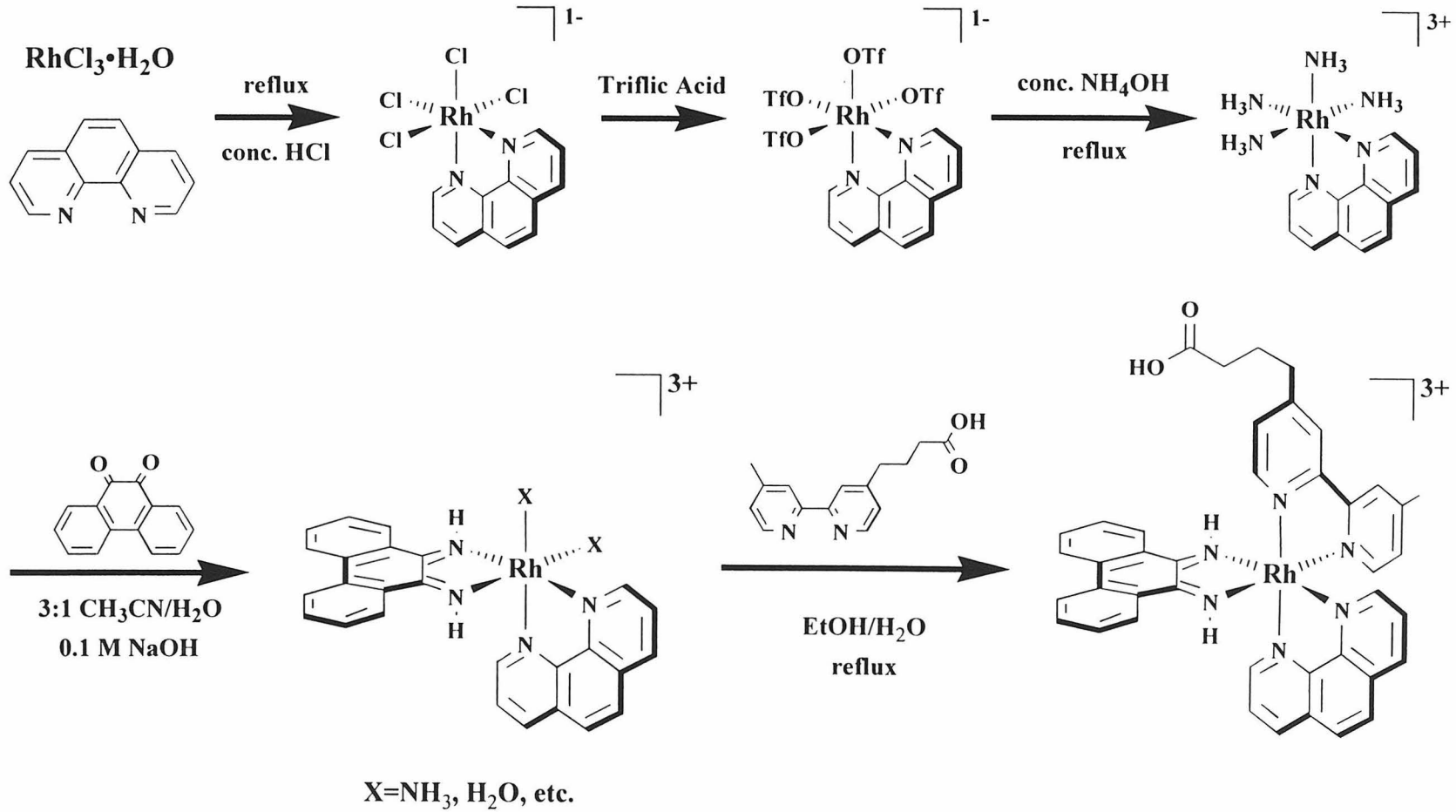
Application of $[Rh(phen)(NH_3)_4]^{3+}$ as a synthetic starting material is not limited to the sequential condensation of two equivalents of aromatic quinone. If only one equivalent of quinone is added, it is possible to use the resulting intermediate material in further synthetic reactions. Displacing the remaining monodentate ligands on the metal with an additional chelating ligand, for example, made it possible to produce tris-heteroleptic rhodium complexes containing only one quinone diimine ligand. A generalized scheme describing this synthetic route is included as Figure 2.7.

$[Rh(phen)(phi)X_2](OTf)_3$: $[Rh(phen)(NH_3)_4]$ $(OTf)_3$ (75 mg, 0.094 mmol) was combined with 9,10-phenanthrenequinone (19.6 mg, 0.094 mmol) in acetonitrile (30 mL), water (5.8 mL) and sodium hydroxide (4.2 mL, 1.06 M). The reaction was stopped after stirring overnight by neutralization with hydrochloric acid. The reaction mixture was decanted from a white precipitated salt product, anion exchanged on a Sephadex QAE-A-25 column which had been equilibrated with magnesium chloride, and lyophillized to dryness. The resulting solid was used in subsequent reaction steps without purification or characterization.

$[Rh(phen)(chrysi)X_2](OTf)_3$: $[Rh(phen)(NH_3)_4](OTf)_3$ (220 mg, 0.276 mmol) was combined with 5,6-chrysenequinone (67.2 mg, 0.261 mmol) in acetonitrile (120 mL) and sodium hydroxide (40 mL, 0.4 M). The reaction was stopped after 8 hr by neutralization with hydrochloric acid. The reaction mixture was anion exchanged on a Sephadex QAE A-25 column which had been equilibrated in 0.05 M magnesium

Figure 2.7. Stepwise Synthesis of Tris-Heteroleptic Complexes of Rhodium(III) Utilizing Both *o*-Quinone Condensation with Coordinated Ammine Ligands and Final Coordination of an Additional Chelating Ligand.

Figure 2.7:


RhCl3•H2O
reflux
conc. HCl
1-
Triflic Acid
1-
conc. NH4OH
reflux
3+
3:1 CH3CN/H2O
0.1 M NaOH
3+
EtOH/H2O
reflux
3+
X=NH3, H2O, etc.

chloride. Product fractions were lyophillized to dryness and the resulting solid was used in subsequent reaction steps without purification or characterization.

[Rh(phen)(chrysi)(bpy')]$^{3+}$: [Rh(phen)(chrysi)X_2]Cl_3 (167 mg, 0.246 mmol) was combined with 4-(4-carboxybutyl)-4'-methyl-2,2'-bypyridine (bpy', 90 mg, 0.351 mmol) in a 50/50 mixture of ethanol and deionized water (100 mL) in a 250 mL round bottom flask equipped with stirrer. The reaction was heated to reflux in an oil bath and stirred for 20 hr. The mixture was then allowed to cool and purified by cation exchange chromatography on a Sephadex SP C-25 column by eluting with a gradient of 0.05M - 0.5 M $MgCl_2$ which had been acidified with a few drops of concentrated hydrochloric acid. The dark brown product band was collected, isolated on a Waters Sep-Pak 5g C_{18} cartridge and washed with copious amounts of water. The metal complex was eluted from the cartridge with a minimum volume of 0.1% TFA in MeCN/water (1:1) and lyophillized to dryness yielding a dark brown powder (27.9 mg, 13%*).

^{1}H NMR, D_2O, TFA: (mixture of two diastereomers) 9.07 ppm (m, 1H); 8.96 ppm (m, 2H); 8.64 ppm (m, 3H); 8.33 ppm (m, 6H); 7.94 ppm (m, 7H); 7.51 ppm (m, 5H); 3.05 ppm (t, 2H); 2.88 ppm (t, 2H); 2.72 ppm (d, 3H); 2.54 ppm (s?, 3H); 2.39 ppm (m, 2H); 2.08 ppm (m, 2H?); 1.95 ppm (m, 2H?).

ESI-MS: 795.0 observed (M^+, also M-H^+, M-2H^+, M-phen, M-bpy'), 795.2 expected.

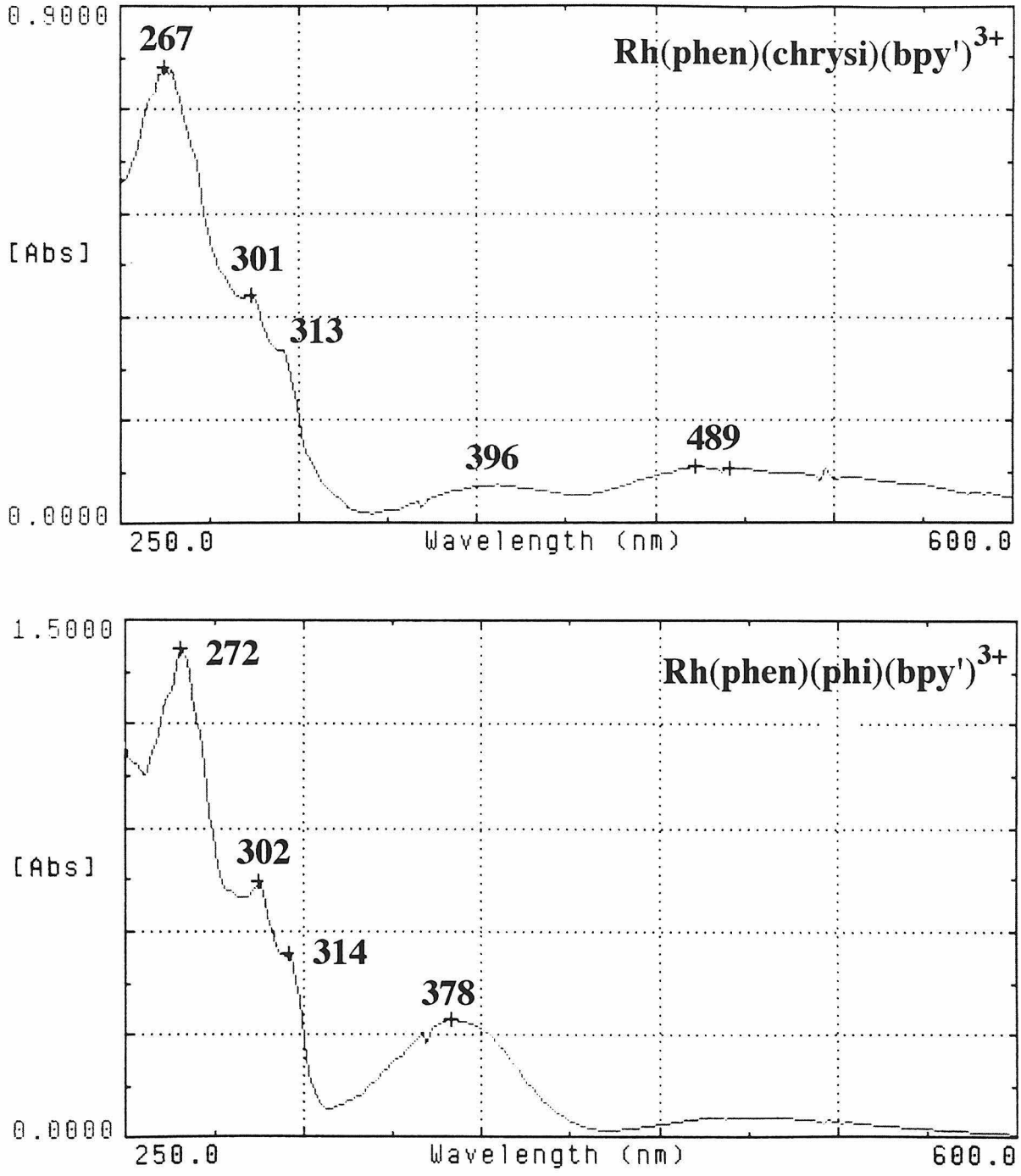
UV-Vis: λ_{max}: 267 nm, 301 nm (shoulder), 313 nm (shoulder), 396 nm, 489 nm. (Figure 2.8)

---

* The reported yield is artificially low as a portion of the unpurified reaction mixture (50-60%) was used for other purposes.

Figure 2.8. Absorption Spectra of the Complex Ions $[Rh(phen)(chrysi)(bpy')]^{3+}$ and $[Rh(phen)(phi)(bpy')]^{3+}$ in Deionized Water (pH ≈ 5).

Figure 2.8:


0.9000
267
Rh(phen)(chrysi)(bpy')3+
[Abs]
301
313
396
489
0.0000
250.0
Wavelength (nm)
600.0
1.5000
272
Rh(phen)(phi)(bpy')3+
[Abs]
302
314
378
0.0000
250.0
Wavelength (nm)
600.0

[Rh(phen)(phi)(bpy')]$^{3+}$: [Rh(phen)(phi)X_2]Cl_3 (59.2 mg, 0.094 mmol) was combined with 4-(4-carboxybutyl)-4'-methyl-2,2'-bypyridine (bpy', 30.3 mg, 0.118 mmol) in a 50/50 mixture of ethanol and deionized water (40 mL) in a 100 mL round bottom flask equipped with stirrer. The reaction was heated to reflux in an oil bath and stirred for 13 hr. The mixture was then allowed to cool and purified by cation exchange chromatography on a Sephadex SP C-25 column by eluting with a gradient of 0.05M - 0.5 M $MgCl_2$ which had been acidified with a few drops of concentrated hydrochloric acid. The major orange product band was collected, isolated on a Waters Sep-Pak 5g C_{18} cartridge and washed with copious amounts of water. The metal complex was eluted from the cartridge with a minimum volume of 0.1% TFA in MeCN/water (1:1) and lyophilized to dryness yielding aN orange powder (67.7 mg, 85%).

^{1}H NMR, D_2O, TFA: (mixture of two diastereomers) 9.06 ppm (d, 1H); 8.92 ppm (t, 2H); 8.62 ppm (s, 1H); 8.37 ppm (m, 7H); 8.10 ppm (m, 3H); 7.79 ppm (m, 4H); 7.69 ppm (t, 1H); 7.38 ppm (m, 3H); 3.03 ppm (t, 2H); 2.89 ppm (t, 2H); 2.70 ppm (s, 3H); 2.54 ppm (s, 3H); 2.49 ppm (t, 2H); 2.39 ppm (t, 2H); 2.09 ppm (quin, 2H); 1.95 ppm (quin, 2H).

ESI-MS: 745.0 observed (M^+, also M-H^+, M-2H^+, M-phen, M-phi, M-bpy'), 745.2 expected.

UV-Vis: λ_{max}: 272 nm, 302 nm (shoulder), 314 nm (shoulder), 378 nm. (Figure 2.8)

2.2.2.4: Ligand Synthesis

5,6-Chrysenequinone: The chrysenequinone starting material was produced by the method of Greabe with minor modifications.[41] Chrysene (5g) was combined with sodium dichromate (21.35 grams) and glacial acetic acid (53 grams) in a 250 mL round bottom flask equipped with a stirrer. The resulting slurry was heated to reflux for eight hr over which it changed from the yellow color of the hydrocarbon to a mixture of green chromium products containing the bright orange chrysenequinone. The reaction was poured into 100 mL of boiling water and the product filtered out on a sintered glass frit. The product was washed with several hundred mL hot water. It is important to note that other dichromate salts should both be substituted for the sodium salt used in this preparation; in the case of the potassium salt, for example, the resulting chromium products are insoluble and the quinone must be obtained by extraction into toluene from the solid mixture. The resulting orange crystals are recrystallized from hot ethanol. Typical yields for this preparation are greater than 80%.[41]

^{1}H NMR, CD_2Cl_2: 9.39 ppm (d, 1H); 8.16 ppm (m, 4H); 7.92 ppm (d, 1H); 7.77 ppm (t of d, 2H); 7.57 ppm (t of d, 2H).

ESI-MS: 258.1 observed (M^+), 258.1 expected.

2.2.3: Characterization Methods

2.2.3.1: Measurement of pH Dependent Optical Changes

A metal complex solution (100-150 mL, 0.5-1.2 Abs units at maximum, one of six phi or chrysi complexes) was prepared in a 250 mL beaker equipped with mechanical stirring. The solution was titrated with concentrated stocks of either sodium hydroxide or hydrochloric acid and the pH monitored by an internal electrode. The

pH of the solution was adjusted from approx. 2.0 to 12.0 and back. At various points in the titration, at least every 0.5 pH unit, an aliquot was removed and its absorption spectrum measured. The aliquot was then returned to the titration reservoir and the experiment continued. In each case, the spectroscopy cell was washed extensively with the complex solution to ensure that the pH in the cuvette matched that in the reservoir. A single wavelength was selected for each metal complex where a large change was observed over the course of the titration. The absorbance at this wavelength was then plotted as a function of pH to generate a titration curve. The pK_a of the metal complex was determined from the inflection point of this sigmoidal curve.

2.2.3.2: Crystallographic Studies of $[Rh(bpy)_2(chrysi)]Cl_3$

The complex crystallized from acetonitrile as dark brown triclinic block crystals in the space group $P\bar{1}$ (#2). The cell parameters of the crystal are described in Table 2.1 on the following page. Crystallographic analysis was performed on a single crystal at 85 K by Lawrence M. Henling of the Caltech X-Ray Crystallography Laboratory. Further detail on the solution and refinement of the structure and crystallographic data tables is included as Appendix I.

Table 2.1: Crystal Data and Structural Analysis Results for $[Rh(bpy)_2(chrysi)]Cl_3$

Crystal Data		
Formula		$C_{44}H_{41}Cl_3N_9O_2Rh$
Formula Weight (g $mole^{-1}$)		937.13
Crystal System		Triclinic
Space Group		$P\bar{1}$ (#2)
Z (formulas per unit cell)		2
Cell Parameters:	a (Å)	9.079(3)
	b (Å)	10.970(3)
	c (Å)	21.192(8)
	α (deg)	86.71(3)
	β (deg)	89.21(3)
	γ (deg)	78.58(3)
	V ($Å^3$)	2065.4(12)
Crystal Size (mm)		0.13 x 0.22 x 0.33
Habit		Block
ρ_{calc} (g cm^{-3})		1.507
μ (cm^{-1})		6.57
F_{000}		960
Data Measurement Parameters and Analysis Results		
Diffractometer		CAD-4, ω scan
Radiation		MoKα (λ=0.7107 Å)
2Θ range (deg)		3-50
Temperature (K)		85
Number of reflections measured		15224
Number of independent reflections		7250
All independent reflections used in refinement		
GOFmerge		0.98 for 7250 multiples
Final $R(F_0)$ [6433 reflections with $F_O^2 > 3\sigma(F_O^2)$]		0.026
Final $R(F_0)$ [7006 reflections with $F_O^2 > 0$]		0.063
Final goodness of fit [728 parameters, 7250 reflections]		1.81
$\Delta\rho_{max}$ (e $Å^{-3}$)		0.75

2.2.3.3: pH Titration of $[Rh(d_8\text{-bpy})_2(chrysi)]Cl_3$ by 1D-^{1}H NMR Spectroscopy

In order to directly observe the effects of changing pH on the geometry of the chrysi intercalating ligand (see pH titrations above), a parallel pH titration was performed on $[Rh(d_8\text{-bpy})_2(chrysi)]Cl_3$ using proton NMR. The complex with deuterated ancillary ligands was used so the multiple bipyridine proton signals would not obscure the chrysi signals of interest. A sample of the complex in 90/10 H_2O/D_2O was studied on the AM-500 MHz NMR using the WATERGATE gradient solvent suppression.[42] The pH of the solution was monitored with an external pH meter equipped with an appropriate probe. The pH was titrated with small aliquots of concentrated aqueous HCl and NaOH solutions between acquiring 1D spectra.

2.3: Results and Discussion

2.3.1: Condensation Chemistry for the Synthesis of Quinone Diimine Complexes

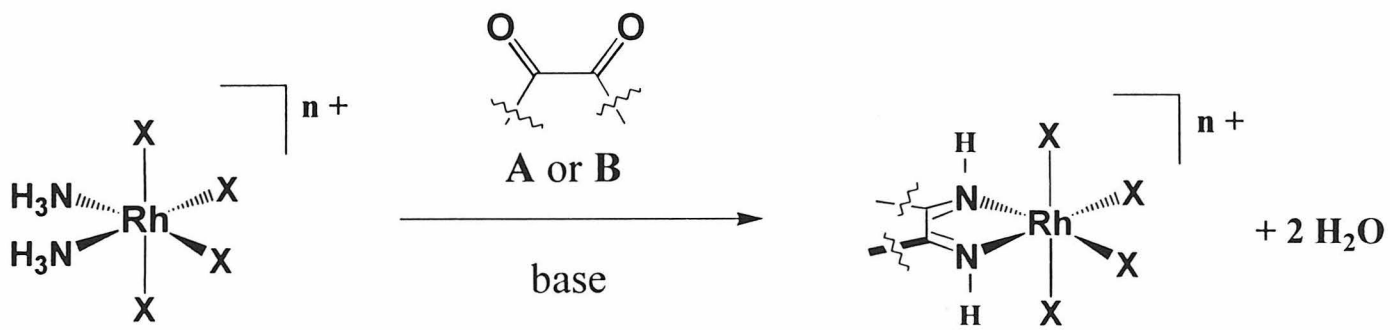
The general synthetic approach for the preparation of quinone diimine ligands by the condensation of aromatic quinones with coordinated ammines is schematized in Figure 2.9. This general scheme and reaction provides a very versatile method for preparing quinone dimmine complexes of varied structure including a straightforward route to tris-heteroleptic compounds of rhodium(III).

2.3.1.1: Addition of One Aromatic Quinone to $Rh(L)_2(NH_3)_2$

Mono(quinone diimine) complexes can be readily synthesized starting from *cis*-diammine rhodium(III) starting materials. A wide variety of such diammine compounds have been prepared in the literature[35] providing starting points for many novel diimine complexes using this synthetic methodology. In this work, both

Figure 2.9. General Synthetic Scheme for the Preparation of Rhodium Complexes Containing Quinone Diimine Ligands by the Condensation of Aromatic Quinones with Coordinated Ammines. The two quinone starting materials applied to the syntheses in this work are shown. It should be noted, however, that these synthetic methods are not limited to these materials and could provide versatile synthetic routes to coordinated diimines from any quinone or diketone starting material.

Figure 2.9:





A **B**

$[Rh(phen)_2(NH_3)_2]^{3+}$ and $[Rh(bpy)_2(NH_3)_2]^{3+}$ were reacted at ambient temperatures under atmospheric conditions with both 9,10-phenanthrenequinone and 5,6-chrysenequinone, two readily available aromatic quinones. These reactions, which proceed in moderate concentrations of base (0.1 M NaOH) in acetonitrile/water mixtures, provide a much milder synthetic alternative to traditional syntheses of phenanthrenequinone diimine intercalators. Because of the mild conditions, the conversions proceed very cleanly as is shown in the HPLC traces of the course of one reaction shown in Figure 2.10. The two starting materials are converted to *only* the desired product; as a result, the yields reported above for this class of reactions are reduced only by mechanical losses during work-up and isolation. The clean progress of the reaction also allows monitoring of its progress visually (shown in Figure 2.11) as the formation of the diimine chromophore causes a significant shift in the color of the reaction mixture.

These reaction conditions have proven to be far superior to previously reported syntheses of quinone diimine intercalators of rhodium(III). Typically complete after a few hours of stirring at ambient temperature, the reactions are simply neutralized and readily purified from the small residual starting materials by cation exchange chromatography. This purification has the added advantage of also providing a product with homogeneous, known counter-ions for subsequent experiments. These facile isolation and purification steps, which result from the high yield and clean progress of the reaction, are a stark contrast to previously described methods of rhodium complex synthesis. Such procedures require isolation of much smaller amounts of the desired complexes from a large number of similar by-products. In addition to these significant advantages, the condensation method of quinone diimine synthesis has been shown by Dr. Hansreudi Mürner to proceed with retention of configuration at the metal center.[36] It was demonstrated that enantiomerically pure

Figure 2.10. Reverse Phase HPLC Traces Showing the Clean Conversion of $[Rh(phen)_2(NH_3)_2]^{3+}$ ($t_{ret} \approx 8$ min) and 9,10-Phenanthrenequinone ($t_{ret} \approx 26$ min) to $[Rh(phen)_2(phi)]^{3+}$ ($t_{ret} \approx 14$ min) as a Function of the Time of Reaction in Acetonitrile/Water, 3:1, 0.1 M in NaOH at Ambient Temperature.

Figure 2.10:

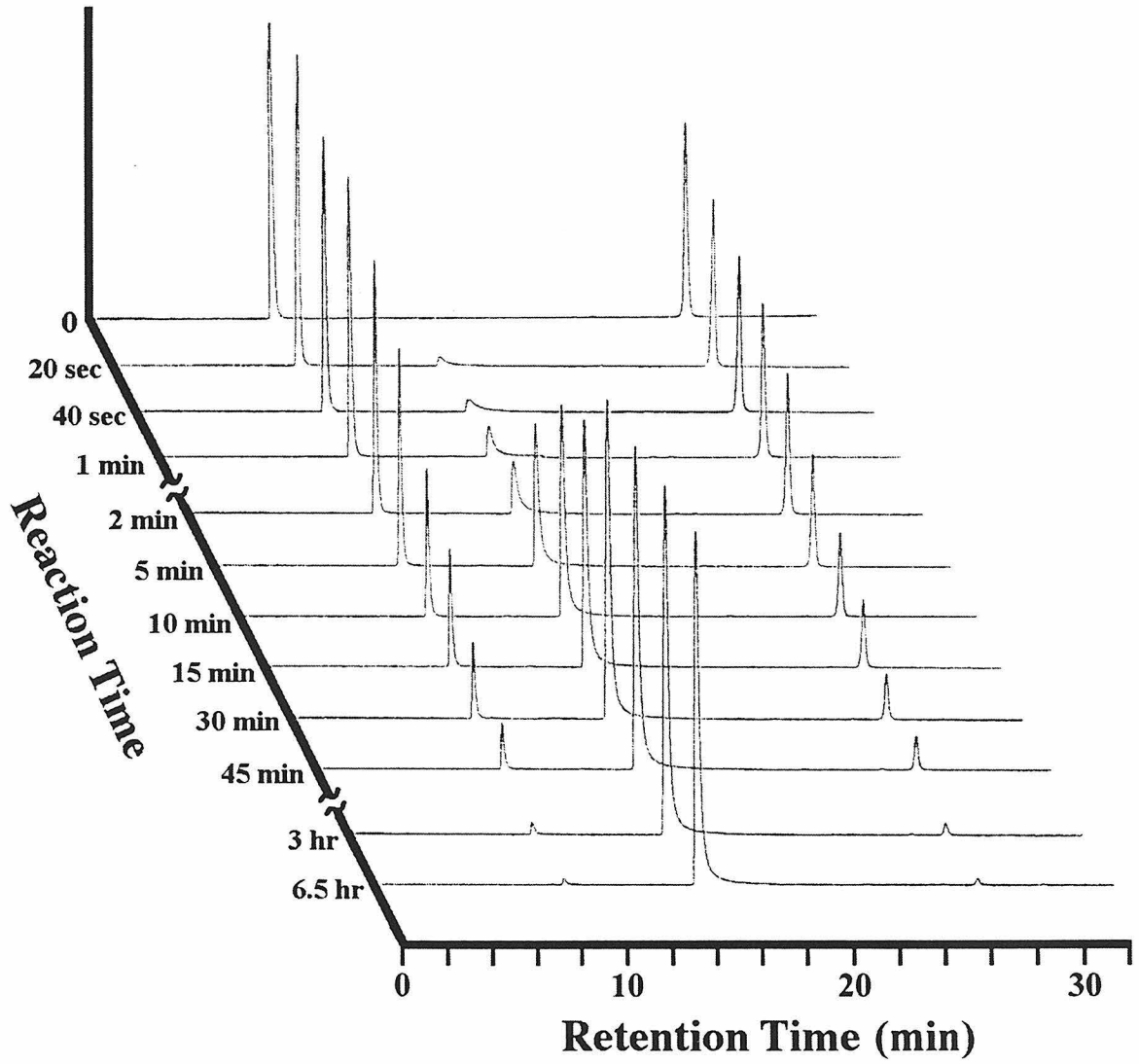
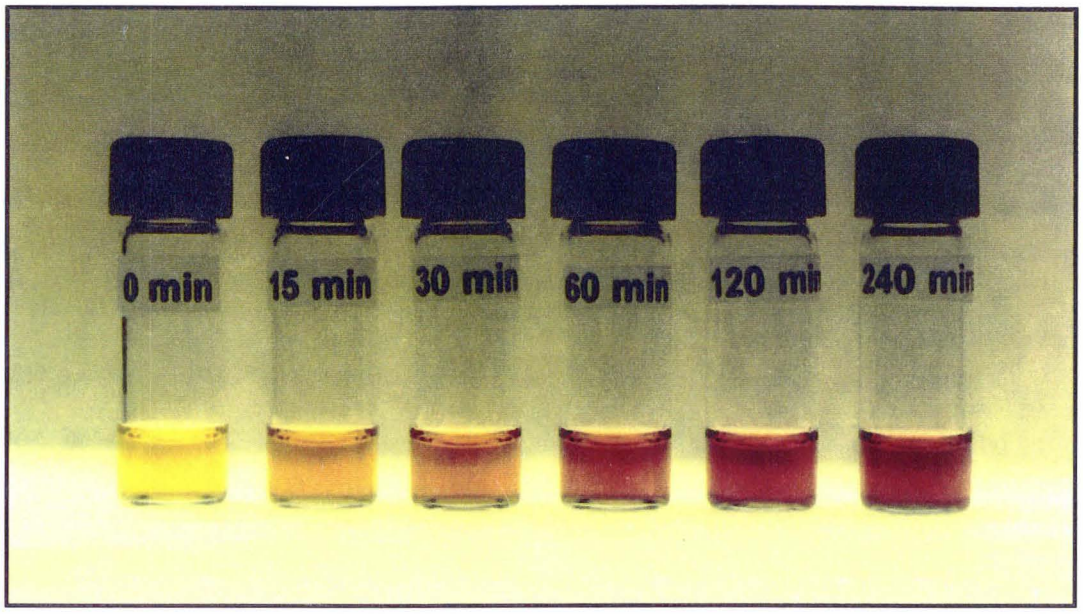

0
20 sec
40 sec
1 min
2 min
5 min
10 min
15 min
30 min
45 min
3 hr
6.5 hr
Reaction Time
0
10
20
30
Retention Time (min)

Figure 2.11. Acidified Aliquots of the Reaction Between $[Rh(bpy)_2(NH_3)_2]^{3+}$ and 5,6-Chrysenequinone Showing the Formation of the Dark Brown $[Rh(bpy)_2(chrysi)]^{3+}$ from the Yellow-Orange Starting Materials as a Function of the Time of Reaction in Acetonitrile/Water, 3:1, 0.1 M in NaOH at Ambient Temperature.

Figure 2.11:



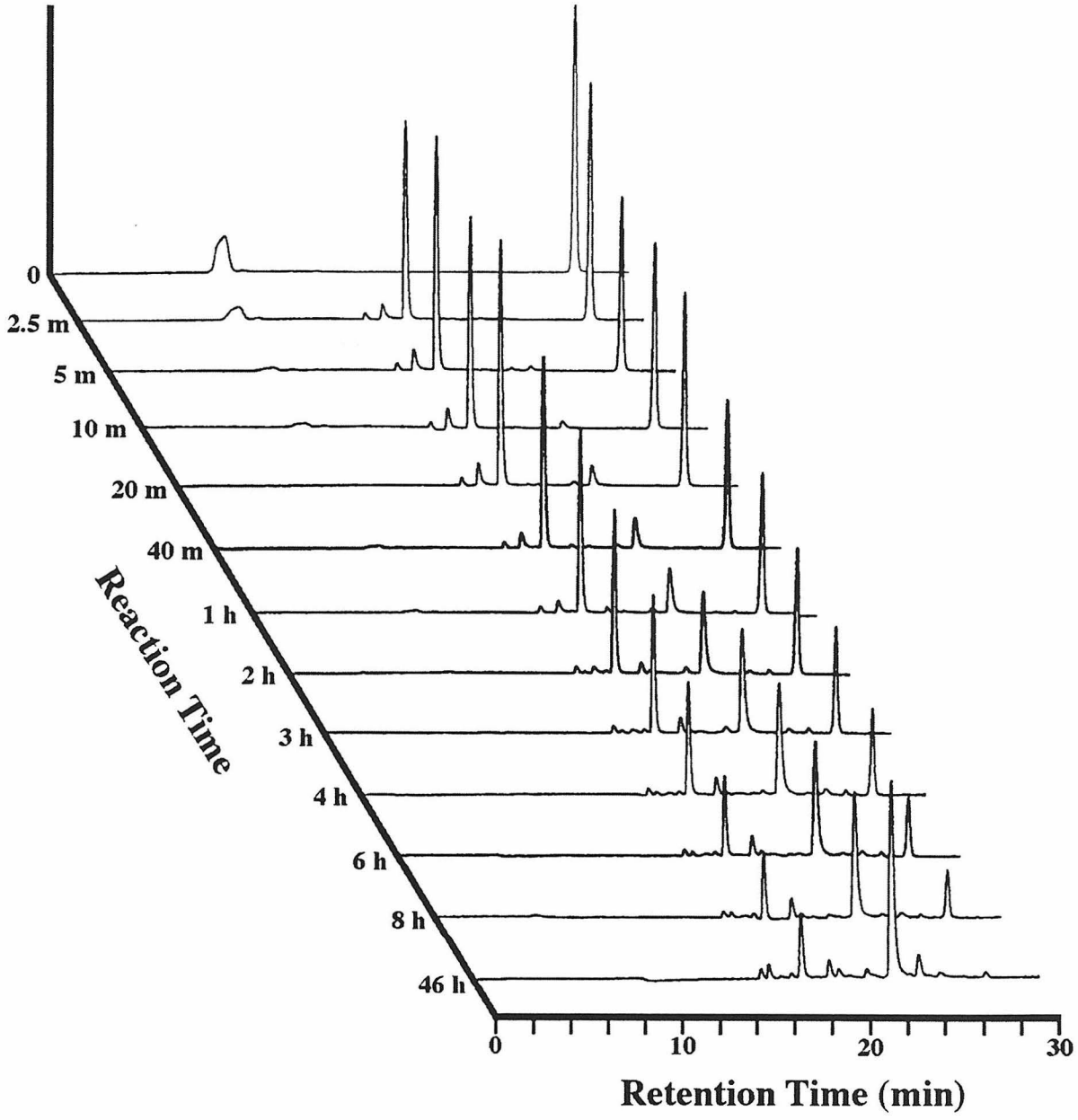
$[Rh(phen)_2(NH_3)_2]^{3+}$, when reacted with 9,10-phenathrenequinone under condensation conditions, produces enantiomerically pure $[Rh(phen)_2(phi)]^{3+}$. In fact, the $\Delta\varepsilon$ values measured for the complex prepared by this method were slightly higher than those previously reported for chromatographically separated material. This result indicates that enantiomerically pure *cis*-diammine complexes are another example of chiral building blocks for the stereo-selective synthesis of transition metal complexes. This has particular relevance for the DNA binding chemistry of these compounds as it has long been established that the complementarily of metal complex chirality with the right handed DNA helix is important for molecular recognition applications.

2.3.1.2: Addition of Two Aromatic Quinones to $Rh(L)(NH_3)_4$

When the condensation reaction is begun with $[Rh(L)(NH_3)_4]^{3+}$, more than one quinone diimine ligand can be introduced. HPLC traces of one example of such a reaction, between $[Rh(phen)(NH_3)_4]^{3+}$ and 9,10-phenanthrenequinone, are included as Figure 2.12. The data shown in Figure 2.12 also demonstrate that the condensation of two equivalents of quinone is more complex that the single condensation described above. The addition of the first phi ligand is very fast and is completed in a few minutes. The condensation of the second equivalent of quinone, however, is much slower and requires many hours to reach completion. This difference in kinetic behavior shows that there is an anti-cooperative effect of the first phi ligand, possibly due to the immediate deprotonation of the phi in the strongly basic reaction conditions; this deprotonation would result in a reduced overall charge of the complex, presumably making it more difficult to deprotonate the remaining ammine ligands. As a result of the much longer required reaction time, this double condensation is not as clean as the cases discussed above. As shown in Figure 2.12,

Figure 2.12. Reverse Phase HPLC Traces Showing the Reaction of $[Rh(phen)(NH_3)_4]^{3+}$ (broad peak at $t_{ret} \approx 8$ min) and 9,10-Phenanthrenequinone ($t_{ret} \approx 26$ min) as a Function of the Time of Reaction in Acetonitrile/Water, 3:1, 0.1 M in NaOH at Ambient Temperature. Formation of both $[Rh(phen)(phi)(NH_3)_2]^{3+}$ ($t_{ret} \approx 17$-18 min) and subsequent conversion to $[Rh(phi)_2(phen)]^{3+}$ ($t_{ret} \approx 22$ min) is observed. Residual mono-phi complex remains in this reaction because less than stoichiometric quantities of quinone were added. Note that, although the desired phi products are by far the primary products of the reaction, this reaction is not as clean as the mono-phi case included in Figure 2.10.

Figure 2.12:


0
2.5 m
5 m
10 m
20 m
40 m
1 h
2 h
3 h
4 h
6 h
8 h
46 h
Reaction Time
0
10
20
30
Retention Time (min)

a number of small side products appear over the course of the reaction incubation. Some of these side products are likely the result of base induced breakdown of the various starting materials; over time, rhodium ammine ligands are known to dissociate[43] and 9,10-phenanthrenequinone is known to decompose to 9-hydroxy-9-carboxy-fluorene.[44] In spite of these small deviations, these methods allow synthesis of bis(quinone diimine) compounds in high yield with purification and isolation procedures only minimally more involved than those described above for the mono(quinone diimine) complexes.

Although the strong anti-cooperative effect of addition of a single quinone diimine ligand to $[Rh(phen)(NH_3)_4]^{3+}$ made the reaction proceed more slowly and slightly less cleanly than the previously described single step condensation chemistry, the strong kinetic separation of the two reaction steps makes this protocol useful for additional synthetic applications. Because the first ligand condensation is essentially complete before any material has proceeded through the second reaction, one might envision stopping the reaction at that step and isolating the [Rh(phen)(quinone diimine L)$(NH_3)_2]^{3+}$ as a synthon for the preparation of other complexes. Unfortunately, attempts to isolate this diammine complex and react it further with an additional equivalent of quinone failed. This is likely a result of the lability of the coordinated ammine ligands one or more of which could have been lost during the work-up; this substitution would eliminate the required *cis*-diammine functionality required for successful quinone condensation. This conclusion was supported by mass spectrometry data consistent with the presence of $[Rh(phen)(phi)(H_2O)(NH_3)]^{3+}$ in the isolated material (data not shown). If no attempt is made to isolate the synthetic intermediate and the second quinone is added *in situ* after sufficient time for completion of the first condensation reaction, tris-heteroleptic complexes containing two different quinone diimine ligands are accessible. In the example described

above, although some non-desired bis(phi) or bis(chrysi) complexes were produced, the great majority of the product was the three-ligand complex of interest. As a result, in addition to providing high yielding routes to both mono and bis(quinone diimine) compounds, these synthetic methods also provide a novel procedure for making tris-heteroleptic complexes of rhodium(III).

2.2.2.3: Use of Condensation Chemistry as an Intermediate Synthetic Step

Although lability of the remaining ammine ligands on [Rh(phen)(quinone diimine L)$(NH_3)_2]^{3+}$ made it impossible to isolate the complex as an intermediate for subsequent *condensation* reactions, the tendency for substitution of the remaining monodentate ligands makes this material applicable to alternative synthetic strategies. The resulting synthetic intermediate, labeled [Rh(phen)(quinone diimine L)$(X)_2]^{3+}$ to represent the presence of either ammine or solvent ligands at the remaining coordination sites, can be reacted with additional chelating ligands to produce another family of tris-heteroleptic rhodium compounds. Two products were prepared by this strategy, [Rh(phen)(phi)(bpy')]Cl_3 and [Rh(phen)(chrysi)(bpy')]Cl_3, which represent new members of a family of rhodium compounds that can be tethered to other molecules through the carboxylic acid group of bpy'; the chrysi compound has already been applied to the construction of rhodium-peptide conjugates for site-specific binding and hydrolysis of DNA.[45]

2.2.2.4: Broader Issues: Ammine Condensation-Based Synthesis of Rhodium(III) Complexes

Although ammine condensation strategies provide versatile preparation methods for a wide variety of compounds, these syntheses are not without complications which must be considered before applying them to the construction of novel compounds.

As a result, it is relevant to consider a somewhat broader view of these reaction schemes in the interests of later workers who might apply them to alternate research goals. Although the condensation reaction lacks the obvious harshness of the extended, high temperature reflux steps used in the traditional synthesis of quinone diimine complexes, the condensation reaction itself and many of the preceding syntheses may pose problems for certain functionalized ligands. It was observed, for example, that the condensation reaction would not proceed when the carboxylate appended bpy' ligand was present on the rhodium ammine complex. Although no definitive cause for this failure was ever determined, it is likely that the pendant carboxylate either sterically interferes with the reaction or, by deprotonating in the basic reaction conditions, reduces the overall pK of the coordinated ammines enough to prevent condensation. As a result, the bpy' ligand represents an example of a case where even a functionality that is stable to the basic condensation conditions can prevent the reaction from taking place. In addition to the potential of ligands interfering with the condensation reaction itself, many of the other reaction conditions involved in these preparations could be incompatible with other more sensitive functionalities. The preparation of the $[Rh(phen)(NH_3)_4]^{3+}$ complex, for example, requires incubation in triflic acid and a subsequent reflux in ammonium hydroxide. These extremes of concentrated strong acid and base could cause degradation of a desired ligand or loss of protecting groups. Also, the reactions described in this work were not found to be synthetically useful for complexes starting with $[Rh(NH_3)_5Cl]^{2+}$ or $[Rh(NH_3)_6]^{3+}$. These reactions, which were examined by Dr. Hansreudi Mürner, proceeded very slowly and, as a result, did not result in clean formation of the desired multi(quinone diimine) complexes.[36]

These limitations having been acknowledged, however, the strategies described in this chapter also provide alternate routes around many of these synthetic challenges.

The introduction of relatively inert and stable ligands like phenathroline in earlier synthetic steps and reserving sensitive functionalities for later addition provide solutions both to the harsh conditions of the first reactions and possible interference by these ligands during the condensation reaction. The preparation of tris-heteroleptic compounds by quinone condensation followed by addition of bpy' provided a method to incorporate a ligand that otherwise disrupted the reaction's progress. Alternatively, the preparation of alternate ligands whose functionalities can be protected also provides a route around these types of roadblocks. The ligand bpy'', an amine functionalized bipyridine whose protected form was observed to be compatible with the condensation conditions, is an example of this later strategy.[46] One could envision further adaptations of this approach where ligands which were compatible with the condensation chemistry could be subsequently modified to append interesting groups after metal complex synthesis was complete. As a result, the ability to vary both the sequence of synthetic steps and the identity of alternate ligands provide routes for the preparation of many novel rhodium complexes using this synthetic methodology. It should be emphasized that the compounds described here represent only a few examples of the large family of possible complexes; this work, rather than being a comprehensive examination, is only the initial proof of what could be a very useful set of concepts and approaches.

2.3.2: Properties of Chrysenequinone Diimine Complexes of Rhodium(III): A New Family of DNA Intercalating Metal Complexes

2.3.2.1: Spectroscopic Properties of Chrysenequinone Diimine Complexes

As expected, the electronic spectra of Rh(III) chrysi complexes are broadly similar in structure to their analogous phi compounds. Like phi complexes, the spectra of chrysi complexes can be generally approximated as combinations of the spectra of

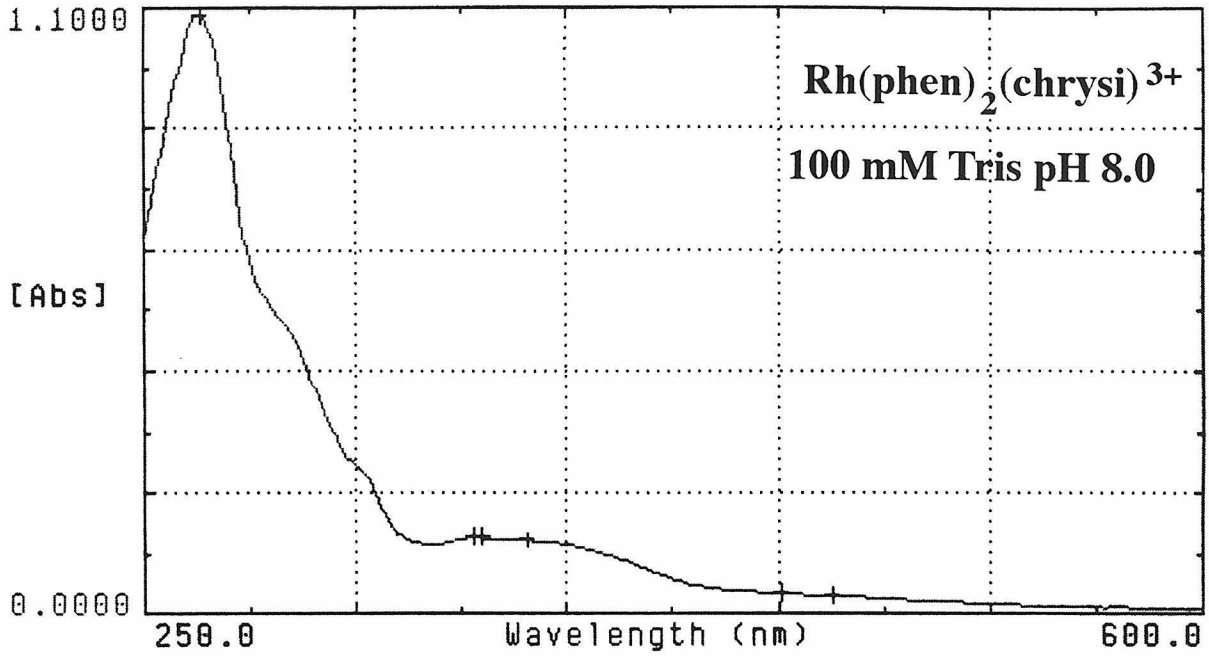
their component ligands. As a result, the spectrum can be broadly characterized as consisting of contributions from the phen or bpy ancillary ligands in the ultraviolet region and visible transitions associated with the diimine intercalator. Furthermore, the differences in the electronic spectra for phen and bpy compounds in the UV can be explained by the different transitions of the ligands themselves in this region.[47] Given the significant differences between the phi and chrysi ligands, including the lack of symmetry the latter, it is not surprising that significant differences exist in the absorption characteristics in the visible – diimine region – of the spectra. Examples of these differences, for the $[Rh(phen)_2(phi)]^{3+}$/ $[Rh(phen)_2(chrysi)]^{3+}$ and $[Rh(phi)_2(phen)]^{3+}$/$[Rh(chrysi)_2(phen)]^{3+}$ pairs, are included as Figures 2.13A and B respectively. In both cases the peaks in the chrysi spectra are broader and extend to longer wavelength than those in the corresponding phi complexes. For comparison, spectra of free chrysenequinone and chrysenediamine are included as Figure 2.14. The differences in the absorbance characteristics of the metal complexes diverge further at acidic pH as shown in Figure 2.15 and discussed more comprehensively in succeeding sections.

2.3.2.2: pK_a Measurement by Spectroscopic Titration

To further characterize the complexes containing the chrysenequinone diimine intercalating ligand, the acidity constants of the complexes were determined by a spectroscopic titration. It has been previously demonstrated that the visible absorbance changes which occur as the pH of a rhodium complex solution is titrated can be used for the determination of the pK values of the compounds.[47] When the pH of a solution of a rhodium(phi) complex is increased from 2 to 10, the visible transition associated with the phi ligand undergoes a smooth blue shift with little change in structure. This behavior can be observed in Figures 2.16, 2.17,

Figure 2.13. (A) Comparison of the Absorption Spectra of $[Rh(phen)_2(chrysi)]^{3+}$ and $[Rh(phen)_2(phi)]^{3+}$ in 100 mM Tris pH 8.0. (B) Comparison of the Absorption Spectra of $[Rh(chrysi)_2(phen)]^{3+}$ and $[Rh(phi)_2(phen)]^{3+}$ in 100 mM Tris pH 8.0. In both cases, note the broader envelope of visible absorbance for the chrysi complex.

Figure 2.13A:


1.1000
[Abs]
0.0000
250.0
Wavelength (nm)
600.0
Rh(phen)2(chrysi)3+
100 mM Tris pH 8.0

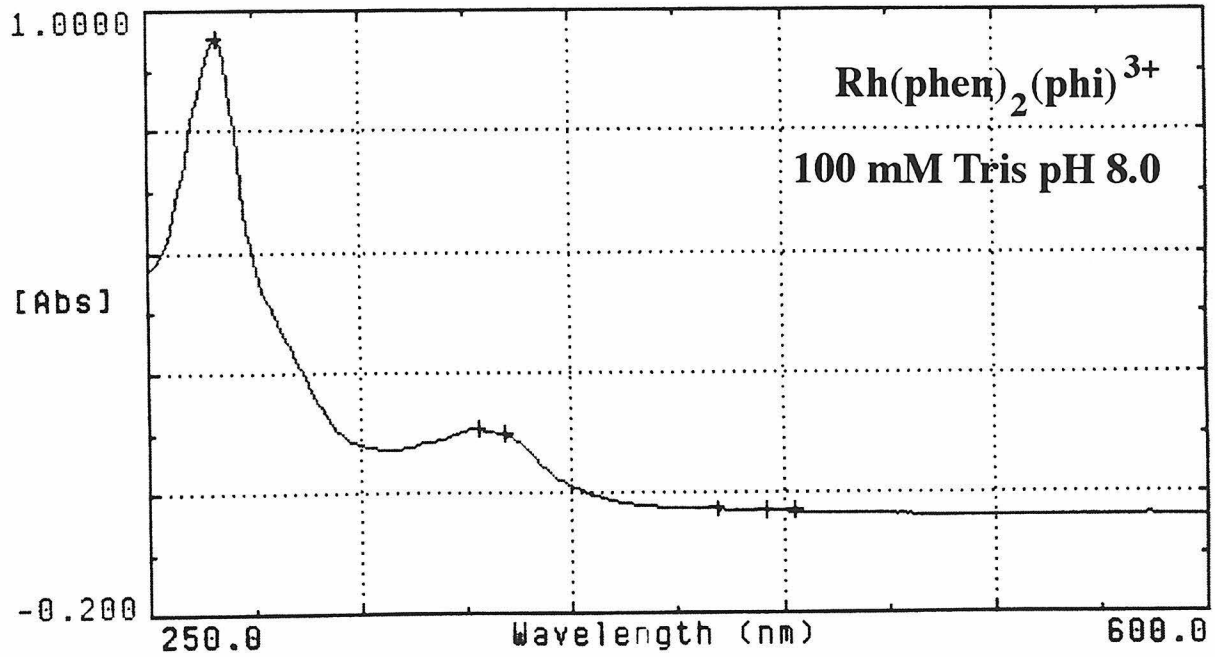
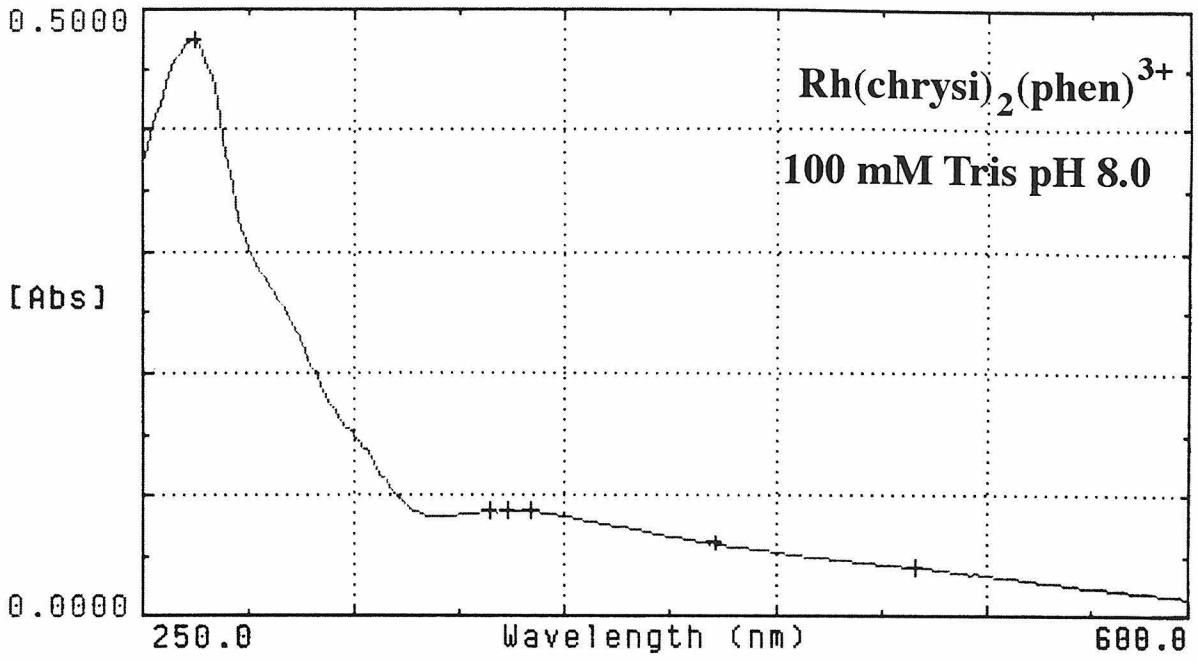

1.0000
[Abs]
-0.200
250.0
Wavelength (nm)
600.0
Rh(phen)2(phi)3+
100 mM Tris pH 8.0

Figure 2.13B:


0.5000
[Abs]
0.0000
250.0
Wavelength (nm)
600.0
Rh(chrysi)$_2$(phen)$^{3+}$
100 mM Tris pH 8.0

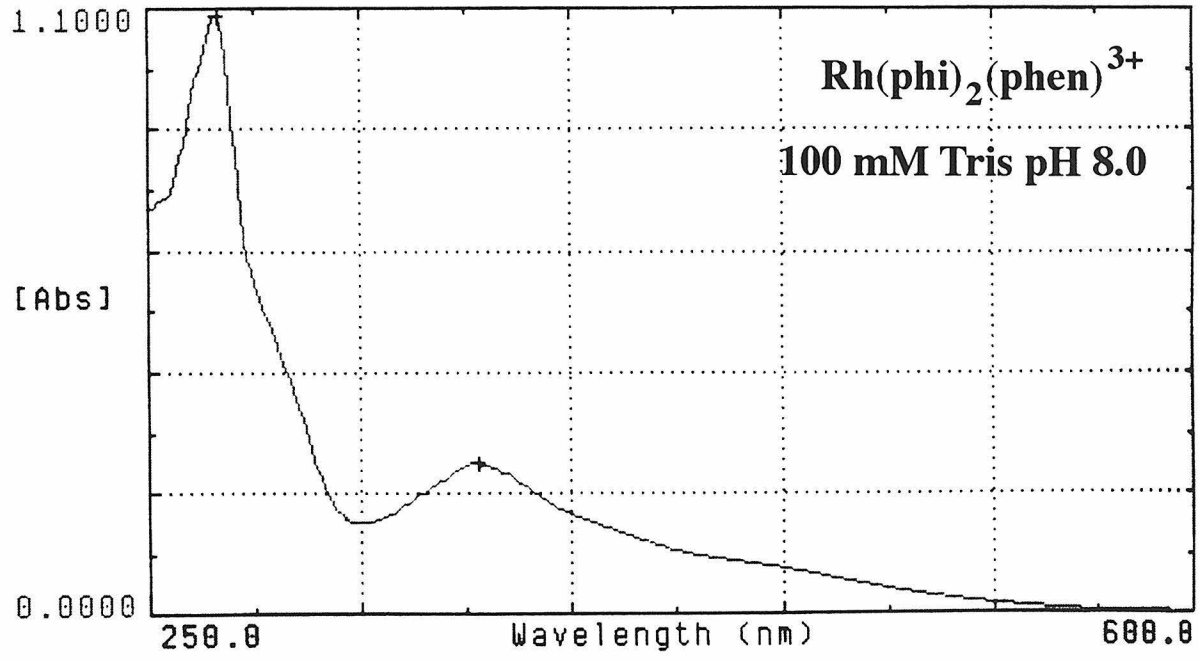
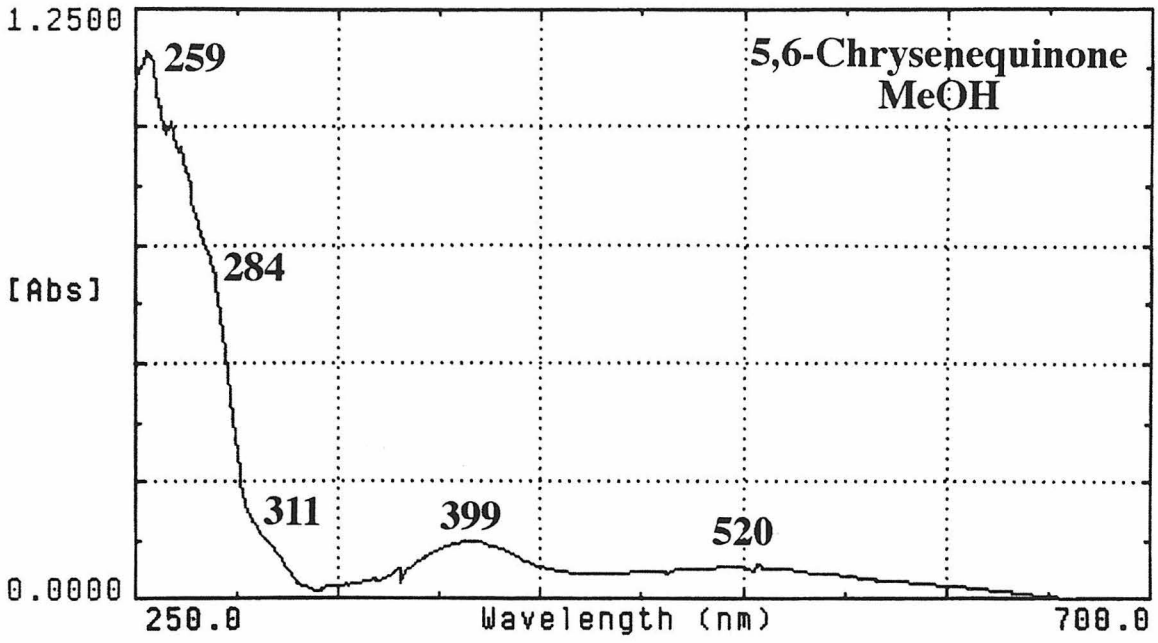

1.1000
[Abs]
0.0000
250.0
Wavelength (nm)
600.0
Rh(phi)$_2$(phen)$^{3+}$
100 mM Tris pH 8.0

Figure 2.14. Absorption Spectra of 5,6-Chrysenequinone and 5,6-Chrysenediammine in MeOH. Although neither of these molecules is an exact analogue for the coordinated chrysenediimine ligand, note the significant differences in spectral structure between them. These characteristics can be compared to the spectra of the metal complexes included in the previous figure.

Figure 2.14:


1.2500
0.0000
[Abs]
259
284
311
399
520
5,6-Chrysenequinone
MeOH
250.0
Wavelength (nm)
700.0

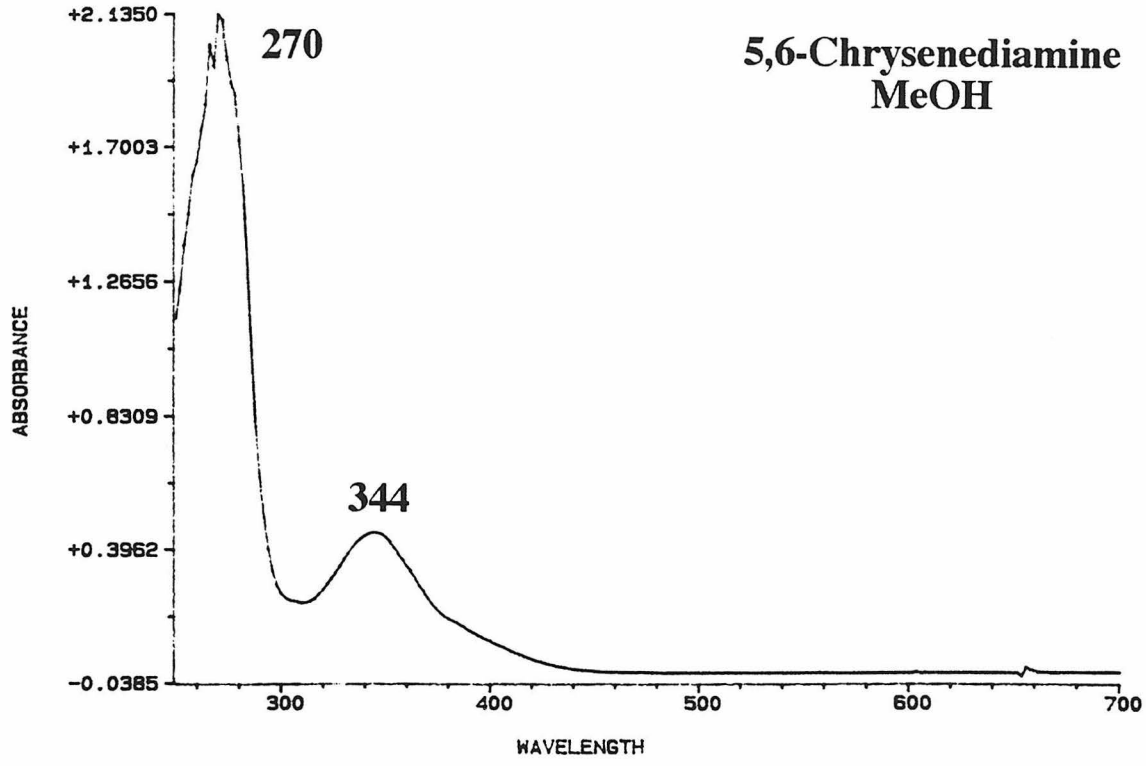

+2.1350
+1.7003
+1.2656
+0.8309
+0.3962
-0.0385
ABSORBANCE
270
344
5,6-Chrysenediamine
MeOH
300
400
500
600
700
WAVELENGTH

Figure 2.15. Comparison of the Absorption Spectra of $[Rh(bpy)_2(phi)]^{3+}$ and $[Rh(bpy)_2(chrysi)]^{3+}$ at both pH 2.5 and pH 9.3. Although the visible absorbance envelope is broader for the chrysi complex even at basic pH, note that the spectral characteristics diverge further when the pH is decreased to 2.5.

Figure 2.15:

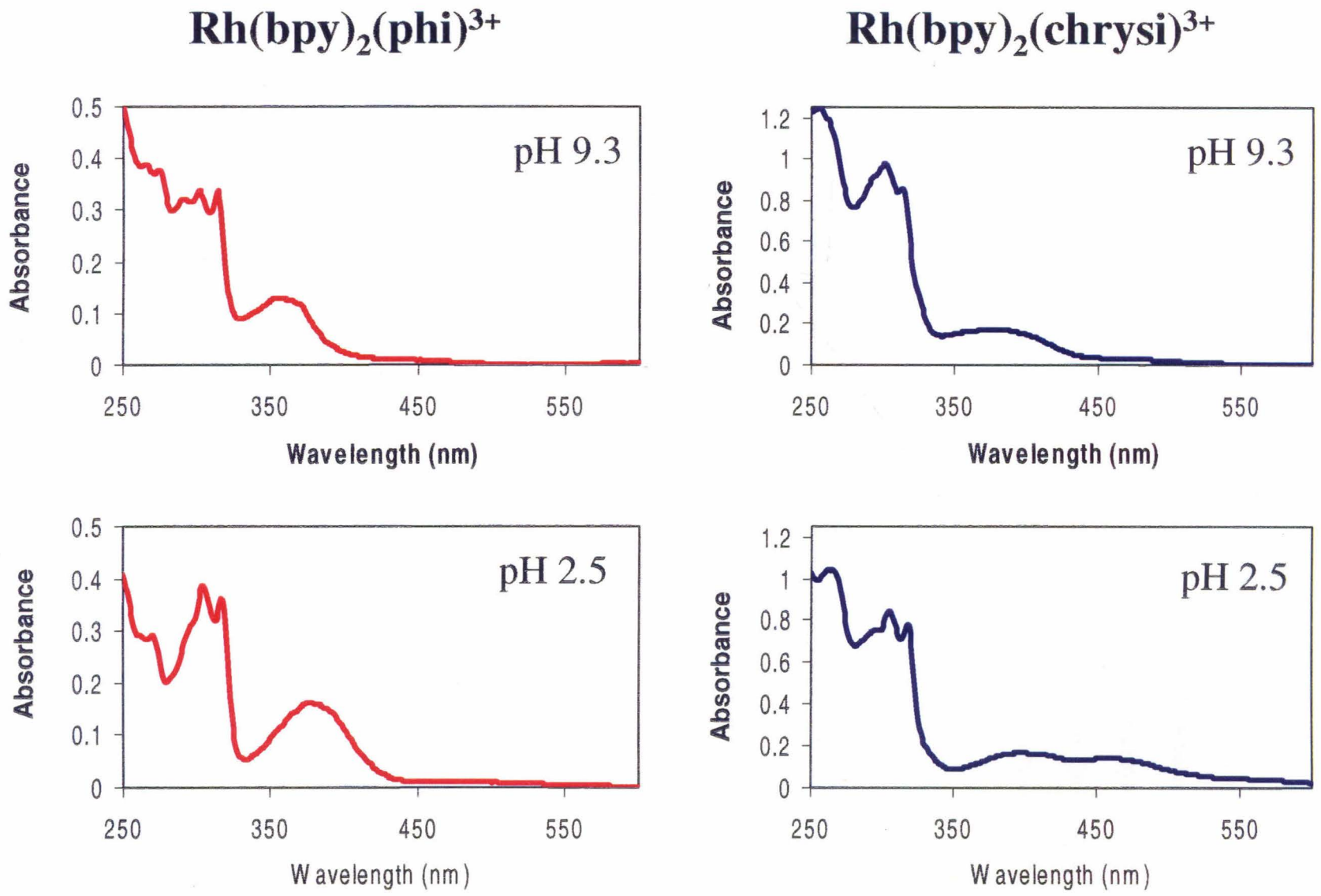

Rh(bpy)2(phi)3+
Rh(bpy)2(chrysi)3+
pH 9.3
pH 2.5
Absorbance
Wavelength (nm)
0.5
0.4
0.3
0.2
0.1
0
1.2
1
0.8
0.6
250
350
450
550

Table 2.2: pKa Values for Phi and Chrysi Complexes of Rh(III) Determined by Spectrophotometric Titration	
$[Rh(phen)_2(phi)]^{3+}$	6.0
$[Rh(phen)_2(chrysi)]^{3+}$	4.9
$[Rh(bpy)_2(phi)]^{3+}$	5.8
$[Rh(bpy)_2(chrysi)]^{3+}$	5.2
$[Rh(phi)_2(phen)]^{3+}$	6.7
$[Rh(chrysi)_2(phen)]^{3+}$	5.5
Error: (estimated by comparison of repeated trials)	(+/- 0.2)

and 2.18 where the absorbance of phi centered transitions shift between 20 and 50 nm. In the chrysi complexes, however, the spectral changes that result from alterations in the pH are much more dramatic. Instead of the smooth shifting behavior, the spectra of the chrysi complexes completely change structure as the pH is decreased. At basic pH, as emphasized in Figure 2.15, the spectral structure of phi complexes and chrysi complexes is relatively similar. At acidic pH, however, they are quite different. As pH is decreased from 10 to 2, the visible absorbance not only dramatically red shifts, but splits into at least two distinct spectral bands. This is most obvious in the $[Rh(bpy)_2(chrysi)]Cl_3$ titration (Figure 2.20) although it can be seen in the phen (Figure 2.19) and bis(chrysi) (Figure 2.21) complexes as well.

When the absorbance at a single wavelength from each point in the spectral titration is plotted as a function of pH, a titration curve can be constructed and the pK value of each metal complex determined from the inflection point of the curve. These titration curves for each complex are included as Figures 2.22-2.27. The data extracted from them is included as Table 2.2.

In all cases, the pK value measured for the chrysi containing complexes is between 0.6 and 1.2 units below that of the corresponding phi complex. This depression in pK of the chrysi compounds, when combined with the variance in pH dependence of

Figure 2.16. Spectral Changes which Occur Upon Titration of a Solution of $[Rh(phen)_2(phi)]^{3+}$ between pH 2.5 and pH 10.5. Visible absorbance transition shifts to the blue and loses intensity with increasing pH (see arrows).

Figure 2.16:

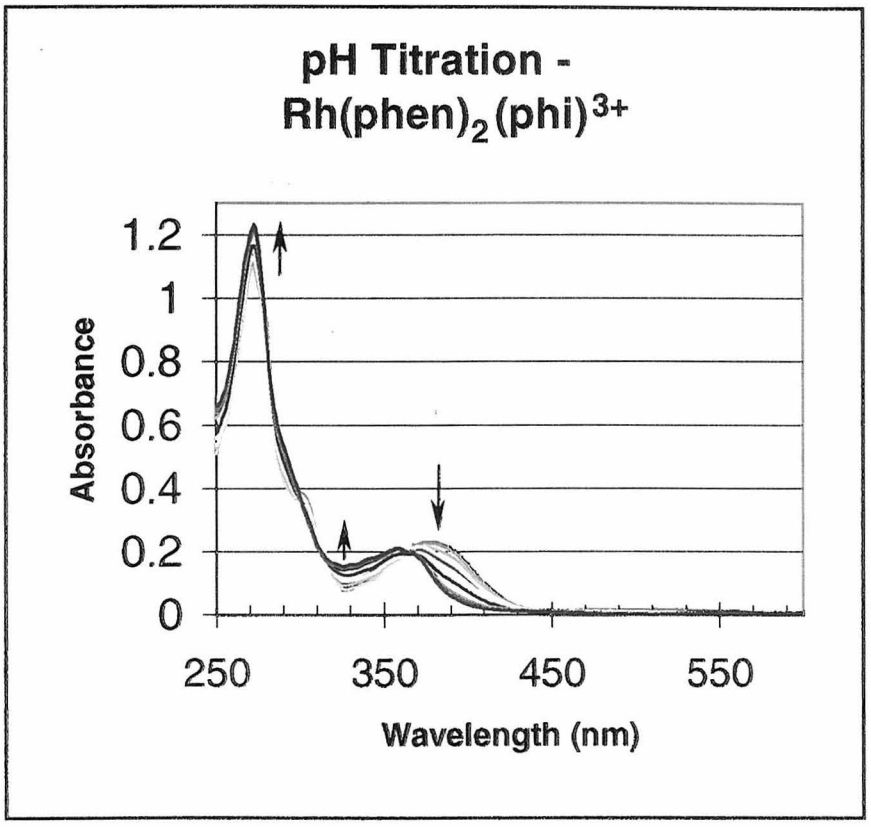

pH Titration -
Rh(phen)2(phi)3+
Absorbance
1.2
1
0.8
0.6
0.4
0.2
0
250
350
450
550
Wavelength (nm)

Figure 2.17. Spectral Changes which Occur Upon Titration of a Solution of $[Rh(bpy)_2(phi)]^{3+}$ between pH 2.5 and pH 10.5. Visible absorbance transition shifts to the blue and loses intensity with increasing pH (see arrows).

Figure 2.17:

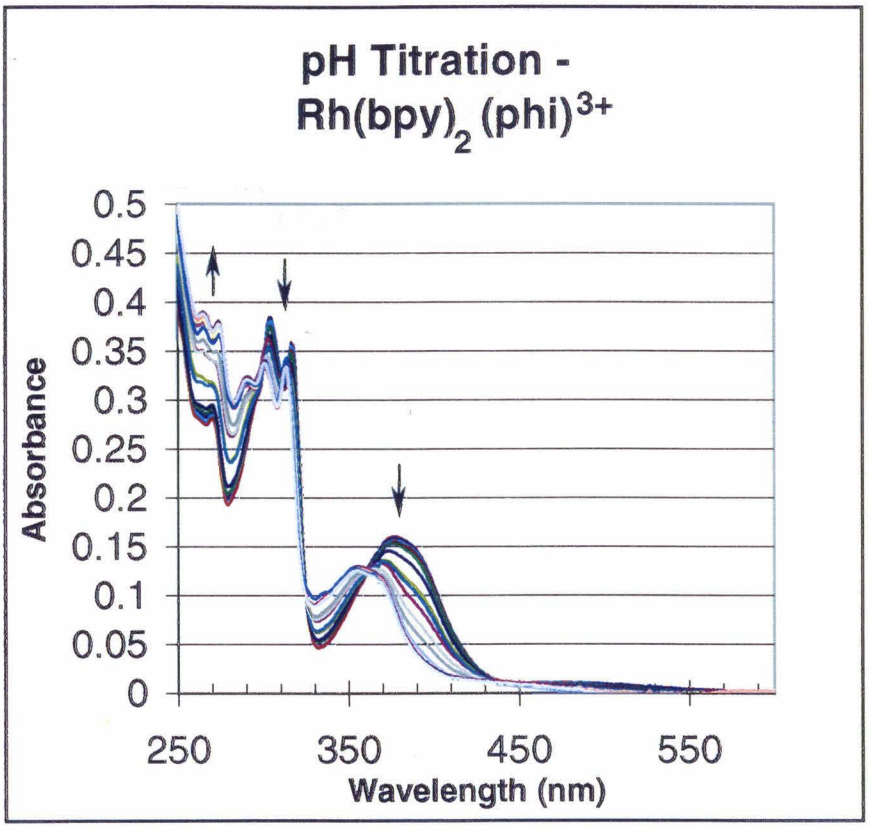

pH Titration -
Rh(bpy)2 (phi)3+
Absorbance
0.5
0.45
0.4
0.35
0.3
0.25
0.2
0.15
0.1
0.05
0
250
350
450
550
Wavelength (nm)

Figure 2.18. Spectral Changes which Occur Upon Titration of a Solution of $[Rh(phi)_2(phen)]^{3+}$ between pH 2.5 and pH 10. Visible absorbance transition shifts to the blue and loses intensity with increasing pH (see arrows).

Figure 2.18:

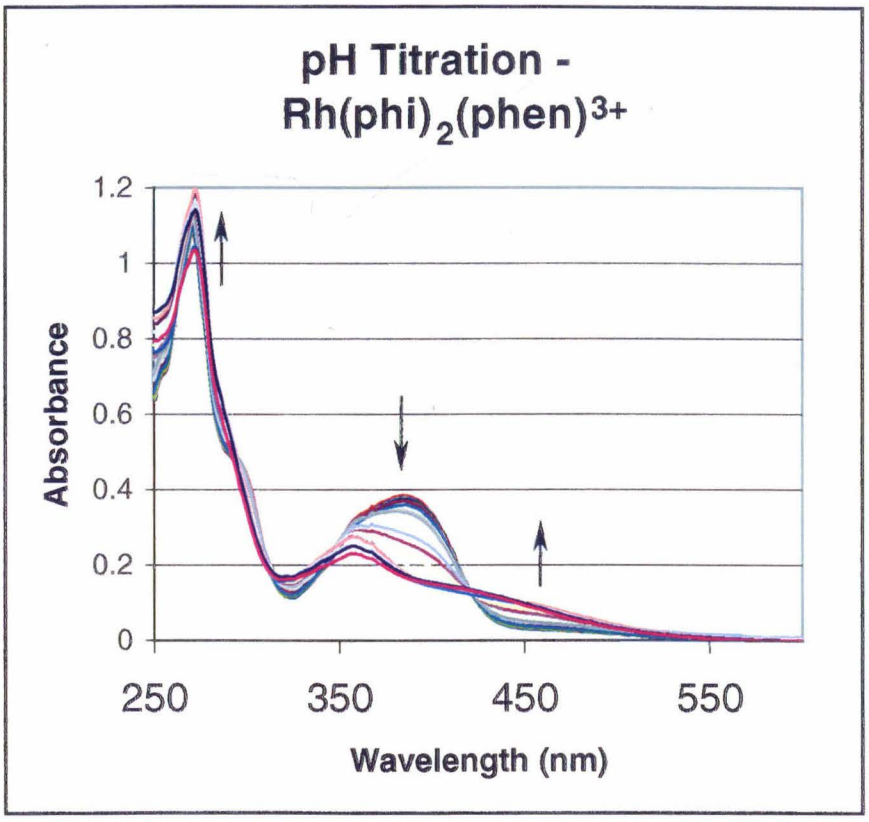

pH Titration -
Rh(phi)2(phen)3+
Absorbance
1.2
1
0.8
0.6
0.4
0.2
0
250
350
450
550
Wavelength (nm)

Figure 2.19. Spectral Changes which Occur Upon Titration of a Solution of $[Rh(phen)_2(chrysi)]^{3+}$ between pH 2.5 and pH 10.5. Visible absorbance bands coalesce and shift to the blue with increasing pH (see arrows).

Figure 2.19:

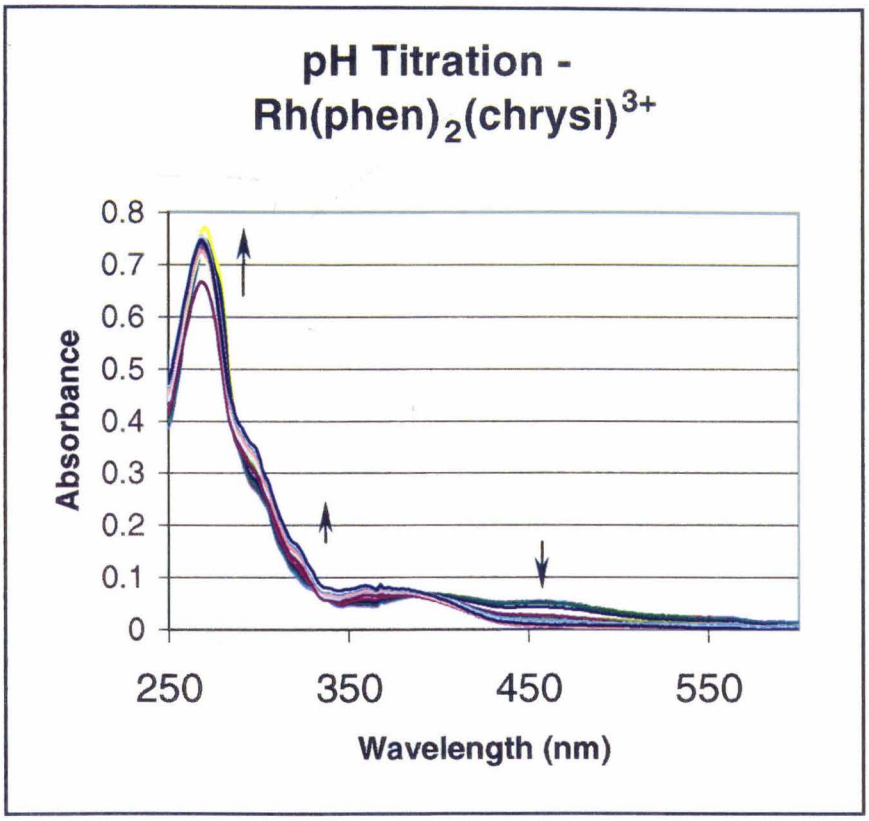

pH Titration -
Rh(phen)2(chrysi)3+
Absorbance
0.8
0.7
0.6
0.5
0.4
0.3
0.2
0.1
0
250
350
450
550
Wavelength (nm)

Figure 2.20. Spectral Changes which Occur Upon Titration of a Solution of $[Rh(bpy)_2(chrysi)]^{3+}$ between pH 2.5 and pH 10.5. Visible absorbance bands coalesce and shift to the blue with increasing pH (see arrows).

Figure 2.20:

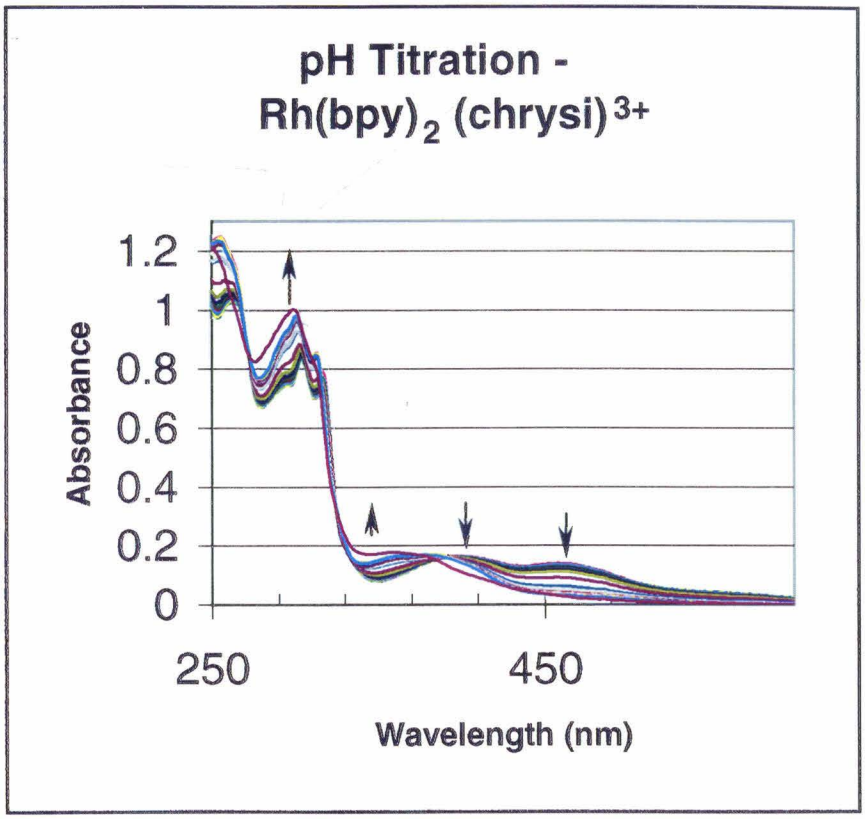

pH Titration -
Rh(bpy)2 (chrysi)3+
Absorbance
1.2
1
0.8
0.6
0.4
0.2
0
250
450
Wavelength (nm)

Figure 2.21. Spectral Changes which Occur Upon Titration of a Solution of $[Rh(chrysi)_2(phen)]^{3+}$ between pH 2.5 and pH 10. Visible absorbance bands coalesce and shift to the blue with increasing pH (see arrows).

Figure 2.21:

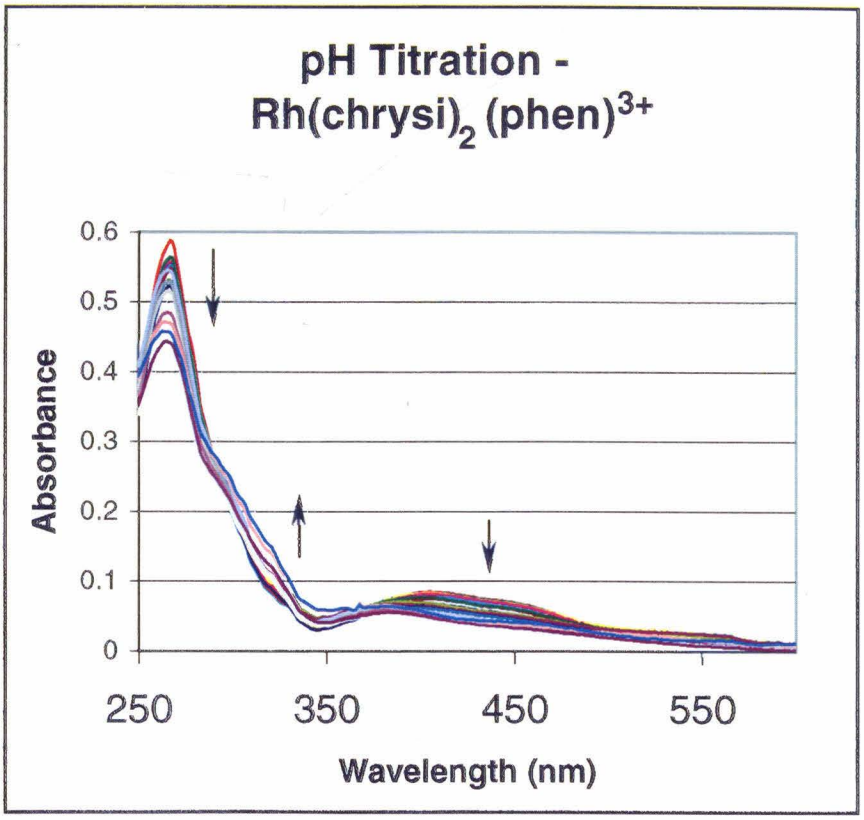

pH Titration -
Rh(chrysi)2 (phen)3+
Absorbance
0.6
0.5
0.4
0.3
0.2
0.1
0
250
350
450
550
Wavelength (nm)

Figure 2.22. Spectrophotometric Titration Curve for $[Rh(phen)_2(phi)]^{3+}$ between pH 2.5 and pH 10.5.

Figure 2.22:

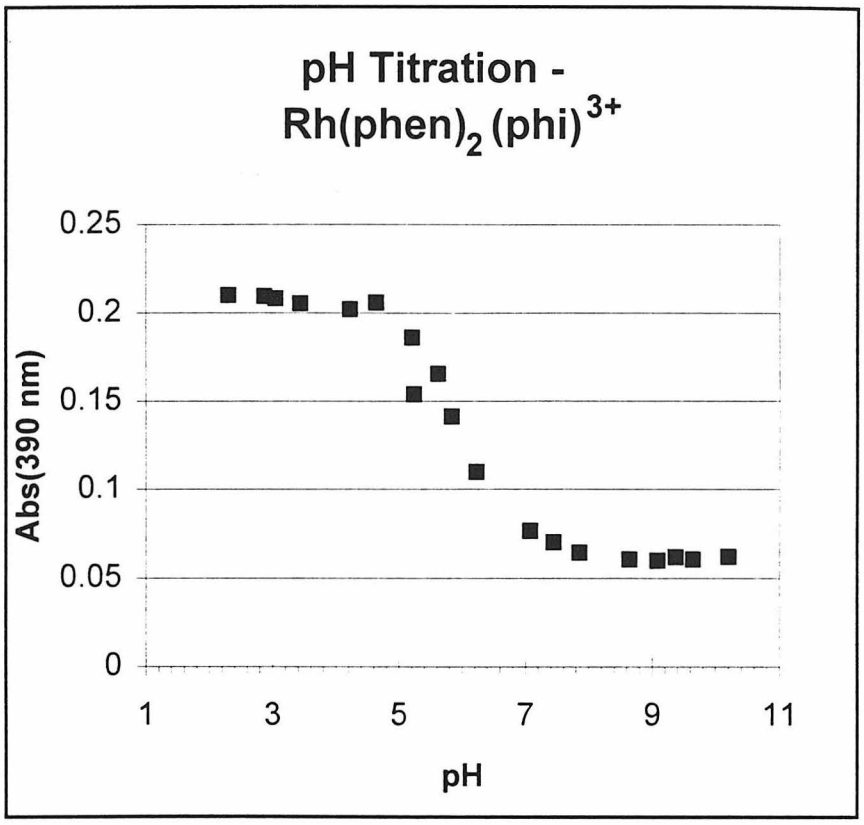

pH Titration -
Rh(phen)2 (phi)3+
Abs(390 nm)
0.25
0.2
0.15
0.1
0.05
0
1
3
5
7
9
11
pH

Figure 2.23. Spectrophotometric Titration Curve for $[Rh(bpy)_2(phi)]^{3+}$ between pH 2.5 and pH 10.5.

Figure 2.23:

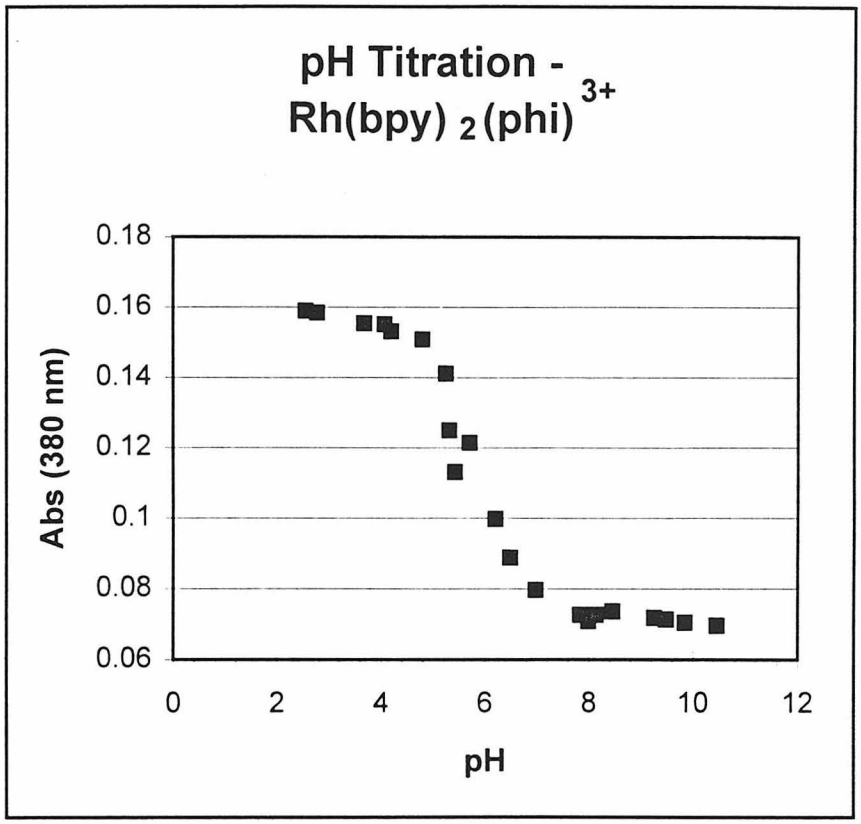

pH Titration -
Rh(bpy) 2 (phi) 3+
Abs (380 nm)
0.18
0.16
0.14
0.12
0.1
0.08
0.06
0
2
4
6
8
10
12
pH

Figure 2.24. Spectrophotometric Titration Curve for $[Rh(phi)_2(phen)]^{3+}$ between pH 2.5 and pH 10.

Figure 2.24:

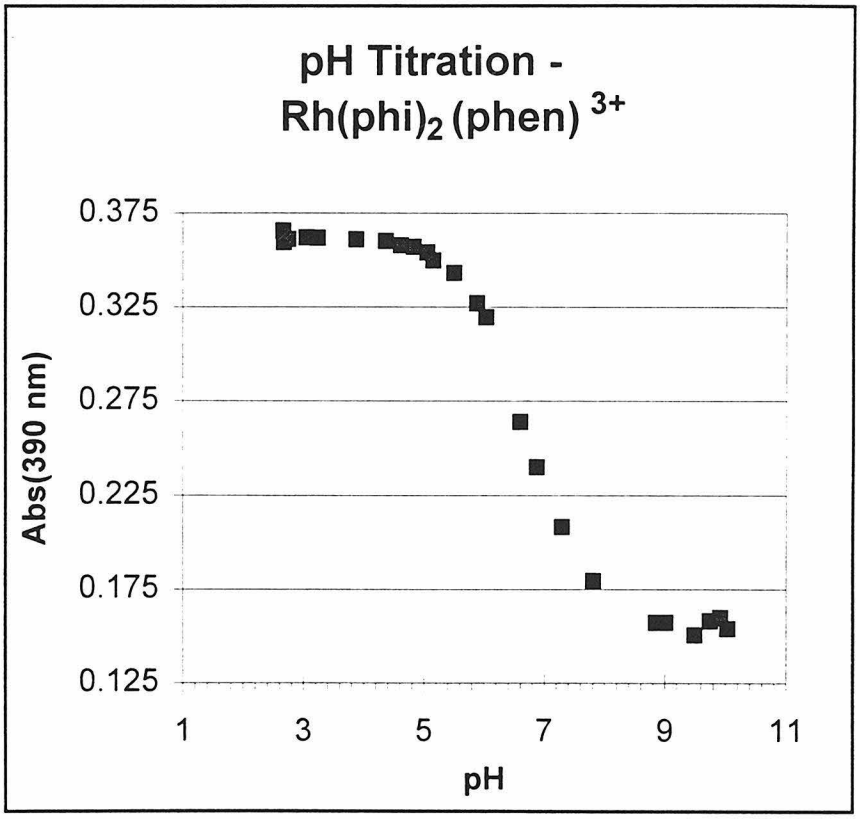

pH Titration -
Rh(phi)2 (phen) 3+
Abs(390 nm)
0.375
0.325
0.275
0.225
0.175
0.125
1
3
5
7
9
11
pH

Figure 2.25. Spectrophotometric Titration Curve for $[Rh(phen)_2(chrysi)]^{3+}$ between pH 2.5 and pH 10.5.

Figure 2.25:

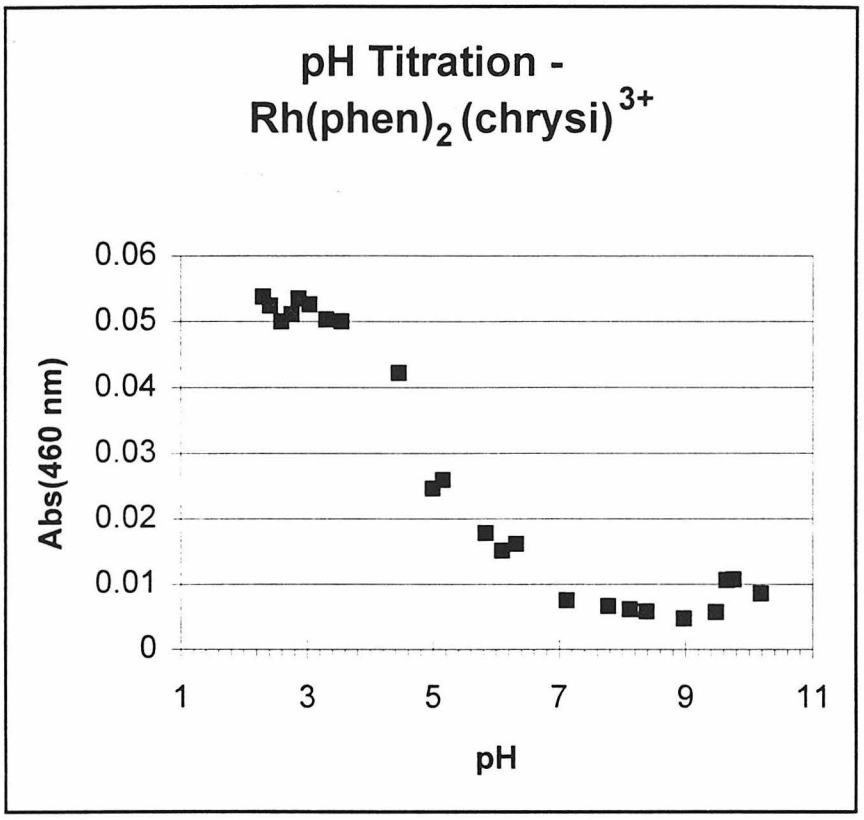

pH Titration -
Rh(phen)2(chrysi)3+
Abs(460 nm)
0.06
0.05
0.04
0.03
0.02
0.01
0
1
3
5
7
9
11
pH

Figure 2.26. Spectrophotometric Titration Curve for $[Rh(bpy)_2(chrysi)]^{3+}$ between pH 2.5 and pH 10.5.

Figure 2.26:

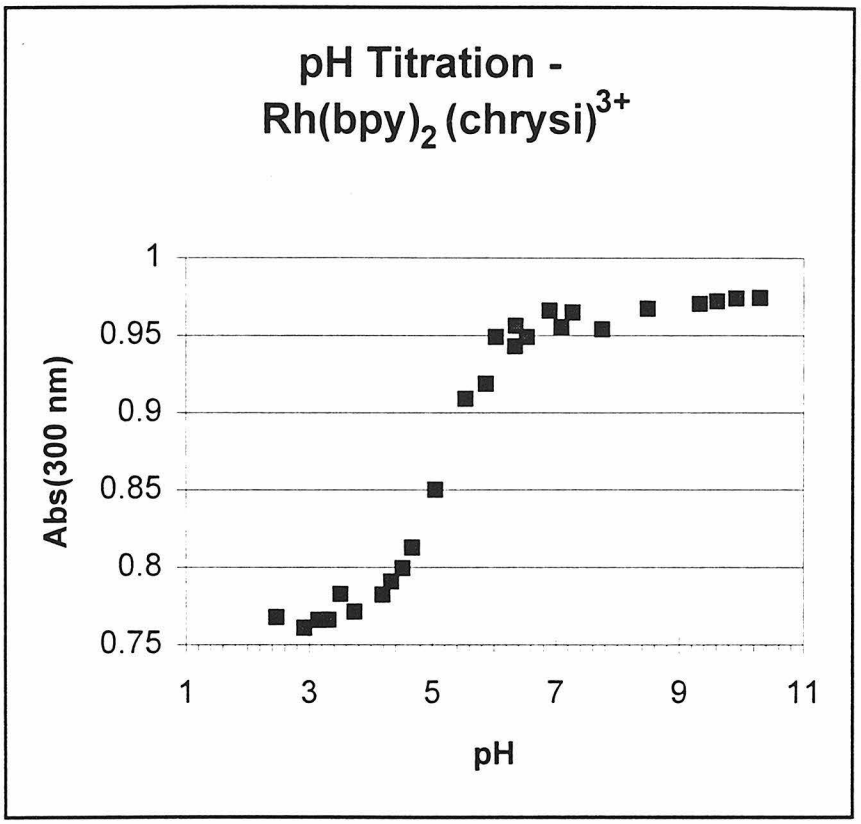
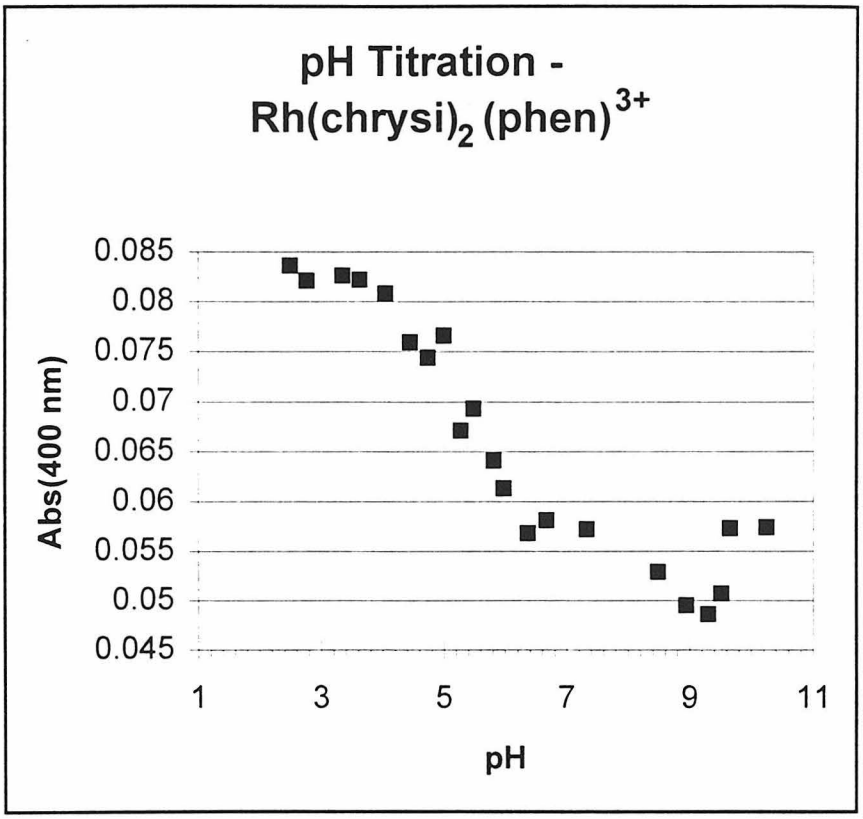

pH Titration -
Rh(bpy)2 (chrysi)3+
Abs(300 nm)
1
0.95
0.9
0.85
0.8
0.75
1
3
5
7
9
11
pH

Figure 2.27. Spectrophotometric Titration Curve for $[Rh(chrysi)_2(phen)]^{3+}$ between pH 2.5 and pH 10.

Figure 2.27:


pH Titration -
Rh(chrysi)2 (phen)3+
Abs(400 nm)
0.085
0.08
0.075
0.07
0.065
0.06
0.055
0.05
0.045
1
3
5
7
9
11
pH

the spectral structures themselves, suggested that significantly different behaviors must occur upon protonation of the immino nitrogen in chrysi complexes than in their phi counterparts. Molecular modeling studies suggested that this difference in acid-base behavior could be traced directly to the presence of the additional aromatic ring in the chrysene ligand. This hypothesis was confirmed by the results of a crystal structure of $[Rh(bpy)_2(chrysi)]Cl_3$ in its protonated form (see below).

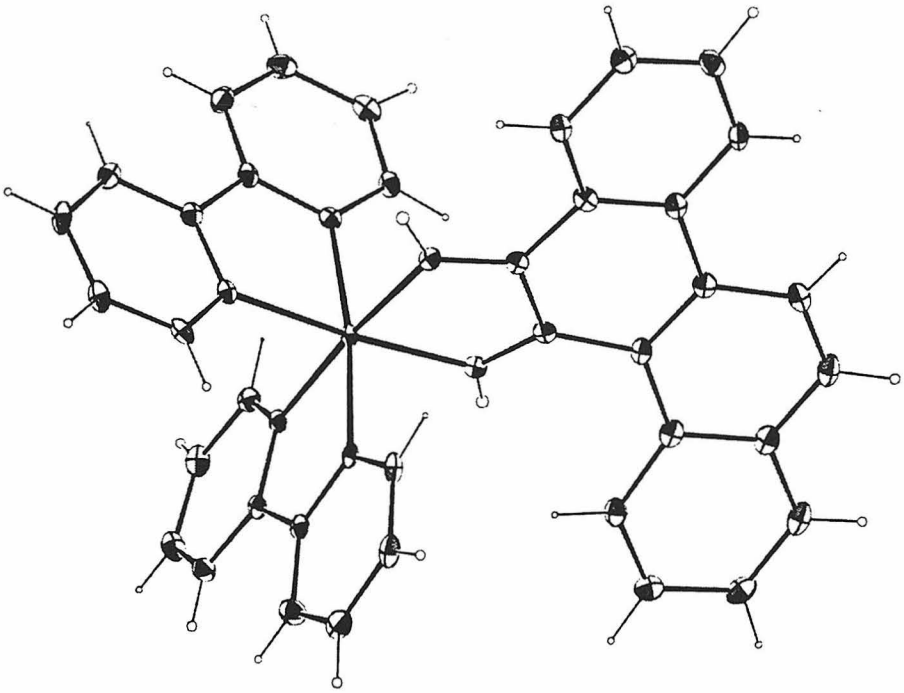
2.3.2.3: Crystallographic Characterization of $[Rh(bpy)_2(chrysi)]Cl_3$

Although previous crystal structures have been determined of metal complexes of both rhodium[18,48] and ruthenium containing phi ligands,[19] the novelty of the chrysenequinone diimine ligand made the atomic structure of a representative complex containing chrysi of considerable interest. An ORTEP drawing of the structure of the complex ion $[Rh(bpy)_2(chrysi)]^{3+}$ is included as Figure 2.28. Additional data on the structure of $[Rh(bpy)_2(chrysi)]Cl_3 \bullet 3CH_3CN \bullet 2H_2O$, including heavy atom parameters, bond distances and angles, and refined hydrogen parameters are included in Appendix I to this thesis. Like the previous structure of the $[Ru(bpy)_2(phi)](BF_4)_3$,[19] the bipyridyl ligands in the $[Rh(bpy)_2(chrysi)]^{3+}$ complex ion are essentially unperturbed. Also like the Ru(phi) complex, the general structure is a distorted octahedron with the N-Rh-N angles for ancillary ligand coordination (bipyridine N-Rh-bipyridine N) varying from 79.9° to 94.9° and averaging to 87.3°. Angles involving the chrysi nitrogens and bipyridine nitrogens are somewhat wider varying from 87.7° to 97.9° and averaging 94.4°. The angle between the chrysi nitrogens themselves is the shortest N-Rh-N angle in the structure at 78.0°.

Examining the angular structure of the complex more comprehensively, more significant differences between the Ru(phi) compound and the Rh(chrysi) complex

Figure 2.28. ORTEP Plot of $[Rh(bpy)_2(chrysi)]^{3+}$ from the X-ray Structure of $[Rh(bpy)_2(chrysi)]Cl_3 \bullet 3CH_3CN \bullet 2H_2O$.

Figure 2.28:



emerge. Unlike the Ru(phi) complex, which displayed an essentially planar structure of the phi ligand itself, the chrysi intercalating ligand is severely distorted from planarity. This distortion can be more clearly seen in Figure 2.29 which includes multiple views of the complex. The source of this distortion from planarity can be traced to a steric clash between the acidic proton on the immino nitrogen and the aromatic proton pointing back toward the rhodium center on the chrysene ring; this determination is made possible by the fact that the quality of the crystal data made it possible to determine the positions of the hydrogen atoms themselves. The interaction of the two atoms is graphically illustrated in Figure 2.30 which includes both a molecular model (panel A), where the chrysi ligand has been forced into planarity, and a view of the crystal structure (panel B) in its observed, distorted state. The van der Waals surfaces of the two involved hydrogen atoms are indicated by the red mesh. It is clear that, in order to force the aromatic rings planar, significant overlap is required between the two atoms; the distortion in the crystal structure relieves this clash. As an added comparison, the crystal structure of the chrysi compound is compared to the crystal structure of $[Rh(Me_2trien)phi]Cl_3$ which was previously determined[49] is shown in Figure 2.31. It is clear that in the phi case, where no aromatic protons are positioned directly back toward the metal center, there is no steric clash and therefore no required distortion.

A closer examination of the Rh-N distances observed in the structure also identify differences from the previously determined Ru structure. In this case, the Rh-N distances for the bipyridine ligands vary from 2.030(2) Å to 2.039(2) Å with the equatorial bonds being the longest. Like the analogous Ru(phi) structure, the bond distances between the immino nitrogen atoms and the rhodium are significantly shorter at 2.005(2) Å and 2.006(2) Å. The difference in these lengths is not as great as that for the ruthenium complex, however, where the phi N-Rh distances also

Figure 2.29. Multiple Views of the Crystal Structure of $[Rh(bpy)_2(chrysi)]^{3+}$ from Varied Angles. Note the severe distortion of the planarity of the chrysi ligand (shown in red).

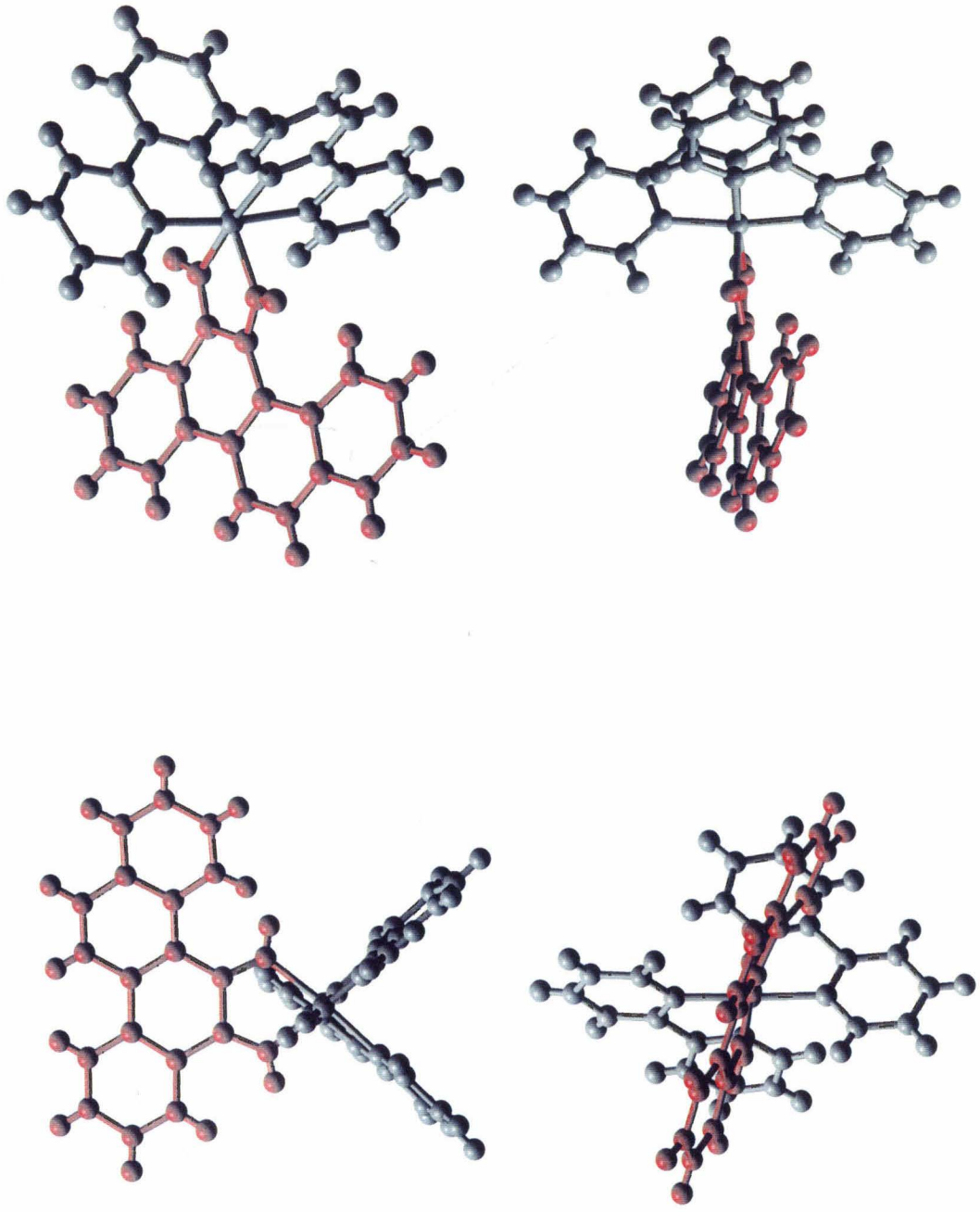
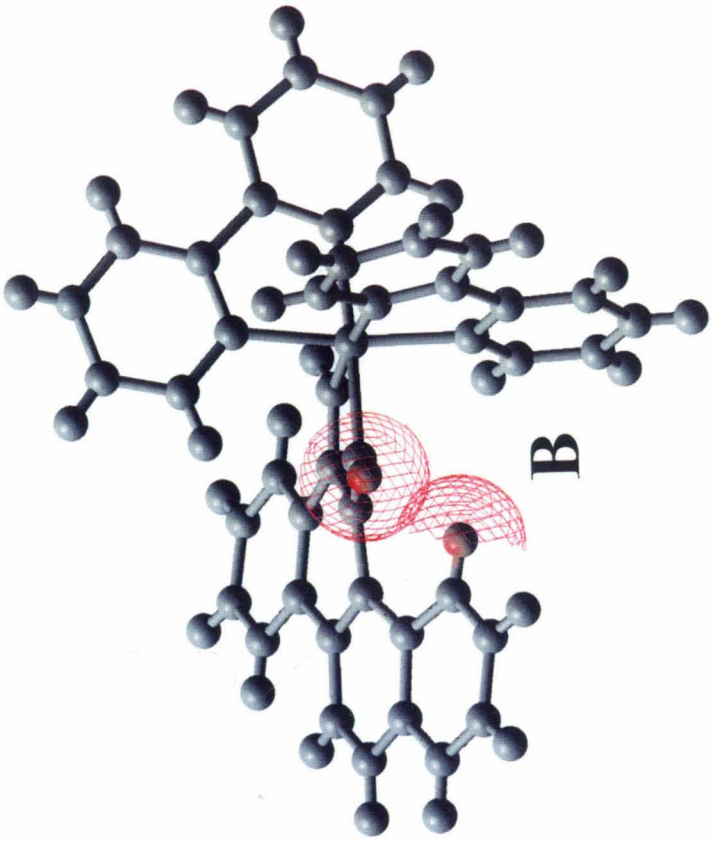


Figure 2.29:

Figure 2.30. Comparison of a Molecular Model (A) of $[Rh(bpy)_2(chrysi)]^{3+}$ whose Chrysenequinone Diimine Ligand has been Forced into Planarity with the Crystal Structure (B) of the Same Molecule. The van der Waals surfaces of the protons of interest are indicated with red mesh. Note the extensive overlap between the aromatic proton and the imino proton required to constrain the ligand to its planar form.



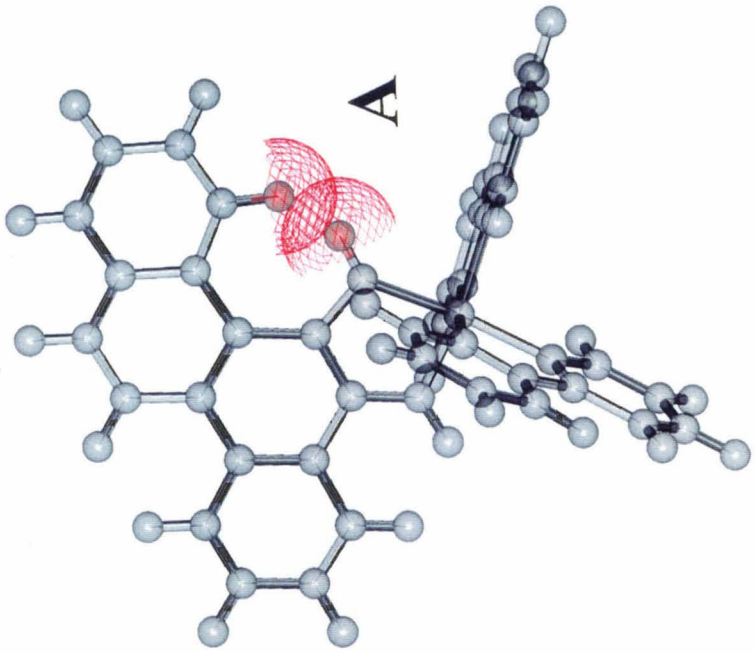
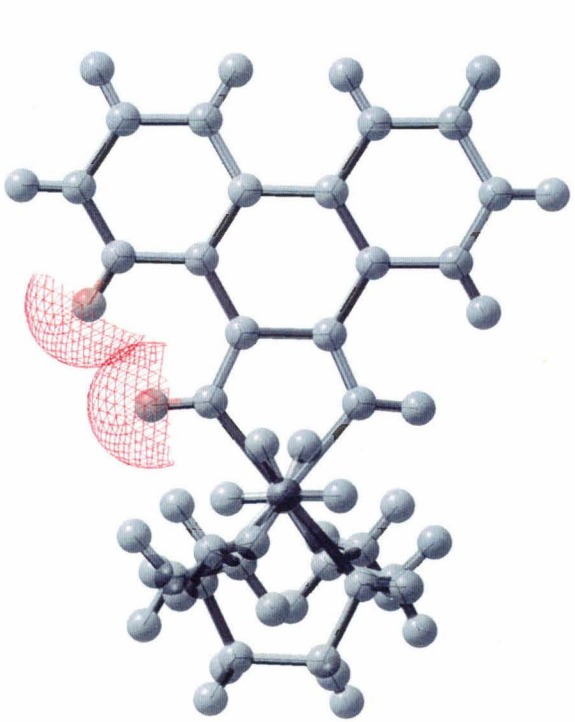


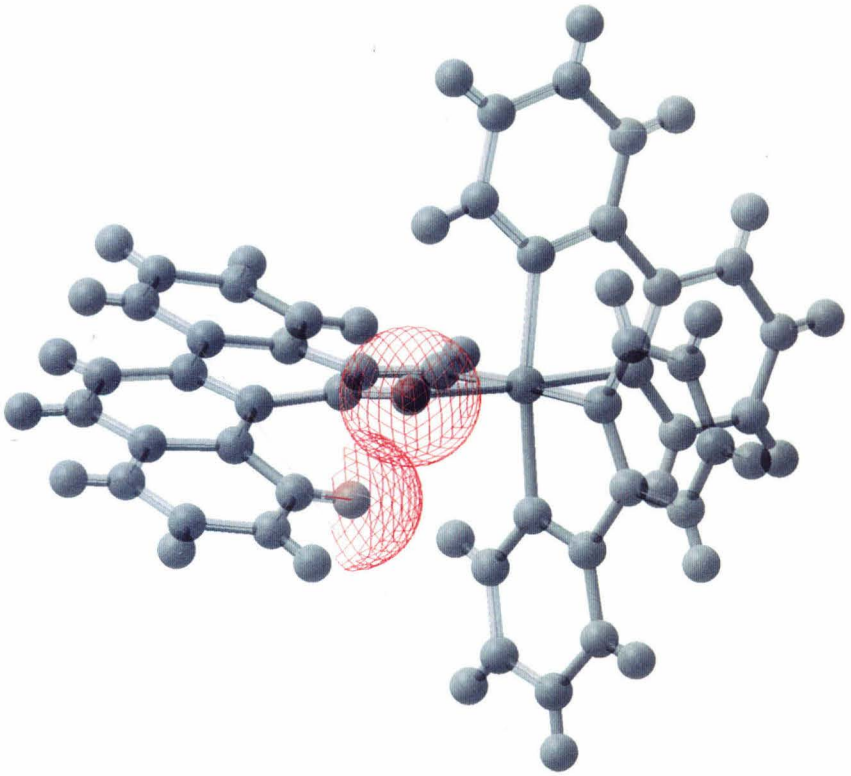
Figure 2.30:

Figure 2.31. Comparison of the Previously Reported Crystal Structure of $[Rh(Me_2trien)phi]^{3+}$ with the Structure of $[Rh(bpy)_2(chrysi)]^{3+}$. Note that in the phi case, where no aromatic protons are positioned pointing directly back towards the metal center, there is no steric clash and therefore no required distortion of the ligand.[49]

Figure 2.31:



$[Rh(Me_2trien)(phi)]^{3+}$



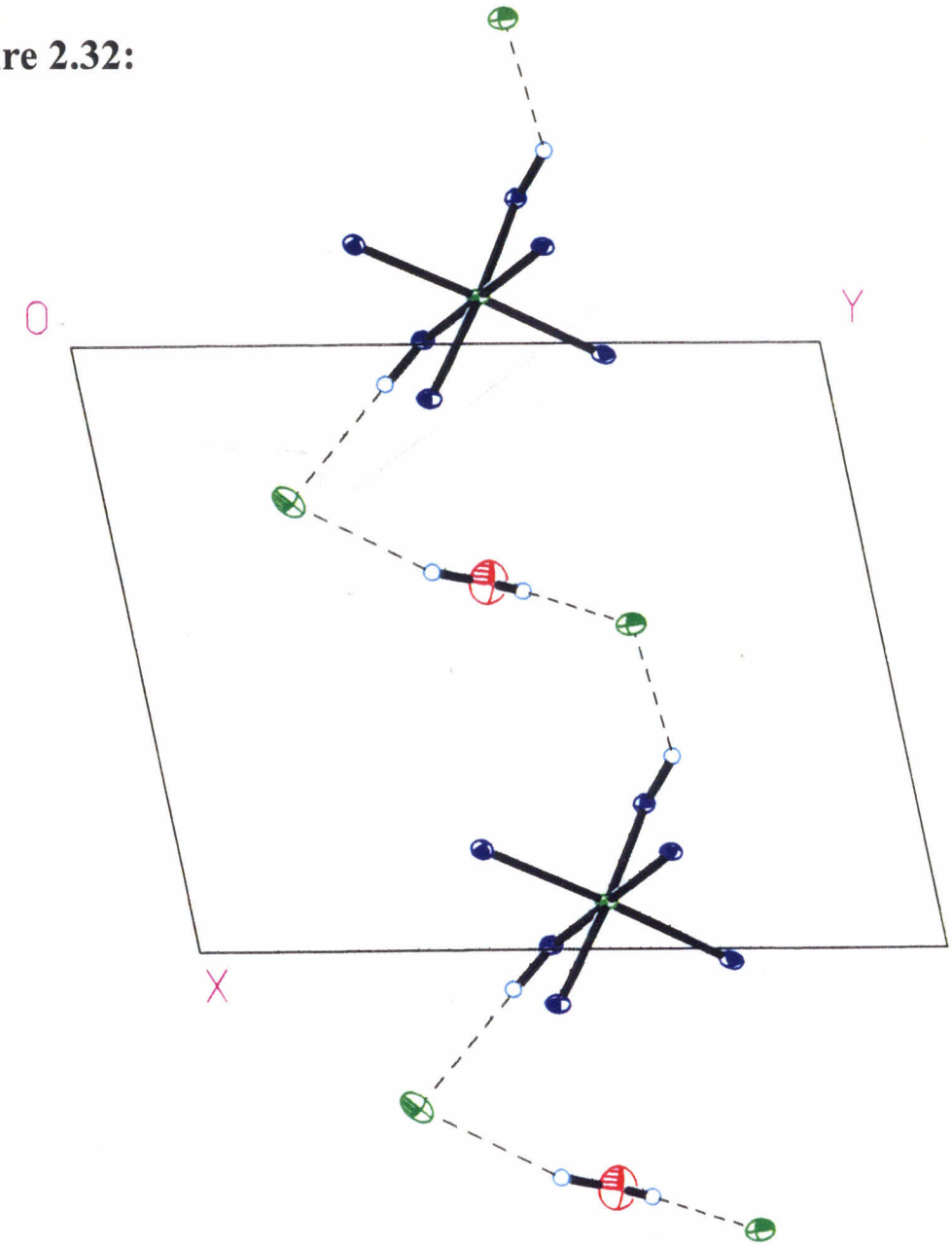
$[Rh(bpy)_2(chrysi)]^{3+}$

averaged 2.006(4) Å but are compared to bpy N-Rh distances averaging 2.064(4) Å. In the ruthenium case the explanation proposed to explain the shortened diimine-Rh distances was that greater back-bonding occurred between the Rh and phi ligand than the bpy ligands.[47] A parallel explanation for the distances in the $[Rh(bpy)_2(chrysi)]Cl_3$ structure could involve two elements. It is possible that the greater charge on the central metal ion in the rhodium case is singularly responsible for the observed shorter bpy N-Rh distances and, therefore, the lower difference between that value and the chrysi N-Rh lengths. It is also possible, however, that the distortion discussed in the previous paragraph also plays a role in the determination of the bond distances; in this case the explanation would be that the disruption caused by the twisted chrysi ligand prevents back-bonding that would otherwise resulted in a ratio between the bpy N-Rh and chrysi N-Rh distances more similar to the Ru(phi) structure. Values of the phi N-Rh distances from other Rh(phi) complex structures lacking the distortion of the chrysi ligand provide little help in distinguishing these mechanisms as they vary from 2.006(3) Å for $[Rh(NH_3)_4phi]Cl_3$, 2.016 to 2.017(17) Å for the isomers of $[Rh(Me_2trien)phi](Cl$, tartrate, or $SCN)_3$ and $[Rh([12]aneN_4)phi](SCN)_3$, and 2.047(4) Å for $[Rh([12]aneS_4)phi]Br_3$.[18,49] These data clearly suggest the influence of *trans* effects of the ancillary ligands on the bond length for the phi or chrysi in addition to steric or electronic concerns specific to the diimine intercalator itself.

Beyond the characteristics of the complex itself, the crystal structure of $[Rh(bpy)_2(chrysi)]Cl_3 \bullet 3CH_3CN \bullet 2H_2O$ is also noteworthy for the extensive hydrogen bonding network that exists within the crystal lattice. The three chloride ions, three acetonitrile and two water molecules contained in the crystal for each equivalent of metal complex form two hydrogen bonding "strings" which go through the unit cell. The more defined bonding string, shown in Figure 2.32, is as follows: a metal

Figure 2.32. Hydrogen Bonding Network in the Crystal of $[Rh(bpy)_2(chrysi)]Cl_3$ Involving the Metal Complex Immino Protons, Two Chloride Counter-ions and Two Ordered Water Molecules. For clarity, all atoms except the central rhodium ion and coordinating nitrogens are omitted from the metal complex. Chloride ions are indicated in green, nitrogen atoms in purple, hydrogen atoms in light blue and oxygen atoms in red.

Figure 2.32:



complex immino proton hydrogen bonds to a chloride ion which bonds to an ordered water which bonds to the next chloride which bonds to the immino of the next complex. A second network of hydrogen bonds goes along the edges of the unit cell made up of the remaining chloride ion, the remaining water molecule, and the acetonitrile molecules. This system is less interesting than the network including the metal complex, however, because it is much less well defined. Positions in this network are partially occupied by either water molecules or chloride ions and there is conformational disorder in the positioning of the acetonitrile molecules. In addition to the hydrogen bonding contacts which occur in the crystal, there are also significant aromatic-aromatic stacking interactions stabilizing the structure. These stacking contacts, which can be seen in the two views of four molecules in the crystal structure included as Figures 2.33 and 2.34, occur between the sides of the chrysi ligand not subject to the protonation-induced distortion and twisting. This partial overlap of the diimine intercalating ligands is similar to that observed in other rhodium(phi) crystal structures; in this case, the lack of more extensive overlap was explained by the interference of the ancillary ligand with stacking.[18] As a result, the extent of overlap between the aromatic ligands in this structure is likely controlled both by these sort of ancillary ligand concerns and the novel geometry of the protonated chrysi ligand.

2.3.2.4: pH Titration of $[Rh(d_8\text{-bpy})_2(chrysi)]Cl_3$ by 1D-^{1}H NMR Spectroscopy

In addition to the solid state demonstration of the conformational shift imposed on the chrysi ligand as a result of protonation, examination of $[Rh(bpy)_2(chrysi)]^{3+}$ by proton NMR further supports this model of the compound's unique spectral and acidic properties. The results of a pH titration performed on $[Rh(d_8\text{-bpy})_2(chrysi)]Cl_3$ in 90/10 H_2O/D_2O are included as Figure 2.35B. This solution study is consistent with

Figure 2.33. Side view of Four Molecules from the Crystal Structure of $[Rh(bpy)_2(chrysi)]Cl_3$. Note the positioning of the chrysi intercalating ligands above one another to participate in aromatic-aromatic stacking interactions.

Figure 2.33:

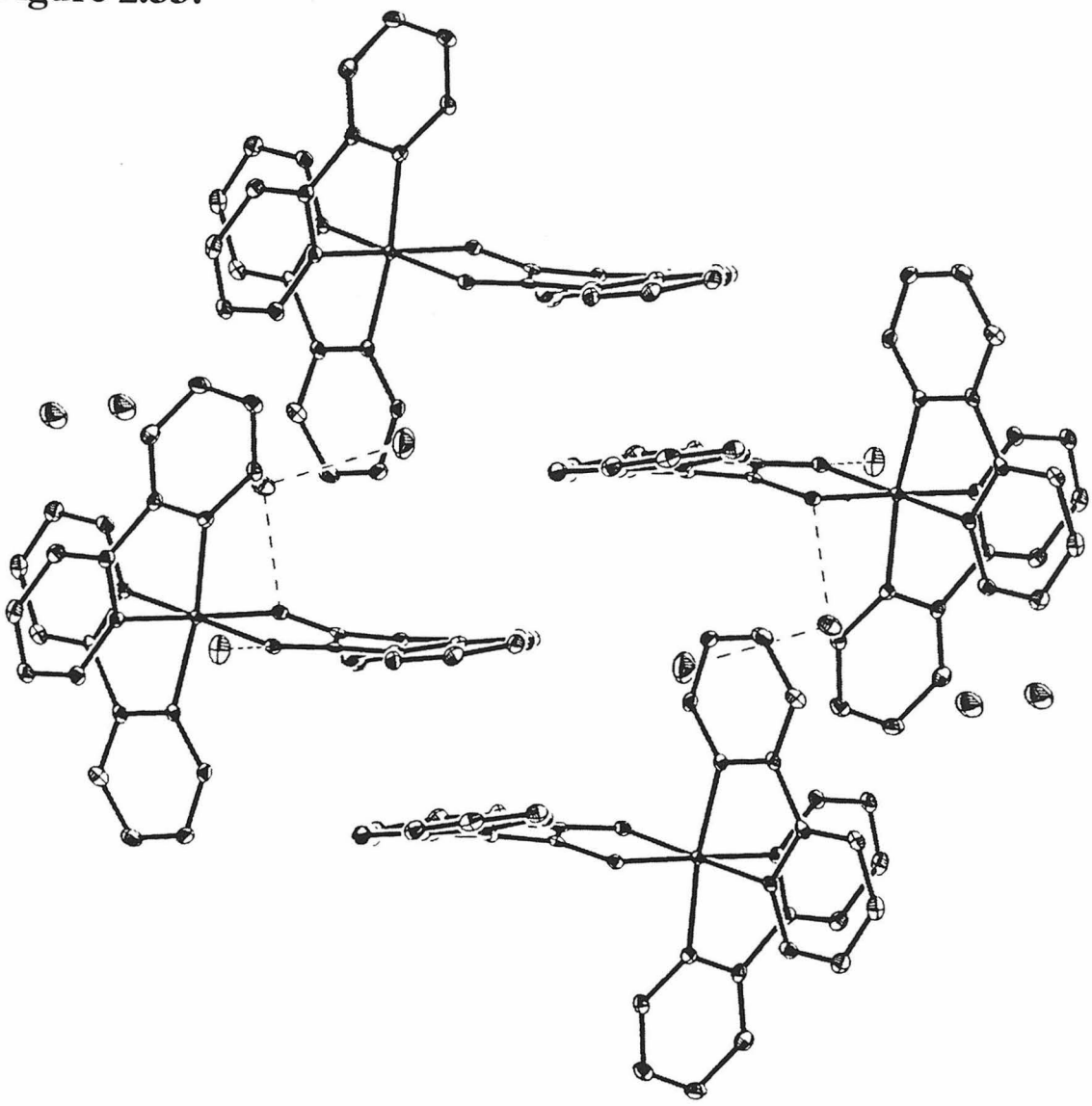


Figure 2.34. Top View of Four Molecules from the Crystal Structure of $[Rh(bpy)_2(chrysi)]Cl_3$. Note that the overlap of the chrysi intercalating ligands for aromatic-aromatic stacking interactions occurs on the side of the molecule not subject to protonation induced distortion. The sites of protonation induced distortion are indicated in the figure by stars.

Figure 2.34:

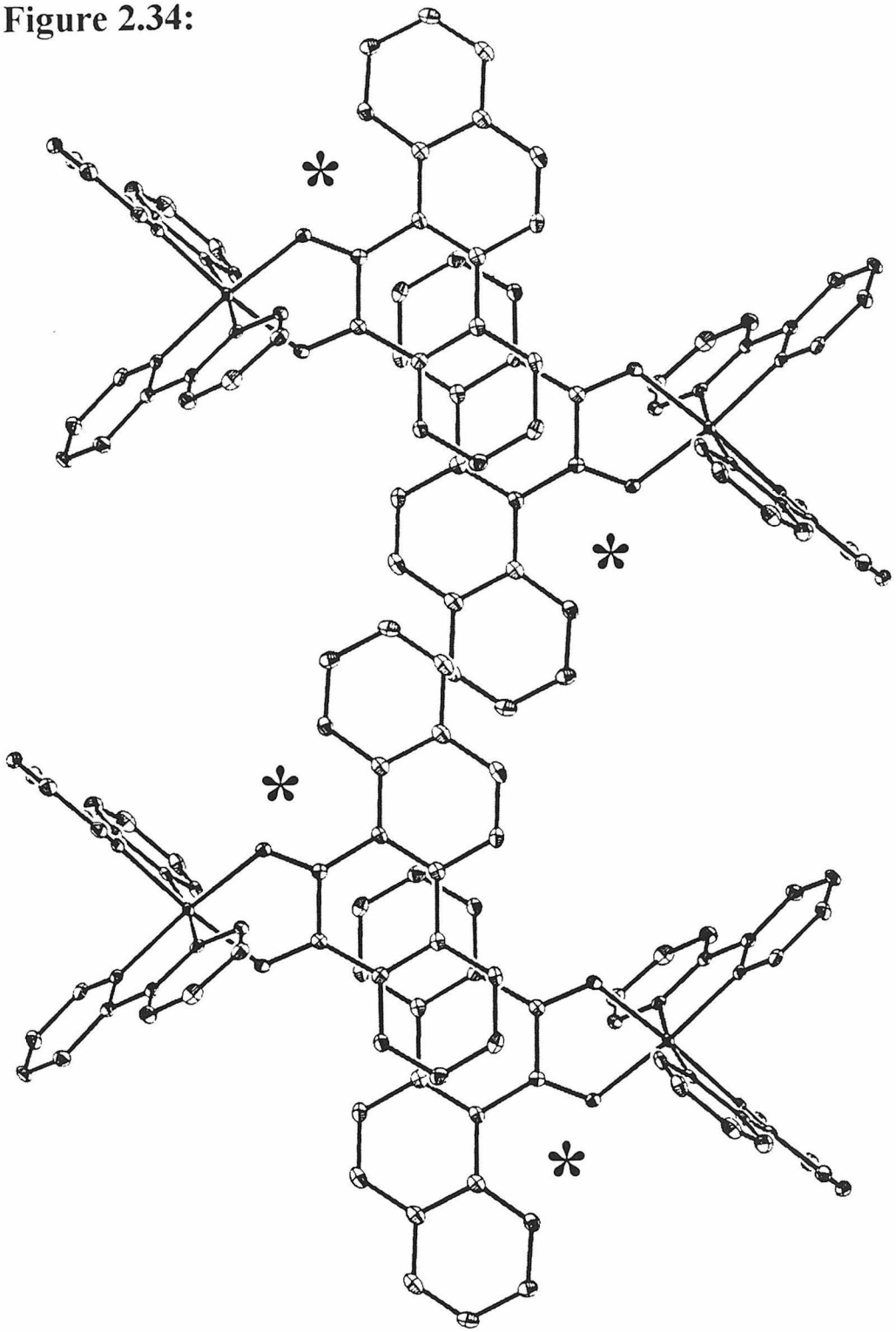


Figure 2.35. (A) Labeled $[Rh(bpy)_2(chrysi)]^{3+}$ for Interpretation of NMR Titration Results. (B) Results of a 1-D 500 MHz ^1H NMR pH Titration of $[Rh(d_8\text{-}bpy)_2(chrysi)]Cl_3$ in 90/10 H_2O/D_2O using WATERGATE Gradient Solvent Suppression. Note that the four doublets labeled "A" in the pH 1.45 (protonated) spectrum are shifted up field from all resonances in the pH 9.60 (deprotonated) spectrum. In addition, these peaks, particularly the three near 7 ppm, are the most rapidly exchange broadened upon increasing the pH of the solution. Note also the single peak labeled "B" in the pH 9.60 spectrum. This peak, shifted far down field from all the remaining peaks is consistent with the placement of the proton at position 4 proximal to the immino anion of the deprotonated complex.

Figure 2.35A:

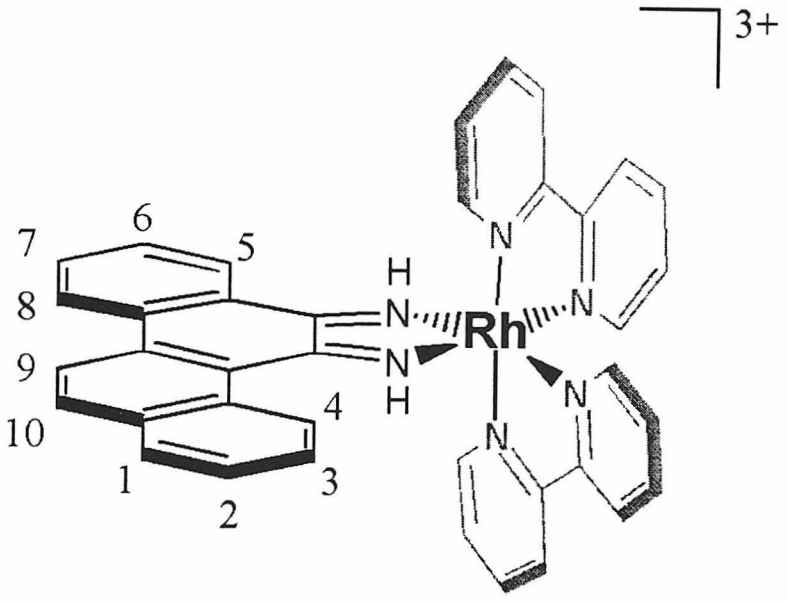
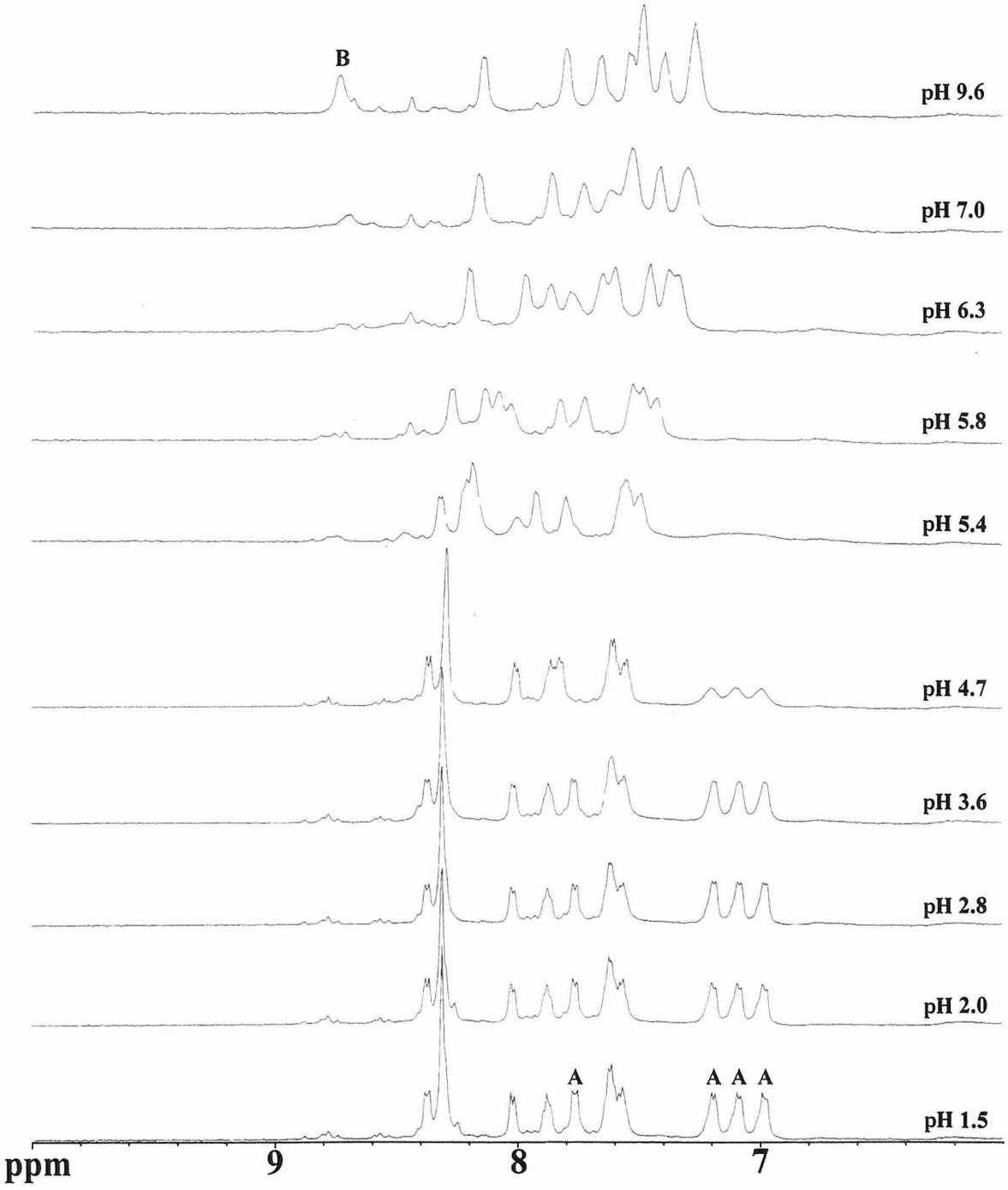


Figure 2.35B:


B
pH 9.6
pH 7.0
pH 6.3
pH 5.8
pH 5.4
pH 4.7
pH 3.6
pH 2.8
pH 2.0
A
A A A
pH 1.5
ppm
9
8
7

the conclusions drawn from the crystal structure data about chrysi ligand conformational distortion. Most generally, it should be noted that distortion of the ligand in its protonated state (low pH, bottom of Figure 2.35B) is supported by the fact that distinct resonances can be discerned for each of the ten aromatic protons on the chrysi intercalator. Under basic conditions (high pH, top of Figure 2.35B), the resonances are far less dispersed and some are coincident with one another implying that, in this state, the protons are in more similar environments. This change from more dispersed to less is consistent with the proposed flattening of the twisted ligand shown in Figure 2.29.

The chemical shifts of protons in both the acidified and basic NMR samples also support this deformation behavior. In the acidified spectrum, a set of three doublets (three of the peaks labeled "A" in Figure 2.35B) are 0.5-1.0 ppm upfield from the remainder of the resonances. This positioning is consistent with these protons being torqued out of plane and, as a result, subject to less of the aromatic ring currents of the chrysene ring system. The rapid exchange broadening of these peaks (in addition to the other doublet labeled "A" in Figure 2.35B) as the pH is increased is also consistent with them being near the acidic site on the metal complex and therefore more subject to the protonation/deprotonation equilibrium as the solution approaches the pKa of the compound. Because of the multiplicity of the peaks (all doublets), these four protons are likely at positions 1,4,9, and 10 on Figure 2.33A; although it is more difficult to determine candidate peaks for protons 2 and 3, they may be the large singlet at approximately 8.25 ppm which also shifts dramatically as the pH approaches the pKa (5.2) of the complex. Beyond the basic argument that the similarity in the aromatic chemical shifts in the high pH spectrum support the planar orientation of the chrysi ligand, the single resonance shifted far downfield is also consistent with this model. In the deprotonated, planar chrysi ligand, one proton (4

in Figure 2.35A) will be very close to the deprotonated immino-anion. It is likely that this positioning so near a negative charge will have a significant effect on the chemical shift of the involved proton. The presence of a single proton in this environment also supports the flattening of the chrysene ring with deprotonation.

2.3.2.5: Chrysenequinone Diimine Ligands: A Consistent Picture

The results presented in the previous sections comprise a complete picture of the interaction between the structural, photophysical and chemical properties of $[Rh(bpy)_2(chrysi)]^{3+}$, a novel complex based on a new quinone diimine ligand. The deformations observed in the crystal structure of the protonated form not only serve as a structural explanation for the depressed pK values observed in all the compounds containing the chrysi ligand but also rationalize the differences between the absorbance characteristics of chrsyi complexes and their analogous phi compounds. Since at basic pH both ligands are planar and deprotonated, the differences in their spectral behavior are minimal (Figure 2.15). At acidic pH, however, where the chrysi ligand is twisted out of plane, the splitting of the spectral transitions into multiple bands of significantly different maxima is entirely reasonable. In the phi case, where no such structural changes occur upon protonation, the spectrum retains its same overall structure and shifts much less dramatically in response to the change in pH. As a result, complexes of chrysenequinone diimine are not only of interest because of their potential as new DNA binding molecules but also as an example of molecules which contain pH "gated" ligand conformational switch. Such a switching mechanism could provide a useful model system to explore the interaction between the structure of transition metal complexes and their photophysical properties.

2.4: Literature Cited

1) Pyle, A. M.; Barton, J. K. *Prog. Inorg. Chem.* **1990**, *38*, 413.

2) Pratviel, G.; Bernadou, J.; Meunier, B. *Adv. Inorg. Chem.* **1998**, *45*, 251.

3) Burrows, C. J.; Muller, J. G. *Chem. Rev.* **1998**, *98*, 1109.

4) Trawick, B. N.; Daniher, A. T.; Bashkin, J. K. *Chem. Rev.* **1998**, *98*, 939.

5) Norden, B.; Lincoln, P.; Ackerman, B.; Tuite, E. *Met. Ions Biol. Sys.* **1996**, *33*, 177.

6) Lippert, B. *Biometals* **1992**, *5*, 195.

7) Pratviel, G.; Bernadou, J.; Meunier, B. *Ang. Chem. Int. Ed. Eng.* **1995**, *34*, 746.

8) Pyle, A. M.; Long, E. C.; Barton, J. K. *J. Am. Chem. Soc.* **1989**, *111*, 4520.

9) Sitlani, A.; Long, E. C.; Pyle, A. M.; Barton, J. K. *J. Am. Chem. Soc.* **1992**, *114*, 2303.

10) Terbrueggen, R. *Exploring the Direct and Indirect Readout of DNA with Phenanthrenequinone Diimine Complexes of Rhodium(III)*. Ph.D. Thesis, Division of Chemistry, California Institute of Technology, 1995.

11) Sitlani, A.; Barton, J. K. *Biochemistry* **1994**, *33*, 12100.

12) David, S. S.; Barton, J. K. *J. Am. Chem. Soc.* **1993**, *115*, 2984.

13) Dupureur, C. M.; Barton, J. K. in *Comprehensive Supramolecular Chemistry*. Lehn, J.-M., ed.; Pergamon Press: Tarrytown, NY, 1996; Vol. 5, 295.

14) Johann, T. W.; Barton, J. K. *Phil. Trans. Royal Soc. A.* **1996**, *354*, 299.

15) Sitlani, A.; Barton, J. K.; in *Handbook on Metal-Ligand Interaction in Biological Fluids, Bioinorganic Chemistry*. Berthon, G., ed.; Marcel Dekker: New York, NY, 1995; Vol. 1, part 2, 466.

16) Chow, C. S.; Barton, J. K. *Methods Enzymol.* **1992**, *212*, 219.

17) Hall, D. B.; Holmlin, R. E.; Barton, J. K. *Nature* **1996**, *382*, 731.

18) Krotz, A. H.; Kuo, L. Y.; Barton, J. K. *Inorg. Chem.* **1993**, *32*, 5963.

19) Pyle, A. M.; Chiang, M. Y.; Barton, J. K. *Inorg. Chem.* **1990**, *29*, 4487.

20) Belser, P.; von Zelewsky, A.; Zehnder, M. *Inorg. Chem.* **1981**, *20*, 3098.

21) Schlosser, K.; Hoyer, E. Z. *Anorg. Allg. Chem.* **1972**, *387*, 91.

22) Bonhôte, P.; Wrighton, M.S. *Synlett* **1997**, 897.

23) Wärnmark, K.; Thomas, J. A.; Heyke, O.; Lehn, J.-M. *J. Chem. Soc. Chem. Commun.* **1996**, 701.

24) Jonasdottir, S.; Kim, C.-G.; Kampf, J.; Coucouvanis, D. *Inorg. Chim. Acta* **1996**, *243*, 255.

25) Hiort, C.; Lincoln, P.; Norden, B. *J. Am. Chem. Soc* **1993**, *115*, 3448.

26) MacDonnell, F. M.; Bodige, S. *Inorg. Chem.* **1996**, *35*, 5758.

27) Bodige, S.; Torres, A. S.; Maloney, D. J.; Tate, D.; Kinsel, G. R.; Walker, A. K.; MacDonnel, F. M. *J. Am. Chem. Soc.* **1997**, *119*, 10364.

28) Golding, B. T.; Harrowfield, J. M.; Robertson, G. B.; Sargeson, A. M. *J. Am. Chem. Soc.* **1974**, *96*, 3691.

29) Creaser, I. I.; Harrowfield, J. M.; Herlt, A. J.; Sargeson, A. M.; Springborg, J.; Geue, R. J.; Snow, M. R. *J. Am. Chem. Soc.* **1977**, *99*, 3181.

30) Creaser, I. I.; Geue, R. J.; Harrowfield, J. M.; Herlt, A. J.; Sargeson, A. M.; Snow, M. R.; Springborg, J. *J. Am. Chem. Soc.* **1982**, *104*, 6016.

31) Geue, R. J.; Korybut-Daszkiewicz, B.; Sargeson, A. M. *J. Chem. Soc. Chem. Commun.* **1993**, 1454.

32) Geue, R. J.; Höhn, A.; Ralph, S. F.; Sargeson, A. M. *J. Chem. Soc. Chem. Commun.* **1994**, 1514.

33) Harrowfield, J. M.; Sargeson, A. M. *J. Am. Chem. Soc.* **1974**, *96*, 2634.

34) Gillard, R. D.; Osborn, J. A.; Wilkinson, G. *J. Chem. Soc.* **1965**, 1951.

35) Gidney, P. M.; Gillard, R. D.; Heaton, B. T. *J. Chem. Soc., Dalton Trans.* **1972**, 2621.

36) Mürner, H.; Jackson, B. A.; Barton, J. K. *Inorg. Chem.* **1998**, *37*, 3007.

37) Yoshikawa, Y.; Yamasaki, K. *Coord. Chem. Rev.* **1979**, *28*, 205.

38) Broomhead, J. A.; Grumley, B. *Inorg. Chem.* **1971**, *10*, 2002.

39) McKenzie, E. D.; Plowman, R. A. *J. Inorg. Nucl. Chem.* **1970**, *32*, 199.

40) Howells, R. D. a. M., J. D. *Chem. Rev.* **1977**, *77*, 69.

41) Greabe, v. C.; Hönigsberger, F. *Ann. Chem.* **1900**, *311*, 257.

42) Piotto, M.; Saudek, V.; Skenar, V. *J. Biomol. NMR* **1992**, *2*, 661.

43) Jardine, F. H.; Sheridan, P. S.; in *Comprehensive Coordination Chemistry*. Wilkinson, G., ed.; Pergamon Press: Oxford, UK, 1987; Vol. 4, 953.

44) Druey, J.; Schmidt, P. *Helv. Chim. Acta* **1950**, *33*, 1080.

45) Copeland, K. D.; Sanford, M. S.; Barton, J. K., unpublished results.

46) Sanford, M. S.; Barton, J. K., unpublished results.

47) Pyle, A. M. *Phenanthrene Diimine Complexes of Ru(II) and Rh(III): Synthesis and Development of a New Class of Shape-Selective Probes for Nucleic Acid Structure*. Ph.D. Thesis, Department of Chemistry, Columbia University, 1989.

48) Schaefer, W. P.; Krotz, A. H.; Kuo, L. Y.; Shields, T. P.; Barton, J. K. *Acta Cryst.* **1992**, *C48*, 2071.

49) Krotz, A. H.; Barton, J. K. *Inorg. Chem.* **1994**, *33*, 1940.

Chapter 3:

Recognition of Base Mismatches in DNA by Chrysenequinone Diimine Complexes of Rhodium(III)*

* Portions of this chapter were adapted from Jackson, B.A. and Barton, J.K. *J. Am. Chem. Soc.* **1997,** *119*, 12986.

3.1: INTRODUCTION

As discussed in Chapter 1 of this thesis, the recognition of base mismatches in DNA is a unique challenge in molecular recognition. Since any of the four naturally occurring DNA bases can exist as part of a mismatched base pair, it is not possible to design a general mismatch recognition agent by taking advantage of direct readout mechanisms of DNA base discrimination. Furthermore, when the structures of base mismatches in DNA are examined crystallographically, no common structural characteristics are apparent which could be exploited as a shape selective handle in the design of small molecule mismatch binding agents. When oligonucleotides containing base mismatches are examined in solution, however, it becomes clear that many mismatches do have a common characteristic: the presence of base mismatches, with their often limited or disrupted hydrogen bonding patterns, thermodynamically destabilizes the DNA double helix. This destabilization is manifest in the reduced melting temperature (T_M) at which the strands of a mismatch-containing duplex separate compared to a correctly base paired analogue. In addition, the stability of the appropriately paired bases near a mismatch site is reduced which results in an increased tendency to open and a breakdown of the regular structure of the double helix. This effect can be directly observed by NMR as an increase in the rate of proton exchange at bases near a mismatch compared to Watson-Crick paired DNA.[1] Although this helix destabilization is a characteristic which clearly distinguishes most mismatch sites from properly paired DNA, use of such a characteristic as a molecular recognition element is a significantly novel approach.

Traditional strategies of molecular recognition design consist of defining the macromolecular surface or cleft with which binding is desired and creating a molecule which is decorated with appropriate functionality to maximize favorable

interactions with the target binding site. Such a strategy was applied, for example, in the design of Δ–α–[Rh[(*R,R*)-Me_2trien]phi]$^{3+}$ where appropriate hydrogen bond donor groups and van der Waals contacts were placed in a geometry complementary to the surface presented by the major groove edge of a 5'-TGCA-3' DNA sequence. The use of helix destabilization as a recognition element for DNA base mismatches is almost the opposite strategy; rather than recognizing the functionality and geometry of a desired binding site, the goal is to recognize the *absence* of such a regular and ordered surface.

Approaching this problem required the application of a shape selective strategy that is seldom intentionally used in the design of small molecule recognition agents but often applied by protein recognition systems. Instead of carefully designing a molecule with an ensemble of interactions to *promote* binding at a target site, the goal was much more straightforward: construct a molecule with the intention of *discouraging* binding at undesirable sites. When this strategy can be applied to a molecular recognition problem, it is often the most effective way to design specific binding agents. For example, while an unpaired hydrogen bond might decrease binding at an undesired site by 10 fold, if an undesired substrate is too large to fit into an enzyme active site, specificity is *absolute*. As a result, in the same way that the binding of the Λ enantiomers of octahedral metallointercalators is prevented because of steric interference with the DNA backbone, molecules might be designed which are prohibited from binding to the ordered structure of properly paired DNA but could bind in the destabilized regions near mismatches.

Since the characteristic targeted for mismatch recognition was structural disorder at the core of the base stack, modifications to the ancillary ligands of the compound would not be effective to impart specificity. Instead, a novel intercalating ligand,

chrysenequinone diimine or chrysi (Figure 3.1), was designed to provide both binding affinity for DNA and impart mismatch specificity to the complex. This strategy is a significant departure from the traditional model of designing these compounds where intercalation provided only sequence neutral binding affinity to deliver recognition elements to the major groove of DNA.

The design of the chrysi intercalating ligand was based on analysis of the NMR solution structure of Δ–α–[Rh[(*R,R*)-Me_2trien]phi]$^{3+}$ bound to DNA. Examination of a space filling model of the abstracted binding site from this structure (Figure 3.2) reveals that the phenanthrenequinone diimine (phi) ligand, when it is intercalated into B-form DNA, snugly fills most available space inside the intercalation site. At the interface between the intercalator and the DNA binding site, sugar protons are almost in contact with the aromatic ligand. As a result, if a wider ligand were introduced as a DNA intercalator, it would sterically clash with these functionalities at the edges of the site and, as a result, be unable to readily bind to B-form DNA. The structural disorder found near mismatch sites, however, might provide a more open and accessible binding site for a more sterically demanding ligand. This recognition strategy was the rationale behind the design of the chrysi ligand; by adding an additional ring to one side of the phi ligand, the width of the intercalator was increased by 2.1 Å (hydrogen to hydrogen, Figure 3.3). Molecular modeling suggested that this increase in width was sufficient to generate clashes between the ligand and the sides of a standard intercalation site in DNA. This strategy made it possible to increase the steric bulk of the ligand while still preserving the planar, aromatic structure necessary to facilitate intercalation.

Figure 3.1. The Chrysenequinone Diimine (chrysi) Intercalating Ligand.

Figure 3.1:

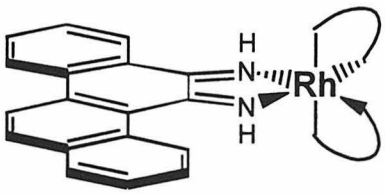


Figure 3.2. Abstracted Metal Complex and Binding Site of Δ–α–[Rh[(*R,R*)-Me_2trien]phi]$^{3+}$. Central two base pairs and metallointercalator were excised from the NMR solution structure of the complex bound to a 10 base pair self complementary oligonucleotide constructed by Dr. B.P. Hudson in this research group. Note that, once the phi intercalating ligand is accommodated in the DNA binding site, little extra space remains unfilled. As a result, because of steric conflicts with the sugar phosphate backbone, binding of a larger intercalating ligand in such a binding site should be disfavored.[7,8]

Figure 3.2:

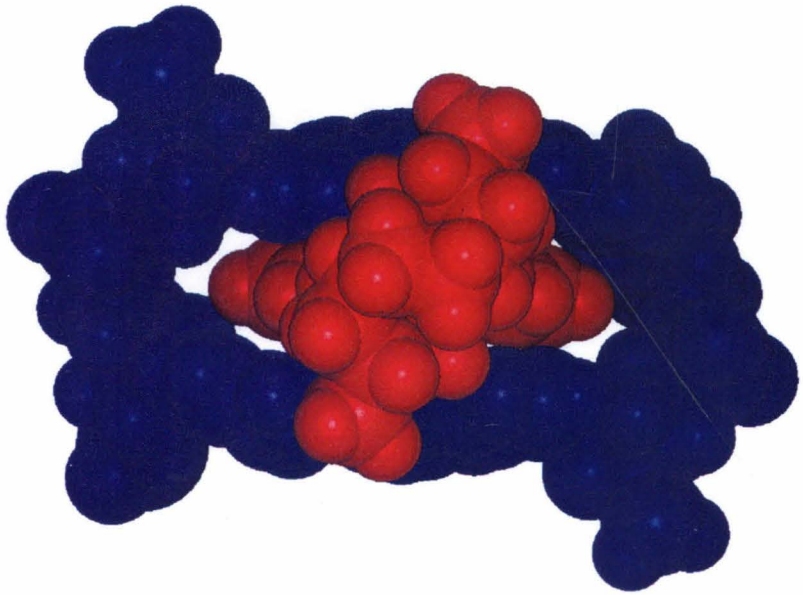
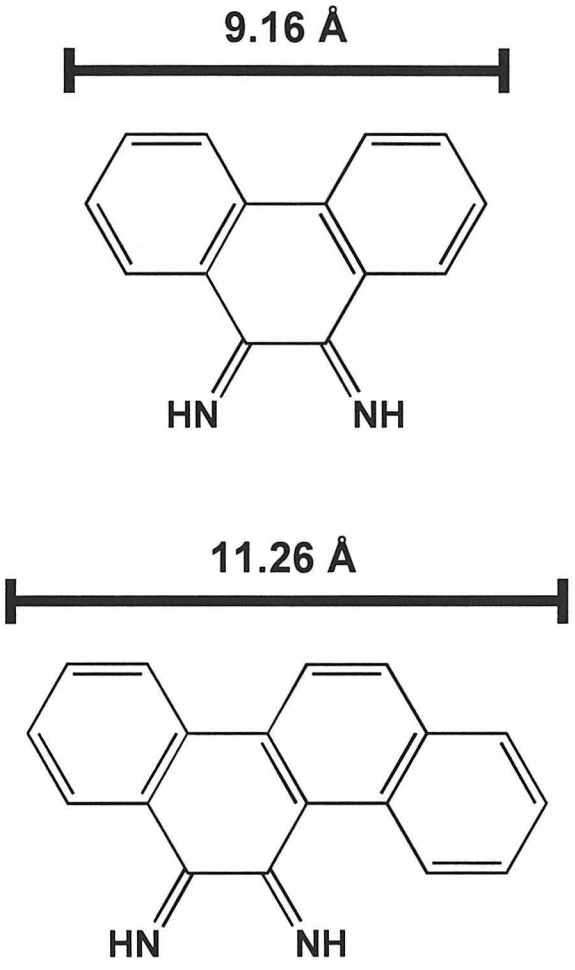


Figure 3.3. Comparison of the Widths of the Chrysenequinone Diimine and Phenanthrenequinone Diimine Intercalators. Width measurements were made on models constructed in Insight II and are the *horizontal* distances from hydrogen nucleus to hydrogen nucleus on the farthest edges of the two ring systems.

Figure 3.3:



3.2: Experimental Methods

3.2.1: Instrumentation and Materials

All reagents were the highest purity commercially available and used as obtained without further purification. Sonicated calf thymus DNA was obtained from Amersham-Pharmacia Biotech, Buckinghamshire, UK. All oligonucleotides were prepared by standard phosphoramidite methods on an ABI 392 DNA/RNA synthesizer and purified either by reverse phase HPLC or on Poly-pak nucleic acid purification cartridges (Glen Research, Sterling, VA). HPLC purification was performed on either a Waters 660E, Hewlett Packard 1050 or 1100 instrument using a Dynamax C_{18} reverse phase column. Absorption spectra were recorded on a Beckman DU 7400 spectrophotometer.

Oligonucleotides were 5'-end-labeled with ^{32}P using γ-^{32}P-ATP and T4 polynucleotide kinase (New England Biolabs, Beverly, MA) and purified by denaturing polyacrylamide gel electrophoresis. Oligonucleotides were isolated from excised polyacrylamide slices by elution into ammonium acetate EDTA buffer (500 mM NH_4OAc, 1 mM EDTA, pH 9) and ethanol precipitated. Chemical sequencing reactions were performed by literature protocols.[2] DNA photocleavage reactions were performed on samples of end-labeled DNA with unlabeled, identical sequence carrier DNA in running buffer (50 mM Tris, 20 mM sodium acetate, 18 mM NaCl, pH 7.0) or in 25 mM ammonium acetate, pH 9.0. DNA samples were annealed by heating to 90°C and controlled cooling to room temperature using a Perkin Elmer Cetus DNA thermocycler. Concentrations of metal complex solutions were determined spectrophotometrically using ε_{271} 63,800 M^{-1} cm^{-1} for $[Rh(bpy)_2(chrysi)]^{3+}$ (determined by atomic absorption spectroscopy) and ε_{358} 19,500

M^{-1} cm^{-1} for $[Rh(bpy)_2(phi)]^{3+}$. For Δ-$[Rh(phen)_2(chrysi)]^{3+}$ and Δ-$[Rh(chrysi)_2(phen)]^{3+}$, extinction coefficients were estimated by comparison to rhodium(III) phi complexes with identical ancillary ligands and known extinction coefficients in areas of the spectrum dominated by ancillary ligand absorbance rather than the quinone diimine transitions. Concentrations of oligonucleotides were determined spectrophotometrically using per-base extinction coefficients of A: 8600 M^{-1} cm^{-1}; C: 6800 M^{-1} cm^{-1}; G: 9700 M^{-1} cm^{-1}; T: 8400 M^{-1} cm^{-1} which are based on values from single stranded DNA homopolymers. Extinction coefficients for the *double stranded regions* of DNA hairpins were systematically reduced 15% from the calculated values based on temperature dependent hypochromicity measurements made on a representative sample of these hairpins. Photocleavage samples were prepared between 5 and 30 min before irradiating on an Oriel Hg/Xe lamp system equipped with a monochromator in open, horizontally positioned 1.7 ml microcentrifuge tubes. Dried irradiation samples were resuspended in denaturing formamide loading dye and electrophoresed on 20% denaturing polyacrylamide gels. Images of the gels were obtained by phosphoimagery (Molecular Dynamics) and quantitated using the Imagequant software package.

3.2.2: Spectrophotometric Titration of the Binding of Δ-$[Rh(bpy)_2(chrysi)]^{3+}$ to B-DNA

Solutions of Δ-$[Rh(bpy)_2(chrysi)]Cl_3$ (30 μM) were prepared in 10 mM Tris, pH 8.0. Identical aliquots of a concentrated DNA solution (either sonicated calf thymus DNA or the Watson-Crick paired 17mer oligonucleotide 5'-CGCGCGCACGACGGCCG-3' annealed to its complement) were added to two cuvettes, one containing the metal solution and one containing only buffer. The spectrum of each solution was measured from 350 nm to 550 nm, far enough to the visible to avoid interference from the DNA absorption. To more completely control for any DNA contribution to

the observed spectrum, the spectra of the metal-DNA solutions was measured using an identical DNA-only solution as a blank. The hypochromicity of the metal complex visible absorbance band was extracted to construct a binding curve for the compound to B-form DNA; a bulk binding constant for this non-specific interaction was extracted by equating the hypochromicity to a fraction bound and fitting the data to a simplified binding model based on the number of base pairs titrated into the metal complex.

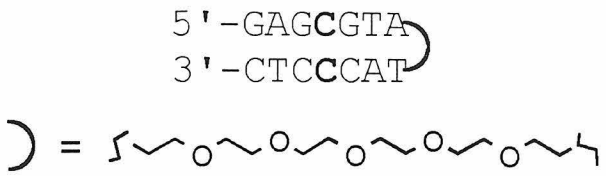
$$\text{Fraction Bound} = [Rh{\bullet}DNA]/[Rh]_T$$

(1)
$$[Rh \cdot DNA] = \frac{\left(K_b([DNA]_T + [Rh]_T) + 1\right) - \sqrt{\left(\left(K_b([DNA]_T + [Rh]_T) + 1\right)^2 - 4 \cdot K_b^2 [Rh]_T [DNA]_T\right.}}{2 \cdot K_b}$$

Where [Rh•DNA] is the concentration of the rhodium complex bound to the nucleic acid, $[Rh]_T$ is the total rhodium complex concentration, $[DNA]_T$ is the total DNA concentration in base pairs, and K_b is the binding constant of the complex for the nucleic acid. (See Appendix 2 for additional detail on determining association constants.)

3.2.3: Examination of the Interaction of Δ-$[Rh(bpy)_2(chrysi)]^{3+}$ and CC Mismatch Containing DNA by NMR

The oligonucleotide hairpin shown below was prepared by standard phosphoramidite synthesis methods using the unnatural phosphoramidite "Spacer 18" (Glen Research, Sterling, VA) – the polyether linker whose structure is shown – to connect the two DNA halves of the hairpin. The resulting 14mer+ oligonucleotide was purified by standard reverse phase HPLC techniques, ion-exchanged to the sodium salt on Sephadex CM C-25 cation exchange resin (equilibrated with NaCl), and separated from exogenous salts using a Waters Sep-pak C_{18} purification cartridge.



The stock solutions (in 10 mM sodium phosphate, 20 mM NaCl, pH 7.0) of the oligonucleotide and Δ-$[Rh(bpy)_2(chrysi)]^{3+}$ used for NMR data acquisition were made at 2.22 mM and 20 mM respectively so that the titration of 450 μl of DNA solution with 50 μl of metal complex solution would produce a bound complex concentration of 2 mM. Both samples were exhaustively exchanged in D_2O before being reconstituted in 99.96% D_2O. The DNA solution contained TMSP as an internal standard (0.00 ppm).

After acquiring a NOESY spectrum of the free DNA (500 MHz Brüker AMX-500 spectrophotometer with variable temperature control, 10 ppm sweep width, TPPI mode, 2048 complex points, 512 t_1 blocks, 128 scans per t_1 block, 1.3 s relaxation delay, 200 ms mixing time, 4°C), the metal complex was titrated into the DNA sample and the progress monitored by 1D spectra. Titration was stopped after addition of 80% of the calculated equimolar amount of metal complex since no further changes were observed in the spectrum. A NOESY spectrum (conditions as above) of the complex was recorded.

3.2.4: Comparison of DNA Photocleavage by Rh(phi) and Rh(chrysi) Complexes

Solutions of both $[Rh(bpy)_2(chrysi)]^{3+}$ and its phenanthrenequinone diimine analogue $[Rh(bpy)_2(phi)]^{3+}$ (concentrations increasing from 2×10^{-9} M to 2×10^{-5} M in 10 fold increments) were prepared in deionized water. DNA solutions of identical concentration were made containing the 5'-end-labeled oligonucleotide shown below

combined with one of two complementary strands, the first producing a properly matched duplex (X=G) and the second (X=C) producing a CC mismatch at the site indicated in boldface italic type.

*5′-GCCCTACGCA***C**GACATGATGCTGCGG-3′
3′-CGGGATGCGT***X***CTGTACTACGACGCC-5′

The labeled strand was added to an excess of its complement, annealed, and purified as the duplex on a non-denaturing, low temperature polyacrylamide gel. Each labeled duplex was combined with annealed carrier DNA of identical sequence to produce solutions of appropriate concentrations in 2x running buffer. Identical aliquots (10 μl) of each metal solution and each DNA solution were mixed (producing a solution 1x in running buffer, with equal concentrations of complex and oligonucleotide duplex ranging from 1 x 10^{-9} M to 1 x 10^{-5} M in 10 fold increments) 4 min before irradiation for 15 min at 365 nm. Dark control samples were prepared containing 1 x 10^{-5} M metal and DNA but were not irradiated; light control samples were prepared containing 1 x 10^{-5} M DNA and irradiated in the absence of metal complex. Samples were dried after irradiation and brought up in formamide loading dye before analysis by gel electrophoresis.

3.2.5: DNA Photocleavage Pattern and Post-Treatment Dependence of Various Rh(chrysi) Complexes

In order to more fully characterize the photoreactivity of all of the synthesized Rh(chrysi) complexes with DNA, two oligonucleotide duplexes were prepared, each containing a CC mismatch binding site in one of two possible orientations. In addition, a double guanine site, known to be sites of low oxidation potential where oxidative damage localizes, was included in each duplex.[3] The sequences of

duplexes is shown below with the CC mismatch binding cassette indicated by a horizontal bar and the GG site in bold-italic type:

5′-GCTAGCGTCGTCAACT***GG***AG-3′
3′-CGATCCCAGCAGTTGACCTC-5′

5′-GCTACCCTCGTCAACT***GG***AG-3′
3′-CGATGCGAGCAGTTGACCTC-5′

The oligonucleotides were purified by HPLC, end-labeled, and isolated as described above. All metal complexes (Δ-[Rh(bpy)$_2$(chrysi)]$^{3+}$, Δ-[Rh(phen)$_2$(chrysi)]$^{3+}$, and Δ-[Rh(chrysi)$_2$(phen)]$^{3+}$) used in irradiation experiments were purified by HPLC. Irradiation samples (10 μM DNA polymers, 5 μM Rh, 20 μl total volume) were prepared as described above in ammonium acetate buffer. Irradiations were performed at 313 nm (10 min), 365 nm (30 min), and 400 nm (30 min). After irradiation, 160 μl of deionized water was added to the samples and 90 μl was removed to a separate tube. Neat piperidine (10 μl) was added to the remaining sample and it was heated at 90°C for 30 min. Both samples were then dried under vacuum and assayed by gel electrophoresis as described. Additional photocleavage samples with Δ-[Rh(chrysi)$_2$(phen)]$^{3+}$ and the second oligonucleotide duplex were prepared by irradiation at 365 nm for 2 hr and piperidine treatment as described above.

3.2.6: Recognition of All Base Mismatches in a Single Sequence Context by [Rh(bpy)$_2$(chrysi)]$^{3+}$

Experiments to examine the recognition of all possible base mismatches in single DNA sequence contexts about the mismatch site were performed by two methods. The first experiments were performed on the 17mer 5'-end-labeled duplexes shown below:

*5′-GCGGAGTC***X**TGCATGTC-3′
3′-CGCCTCAG**Y**ACGTACAG-5′

where ***XY*** was substituted for the basepairs CC, CA, TT, AA, TC, TG, GA, GG, AT and GC. DNA photocleavage was performed with Δ– and Λ–$[Rh(bpy)_2(chrysi)]^{3+}$ (10 μM DNA duplex, 1 μM Rh complex, 1x running buffer) for 13 min at 365 nm after 11 min pre-equilibration. Samples were dried and electrophoresis was performed as described above.

In a second experiment, mismatch specific photocleavage was examined on a set of hairpin oligonucleotides as shown below:

$$\begin{array}{l} 5'\text{-GGCAGTXCTGGC}\overset{*}{\text{T}}\text{T}_{\text{T}} \\ 3'\text{-CCGTCAYGACCG}_{\text{TT}}\overset{*}{\text{T}} \end{array}$$

where ***XY*** was substituted with all the possible combinations of DNA base mismatches (CC, AC, CA,… etc.) and the two Watson-Crick base pairs. Photocleavage samples (6.7 μM DNA, 1.7 μM Δ- or Λ-$[Rh(bpy)_2(chrysi)]^{3+}$, 1x running buffer) were prepared 4 min before irradiation at 313 nm for 5 min. Samples were dried and electrophoresed as described.

3.3: Results and Discussion

3.3.1: Probing the Interaction of Chrysenequinone Diimine Complexes with B-form DNA Spectrophotometrically

The use of absorbance titrations is an established technique to examine the binding of dye molecules to DNA.[4] The octahedral metallointercalators of interest to this work, because of their visible absorbance transitions which are well separated from otherwise confounding DNA absorption bands, are ideally suited for this technique.

It has been previously demonstrated that the ligand centered π^* transition of phi complexes of rhodium(III) is dramatically affected upon binding to DNA; in addition to demonstrating significant hypochromicity upon binding, the transition also red shifts by 16 nm. These spectral changes have been used to extract average binding constants of phi complexes to B-DNA in the 3×10^5 M^{-1} regime.[4]

Titration of solutions of Δ-$[Rh(bpy)_2(chrysi)]Cl_3$ with either short oligonucleotide or sonicated calf thymus DNA produces spectral changes consistent with those observed for the phenanthrenequinone diimine complexes. Figure 3.4 shows representative data for the titration of the complex with calf thymus DNA; curves for oligonucleotide trials are qualitatively identical. Significant hypochromism is observed in the visible absorbance bands. At 380 nm, the wavelength of maximal change, binding to DNA causes a hypochromism of between 43 and 45% in the visible absorption of the complex. This value agrees very well with the comparable value of 42% measured for $[Rh(phen)_2(phi)]^{3+}$.[4] Unlike the phi complex, however, instead of a smooth red shift, the visible transition of $[Rh(bpy)_2(chrysi)]^{3+}$ broadens to the red to form a wider absorption envelope. This observation is not inconsistent with the asymmetry of the chrysi ligand compared to the symmetrical phi and is similar to the more complex spectroscopic behavior observed for this compound as a function of pH (see **2.3.2.2**).

Hypochromism upon binding to DNA is believed to result from the parallel orientation of the dipoles of DNA base pairs with the dipole of an *intercalated* dye.[5] As a result, the presence of hypochromism in the absorption spectrum is consistent with this binding mode. When the data are examined more quantitatively, the amount of hypochromism at the wavelength of maximal change (380 nm) can be plotted and a binding curve constructed. Such a curve, for the CT DNA data

included in Figure 3.4, is shown in Figure 3.5. When these binding data are converted to a fraction of metal complex bound, they can be fit and a value of the binding constant for B-form DNA estimated (Figure 3.6). The values measured both on the oligonucleotide and calf thymus DNA systems varied between 9.5 x 10^4 M^{-1} and 1.6 x 10^5 M^{-1} with an average value of 1.2 (+/- 0.4) x 10^5 M^{-1}. As expected for the sterically demanding chrysi ligand, this value is lower than that obtained for the rhodium(III) phi intercalators. It should be noted, however, that this value should be viewed as only an estimate of the affinity of the complex for B-DNA. Fitting these data to such a simple binding model is an oversimplification of the behavior which is likely occurring in solution; this can be observed in the systematic deviation from the fitted function at low concentrations of DNA (Figure 3.6). It is has also been previously demonstrated that certain rhodium(III) phi compounds, specifically $[Rh(phi)_2(bpy)]^{3+}$, can undergo complex spectral changes upon association with DNA.[4] Although it is known to bind intercalatively into the double helix, $[Rh(phi)_2(bpy)]^{3+}$ displays both hypochromism and hyperchromism depending on the ratio of metal complex to DNA.[4] In the present case, similar spectral complexity might make the simple equation of hypochromism with intercalative binding problematic.

3.3.2: NMR Examination of the Binding of Δ-$[Rh(bpy)_2(chrysi)]^{3+}$ to Mismatch Containing DNA

In an attempt to gain access to better information on the binding of Δ-$[Rh(bpy)_2(chrysi)]^{3+}$ to DNA, characterization was attempted by NMR spectroscopy. Examination of the binding of the complex to DNA by NMR, however, proved to be particularly challenging. Accompanying the stability and structural problems posed by mismatch containing DNA by itself, the examination of the bound complex in several oligonucleotide systems was made difficult by intermediate exchange

Figure 3.4. Absorbance Titration of Δ-[$Rh(bpy)_2(chrysi)]Cl_3$ with Calf Thymus DNA. Upon addition of DNA to a solution of metal complex, the visible absorption bands exhibit hypochromicity consistent with intercalative binding into DNA.

Figure 3.4:

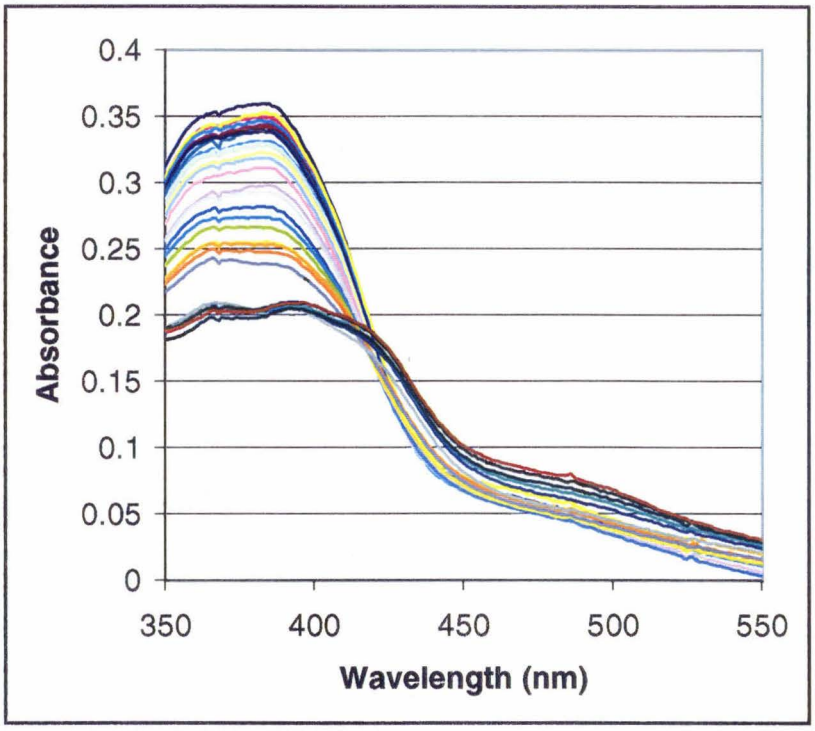

0.4
0.35
0.3
0.25
0.2
0.15
0.1
0.05
0
Absorbance
350
400
450
500
550
Wavelength (nm)

Figure 3.5. Binding Curve of Δ-[$Rh(bpy)_2(chrysi)]Cl_3$ for Calf Thymus DNA. The absorbance of a solution of metal complex at 380 nm is plotted as the amount of nucleic acid in the sample is increased. Regimes at low DNA concentration and high DNA concentration are apparent where very small changes in absorbance occur indicating that the experimental window included the entire progress of the complex binding curve.

Figure 3.5:

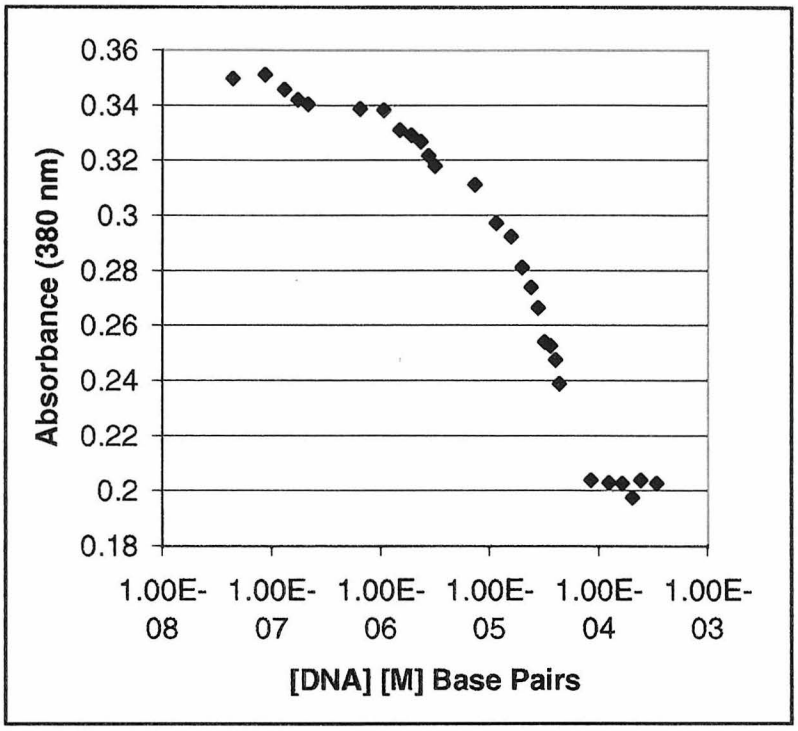
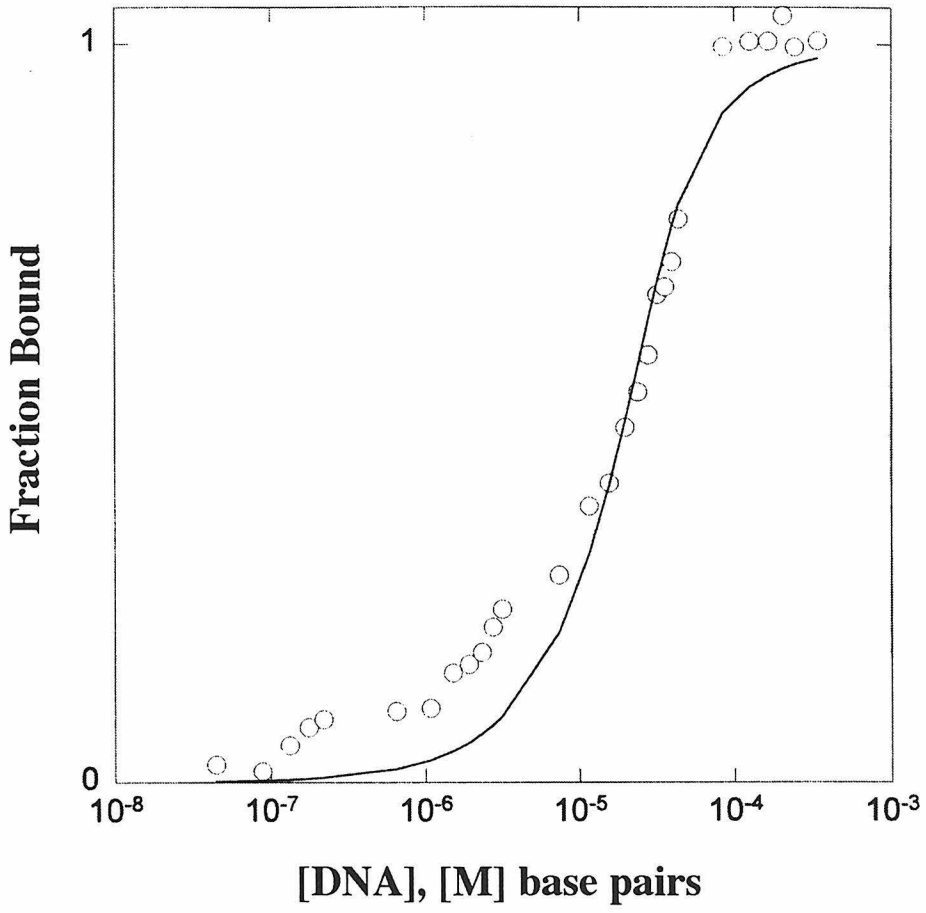

0.36
0.34
0.32
0.3
0.28
0.26
0.24
0.22
0.2
0.18
Absorbance (380 nm)
1.00E-08
1.00E-07
1.00E-06
1.00E-05
1.00E-04
1.00E-03
[DNA] [M] Base Pairs

Figure 3.6. Fitted Binding Curve of Δ-[Rh(bpy)$_2$(chrysi)]Cl$_3$ for Calf Thymus DNA. The data shown in Figure 3.5 were converted to percentage changes and normalized to represent the fraction of total metal complex in the sample bound to DNA. These data were fitted to equation 1 in the text where the dependent variable was the fraction of complex bound and the independent variable was $[DNA]_T$, the concentration of added DNA in base pairs.

Figure 3.6:



kinetics; in addition to serious exchange broadening, the heterogeneity of the spectra suggested that more than one complex was formed between certain small oligonucleotides and the rhodium complex. The small hairpin system shown in the experimental section above, however, proved to be somewhat more amenable to study. The system, particularly the polyether linker arm, was selected to minimize the number of unique bases in the hairpin to make interpretation as straightforward as possible.

As shown in Figure 3.7, when the metal complex is titrated into the DNA, formation of a complex can be observed with at least some peaks indicating relatively slow exchange behavior. Two of the clearest examples of this are highlighted with asterisks near 1.7 ppm and 3.8 ppm. Unlike the Δ–α–[Rh[(*R,R*)-Me_2trien]phi]$^{3+}$ - DNA system which was previously characterized by NMR,[8] it is also obvious from the 1D titration that the linewidths of the DNA resonances increase markedly upon addition of metal. As a result, the exchange rate for this metallointercalator-DNA system is likely significantly greater than that observed for the binding of the Me_2trien complex to DNA and parts of the spectra are definitely in the intermediate exchange regime. Given the destabilized nature of mismatch containing duplexes and the tendency of CC mispairs to be in dynamic equilibrium between intra- and extra-helical conformations even in the absence of a binding molecule, the fact that different regions of the molecule might have different exchange kinetics should not be surprising. Problems with exchange processes associated with mismatched bases in the NMR spectroscopy of DNA is well documented in the literature.[6] The effect that the exchange behaviors have on 2D data acquired on this system is obvious in Figures 3.8 and 3.9. Although the spectrum of the DNA alone is relatively clean (Figure 3.8), once the metal complex is added (Figure 3.9), many peaks disappear and the quality of the data deteriorates markedly.

Figure 3.7. 1D NMR Titration of a CC Mismatch Containing Hairpin Oligonucleotide with Δ-[$Rh(bpy)_2(chrysi)]Cl_3$. Although some peaks indicate slow exchange behavior (asterisks), the broadening of the DNA resonances clearly indicates that parts of this system are in intermediate exchange. However, chrysene intercalator peaks do appear (arrows) in a region upfield from all metal complex resonances when the compound is in solution (Figure 10). This shielding of these protons is consistent with an intercalative binding mode of the complex.

Figure 3.7:

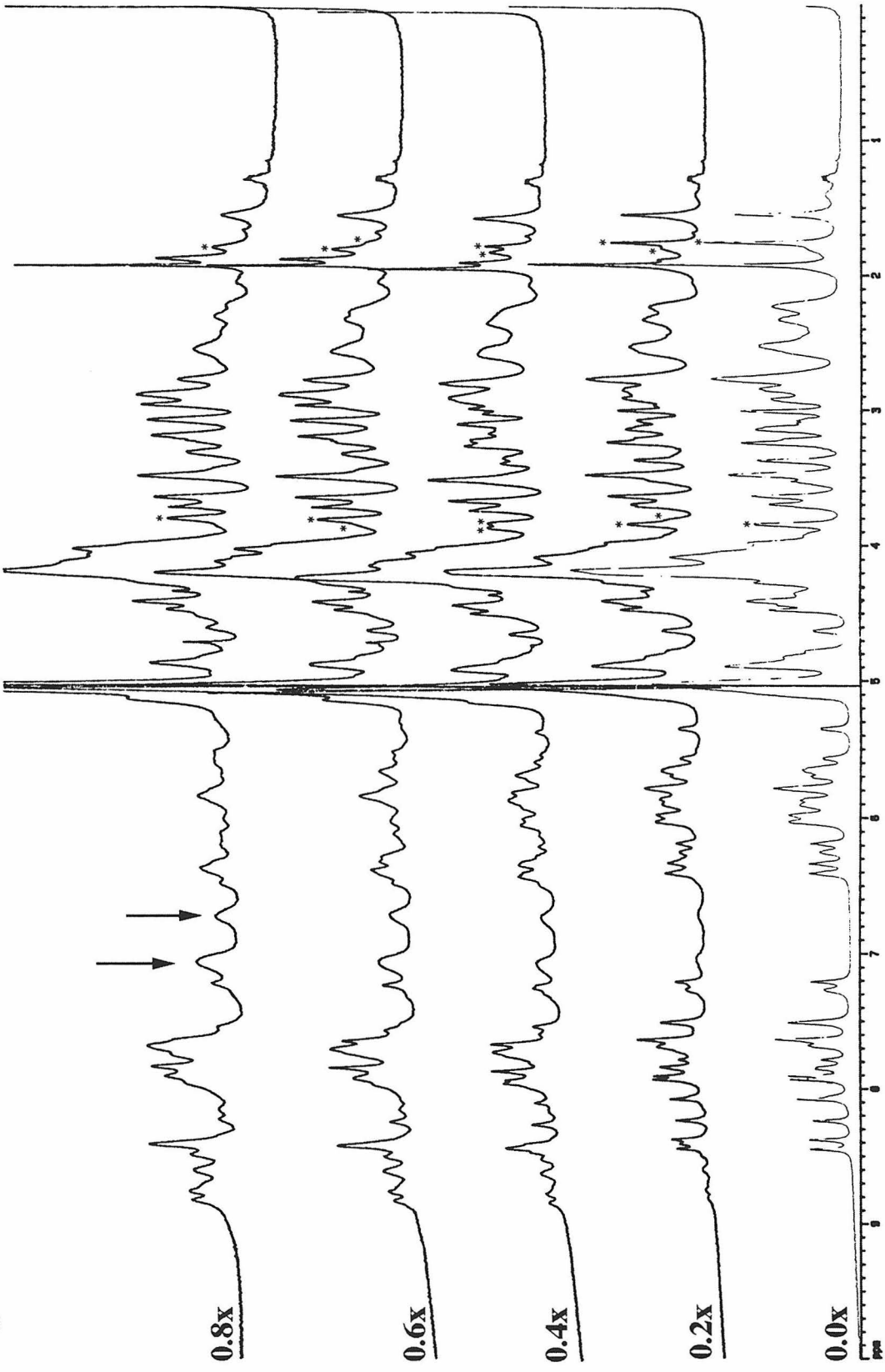


Figure 3.8. 2D NOESY spectrum of a CC Mismatch Containing Hairpin Oligonucleotide in the Absence of Rhodium Complex. Conditions of acquisition are included in the text. Note that in the free DNA spectrum, a large number of NOESY crosspeaks are observed.

Figure 3.8:

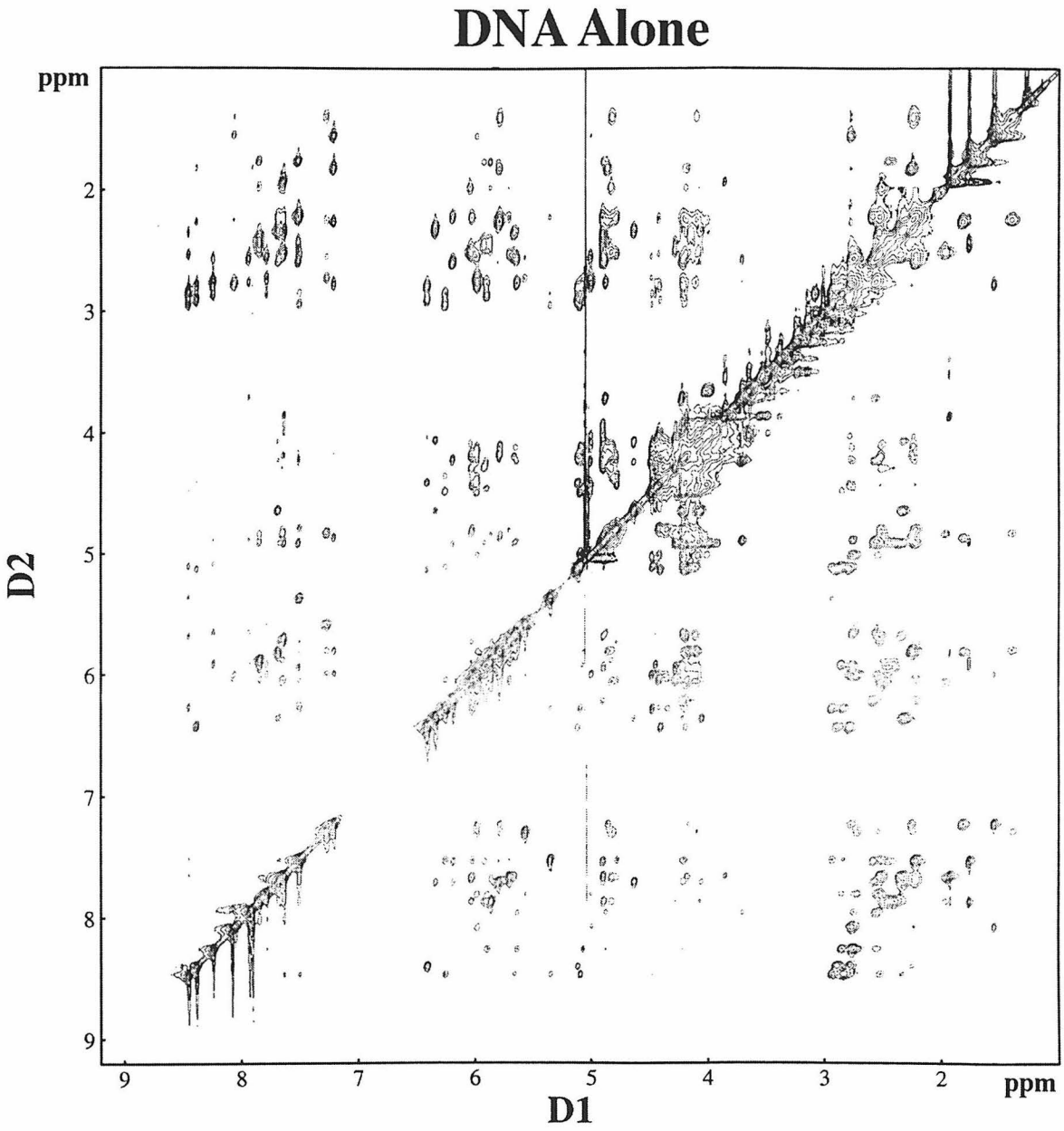
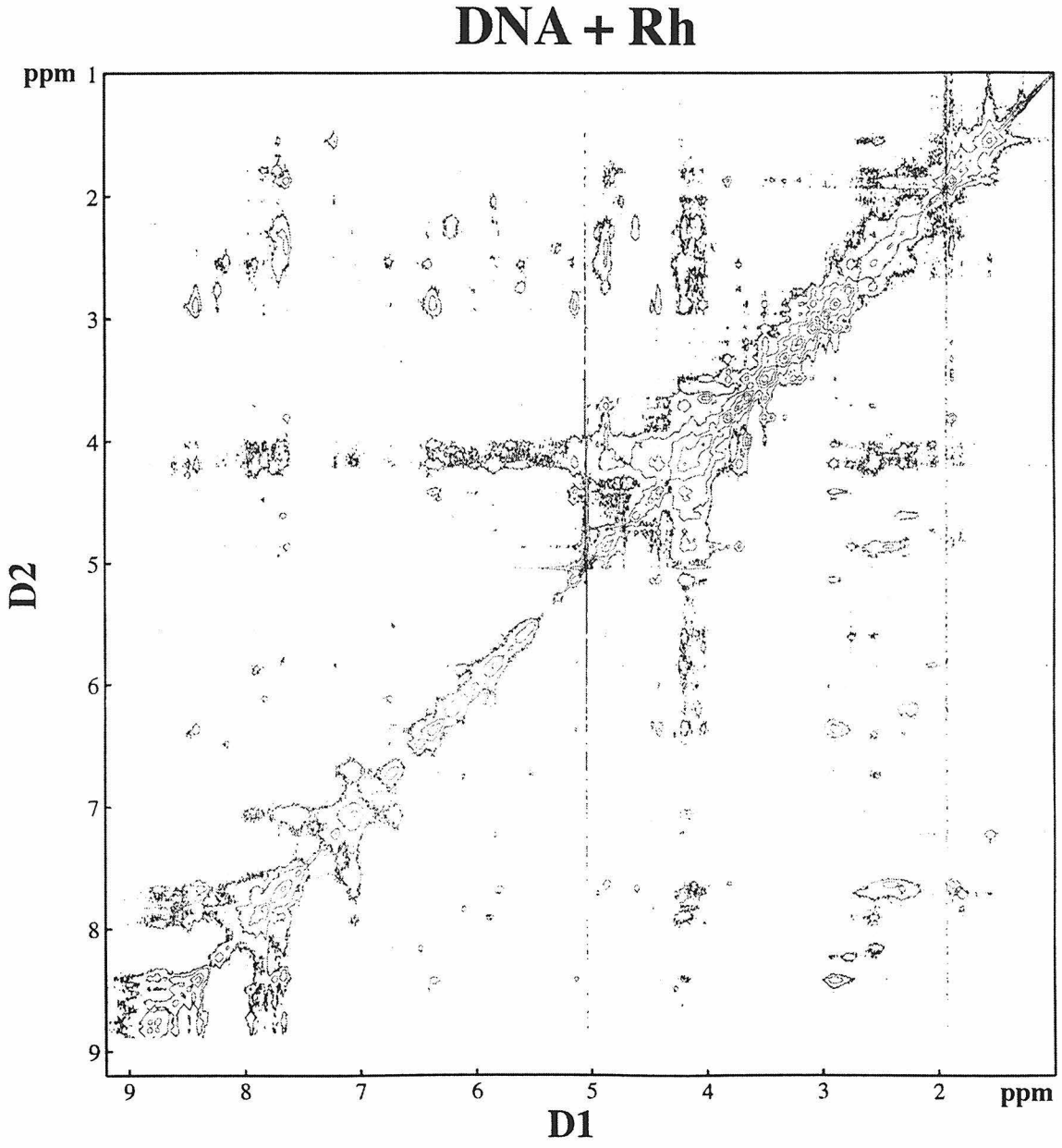


Figure 3.9. 2D NOESY spectrum of a CC Mismatch Containing Hairpin Oligonucleotide bound by Δ-[$Rh(bpy)_2(chrysi)]Cl_3$. Conditions of acquisition are included in the text. Note that in this spectrum, the number of NOESY crosspeaks is much reduced from the free DNA spectrum suggesting significant exchange broadening.

Figure 3.9:



Even considering the complications generated by this faster exchange behavior, some information about the binding of Δ-$[Rh(bpy)_2(chrysi)]^{3+}$ to this mismatch site can be extracted from this experiment. The 1D titration clearly includes the appearance of peaks in the 6.5-7.0 ppm region as the metal complex concentration is increased. These peaks are indicated by the arrows over the highest Rh concentration spectrum in Figure 3.7. The appearance of peaks in this region, which is significantly upfield from any resonances in the spectrum of the free metal complex (see Figure 3.10), is consistent with an intercalative mode of binding due to greater shielding of the intercalated protons by the ring currents of the bases above and below.[7-11]

Because of the non-optimal characteristics of this system, the 2D NOESY spectrum of the Rh-DNA complex (Figure 3.9) is difficult to interpret. Although assignments could be made of the spectrum of the DNA alone, the complexity of the metal containing spectrum made accurate assignments impossible. Some features can be identified, however. There are clear intramolecular NOE crosspeaks in the aromatic ligand-DNA H2'/H2'' region. These crosspeaks, between protons at 6.75 ppm-2.55 ppm and 6.71 ppm-2.91 ppm, lie in an area of the spectrum which is typically empty in DNA. These crosspeaks are highlighted in Figure 3.11. Unfortunately, because of exchange broadening coupled with chemical shift changes upon binding, the identification of other intramolecular NOE connectivities in more populated regions of the spectrum is not possible. Given that parts of the system are clearly in intermediate exchange, these additional connectivities may not even appear.

As a result, examination of the binding of Δ-$[Rh(bpy)_2(chrysi)]^{3+}$ at a CC mismatch by NMR suggests that the metal complex binds, as expected, by intercalation into the DNA base stack; this supports the spectroscopic studies discussed in the previous section which were also consistent with an intercalative binding mode. The fact that

Figure 3.10. 1D Proton NMR spectrum of Δ-[$Rh(bpy)_2(chrysi)]Cl_3$ in 25 mM phosphate buffer, pH 7.0. Note that no metal complex resonances appear below 7.0 ppm.

Figure 3.10:

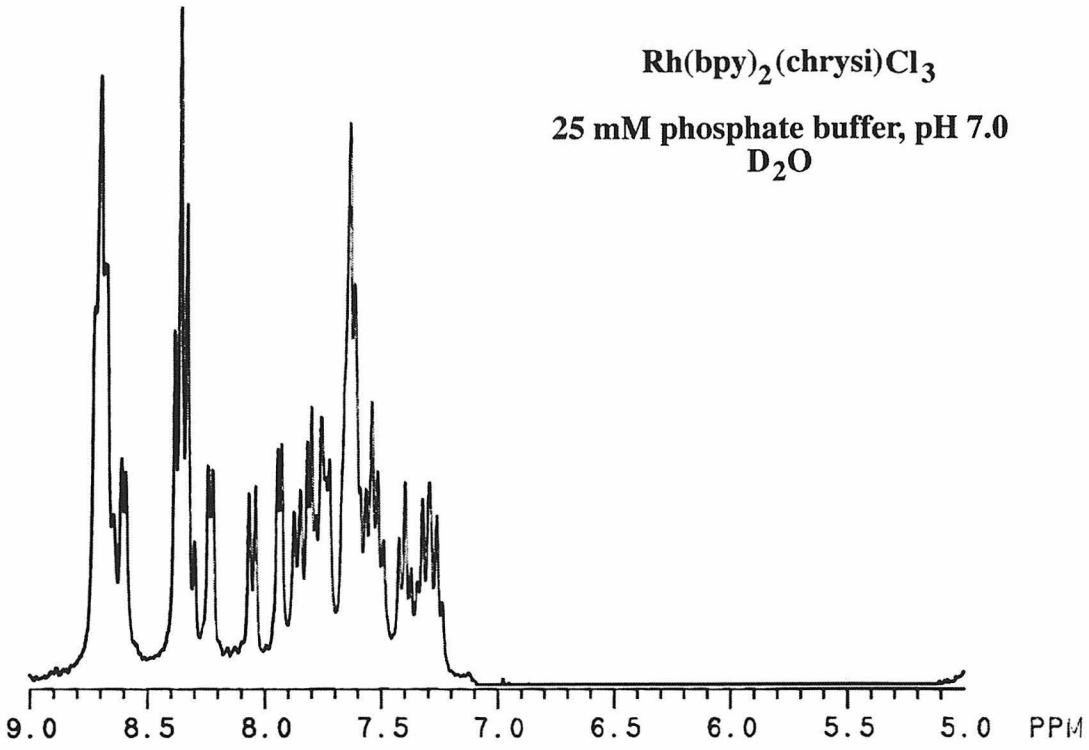
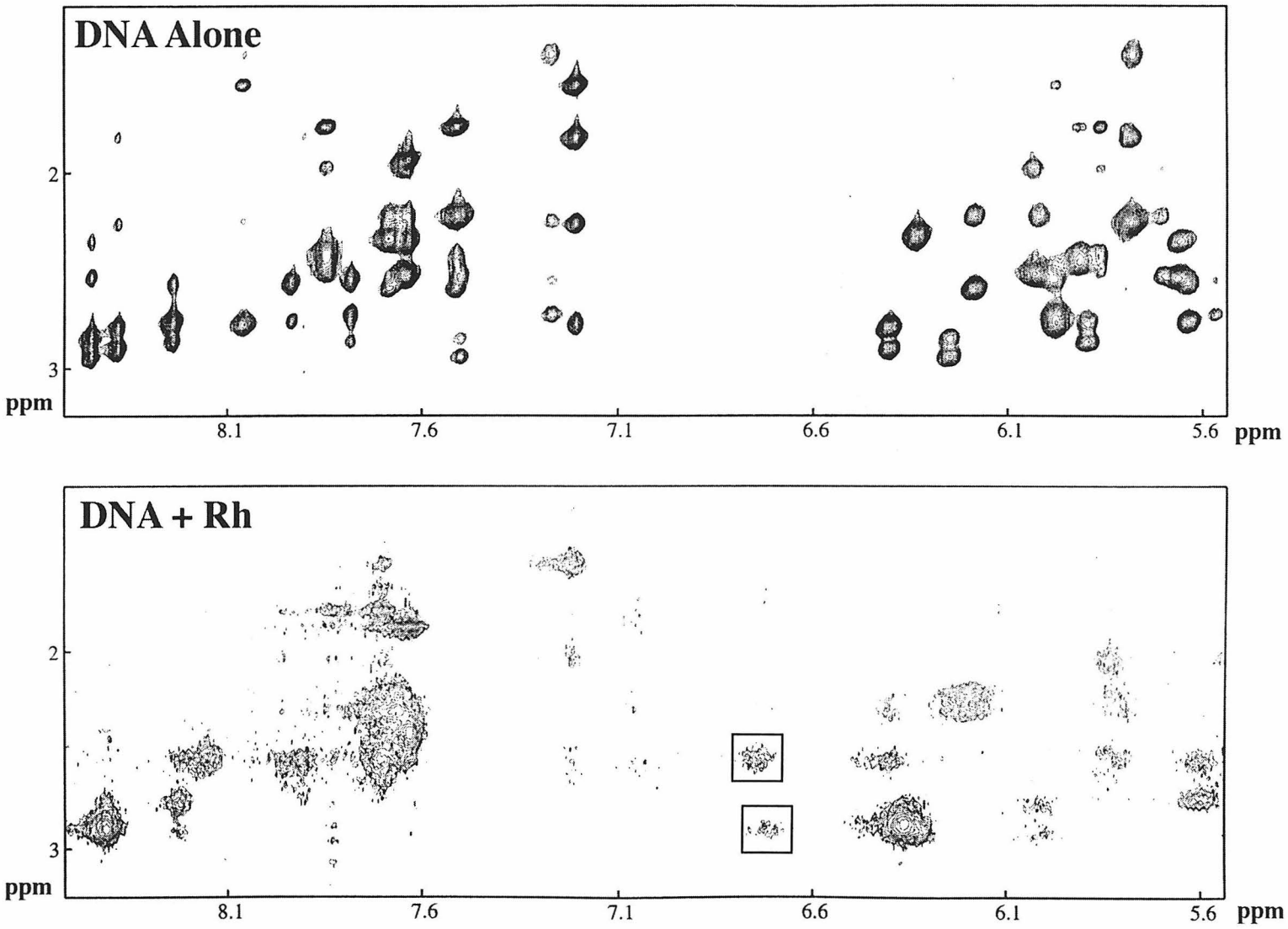

Rh(bpy)2(chrysi)Cl3
25 mM phosphate buffer, pH 7.0
D2O
9.0
8.5
8.0
7.5
7.0
6.5
6.0
5.5
5.0
PPM

Figure 3.11. Excised Section of the 2D NOESY Spectra of the Free and Metal Bound CC Mismatch Containing Hairpin Oligonucleotide. These sections of the NOESY spectra included in Figures 3.8 and 3.9 highlight the two intermolecular NOE connectivities (squares) that could be identified in the Δ-[$Rh(bpy)_2(chrysi)]Cl_3$ bound complex.

Figure 3.11:


DNA Alone
2
3
ppm
8.1
7.6
7.1
6.6
6.1
5.6
ppm
DNA + Rh
2
3
ppm
8.1
7.6
7.1
6.6
6.1
5.6
ppm

more definitive structural conclusions were not accessible from this data set, while disappointing, is fully consistent with the design strategy used in the construction of $[Rh(bpy)_2(chrysi)]^{3+}$. Given that the molecule is intended to interact with regions of the DNA which are destabilized or base pairs which are transiently extra-helical, it is not surprising that the bound complex and the DNA itself might have kinetic exchange properties which are non-optimal for characterization by NMR.

3.3.3: DNA Photocleavage by Chrysenequinone Diimine Complexes of Rhodium(III)

3.3.3.1: Comparison of DNA Photocleavage by Chrysenequinone Diimine and Phenanthrenequinone Diimine Complexes

The most noteworthy observation which emerges from the experimental results included as Figure 3.12 is that chrysenequinone diimine complexes of rhodium(III) cleave DNA upon photoactivation. Although there is no clear rationale why the addition of another aromatic ring to the side of the phenanthrenequinone diimine ligand would eliminate the DNA photocleavage properties of the resulting rhodium complexes, there was no way to predict, *a priori*, the photochemical properties of rhodium(III) chrysi complexes. The fact that this property was preserved in this new family of intercalators was of critical importance for the study of their DNA binding properties.

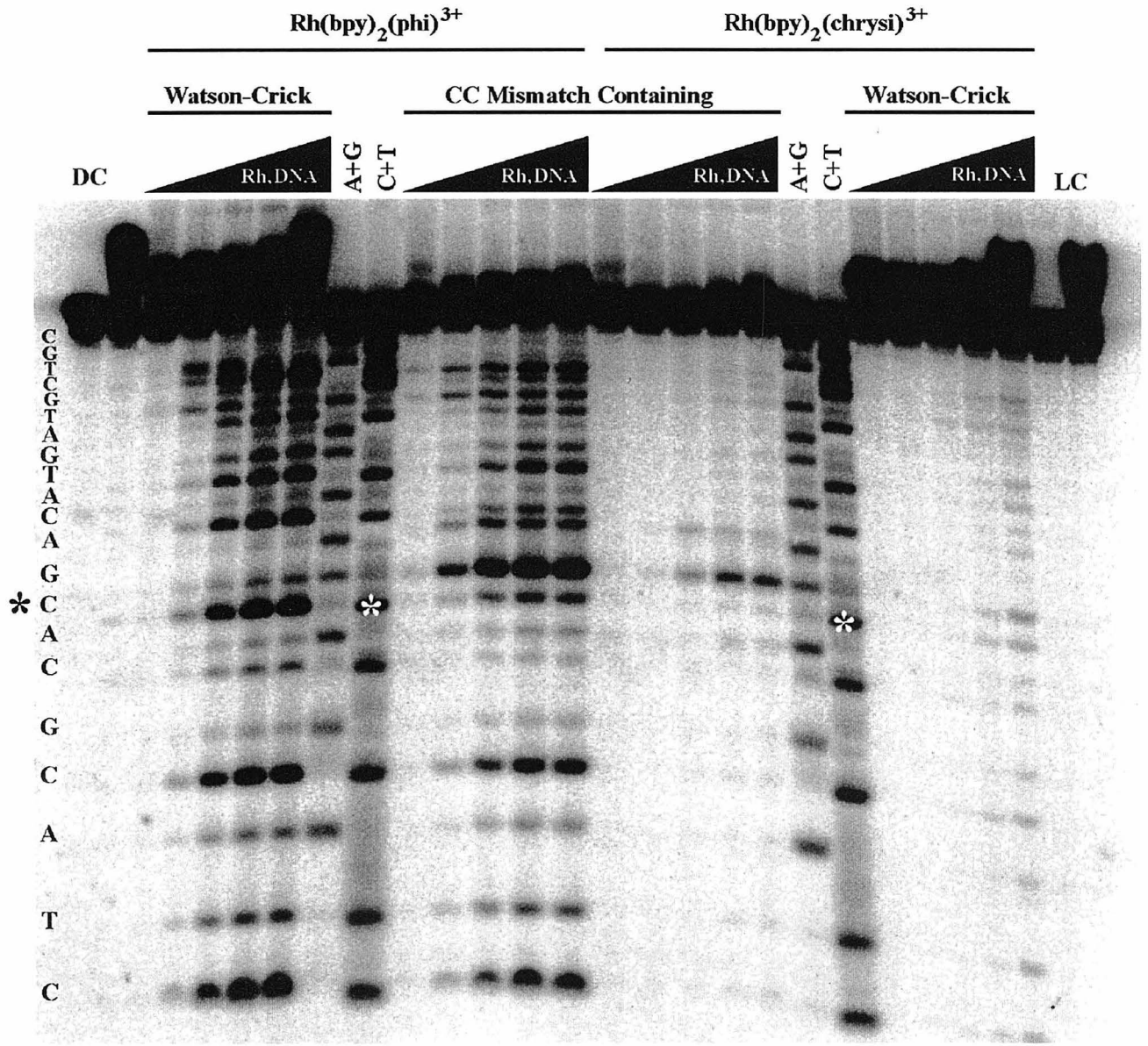
Examination of the sites of DNA photocleavage by $[Rh(bpy)_2(chrysi)]^{3+}$ and $[Rh(bpy)_2(phi)]^{3+}$ clearly demonstrates that the chrysenequinone diimine intercalating ligand produces dramatic changes in DNA cleavage specificity. As shown in Figure 3.12, $[Rh(bpy)_2(chrysi)]^{3+}$ specifically cleaves the DNA immediately to the 3' side of the CC base mismatch; in the absence of the mismatch site, no DNA cleavage is

Figure 3.12. DNA Photocleavage by $[Rh(bpy)_2(chrysi)]^{3+}$ and $[Rh(bpy)_2(phi)]^{3+}$ on DNA samples with and without a CC base mismatch. Samples of the 26mer 5'-endlabeled oligonucleotide:

5'-GCCCTACGCA***C***GACATGATGCTGCGG-3'

combined with one of two complementary strands (one producing a properly paired "Watson-Crick" duplex and the other containing a CC mismatch at the site indicated by boldface italic in the sequence and with asterisks on the gel) were irradiated for 15 min with equal concentrations of either $[Rh(bpy)_2(chrysi)]^{3+}$ and $[Rh(bpy)_2(phi)]^{3+}$. Sample concentrations increased from 1×10^{-9} M to 1×10^{-5} M in 10 fold increments as indicated by the gradient bars above the lanes. Lanes marked DC are DNA samples incubated with metal in the absence of light; those labeled LC are DNA samples irradiated in the absence of metal. Note the high level of specificity shown by the chrysi complex for the mismatch site; in addition, in the absence of a mismatch, cleavage of the DNA by the complex is only observed at the highest concentrations. In contrast, although the phi complex does show some affinity for the mismatch site, its level of specificity is very low as numerous other high affinity sites for the complex exist both in the presence and the absence of the mispaired bases.

Figure 3.12:


Rh(bpy)2(phi)3+
Rh(bpy)2(chrysi)3+
Watson-Crick
CC Mismatch Containing
Watson-Crick
DC
Rh,DNA
A+G
C+T
Rh,DNA
Rh,DNA
A+G
C+T
Rh,DNA
LC
CGTCGTAGTACAGCACGCATC

observed until the highest concentrations of oligonucleotide (10 μM) and metal complex (10 μM) are reached. In contrast, the parent complex, $[Rh(bpy)_2(phi)]^{3+}$, has a large number of intense cleavage sites even in the absence of the base mismatch. There are significant changes in the cleavage preferences of the phi compound in the presence of the mismatch, including an intense band at the same 3' base where cleavage by the chrysi complex is observed. Although this does indicate a probable high *affinity* interaction of the rhodium(III) phi complex with the mismatch site, the *specificity* of this interaction is low. In contrast, $[Rh(bpy)_2(chrysi)]^{3+}$ interacts with the mismatch site with a high degree of specificity; as shown in Figure 3.12, the mismatch specific product is, by far, the predominant cleavage product.

In addition to demonstrating that $[Rh(bpy)_2(chrysi)]^{3+}$ does display the desired cleavage behavior and possesses a dramatically increased specificity over an analogous phi intercalator, some insights regarding recognition design can also be drawn from this experiment. The rationale behind the design of the chrysi ligand was that the increased breadth of the intercalating ligand would disfavor binding to B-form DNA. This is clearly the case. Examining only the photocleavage reactions on B-form DNA (sets of lanes to each side of the gel), it is clear that, in the high concentration limit, the binding site preferences of the chrysi and phi compounds are the same. The faint bands that appear in the high concentration $[Rh(bpy)_2(chrysi)]^{3+}$ photocleavage reactions correspond in mobility to much darker bands observed in the phi lanes. Given what is known about the binding of transition metal complexes to DNA, it is not unexpected that these two compounds would bind to the same sites on B-DNA; since their ancillary ligands are the same, their shape-selective preferences for binding are likely to be similar. That these cleavage products only appear at much higher concentration of metal complex and DNA indicate that the modification

to the intercalator directly disfavors binding to B-form DNA and that this mechanism is an important source of the molecule's specificity. It should also be noted that the similar shape-selective cleavage behavior in the high concentration limit also suggests that the chrysi complex is interacting with the DNA in a similar manner, i.e., with a major groove orientation, as its phi analogue. Confirmation of this binding mode hypothesis, however, would require significant additional structural characterization.

In a complementary manner, the behavior of the two complexes in the presence of a CC mismatch (center sets of lanes) also validates the assumptions which underlie the design strategy. Both the phi and chrysi compounds show strong photocleavage at the base 3' to the mismatch site. Furthermore, in both compounds this band is the *most* intense cleavage site on the mismatch containing oligonucleotide. This result is not unexpected. As discussed in previous section on small molecule recognition of nucleic acids, all intercalators must disrupt the structure of DNA in order to bind. This disruption, which includes forcing apart a stacked base pair and disturbing the winding of the helix, has an associated energetic cost which is compensated for by the binding energy of the intercalator interacting with the core of the helix. The disorder which exists at DNA mismatch sites must, almost by definition, favor the binding of intercalating molecules. Because of the reduced structure and stacking at these sites, a portion of the cost associated with binding will "have already been paid." This observation is consistent with current hypotheses of protein recognition of disordered sites in DNA as well (See **1.3**.) As discussed above, however, the difference between the two molecules is in their level of specificity. The phi compound, even with an energetic incentive to bind at the mismatch, still binds and cleaves at numerous other sites on the DNA. Conversely, the chrysi complex, is selective for the mismatch site because of its disincentive to bind to B-DNA. Once again,

the similarity in the cleavage patterns of the phi and chrysi complexes at the mismatch site (with both showing a strong 3' asymmetry) suggests that they are binding in a similar manner; in the geometrical uncertainty about a mismatch site, however, this similarity is more difficult to interpret than in the B-DNA case discussed in the previous paragraph.

3.3.3.2: DNA Photocleavage by Chrysenequinone Diimine Containing Complexes is Observed Primarily Near the Site of Destabilization in DNA

The results of DNA cleavage by Δ-$[Rh(bpy)_2(chrysi)]^{3+}$, Δ-$[Rh(phen)_2(chrysi)]^{3+}$, and Δ-$[Rh(chrysi)_2(phen)]^{3+}$ on CC mismatch containing oligonucleotide duplexes are included as Figures 3.13-3.15. The data in this single set of gels include several unexpected and interesting results. As such, in addition to considering these experiments in their own right, the following discussion serves to introduce points which will be subsequently explored in the remainder of the thesis.

All of the Chrysi Complexes Cleave DNA Proximal to the Mismatch Site: At the most basic level, it is clear that all three of these complexes cleave DNA upon photoactivation and, in contrast to some DNA cleavage chemistries, without the necessity of post treatment by piperidine. Examining the reactions for each of the complexes at 313 nm without piperidine treatment, it is clear that there are both similarities and differences in the cleavage behavior of the compounds. As expected from their similar geometry, the cleavage produced by Δ-$[Rh(bpy)_2(chrysi)]^{3+}$ and Δ-$[Rh(phen)_2(chrysi)]^{3+}$ are very similar. Both compounds cleave very strongly at the 3' C of the 5'-C***C***C-3' (where the italicized C is the mismatched base) (Figures 3.14 & 3.15); when the site is inverted, both compounds still cleave the labeled DNA strand although less intensely. This strand preference for photocleavage, which is not unreasonable given the significant asymmetry of the chrysi intercalating ligand,

Figure 3.13. Wavelength and Piperidine Post-Treatment Dependence of DNA Photocleavage by Δ-$[Rh(phen)_2(chrysi)]^{3+}$ and Δ-$[Rh(chrysi)_2(phen)]^{3+}$ in the Binding Site 5'-G***C***G-3'. DNA photocleavage was performed on the 5'-endlabeled DNA oligonucleotide 5'-GCTAG***C***GTCGTCAACTGGAG-3' annealed to its complement. The CC mismatch binding site is underlined with the mismatched C itself indicated by bold-italic type. Samples (10 μM DNA polymers, 5 μM Rh, 20 μl total volume) were irradiated at 313 nm (10 min), 365 nm (30 min), or 400 nm (30 min). After irradiation, the samples were split and half was treated with 1 M piperidine (90°C for 30 min). DC lanes indicate samples incubated with metal complex in the absence of light; LC lanes indicate samples which were irradiated in the absence of metal complex. Both treated and untreated samples were dried before resuspension and electrophoresis as described in the text.

Figure 3.13:

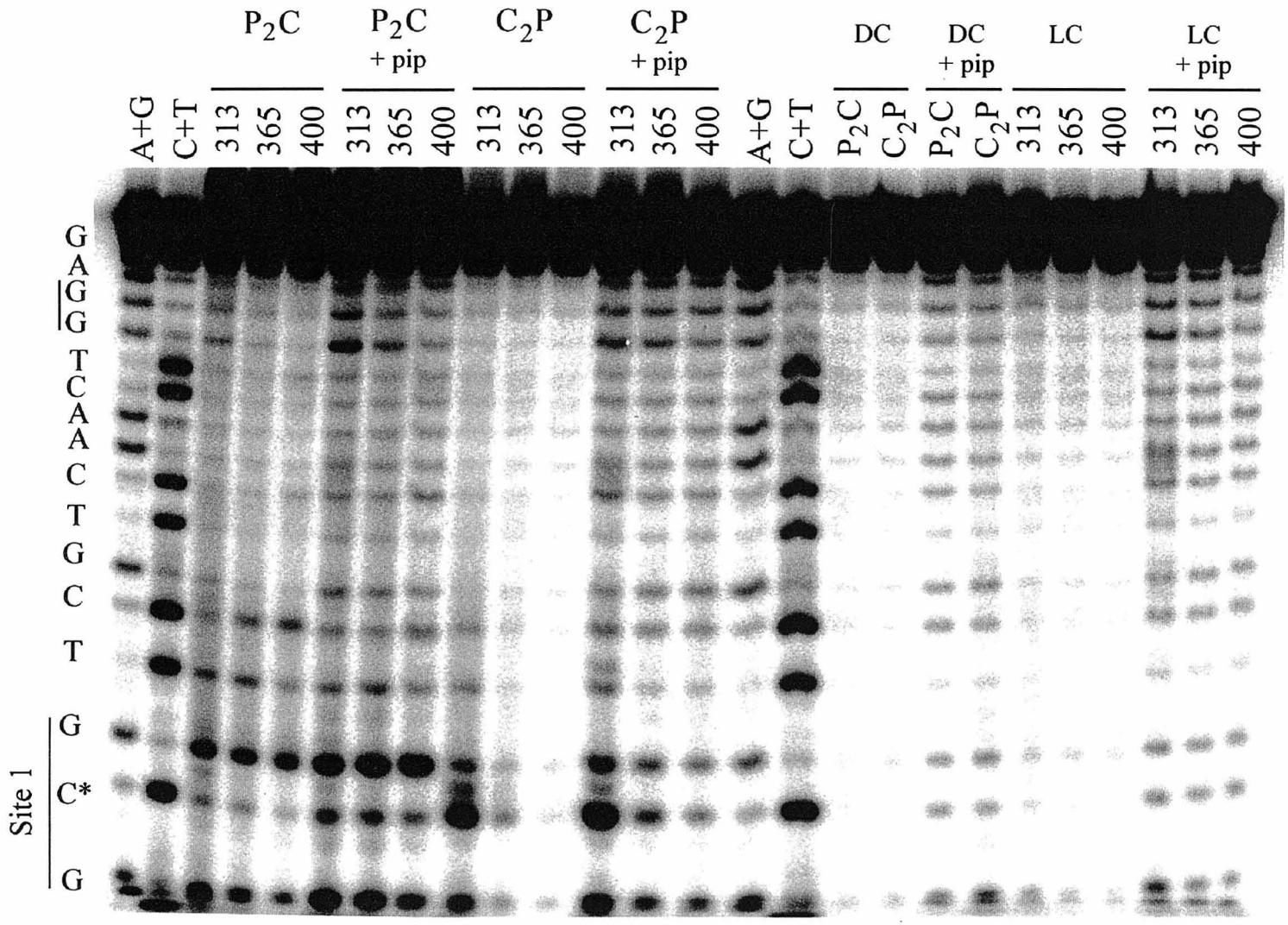

P2C
P2C + pip
C2P
C2P + pip
DC
DC + pip
LC
LC + pip
A+G
C+T
313
365
400
P2C
C2P
Site 1
G
A
G
G
T
C
A
A
C
T
G
C
T
G
C*
G

Figure 3.14. Wavelength and Piperidine Post-Treatment Dependence of DNA Photocleavage by Δ-$[Rh(phen)_2(chrysi)]^{3+}$ and Δ-$[Rh(chrysi)_2(phen)]^{3+}$ in the Binding Site 5'-C***C***C-3'. DNA photocleavage was performed on the 5'-endlabeled DNA oligonucleotide 5'-GCTAC***C***CTCGTCAACTGGAG-3' annealed to its complement. The CC mismatch binding site is underlined with the mismatched C itself indicated by bold-italic type. Samples (10 μM DNA polymers, 5 μM Rh, 20 μl total volume) were irradiated at 313 nm (10 min), 365 nm (30 min), or 400 nm (30 min). After irradiation, the samples were split and half was treated with 1 M piperidine (90°C for 30 min). DC lanes indicate samples incubated with metal complex in the absence of light; LC lanes indicate samples which were irradiated in the absence of metal complex. Both treated and untreated samples were dried before resuspension and electrophoresis as described in the text.

Figure 3.14:

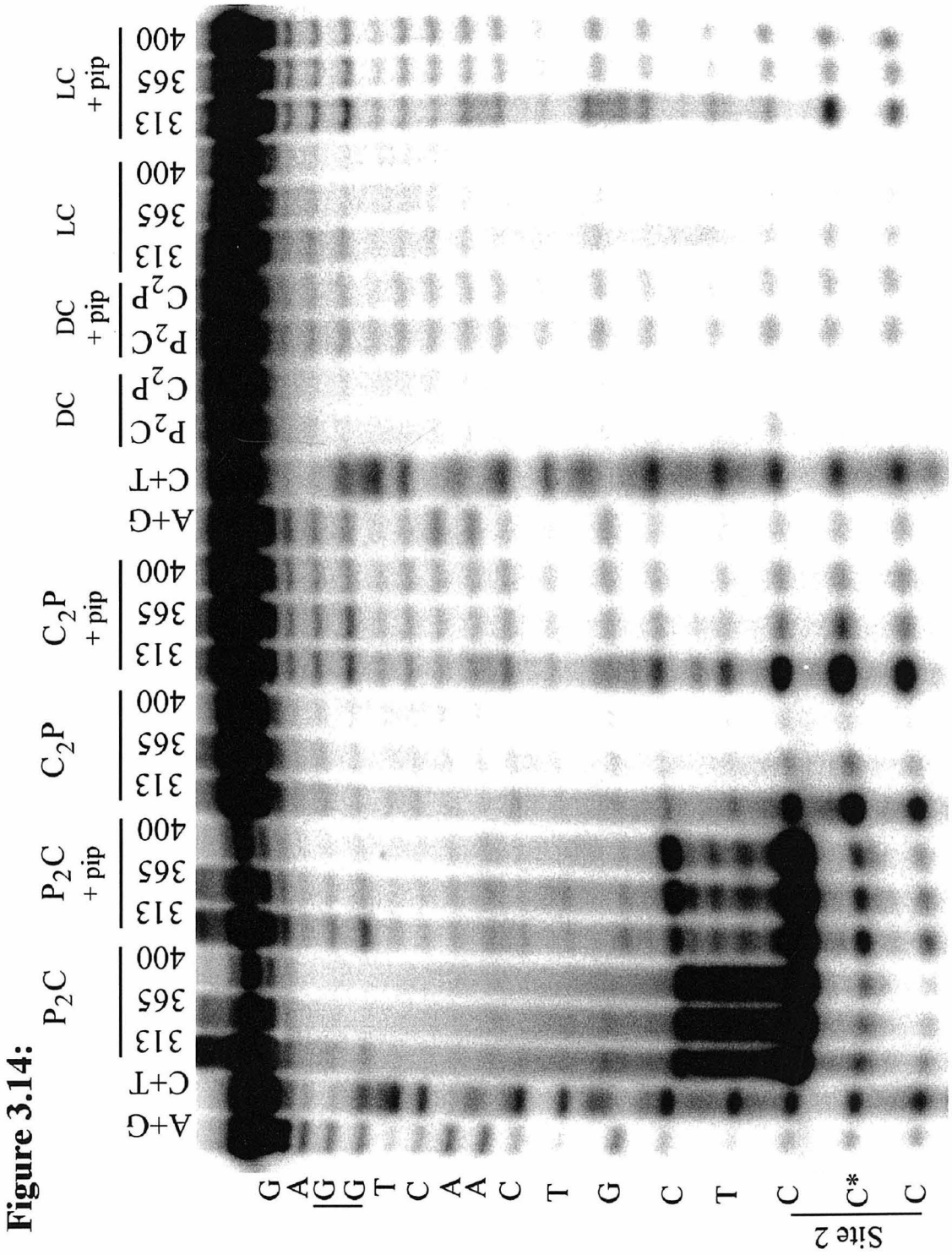

A+G
C+T
P2C
313
365
400
P2C + pip
313
365
400
C2P
313
365
400
C2P + pip
313
365
400
A+G
C+T
DC
P2C
C2P
DC + pip
P2C
C2P
LC
313
365
400
LC + pip
313
365
400
G A G G T C A A C T G C T C C* C
Site 2

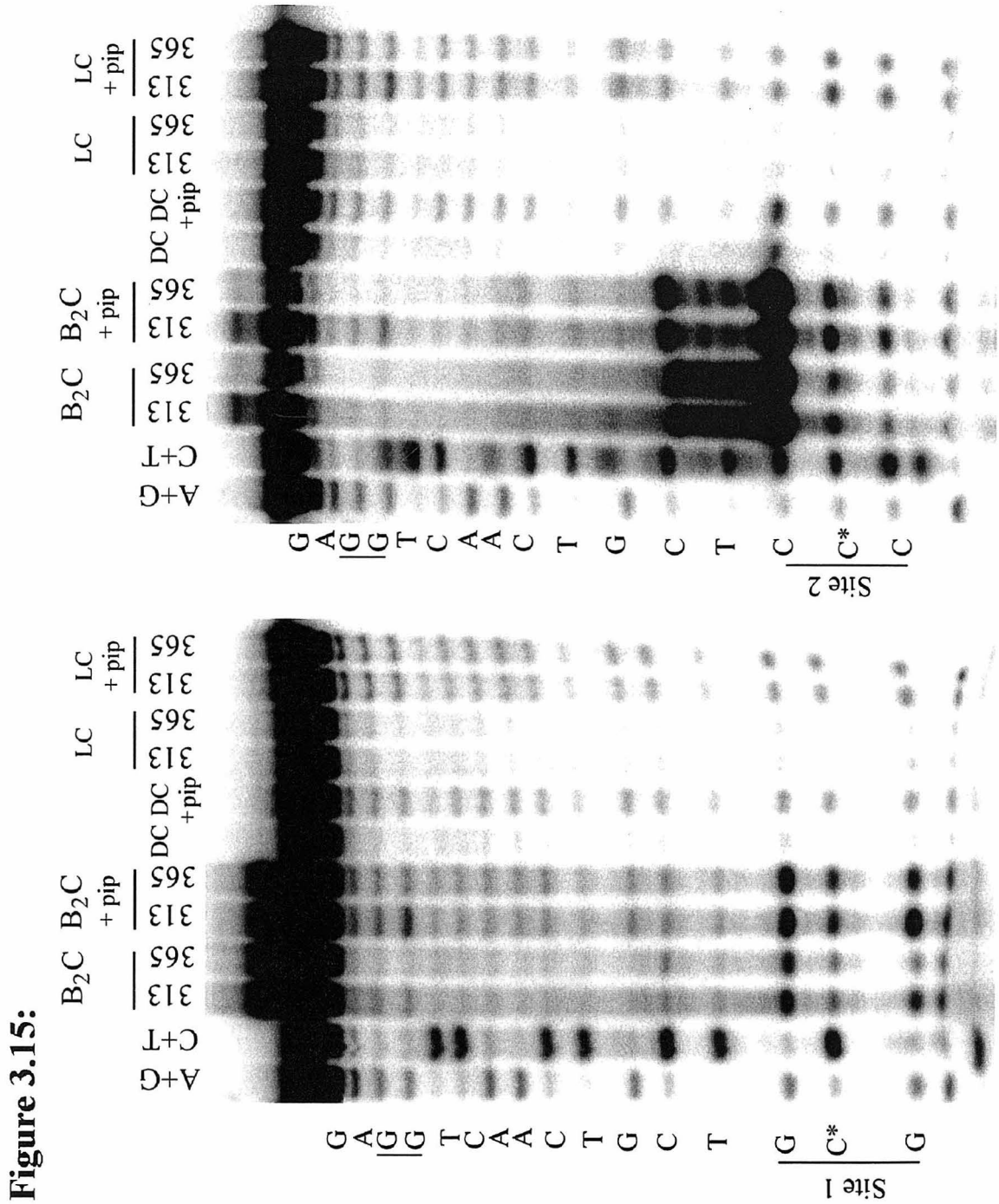
Figure 3.15. Wavelength and Piperidine Post-Treatment Dependence of DNA Photocleavage by Δ-$[Rh(bpy)_2(chrysi)]^{3+}$ at the Binding Sites 5'-G***C***G-3' and 5'-C***C***C-3'. DNA photocleavage was performed on the 5'-endlabeled DNA oligonucleotides,

5'-GCTAC***C***CTCGTCAACTGGAG-3'

5'-GCTAG***C***GTCGTCAACTGGAG-3'

annealed to their complements. The CC mismatch binding sites are underlined with the mismatched C bases indicated by bold-italic type. Samples (10 μM DNA polymers, 5 μM Rh, 20 μl total volume) were irradiated at 313 nm (10 min) and 365 nm (30 min). After irradiation, the samples were split and half was treated with 1 M piperidine (90°C for 30 min). DC lanes indicate samples incubated with metal complex in the absence of light; LC lanes indicate samples which were irradiated in the absence of metal complex. Both treated and untreated samples were dried before resuspension and electrophoresis as described in the text.

Figure 3.15:


A+G
C+T
B2C
313
365
B2C + pip
313
365
DC
DC +pip
LC
313
365
LC + pip
313
365
G A G G T C A A C T G C T C C* G
Site 1
Site 2

will be explored more comprehensively in the following chapter. When irradiated at 313 nm, Δ-$[Rh(chrysi)_2(phen)]^{3+}$ also cleaves DNA although with a markedly different specificity than the mono-chrysi complexes (Figures 3.13 & 3.14). Independent of the orientation of the site, the bis-chrysi compound cleaves strongly at the mismatched C base. In addition, it also cleaves at the bases to either side of the mismatch although less intensely. Such changes in recognition specificity are similar to those observed with the phi analogues of these compounds. $[Rh(phi)_2(phen)]^{3+}$ is essentially sequence neutral compared to $[Rh(phen)_2(phi)]^{3+}$ because of the two compounds' very different steric requirements for binding. In a similar fashion, the markedly different cleavage patterns between the mono- and bis-chrysi compounds are likely the result of differences in binding geometry at the mismatch site.

Direct Photocleavage by Mono-Chrysi Compounds Shows an Unexpected Wavelength Behavior: When the wavelength of irradiation is increased beyond the high energy UV, direct photocleavage of DNA by $[Rh(chrysi)_2(phen)]^{3+}$ is no longer observed. This can be clearly seen in Figures 3.13 and 3.14 where photocleavage by the bis-chrysi complex is markedly reduced at 365 nm and undetectable at 400 nm. This observation corresponds to behavior seen in previously reported experiments with $[Rh(phi)_2(phen)]^{3+}$.[4] In contrast, both the phen and bpy compounds continue to cleave DNA very efficiently with 365 nm irradiation; the phen compound also cleaves upon irradiation at 400 nm (Figure 3.13, 3.14 & 3.15). A more complete exploration of the wavelength dependence of cleavage by $[Rh(bpy)_2(chrysi)]^{3+}$ follows in Chapter 5; as observed for the phen complex, $[Rh(bpy)_2(chrysi)]^{3+}$ also cleaves DNA with wavelengths well into the visible region of the spectrum.

Also worthy of note in these results is the fact that, in the samples of DNA irradiated with either Δ-$[Rh(bpy)_2(chrysi)]^{3+}$ or Δ-$[Rh(phen)_2(chrysi)]^{3+}$ bound to the 5'-C***C***C-3' site at 365 or 400 nm (Figures 3.14 & 3.15), significantly more than half of the full length DNA band has been cleaved 3' to the mismatch site. Since the ratio of Rh complex to DNA is held constant in all of the samples at 1:2, this level of cleavage would require that a single metal complex cleave more than one DNA polymer. This observation has also been confirmed at much lower ratios of metal complex to DNA polymers and is discussed in greater detail in Chapter 5.

Treatment with Piperidine Causes Changes in DNA Cleavage Pattern: It has been previously observed that irradiation of $[Rh(phi)_2(bpy)]^{3+}$ bound to DNA with 365 nm light results in oxidation of guanine bases by photoinduced electron transfer.[3] Conversion of these oxidative lesions to DNA strand breaks which can be resolved by electrophoretic methods requires treatment with hot piperidine. As a result, the effect of piperidine treatment on the DNA cleavage patterns produced by these three compounds was explored. In the case of the $[Rh(bpy)_2(chrysi)]^{3+}$ and $[Rh(phen)_2(chrysi)]^{3+}$ complexes, piperidine treatment after irradiation causes small changes in the observed photocleavage pattern. In the samples bound to the 5'-C***C***C-3' site (Figure 3.14 & 3.15), treatment with the base "cleans up" the broad smear of cleavage products at the cytosine bases 3' to the mismatch site and resolves it into two clear bands. This is likely due to subsequent conversion of base labile cleavage products to species with less heterogeneous mobility on the electrophoretic gel. In the case of the 5'-G***C***G-3' site, piperidine treatment generates an enhancement of cleavage at the guanines to either side of the mismatch site. This level of piperidine sensitive guanine damage is comparable to that observed when similar experiments are performed with $[Rh(phen)_2(phi)]^{3+}$.[12] Although there appears to be some formation of piperidine-sensitive damage at the double guanine site on the other end

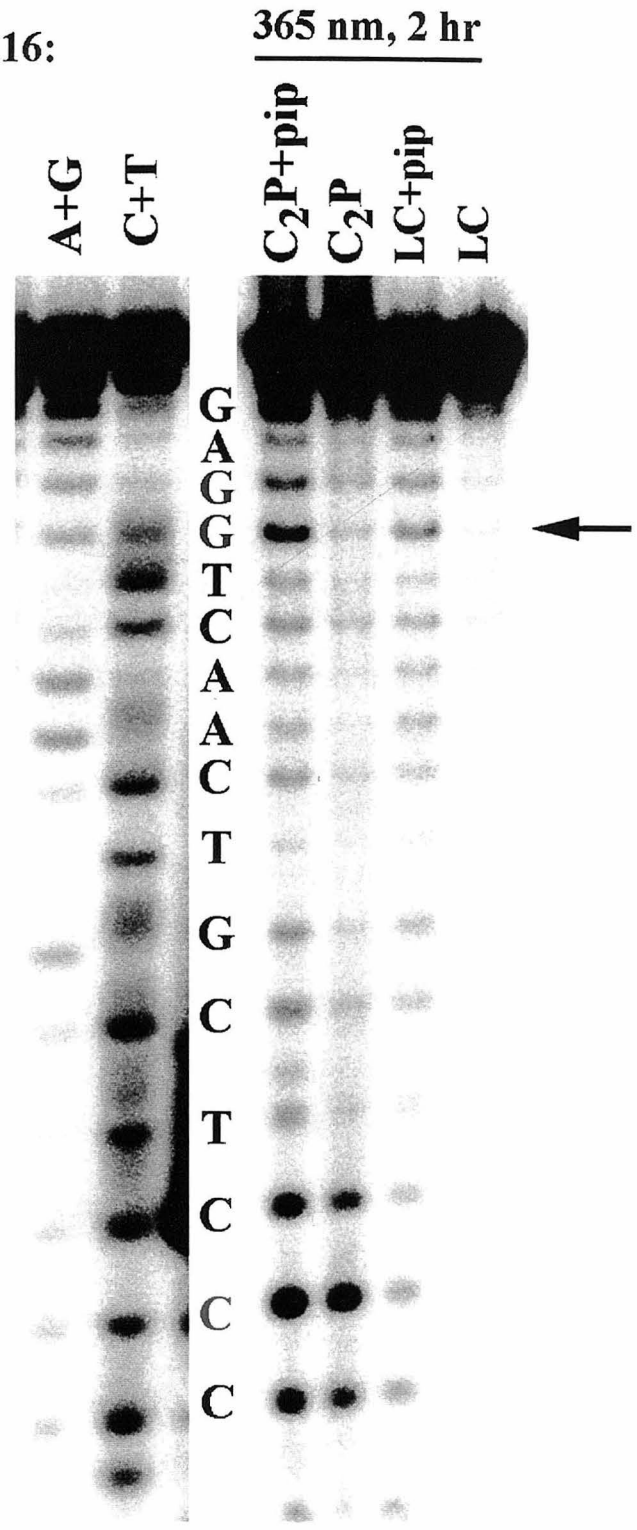
of the duplex, this damage is not greater than that observed in the non-metal containing light controls.

Because of its similar structure to $[Rh(phi)_2(bpy)]^{3+}$, it was expected that photolysis with $[Rh(chrysi)_2(phen)]^{3+}$ would generate piperidine-sensitive guanine damage, possibly at sites separated from the binding site of the complex. As a result, the relative lack of such damage in the experiments in Figures 3.13 and 3.14 was somewhat surprising. With both binding site orientations, only very small amounts of piperidine sensitive damage (over control samples) were observed. Subsequent experiments with lengthened irradiation times did produce a significant amount of guanine damage. As shown in Figure 3.16, irradiation of the complex with DNA for 2 hr produced preferential damage at the 5' G of a guanine-guanine site 11 base pairs from the mismatch site.

Overview of DNA Photocleavage Properties of Chrysenequinone Diimine Complexes: Like their phenanthrenequinone diimine counterparts, it is clear that chrysenequinone diimine complexes have a very rich photoreactivity with DNA. In all three complexes which were examined, direct photocleavage is primarily observed near the site of the DNA mismatch. This observation is consistent with the design strategy for these molecules and suggests that the chrysi ligand does, indeed, confer selectivity for destabilized regions of DNA independent of the ancillary ligands on the complex. The observations that the mono-chrysi complexes continue to cleave DNA even with irradiation with visible light and seem to do so non-stoichiometrically suggests that reaction pathways must exist which result in DNA cleavage without concurrent destruction of the metal complex. Furthermore, although the changes in photocleavage pattern after piperidine treatment are small, the production of base sensitive lesions at guanine bases suggests another possible reaction manifold. These

Figure 3.16. Piperidine Sensitive Guanine Damage Induced by Irradiation of $[Rh(chrysi)_2(phen)]^{3+}$ bound to DNA with 365 nm light. DNA photocleavage was performed on the 5'-endlabeled DNA oligonucleotide 5'-GCTA<u>C***C***C</u>TCGTCAACTGGAG-3' annealed to its complement. The CC mismatch binding site is underlined with the mismatched C itself indicated by bold-italic type. Samples (10 μM DNA polymers, 5 μM Rh, 20 μl total volume) were irradiated at 365 nm (2 hr). After irradiation, the samples were split and half was treated with 1 M piperidine (90°C for 30 min). LC lanes indicate samples which were irradiated in the absence of metal complex. Both treated and untreated samples were dried before resuspension and electrophoresis as described in the text.

Figure 3.16:



behaviors are consistent with previous work done on phi analogues of these compounds.[12]

3.3.3.3: Recognition of Multiple Mismatches in a Single Sequence Context by $[Rh(bpy)_2(chrysi)]^{3+}$

Photocleavage data for the enantiomers of $[Rh(bpy)_2(chrysi)]^{3+}$ on oligonucleotides containing varied DNA base mismatches is included in Figures 3.17 and 3.18. From these data, it is clear that the complex specifically recognizes a large fraction of the possible base mispairs. In the first experiment (Figure 3.17), for example, the strongest cleavage is observed with the Δ enantiomer on the duplex containing the CC mismatch to the 3' side of the mispaired base. Similar but less intense cleavage is observed at the other pyrimidine-pyrimidine mismatches TT and TC. CA, the single purine-pyrimidine mismatch that is recognized, shows a very different cleavage pattern. Strong cutting is evident at the mismatched C and neighboring the base 3' to the mismatch site. Unlike the other recognized mismatches, the cleavage 3' to CA results in two products of differing gel mobility. Photocleavage on the duplex containing AA, the only purine-purine mismatch recognized by the complex, also shows distinctive characteristics. Δ-$[Rh(bpy)_2(chrysi)]^{3+}$ promotes strong cleavage at the base 3' to AA and a small amount of cleavage at the mismatched A itself. On this set of DNA duplexes, the AA mismatch is also the only site where the Λ enantiomer shows detectable recognition with a cleavage pattern similar to, but weaker than, its Δ counterpart. When the end-label is placed on the other strand of the duplex, significant cleavage is observed only with the CC and TC mispairs (data not shown); in that case, cleavage occurs at the guanine 3' of the mismatch site.

In the second case (Figure 3.18), performed at a somewhat higher Rh complex:DNA ratio and on hairpin oligonucleotides so cleavage on both strands is visible, the

Figure 3.17. Mismatch Specific DNA Photocleavage by the Enantiomers of $[Rh(bpy)_2(chrysi)]^{3+}$ on double stranded oligonucleotides with 313 nm light. DNA photocleavage reactions were performed on the 17mer 5'-end-labeled duplexes shown below:

```
*5'-GCGGAGTCXTGCATGTC-3'
 3'-CGCCTCAGYACGTACAG-5'
```

where ***XY*** was substituted for the basepairs CC, CA, TT, AA, TC, TG, GA, GG, AT and GC. DNA photocleavage was performed with Δ– and Λ–$[Rh(bpy)_2(chrysi)]^{3+}$ (10 μM DNA duplex, 1 μM Rh complex, 1x running buffer) for 13 min at 365 nm after an 11 min pre-equilibration. Samples were dried and electrophoresis performed as described in the text.

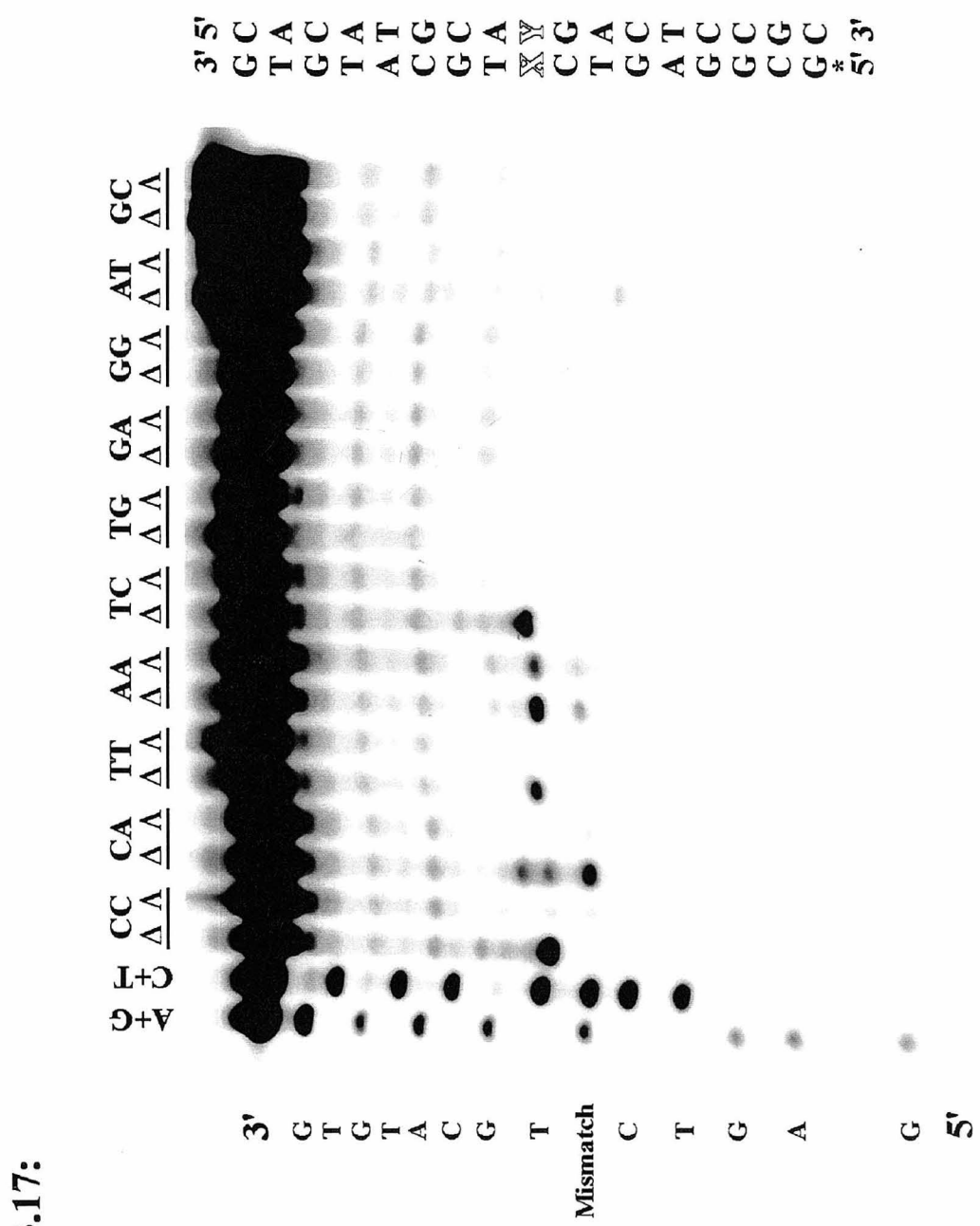

A+G
C+T
CC
CA
TT
AA
TC
TG
GA
GG
AT
GC
3' 5'
G C
T A
G C
T A
A T
C G
G C
T A
X Y
C G
T A
G C
A T
G C
G C
C G
G C
* 5' 3'
3'
G
T
G
T
A
C
G
T
Mismatch
C
T
G
A
G
5'

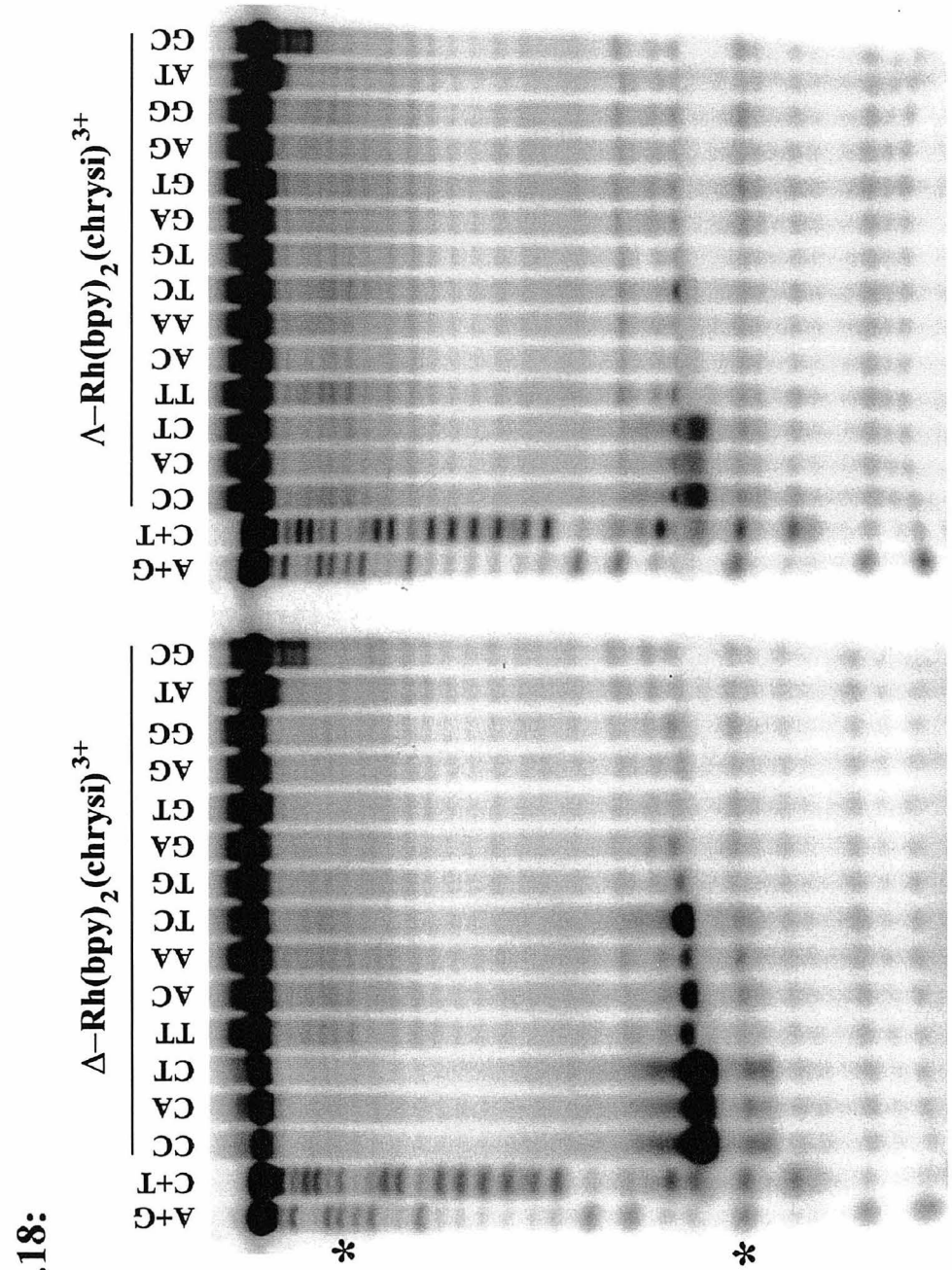
Figure 3.17:

Figure 3.18. Mismatch Specific DNA Photocleavage by the Enantiomers of $[Rh(bpy)_2(chrysi)]^{3+}$ on a family of hairpin oligonucleotides with 365 nm light. Mismatch specific photocleavage was examined on a set of hairpin oligonucleotides as shown below:



where ***XY*** was substituted with all the possible combinations of DNA base mismatches (CC, AC, CA,… etc.) and the two Watson-Crick base pairs. Photocleavage samples (6.7 μM DNA, 1.7 μM Δ- or Λ-$[Rh(bpy)_2(chrysi)]^{3+}$, 1x running buffer) were prepared 4 min before irradiation at 313 nm for 5 min. Samples were dried and electrophoresed as described.

Figure 3.18:


Δ–Rh(bpy)2(chrysi)3+
Λ–Rh(bpy)2(chrysi)3+
A+G
C+T
CC
CA
CT
TT
AC
AA
TC
TG
GA
GT
AG
GG
AT
GC
*
*
5'–GGCAGTXCTGGCTT
3'–CCGTCAYGACCGTT
*
*

general pattern of recognition is quite similar. Strongest recognition is observed at the CC, CA and CT sites. An intermediate level of cleavage occurs at the TC, AC, TC, and TT sites. A much smaller, but still detectable, level of cleavage is observed at the GA, GG, TG and AG sites. Negligible levels of photocleavage are observed in the absence of a mismatch site; the bands at the very top of the GC Watson-Crick paired gel lane to the far right are artifactual and were observed in the light and dark control samples. In this case, the specificity of cleavage by the Λ enantiomer of the complex is essentially the same as that observed for the Δ.

Unlike previous rhodium complexes constructed for DNA recognition, it was not initially clear whether there would be a strong enantiomeric preference in the binding of chrysi complexes to DNA. For metal complexes whose entire specificity is determined by the structure of their ancillary ligands, one would expect that the geometrical disposition of those ligands should have a strong effect on binding properties. In this case, where specificity was generated by the intercalating ligand, it was possible that, if the complex bound by very shallow intercalation, the chiral arrangement of the ancillary ligands might not affect binding. That the complex does have preferences similar to those previously observed for phi complexes of rhodium(III) implies that it is binding deeply enough into the DNA helix that the ancillary ligands can interact with the sugar-phosphate backbone. The slight differences which were observed in the cleavage properties of the two enantiomers of the complex between the two experiments discussed here are likely due to geometrical differences which exist among the mismatch sites in the two different sequence contexts.[13-17]

The data shown here clearly indicate that $[Rh(bpy)_2(chrysi)]^{3+}$ photocleaves DNA near a variety of mismatch sites. Although differences exist in the cleavage patterns

observed at the various sites, in general, photocleavage occurs at the base to 3' side of the mismatch. The Δ and Λ enantiomers of the complex do display differences in photocleavage behavior which are explicable both in terms of the differential binding of chiral complexes to the right-handed helix of DNA and also the heterogeneity which exists in the structure of mismatch sites in different sequence contexts. This dependence on sequence context for mismatch recognition will be comprehensively explored in the next chapter.

3.3.4: Qualitative Relationship between Thermodynamic Destabilization and Mismatch Recognition

Since the design of the chrysi ligand was based on the assumption that its larger surface area would allow recognition of regions where the structure of the DNA helix was destabilized by base mismatches, it is relevant to pose the question whether this is indeed the characteristic recognized by the complex. To approach this problem, data on the thermodynamic consequences of mismatch incorporation into DNA duplexes was obtained from Professor John SantaLucia Jr. at Wayne State University.[13-18] These data, based on extensive analysis of melting curves of DNA duplexes containing all possible base mismatches, allow calculation of the helix destabilization which results from the incorporation of a given mismatch in a given single base sequence context.

An analysis to assess whether the recognition of mismatches is directly related to the helix destabilization caused by the mismatch would ideally be based on direct information about the binding of the metal complex to different mismatch sites. The binding of the complex in this experiment, however, is detected using DNA photocleavage chemistry which has the potential to differ in efficiency among the

various sites. This could be particularly problematic in the case of DNA mismatches where the structural instability and heterogeneity of the binding sites could lead to very different binding geometries for the rhodium complex from site to site. These varied geometries could place the photo-generated radical which causes strand cleavage in positions with markedly different access to the DNA backbone. In these experiments, however, where the base sequence around the mismatch is held constant, the assumption will be made that, to first order, the efficiencies are similar enough to allow direct comparison of photocleavage intensities from mismatch site to mismatch site. Such an assumption has a basis in the fact that the stacking of the intercalator against these constant flanking sequences is likely to provide a significant fraction of the binding affinity to complex for DNA. As a result, it might be inferred that the constant flanking sequence will also impose some consistency in binding geometry between sites where the identity of the mismatches differ.

As a result, an absolute value of DNA photocleavage for Δ-$[Rh(bpy)_2(chrysi)]^{3+}$ at each mismatch in the experiments included as Figures 3.17 and 3.18 was determined by integration using the Imagequant software package; non-specific light damage was controlled by subtracting an identical integrated volume from the control samples for each irradiation lane. The resulting values were plotted versus the thermodynamic destabilization caused by the incorporation of each mismatch into the DNA helix.[13-18] These graphs are included as Figures 3.19 and 3.20. It is clear from these plots that there is a correlation between the thermodynamic destabilization at the mismatch sites and the extent to which Δ-$[Rh(bpy)_2(chrysi)]^{3+}$ promotes DNA photocleavage. As a result, it is probable, especially when combined with the photocleavage results on B-DNA discussed above, that the destabilization of the DNA helix is the structural characteristic recognized by the chrysi intercalating ligand.

Figure 3.19. Plot of Photocleavage at the Mismatch Site versus Mismatch Induced Thermodynamic Destabilization in the 5'-C*X*T-3' Sequence Context. Data from the photocleavage gels shown in Figure 3.17 was extracted and quantitated using the Imagequant software package. Cleavage at the mismatch site was expressed as a fraction of the parent DNA band and plotted versus the thermodynamic destabilization caused by the mismatch as described in the text.

Figure 3.19:

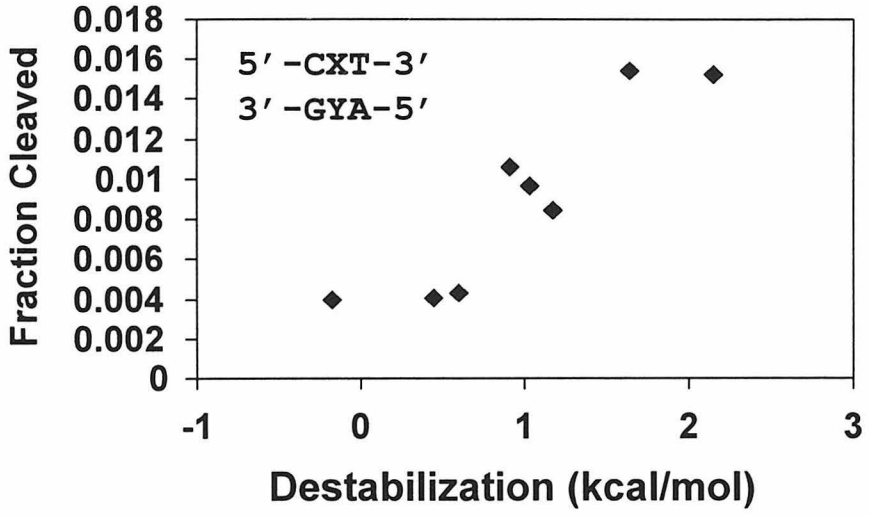
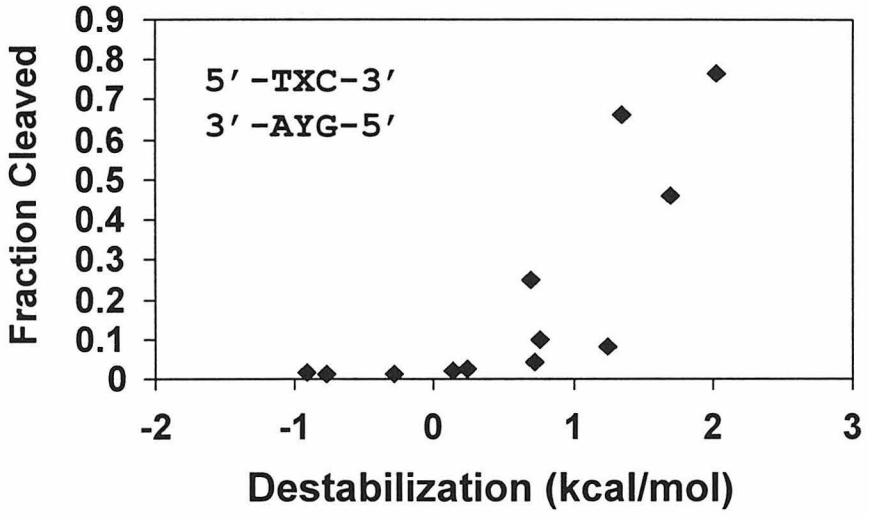

0.018
0.016
0.014
0.012
0.01
0.008
0.006
0.004
0.002
0
Fraction Cleaved
5′-CXT-3′
3′-GYA-5′
-1
0
1
2
3
Destabilization (kcal/mol)

Figure 3.20. Plot of Photocleavage at the Mismatch Site versus Mismatch Induced Thermodynamic Destabilization in the 5'-T*X*C-3' Sequence Context. Data from the photocleavage gels shown in Figure 3.18 was extracted and quantitated using the Imagequant software package. Cleavage at the mismatch site was expressed as a fraction of the parent DNA band and plotted versus the thermodynamic destabilization caused by the mismatch as described in the text.

Figure 3.20:


Fraction Cleaved
0.9
0.8
0.7
0.6
0.5
0.4
0.3
0.2
0.1
0
5′-TXC-3′
3′-AYG-5′
-2
-1
0
1
2
3
Destabilization (kcal/mol)

The shape of these plots is also noteworthy with respect to the recognition of destabilized sites by chrysenequinone diimine intercalators. As the identity of the base mismatch is changed and thermodynamic destabilization increased, the amount of DNA photocleavage displays a roughly sigmoidal dependence. This behavior is observed most clearly in Figure 3.19 but also to a lesser extent in Figure 3.20. The latter case is explainable by the fact that, in the experiment analyzed in Figure 3.20, a greater than stoichiometric amount of the DNA has been cleaved at the mismatch site as a result of the higher wavelength used in the irradiations. As a result, the fraction cleaved values plotted are convoluted by the effect of multiple cleavage events in the more completely reacted samples. In Figure 3.19, where the higher energy irradiation minimizes the contribution of these multiple cleavage events, it is reasonable to assume that the curve more closely represents the populations of bound species.*

Irrespective of the potential for differences in photocleavage efficiency or multiple cleavage events by the complex, the sigmoidal dependence of the photocleavage intensity on destabilization can be used to suggest a model of recognition of disordered sites in DNA by $[Rh(bpy)_2(chrysi)]^{3+}$. At the bottom of the curve, where the destabilization at the mismatch site is the least, the intercalator has difficulty gaining access to the base stack to bind. As destabilization reaches a lower threshold value and continues to grow, the incremental increase in the opening of the base pairs and breakdown of the helical structure will allow incremental increases in binding and photocleavage. This corresponds to the central "pseudo-linear" region of the sigmoidal curve. At some point, however, the destabilization of the helix will no

---

* These issues of multiple cleavage events by a single metal complex will be discussed in greater detail in Chapter 5 of this thesis.

longer be the dominant factor controlling the binding of the intercalating ligand to the helix. Once this point is reached, other factors such as the stacking of the ligand on the adjacent base pairs will determine the extent that the molecule can bind to a given site. This situation would correspond to the region at the top of the sigmoidal curve where photocleavage intensity levels out even with increasing destabilization. A useful analogy for this model of molecular recognition is that of an opening door: At the bottom of the curve, where the door is closed or only slightly ajar, binding is still prohibited or strongly disfavored. As the door opens, the increasing access will allow better and better binding. Once the door is sufficiently open to allow "complete" access, however, opening it even wider results in no added benefit. In addition to being a relevant summary of the recognition properties of the rhodium complex, the fact that the relationship between photocleavage and helix destabilization can be reduced to a physically reasonable binding model provides a measure of circumstantial support for the assumption that cleavage intensity is an acceptable proxy for binding in these constant sequence context experiments.

3.4: CONCLUSIONS

The results discussed in the preceding sections clearly indicate that $[Rh(bpy)_2(chrysi)]^{3+}$ photocleaves DNA at sites of destabilization in the DNA helix. Specific cleavage was observed at a majority of the mismatch sites examined in two experiments where the sequence contexts around the mispairs were held constant. In addition, the extent of photocleavage at these mismatch sites increased as the amount of thermodynamic destabilization at the mismatch site increased. This is suggestive that it is indeed the helix destabilization, which allows access for intercalation by the chrysi ligand, which generates the specificity for mismatch sites. This conclusion is also supported by the comparison between DNA photocleavage by

$[Rh(bpy)_2(chrysi)]^{3+}$ and $[Rh(bpy)_2(phi)]^{3+}$. The phi intercalator shows a similar preference for cleaving at the destabilized region near the CC mismatch but lacks the selectivity of the sterically larger rhodium(III) chrysi complex.

In addition to providing support for this strategy of molecular recognition design, these photocleavage results also highlight other characteristics of rhodium(III) chrysi complexes which are of interest. The cleavage behavior observed with $[Rh(chrysi)_2(phen)]^{3+}$ and post-treatment with piperidine suggests that, like the analogous bis-phi compounds, these complexes also produce alkaline labile damage at guanine residues. More dramatic, however, is the unexpected wavelength dependence and non-stoichiometric nature of the photocleavage by the mono-chrysi complexes. This property, which could be of particular importance to many of the possible applications of these molecules, will be explored in greater detail in Chapter 5.

3.5: Literature Cited

1) Patel, D. J.; Kozlowski, S. A.; Ikuta, S.; Itakura, K. *Fed. Proc.* **1984**, *43*, 2663.

2) Sambrook, J.; Fritsch, E. F.; Maniatis, T. *Molecular Cloning: A Laboratory Manual*; 2nd ed.; Cold Spring Harbor Laboratory Press: Cold Spring Harbor, NY, 1989.

3) Hall, D. B.; Holmlin, R. E.; Barton, J. K. *Nature* **1996**, *382*, 731.

4) Pyle, A. M. *Phenanthrene Diimine Complexes of Ru(II) and Rh(III): Synthesis and Development of a New Class of Shape-Selective Probes for Nucleic Acid Structure*. Ph.D. Thesis, Department of Chemistry, Columbia University, 1989.

5) Bloomfield, V. A.; Crothers, D. M.; Tinoco, I. *Physical Chemistry of Nucleic Acids*; Harper and Row: New York, NY, 1974; Vol., 432.

6) Fazakerley, G. V.; Boulard, Y. *Meth. Enzymol.* **1995**, *261*, 145.

7) Hudson, B. P.; Dupureur, C. M.; Barton, J. K. *J. Am. Chem. Soc.* **1995**, *117*, 9379.

8) Hudson, B. P.; Barton, J. K. *J. Am. Chem. Soc.* **1998**, *120*, 6877.

9) Collins, J. G.; Shields, T. P.; Barton, J. K. *J. Am. Chem. Soc.* **1994**, *116*, 9840.

10) David, S. S.; Barton, J. K. *J. Am. Chem. Soc.* **1993**, *115*, 2984.

11) Dupureur, C. M.; Barton, J. K. *J. Am. Chem. Soc.* **1994**, *116*, 10286.

12) Hall, D. B. *Oxidative DNA Damage Through Long Range Electron Transfer*. Ph.D. Thesis, Division of Chemistry, California Institute of Technology, 1998.

13) Allawi, H. T.; SantaLucia, Jr., J. *Biochemistry* **1997**, *36*, 10581.

14) Allawi, H. T.; SantaLucia, Jr., J. *Biochemistry* **1998**, *37*, 2170.

15) Allawi, H. T.; SantaLucia, Jr., J. *Biochemistry* **1998**, *37*, 9435.

16) Allawi, H. T.; SantaLucia, Jr., J. *Nuc. Acids. Res.* **1998**, *26*, 2694.

17) Peyret, N.; Seneviratne, P. A.; Allawi, H. T.; SantaLucia, Jr., J. *Biochemistry* **1999**, *38*, 3468.

18) SantaLucia, Jr., J., Personal Communication.

Recognition of Base Mismatches in DNA by Chrysenequinone Diimine Intercalators of Rhodium (III)

Thesis by
Brian Anthony Jackson

Submitted in Partial Fulfillment of
the Requirements for the Degree of
Doctor of Philosophy

California Institute of Technology
Pasadena, California

1999
(submitted April 22, 1999)

Chapter 4:

$[Rh(bpy)_2(chrysi)]^{3+}$: Characterization of the Breadth and Specificity of Mismatch Recognition by a Chrysenequinone Diimine Complex*

* Portions of this chapter were adapted from Jackson, B.A., Alekseyev, V.Y., and Barton, J.K. *Biochemistry,* **1999**, *38*, 4655 and from Jackson, B.A. and Barton, J.K. *J. Amer. Chem. Soc.* **1997**, *119*, 12986.

4.1: INTRODUCTION

Although the results discussed in the previous chapter clearly indicate that the chrysenequinone diimine intercalating ligand produces DNA photocleavage specificity for the destabilized regions near base mismatches, such a demonstration is not sufficient to show if this molecule, or molecules designed using similar recognition mechanisms, would be appropriate for *applied* tasks of mismatch recognition. If such a compound is to be used either as a chemotherapeutic drug or as a laboratory mismatch recognition agent, its mismatch binding and cleavage properties must be more comprehensively characterized. For both these tasks, examining DNA binding and photocleavage of mismatches on defined oligonucleotides with constant DNA sequences surrounding the mispairs does not provide enough information. Ideally, a mismatch recognition agent suitable for medical applications would be able to bind and cleave at every possible mispair; such an idealized reagent would also be unaffected by the sequence context found around the mismatch site. Furthermore, since DNA molecules of biological relevance tend to be very large, it would also be desirable that a mismatch recognition agent have a high degree of specificity to make it possible to identify a single mismatch site even in the presence of a large excess of properly paired DNA. The experiments which follow address whether $[Rh(bpy)_2(chrysi)]^{3+}$, as a representative member of the family of chrysenequinone diimine metallointercalators, possesses the requisite level of both broad specificity and high selectivity.

4.2: Experimental Methods

4.2.1: Instrumentation and Materials

All reagents were the highest purity commercially available, and unless otherwise noted, were used as obtained without further purification. $[Rh(bpy)_2(chrysi)]Cl_3$ was synthesized, purified, and its enantiomers resolved as described in Chapter 2. Sonicated calf thymus DNA was obtained from Amersham Pharmacia Biotech, Buckinghamshire, UK. DNA synthesis was performed either on an ABI 392 DNA/RNA synthesizer (reagents from Glen Research, Sterling, VA) or at the Caltech Biopolymer Synthesis Facility. Oligonucleotides were purified on Poly-Pak II purification cartridges (Glen Research) according to the manufacturer's instructions or by reverse phase HPLC. HPLC purification was performed on either a Waters 660E, Hewlett Packard 1050 or 1100 instrument using a Dynamax C_{18} reverse phase column. Absorption spectra were recorded on a Beckman DU 7400 spectrophotometer.

Enzymes used in plasmid preparation and cleavage were obtained from either New England Biolabs (Beverly, MA), USB (Cleveland, OH), or Boehringer Mannheim (Indianapolis, IN). Oligonucleotides were 5'-end-labeled with ^{32}P using γ-^{32}P-ATP and T4 polynucleotide kinase (New England Biolabs) and purified by denaturing polyacrylamide gel electrophoresis. Oligonucleotides were isolated from excised polyacrylamide slices by elution into ammonium acetate EDTA buffer (500 mM NH_4OAc, 1 mM EDTA, pH 9) and ethanol precipitated. DNA photocleavage reactions were performed on samples of end-labeled DNA with unlabeled, identical sequence carrier DNA in running buffer (50 mM Tris, 20 mM sodium acetate, 18 mM NaCl, pH 7.0) or in Tris buffer alone (10 mM Tris, pH 8.5). DNA samples were annealed by heating to 90°C and controlled cooling to room temperature using a

Perkin Elmer Cetus DNA thermocycler. Concentrations of metal complex solutions were determined spectrophotometrically using ε_{271} 63,800 M^{-1} cm^{-1} for $[Rh(bpy)_2(chrysi)]^{3+}$. Concentrations of oligonucleotides were determined spectrophotometrically using per-base extinction coefficients of A: 8600 M^{-1} cm^{-1}; C: 6800 M^{-1} cm^{-1}; G: 9700 M^{-1} cm^{-1}; T: 8400 M^{-1} cm^{-1} which are based on values from single stranded DNA homopolymers. Extinction coefficients for the *double stranded regions* of DNA hairpins were systematically reduced 15% from the calculated values based on temperature dependent hypochromicity measurements made on a representative sample of these hairpins. Samples were prepared between 5 and 30 min before irradiating on an Oriel Hg/Xe lamp system equipped with a monochromator, IR filter, and 300 nm cut-off filter. The irradiations were performed in open, horizontally positioned 1.7 ml microcentrifuge tubes. Dried irradiation samples were resuspended in denaturing formamide loading dye and electrophoresed on 20% denaturing polyacrylamide gels unless indicated otherwise. Images of the gels were obtained by phosphoimagery (Molecular Dynamics) and quantitated using the Imagequant software package.

4.2.2: Sequence Context Dependence of Mismatch Recognition

Individual primer scale (0.04 μM) preparations of 29 base pair oligonucleotide hairpins containing one of the eight possible DNA mispairs in a unique single base sequence context were synthesized and purified by the Caltech Biopolymer Synthesis Facility. The general structure of these oligonucleotides, containing a mismatch PQ flanked by base pairs XW and YZ, is shown below; in this scheme, the nomenclature for individual oligonucleotides was defined as PQ/XY, denoting both the mismatch and the sequence context around it on the upper strand.

5'-GGCAG**XPY**TGGC $^{T}_{T}$
3'-CCGTC**WQZ**ACCG $^{T}_{TT}$

In total, 104 oligonucleotides were made which represent all the possible single base contexts around the eight mispairs when rotational symmetry is taken into account. The oligonucleotides were 5' end-labeled with ^{32}P and purified as described above. Samples of labeled DNA were combined with unlabeled carrier and annealed as described. Aliquots of each oligonucleotide solution (10 μl, 20 μM DNA polymers, 10 mM Tris pH 8.0) were combined with an equal volume of metal complex solution, either Δ- or Λ-$[Rh(bpy)_2(chrysi)]Cl_3$ (10 μM in deionized H_2O), producing irradiation samples 10 μM in DNA and 5 μM in metal complex. Irradiations were performed on both sets of samples at 313 nm for 10 min. DNA samples of identical concentration were incubated with metal complex in the absence of light (dark controls) or irradiated in the absence of metal complex (light controls). In addition, one set of Δ-$[Rh(bpy)_2(chrysi)]Cl_3$ samples was irradiated at 440 nm for 30 min. Samples were dried under vacuum, resuspended and electrophoresed as described without any additional post treatment.

4.3.3: Measurement of the Binding Constant of Δ-$[Rh(bpy)_2(chrysi)]^{3+}$ at Mismatch Sites

To determine the thermodynamic association constants of Δ-$[Rh(bpy)_2(chrysi)]^{3+}$ for a number of mismatch sites of interest, photocleavage titrations were performed on a variety of oligonucleotide hairpins. Calling on the same scheme used for describing the sequences in the context experiment above, the sequences of the hairpins used were PQ/XY: CC/GC, TT/GC, CT/GC, AC/GC, AA/GC, and CC/AT. In addition,

experiments were performed on the slightly longer hairpin:

$$\begin{matrix} {}^{T}_{T}{}^{T}\text{GGGCA}\mathbf{C}\text{GACATGATG-3'} \\ {}^{T}_{T}{}_{T}\text{CCCGT}\mathbf{C}\text{CTGTACTAC-5'} \end{matrix}$$

Although more extensive discussion of these experiments and their associated data analysis is included in Appendix 2, a brief summary follows. Photocleavage was performed with Δ-$[Rh(bpy)_2(chrysi)]^{3+}$ at concentrations from 3 x 10^{-10} M to 1 x 10^{-3} M DNA polymers in 1x running buffer. The Rh:DNA ratio was held constant at a value of 1:10. Samples were photolyzed at 313 nm for 5 min after preincubation of 4 min. Samples were dried under vacuum and electrophoresis performed as described. The fraction cleaved at the mismatch site was quantitated, expressed as a fraction of the uncleaved parent DNA band, and fit to a single site, one parameter binding model. As discussed in the appendix, under such conditions of low complex to DNA ratios, the effects of non-specific binding can be neglected.

4.2.4: Measurement of the Binding Constant of Δ-$[Rh(bpy)_2(chrysi)]^{3+}$ to B-DNA by Direct Photocleavage Titration

To determine the binding constant of Δ-$[Rh(bpy)_2(chrysi)]^{3+}$ for B-DNA, a photocleavage titration was performed on the following Watson-Crick base paired oligonucleotide hairpin:

$$\begin{matrix} \text{5'-GCGGTTGAATGAGC}^{T}_{T}{}^{T} \\ \text{3'-CGCCAACTTACTCG}_{TT}{}^{T} \end{matrix}$$

Although more specific information on this experiment and the analysis of the resulting data is included in Appendix 2, a brief summary of the procedure follows. Photocleavage was performed with Δ-$[Rh(bpy)_2(chrysi)]^{3+}$ at concentrations from

1 x 10^{-9} M to 1 x 10^{-4} M DNA polymers in 1x running buffer. The Rh:DNA ratio was held constant at a value of 1:2. Samples were photolyzed at 365 nm for 15 min after preincubation for 30 min. Samples were dried under vacuum and electrophoresis performed as described. The fraction cleaved over the entire gel lane was quanititated and fit to a multi-site binding model to obtain an average value of the non-specific binding constant as described in Appendix 2.

4.3.5: Measurement of the Binding Constant of Δ-[Rh(bpy)$_2$(chrysi)]$^{3+}$ to B-DNA by Photocleavage Competition Titration

If the association constant at a given high-affinity DNA site is known, it is possible to measure an average association constant for mixed sequence (in this case, B-form) DNA by a competition titration. This was performed by titration of Δ-[Rh(bpy)$_2$(chrysi)]$^{3+}$ bound to the CC mismatch hairpin shown below:

```
 T T
T  GGGCACGACATGATG-3'
 T T
T  CCCGTCCTGTACTAC-5'
 T T
```

whose corresponding association constant was known (see **4.3.2.1** below) to be 8.4 x 10^5 M^{-1}. Samples were prepared at 0.5 to 0.1 μM hairpin and 0.5 to 0.04 μM Δ-[Rh(bpy)$_2$(chrysi)]$^{3+}$ in 1x running buffer with carrier DNA concentration increasing from a base pair ratio (Carrier Base Pairs:CC Mismatches) of 0 to 25,000. Both sonicated calf thymus DNA and a 25 base pair oligonucleotide DNA duplex (5'-GCGGTATCTAGAGCGCATCTGGGCG-3' annealed to its complement) were used as the titrant. Samples were irradiated for 15 minutes at 365 nm, dried down and electrophoresed as described. Data were fit to a two parameter binding model analogous to that described in Appendix 2 with the exception that the independent variable was set to the number of non-specific (low-affinity) sites in the sample and

the dependent variable was the fraction of the mismatch (high-affinity) site bound by metal complex.

4.3.6: Specific Cleavage of a Plasmid DNA at a Single Base Mismatch

4.3.6.1: Plasmid Construction

The oligonucleotide inserts,

```
5'-TCGACACTCAAGTGAGCCAAGGTAGGACCTACTTGAGXCATCAAAGGGCCCTTTATT-----3'
3'-----GTGAGTTCACTCGGTTCCATCCTGGATGAACTCYGTAGTTTCCCGGGAAATAATCGA-5'
```

where XY is either a GC or CG base pair, were synthesized and purified on Poly-Pak II cartridges as described. In addition, the oligonucleotides were purified by gel electrophoresis (19.5% non-denaturing gel), identified by UV shadowing, and excised and eluted as described. The purified DNA was ion-exchanged to the chloride salt by elution through Sephadex CM-C25 equilibrated in NaCl and lyophilized to dryness.

Commercially available pUC19 DNA (5 μg) was doubly digested with the restriction endonucleases *SalI* and *HindIII* (37°C, 12 hr). The progress of the reactions were monitored by running parallel individual digestions and assaying reaction completion by agarose gel electrophoresis. The cleaved products were dephosphorylated with alkaline phosphatase (calf intestinal, 37°C, 1 hr). The plasmid DNA was then purified from the enzymes by phenol-chloroform extraction and ethanol precipitation. The oligonucleotide inserts were phosphorylated with polynucleotide kinase and ATP (37°C, 12 hr). The inserts (at molar ratios of 1x, 0.5x, 0.2x and 0.1x to the linearized plasmid) were ligated into pUC 19 by treatment with T4 DNA ligase (16°C, 12 hr). Aliquots of these plasmid ligations, labeled $pVYA_C$ or $pVYA_G$ depending on which base was included in the variable position on the upper strand,

were transformed into competent DH5α *E.Coli* (Gibco BRL Life Technologies) according to the manufacturer's protocols. After plating of the transformed bacteria on selective media (Terrific Broth/Agar plates, 200 μg/ml ampicillin) a single transformed colony was selected for each plasmid and grown in a 15 ml culture (Terrific Broth, 200 μg/ml ampicillin). The plasmid DNA was isolated from these cultures using a Qiagen (Valencia, CA) plasmid isolation spin column (QIAprep Spin Miniprep Kit) according to the manufacturer's instructions. After sequencing of the resulting plasmid DNA by the Caltech Core DNA Sequencing Facility, larger 500 ml cultures of each plasmid-expressing bacterial strain were grown. Milligram quantities of plasmid were extracted from these cultures using a Qiagen Maxi-Prep (Tip 500) according to the manufacturer's protocols.

4.3.6.2: Recognition of a CC Mispair on a Plasmid Heteroduplex

Samples of $pVYA_C$ and $pVYA_G$ (26 μg each) were linearized with *ScaI* (37°C, 4 hr) and dephosphorylated with shrimp alkaline phosphatase (37°C, 90 min). After ethanol precipitation, samples of each plasmid were combined (a total of 52 μg in 40 μl 10 mM Tris) and denatured by addition of 10 M NaOH (2 μl) according to the method of Smith and Modrich.[1] After incubation for five min, the samples were neutralized with acetic acid, sodium chloride was added (1 M, 3 μl), and they were buffered by addition of 1 M Tris pH 8.5 (18 μl). The samples were then annealed by 30 min incubations at 65°C and 37°C. This mixture of heteroduplexes (some containing CC and GG mispairs) was desalted and exchanged into 10 mM Tris buffer (pH 8.5) on a Microcon 10 spin filter (Millipore, Bedford, MA). Similar base treatment and reannealing procedures were performed on samples of $pVYA_C$ and $pVYA_G$ separately for control purposes. These samples were combined before desalting to provide a sample with the same DNA composition as the heteroduplex

sample but lacking base mismatches. Samples of both the heteroduplex and control plasmid samples were end-labeled (on both ends of the plasmid) with ^{32}P ATP and polynucleotide kinase (37°C, 2 hr). Stocks of labeled plasmid for photocleavage were prepared from 2 μg of the plasmid in 100 μl 2x running buffer. Aliqouts of these plasmid stocks (10 μl) were combined with an equal volume of a solution of Δ-$[Rh(bpy)_2(chrysi)]^{3+}$ (200 nM, 20 nM, 2 nM, or 0.2 nM, in deionized water) at least 20 min before irradiation for 10 min at 440 nm. Samples were combined with 1 vol. alkaline agarose loading dye (50 mM NaOH, 1 mM EDTA, 2.5% Ficoll, 0.25% bromocresol green) and run on an alkaline agarose gel (1% agarose, 50 mM NaOH, 1 mM EDTA).[2] The gel was fixed in 7% trichloroacetic acid, dried under vacuum, and visualized by phosphorimagery. The lengths of the mismatch-specific photocleavage products (974 and 1751 bp) were verified by comparison with a *SalI* digest of the labeled plasmid (producing fragments of 936 and 1789 bp).

4.3.6.3: Determination of the Δ-$[Rh(bpy)_2(chrysi)]^{3+}$ Cleavage Site in $pVYA_{C/G}$ Heteroduplexes at High Resolution

A sample of $pVYA_C$ (26 μg) was digested with *EcoRI* (37°C, 3.5 hr) and dephosphorylated with shrimp alkaline phosphatase (37°C, 3.5 hr), and 5' end-labeled with polynucleotide kinase and ^{32}P ATP (37°C, 1 hr). The labeled plasmid was then treated with *PvuII* (37°C, 4 hr) yielding three restriction fragments. The fragment of interest (273 base pairs) was separated on a 6% non-denaturing polyacrylamide gel and isolated from the gel slice by extraction into NH_4OAc buffer and EtOH precipitation as described. Samples of the labeled restriction fragments were combined with a large excess (25 μg) of either $pVYA_G$ or $pVYA_C$ that had been treated with both *EcoRI* and *PvuII* (37°C, 6 hr). This mixture of labeled 273mer and all three unlabeled fragments resulting from the double digests were alkaline denatured and reannealed as described in the previous procedure. This treatment

produced two samples, depending on whether the labeled material was combined with fragments of $pVYA_G$ or $pVYA_C$, one containing labeled CC mispairs (and CG base pairs) and the other containing only Watson-Crick DNA. Samples of these DNA solutions were diluted in 2x running buffer and mixed with an equal volume of Δ-$[Rh(bpy)_2(chrysi)]^{3+}$ (2 μM, 200 nm, or 20 nm, in deionized water) solution 10 min before irradiation at 440 nm for 10 min. Samples were dried, resuspended in formamide loading dye, electrophoresed on a 6% denaturing polyacrylamide gel, and visualized as described.

4.3: Results and Discussion

4.3.1: Broad Specificity

4.3.1.1: DNA Base Mismatch Recognition in Variable Sequence Contexts

For a mismatch-specific cleavage agent to be generally applicable to problems in either a medical or laboratory setting, it must be able to recognize many if not all of the broad range of possible mismatch sites that can occur in DNA. Without a broad specificity, such a compound could only be applied to specific uses in the laboratory and, if used as a drug, would have a much reduced therapeutic benefit. This generality in recognition must include not only the bases involved in the mismatch itself, but the different sequence contexts that can arise around individual mispaired sites. In order to test the breadth of recognition by $[Rh(bpy)_2(chrysi)]^{3+}$, 104 DNA hairpins were synthesized, 10 for each homo-mismatch (CC, AA, etc). and 16 for each hetero-mismatch. The group includes all possible single base sequence contexts around the mismatches when rotational symmetry about the homo-mismatches is considered. For example, the CC mismatch site 5'-G**C**G-3' (CC/GG in the nomenclature of **4.2.2** above and Figure 4.1) occupying the XPY sites is equivalent

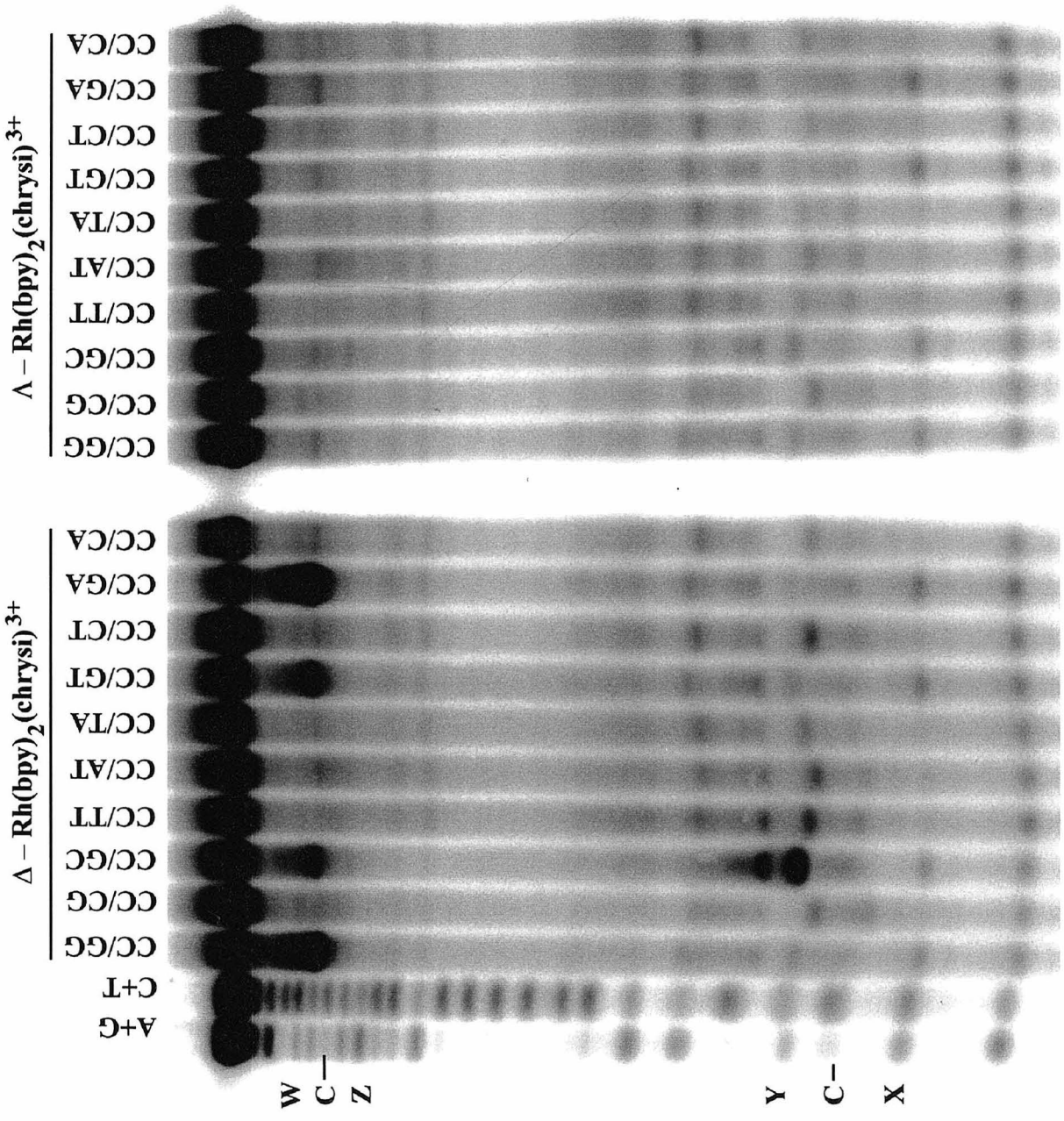
to 5'-C**C**C-3' (CC/CC) occupying those sites since they appear on the opposite strand of the same hairpin and can be inter-converted by rotation. Consideration of the rotational symmetry allows study of the 128 possible mismatch sites (8 mismatches each of which have 16 possible single base contexts) on only 104 individual DNA substrates. The use of DNA hairpins, in addition to minimizing problems associated with the reduced melting temperature of mismatch-containing duplexes, makes it possible to observe cleavage events that occur on both strands of the complex binding site.

Examination of the photocleavage products produced when the mismatch-containing hairpins were photolyzed at either 313 nm and 440 nm in the presence of metal complex immediately demonstrates that $[Rh(bpy)_2(chrysi)]^{3+}$ is an extremely general mismatch recognition agent. The results of photocleavage at 313 nm, which compares the behavior of the Δ and Λ enantiomers of the complex, are included as Figure 4.1. As observed in the constant context experiments described in the previous chapter, the cleavage pattern of the Λ enantiomer of the complex is generally similar to the Δ complex although much weaker in intensity. Also apparent in these autoradiograms is a relatively high background level of damage observed on the entire double stranded regions of the DNA hairpins; this non-specific light damage along the length of the double stranded region is also observed in the light control samples and is not due to the metal complex. The ratio of this background damage to site specific cleavage at the mismatch site is much reduced when the irradiation wavelength of the photolysis reaction is increased to 440 nm. This can be clearly seen in the autoradiogram images included as Figure 4.2 which compare the photocleavage behavior of Δ-$[Rh(bpy)_2(chrysi)]^{3+}$ at both wavelengths. In addition to the reduction in the non-specific light damage to the DNA at these higher wavelengths, it is clear that the amount of mismatch-specific cleavage at 440 nm

Figure 4.1. DNA Photocleavage of DNA Hairpins Containing All Base Mismatches in All Single Base Sequence Contexts by Δ and Λ-$[Rh(bpy)_2(chrysi)]^{3+}$ at 313 nm. DNA hairpins of the general sequence,

5'-GGCAG**XPY**TGGC $^{T}_{T}$
3'-CCGTC**WQZ**ACCG $_{T}^{T}$

were prepared and purified as described in the text. The nomenclature for individual oligonucleotides shown in the figure is defined as PQ/XY, denoting both the mismatch and the sequence context around it on the upper strand. In total, 104 hairpins represent all the possible single base contexts around the eight mispairs when rotational symmetry is taken into account. The oligonucleotides were 5' end-labeled with ^{32}P and purified as described above. Samples (20 μl, 10 μM DNA polymers, 5 μM Δ- or Λ-$[Rh(bpy)_2(chrysi)]Cl_3$, 5 mM Tris pH 8.0) were irradiated at 313 nm for 10 min. Samples were dried under vacuum, resuspended, electrophoresed, and imaged as described. Although Δ-$[Rh(bpy)_2(chrysi)]^{3+}$ does recognize most mismatch sites, it is clear that the sequence context, either by changing the structure or destabilization at the site, has a strong effect on the intensity of observed DNA photocleavage.

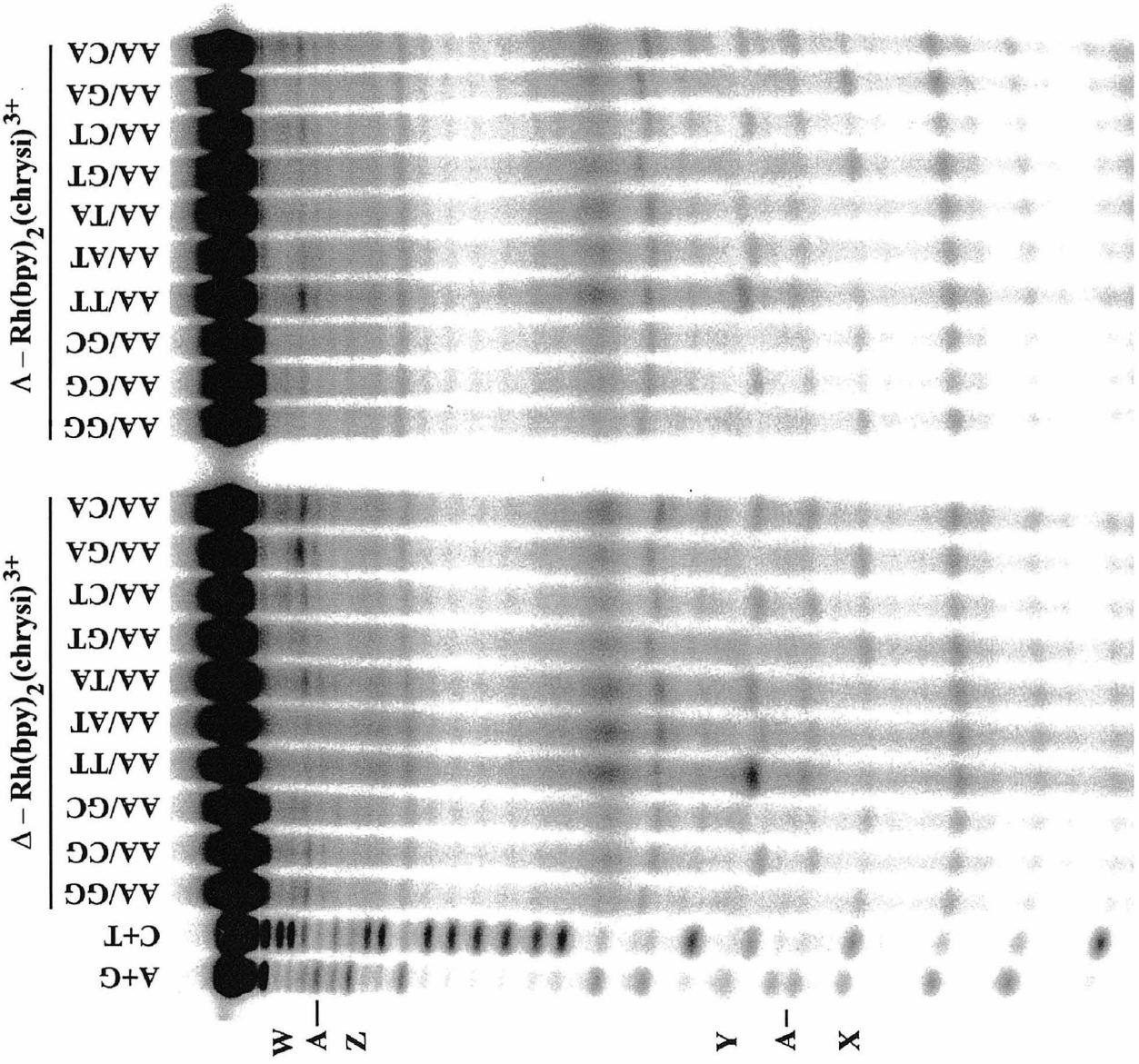

Δ – Rh(bpy)2(chrysi)3+
Λ – Rh(bpy)2(chrysi)3+
CC/GG
CC/CG
CC/GC
CC/TT
CC/AT
CC/TA
CC/GT
CC/CT
CC/GA
CC/CA
A+G
C+T
W
C
Z
Y
C
X
TTT
T T
C G
G C
G C
T A
Y Z
C C
X W
G C
A T
C G
G C
G C
5' 3'
10 μM DNA
(hairpin)
5 μM Rh(B)2C
313 nm
10 min

Δ – Rh(bpy)2(chrysi)3+
A+G
C+T
CT/GG
CT/CG
CT/CC
CT/GC
CT/TT
CT/AT
CT/TA
CT/AA
CT/CA
CT/GA
CT/CT
CT/GT
CT/AC
CT/TC
CT/TG
CT/AG
W
T
Z
Y
C
X
Λ – Rh(bpy)2(chrysi)3+
A+G
C+T
CT/GG
CT/CG
CT/CC
CT/GC
CT/TT
CT/AT
CT/TA
CT/AA
CT/CA
CT/GA
CT/CT
CT/GT
CT/AC
CT/TC
CT/TG
CT/AG
TTTT
T T
C G
G C
G C
T A
Y Z
C T
X W
G C
A T
C G
G C
G C
5' 3'
10 μM DNA
(hairpin)
5 μM RhBpy2C
313 nm
10 min

Δ – Rh(bpy)2(chrysi)3+
Λ – Rh(bpy)2(chrysi)3+
A+G
C+T
TT/GG
TT/CG
TT/GC
TT/TT
TT/AT
TT/TA
TT/GT
TT/CT
TT/GA
TT/CA
W
T—
Z
Y
T—
X
10 μM DNA (hairpin)
5 μM Rh2
313 nm
10 min
5' TTTT 3'
T T C G G C G C T A Y Z T T X W G C A T C G G C G C

Δ – Rh(bpy)2(chrysi)3+
Λ – Rh(bpy)2(chrysi)3+
A+G
C+T
AC/GG
AC/CG
AC/CC
AC/GC
AC/TT
AC/AT
AC/TA
AC/AA
AC/CA
AC/GA
AC/CT
AC/GT
AC/AC
AC/TC
AC/TG
AC/AG
W
C
Z
Y
A
X
10 μM DNA (hairpin)
5 μM Rh
313 nm
10 min
5' 3'
T T T T
C C G G
G C C G
G C G C
T A Y Z
A C X W
G C G C
A T C G
C G G C
G C C G
G C G C

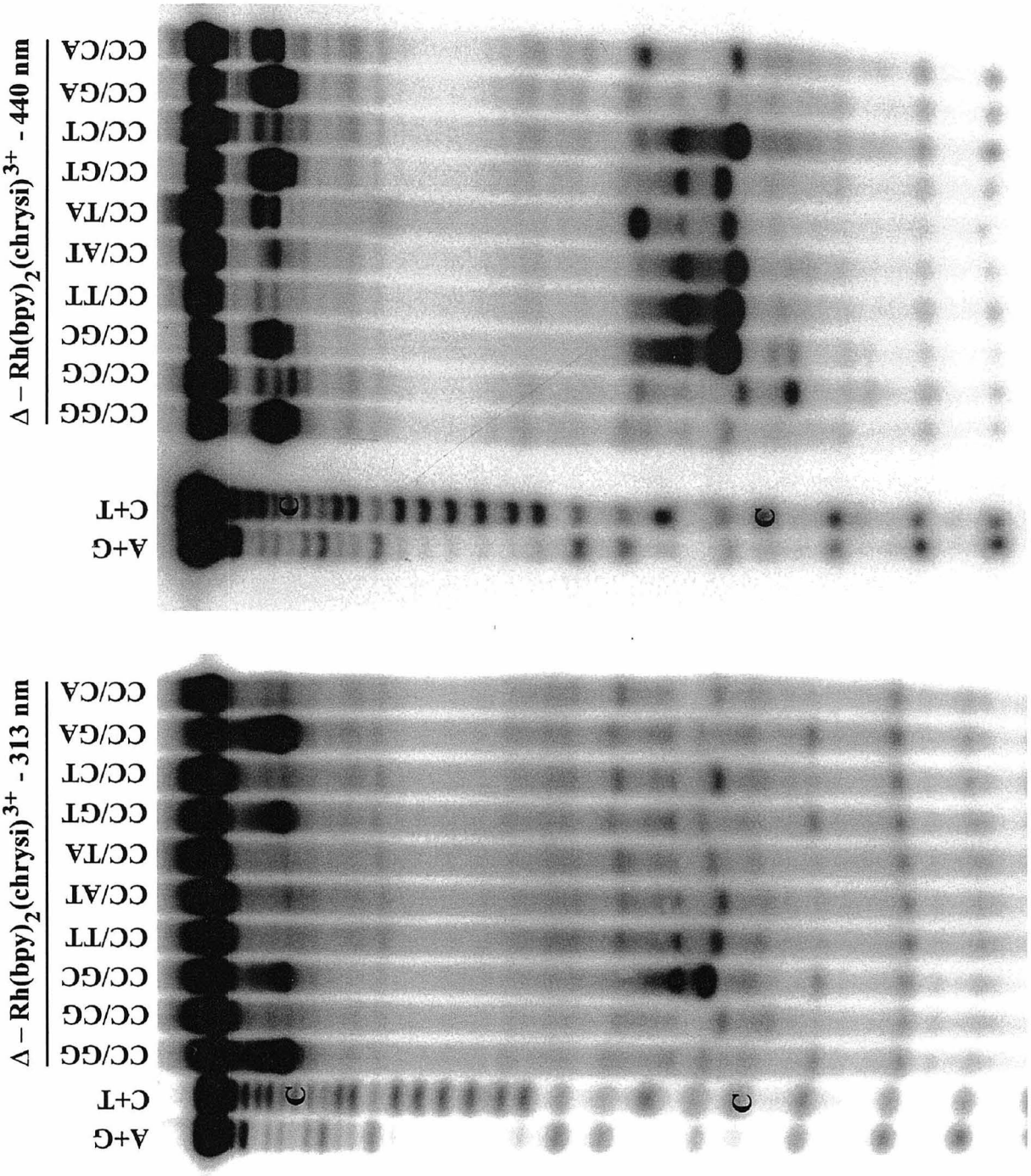
Δ – Rh(bpy)2(chrysi)3+
A+G
C+T
GT/GG
GT/CG
GT/CC
GT/GC
GT/TT
GT/AT
GT/TA
GT/AA
GT/CA
GT/GA
GT/CT
GT/GT
GT/AC
GT/TC
GT/TG
GT/AG
W
T
Z
Y
G
X
Λ – Rh(bpy)2(chrysi)3+
A+G
C+T
GT/GG
GT/CG
GT/CC
GT/GC
GT/TT
GT/AT
GT/TA
GT/AA
GT/CA
GT/GA
GT/CT
GT/GT
GT/AC
GT/TC
GT/TG
GT/AG
T T T T
C C G G
G C C G
G C C T
T A G C
Y Z G C
G T X W
X W
5' 3'
10 μM DNA
(hairpin)
5 μM Rh(bpy)2C
313 nm
10 min

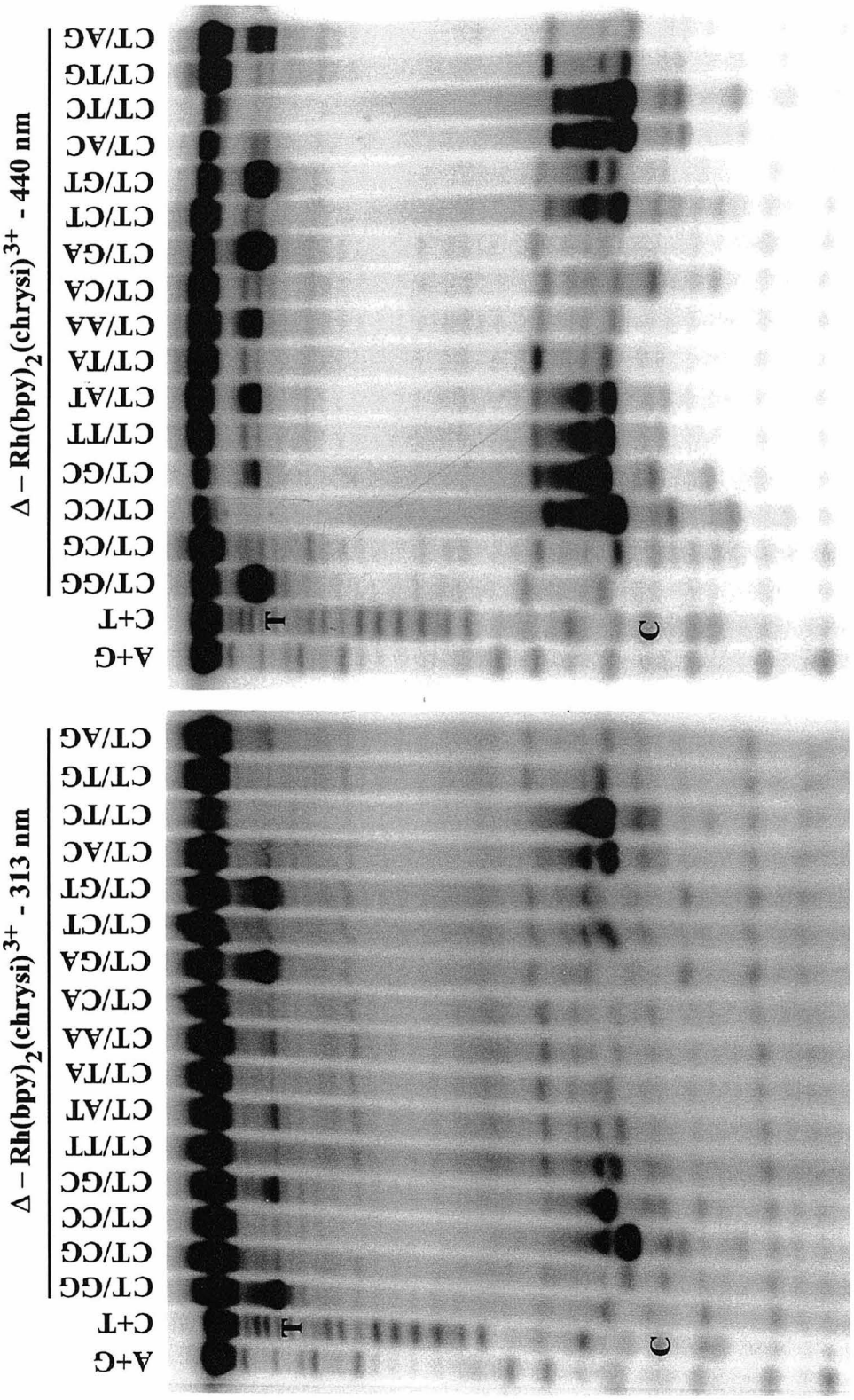

10 μM DNA
(hairpin)
5 μM $Rh(B_2C$
313 nm
10 min
5' 3'
TTT
T T
C G
G C
G C
T A
Y Z
A A
X W
G C
A T
C G
G C
G C
W
A—
Z
Y
A—
X
Δ – $Rh(bpy)_2(chrysi)^{3+}$
Λ – $Rh(bpy)_2(chrysi)^{3+}$
A+G
C+T
AA/GG
AA/CG
AA/GC
AA/TT
AA/AT
AA/TA
AA/GT
AA/CT
AA/GA
AA/CA

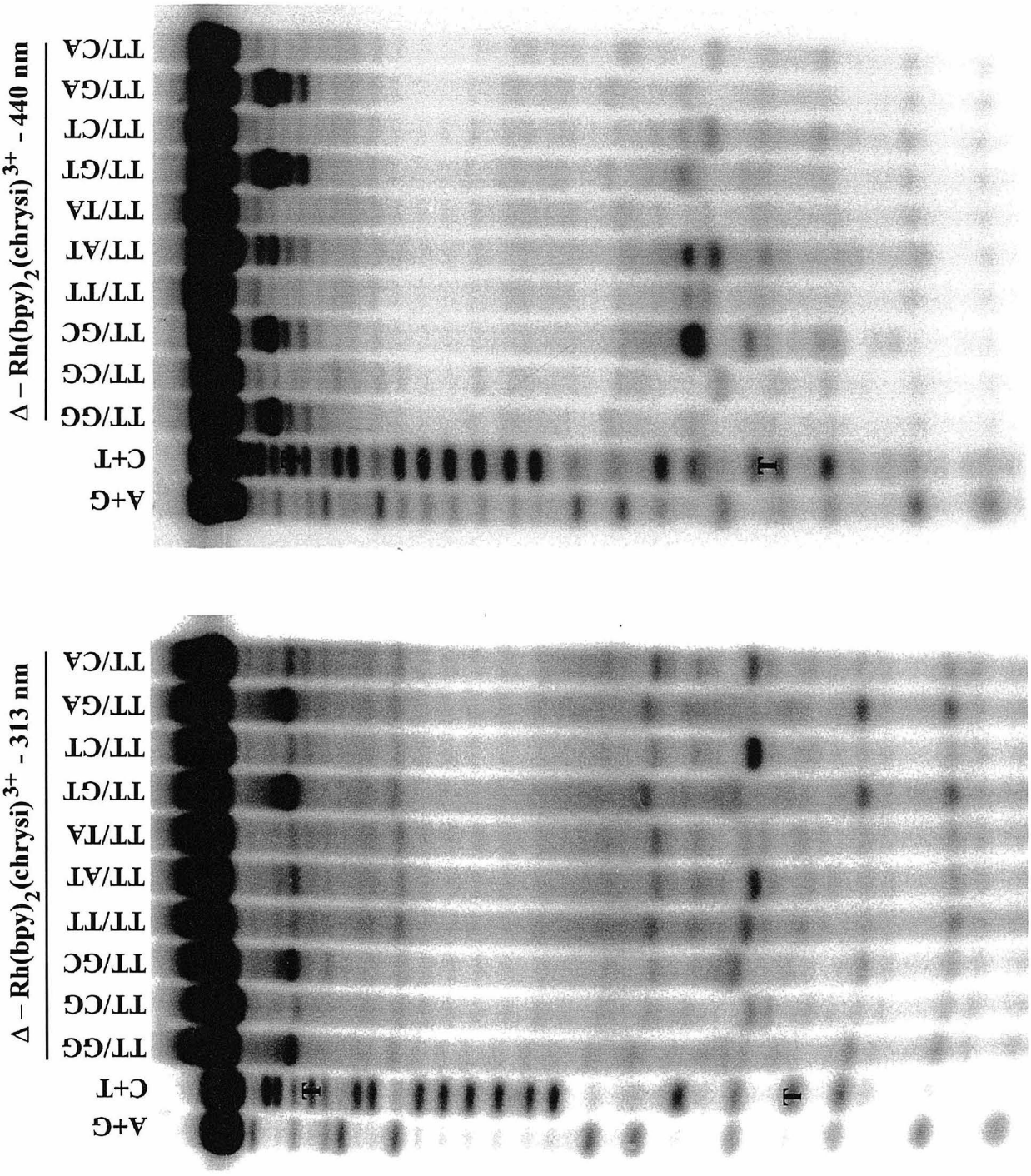
Δ – Rh(bpy)2(chrysi)3+
A+G
C+T
AG/GG
AG/CG
AG/CC
AG/GC
AG/TT
AG/AT
AG/TA
AG/AA
AG/CA
AG/GA
AG/CT
AG/GT
AG/AC
AG/TC
AG/TG
AG/AG
W
G
Z
Y
A
X
Λ – Rh(bpy)2(chrysi)3+
A+G
C+T
AG/GG
AG/CG
AG/CC
AG/GC
AG/TT
AG/AT
AG/TA
AG/AA
AG/CA
AG/GA
AG/CT
AG/GT
AG/AC
AG/TC
AG/TG
AG/AG
TTTT
T C G T
C G C G
G C G C
T A G C
Y Z A T
A G C G
X W G C
G C G C
5' 3'
10 μM DNA (hairpin)
5 μM RhbiC
313 nm
10 min

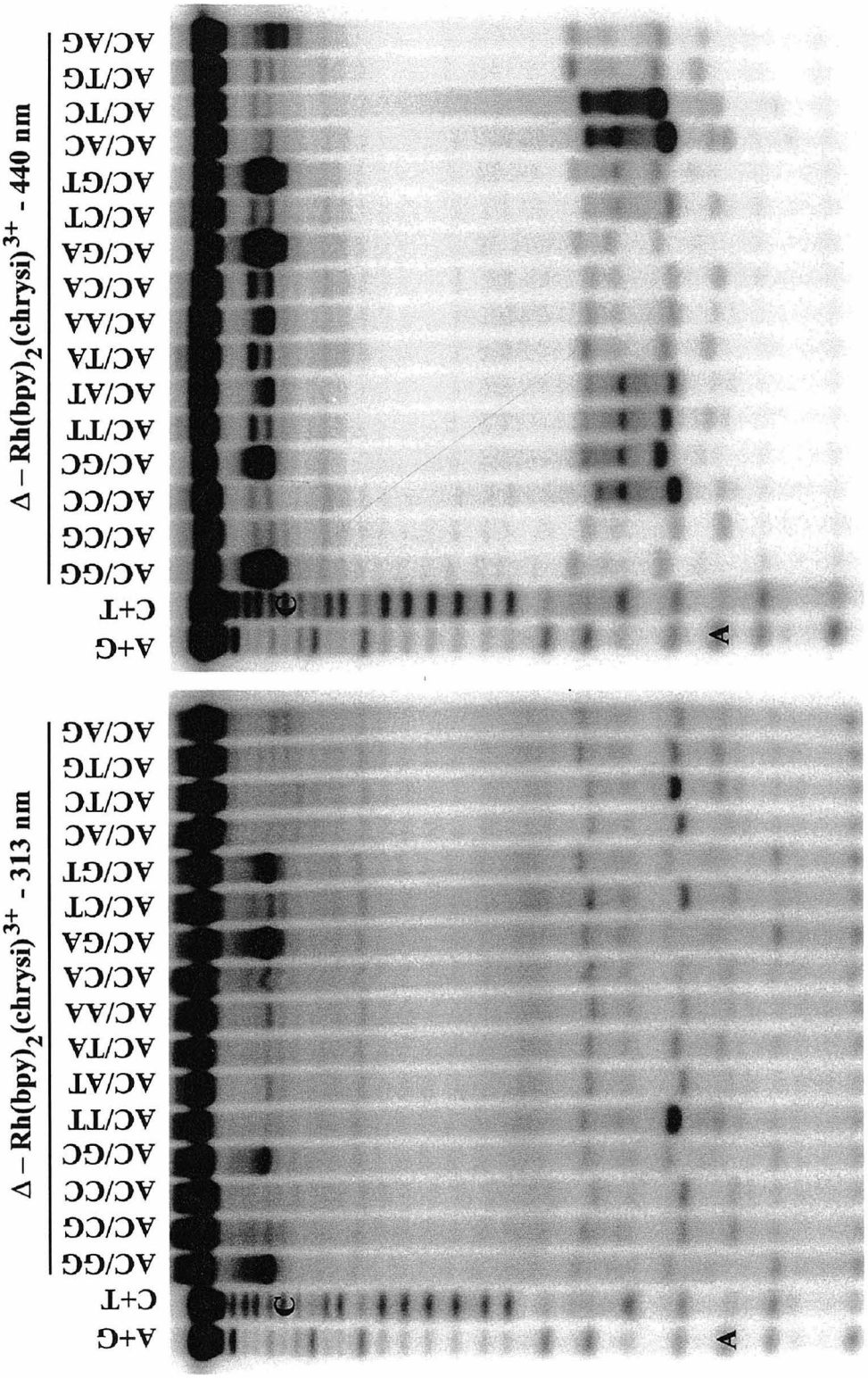
Δ – Rh(bpy)2(chrysi)3+
Λ – Rh(bpy)2(chrysi)3+
A+G
C+T
GG/GG
GG/CG
GG/GC
GG/TT
GG/AT
GG/TA
GG/GT
GG/CT
GG/GA
GG/CA
W
G–
Z
X
Y
G–
5' TTTT
T L
C G
G C
G C
T A
Y Z
G G
X W
G C
A T
C G
G C
G C
5' 3'
10 μM DNA
(hairpin)
5 μM Rh
313 nm
10 min

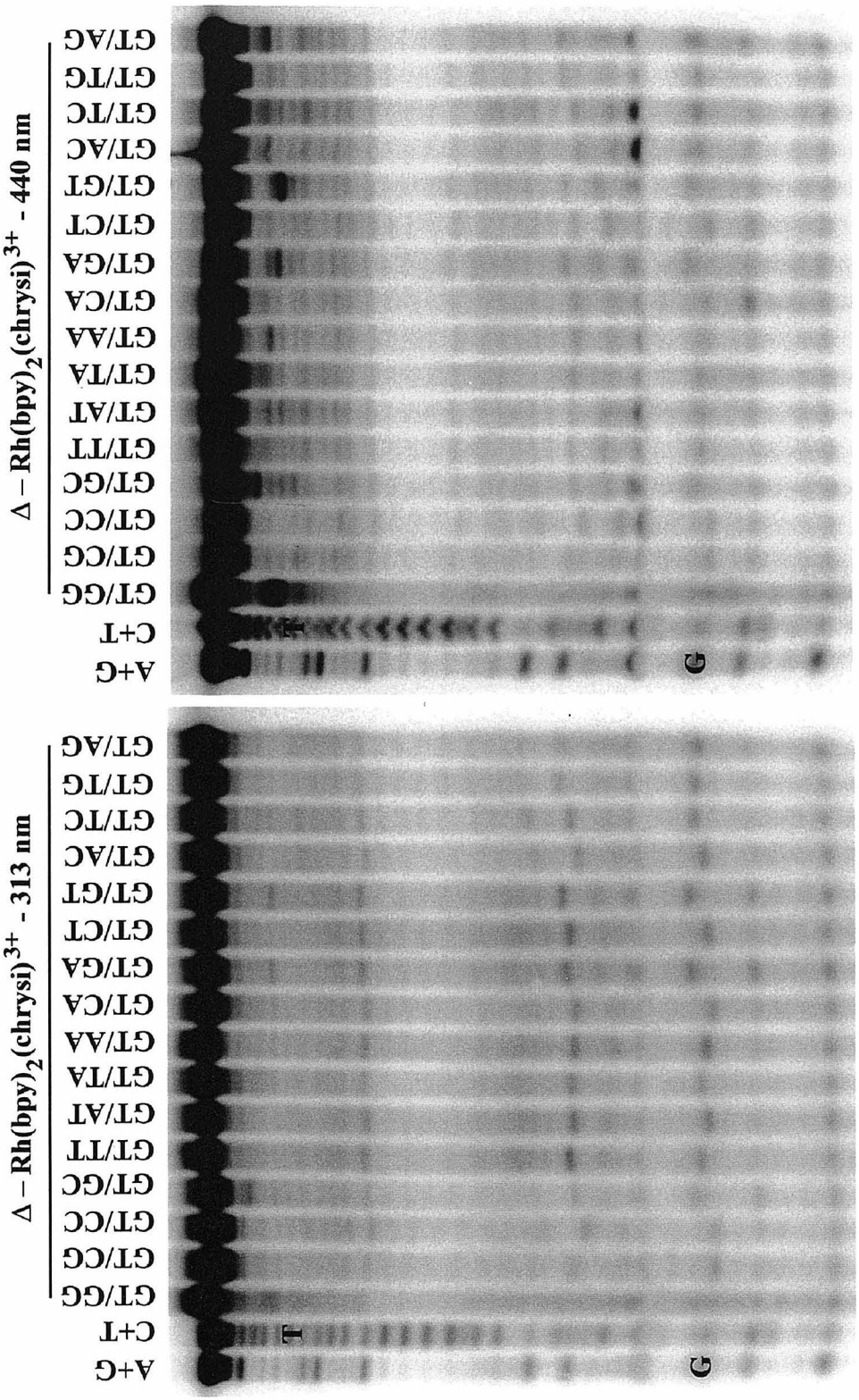
Figure 4.2. Comparison of DNA Photocleavage by Δ-$[Rh(bpy)_2(chrysi)]^{3+}$ on DNA Hairpins Containing All Base Mismatches in All Single Base Sequence Contexts at 313 nm and 440 nm. Samples identical to those described in the caption to Figure 4.1 were prepared of each DNA hairpin with Δ-$[Rh(bpy)_2(chrysi)]Cl_3$ and irradiated at 440 nm for 30 min. These samples were subsequently treated identically as described in the previous figure caption. The results from the analogous 313 nm irradiations are reproduced next to the 440 nm PAGE autoradiograms for comparison. Although Δ-$[Rh(bpy)_2(chrysi)]^{3+}$ does recognize most mismatch sites, it is clear that the sequence context, either by changing the structure or destabilization at the site, has a strong effect on the intensity of observed DNA photocleavage.

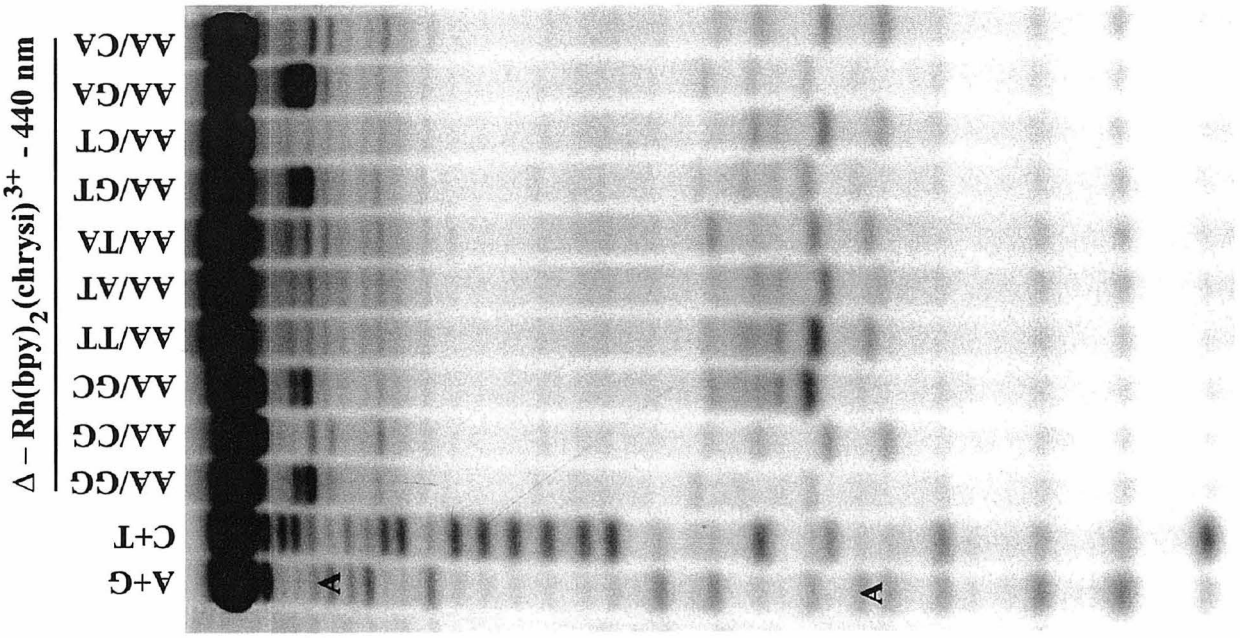

Δ – Rh(bpy)2(chrysi)3+ - 440 nm
CC/CA
CC/GA
CC/CT
CC/GT
CC/TA
CC/AT
CC/TT
CC/GC
CC/CG
CC/GG
C+T
A+G
Δ – Rh(bpy)2(chrysi)3+ - 313 nm
CC/CA
CC/GA
CC/CT
CC/GT
CC/TA
CC/AT
CC/TT
CC/GC
CC/CG
CC/GG
C+T
A+G

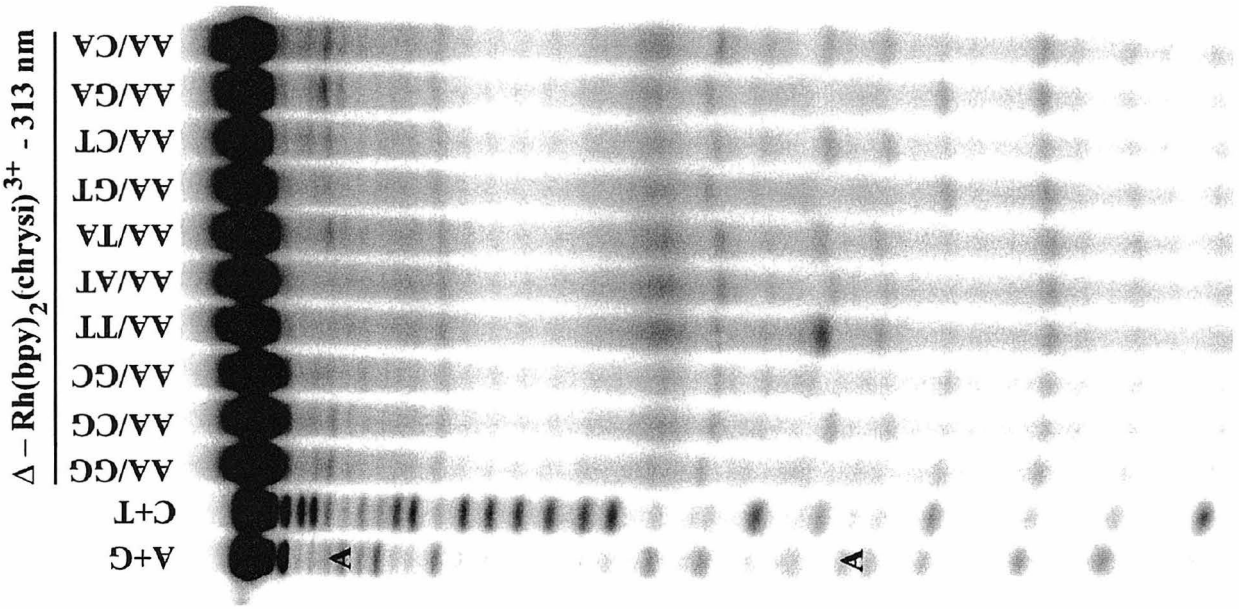

Δ – Rh(bpy)2(chrysi)3+ - 440 nm
Δ – Rh(bpy)2(chrysi)3+ - 313 nm
A+G
C+T
CT/GG
CT/CG
CT/CC
CT/GC
CT/TT
CT/AT
CT/TA
CT/AA
CT/CA
CT/GA
CT/CT
CT/GT
CT/AC
CT/TC
CT/TG
CT/AG
T
C

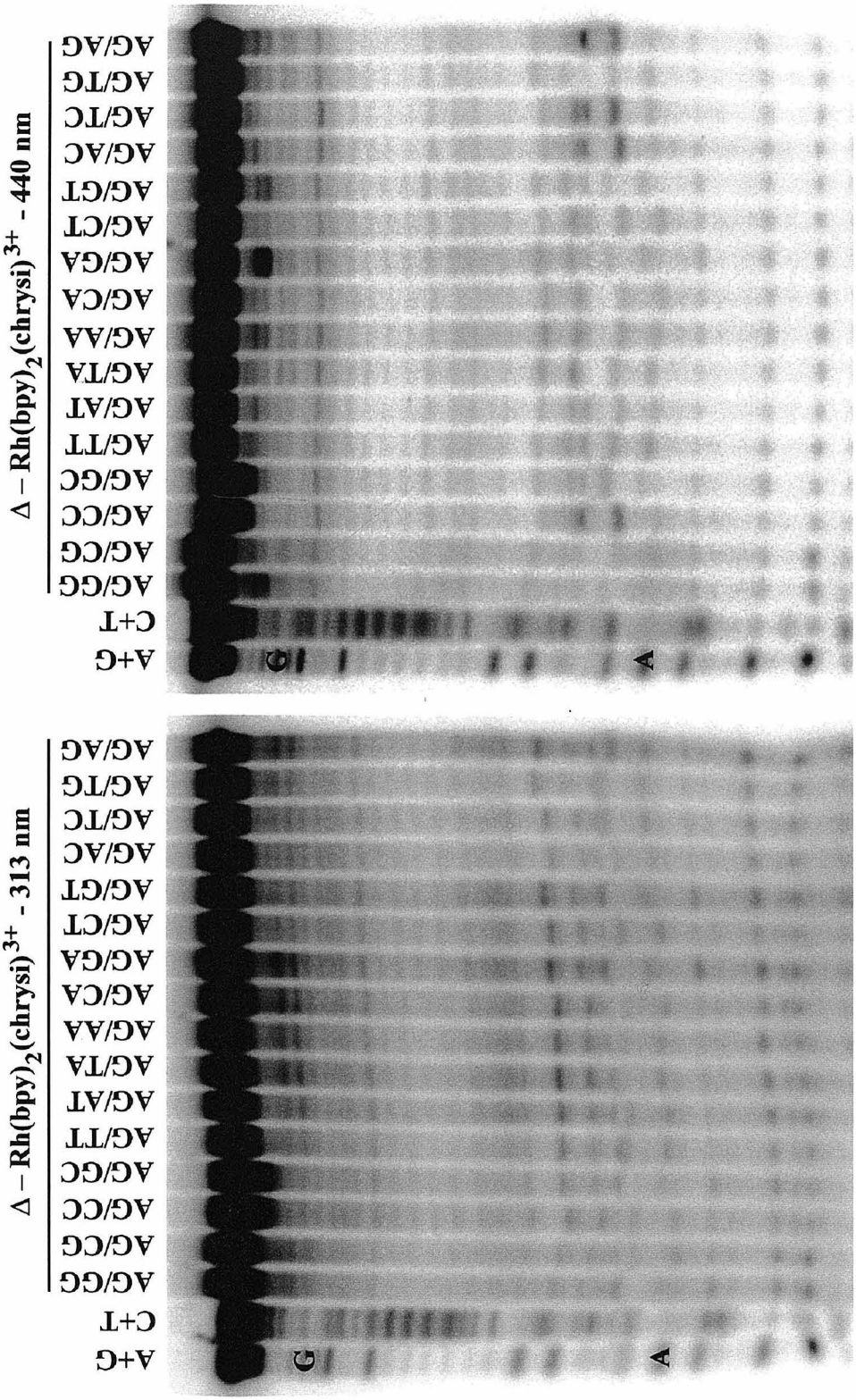

Δ – Rh(bpy)2(chrysi)3+ - 440 nm
TT/CA
TT/GA
TT/CT
TT/GT
TT/TA
TT/AT
TT/TT
TT/GC
TT/CG
TT/GG
C+T
A+G
Δ – Rh(bpy)2(chrysi)3+ - 313 nm
TT/CA
TT/GA
TT/CT
TT/GT
TT/TA
TT/AT
TT/TT
TT/GC
TT/CG
TT/GG
C+T
A+G

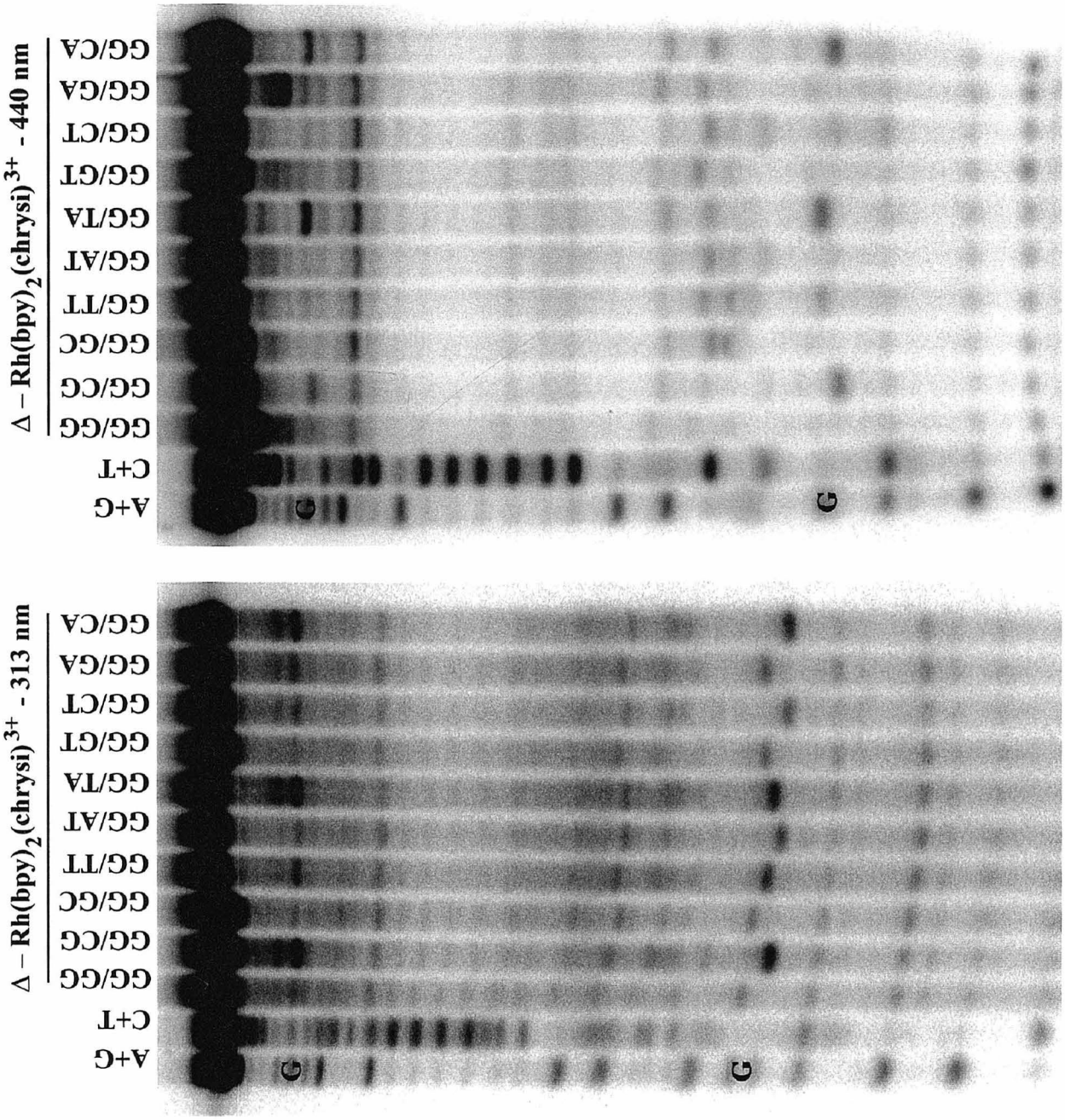

Δ – Rh(bpy)2(chrysi)3+ - 440 nm
Δ – Rh(bpy)2(chrysi)3+ - 313 nm
A+G
C+T
AC/GG
AC/CG
AC/CC
AC/GC
AC/TT
AC/AT
AC/TA
AC/AA
AC/CA
AC/GA
AC/CT
AC/GT
AC/AC
AC/TC
AC/TG
AC/AG


Δ – Rh(bpy)2(chrysi)3+ - 440 nm
Δ – Rh(bpy)2(chrysi)3+ - 313 nm
A+G
C+T
GT/GG
GT/CG
GT/CC
GT/GC
GT/TT
GT/AT
GT/TA
GT/AA
GT/CA
GT/GA
GT/CT
GT/GT
GT/AC
GT/TC
GT/TG
GT/AG
T
G


Δ – Rh(bpy)2(chrysi)3+ - 440 nm
AA/CA
AA/GA
AA/CT
AA/GT
AA/TA
AA/AT
AA/TT
AA/GC
AA/CG
AA/GG
C+T
A+G
A
A


Δ – Rh(bpy)2(chrysi)3+ - 313 nm
AA/CA
AA/GA
AA/CT
AA/GT
AA/TA
AA/AT
AA/TT
AA/GC
AA/CG
AA/GG
C+T
A+G
A
A


Δ – Rh(bpy)2(chrysi)3+ - 440 nm
Δ – Rh(bpy)2(chrysi)3+ - 313 nm
A+G
C+T
AG/GG
AG/CG
AG/CC
AG/GC
AG/TT
AG/AT
AG/TA
AG/AA
AG/CA
AG/GA
AG/CT
AG/GT
AG/AC
AG/TC
AG/TG
AG/AG
G
A


Δ – Rh(bpy)2(chrysi)3+ - 313 nm
Δ – Rh(bpy)2(chrysi)3+ - 440 nm
A+G
C+T
GG/GG
GG/CG
GG/GC
GG/TT
GG/AT
GG/TA
GG/GT
GG/CT
GG/GA
GG/CA
G
G
G
G

(30 min irradiation) is much greater than that observed at 313 nm (10 min irradiation). As a result, some mismatches whose recognition was impossible to discern with the higher energy irradiation (GT/GT, for example) is resolved from the background damage and becomes clear. In addition, the non-stoichiometric cleavage behavior which was alluded to in the previous chapter is also observed here. In several lanes (CT/CC and CT/TC in particular), most of the full length DNA strand has been cleaved at the mismatch site. This level of cleavage is unexpected given the ratio of Rh complex to DNA polymers in the irradiation sample is 1:2.*

Although the metal complex does cleave at a great variety of mismatch sites, it is important to note that the intensity of DNA cleavage varies greatly as the sequence context around the mismatch site is changed (Figure 4.1 & 4.2). These differences in cleavage intensity likely arise as a result of variations in the geometry of the mismatch sites in different sequence contexts; these different geometries could exert a number of influences including effects on rhodium complex binding and, once bound, on its efficiency of DNA photocleavage. Cleavage is usually observed 3' to the mismatch site although cutting also occasionally occurs at the mismatched base itself. This cleavage at the mismatched base can be the primary cleavage product, as observed in the GG mismatches, or can appear as a minor product in addition to the primary cleavage at the 3' base. This case is observed, for example, in members of

---

* It is also interesting to note that when the wavelength is changed, certain photocleavage reactions also seem to show a change in cleavage specificity. This is particularly clear in the GG mismatch case where cleavage appears in almost every lane at a cytosine base to the 5' of the mismatch site (Figure 4.2). This cleavage product, which is observed to varying extents in all the GG containing cleavage experiments, occurs in the 440 nm irradiation samples but not in the 313 nm irradiations. This change in the specificity of cleavage with a change in irradiation wavelength suggests another photochemical reaction with DNA. This will be discussed in more depth in the subsequent chapter.

the AC, TT, and AA mismatch families. In a very few cases, cleavage is observed at bases to the 5' side of the mismatch site (TT/GC, TT/CT, CT/CC, CT/TC & CT/GC). In all cases, DNA irradiated in the absence of metal complex or DNA incubated with metal complex in the absence of light showed no significant strand cleavage (data not shown).

In addition to variations in the position of DNA cleavage relative to the mismatch site, different mismatch-sequence context combinations also display markedly different strand distributions of DNA photocleavage. Taking photocleavage at the CT mismatch as an example, it is readily apparent that the sequence context around the mismatch can have a very significant effect on which DNA strand is cleaved. In some cases, like CT/CC and CT/GG, cleavage is very asymmetric with a strong preference for one strand over another.* In a more symmetrical sequence context, like CT/AT, cutting is much more evenly distributed between the two strands. These differences in both the exact position and distribution of photocleavage are likely determined by the complex interaction of the asymmetrical chrysi intercalating ligand with the various DNA sites.

Although it is well known that differences in the sequence context around mismatches have significant effects on the stability of the sites,[3-8] no comparably exhaustive studies have been done to characterize the exact structural consequences of differences in sequence context around a mismatch site. It is reasonable to assume, however, that the differences in base stacking, hydrogen bonding, and base pair geometry which generate the varied thermodynamic consequences of mismatch

---

* It is also possible that a reactivity preference with one base over another could explain the strand preferences for DNA photocleavage. This possibility will be more completely explored in the subsequent chapter.

incorporation in the helix result in different geometries from site to site. As will be discussed in more detail in the following section, it is only reasonable that such differences in site geometry would affect the interaction of the metal complex with the mismatch binding site and its subsequent photocleavage of DNA. These effects could include, but are not necessarily limited to, influencing the binding constant of the complex and therefore affecting the fractional occupancy of different mismatch sites, generating differences in the kinetics of association of the complex and various sites, and placing constraints on the exact geometry of the interaction between the complex and a given mismatch. Because of the nature of the DNA photocleavage reaction, which requires the abstraction of a sugar hydrogen atom by a photo-generated radical, such differences in the geometry of the bound complex could produce significant differences in the photocleavage efficiency of the complex from site to site.

Moving away from discussion of the exact positions and intensities of photocleavage, some generalizations about the recognition characteristics of $[Rh(bpy)_2(chrysi)]^{3+}$ can be made. The most readily recognized mismatches, CC, TT, CT, AC and AA, show cleavage in all the mismatch sequence context combinations but to varying extents. Of these cases, the pyrimidine-pyrimidine mismatches (CC, CT and TT) and the purine-pyrimidine mismatch (AC) show the most intense cleavage. Of the remaining cases, the AG, GG, and GT mispairs all show cleavage in a few sequence contexts, but all cleavage is much less intense than that observed with the other mismatches. This weaker recognition of these mainly purine containing mispairs is understandable given that these mismatches are generally the least destabilizing of the DNA duplex. In addition, these results also confirm the correlation discussed in the previous chapter between thermodynamic destabilization at the mismatch site and photocleavage by $[Rh(bpy)_2(chrysi)]^{3+}$. When the average values of the

Table 4.1: Average Free Energy Change as a Result of Mismatch Incorporation – All Sequence Contexts‡

Mismatch:*	$\Delta G°_{37}$:† (kcal/mol)
CC	2.1 (0.1)
TT	1.2 (0.1)
CT	1.1 (0.2)
CA	1.0 (0.2)
AA	0.88 (0.1)
GT	0.09 (0.1)
GA	-0.04 (0.2)
GG	-0.54 (0.1)

‡ Computed from data derived from references 3-8.

* Values are averages computed for all the possible sequence-context combinations for a given mismatch.

† Destabilization values generated from literature values of thermodynamic parameters of duplex formation measured from thermal melting of oligonucleotides in 1 M NaCl, 10 mM sodium cacodylate, and 0.5 mM Na_2EDTA, pH 7.0. Errors indicated in parentheses.

thermodynamic destabilization caused by each mismatch in all its possible sequence contexts are calculated,[3-8] the trend in the values is the same as that identified in the photocleavage experiments (Table 4.1).

When all the experiments in Figures 4.1 and 4.2 are considered, the metal complex shows detectable DNA cleavage at approximately 80% (83 of 104) of the mismatch/sequence context combinations shown and, when symmetry is taken into account, 82% (105 of 128) of the total possible mismatch sites.

4.3.1.2: A Closer Examination of Recognition of Mismatch Recognition by $[Rh(bpy)_2(chrysi)]^{3+}$ – Implications for a Recognition Model

Although there is clearly a relationship between increased thermodynamic destabilization and more facile recognition of a given mismatch by $[Rh(bpy)_2(chrysi)]^{3+}$, a closer examination of individual mismatch-specific cleavage shows that this correlation is somewhat limited. To make this examination, the DNA photocleavage by $[Rh(bpy)_2(chrysi)]^{3+}$ at 313 nm (shown in Figure 4.1) was quantitated using the Imagequant software package. The 313 nm data set was

selected over the longer wavelength irradiations in an attempt to avoid any interference from the non-stoichiometric cleavage behavior discussed previously. The intensities of the photocleavage bands two bases to the 3' of the mismatch site on each strand of the DNA hairpin were calculated and expressed as a cleavage fraction.* This cleavage fraction was adjusted by identical measurements made on the light control samples for each irradiation lane. Plots of the resulting metal-complex-specific cleavage fractions versus the thermodynamic destabilization associated with each individual mismatch site are included as Figure 4.3 and 4.4. When these data are examined, it is clear that there is not a simple correlation between the thermodynamic destabilization and photocleavage intensity at a site. In some cases, like the AC mismatch, for example, sites with negative destabilization values (i.e., the presence of the mismatch actually stabilizes the duplex compared to the Watson-Crick DNA) show a higher cleavage fraction than more destabilized sites. In addition, there are many examples, in virtually all the mismatch families, of sites with greater destabilization displaying less photocleavage than other, less thermodynamically perturbed, mismatches.

It is not surprising that the single characteristic of thermodynamic destabilization does not show a tight correlation with these DNA photocleavage data. The chrysenequinone diimine ligand, because of its steric bulk, was designed to be selective for open or disordered sites in DNA. Although it is reasonable to assume that mismatch sites which have a destabilizing effect on the thermodynamics of the DNA duplex will be more likely to have such open and disordered sites at or near the mismatch, it is the DNA structure, not the thermodynamic destabilization itself,

---

* The denominator of this fraction cleaved was the sum of both the uncleaved, parent DNA band and the quantitated mismatch-specific cleavage bands.

Figure 4.3. Quantitated 313 nm Photocleavage by Δ-$[Rh(bpy)_2(chrysi)]^{3+}$ on DNA Hairpins Containing CC, TT, CT, and AC Base Mismatches. Data from the autoradiograms included in Figure 4.1 was quantitated using the Imagequant software package as described in the text. Photocleavage intensity, adjusted for damage observed in irradiations of the DNA in the absence of metal complex, was quantitated at the two bases to the 3' side of each mismatch site on both strands of the DNA. This value, serving as an approximation of the total cleavage at each mismatch in each sequence context, was expressed as a cleavage fraction by dividing by the sum of the quantitated photocleavage bands and the uncleaved full length DNA band. This data was plotted as a function of the thermodynamic destabilization at each mismatch site.[3-8] Note that in these more destabilizing mismatches there is little correlation between increasing photocleavage and increasing thermodynamic destabilization. In the terms of the binding model described in the text, this implies that factors other than access to the DNA helix control binding affinity at these sites.

Figure 4.3:

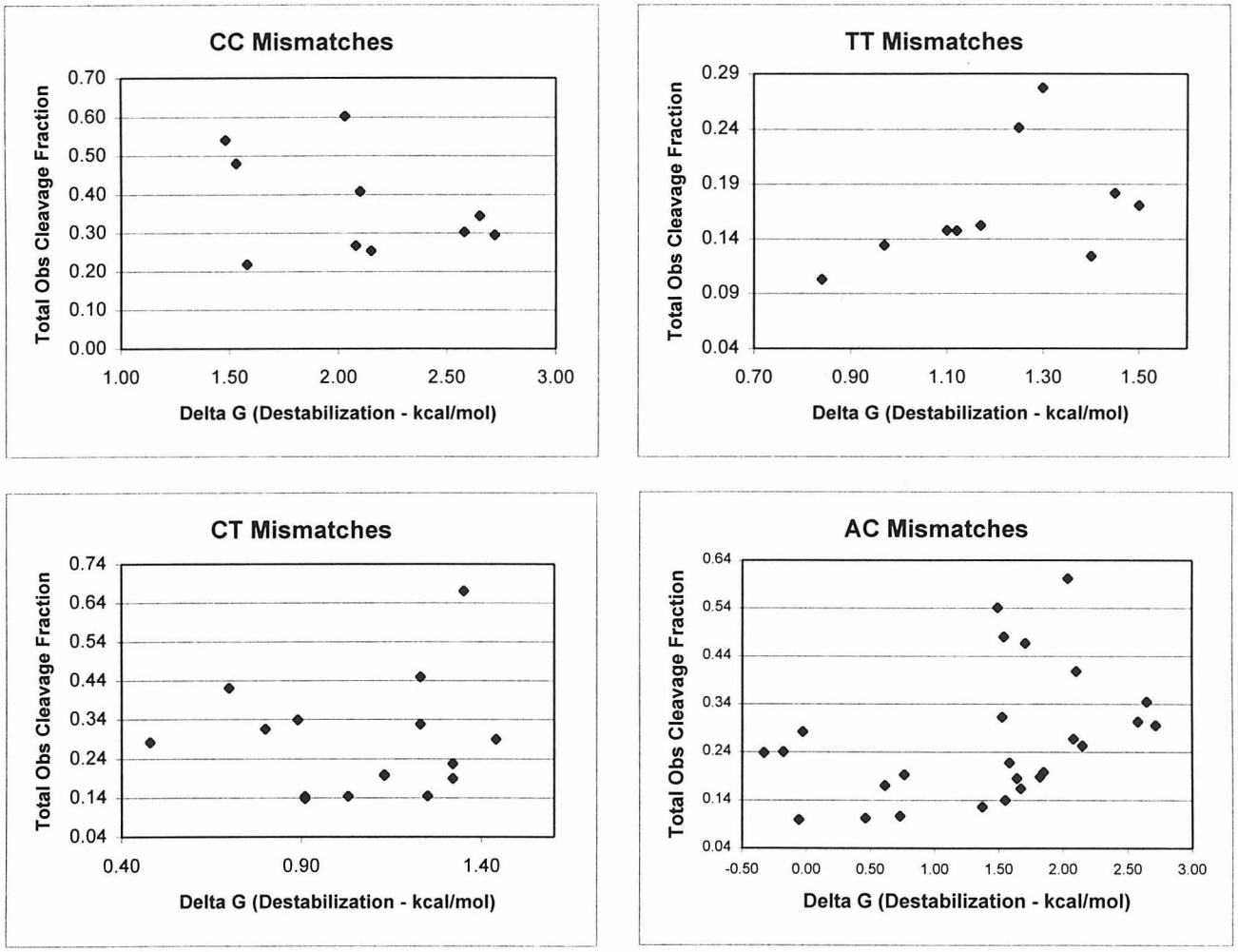
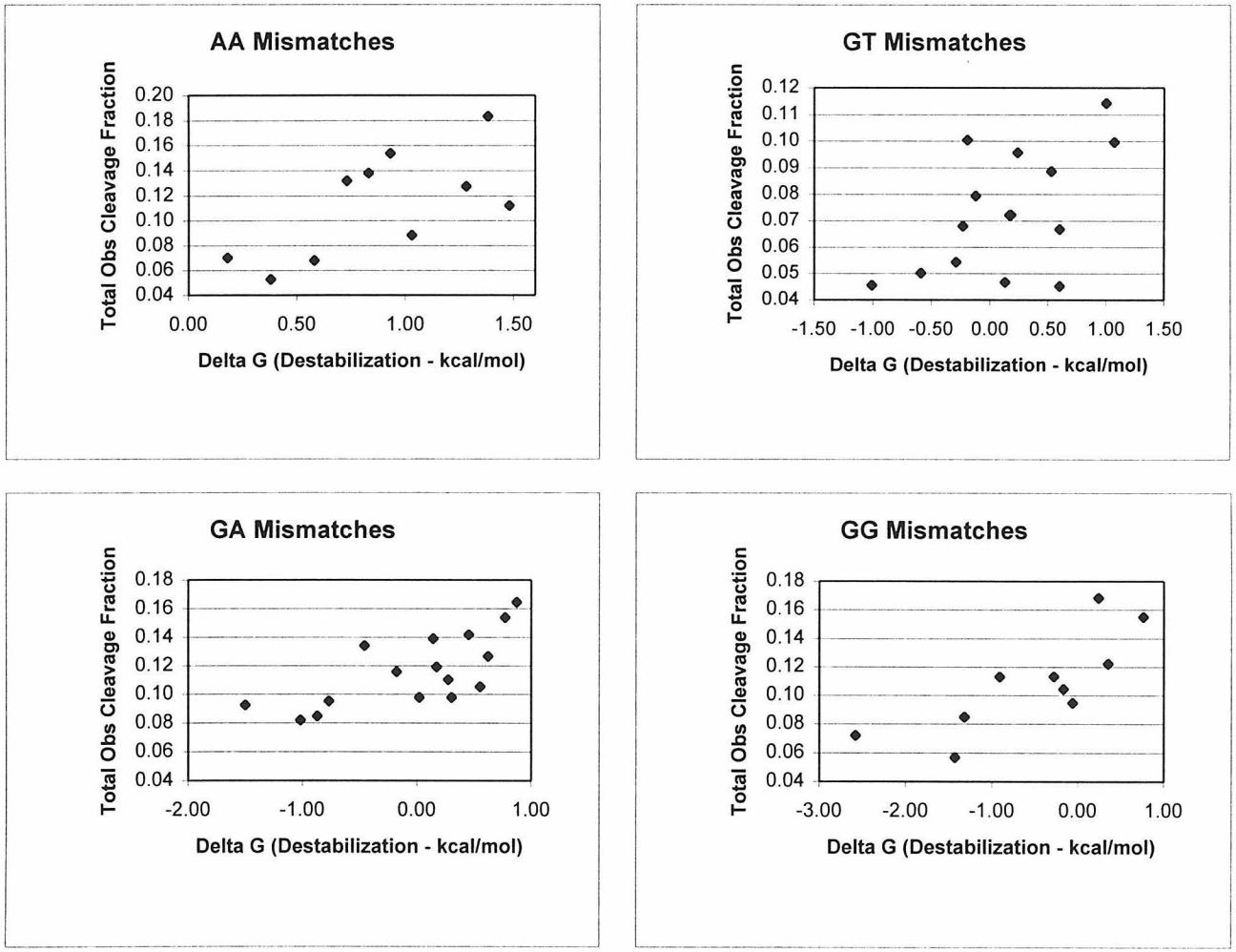

CC Mismatches
Total Obs Cleavage Fraction
0.70
0.60
0.50
0.40
0.30
0.20
0.10
0.00
1.00
1.50
2.00
2.50
3.00
Delta G (Destabilization - kcal/mol)
TT Mismatches
Total Obs Cleavage Fraction
0.29
0.24
0.19
0.14
0.09
0.04
0.70
0.90
1.10
1.30
1.50
Delta G (Destabilization - kcal/mol)
CT Mismatches
Total Obs Cleavage Fraction
0.74
0.64
0.54
0.44
0.34
0.24
0.14
0.04
0.40
0.90
1.40
Delta G (Destabilization - kcal/mol)
AC Mismatches
Total Obs Cleavage Fraction
0.64
0.54
0.44
0.34
0.24
0.14
0.04
-0.50
0.00
0.50
1.00
1.50
2.00
2.50
3.00
Delta G (Destabilization - kcal/mol)

Figure 4.4. Quantitated 313 nm Photocleavage by Δ-$[Rh(bpy)_2(chrysi)]^{3+}$ on DNA Hairpins Containing AA, GT, GA, and GG Base Mismatches. Data from the autoradiograms included in Figure 4.1 was quantitated using the Imagequant software package as described in the text. Photocleavage intensity, adjusted for damage observed in irradiations of the DNA in the absence of metal complex, was quantiated at the two bases to the 3' side of each mismatch site on both strands of the DNA. This value, serving as an approximation of the total cleavage at each mismatch in each sequence context, was expressed as a cleavage fraction by dividing by the sum of the quantitated photocleavage bands and the uncleaved full length DNA band. This data was plotted as a function of the thermodynamic destabilization at each mismatch site.[3-8] Note that in these less destabilizing mismatches there is a correlation between increasing photocleavage and increasing thermodynamic destabilization. In the terms of the binding model described in the text, this implies that these cases are likely "access limited" where the ability of the chrysi intercalator to bind into the helix is the primary determinant of binding affinity at these sites.

Figure 4.4:


AA Mismatches
Total Obs Cleavage Fraction
0.20
0.18
0.16
0.14
0.12
0.10
0.08
0.06
0.04
0.00
0.50
1.00
1.50
Delta G (Destabilization - kcal/mol)
GT Mismatches
Total Obs Cleavage Fraction
0.12
0.11
0.10
0.09
0.08
0.07
0.06
0.05
0.04
-1.50
-1.00
-0.50
0.00
0.50
1.00
1.50
Delta G (Destabilization - kcal/mol)
GA Mismatches
Total Obs Cleavage Fraction
0.18
0.16
0.14
0.12
0.10
0.08
0.06
0.04
-2.00
-1.00
0.00
1.00
Delta G (Destabilization - kcal/mol)
GG Mismatches
Total Obs Cleavage Fraction
0.18
0.16
0.14
0.12
0.10
0.08
0.06
0.04
-3.00
-2.00
-1.00
0.00
1.00
Delta G (Destabilization - kcal/mol)

which is recognized by the complex. As a result, in these analyses, the measured thermodynamic parameter is actually standing proxy for an unknown quantity – the extent that each of these mismatches, in all their different sequence contexts, generate open and accessible structures in the DNA which facilitate binding of the metal complex.

It is also important to note that such open and disordered structures are not the *only* parameters which dictate the binding affinity of $[Rh(bpy)_2(chrysi)]^{3+}$ for a given mismatch site. The binding affinity of this metal complex for the DNA is primarily provided by the stacking of the intercalating ligand into the DNA helix. This interaction will clearly be influenced by the identity of the bases on either side of the mismatch and how those bases are positioned to participate in stacking. In a related manner, this binding energy will be affected by the nature of the mismatch itself. If the mismatched base is forced into an extrahelical conformation by the binding of the complex, any stacking interactions with the mismatch will not occur; if the mismatch is still within the helix, however, the particular geometry and stacking surface which it provides for the ligand will have a large effect on the binding affinity.

The binding of rhodium polypyridyl complexes to DNA is also influenced the shape and identity of their ancillary ligands. These shape-selective interactions have been used to generate geometry selective probes of DNA structure. As a result, it is also likely that the binding of $[Rh(bpy)_2(chrysi)]^{3+}$ to particular mismatch sites is affected not only by the accessibility of the helix for chrysi intercalation, but also by the more qualitative shape of the DNA binding site. There is no reason why these differences in geometry, although related to the destabilizing consequences of the DNA mismatch, would vary regularly with the thermodynamic parameters of the mismatch sites. It is also relevant to note that the differences in geometry, both inside the helix

and more generally, could have significant effects on the efficiency with which the complex can photocleave the DNA. If, for example, the compound bound in a way where the DNA backbone was inaccessible to the photo-generated radical on the intercalated ligand, it is possible that sites where the complex binds strongly might not result in intense photocleavage bands.

Acknowledging the many factors which likely affect the binding of particular mismatch sites by $[Rh(bpy)_2(chrysi)]^{3+}$, it is still worthwhile to examine this cleavage data from the point of view of the binding model discussed in the previous chapter. The premise of that model, based on photocleavage experiments performed on various mismatches in constant sequence contexts, was that thermodynamic destabilization acted as a "door" which controlled the access of the chrysi intercalator to the DNA helix. In that formalism, destabilization increasing from very low values allowed an increase in access and therefore a corresponding increase in binding and photocleavage. Once the helix was sufficiently destabilized to allow binding, however, additional destabilization caused no additional increase in binding or cleavage. The data included in Figures 4.3 and 4.4 are broadly consistent with this description of the binding of DNA by $[Rh(bpy)_2(chrysi)]^{3+}$. In the mismatches which are either stabilizing or destabilize the helix to a small extent (GG, GA, AA; Figure 4.4), increases in thermodynamic destabilization do result in corresponding increases in DNA photocleavage. This is consistent with these sites being "access limited" where small increases in the amount of destabilization have a direct and proportional effect on the amount of metal complex which is able to bind. In case of the more destabilizing mismatches, however, there is no indication of a direct relationship between thermodynamic destabilization and the extent of DNA photocleavage (Figure 4.3). Especially in the CC and CT cases, there is *no* trendline which one could envision putting through the data. This observation is consistent with these

mismatches being above the threshold level of destabilization where additional disorder does not translate into additional metal complex binding. In these cases it is likely that the other factors discussed above, including stacking of the chrysi ligand and the overall structure of the sites, dominate the binding affinity and subsequent photocleavage. As a result, increases in destabilization would not have a positive effect on binding and, depending on their geometrical consequences, might result in reduced cleavage.

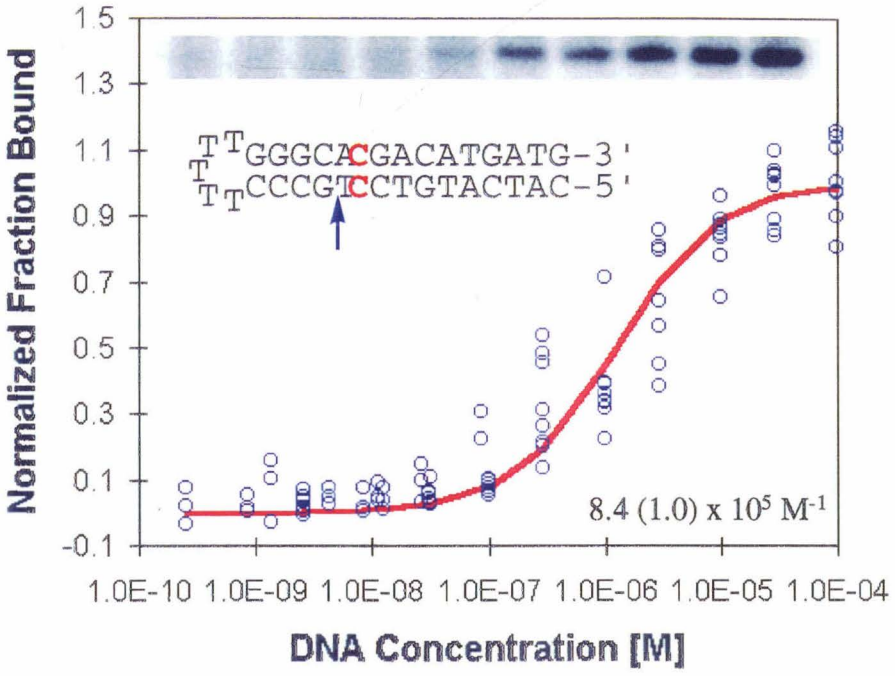
4.3.2: High Selectivity

4.3.2.1: Measurement of Binding Constants of Δ-$[Rh(bpy)_2(chrysi)]^{3+}$ to Mismatch Sites

In an attempt to remove a level of the uncertainty associated with discussing DNA mismatch recognition in terms of DNA photocleavage intensities, significant work was devoted to both the development of methodology and the direct measurement of the thermodynamic association constants of Δ-$[Rh(bpy)_2(chrysi)]^{3+}$ at a variety of mismatch sites. These experiments, the theoretical basis of which is discussed in Appendix 2, consisted of constructing an equilibrium binding isotherm for the complex at mismatch sites by photocleavage titration. By increasing both the concentration of the rhodium complex and a short DNA oligonucleotide hairpin containing the mismatch site, it is possible to generate binding curves which are independent of any differences in DNA photocleavage efficiency from site to site. An example of such a binding curve, assembled from data derived from a number of independent binding trials, is included as Figure 4.5. Similar experiments were run on a number of mismatch-containing oligonucleotide hairpins. The resulting binding

Figure 4.5. Binding isotherm for Δ-$[Rh(bpy)_2(chrysi)]^{3+}$ targeted to a CC mismatch-containing oligonucleotide. Top Inset: Excised gel bands from a representative photocleavage titration experiment. The binding constant was determined on a hairpin oligonucleotide, 5'-CATCATGTC**C**TGCCCTTTTTGGGCA**C**GACATGATG-3' (Bottom Inset), containing a single CC base mismatch (involved bases boldface). Photocleavage reactions were performed at either 313 nm or 365 nm for 7.5 to 15 min. The concentration of hairpin DNA varied from 3×10^{-10} M to 1×10^{-4} M with the rhodium complex at tenfold lower concentration. After photocleavage, samples were electrophoresed and quantitated as described. Cleavage is observed 3' to the CC mismatch on both sides of the hairpin; only the cleavage band closest to the end label (indicated by the arrow) was quantitated. Data from multiple trials were normalized (open circles) and fit to a standard single binding site binding model (solid line) as described in the text and in Appendix 2.

Figure 4.5:


Normalized Fraction Bound
1.5
1.3
1.1
0.9
0.7
0.5
0.3
0.1
-0.1
TTGGGCACGACATGATG-3'
TTCCCGTCCTGTACTAC-5'
8.4 (1.0) x 10^5 M^-1
1.0E-10 1.0E-09 1.0E-08 1.0E-07 1.0E-06 1.0E-05 1.0E-04
DNA Concentration [M]

constants, identified with the same nomenclature defined for the context experiments above and discussed in the experimental section, is summarized in Table 4.2.

Table 4.2: Thermodynamic Binding Constants of Δ-$[Rh(bpy)_2(chrysi)]^{3+}$ at Varied Mismatch Sites‡

Mismatch Site:*	Thermodynamic Destabilization:℘ (kcal/mol)	K_B:† (x 10^6 M^{-1})
CC/GC	1.48 (0.20)	10.4 (7.3)
TT/GC	1.10 (0.20)	2.31 (0.36)
CT/GC	0.80 (0.72)	3.28 (0.65)
CA/GC	0.61 (0.51)	2.71 (0.50)
AA/GC	0.18 (0.30)	0.29 (0.26)
CC/AT	2.72 (0.16)	21.6 (11.4)
CC/AG	2.15 (0.18)	0.84 (0.10)

‡ Mismatch thermodynamic values obtained from references 3-8.

* Mismatch sites are identified with the general nomenclature PQ/XY where PQ identifies the nature of the base mismatch itself and XY the bases flanking the site to the 5' and 3' sides respectively on one strand of a DNA duplex.

℘ Mismatch destabilization values from references 3-8 were generated from thermodynamic parameters of duplex formation measured from thermal melting of oligonucleotides in 1 M NaCl, 10 mM sodium cacodylate, and 0.5 mM Na_2EDTA, pH 7.0. Errors indicated in parentheses.

† Binding constants of Δ-[Rh(bpy)2(chrysi)]3+ to mismatch-containing oligonucleotides were measured by photocleavage titration in 1x running buffer (50 mM Tris, 20 mM NaOAc, 18 mM NaCl, pH 7.0) at ambient temperature. Errors indicated in parentheses.

Although these data demonstrate that Δ-$[Rh(bpy)_2(chrysi)]^{3+}$ can bind very strongly to mismatch sites with association constants as high as 2 x 10^7 M^{-1}, like the photocleavage data discussed above, they do not unambiguously define a molecular recognition mechanism for the molecule. Even though these values eliminate the possible convolution of photocleavage efficiency with binding affinity, the correlation between these binding constant values and the thermodynamic destabilization at the mismatch sites is weak. Although it is true for the first series of constant-context association constants (Table 4.2, top) that the more destabilized sites generally have higher binding constants, this

relationship is not even fully preserved in this small data set. Comparing the association constants at the TT and CT mismatches, for example, even though the TT has a higher destabilization value by approx. 38%, the binding constant at CT exceeds TT by 42%. When the measurements on CC mismatch sites in other sequence contexts (Table 4.2, bottom) are considered as well, it is clear that there is no solid correlation.

These particular data on the CC mismatch sites also highlight the risk associated with equating photocleavage intensity with the binding affinity of the metal complex at a mismatch site. When the photocleavage intensity at the three measured CC mismatch binding sites are compared, it becomes clear that, not only is there little relationship between the thermodynamic destabilization and binding affinity, but there is also no relationship between their photocleavage intensities and the association constants at the site. The tightest binding site, CC/AT, has an observed cleavage fraction of 0.14. The weakest binding site, CC/AG (CC/CT reversed), has a comparable observed cleavage fraction of 0.13. It is the site with intermediate binding affinity, CC/GC, which shows the strongest cleavage at 0.40. It is not surprising that the binding of the rhodium complex to the highly disordered CC mismatch sites might result in markedly different photocleavage efficiencies depending on the orientation adopted by the intercalator in the DNA. It is also possible, which will be discussed in some detail later, that characteristics other than binding geometry could also influence photocleavage efficiency of the rhodium complex. Of these three sites, it is only the CC/GC site which has a cytosine in the position 3' to the mismatched C. Irrespective of the mismatch, the greatest levels of cleavage observed in the sequence context experiment discussed above (Figure 4.2) were observed when a cytosine occupied this position relative to the mismatch.

As a result, it can be concluded that characteristics of these mismatch binding sites which are not adequately represented by the thermodynamic destabilization caused by the mismatch have a significant effect on the binding affinity and photocleavage efficiency of Δ-$[Rh(bpy)_2(chrysi)]^{3+}$ at mismatch sites. Whether these characteristics are the stacking of the ligand into the DNA, the overall geometry of the mismatch site, or other reactivity considerations is not readily apparent. Independent of these concerns, however, these data do support a *qualitative* relationship between destabilization and chrysi intercalator binding and are consistent with a model of complex recognition based on destabilization "opening" the DNA helix for access by the sterically demanding intercalator.

4.3.2.2: Measurement of Δ-$[Rh(bpy)_2(chrysi)]^{3+}$ Binding Constants to B-DNA by Photocleavage Titrations

Although knowledge of the thermodynamic binding constants of Δ-$[Rh(bpy)_2(chrysi)]^{3+}$ at mismatch sites of interest is important to characterize the binding properties of the complex, those values alone are insufficient to define the specificity of the metal complex. In order to make this determination, it is necessary to have access to quantitative measurements of the binding affinity of the complex for mixed sequence, properly paired DNA so that the association constants at desired sites can be compared to this "non-specific" binding affinity to DNA independent of its sequence or level of destabilization. Although the spectrophotometric titrations discussed in the previous chapter did provide an estimate of this binding affinity, more accurate values are desirable for comparison with the compound's mismatch-specific association constants.

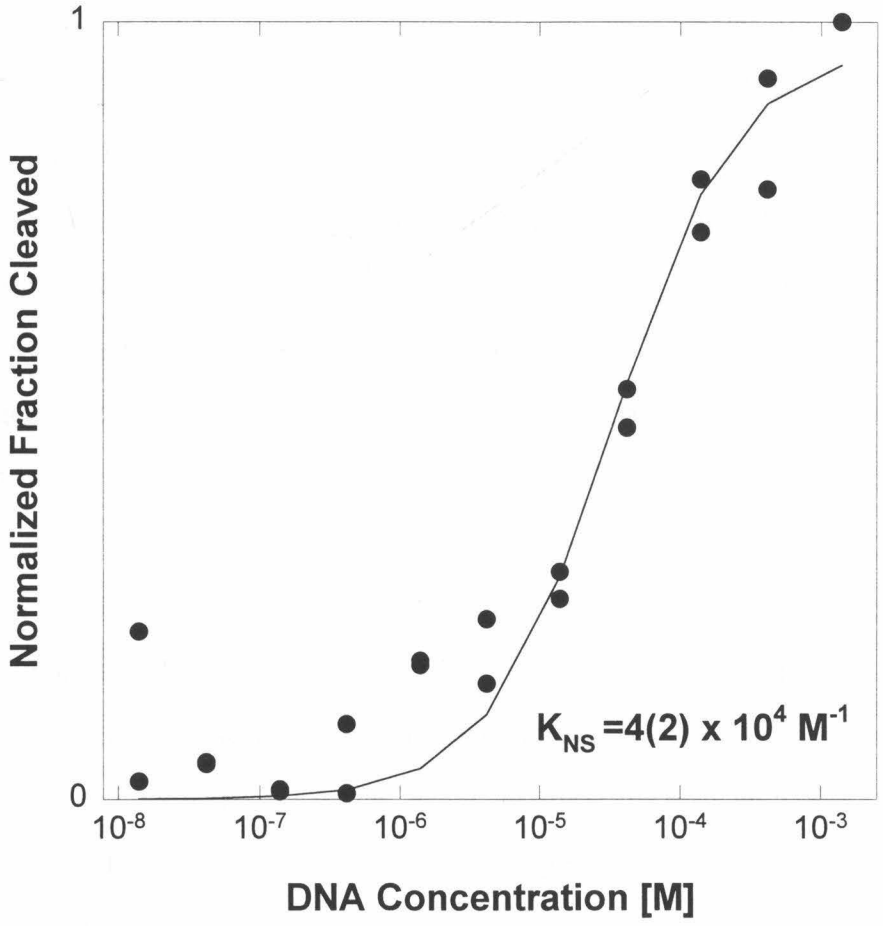
Measurement by Direct Photocleavage Titration: The task of measuring the association constant of Δ-$[Rh(bpy)_2(chrysi)]^{3+}$ for B-form DNA was approached in two ways. The first method, which is discussed at length in the appendix, was a direct photocleavage titration on a hairpin DNA which contained no high-affinity sites for the compound. After performing a photocleavage titration analogous to that described in the previous section for mismatch-containing hairpins, the cleavage over the entire "non-specific" hairpin is quantitated and an average binding isotherm fit to the data. This method, unlike the spectroscopic titration discussed above, has the advantage that it measures only binding modes which lead to photo-induced strand scission. As a result, spectral changes that might be associated with less intimate association between the nucleic acid and the rhodium complex which might be included in the earlier measurements will not affect measurements made using this methodology. A fitted isotherm generated using this procedure is included as Figure 4.6. As indicated in the figure, the association constant of Δ-$[Rh(bpy)_2(chrysi)]^{3+}$ for B-DNA measured in this titration is $4(2) \times 10^4\ M^{-1}$. This value is smaller, by an order of magnitude, than the value determined in the spectroscopic titrations discussed previously. This suggests that the spectral measurements do contain significant interference from binding modes which do not lead to strand scission upon photo-activation. It should also be noted that this binding curve may still represent an over-estimate of the binding affinity of Δ-$[Rh(bpy)_2(chrysi)]^{3+}$ for this hairpin DNA. Although the trend in the data near the top of the binding isotherm does appear to be beginning to form the asymptotic plateau characteristic of saturation, this trend is not as unambiguous as, for example, that observed in Figure 4.5. Increasing the concentration of the DNA beyond those included in the figure is not readily practical. As a result, the possibility exists that, if the titration could be continued, the measured association constant would be even lower in magnitude.

Figure 4.6. Binding isotherm for Δ-$[Rh(bpy)_2(chrysi)]^{3+}$ targeted to a non-specific hairpin oligonucleotide. Photocleavage titration analagous to that described in Figure 4.5 was performed using the B-form hairpin oligonucleotide:

5'-GCGGTTGAATGAGCTTTTTGCTCATTCAACCGC-3'

from a concentration of 1 x 10^{-9} M to 1 x 10^{-4} M DNA polymers. Δ-$[Rh(bpy)_2(chrysi)]^{3+}$ was held at a constant Rh:DNA ratio of 1:2. Samples were mixed 30 min before irradiation at 365 nm for 15 min. Reactions were electrophoresed and analyzed as described. Fraction cleavage over the entire gel lane was quanititated and fit to a multi-site binding model as described in Appendix 2.

Figure 4.6:


1
0
Normalized Fraction Cleaved
K_{NS} =4(2) x 10^4 M^{-1}
10^{-8}
10^{-7}
10^{-6}
10^{-5}
10^{-4}
10^{-3}
DNA Concentration [M]

Measurement by Competition Titration: In an attempt to address the possibility that the association constant of Δ-$[Rh(bpy)_2(chrysi)]^{3+}$ for B-DNA might be lower than could be practically measured by direct titration, a second approach to determine this value was developed. In this alternate procedure, a rhodium-DNA system with a known, high-affinity association constant was titrated with increasing concentrations of B-form DNA; this made it possible to determine the concentration at which binding to this added DNA successfully competed with binding and photocleavage at the high-affinity site. An example of the data obtained in such an experiment is included as Figure 4.7. Such an approach has both advantages and disadvantages over the direct measurement discussed in the previous paragraphs. Most significant among its advantages is that it is not limited as readily by the upper concentration limits discussed above. Since there are no sequence "requirements" for the exogenous competitor DNA, virtually any commercially available polymers can be used.

Unlike the direct titration, however, this competitive titration is not restricted to the measurement of binding modes which lead to photo-induced strand scission. As a result, similar to the spectroscopic titration, the possibility exists that other, non-intercalative binding modes will contribute to the value measured using this technique. In reality, however, this is not a significant disadvantage. Although alternate binding modes were problematic for spectroscopic titrations because of their potential to convolute the hypochromicity measurements in unclear ways, they do not pose such difficulty in this system. In this case, since what is being observed is the loss of photocleavage at a site of known binding constant, there is no ambiguity about the contributions that varied binding modes could make to the measurement of the average B-DNA binding constant. Other modes *will* contribute to the titration of photocleavage but, unlike the spectroscopic case, they will necessarily contribute

Figure 4.7. Titration of Specific Binding and Photocleavage by Δ-$[Rh(bpy)_2(chrysi)]^{3+}$ at the CC Mismatch Site 5'-C***C***T-3' with Increasing Amounts of Added Carrier DNA. Samples of the hairpin DNA,



combined with the rhodium complex (0.5 μM in each) were combined with increasing amounts of either the oligonucleotide,

5'-GCGGTATCTAGAGCGCATCTGGGCG-3'

annealed to its complement or with sonicated calf thymus DNA. The ratio between the mismatch sites and the carrier base pairs increase from 0 (No Carrier) to 25,000 as shown above the gel lanes. Irradiation samples were irradiated for 15 min at 365 nm after a 14 min preincubation period. Lanes labeled DC and LC correspond to DNA incubated with the metal complex in the absence of light and DNA irradiated in the absence of the metal complex respectively. Lanes labeled A+G and C+T are standard Maxam-Gilbert chemical sequencing as described in the text. All samples were treated and electrophoresed as described in the text.

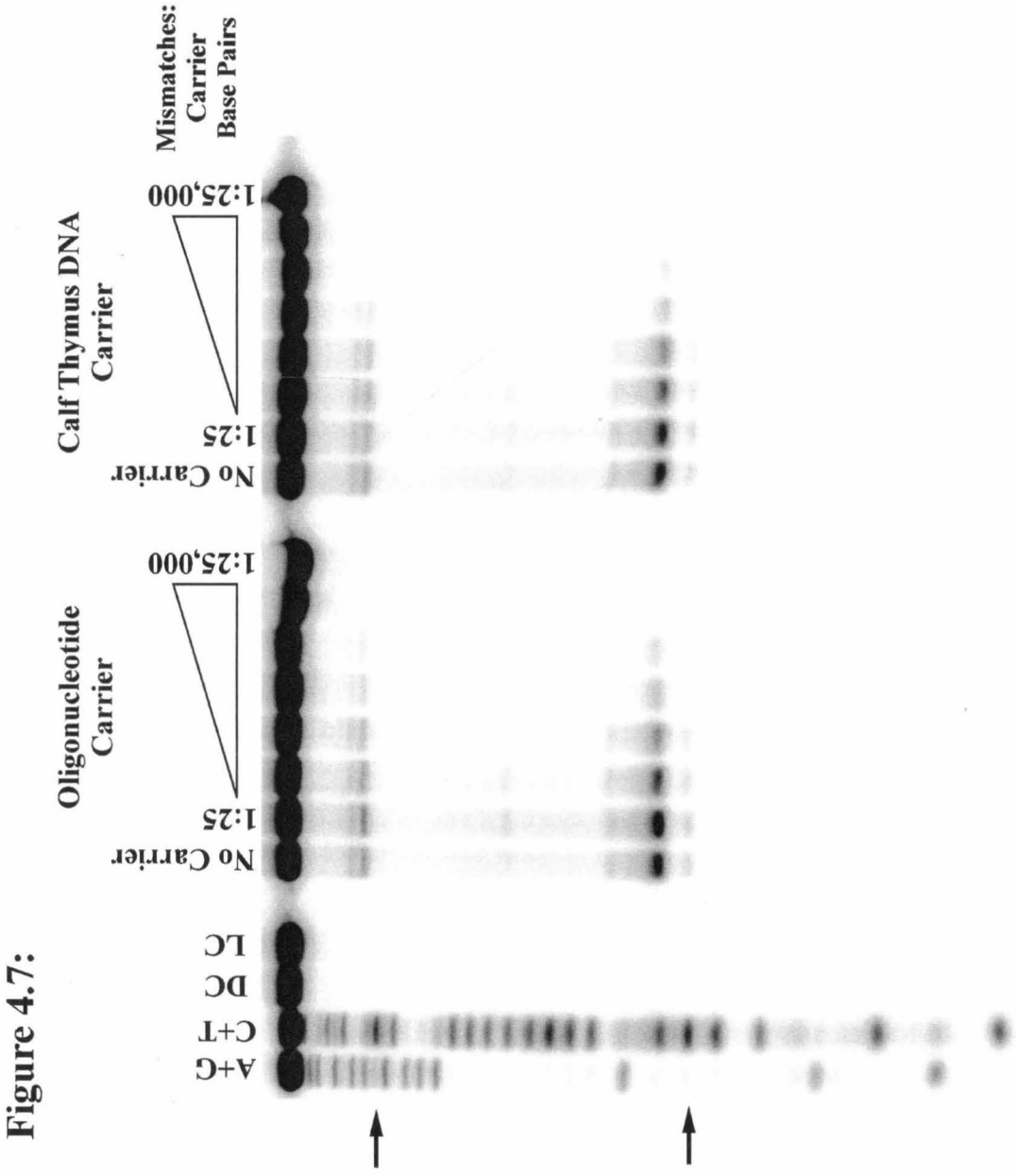

Mismatches:
Carrier
Base Pairs
Calf Thymus DNA
Carrier
1:25,000
1:25
No Carrier
Oligonucleotide
Carrier
1:25,000
1:25
No Carrier
LC
DC
C+T
A+G

Figure 4.7:

proportionally with the magnitude of their different association constants. As a result, the measurement of the average binding constant using this method is likely to be superior to other methods as it most closely captures the situation which exists in the actual application of these molecules to molecular recognition. If a molecule is intended to recognize a given site on a long DNA molecule, *all* competitive binding modes which interfere with that recognition must be taken into account when the desired binding behavior is evaluated.

When the data from this type of titration (Figure 4.7) is treated quantitatively, a titration curve can be extracted. A sample of such a curve, along with its fitted "titration isotherm" is included as Figure 4.8. As the number of competitor base pairs are increased, the complex bound at the high-affinity mismatch site is gradually titrated off and photocleavage decreases. These data are then fit to a multi-site binding model, a modification of the binding models included in Appendix 2 as discussed in **4.3.5** above, and an average binding constant to B-DNA extracted. When the defined sequence oligonucleotide is used as carrier, the resulting average association constant measured by this technique is 4 (3) x 10^4 M^{-1}; with mixed sequence calf thymus DNA as carrier, the value is 5 (4) x 10^4 M^{-1}. These values are comparable to those measured using the direct titration method discussed above.

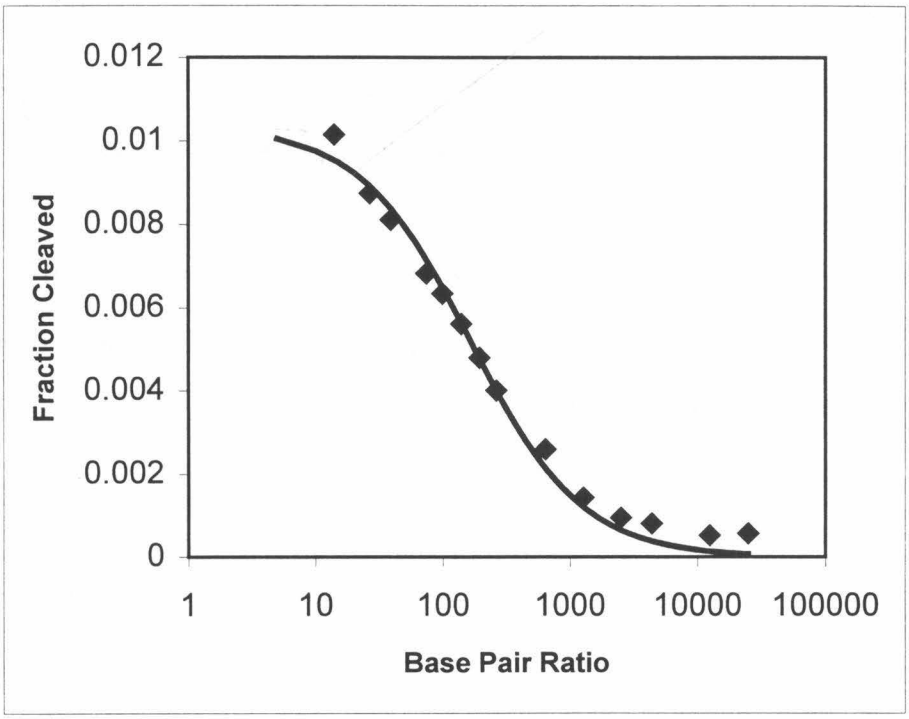
It should be noted that these values for the "non-specific" binding constant of Δ-$[Rh(bpy)_2(chrysi)]^{3+}$ for B-DNA compare very favorably with the mismatch-specific binding sites discussed in the previous section. In the best case comparison, between the highest-affinity CC binding site and the lowest measured affinity for B-DNA, the ratio of the binding constants is 540 indicating discrimination between this site and "non-specific" DNA of more than five hundred fold. Even the lowest affinity site

Figure 4.8. Titration of Δ-$[Rh(bpy)_2(chrysi)]^{3+}$ bound to the CC mismatch hairpin described in Figure 4.5 in the text was performed with the unlabeled oligonucleotide:

5'-GCGGTATCTAGAGCGCATCTGGGCG-3'

annealed to its complement. Samples were prepared at 0.5 to 0.1 μM hairpin and 0.5 to 0.04 μM Δ-$[Rh(bpy)_2(chrysi)]^{3+}$ with carrier DNA concentration increasing from a base pair ratio (Carrier Base Pairs:CC Mismatches) of 0 to 25,000. Samples were irradiated for 15 min at 365 nm. After electrophoresis, data was quantitated as described previously and, when combined with the measured CC specific binding constant, was fit to a two parameter binding model describing binding at the mismatch as a function of competing non-specific DNA concentration. Details are included in Appendix 2.

Figure 4.8:


0.012
0.01
0.008
0.006
0.004
0.002
0
Fraction Cleaved
1
10
100
1000
10000
100000
Base Pair Ratio

which was measured, the AA/GC site, shows a level of discrimination of almost ten fold.

4.3.2.3: Discrimination of a Single Mismatch in a Plasmid DNA

Although the work discussed in the previous section has clearly shown that the sterically bulky chrysene intercalating ligand provides binding specificity for mismatch sites on small oligonucleotide substrates, demonstrating that the compound can specifically recognize base mispairs on long DNA polymers of biological origin is critical to its potential applicability and usefulness. It is only with high specificity that such a molecule could select its binding sites from the large excess of properly paired DNA that would exist in a cell or in any biologically derived nucleic acid sample. From the association constants discussed in the previous section, it was clear that Δ-$[Rh(bpy)_2(chrysi)]^{3+}$ likely possessed sufficient specificity to perform such recognition tasks. As a result, the construction of a system where this level of base mismatch discrimination could be demonstrated was highly desirable.

In order to determine if Δ-$[Rh(bpy)_2(chrysi)]^{3+}$ could be used for the specific recognition of base mismatches in a biologically derived, high molecular weight DNA sample, an experiment on two plasmids was performed. Each plasmid had an oligonucleotide segment (57 bp) inserted between the *SalI* and *HindIII* sites in the polycloning site of pUC19. The two inserts differed in only one base pair producing plasmids with either a cytosine ($pVYA_C$) or a guanine ($pVYA_G$) at position 467 (as numbered from the first base pair of pUC19). The plasmids were introduced into competent cells and milligram quantities produced by routine methods. Such a system provided ready access to significant quantities of DNA which could be used to

model, for example, copies of a known genetic sequence and a laboratory isolated, unknown sequence containing a single base mutation.

Samples of each plasmid were cut with the restriction endonuclease *ScaI* producing a linear 2725mer with the C/G variable site 975 base pairs from one end (see Figure 4.9). Equal amounts of the C and G containing plasmids were combined and the DNA strands denatured under alkaline conditions.[1] After re-annealing, the resulting mixture should recombine statistically to produce correctly matched plasmids (one half of the sample with either CG or GC pairs at site 467) and plasmids containing one base mismatch each (one quarter each with either CC or GG mispairs at site 467). Each end of the 2725mer was radioactively labeled and the plasmid was photolyzed at 440 nm for 10 min in the presence of increasing concentrations of Δ-$[Rh(bpy)_2(chrysi)]^{3+}$.

Because the plasmid was labeled at each end, both segments of the plasmid produced by cleavage at the mismatch site are visible on the denaturing alkaline agarose gel[2] included as Figure 4.10. The longer of the two products corresponds to cleavage on the "upper strand" in Figure 4.9 and the shorter to cleavage at the analogous site on the lower strand. The lengths of the two cleavage bands were confirmed by comparison with *SalI* cleavage of the linear plasmid which produced two fragments of similar lengths (data not shown). Irradiation of identically treated DNA not containing mismatches (samples of the two plasmids that were alkaline denatured and re-annealed separately) shows no specific cleavage (Figure 4.10). It is interesting to note that the molecule appears to cleave more readily at the site on the "upper strand" as its cleavage band grows in at a lower concentration of metal complex. This suggests that the geometry of this locally (3 base pair) symmetrical site (5'-GA**GXC**AT-3') is likely affected by the identity of the bases further away from the

Figure 4.9. Schematic of the application of plasmids $pVYA_C$ and $pVYA_G$, derivatives of pUC19 differing in a single base pair, to the generation of a 2725 base pair plasmid heteroduplex containing a single base mismatch. After linearization and denaturation/re-annealing, a mixture of the two plasmids produces a statistical population of heteroduplexes one quarter of which contain CC mispairs.

Figure 4.9:

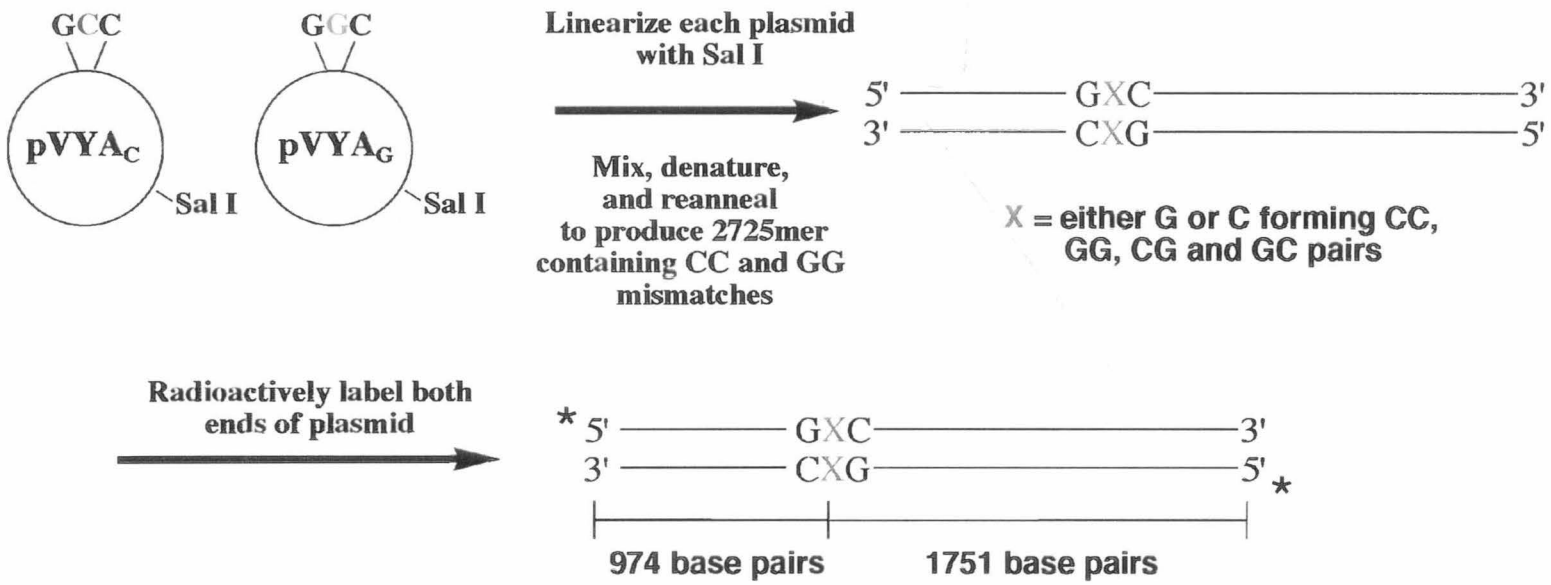

GCC
GGC
pVYA$_C$
pVYA$_G$
Sal I
Sal I
Linearize each plasmid with Sal I
5' GXC 3'
3' CXG 5'
Mix, denature, and reanneal to produce 2725mer containing CC and GG mismatches
X = either G or C forming CC, GG, CG and GC pairs
Radioactively label both ends of plasmid
* 5' GXC 3'
3' CXG 5' *
974 base pairs
1751 base pairs

Figure 4.10. Image of an alkaline agarose gel of the photolysis (440 nm, 10 min) products of the plasmid mixture described in Figure 4.9 with varying amounts of Δ-$[Rh(bpy)_2(chrysi)]^{3+}$. As the concentration of rhodium complex is increased from 0.1 to 100 nm, conversion of the full length plasmid to segments of lengths consistent with specific cleavage at the mismatch site is observed. Samples without mismatches (Watson-Crick), samples incubated with metal complex in the absence of light (DC), and samples irradiated without metal complex (LC) show no cleavage.

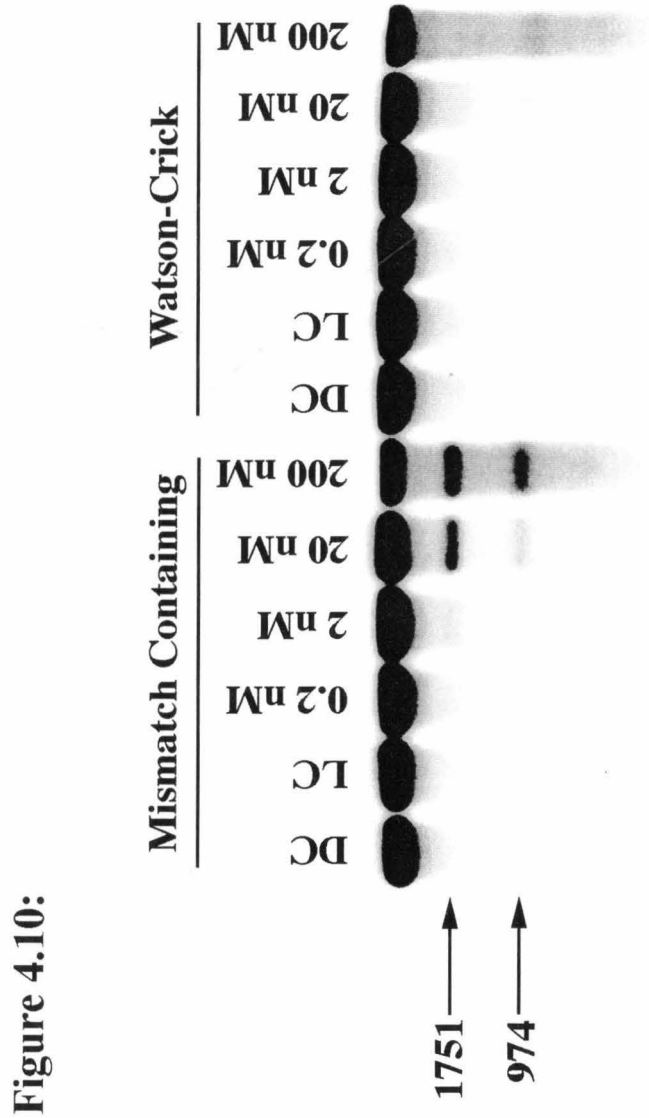

Mismatch Containing
Watson-Crick
DC
LC
0.2 nM
2 nM
20 nM
200 nM
DC
LC
0.2 nM
2 nM
20 nM
200 nM
1751
974

Figure 4.10:

mismatch. This specific binding and recognition of a single mismatch site in a multi-kilobase DNA duplex by a small molecule is, to our knowledge, unprecedented.

In order to identify the specific site of DNA cleavage within the plasmid, an experiment analogous to that described above was performed on a combination of plasmid restriction fragments from $pVYA_C$ and $pVYA_G$. A 273 base pair, singly labeled fragment, was obtained from $pVYA_C$ by sequential cleavage and phosphorylation of the plasmid with *EcoRI*, T4 polynucleotide kinase, and *PvuII*. The resulting radio-labeled restriction fragment containing site 467 (the variable base site in the inserted DNA sequence) was isolated on a non-denaturing gel. Samples of the fragment were combined with doubly digested samples of each plasmid and denatured/re-annealed as described previously.[1] This procedure produced DNA samples identical in DNA composition to those described above (i.e., containing the plasmid DNA in its entirety) but with the DNA cleaved into a number of fragments and labeled only at one end of the fragment of interest (Figure 4.11). This mixture of DNA, which has the same ratio of mismatches to total plasmid base pairs as in the first experiment, was photolyzed in the presence of increasing amounts of Δ-$[Rh(bpy)_2(chrysi)]^{3+}$.

The results, shown in Figure 4.12, indicate that the complex cleaves to the 3' side of the mismatch site as expected. Samples irradiated without metal complex, treated with metal complex in the absence of light, or non-mismatch-containing samples irradiated with metal show no cleavage. The cleavage pattern on the plasmid restriction fragment, in addition to corresponding well to that observed in the sequence context experiments described above (see CC/GC in Figure 4.2), shows at high resolution that cleavage of the plasmid occurs specifically at the mismatch site.

Figure 4.11. Experimental procedure for the determination of the site of $pVYA_C$/$pVYA_G$ heteroduplex photocleavage at high resolution. A singly end-labeled $pVYA_C$ restriction fragment is combined with a doubly digested sample of $pVYA_G$ to produce heteroduplex samples with comparable DNA content to those described in Figures 4.9 and 4.10 but with the DNA in multiple fragments and only a single radioactive label.

Figure 4.11:

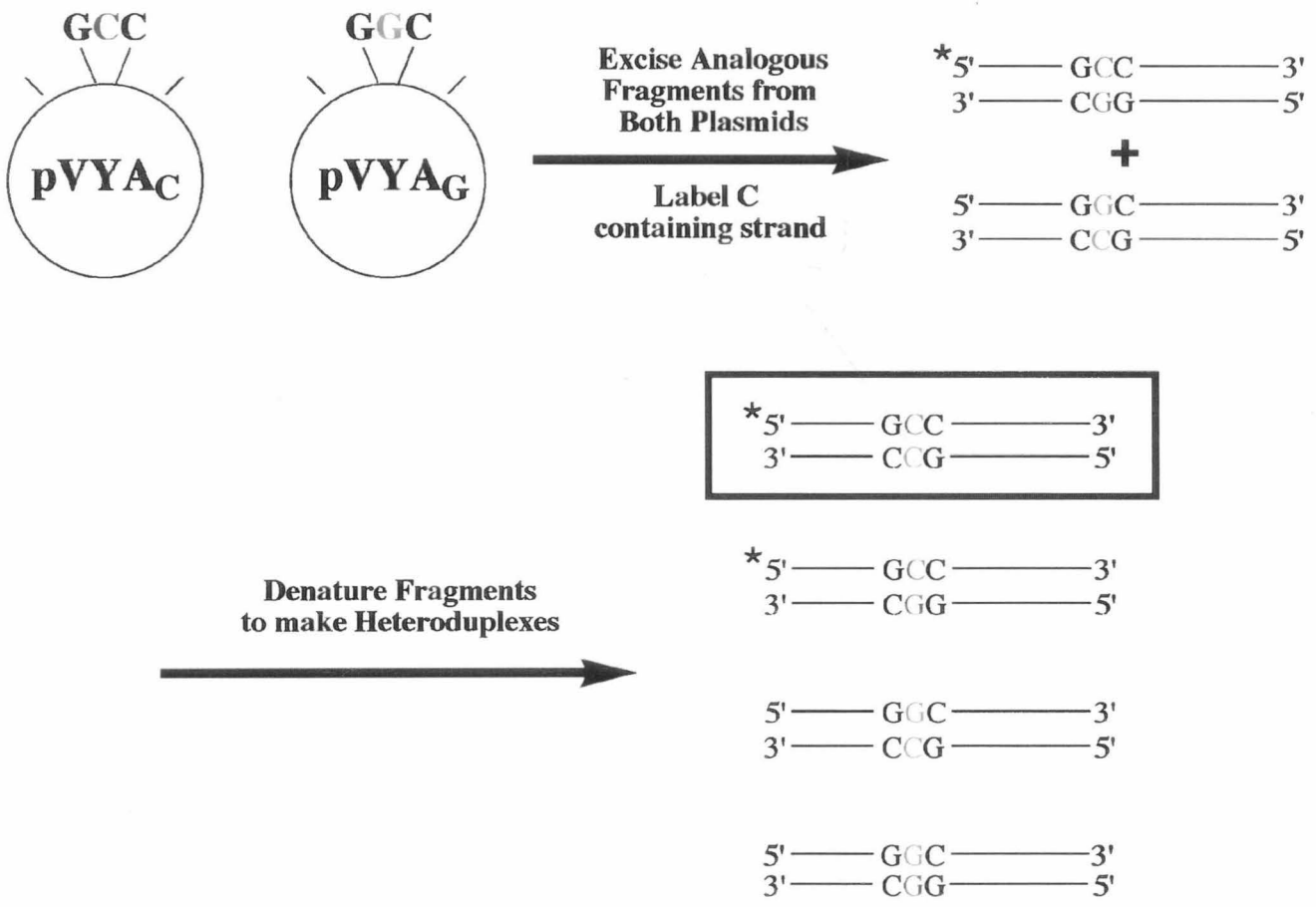
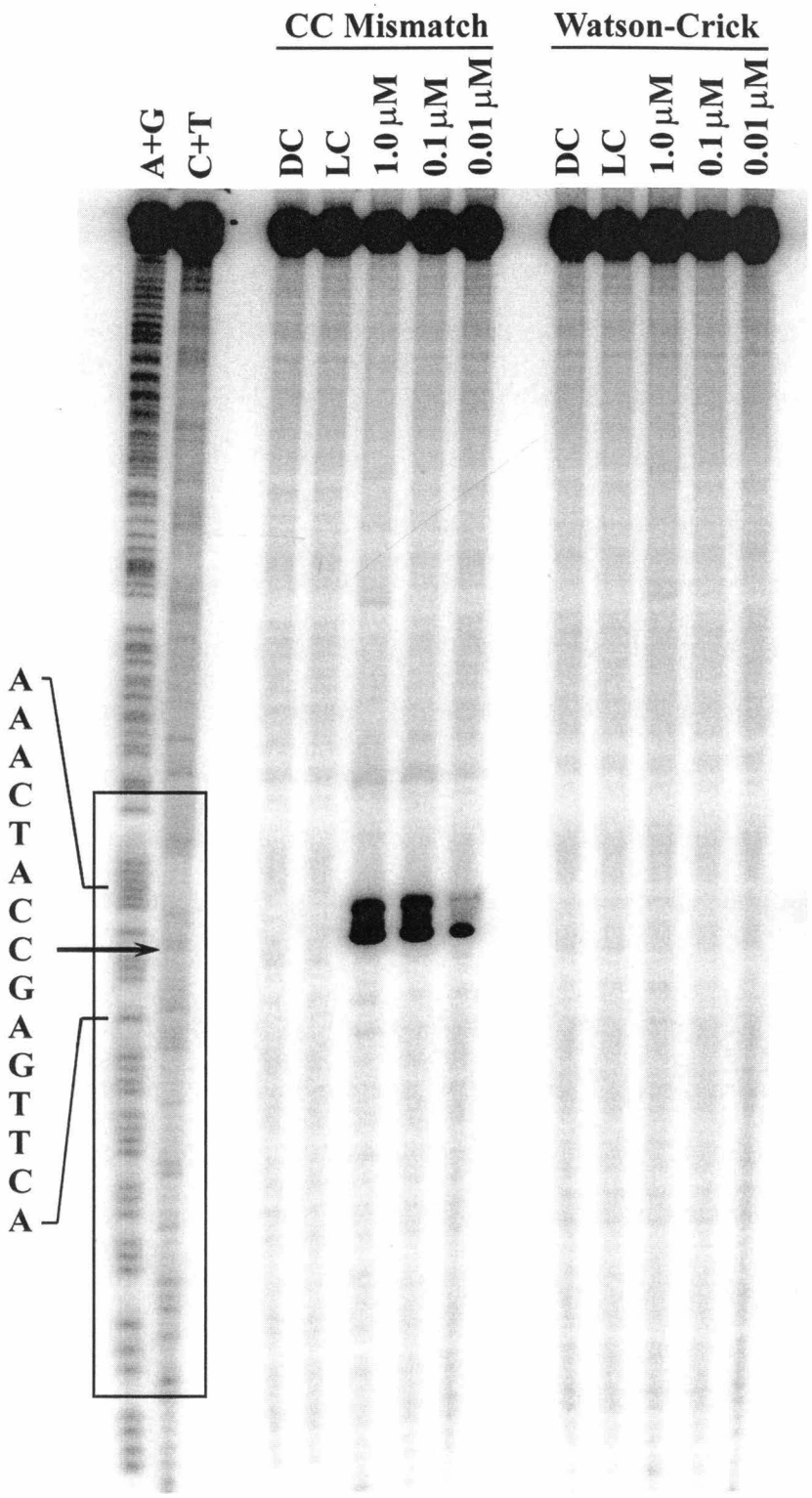

GCC
GGC
pVYA$_C$
pVYA$_G$
Excise Analogous Fragments from Both Plasmids
Label C containing strand
*5'—— GCC ——3'
3'—— CGG ——5'
+
5'—— GGC ——3'
3'—— CCG ——5'
*5'—— GCC ——3'
3'—— CCG ——5'
Denature Fragments to make Heteroduplexes
*5'—— GCC ——3'
3'—— CGG ——5'
5'—— GGC ——3'
3'—— CCG ——5'
5'—— GGC ——3'
3'—— CGG ——5'

Figure 4.12. Identification of the Site of Plasmid Cleavage by $[Rh(bpy)_2(chrysi)]^{3+}$ in the $pVYA_C/pVYA_G$ Heteroduplex at High Resolution. Image of a 6% denaturing PAGE gel of photolysis (440 nm, 10 min) products of the restriction fragment heteroduplex mixture described in Figure 4.11 with varying amounts of Δ-$[Rh(bpy)_2(chrysi)]^{3+}$. Specific recognition of the mismatch site with cleavage to the 3' of the mismatch is observed at concentrations as low as 10 nm. Samples without mismatches, samples incubated with metal complex in the absence of light (DC), and samples irradiated without metal complex (LC) show no cleavage.

Figure 4.12:


CC Mismatch
Watson-Crick
A+G
C+T
DC
LC
1.0 μM
0.1 μM
0.01 μM
DC
LC
1.0 μM
0.1 μM
0.01 μM
A
A
A
C
T
A
C
C
G
A
G
T
T
C
A

4.4: CONCLUSIONS

4.4.1: Mismatch Discrimination and Recognition Design

The results discussed in this chapter clearly and unambiguously demonstrate that $[Rh(bpy)_2(chrysi)]^{3+}$ is a versatile and specific mismatch recognition agent. In addition to demonstrating that the complex cleaves at an impressive 82% of the possible mismatch-single base sequence context combinations, the level of specificity of the complex for a CC mismatch site was sufficient to allow discrimination of a single CC mispair in a 2725 base pair plasmid DNA heteroduplex. Even in light of these impressive properties for a small molecule recognition agent, it is important to realize that the studies described in this work may not fully capture the magnitude of this compound's recognition behavior. Because of the labor intensive and time consuming nature of the experiments, thermodynamic binding constants at only a few representative mismatch sites could be determined. As a result, it is possible that other families of sites contain examples where even tighter binding is observed at the mismatch site leading to even greater specificity over properly paired DNA.

When the results obtained with $[Rh(bpy)_2(chrysi)]^{3+}$ are compared to naturally occurring mismatch recognition proteins, some interesting similarities and contrasts emerge. Depending on the natural protein system, different mismatches are recognized to different extents. The mismatch recognition hierarchies of $[Rh(bpy)_2(chrysi)]^{3+}$ and some protein examples from the literature are included as Table 4.3 (next page).

Although there are some similarities in the preferences of individual mismatch recognition proteins and the recognition characteristics of $[Rh(bpy)_2(chrysi)]^{3+}$, it is clear that there are also significant differences. For example, the CC mismatch,

Table 4.3: Comparison of Specificity of $[Rh(bpy)_2(chrysi)]^{3+}$ and Natural Mismatch Recognition Proteins

Recognition Molecule:	Strongly Recognized Mismatches:	Moderately Recognized Mismatches:	Weakly Recognized Mismatches:	Citation:
$[Rh(bpy)_2(chrysi)]^{3+}$	CC, CT, AC	TT,AA	GT, AG, GG	
E.Coli MutS	GT,AC	AA,TT,GG	AG,CT,CC	9
S.Cerevisiae MutS	GT,AC,AA,GG	TT,TC,AG	CC	10
Human hMSH2	GT,GG.GA	AC,CT,TT	AC,CC	11
Taq. HB8 MutS	TT,CT	CC,GT,GG	GA,AC,AA	12

which is by far the most readily recognized by the complex, is in general poorly recognized by the protein systems. Of these protein examples, the metal complex is most similar to the *Taq HB8* MutS although the significance of such a similarity is difficult to define. Although numerous other parallels could be drawn between these systems and the recognition pattern of the metal complex, it is more relevant to simply acknowledge that the recognition profiles are likely different since the proteins must, by definition, be using different functional groups and molecular architectures for mismatch discrimination. A more laudatory comparison between the metal complex and certain mismatch recognition proteins is in the area of binding affinity and specificity. Two examples of proteins whose binding parameters have been determined are the *E.Coli* MutS[10] and human MutY, a GA mismatch-specific protein.[13] Binding affinities of the *E.Coli* protein for its various mismatch targets vary from 3×10^7 M^{-1} to 2×10^6 M^{-1}. These values are very comparable to those obtained for the rhodium complex. Further, in the MutY case, the specific binding constant for the GA mismatch is 3×10^7 M^{-1} with a non-specific binding constant as high as 4×10^6 M^{-1}.* Although the specific association constant is very similar to

* It should be noted, however, that this comparison is not entirely "fair" to the protein as it is not wholly dependent on differential binding and derives a much greater proportion of its selectivity based on differential reaction at specific vs. non-specific sites.

some of the values for the chrysi compound, the metal complex has a far superior selectivity in binding. Given these data, although $[Rh(bpy)_2(chrysi)]^{3+}$ does display clear preferences in binding for certain mismatches, such differences in activity are also observed in the cases of natural mismatch recognition proteins. As a result, in both affinity and selectivity, this small molecule has proven to be a superior mismatch recognition system compared with some of its far larger and more evolutionarily optimized natural counterparts.

From the point of view of a molecular recognition model to explain the preferential binding and photocleavage of mismatch sites by $[Rh(bpy)_2(chrysi)]^{3+}$, the data described here are also broadly consistent with the design strategy of the molecule. On the most basic level, it is the mismatches which are the most destabilized which are most readily recognized by the rhodium complex. In addition, the trends in the photocleavage of the complex on varied mismatch sites also support the idea that helix destabilization, and the structural disorder it implies, is an important factor in the binding of $[Rh(bpy)_2(chrysi)]^{3+}$ to the DNA helix. In mismatch families which are stabilizing or only minimally destabilizing, small increases in destabilization are observed to be correlated with corresponding increases in photocleavage at the mismatch sites. In the limit of great helix destabilization, the exact value of the thermodynamic destabilization at the mismatch site is less relevant. At this point, other factors seem to dominate binding as the molecule has all the "access" required for intercalation. When the data are examined more closely, however, there is a great deal of scatter in the individual data points along this general trend. Examples exist of mismatch sites which are very destabilized which show less photocleavage than much less destabilized sites; this is also observed in the thermodynamic binding constants measured for the complex at a set of mismatch sites. This observation underscores the other factors like site geometry which *must* be involved in

determining the binding affinity and photocleavage efficiency of $[Rh(bpy)_2(chrysi)]^{3+}$ at these many different mismatch sites.

4.4.2: Mismatch Structure and Metal Complex Binding

The formation of hypotheses about these "geometrical factors" which likely play an important role in the binding of chrysi intercalators to mismatch sites is hampered by the lack of structural information about base mismatch sites themselves. Although a few structures of mismatches in solution and descriptions of their kinetic behavior are available,[14-27] there is not enough information to really make any general conclusions possible. As a larger database of information about base mismatch sites and structural information about the nature of the complexes between mismatches and metallointercalators like $[Rh(bpy)_2(chrysi)]^{3+}$ become available, the photocleavage patterns shown in Figure 4.1 and 4.2 will acquire additional levels of significance. This is analogous to the application of compounds like $[Rh(phen)_2(phi)]^{3+}$ as shape selective probes of DNA for the examination of uncharacterized DNA sequences which became possible once their DNA photocleavage patterns were calibrated against known structural parameters of DNA sites.[28-32] Similarly, once a general model of the interaction of chrysi intercalators with mismatches can be constructed, the photocleavage patterns reported here can be reinterpreted not only from the perspective of what they imply about the mismatch recognition capabilities of $[Rh(bpy)_2(chrysi)]^{3+}$ but also about what they imply about the structures of the mismatches themselves.

4.4.3: Speculation on Strand Selectivity of Photocleavage

Structural information about the interaction of $[Rh(bpy)_2(chrysi)]^{3+}$ with DNA mismatch sites is also necessary to more completely rationalize the photocleavage

behavior observed in the experiments reported in this chapter. Although rhodium complexes which exhibit strand selectivity in their photocleavage behaviors are not unprecedented (see experiments with $[Rh(MGP)_2(phi)]^{5+}$ in Appendix 2), the level of selectivity displayed by $[Rh(bpy)_2(chrysi)]^{3+}$ at some mismatch sites is very dramatic. Given the asymmetry inherent in the chrysenequinone diimine intercalating ligand, the asymmetric photocleavage behavior could reflect differences in binding or reactivity. Such a preference could be generated by one or more different mechanisms. It has been previously observed[33] that phi intercalators preferentially stack over the purine bases adjacent to their intercalation site. As a result, it is possible that the aromatic ring structure of the chrysi intercalator generates a strong preference for stacking on the purines positioned in certain sequence contexts which constrains photocleavage to a single strand of the helix. Even in the absence of the purine preference that was observed for the phi intercalator, it is possible that some other binding-related constraints imposed by the sterically large intercalator result in the asymmetry observed in photocleavage.

The novel protonation behavior of this complex provides an additional possible explanation for the directionality observed in photocleavage by $[Rh(bpy)_2(chrysi)]^{3+}$. It was previously demonstrated that, for photocleavage at 365 nm with $[Rh(phen)_2(phi)]^{3+}$, the amount of photocleavage increased by approximately 400% as pH was increased from pH 5 (below the pK of the complex) to pH 9 (well above the pK).[34] This indicates that the deprotonation of the metal complex greatly facilitates photocleavage at long wavelengths of light. The mechanism by which deprotonation promotes photocleavage is not clear; one could envison the absence of that proton and the changes to the electronic structure of the ligand affecting the photocleavage reaction itself or some subsequent step in the reactions which follow the direct strand scission. If the effect is exerted at the point where photocleavage

occurs, however, the structure of the chrysi ligand could result in the strand asymmetry observed in the photocleavage experiments. Because of the steric interference discussed in Chapter 2 which results in the novel spectral and acidic properties of this compound, when $[Rh(bpy)_2(chrysi)]^{3+}$ is deprotonated, it will preferentially deprotonate on the side of the molecule with the additional aromatic ring. Assuming that stacking considerations cause the chrysi intercalator to bind in a single orientation within a given mismatch site, the preferential deprotonation of one side of the ligand could lead to only a single "half" of the molecule being active for photocleavage. Depending on the exact positioning of the intercalator in the binding site, this restriction could lead to cleavage occurring only on a single strand or, in some cases, it might lead to a reduction in cleavage efficiency if the "active site" of the molecule was not properly positioned to react with the DNA. As discussed in the previous sections, determining the source of this directionality in photocleavage must await structural information about how this molecule binds to sites on DNA where asymmetric photocleavage is observed.

4.4.4: General Lessons from Mismatch Recognition by Steric Exclusion

The level of specificity and generality of the mismatch recognition properties of $[Rh(bpy)_2(chrysi)]^{3+}$ is exciting. To our knowledge, this molecule is the first designed to recognize sites in DNA by exploiting this "site selection by steric exclusion" mechanism of molecular recognition. As such, it is a dramatic demonstration of the ability of such a simple strategy to generate very specific binding agents. As discussed in the introductory material to this thesis, while the difference in specificity provided by an unpaired hydrogen bond might only be ten fold, if a molecule is sterically prevented from binding to an undesirable site, specificity could theoretically be *absolute*. It should be noted that the use of this

recognition is made possible by the high binding affinity that is provided by the intercalative interaction of the chrysi ligand with the DNA base stack. Without that interaction to provide binding affinity to the complex, the generation of specificity by disfavoring binding at undesired sites would not be possible.

As a result, even with the limitations inherent in such a simple design procedure, the performance of $[Rh(bpy)_2(chrysi)]^{3+}$ indicates that these types of *binding-selective* agents are applicable to mismatch detection tasks required for molecular diagnosis and mutation detection *in vitro*. Furthermore, it is possible that these kinds of compounds may also represent a novel route for the design of mismatch-specific chemotherapeutic agents for the treatment of certain varieties of cancer. Testing of $[Rh(bpy)_2(chrysi)]^{3+}$, which represents the first example of such a mismatch-specific drug candidate, is already underway on such MMR deficient cancer cell lines.

4.5: Literature Cited

1) Smith, J.; Modrich, P. *Proc. Natl. Acad. Sci. USA.* **1996**, *93*, 4374.

2) Cech, T. R. *Biochemistry* **1981**, *20*, 1431.

3) Allawi, H. T.; SantaLucia, Jr., J. *Biochemistry* **1997**, *36*, 10581.

4) Allawi, H. T.; SantaLucia, Jr., J. *Biochemistry* **1998**, *37*, 2170.

5) Allawi, H. T.; SantaLucia, Jr., J. *Nucleic Acids Res.* **1998**, *26*, 2694.

6) Allawi, H. T.; SantaLucia, Jr., J. *Biochemistry* **1998**, *37*, 9435.

7) Peyret, N.; Seneviratne, P. A.; Allawi, H. T.; SantaLucia, Jr., J. *Biochemistry* **1999**, *38*, 3468.

8) SantaLucia Jr., J., Personal Communication.

9) Fishel, R.; Kolodner, R. D. *Curr. Opin. Gen. Dev.* **1995**, *5*, 382.

10) Su, S.-S.; Lambert, R. S.; Au, K. G.; Modrich, P. *J. Biol. Chem.* **1988**, *263*, 6829.

11) Whitehouse, A.; Taylor, G. R.; Deeble, J.; Phillips, S. E. V.; Meredith, D. M.; Markham, A. F. *Biochem. Biophys. Res. Comm.* **1996**, *225*, 289.

12) Whitehouse, A.; Deeble, J.; Parmar, R.; Taylor, G. R.; Markham, A. F.; Meredith, D. M. *Biochem. Biophys. Res. Comm.* **1997**, *233*, 834.

13) Porello, S. L.; Williams, S. D.; Kuhn, H.; Micheals, M. L.; David, S. S. *J. Am. Chem. Soc.* **1996**, *118*, 10684.

14) Allawi, H. T.; SantaLucia, Jr., J. *Nucleic Acids Res.* **1998**, *26*, 4925.

15) Patel, D. J.; Kozlowski, S. A.; Ikuta, S.; Itakura, K. *Fed. Proc.* **1984**, *43*, 2663.

16) Carbonnaux, C.; van der marel, G. A.; van Boom, J. H.; Guschlbauer, W.; Fazakerley, G. V. *Biochemistry* **1991**, *30*, 5449.

17) Lane, A. N.; Jenkins, T. C.; Brown, D. J. S.; Brown, T. *Biochem. J.* **1991**, *279*, 269.

18) Lane, A. N.; Peck, B. *Eur. J. Biochem.* **1995**, *230*, 1073.

19) Li, Y.; Agrawal, S. *Biochemistry* **1995**, *34*, 10056.

20) Gervais, V.; Cognet, J. A. H.; Le Bret, M.; Sowers, L. C.; Fazakerley, G. V. *Eur. J. Biochem.* **1995**, *228*, 279.

21) Cognet, J. A. H.; Boulard, Y.; Fazakerley, G. V. *J. Mol. Biol.* **1995**, *246*, 209.

22) Guest, C. R.; Hochstrasser, R. A.; Sowers, L. C.; Millar, D. P. *Biochemistry* **1991**, *30*, 3271.

23) Salisbury, S. A.; Anand, N. N. *J. Chem. Soc. Chem. Commun.* **1985**, 985.

24) Gao, X.; Patel, D. J. *J. Biol. Chem.* **1987**, *262*, 16973.

25) Kuwata, K.; Liu, H.; Schleich, T.; James, T. L. *J. Mag. Res.* **1997**, *128*, 70.

26) Moe, J. G.; Russu, I. M. *Biochemistry* **1992**, *31*, 8421.

27) Borden, K. L. B.; Jenkins, T. C.; Skelly, J. V.; Brown, T.; Lane, A. N. *Biochemistry* **1992**, *31*, 5411.

28) Sitlani, A.; Barton, J. K. *Biochemistry* **1994**, *33*, 12100.

29) Campisi, D.; Morii, T.; Barton, J. K. *Biochemistry* **1994**, *33*, 4130.

30) Sitlani, A.; Long, E. C.; Pyle, A. M.; Barton, J. K. *J. Am. Chem. Soc.* **1992**, *114*, 2303.

31) Pyle, A. M.; Long, E. C.; Barton, J. K. *J. Am. Chem. Soc.* **1989**, *111*, 4520.

32) Pyle, A. M.; Morii, T.; Barton, J. K. *J. Am. Chem. Soc.* **1990**, *112*, 9432.

33) Hudson, B. P.; Barton, J. K. *J. Am. Chem. Soc.* **1998**, *120*, 6877.

34) Hall, D. B. *Oxidative DNA Damage Through Long Range Electron Transfer*. Ph.D. Thesis, Division of Chemistry, California Institute of Technology, 1998.

Chapter 5:

Characterization of Aspects of the Photochemistry of Chrysenequinone Diimine Complexes of Rhodium(III)

5.1: INTRODUCTION

The direct photocleavage of DNA by phenanthrenequinone diimine rhodium intercalators has been extensively investigated by this research group over the last ten years. From the first examinations of these materials, it was clear that they had a rich photochemistry which led to very useful reactions with nucleic acids. Unlike compounds which promote DNA damage by the generation of diffusible radicals or singlet oxygen and therefore produce distributions of cleavage around a single binding site, these complexes generate sharp cleavage bands. This suggested that the species produced upon irradiation of the metal complexes bound to DNA caused cleavage immediately adjacent to the site of binding.

Research by many investigators has firmly established that rhodium polypyridyl complex are potent photo-oxidants with irradiation leading to ligand-to-metal-charge-transfer (LMCT) transitions.[1-7] In addition, it has also been demonstrated that irradiation into phi transitions promotes preferential photochemistry of the phi ligand.[1] It was therefore suggested that the active species responsible for DNA cleavage by these metal complexes was the photo-generated phi cation radical. This radical, produced by absorption of light when the metal complex is already intimately associated with the nucleic acid *via* intercalation, was proposed to abstract a hydrogen atom from the deoxyribose sugar proximal to the binding site. Analysis of the products of the photocleavage of DNA by metal complexes like $[Rh(phen)_2(phi)]^{3+}$ and $[Rh(phi)_2(bpy)]^{3+}$ were consistent with reaction at the C3' position on the sugar ring.[8] Subsequent reaction of the sugar radical and the metal complex was proposed to lead to the formation of strand breaks in the DNA; these reactions, however, were thought to involve consumption of the rhodium complex as part of the reaction pathway producing DNA cleavage.[7,8]

Considering this model of DNA photocleavage by phenanthrenequinone diimine complexes of rhodium(III), the observation that chrysi compounds appear to cleave DNA photocatalytically, introduced in Chapter 3 of this thesis, was very unexpected. The fact that this photocleavage was effected by low energy, visible light in addition to the ultraviolet radiation usually applied in these DNA photocleavage assays was also novel. Beyond being interesting from a scientific perspective, both of these properties would also be very advantageous if such compounds were ever applied to chemotherapeutic tasks. When treating a patient with a photoactivated drug, it is highly preferable to irradiate with visible light which is far gentler on tissues than a high intensity beam of ultraviolet radiation. Furthermore, if a single drug molecule can cleave DNA numerous times before being degraded, it is also possible to generate high levels of pharmacological effect with a reduced dose of drug; side effects generated by the drug itself or its metabolism products can then be minimized while still preserving efficacy.

Due to the relatively recent discovery of the photocatalytic cleavage behavior of these complexes, we have only begun a detailed characterization of the novel photo-reactivity of these compounds. As a result, the work described in this chapter represents the summation of the experiments performed to date which, in addition to dramatically demonstrating the scope of this photocatalytic DNA cleavage, also suggest some intriguing possibilities for its source. The experiments described here are therefore intended to serve as a guide to future research.

5.2: Experimental Methods

5.2.1: Instrumentation and Materials

All reagents were the highest purity commercially available and, unless otherwise noted, used as obtained without further purification. Sonicated calf thymus DNA was obtained from Amersham-Pharmacia Biotech, Buckinghamshire, UK. Oligonucleotides were made and purified as described in the previous chapters. Analytical HPLC was performed either on a Hewlett Packard 1050 or 1100 instrument equipped with a diode array UV/Vis detector using a Microsorb-MV C_{18} reverse phase column. Absorption spectra were recorded on a Beckman DU 7400 spectrophotometer. HPLC mass spectrometry was performed by the Macromolecular Resources Center at the Colorado State University, Fort Collins. DNA photocleavage reactions were performed on samples of end-labeled DNA (prepared as described previously) with unlabeled, identical sequence carrier DNA in running buffer (50 mM Tris, 20 mM sodium acetate, 18 mM NaCl, pH 7.0), in 25 mM ammonium acetate, pH 9.0, or in 5 mM Tris pH 8.5. Concentrations of all materials were determined spectrophotometrically, solutions prepared, and DNA photocleavage and analysis performed as described. Irradiations were performed on a Hg/Xe arc lamp system equipped with a IR filter, 300 nm cut-off filter, and a monochrometer. The wavelength range passed by the monochrometer, as determined by laser calibration, is approximately 25 nm centered on the selected wavelength of irradiation. Power values for lamp emission at the selected wavelength were taken as the maximum value in this window of "passed wavelengths" from data provided by the lamp manufacturer.

5.2.2: Wavelength Dependence of Photocatalytic DNA Cleavage

5.2.2.1: Photocleavage Saturation Experiments with $[Rh(bpy)_2(chrysi)]^{3+}$

The two strands of the following CC mismatch (indicated in bold-italic) containing DNA duplex were made and purified by reverse phase HPLC by standard methods.

5′-GCTAC***C***CTCGTCAACTGGAG-3′
3′-CGATG***C***GAGCAGTTGACCTC-5′

The upper strand was 5' end-labeled and purified from unincorporated label as described earlier. A solution of the both upper and lower strands (20 μM polymers each) was prepared and annealed in ammonium acetate buffer (50 mM, pH 9). Multiple irradiation samples were assembled by combining an aliquot of the DNA solution (5 μl) with an equal volume of Δ-$Rh(bpy)_2(chrysi)Cl_3$ solution (2 μM in deionized water) producing a solution 25 mM in ammonium acetate with a 1:10 ratio of metal complex to DNA duplexes. These solutions were incubated in the dark for at least 30 min before irradiation. Individual samples were then photolyzed on the Hg/Xe lamp system described above in horizontally positioned, open 1.7 ml microcentrifuge tubes for steadily increasing periods ranging from 1 minute to 120 min. Groups of samples were irradiated at 313 nm, 365 nm, 405 nm, 450 nm, 500 nm, 525 nm, 550 nm, and 600 nm with the time of longest irradiation varying with the wavelength. Groups of samples irradiated at higher energies (313 nm, 365 nm) were irradiated for much shorter times than those at longer wavelengths. Samples were stored in the dark before and after irradiation. The photocleavage reactions were then dried under vacuum and electrophoresed as described. The extent of photocleavage was quantitated using phosphorimagery and the fraction cleaved plotted versus the time of irradiation.

5.2.2.2: Photocleavage Saturation Experiments with $[Rh(phen)_2(phi)]^{3+}$ on Mismatch-Containing DNA

The following oligonucleotide hairpin was synthesized and purified as described previously.

5'-GGCAGT**C**TTGGC$^{T}_{T}$
3'-CCGTCA**C**AACCG$_{T}^{T}$

Aliquots of a solution of the nucleic acid (40 μl, 20 μM polymers, 10 mM Tris, pH 8) were mixed with a solution of Δ-$[Rh(phen)_2(phi)]^{3+}$ (4 μl, 20 μM, 10 mM Tris, pH 8) producing irradiation samples of 44 μl total volume. Groups of samples were photolyzed in horizontally positioned, open 1.7 ml microcentrifuge tubes at 365 nm, 400 nm, 450 nm, and 500 nm with the time of longest irradiation varying with the wavelength. Samples irradiated at 365 nm were photolyzed for shorter periods (maximum time of 60 min vs. 120 min and greater for 400 nm and above) than those at longer wavelengths. Aliquots (11 μl) were removed from the samples throughout the course of a single long irradiation to track the course of the photolysis. Samples were stored in the dark after removal from the irradiation vial. The photocleavage reactions were then dried under vacuum, electrophoresed and quantitated as described.

5.2.2.3: Photocleavage Saturation Experiments with $[Rh(phen)_2(phi)]^{3+}$ and $[Rh(bpy)_2(chrysi)]^{3+}$ on Properly Paired DNA

The following oligonucleotide hairpin was synthesized and purified as described previously.

5'-GGCAGTGTTGGC$^{T}_{T}$
3'-CCGTCACAACCG$_{T}^{T}$

Aliquots of a solution of the nucleic acid (10 μl, 400 μM polymers, 2x running buffer, pH 7) were mixed with either a solution of Δ-$[Rh(phen)_2(phi)]^{3+}$ (10 μl, 40 μM, deionized water) or Δ-$[Rh(bpy)_2(chrysi)]^{3+}$ (10 μl, 40 μM, deionized water) producing irradiation samples 200 μM in DNA and 20 μM Rh. Groups of samples were photolyzed in horizontally positioned, open 1.7 ml microcentrifuge tubes at 400 nm and 450 nm for 90 min on the Hg/Xe lamp system described previously. Dark control samples of DNA incubated with metal in the absence of light and light control samples of DNA irradiated in the absence of metal were also prepared. Additionally, samples were also irradiated in outdoor sunlight (see **5.2.6** below) for 4 and 8 hr. Samples were stored in the dark after irradiation. Photocleavage reactions were then dried under vacuum, electrophoresed and cleavage quantitated as described; in this case, where cleavage occurred at several sites on the oligonucleotide, cleavage intensity by the compounds at all sites on the hairpin was summed and corrected for damage also observed in the light control lanes.

5.2.3: Estimation of the Maximal Extent of Photocatalytic Cleavage of DNA by $[Rh(bpy)_2(chrysi)]^{3+}$

The following hairpin oligonucleotide (CC/GC as included in the sequence context experiments discussed in the previous chapter) was synthesized and purified by previously described methods.

5'-GGCAGG**C**CTGGC$^{T}_{T}$T
3'-CCGTCC**C**GACCG$_{T}$T

A concentrated solution of the nucleic acid (600 μM hairpin, 60 μl) was combined with a small amount of Δ-$[Rh(bpy)_2(chrysi)]^{3+}$ (1.07 μl of a 83.6 μM solution, 0.25% mole percent versus the DNA). The sample was irradiated at either 440 or 525 nm in a horizontally placed, open 1.7 mL microcentrifuge tube for a total of 18 to 21 hr.

Over the course of the irradiation, aliquots of the solution (6 μl) were removed and dried. Evaporation gradually reduced the volume of the sample over the course of the irradiation such that, by the time the irradiation was stopped, the remaining sample had dried. After removal, all samples were kept dark to prevent further photolysis. Samples were resuspended, electrophoresed and quantitated as described.

5.2.4: Wavelength Dependence of the Photoaquation of $[Rh(bpy)_2(chrysi)]^{3+}$ in the Presence of DNA

A DNA duplex containing a single CC mismatch (sequence included in **5.2.2**) was dissolved in ammonium acetate buffer (50 μM DNA duplex, 25 mM NH_4OAc, pH 9, 300 μl total sample volume). The absorption spectrum of the solution was determined from 300 nm to 500 nm in a 500 μl capped cuvette and set as the spectrometer blank. A small aliquot (2 μl) of a 1.5 mM solution of Δ-$[Rh(bpy)_2(chrysi)]Cl_3$ was added producing a final metal concentration of approximately 10 μM. The absorption spectrum of this solution was determined to serve as the T=0 point for the experiment. The sample was then irradiated on the Hg/Xe lamp system described above at either 313 nm (total time, 1 hr), 365 nm (1 hr), 405 nm (1 hr), 450 nm (4 hr), 475 nm (4 hr), 500 nm (4 hr), 525 nm (4 hr), 550 nm (4 hr), or 600 nm (4 hr). The absorption spectrum of the photocleavage/photoaquation reaction was measured periodically over the course of each reaction; the total length of irradiation was selected based on the extent of change observed with increasing reaction time.

5.2.5: Characterization of $[Rh(bpy)_2(chrysi)]^{3+}$ Photochemistry in the Presence and Absence of DNA by Analytical HPLC

The following hairpin oligonucleotide was made and purified by standard methods.

5'-AGAGACACTCCTATC $^{TT}_{T}$
3'-TGTGACGATAG $_{TT}^{T}$

Aliquots of a stock solution of the nucleic acid (75 μl, 1.2 mM polymers, 20 mM Tris pH 8.5) were combined with Δ-$[Rh(bpy)_2(chrysi)]^{3+}$ (75 μl, 600 μM, deionized water). Control samples in the absence of nucleic acid were also prepared by mixing the metal complex solution with 75 μl of buffer alone. Both classes of samples were irradiated using the Hg/Xe lamp system described above at one of three wavelengths: 313 nm, 400 nm, or 500 nm. Three samples were irradiated at each wavelength with increasing times of photolysis. Samples at 313 nm were irradiated for 5, 15 or 30 min, those at 400 nm for 15, 30 or 120 min, and those at 500 for 30, 60, or 120 min. Aliquots of the irradiation reactions (35 μl) were diluted into triethylamine acetate buffer (315 μl , TEAA, 100 mM, pH 7) and 50 μl analyzed by HPLC using a Microsorb-MV C_{18} analytical HPLC column and a TEAA/CH_3CN mobile phase (95:5 TEAA:CH_3CN ➔ 30:70 TEAA:CH_3CN; linear gradient over 45 min, 1.0 mL/min). Absorbance chromatograms were generated by monitoring at 260 nm (DNA λ_{max}), 313 nm (a rhodium complex λ_{max} associated primarily with the bpy ancillary ligands), and 370 nm (chrysi ligand transition).

5.2.6: Photocleavage of DNA by $[Rh(bpy)_2(chrysi)]^{3+}$ using "Non-Traditional" Light Sources

Samples of the 5' end-labeled, CC mismatch-containing duplex described in **5.2.2.1** (5 μl, 20 μM duplex, 37.5 mM NH_4OAc, pH 9) were combined with equal volumes of a Δ-$[Rh(bpy)_2(chrysi)]^{3+}$ solution (10 μM in deionized water). A dark control sample (rhodium complex incubated with DNA without irradiation) and a light control sample (DNA irradiated in the absence of metal complex) were also prepared. Samples were placed in closed 1.7 mL microcentrifuge tubes and placed in a Lucite

radioactivity isolation box. Individual samples were irradiated either under California sunlight or with ambient fluorescent room lighting for between 2 and 8 hr in two hour subdivisions. The samples were kept dark before and after irradiation. The reactions were dried under vacuum, resuspended, electrophoresed, and quantitated as described.

5.2.7: Oxygen Dependence of $[Rh(bpy)_2(chrysi)]^{3+}$ Photoreaction with DNA

The following oligonucleotide hairpins were synthesized and purified as described previously.

5'-CCTGGGC**C**CCCG $^{T}_{T}$
3'-GGACCCG**T**GGGC $_{TT}^{T}$

5'-GCTAC**C**CTCGTCAAC $^{TT}_{T}$
3'-CGATG**C**GAGCAGTTG $_{TT}^{T}$

Irradiation samples were prepared from solutions of each 5' end-labeled oligonucleotide (24-50 μM hairpin, 30-50 μl, 10 mM Tris pH 8.5 or 50 mM NH_4OAc, pH 9.0) and Δ-$[Rh(bpy)_2(chrysi)]^{3+}$ (6-10 μM, equal volume, in deionized water). These samples (12-25 μM nucleic acid, 3-5 μM Rh complex) were sealed in 1 mL, glass HPLC autosampler vials with 0.2 mL glass inserts. The vials were crimp-sealed with a pierceable septum through which syringe needles were inserted and the samples purged with argon or molecular oxygen by either bubbling through the solution or two cycles of freeze-pump-purge-thaw flushes. Light and dark control samples for each different oligonucleotide, irradiation wavelength, and sample buffer were also prepared. The vials were positioned as close as possible to the focal point of the monochromatic radiation from the Hg/Xe arc lamp system described above and irradiated at 313 nm, 440 nm, or 525 nm for between 30 and 60 min depending on the wavelength in use. Samples were stored under as dark conditions as possible before and after irradiation. When photolysis was complete,

the samples were removed from the sealed vials, split into two microcenrifuge vials and half treated with hot 1M piperidine for 25 min at 90°C. Both treated and untreated samples were then dried under vacuum, resuspended, electrophoresed, and quantitated as described.

5.2.8: Products of $[Rh(bpy)_2(chrysi)]^{3+}$ Photoreaction with DNA

5.2.8.1: Free Base Release

Metal dependent photolysis samples were prepared by combining one volume of a solution of sonicated calf thymus DNA (50-100 µl, 4-9 mM base pairs in 10 mM Tris pH 8.5) with one volume of a rhodium complex solution (Δ-$[Rh(bpy)_2(chrysi)]^{3+}$, *rac*-$[Rh(bpy)_2(chrysi)]^{3+}$, *rac*-$[Rh(phen)_2(phi)]^{3+}$ (50 µl, 400 µM- 2 mM in deionized water). Samples were irradiated at 313 nm (30-60 min), 440 nm (120 min), 525 nm (120 min) or 540 nm (120 min). In addition, light control samples of DNA in the absence of metal complex were prepared in an analogous manner with deionized water substituted for the rhodium complex solution and customarily irradiated at 313 nm for 30-60 min. Dark control samples consisting of DNA incubated with the metal complex in the absence of light were also prepared. After irradiation, the reactions were diluted with deionized water and a portion (between 1/3 and all of each sample) was analyzed by HPLC on a Microsorb-MV C_{18} analytical HPLC column using an ammomium formate/acetonitrile mobile phase (50 mM. pH 7) in a modification of the method described by A. Sitlani.[7] After injection of the photolysis sample, the column was eluted with buffer for 10 min followed by a linear increase in the percentage of acetonitrile to 20% over 30 min. The identity of reaction products were established by comparison with the retention times and spectral characteristics of commercially available standards. Free base standards for

cytosine, guanine, thymine, and adenine eluted at 5.8 min, 12.4 min, 18.5 min, and 21.8 min respectively.

Analogous experiments were also performed on CC mismatch-containing oligonucleotide hairpins which had been prepared and purified by previously described methods.

5'-GGCAGG**C**GTGGC^{T}T
3'-CCGTCC**C**CACCG$_{T}$T^{T}

5'-GGCAGT**C**TTGGC^{T}T
3'-CCGTCA**C**AACCG$_{T}$T^{T}

Solutions (400 μM) of both the hairpins CC/GG and CC/TT (see Chapter 4 for nomenclature description) were prepared in 10 mM Tris, pH 8.5. Aliquots of these oligonucleotides (50-200 μl) were combined with equal volumes of a 400 μM solution of Δ-$[Rh(bpy)_2(chrysi)]^{3+}$ and the resulting samples irradiated at 525 nm (60-180 min). As in previous experiments, light control reactions of DNA irradiated in the absence of the metal complex were also prepared. Samples were assayed by HPLC as described in the previous paragraph.

5.2.8.2: Nucleoside Analysis

Nucleic acid samples, either calf thymus DNA (4 mM base pairs, 50 μl) or CC mismatch-containing hairpin oligonucleotides (synthesized and purified as described, sequences in **5.2.8.1** (first sequence, CC/GG) and **5.2.7** (second sequence), 400 μM, 50-100 μl), were prepared in 10 mM Tris, pH 8.5. These were combined with equal volumes of either $[Rh(bpy)_2(chrysi)]^{3+}$ (400 μM Δ-) or $[Rh(phen)_2(phi)]^{3+}$ (400 μM *rac*-) and irradiated at 313 nm (30-60 min), 440 nm (120-180 min), or 525 nm (120-180 min). Analogous dark and light control samples were also prepared. After irradiation, the samples were ethanol precipitated and dried. The pellets were

redissolved in deionized water (26 μl) and sodium acetate (4 μl, 200 mM solution in deionized water, pH 5.2) was added. A solution of nuclease P1 (20 μl, 0.6 units/μl in 10 mM NaOAc, pH 5, Boehringer Mannheim, Indianapolis, IN) was added. The digestion was incubated at 37°C for between 4 and 6 hr at which point Tris buffer (10 μl, 1 M, pH 8.5), deionized water (37 μl), and calf intestine alkaline phosphatase (3 μl, 1 unit/μl, Boehringer Mannheim, Indianapolis, IN) were added. The dephosphorylation reaction was incubated at 37°C for between 5 and 10 hr. The samples were then customarily diluted to 300 μl and a third analyzed by analytical HPLC. Two elution procedures were applied to the analysis of the nucleoside products. The first, taken from Ito et al.,[9] consisted of a 90:10 aqueous:methanol system containing citric acid (12.5 mM), ammonium acetate (25 mM), sodium hydroxide (30 mM), and acetic acid (10 mM). This mixture was used for isocratic elution of the samples and provides good separation between all the nucleoside products. Such a system is not, however, ideal for other characterization methods as the eluted samples contain a great deal of salt. As a result, samples were also eluted with gradient combinations of acetonitrile and water each containing 0.1% trifluoroacetic acid. The four standard nucleoside products could be identified using shallow gradients (0%-10% CH_3CN over 60 min). The identity of products was established by comparison of their relative retention times and absorption spectra to the commercially available *ribo*-nucleoside products.

5.2.9: Electrochemical Characterization of $[Rh(bpy)_2(chrysi)](PF_6)_3$

Cyclic voltammetry was performed on samples of $[Rh(bpy)_2(chrysi)]^{3+}$ which had been ion exchanged to the PF_6^{1-} salt using Sephadex QAE A-25 anion exchange resin equilibrated in potassium hexafluorophosphate. The complex was dissolved in acetonitrile containing 0.1 M tetrabutylammonium tetrafluoroborate and degassed by

bubbling with argon. Cyclic voltammetry was performed using a standard three electrode configuration consisting of a glassy carbon working electrode, a platinum wire auxiliary electrode, and a saturated calomel reference electrode (0 V starting potential, -1.5 V to +1.5 V sweep, initially swept positive, 100 mV/s).

5.3: RESULTS

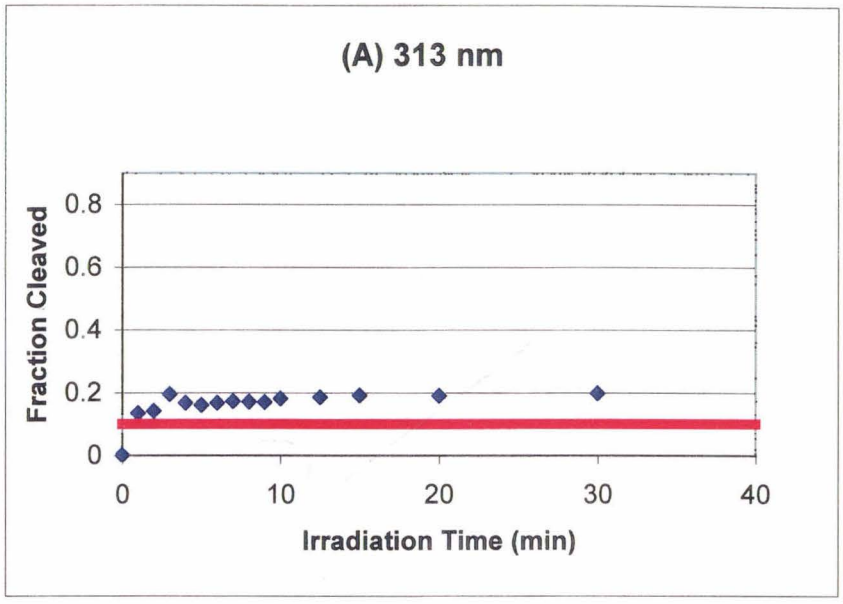
5.3.1: Photocleavage Saturation Experiments using $[Rh(bpy)_2(chrysi)]^{3+}$

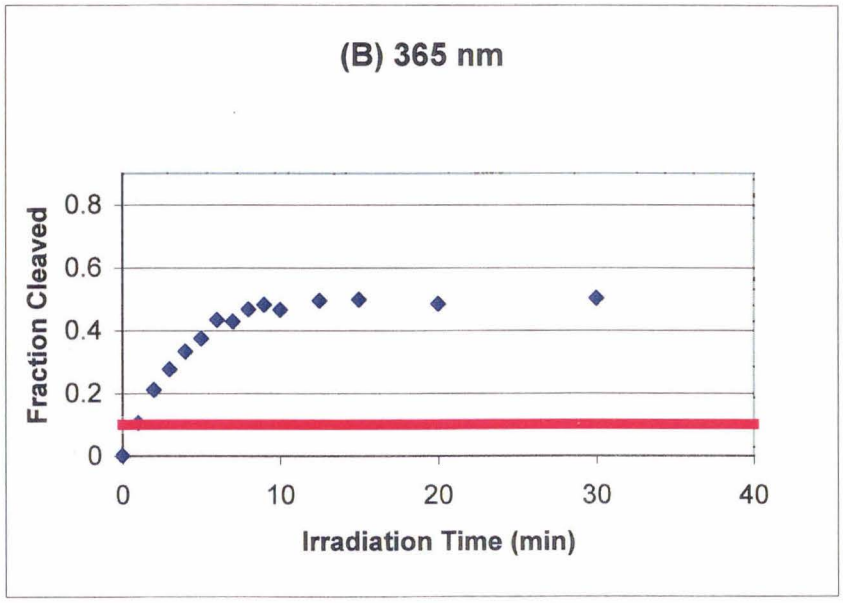
In order to assess the ability of $[Rh(bpy)_2(chrysi)]^{3+}$ to cut DNA when activated by various wavelengths of light, a series of photocleavage saturation experiments was performed. These experiments, which consisted of progressively longer irradiations of many identical rhodium complex-DNA samples, sought to determine the maximal DNA photocleavage which would be observed at a given wavelength extrapolated to an infinitely long photolysis time. At the ratio of rhodium complex to DNA (1:10) used in these experiments, stoichiometric cleavage would result in cutting of 10% of the DNA. In addition, this low loading of Rh to DNA ensured that essentially all cleavage was observed at the single base 3' to the CC mismatch; cleavage at this single site was quantitated, expressed as a cleavage fraction and is summarized graphically as photocleavage build-up curves as a function of irradiation time in Figure 5.1.

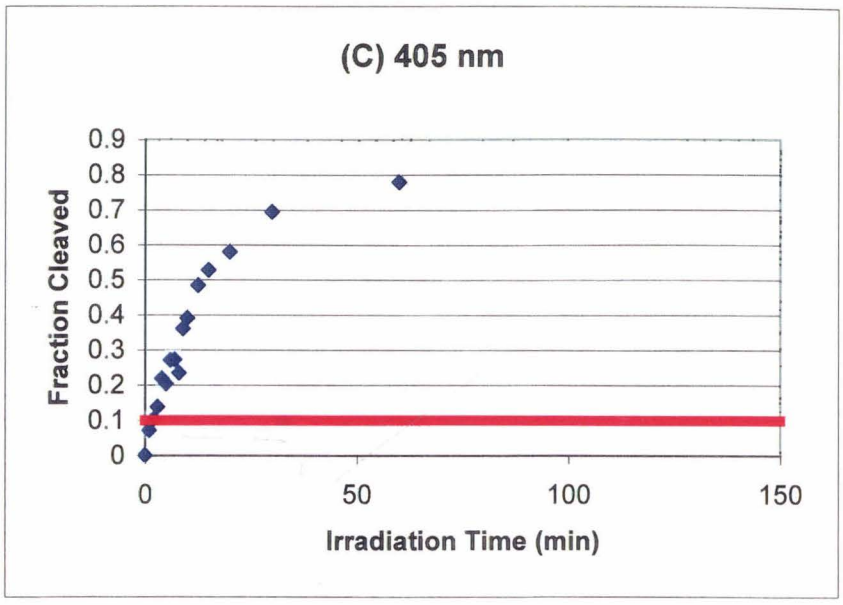
Examination of the photocleavage curves resulting from this experiment dramatically demonstrates both the exceedingly efficient, *photocatalytic* DNA cleavage properties of $[Rh(bpy)_2(chrysi)]^{3+}$ and the broad range of wavelengths of incident light with which it is capable of producing direct DNA strand scission. The levels of maximal cleavage, extrapolated from the apparent asymptotic limits of these build up curves, vary from a low value of about 0.2 (313 and 600 nm) to high values greater than 0.8

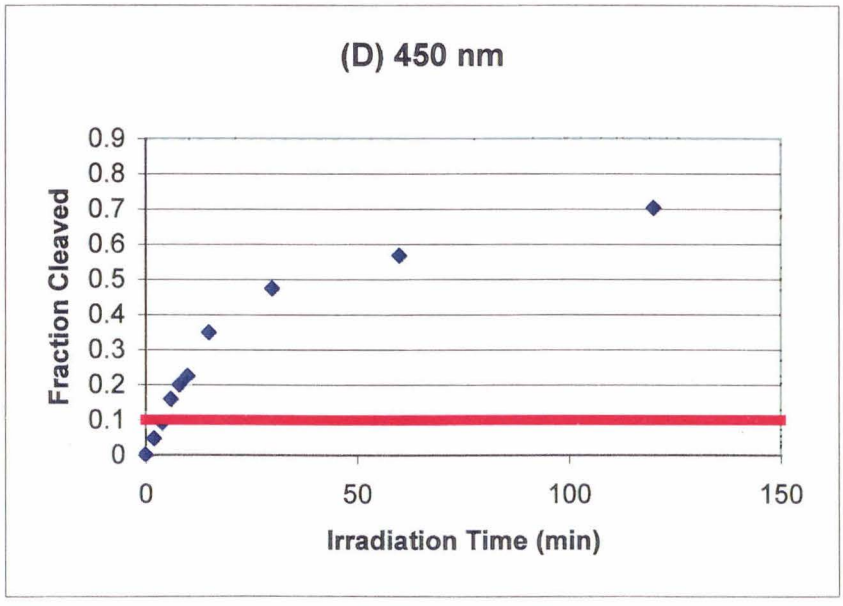
Figure 5.1. Photocleavage by Δ-$[Rh(bpy)_2(chrysi)]^{3+}$ at a CC Mismatch as a Function of Irradiation Wavelength and Photolysis Time. The amount of DNA cleaved at the mismatch site expressed as a fraction of the total radioactivity in the gel lane is plotted as a function of irradiation time. Vertical axes are held constant to facilitate comparison of total photocleavage at each wavelength. Horizontal axes are constant in all cases except Panels A and B (313 and 365 nm) where they have been shortened. Photocatalytic DNA cleavage over the stoichiometric value of 0.1 (red bar) is observed with irradiation at *all* wavelengths.

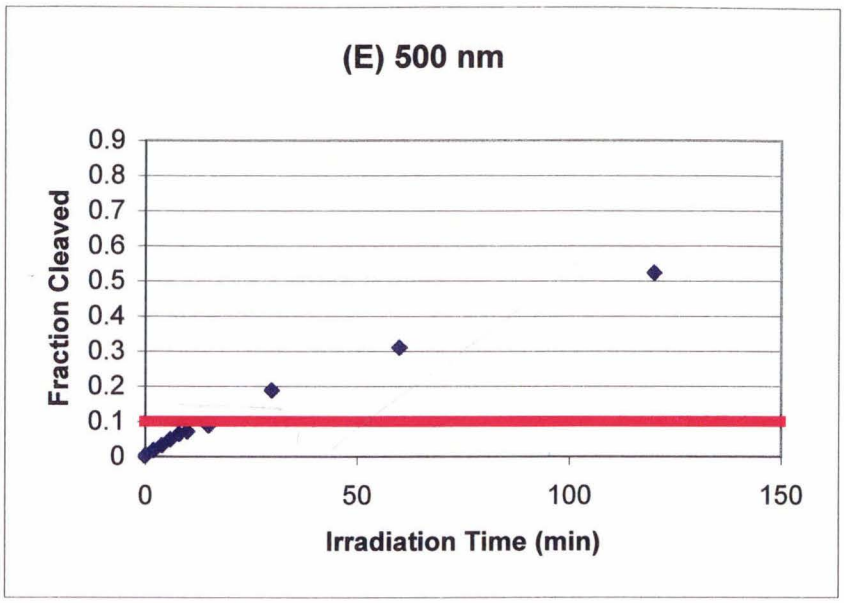
Figure 5.1:

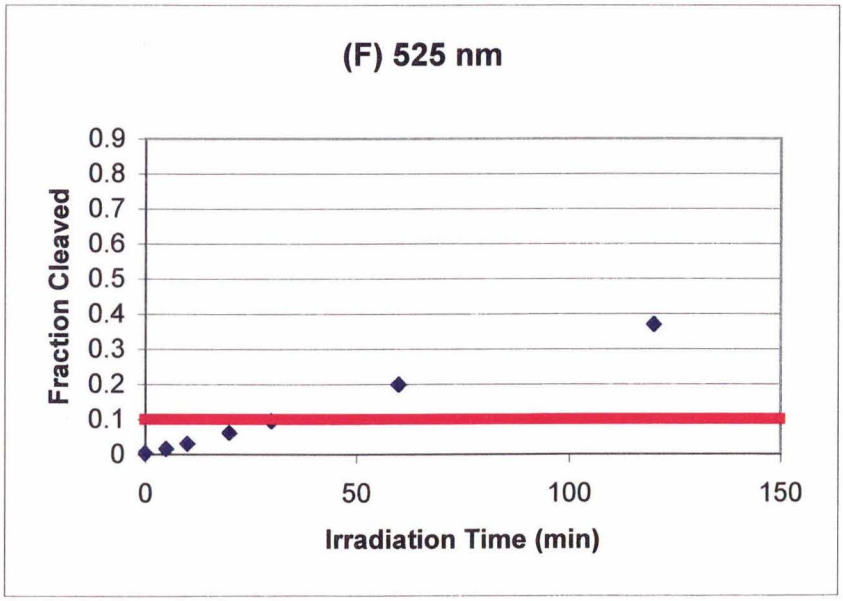

(A) 313 nm
Fraction Cleaved
0.8
0.6
0.4
0.2
0
0
10
20
30
40
Irradiation Time (min)

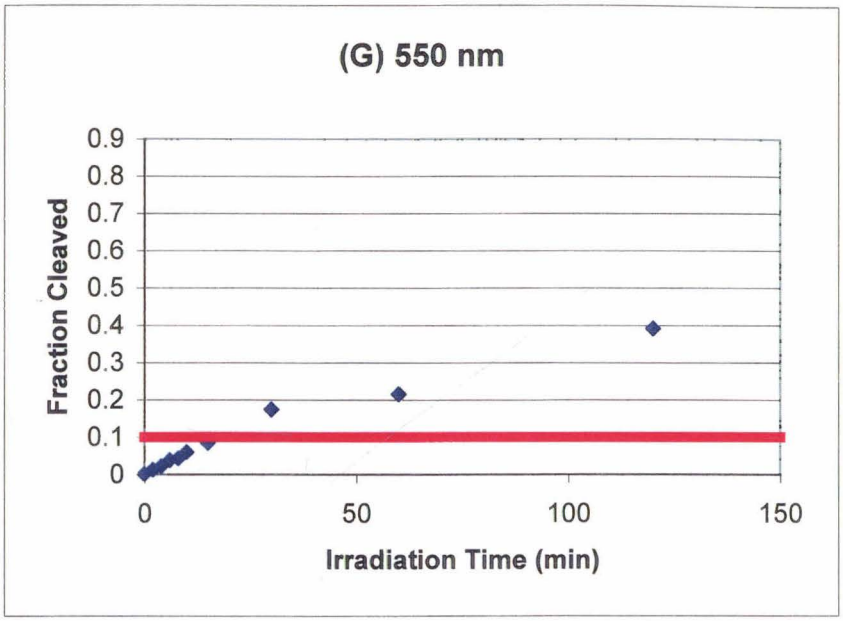

(B) 365 nm
Fraction Cleaved
0.8
0.6
0.4
0.2
0
0
10
20
30
40
Irradiation Time (min)

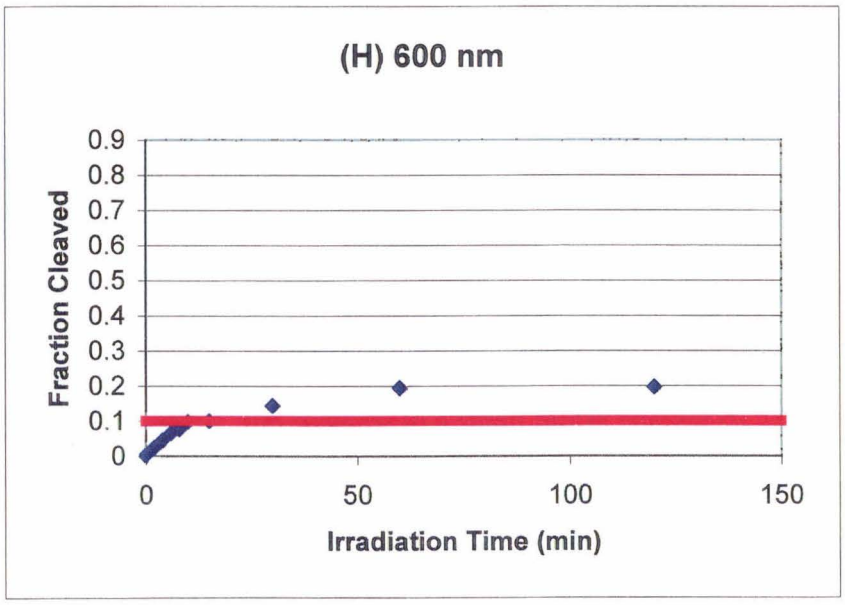

(C) 405 nm
Fraction Cleaved
0.9
0.8
0.7
0.6
0.5
0.4
0.3
0.2
0.1
0
0
50
100
150
Irradiation Time (min)


(D) 450 nm
Fraction Cleaved
0.9
0.8
0.7
0.6
0.5
0.4
0.3
0.2
0.1
0
0
50
100
150
Irradiation Time (min)


(E) 500 nm
Fraction Cleaved
0.9
0.8
0.7
0.6
0.5
0.4
0.3
0.2
0.1
0
0
50
100
150
Irradiation Time (min)


(F) 525 nm
Fraction Cleaved
0.9
0.8
0.7
0.6
0.5
0.4
0.3
0.2
0.1
0
0
50
100
150
Irradiation Time (min)


(G) 550 nm
Fraction Cleaved
0.9
0.8
0.7
0.6
0.5
0.4
0.3
0.2
0.1
0
0
50
100
150
Irradiation Time (min)

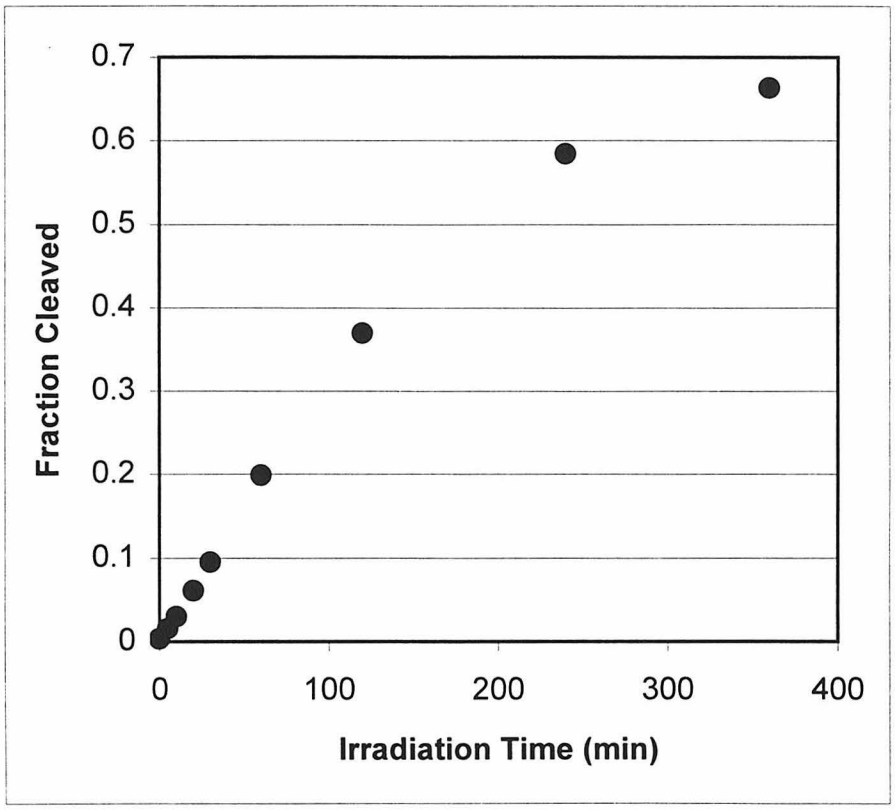

(H) 600 nm
Fraction Cleaved
0.9
0.8
0.7
0.6
0.5
0.4
0.3
0.2
0.1
0
0
50
100
150
Irradiation Time (min)

(405 nm). These values are particularly impressive given that in the irradiation samples the ratio of rhodium complex to DNA duplexes is 1:10; as a result, even at the wavelengths where photocleavage is the least, the observed value is twice the stoichiometric amount.

In addition to the maximal level of DNA cutting, the shape of the photocleavage saturation curves also varies dramatically from wavelength to wavelength. At the shortest wavelengths of irradiation, the cleavage of DNA is efficient with the great majority of cleaved product appearing in only a few min of irradiation. After this initial "burst" of reaction, photocleavage drops off and little additional product is observed. As the wavelength of irradiation is increased, the slope of the saturation curve is reduced. Instead of the almost vertical increase observed at 313 nm, at higher wavelengths the slope is much smoother and gradual. More importantly, however, at some of these higher wavelengths, the clear asymptotic behavior observed in the cleavage curves at 313 or 365 nm is absent. Between 500 and 550 nm, for example, the plots appear almost linear. This behavior was confirmed by performing additional, longer irradiations at 525 nm. When irradiation was continued past the 150 min limit of the graphs included in Figure 5.1, the fraction cleaved continued to increase and only began to show signs of curvature as it approached 0.7 after six hr of irradiation (Figure 5.2). When the ratio of $[Rh(bpy)_2(chrysi)]^{3+}$:DNA was reduced to a small molar percent (0.25%) and the concentration of DNA increased to eliminate any reduction in cleavage which might be caused by consumption of the DNA substrate, levels up to 13 times stoichiometric cleavage were observed. These values also likely do not represent the maximal level of cleavage as drying of the sample by evaporation over the long irradiation times limited the effective length of the solution phase reaction.

Figure 5.2. Photocleavage by Δ-$[Rh(bpy)_2(chrysi)]^{3+}$ at the CC/CC Mismatch Irradiated at 525 nm for Extended Time. The amount of DNA cleaved at the mismatch site expressed as a fraction of the total radioactivity in the gel lane is plotted as a function of irradiation time.

Figure 5.2:


0.7
0.6
0.5
0.4
0.3
0.2
0.1
0
Fraction Cleaved
0
100
200
300
400
Irradiation Time (min)

5.3.2: Photocatalytic DNA Cleavage by $[Rh(phen)_2(phi)]^{3+}$

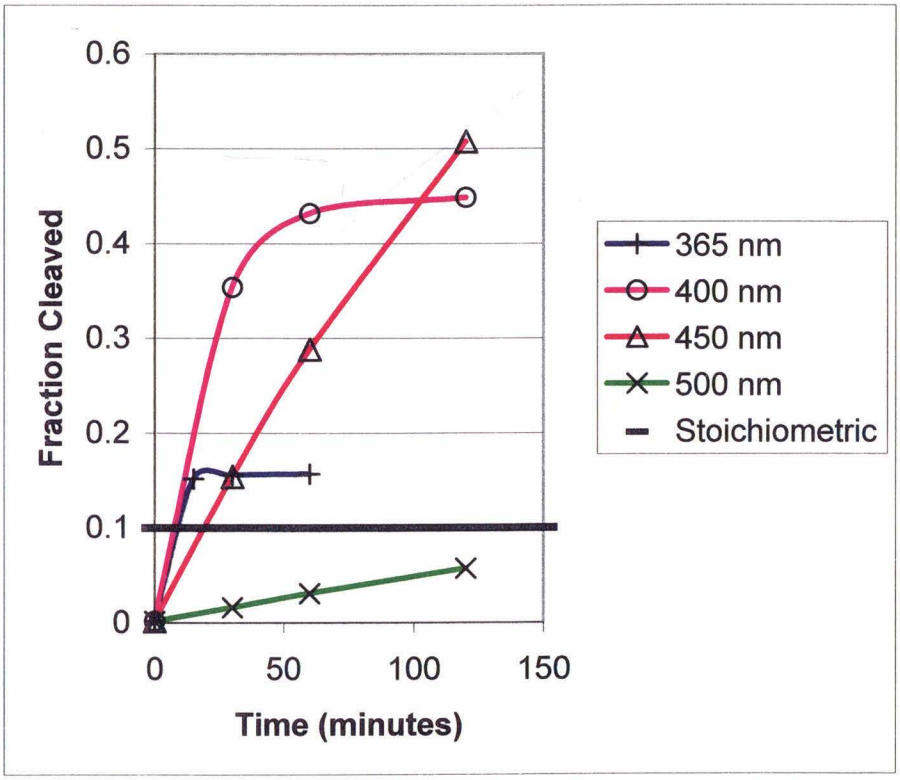
Having established that $[Rh(bpy)_2(chrysi)]^{3+}$ photocleaved DNA catalyticaly upon photo-activation with visible light, determining if this behavior was unique to complexes containing the chrysenequinone diimine intercalating ligand was of substantial interest. As a result, experiments analogous to those described above were performed with $[Rh(phen)_2(phi)]^{3+}$ to determine not only how far into the visible region of the spectrum its photocleavage behavior would extend but also if it would exhibit photocatalytic DNA cleavage. The results of these experiments on a hairpin oligonucleotide containing a CC mismatch* are included as Figure 5.3. It is clear from these results that, like the chrysi complex, the phi intercalator exhibits significant *photocatalytic* cleavage of DNA. In the most dramatic case, at 450 nm, $[Rh(phen)_2(phi)]^{3+}$ cleaved more than 50% of the full length DNA strand after two hr of irradiation and, even at that impressive level of reaction, the resulting saturation curve (Figure 5.3) shows no sign of leveling off. Similar experiments on Watson-Crick base paired DNA, while more difficult to analyze due to the multiple sites of complex binding and photocleavage, also exhibit greater than stoichiometric levels of strand cutting (data not shown). As a result, it can be concluded that photocatalytic cleavage of DNA stimulated by visible light is not a property unique to complexes containing the chrysenequinone diimine intercalating ligand.

---

* As discussed in Chapter 3, like the chrysi complex, the phi compound binds preferentially to the mismatch and, under the low loading conditions of this experiment, the majority of the compound's photocleavage is observed at that site.

Figure 5.3. Photocleavage by Δ-$[Rh(phen)_2(phi)]^{3+}$ at a CC Mismatch as a Function of Irradiation Wavelength and Photolysis Time. The amount of DNA cleaved at the mismatch site expressed as a fraction of the total radioactivity in the gel lane is plotted as a function of irradiation time. The ratio between the rhodium complex and the hairpin DNA polymers was 1:10; the level of cleavage expected if the reaction was stoichiometric is indicated by the heavy line near the bottom of the graph. Not only does $[Rh(phen)_2(phi)]^{3+}$ continue to cleave DNA with irradiation wavelengths as high as 500 nm, but also the photocleavage at 450 nm shows no sign of saturation in this experiment.

Figure 5.3:


0.6
0.5
0.4
0.3
0.2
0.1
0
Fraction Cleaved
0
50
100
150
Time (minutes)
365 nm
400 nm
450 nm
500 nm
Stoichiometric

5.3.3: Photoaquation of Chrysenequinone Diimine Complexes Upon Irradiation when Bound to DNA

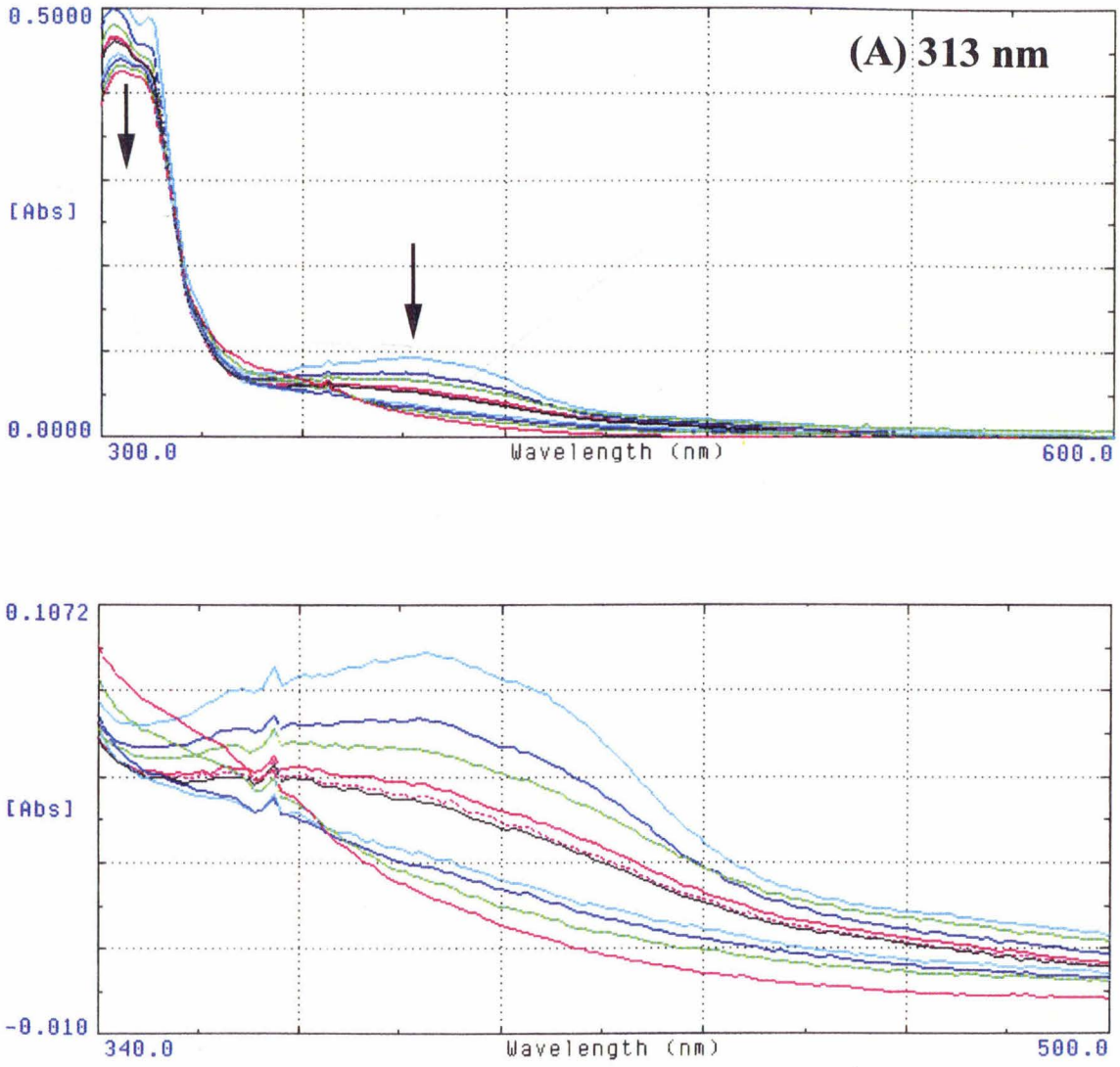
Because of the strong chromophores associated with phenanthrenequinone diimine complexes of rhodium(III) and the sensitivity of their absorption characteristics to changes in the ligand field or at the metal center, absorption spectroscopy has been used extensively to examine the photochemical reactions of these compounds. It has already been demonstrated in this work that absorption spectroscopy can be utilized to observe the electronic changes which occur with deprotonation of the metal complex immino groups (**2.3.2.1** and **2.3.2.2**) or with intercalation of the chrysi ligand into DNA (**3.2.2**). As a result, such studies seemed an ideal way to characterize any changes which might occur in the metal complex during the course of irradiation and DNA cleavage.

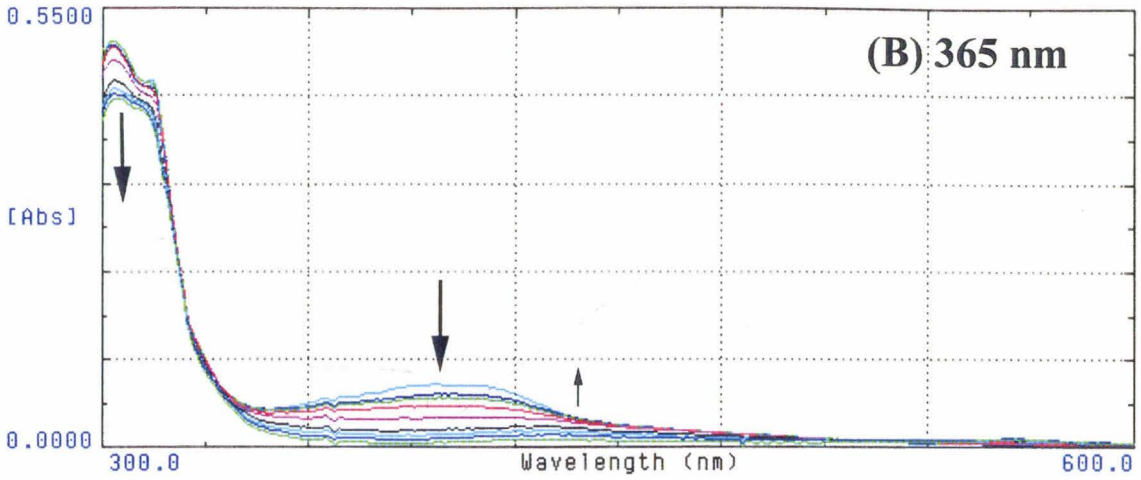
Experiments were performed on $[Rh(bpy)_2(chrysi)]^{3+}$ bound to a CC mismatch-containing oligonucleotide. Concentration conditions (50 μM DNA polymers, 10 μM Δ-$[Rh(bpy)_2(chrysi)]^{3+}$) were selected at which the complex would be completely bound to the DNA and the spectral window of the experiment (300 – 600 nm) chosen to minimize any interference from the DNA absorbance at 260 nm. Periodic spectra obtained over the course of irradiation of many identical samples at different wavelengths demonstrated that the photochemistry of $[Rh(bpy)_2(chrysi)]^{3+}$ is highly dependent on the wavelength of irradiation. As the photolysis wavelength is increased from 313 nm to 600 nm, the photochemical behavior of the complex passes through several distinct regions.

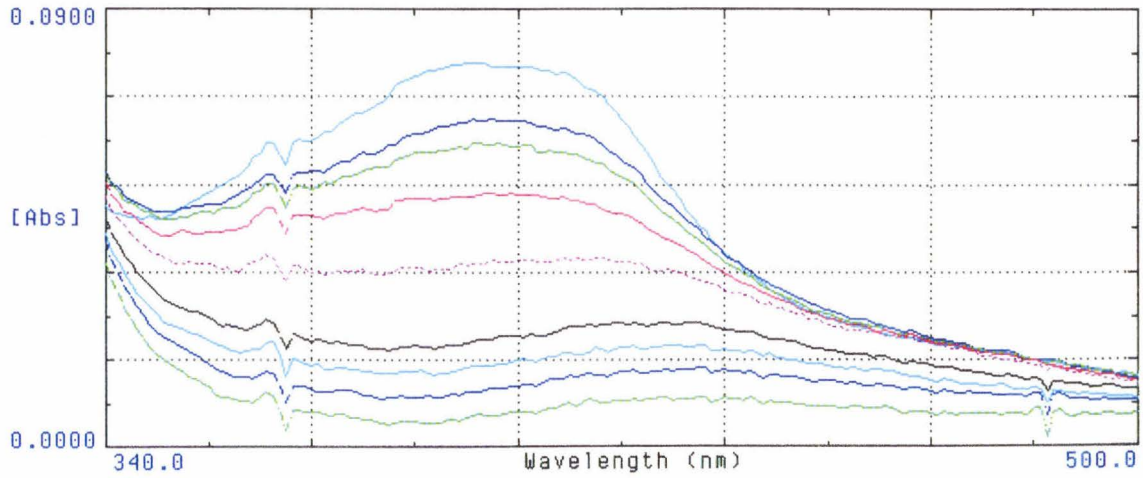
At high energy (313 nm and 365 nm, Figure 5.4A and B), loss of intensity is observed in the visible transitions associated with the quinone diimine ligand suggesting

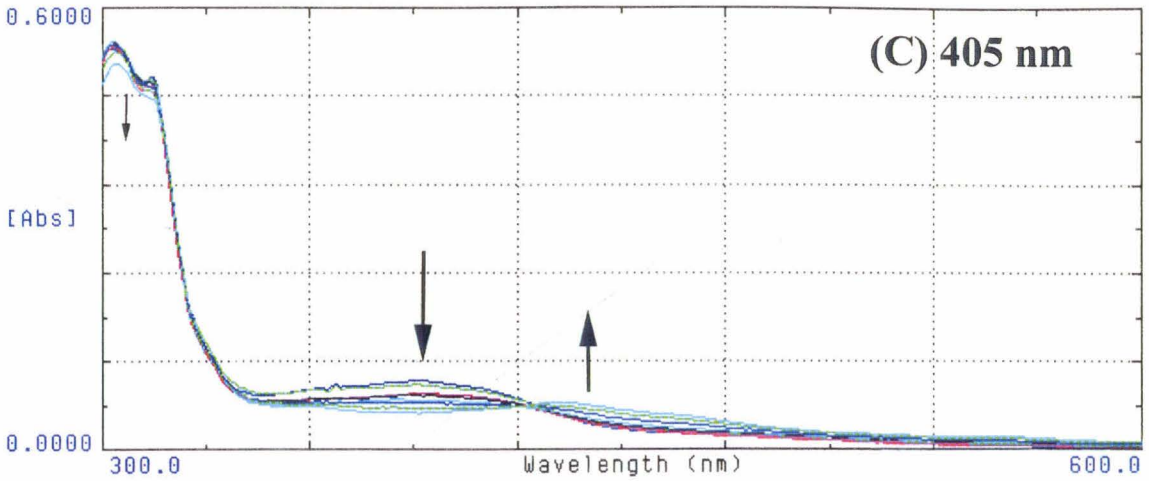
Figure 5.4. Examination of the Spectroscopic Changes which Occur in Δ-$[Rh(bpy)_2(chrysi)]^{3+}$ Bound to DNA over the course of Irradiation. Changes in the absorption spectrum, which are diagnostic of reaction or degradation pathways affecting the rhodium(III) chrysi chromophore are monitored at various wavelengths through the ultraviolet and visible regions of the spectrum. The maximum irradiation time at each wavelength is included in brackets. (A) 313 nm, [1 hr] (B) 365 nm, [1 hr] (C) 405 nm, [1 hr] (D) 450 nm, [4 hr] (E) 500 nm, [4 hr] (F) 525 nm, [4 hr] (G) 550 nm, [4 hr] (H) 600 nm, [4 hr]

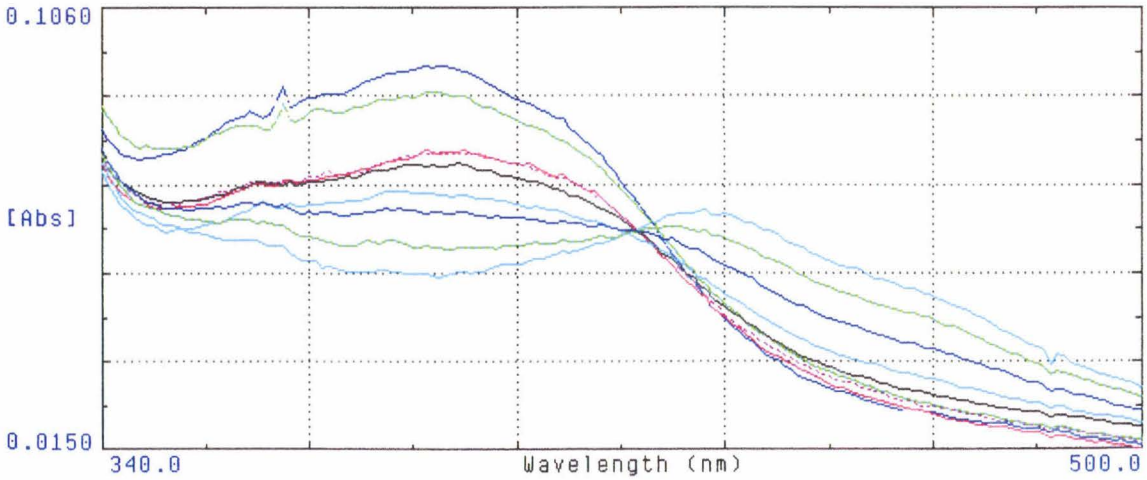
Figure 5.4:

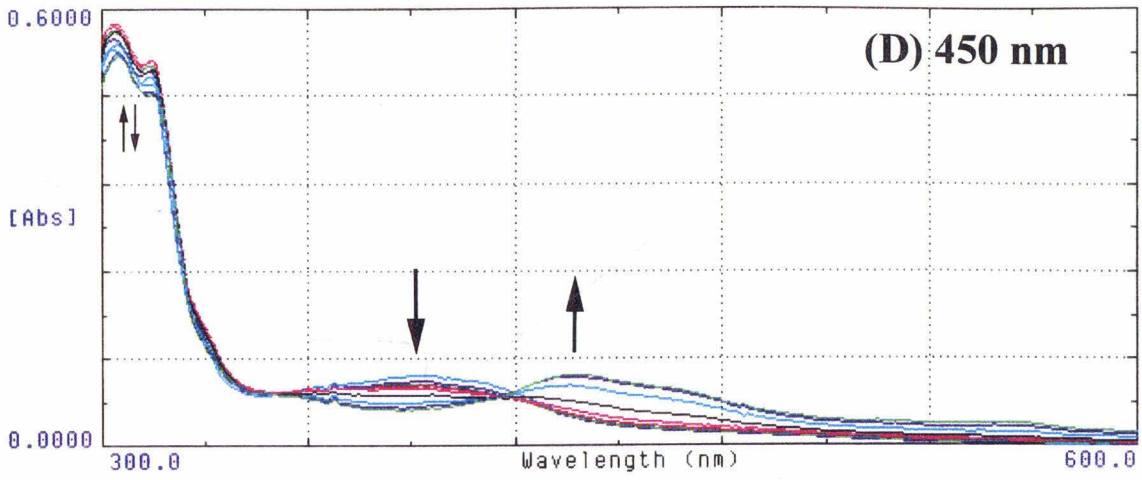

0.5000
[Abs]
0.0000
300.0
Wavelength (nm)
600.0
(A) 313 nm
0.1072
[Abs]
-0.010
340.0
Wavelength (nm)
500.0

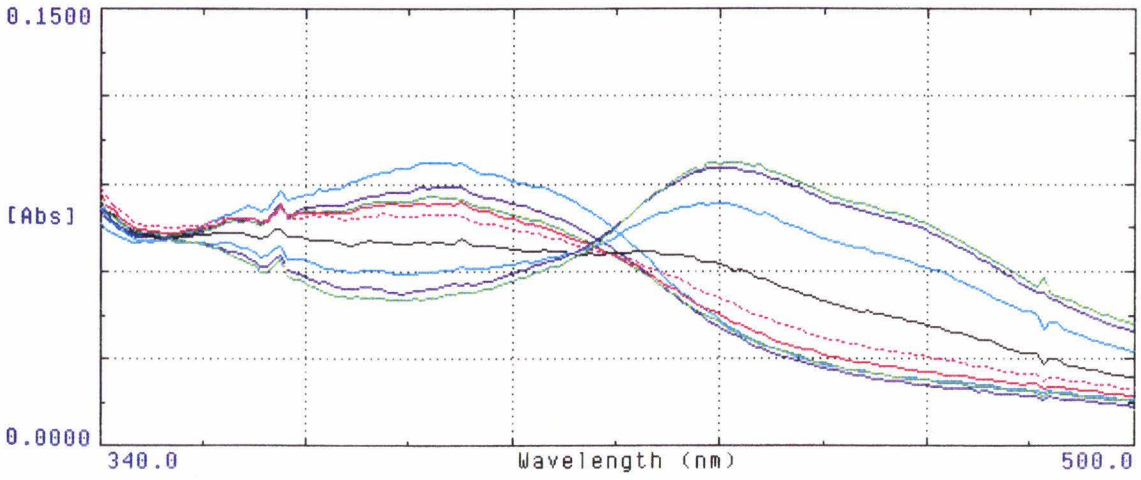

0.5500
[Abs]
0.0000
(B) 365 nm
300.0
Wavelength (nm)
600.0

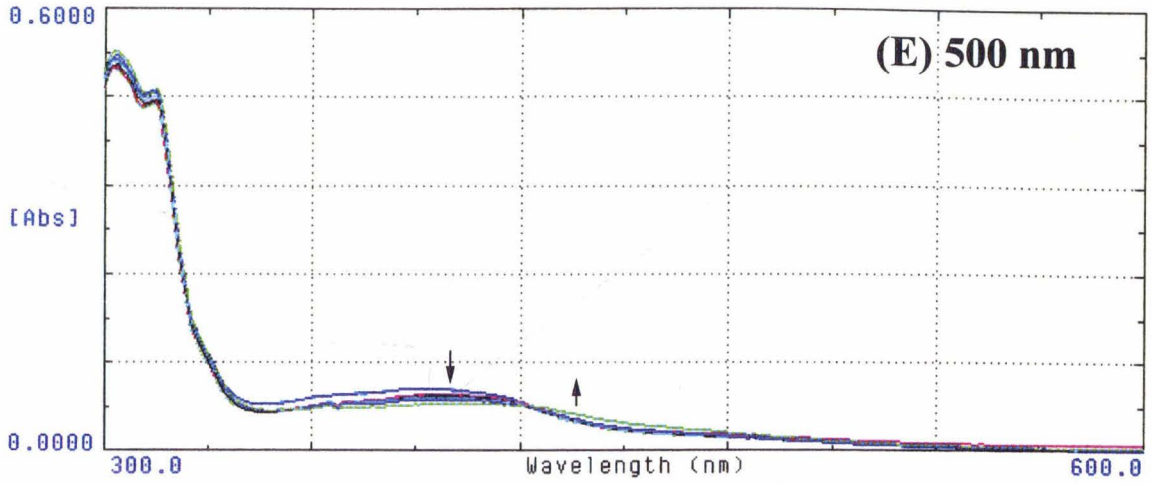

0.0900
[Abs]
0.0000
340.0
Wavelength (nm)
500.0

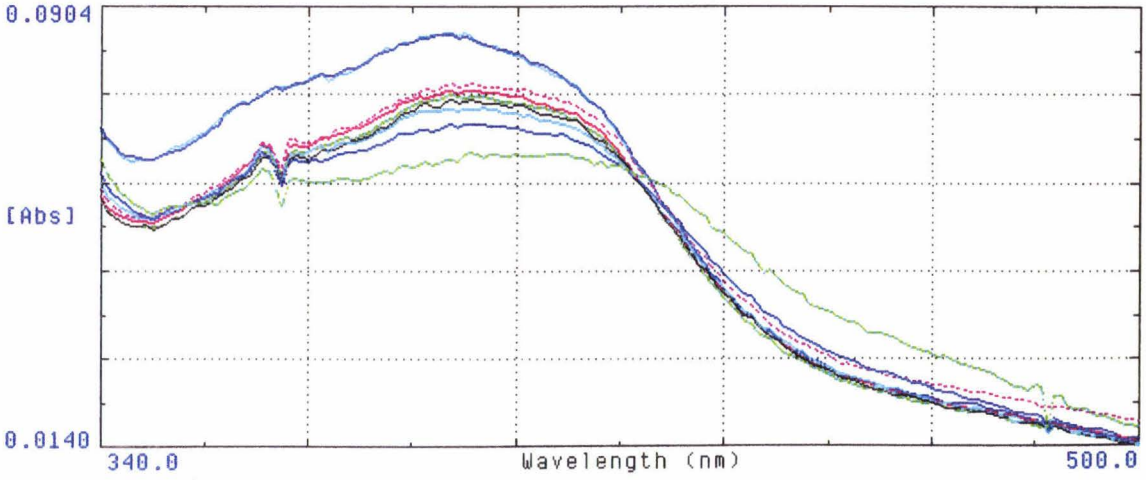

0.6000
[Abs]
0.0000
300.0
Wavelength (nm)
600.0
(C) 405 nm

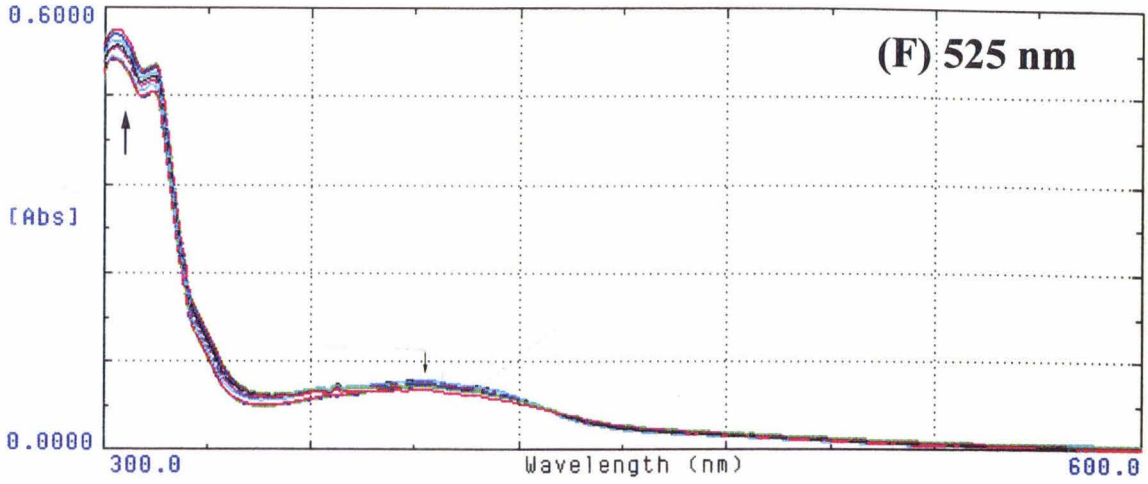

0.1060
[Abs]
0.0150
340.0
Wavelength (nm)
500.0

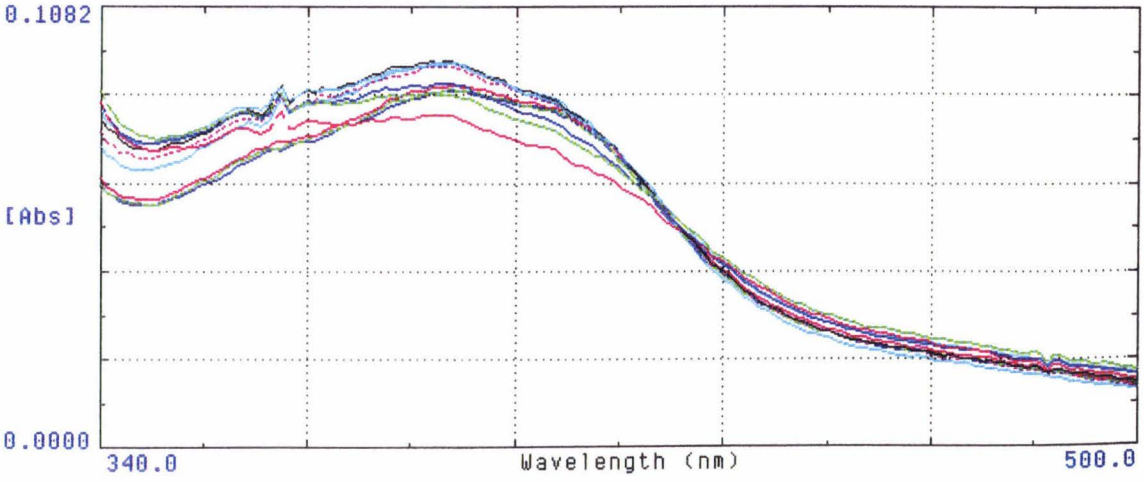

0.6000
[Abs]
0.0000
300.0
Wavelength (nm)
600.0
(D) 450 nm

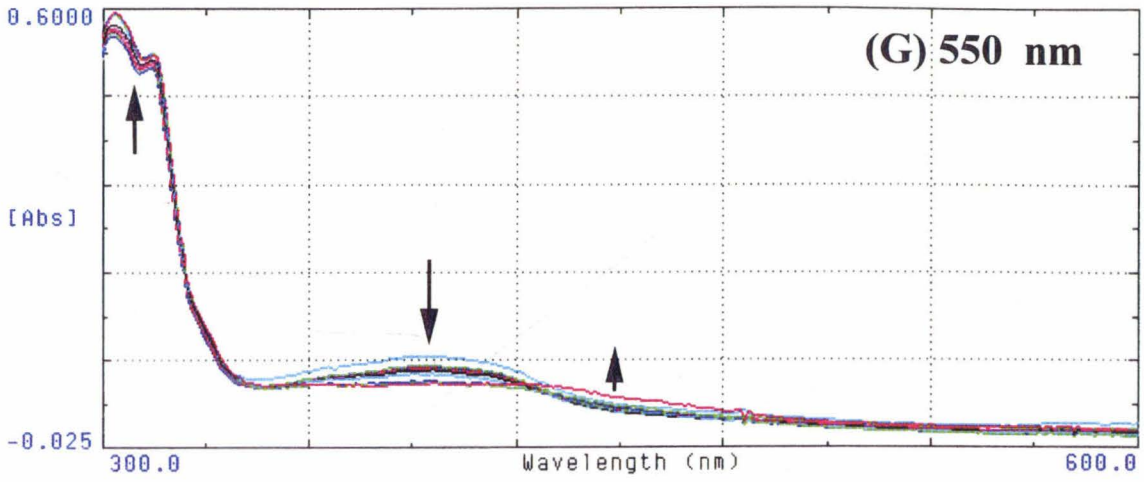

0.1500
[Abs]
0.0000
340.0
Wavelength (nm)
500.0

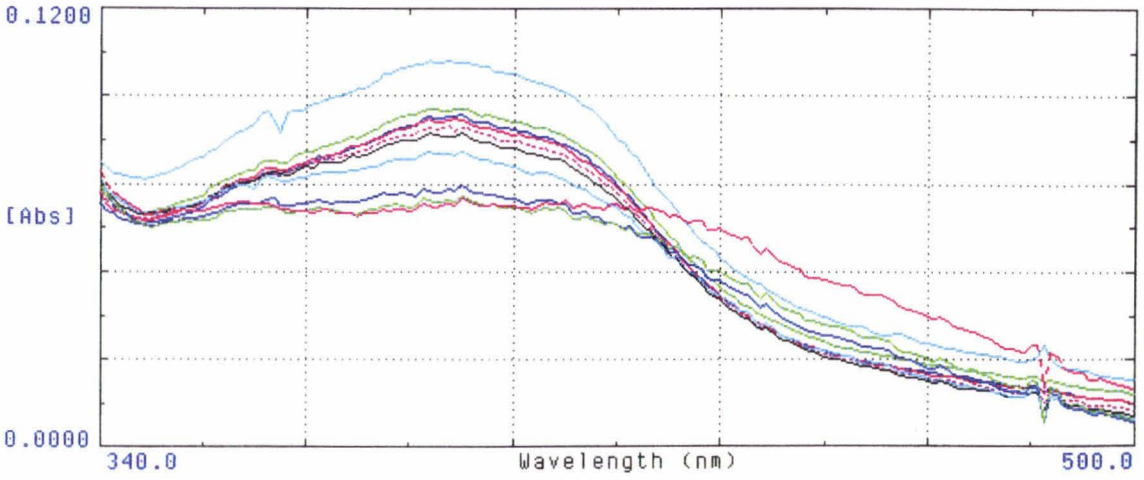

0.6000
[Abs]
0.0000
300.0
Wavelength (nm)
600.0
(E) 500 nm

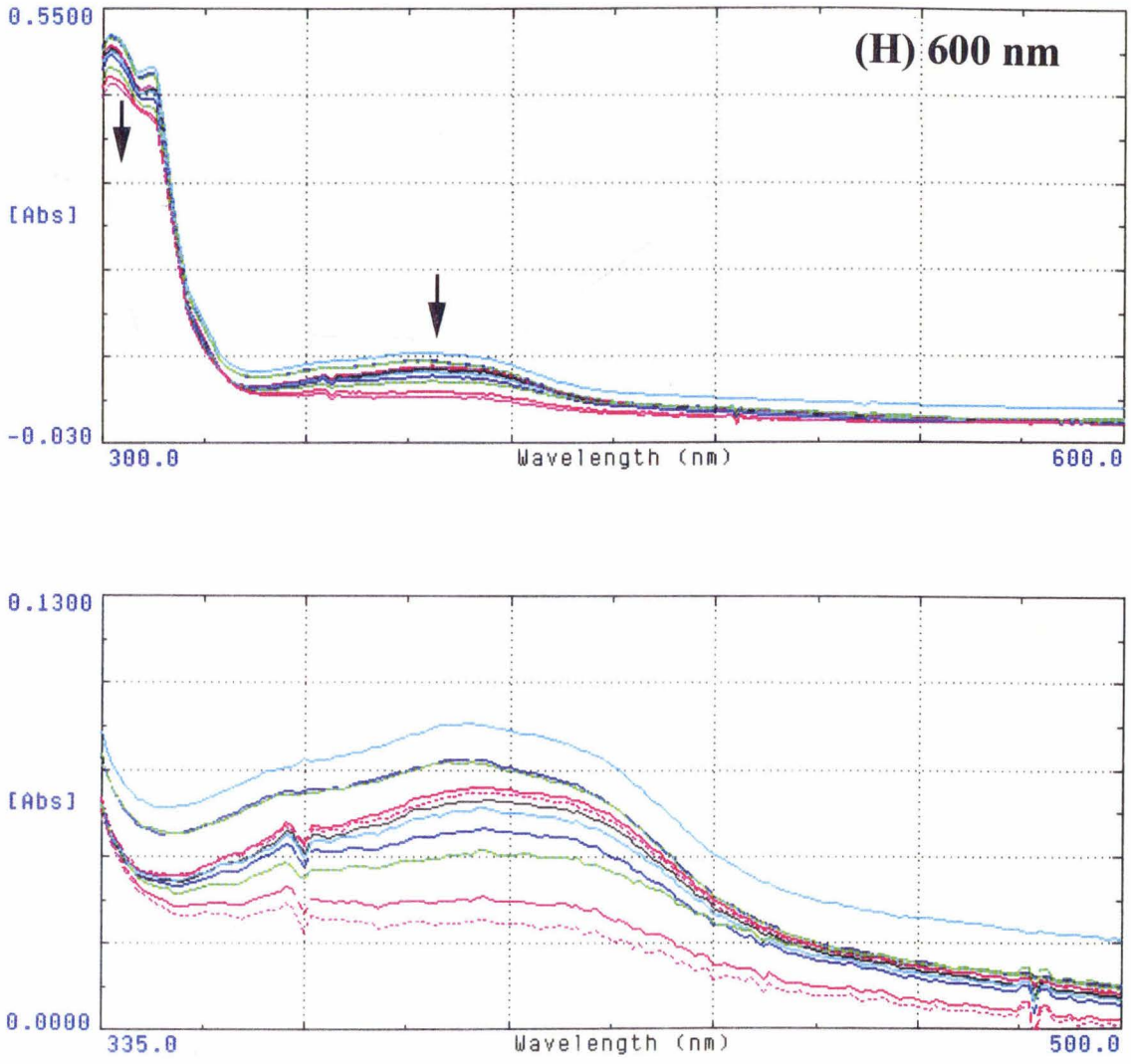

0.0904
[Abs]
0.0140
340.0
Wavelength (nm)
500.0


0.6000
[Abs]
0.0000
300.0
Wavelength (nm)
600.0
(F) 525 nm


0.1082
[Abs]
0.0000
340.0
Wavelength (nm)
500.0


0.6000
[Abs]
-0.025
(G) 550 nm
300.0
Wavelength (nm)
600.0


0.1200
[Abs]
0.0000
340.0
Wavelength (nm)
500.0


(H) 600 nm
0.5500
[Abs]
-0.030
300.0
Wavelength (nm)
600.0
0.1300
[Abs]
0.0000
335.0
Wavelength (nm)
500.0

photoaquation of the complex and loss of the intercalating ligand. Like the DNA cleavage saturation curves, these spectral changes also occur relatively rapidly with large percentage changes observed within one hour of irradiation. This is consistent with analogous behavior previously observed for rhoduim(III) phi complexes.[10,11] As the photolysis wavelength was increased, the photochemical behavior of the metal complex entered a second regime distinctly different from simple photoaquation. Beginning at 365 nm and increasing to a maximum at 450 nm (Figure 5.4B, C, and D), the original absorbance of the metal complex centered at approx. 390 nm is bleached and the appearance of a new set of absorbance transitions is observed over the course of the 4 hour photolysis reaction. This new absorbance appears as a broad peak containing at least two features, one centered at approx. 440 nm and the other near 465 nm. A clear isosbestic point exists (420 nm) between the two sets of peaks suggesting the conversion of one chemical species into another. This will be addressed more fully in section **5.3.4** below.

As the irradiation wavelength is further increased, the photochemistry of the compound enters a third region. In the reaction irradiated at 500 nm (Figure 5.4E), there is very little evidence of the proposed photochemical conversion seen at 450 nm. Instead, even over the course of 4 hr of irradiation, the spectrum is quite stable with a loss of only 24% of its absorbance intensity. Of the wavelengths tested, the absorbance spectrum of the metal complex was the most stable at the slightly higher wavelength of 525 nm (Figure 5.4F). Over its 4 hr photolysis, the transition centered at 390 nm decreases by only 11%. Once the wavelength is increased further to 550 nm and 600 nm (Figure 5.4G and H), the photochemistry enters its final domain. At these highest wavelengths, the behavior is much more reminiscent of that seen with irradiation in the ultraviolet. Particularly at 600 nm, the visible absorption band is

bleached over the course of photolysis as would be expected for photodissociation of the quinone diimine ligand and breakdown of the complex.

5.3.4: Analysis of the Photo-Induced Reaction between $[Rh(bpy)_2(chrysi)]^{3+}$ and DNA by Analytical HPLC

Although monitoring the reactions of $[Rh(bpy)_2(chrysi)]^{3+}$ over the course of irradiation by spectroscopic methods does provide a straightforward and sensitive assay for the integrity and photochemical characteristics of the metal complex, such studies provide only an average view of the species which might exist in the solution reaction. To obtain more specific information about the number of different products produced or the spectroscopic characteristics of individual components of the system, other techniques are required. Toward these ends, the photo-reaction of Δ-$[Rh(bpy)_2(chrysi)]^{3+}$ with a CC mismatch-containing hairpin was monitored by analytical HPLC. In addition to the information provided by the chromatographic separation of the components of the system, the use of a diode array detector also makes spectral information on each individual material accessible.

5.3.4.1: Irradiation of the Metal Complex Alone

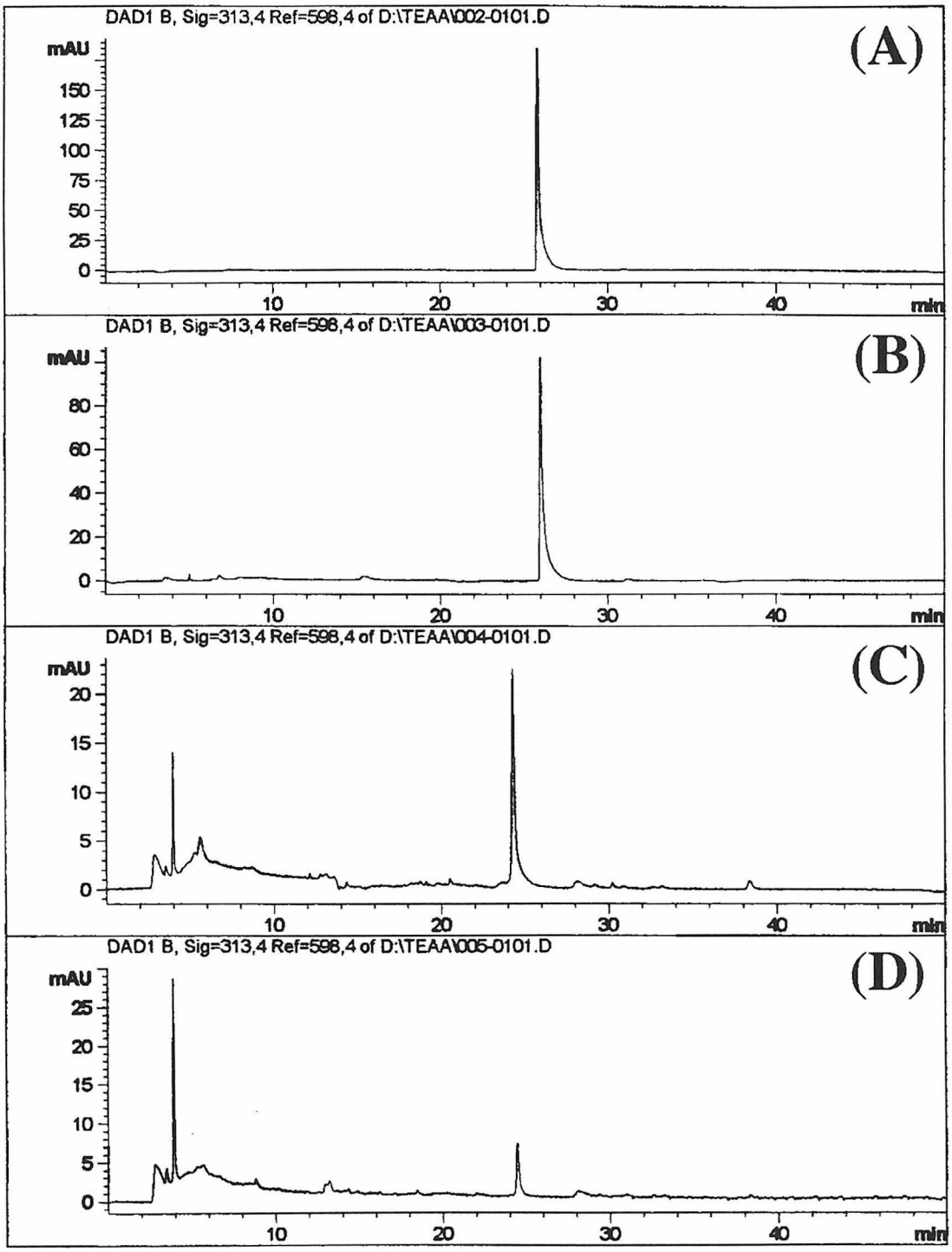
HPLC examination of samples of the rhodium complex irradiated in the absence of DNA demonstrates that there are significant wavelength dependent differences in the photoreactivity of $[Rh(bpy)_2(chrysi)]^{3+}$ *unrelated to DNA photocleavage*. With irradiation at 313 nm, the metal complex (Figure 5.5, retention time of 24-26 min)* is

---

* Although the retention time of the intact metal complex in these experiments was observed to shift from injection to injection presumably as a result of the changes in solution conditions generated over the course of the irradiation experiments, the identity of the peak was confirmed by examination of the absorption spectrum.

Figure 5.5. HPLC Analysis of the Photolysis Products of $[Rh(bpy)_2(chrysi)]^{3+}$ Irradiated at 313 nm. Analytical chromatographic traces of metal complex photolysis products as time of irradiation at 313 nm is increased: (A) T=0, (B) 5 min, (C) 15 min, (D) 30 min. Chromatograms were constructed by monitoring the absorbance of eluted products at 313 nm, an absorption maximum of the metal complex associated with its ancillary bpy ligands. The intact metal complex (retention times of 24-26 min as assigned by absorption spectral measurement) is rapidly converted to products of very short retention time under these chromatographic conditions. Reaction and chromatography conditions are provided in the text.

Figure 5.5:


DAD1 B, Sig=313,4 Ref=598,4 of D:\TEAA\002-0101.D
(A)
mAU
150
125
100
75
50
25
0
10
20
30
40
min
DAD1 B, Sig=313,4 Ref=598,4 of D:\TEAA\003-0101.D
(B)
mAU
80
60
40
20
0
10
20
30
40
min
DAD1 B, Sig=313,4 Ref=598,4 of D:\TEAA\004-0101.D
(C)
mAU
20
15
10
5
0
10
20
30
40
min
DAD1 B, Sig=313,4 Ref=598,4 of D:\TEAA\005-0101.D
(D)
mAU
25
20
15
10
5
0
10
20
30
40
min

observed to quickly fragment to materials with greatly reduced retention times; this breakdown process is observable in chromatograms monitored at both 313 nm (Figure 5.5), a transition primarily associated with the bipyridine ligands, and at the 370 nm absorbance associated with the chrysi ligand. This facile fragmentation of the complex when irradiated at high energy in basic solution is entirely consistent with previous studies of phenanthrenequinone diimine compounds.[7,12]

Irradiation of the metal complex at 400 nm also produces photoinduced breakdown of the complex. At this intermediate wavelength, however, the fragmentation is not as efficient as that observed at higher energy. By thirty min, at which point the complex was entirely destroyed at 313 nm, the complex photolyzed at 400 nm is only slightly depleted (Figure 5.6). In addition, in this case the intact metal complex (24-26 min) is converted first to a single product (Figure 5.6B and C, retention time of 20 min). Although this product is degraded further with additional irradiation, even at 120 min (Figure 5.6D) it is still the primary component of the reaction. The absorption spectrum of this compound (Figure 5.7B) is noteworthy as it is significantly different from the starting complex (Figure 5.7A). Although some absorbance does remain in the region of the spectrum associated with the chrysi transitions, it is much weaker than the parent complex; more dramatically, however, the transitions in the 300 nm region have significantly changed in structure and two entirely new features have arisen at approx. 520 nm and 560 nm. Although these transitions are approx. 80 nm longer wavelength than the increases in absorbance observed in the complex photoaquation experiments in the previous section (see Figure 5.4D), this is likely one species responsible for the spectral changes observed when the complex was irradiated at these wavelengths. It should be noted that the pH of the HPLC elution buffer (TEAA, pH 7) is significantly different from the buffer system utilized in the spectroscopic experiments (ammonium acetate, pH 9).

Figure 5.6. HPLC Analysis of the Photolysis Products of $[Rh(bpy)_2(chrysi)]^{3+}$ Irradiated at 400 nm. Analytical chromatographic traces of metal complex photolysis products as time of irradiation at 400 nm is increased: (A) T=0, (B) 15 min, (C) 30 min, (D) 120 min. Chromatograms were constructed by monitoring the absorbance of eluted products at 313 nm, an absorption maximum of the metal complex associated with its ancillary bpy ligands. The intact metal complex (retention times of 24-26 min as assigned by absorption characteristics) is converted gradually to a product of shorter retention time (20 min). Over extended irradiation, this product appears to be further converted to many other materials. Reaction and chromatography conditions are provided in the text.

Figure 5.6:

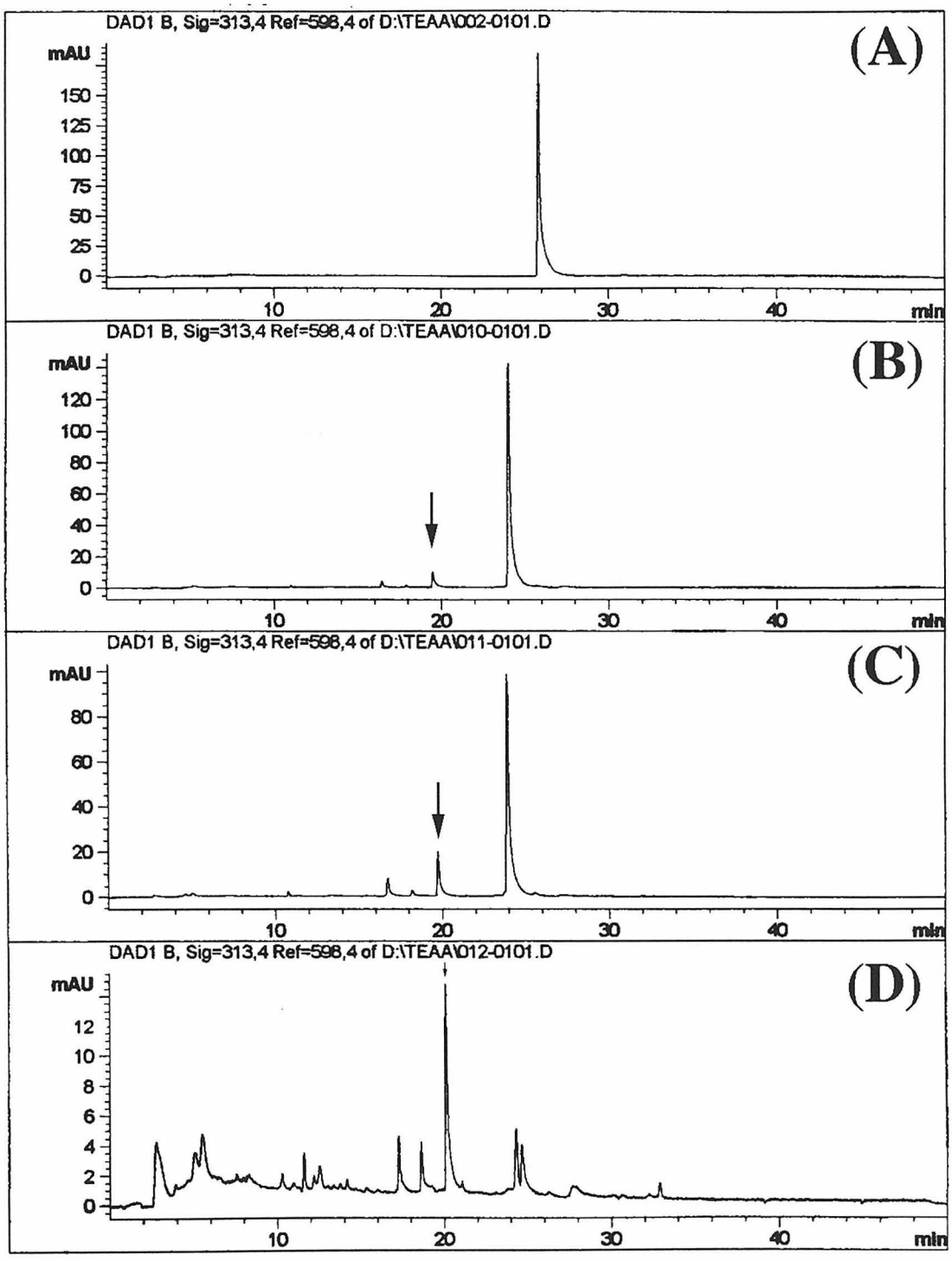
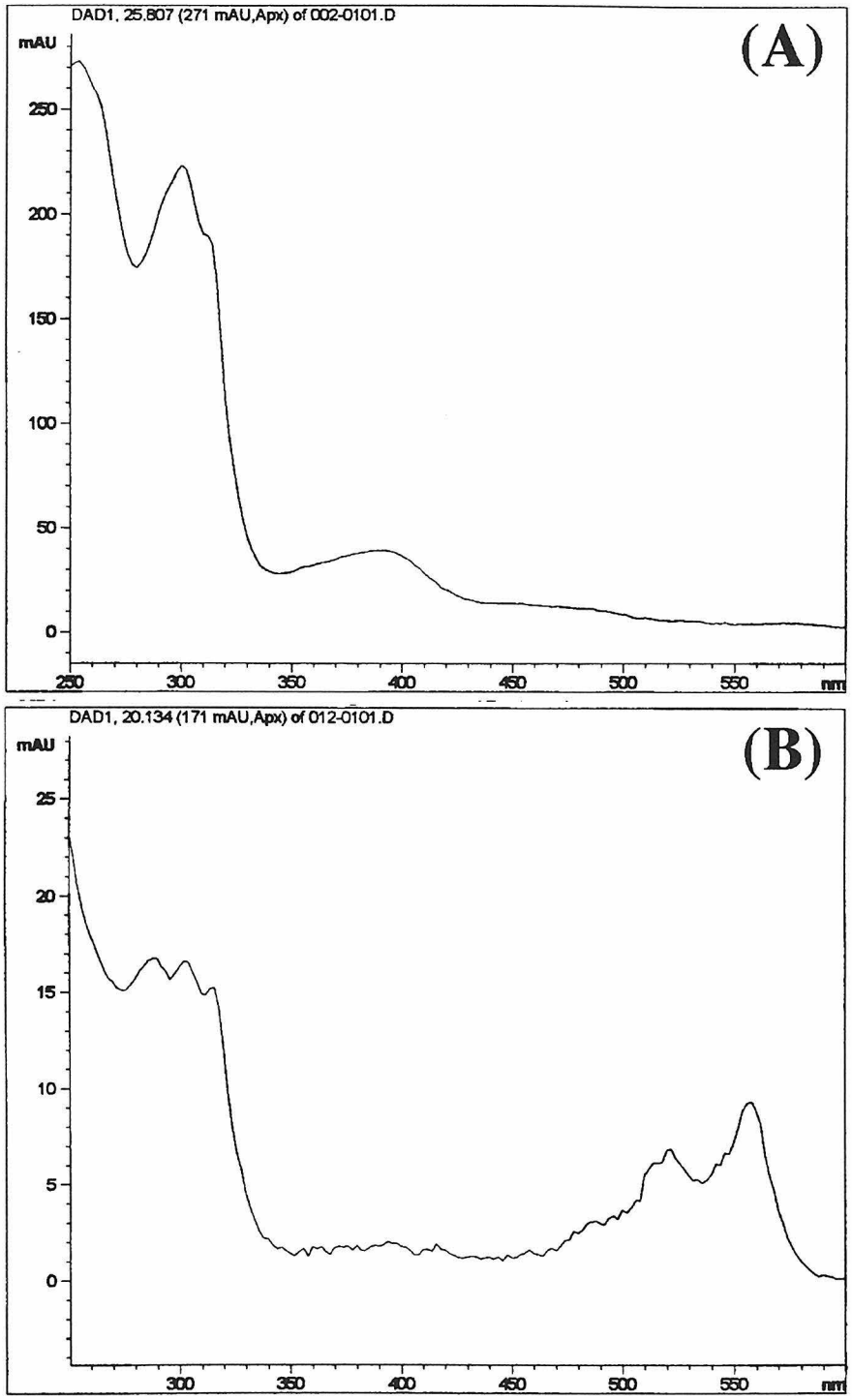

DAD1 B, Sig=313,4 Ref=598,4 of D:\TEAA\002-0101.D
(A)
mAU
150
125
100
75
50
25
0
10
20
30
40
min
DAD1 B, Sig=313,4 Ref=598,4 of D:\TEAA\010-0101.D
(B)
mAU
120
100
80
60
40
20
0
10
20
30
40
min
DAD1 B, Sig=313,4 Ref=598,4 of D:\TEAA\011-0101.D
(C)
mAU
80
60
40
20
0
10
20
30
40
min
DAD1 B, Sig=313,4 Ref=598,4 of D:\TEAA\012-0101.D
(D)
mAU
12
10
8
6
4
2
0
10
20
30
40
min

Figure 5.7. Absorption Spectra of $[Rh(bpy)_2(chrysi)]^{3+}$ and its Primary Photochemical Breakdown Product when Irradiated at 400 nm in Buffered Aqueous Solution. Absorption spectra obtained from diode array spectral measurements of the primary chromatographic peaks in (A) Figure 5.6A, the parent complex $[Rh(bpy)_2(chrysi)]^{3+}$ and (B) Figure 5.6D, the primary photolysis product resulting from 400 nm irradiation with a retention time of approx. 20 min.

Figure 5.7:


DAD1, 25.807 (271 mAU,Apx) of 002-0101.D
mAU
(A)
250
200
150
100
50
0
250
300
350
400
450
500
550
nm
DAD1, 20.134 (171 mAU,Apx) of 012-0101.D
mAU
(B)
25
20
15
10
5
0
300
350
400
450
500
550
nm

Differences in solution pH have already been demonstrated to cause very significant changes in the absorbance characteristics of chrysi complexes (see **2.3.2.1** and **2.3.2.2**). It is also possible that in the spectroscopic samples, where the complex is still associated with DNA, the absorbance maxima have been shifted as a result of nucleic acid binding.

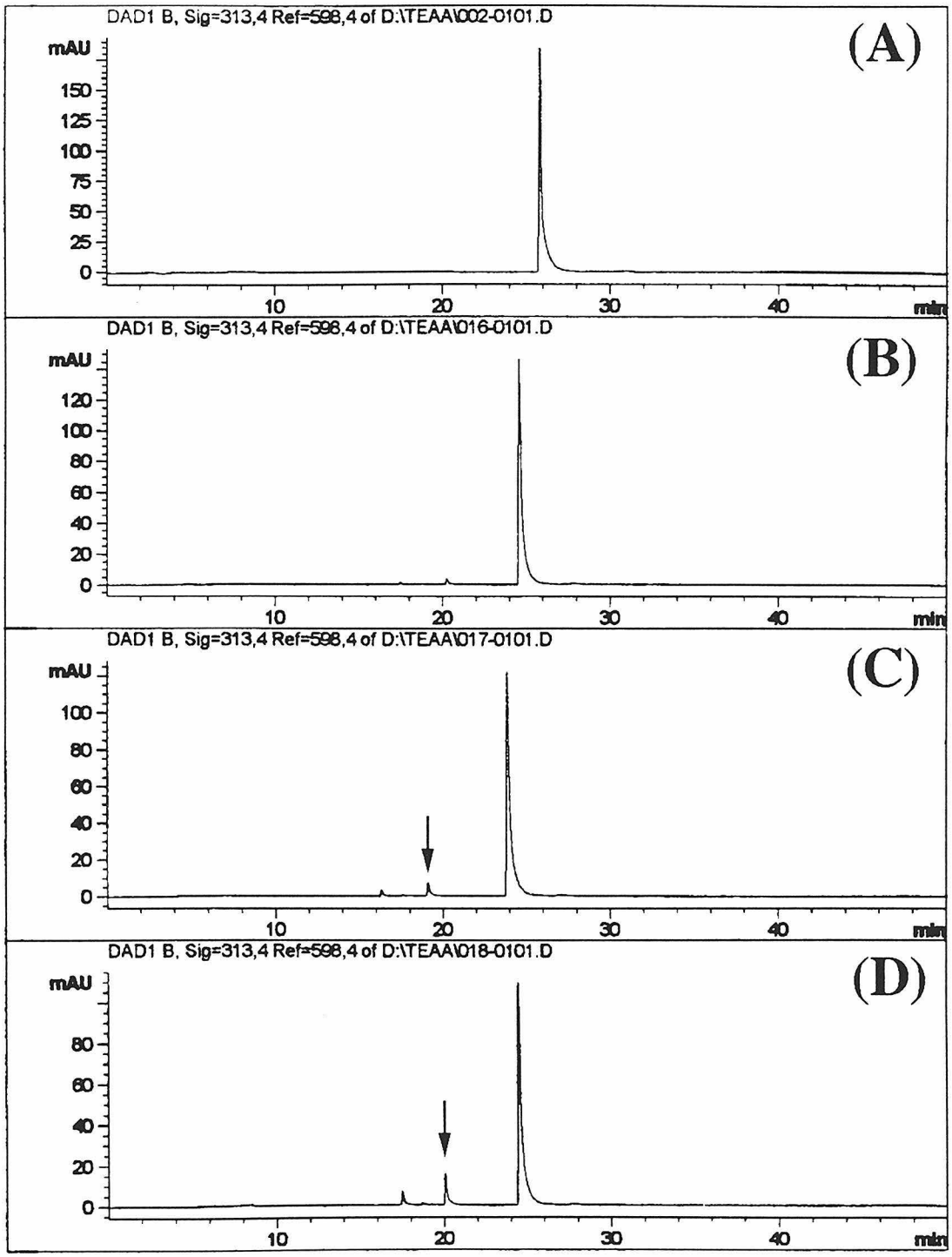
The irradiation of $[Rh(bpy)_2(chrysi)]^{3+}$ in buffer at 500 nm is noteworthy for the miniscule extent of photochemical reactivity at this wavelength (Figure 5.8). Even after two hr of irradiation, only a small amount of the metal complex has been depleted. This observation is consistent with the results of Turro and co-workers[12] which indicated that visible irradiation of phi complexes produced an excited state which did not result in photochemical degradation of the complex. The primary product of the limited photo-conversion which does occur (20 min retention time) is spectrally identical to the product observed in greater quantity after 400 nm irradiation discussed above.

5.3.4.2: Irradiation of the Metal Complex with DNA

Although establishing the stability of $[Rh(bpy)_2(chrysi)]^{3+}$ during photolysis in solution is of interest from a photochemical point of view, such a demonstration does not directly address the photocatalytic cleavage of DNA by these compounds. As a result, an analogous set of experiments were performed to those discussed above where DNA was added to the metal solution before irradiation. In these samples, a CC mismatch-containing hairpin oligonucleotide with an overhanging 5' end (see **5.2.5**) was used; this particular sequence was designed such that cleavage on either strand of the 31mer hairpin would produce fragments distinguishable by HPLC retention time. These experiments were performed at very high concentration and

Figure 5.8. HPLC Analysis of the Photolysis Products of $[Rh(bpy)_2(chrysi)]^{3+}$ Irradiated at 500 nm. Analytical chromatographic traces of metal complex photolysis products as time of irradiation at 500 nm is increased: (A) T=0, (B) 30 min, (C) 60 min, (D) 120 min. Chromatograms were constructed by monitoring the absorbance of eluted products at 313 nm, an absorption maximum of the metal complex associated with its ancillary bpy ligands. The intact metal complex (retention times of 24-26 min as assigned by absorption spectral measurement) is only slightly converted to a product of shorter retention time (20 min). This product has the same absorption spectrum as the peak of similar retention time observed after 400 nm irradiation (Figure 5.7). Reaction and chromatography conditions are provided in the text.

Figure 5.8:


DAD1 B, Sig=313,4 Ref=598,4 of D:\TEAA\002-0101.D
(A)
mAU
150
125
100
75
50
25
0
10
20
30
40
min
DAD1 B, Sig=313,4 Ref=598,4 of D:\TEAA\016-0101.D
(B)
mAU
120
100
80
60
40
20
0
10
20
30
40
min
DAD1 B, Sig=313,4 Ref=598,4 of D:\TEAA\017-0101.D
(C)
mAU
100
80
60
40
20
0
10
20
30
40
min
DAD1 B, Sig=313,4 Ref=598,4 of D:\TEAA\018-0101.D
(D)
mAU
80
60
40
20
0
10
20
30
40
min

ratio of Rh complex to DNA (600 μM DNA polymers, 300 μM Δ-Rh) to ensure the formation of adequate amounts of reaction products for HPLC analysis.

As was observed during photolysis in the absence of nucleic acid, irradiation at 313 nm in the presence of DNA results in efficient consumption of the rhodium complex. This degradation can be observed as the shrinking of the metal complex peak (retention time 24-26 min) with spectrophotometric observation at either 313 nm (ancillary ligand absorbances) or at 370 nm (chrysi ligand absorbance). The chromatograms generated by monitoring at 313 nm are included as Figure 5.9. The cleavage of DNA is also clearly observed as photolysis time is increased. With monitoring at 260 nm, the absorption maximum of DNA, it is clear that the full length DNA strand (Figure 5.10A) is converted to several products (Figure 5.10B-D) over the course of the irradiation. When the chromatogram generated at 260 nm is directly compared to the metal complex focused trace constructed at 313 nm (Figure 5.11), it is clear that some peaks in this region have significant absorbance at both wavelengths. The spectrum of the major product (retention time approx. 7.5 min) is included as Figure 5.12. Although this observation could be the result of co-migration of metal complex breakdown products and nucleic acid components under these LC conditions, this combination of intense absorbance at 260 nm and absorbance in the 310 nm region characteristic of the metal complex is also consistent with the formation of crosslinks between cleaved DNA and breakdown photo-products of the rhodium compound. This agrees with previous work on rhodium(III) phi complexes which demonstrated the formation of nucleic acid-metal complex covalent adducts upon irradiation with UV light.[7] In addition, these low retention time products are almost entirely depleted of absorbance at 370 nm. The maximal absorbance observed at 313 nm in the putative crosslink peak is only approx. 25 mAU (Figure 5.9E) compared to the 200 mAU observed in the unirradiated sample

Figure 5.9. HPLC Analysis of the Photolysis Products of $[Rh(bpy)_2(chrysi)]^{3+}$ Irradiated at 313 nm in the Presence of CC Mismatch-Containing DNA. Analytical chromatographic traces of metal complex photolysis products as time of irradiation at 313 nm is increased: (A) T=0, (B) 5 min, (C) 15 min, (D) 30 min. Chromatograms were constructed by monitoring the absorbance of eluted products at 260 nm, the absorbance maximum of DNA (Panel A) and 313 nm, an absorption maximum of the metal complex associated with its ancillary bpy ligands (Panels B-E). The intact metal complex (retention times of 24-25 min as assigned by absorption spectral measurement) is rapidly depleted over the course of irradiation. Unlike when the complex is irradiated without DNA (Figure 5.5), formation of a significant product with a retention time of approx. 8 min is observed (indicated by the square brackets.) Reaction and chromatography conditions are provided in the text.

Figure 5.9:

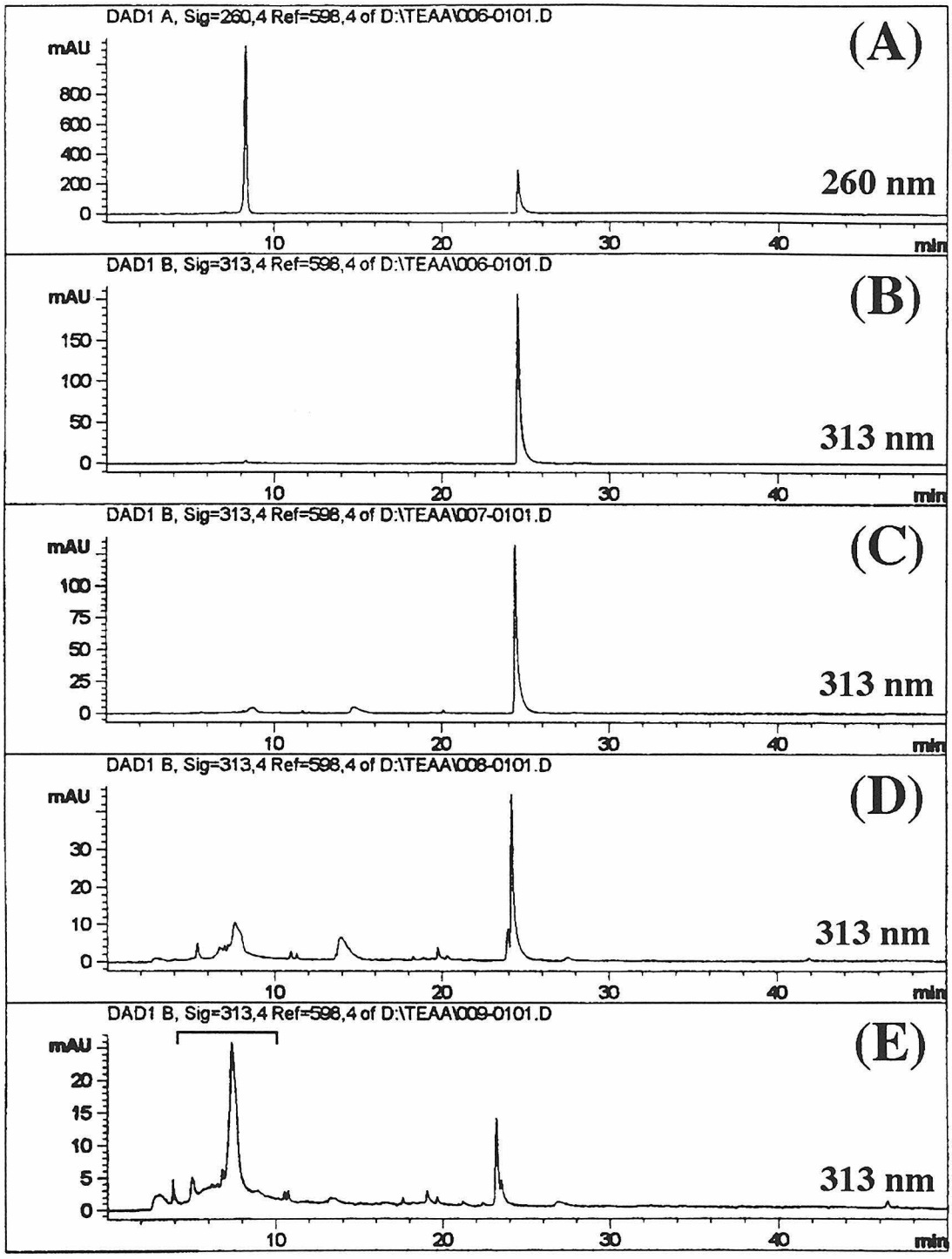

DAD1 A, Sig=260,4 Ref=598,4 of D:\TEAA\006-0101.D
mAU
800
600
400
200
0
10
20
30
40
min
(A)
260 nm
DAD1 B, Sig=313,4 Ref=598,4 of D:\TEAA\006-0101.D
mAU
150
100
50
0
10
20
30
40
min
(B)
313 nm
DAD1 B, Sig=313,4 Ref=598,4 of D:\TEAA\007-0101.D
mAU
100
75
50
25
0
10
20
30
40
min
(C)
313 nm
DAD1 B, Sig=313,4 Ref=598,4 of D:\TEAA\008-0101.D
mAU
30
20
10
0
10
20
30
40
min
(D)
313 nm
DAD1 B, Sig=313,4 Ref=598,4 of D:\TEAA\009-0101.D
mAU
20
15
10
5
0
10
20
30
40
min
(E)
313 nm

Figure 5.10. HPLC Analysis of the DNA Photolysis Products Produced by $[Rh(bpy)_2(chrysi)]^{3+}$ Irradiated at 313 nm in the Presence of CC Mismatch-Containing DNA. Analytical chromatographic traces of metal complex photolysis products as time of irradiation at 313 nm is increased: (A) T=0, (B) 5 min, (C) 15 min, (D) 30 min. Chromatograms were constructed by monitoring the absorbance of eluted products at 260 nm, the absorption maximum of DNA. The full length DNA strand (retention time approx. 8.25 min) is rapidly fragmented to form several products. Reaction and chromatography conditions are provided in the text.

Figure 5.10:

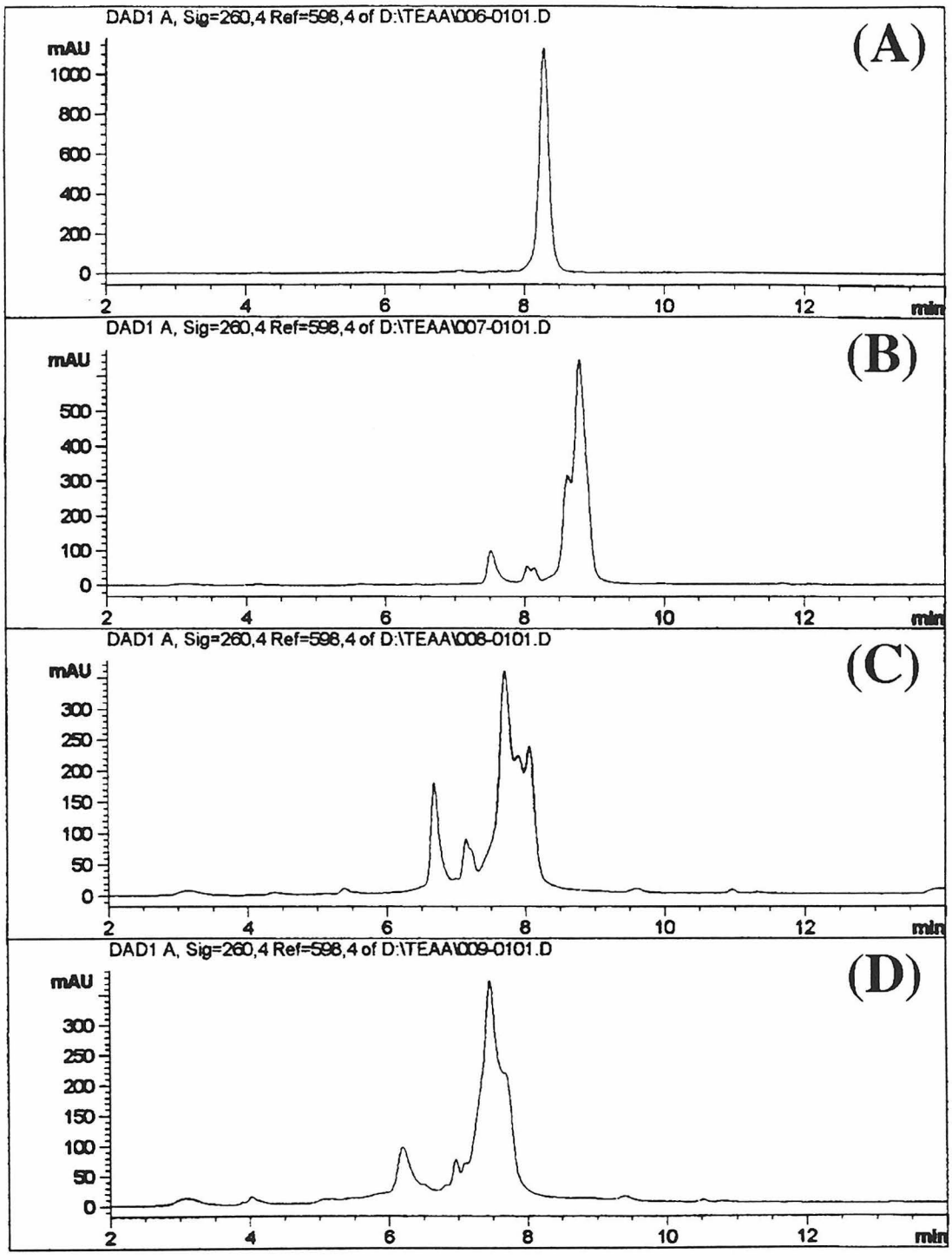

DAD1 A, Sig=260,4 Ref=598,4 of D:\TEAA\006-0101.D
(A)
mAU
1000
800
600
400
200
0
2
4
6
8
10
12
min
DAD1 A, Sig=260,4 Ref=598,4 of D:\TEAA\007-0101.D
(B)
mAU
500
400
300
200
100
0
2
4
6
8
10
12
min
DAD1 A, Sig=260,4 Ref=598,4 of D:\TEAA\008-0101.D
(C)
mAU
300
250
200
150
100
50
0
2
4
6
8
10
12
min
DAD1 A, Sig=260,4 Ref=598,4 of D:\TEAA\009-0101.D
(D)
mAU
300
250
200
150
100
50
0
2
4
6
8
10
12
min

Figure 5.11. Comparison of 260 nm and 313 nm Chromatograms of $[Rh(bpy)_2(chrysi)]^{3+}$ Irradiated for 30 min at 313 nm in the Presence of CC Mismatch-Containing DNA. Comparison of the two chromatograms reveal that the materials eluted in this region appear to absorb both at 313 nm and 260 nm. Although this observation could result from comigration of rhodium photolysis (absorbing at 313 nm) products and DNA cleavage fragments (absorbing at 260 nm) under these LC conditions, if this chromatographic peak does represent one chemical species the dual absorbance also might reflect the formation of crosslinks between rhodium(bipyridine) fragments and the nucleic acid. Such crosslinking is analogous to similar reactivity observed for rhodium(III) phi compounds.[7] Reaction and chromatography conditions are provided in the text.

Figure 5.11:

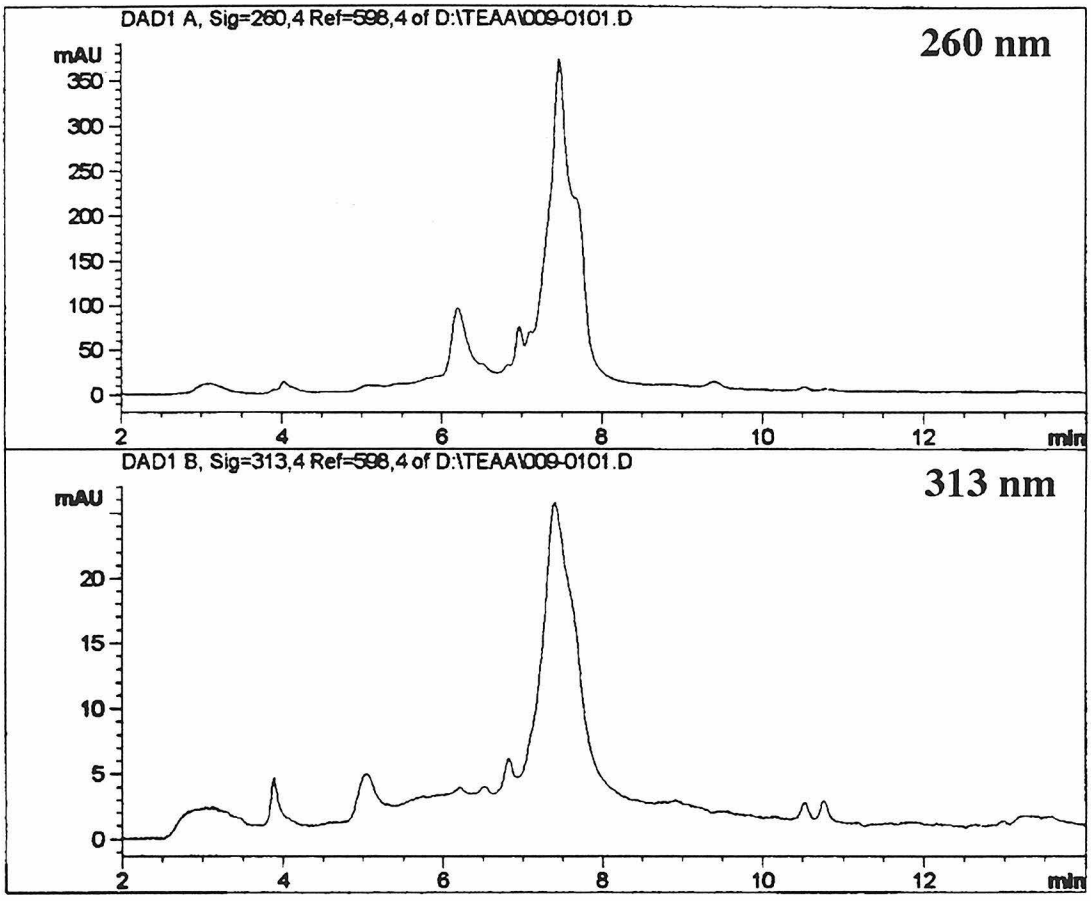
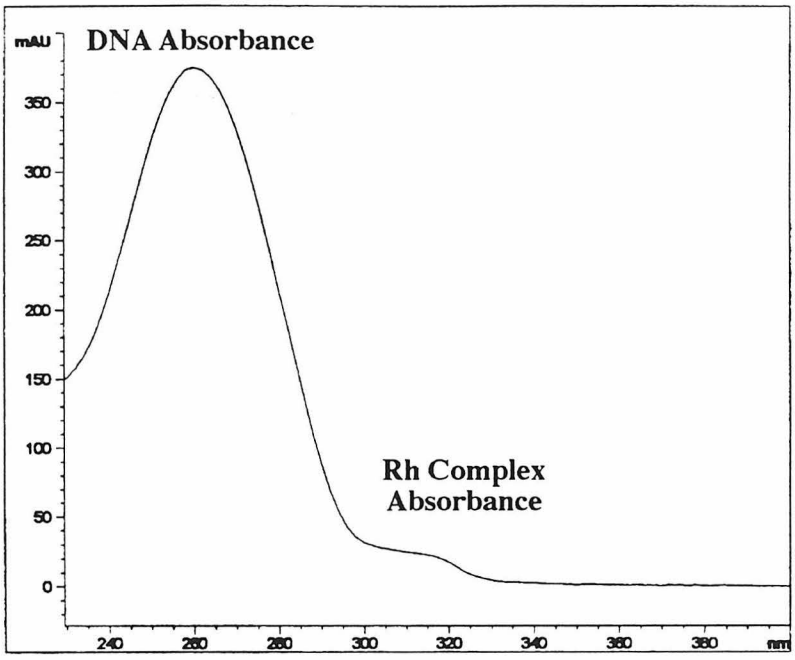

DAD1 A, Sig=260,4 Ref=598,4 of D:\TEAA\009-0101.D
260 nm
mAU
350
300
250
200
150
100
50
0
2
4
6
8
10
12
min
DAD1 B, Sig=313,4 Ref=598,4 of D:\TEAA\009-0101.D
313 nm
mAU
20
15
10
5
0
2
4
6
8
10
12
min

Figure 5.12. Absorption Spectrum of the Major Photolysis Product of $[Rh(bpy)_2(chrysi)]^{3+}$ Irradiated for 30 min at 313 nm in the Presence of CC Mismatch-Containing DNA Displaying both 260 nm and 313 nm Absorbance.

Figure 5.12:


mAU
DNA Absorbance
350
300
250
200
150
100
50
0
Rh Complex
Absorbance
240
260
280
300
320
340
360
380
nm

(Figure 5.9B). Analogous values for 370 nm are 1.4 mAU and 40 mAU respectively (data not shown). This is consistent with preferential loss of the chrysi ligand upon photolysis at 313 nm which would generate $[Rh(bpy)_2(H_2O)_2]^{3+}$ photolysis products which would be chemically able to bind covalently to the nucleic acid. This pathway of reactivity is also consistent with the previous studies of phi complexes.[7]

Irradiation of $[Rh(bpy)_2(chrysi)]^{3+}$ bound to DNA at 400 nm generates products somewhat different than those observed at 313 nm. As in the samples irradiated at this wavelength in the absence of nucleic acid, the complex is broken down over the course of increasing reaction but much less efficiently than with irradiation at 313 nm (Figure 5.13). The DNA substrate of the reaction is efficiently cleaved at this wavelength (Figure 5.14). The cleavage of the nucleic acid at 400 nm produces more product peaks which are better resolved and have different retention times than those observed at 313 nm (compare Figure 5.14D and Figure 5.10D). The production of the novel photoproduct with a retention time of 20 min (spectrum identical to that included in Figure 5.7B) is also observed; in the presence of DNA there appears to be more of this material formed than in its absence. This could either reflect stabilization of the product by the nucleic acid – which is supported by the reduction in the number and amount of other breakdown products (retention times between 10 min and 20 min) – or by increased formation of the product in the presence of DNA. The stabilization of the material is also supported by the fact that the size of the 20 min peak is essentially identical in the intermediate irradiation time samples of metal complex irradiated alone (Figure 5.6C) and with DNA (Figure 5.13D) but that more remains in the DNA-containing sample (Figure 5.13E versus 5.6D) after two hr of irradiation. Like the previous ultraviolet irradiation samples, photolysis at 400 nm also produces species with absorbance at 313 nm with retention times between 2 and 10 min. Unlike the 313 nm samples where there was one predominant peak, in this

Figure 5.13. HPLC Analysis of the Photolysis Products of $[Rh(bpy)_2(chrysi)]^{3+}$ Irradiated at 400 nm in the Presence of CC Mismatch-Containing DNA. Analytical chromatographic traces of metal complex photolysis products as time of irradiation at 400 nm is increased: (A) T=0, (B) 15 min, (C) 30 min, (D) 120 min. Chromatograms were constructed by monitoring the absorbance of eluted products at 260 nm, the absorbance maximum of DNA (Panel A) and 313 nm, an absorption maximum of the metal complex associated with its ancillary bpy ligands (Panels B-E). The intact metal complex (retention times of 24-25 min as assigned by absorption spectral measurement) is slowly depleted over the course of irradiation with the formation of the novel photoproduct (retention time, approx. 20 min, indicated by the arrow in panel D) discussed regarding the irradiations performed in the absence of DNA (Figure 5.7B). Unlike when the complex is irradiated without DNA (Figure 5.6), formation of several products (indicated by the arrows in panel E) with a retention times between 2 and 10 min is observed. Reaction and chromatography conditions are provided in the text.

Figure 5.13:

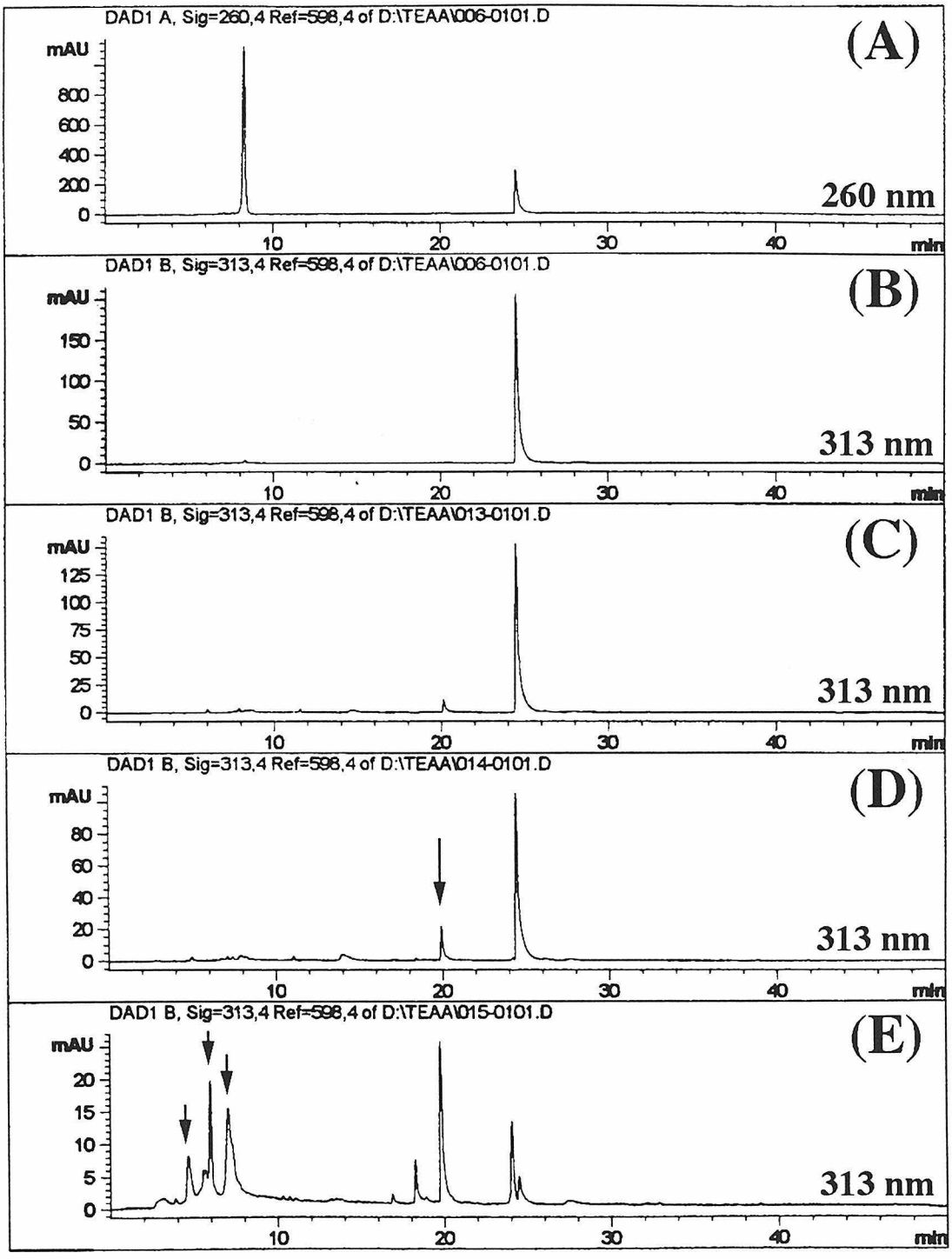
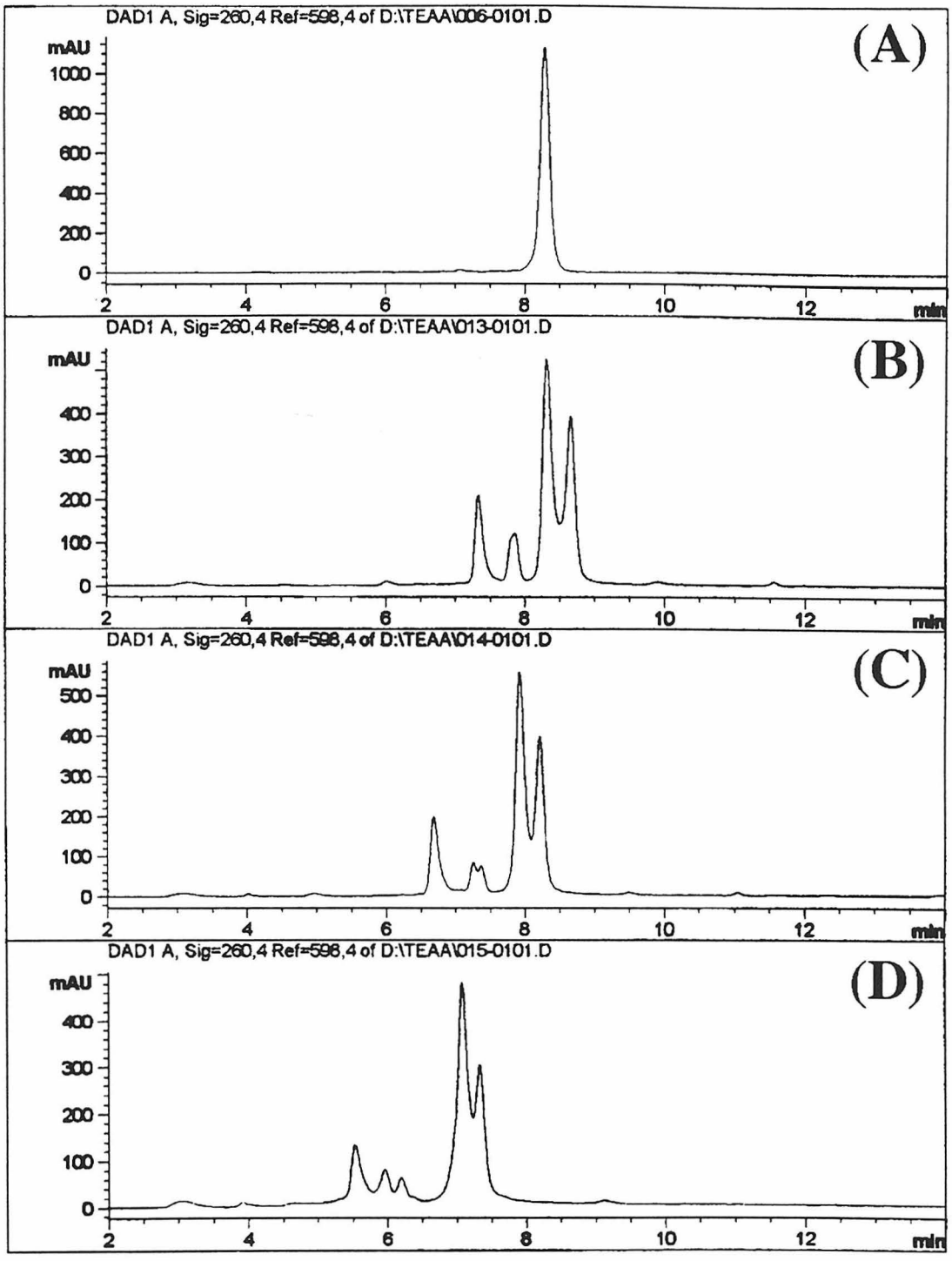

DAD1 A, Sig=260,4 Ref=598,4 of D:\TEAA\006-0101.D
(A)
mAU
800
600
400
200
0
260 nm
10
20
30
40
min
DAD1 B, Sig=313,4 Ref=598,4 of D:\TEAA\006-0101.D
(B)
mAU
150
100
50
0
313 nm
10
20
30
40
min
DAD1 B, Sig=313,4 Ref=598,4 of D:\TEAA\013-0101.D
(C)
mAU
125
100
75
50
25
0
313 nm
10
20
30
40
min
DAD1 B, Sig=313,4 Ref=598,4 of D:\TEAA\014-0101.D
(D)
mAU
80
60
40
20
0
313 nm
10
20
30
40
min
DAD1 B, Sig=313,4 Ref=598,4 of D:\TEAA\015-0101.D
(E)
mAU
20
15
10
5
0
313 nm
10
20
30
40
min

Figure 5.14. HPLC Analysis of the DNA Photolysis Products Produced by $[Rh(bpy)_2(chrysi)]^{3+}$ Irradiated at 400 nm in the Presence of CC Mismatch-Containing DNA. Analytical chromatographic traces of metal complex photolysis products as time of irradiation at 400 nm is increased: (A) T=0, (B) 15 min, (C) 30 min, (D) 120 min. Chromatograms were constructed by monitoring the absorbance of eluted products at 260 nm, the absorption maximum of DNA. The full length DNA strand (retention time approx. 8.25 min) is converted to several products. Reaction and chromatography conditions are provided in the text.

Figure 5.14:


DAD1 A, Sig=260,4 Ref=598,4 of D:\TEAA\006-0101.D
(A)
mAU
1000
800
600
400
200
0
2
4
6
8
10
12
min
DAD1 A, Sig=260,4 Ref=598,4 of D:\TEAA\013-0101.D
(B)
mAU
400
300
200
100
0
2
4
6
8
10
12
min
DAD1 A, Sig=260,4 Ref=598,4 of D:\TEAA\014-0101.D
(C)
mAU
500
400
300
200
100
0
2
4
6
8
10
12
min
DAD1 A, Sig=260,4 Ref=598,4 of D:\TEAA\015-0101.D
(D)
mAU
400
300
200
100
0
2
4
6
8
10
12
min

experiment there are several products produced with these characteristics (Figure 5.15). Analogous to the putative crosslink products observed with irradiation at 313 nm, these products do not display any relevant amount of absorbance at 370 nm (data not shown).*

Photolysis of $[Rh(bpy)_2(chrysi)]^{3+}$ with DNA at 500 nm is also very similar to that observed in the absence of the nucleic acid. Even though the complex readily cleaves DNA (see Figure 5.16), there is little evidence of photochemical breakdown products of the complex (Figure 5.17). There is also no evidence of any products in the region populated by cleaved DNA fragments which possess absorption in the 313 nm range; this could simply be a reflection of the fact that the complex is not degraded thus producing no products suitable to either comigrate with the DNA cleavage peaks or to participate in hypothetical DNA crosslinking reactions.

5.3.5: Cleavage of DNA with Fluorescent Roomlight and Sunlight Irradiation

The very broad wavelength window in which $[Rh(bpy)_2(chrysi)]^{3+}$ catalytically cleaved DNA led to the proposal that light sources other than the high intensity Hg/Xe arc lamp system might be sufficient to promote strand cleavage. As a result, a series of samples were prepared and placed in Lucite radiation isolation boxes. Examination of the absorption characteristics of the boxes indicated that they served as an efficient cut-off filter of all UV radiation beginning at approximately 370 nm.

---

* It should also be noted that this experiment also demonstrates that comigration of different products could explain the presence of some or all of these low retention time peaks. In the 313 nm trace (Figure 5.15 bottom) there is a peak with a retention time of approx. 4.75 min which does not appear in the 260 nm trace (5.15 top). Other such peaks unassociated with the DNA might be chromatographically coincident with the nucleic acid products making it appear that the two species were bonded to one another.

Figure 5.15. Comparison of 260 nm and 313 nm Chromatograms of $[Rh(bpy)_2(chrysi)]^{3+}$ Irradiated for 120 min at 400 nm in the Presence of CC Mismatch-Containing DNA. Although this observation could result from comigration of rhodium photolysis (absorbing at 313 nm) products and DNA cleavage fragments (absorbing at 260 nm) under these LC conditions, if these chromatographic peaks represent single chemical species, the dual absorbance also might reflect the formation of crosslinks between metal complex fragments and the nucleic acid. Reaction and chromatography conditions are provided in the text.

Figure 5.15:

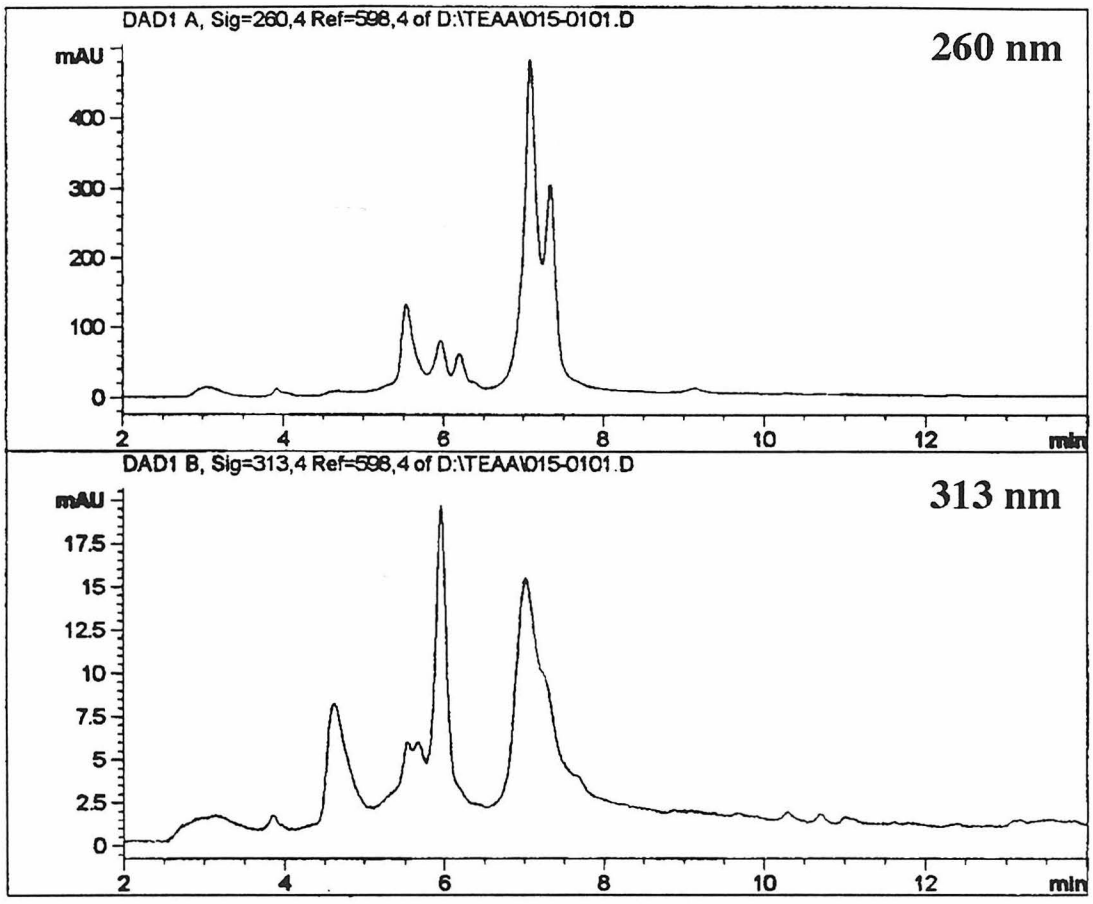

DAD1 A, Sig=260,4 Ref=598,4 of D:\TEAA\015-0101.D
260 nm
mAU
400
300
200
100
0
2
4
6
8
10
12
min
DAD1 B, Sig=313,4 Ref=598,4 of D:\TEAA\015-0101.D
313 nm
mAU
17.5
15
12.5
10
7.5
5
2.5
0
2
4
6
8
10
12
min

Figure 5.16. HPLC Analysis of the DNA Photolysis Products Produced by $[Rh(bpy)_2(chrysi)]^{3+}$ Irradiated at 500 nm in the Presence of CC Mismatch-Containing DNA. Analytical chromatographic traces of metal complex photolysis products as time of irradiation at 500 nm is increased: (A) T=0, (B) 30 min, (C) 60 min, (D) 120 min. Chromatograms were constructed by monitoring the absorbance of eluted products at 260 nm, the absorption maximum of DNA. The full length DNA strand (retention time approx. 8.25 min) is converted to several products. Reaction and chromatography conditions are provided in the text.

Figure 5.16:

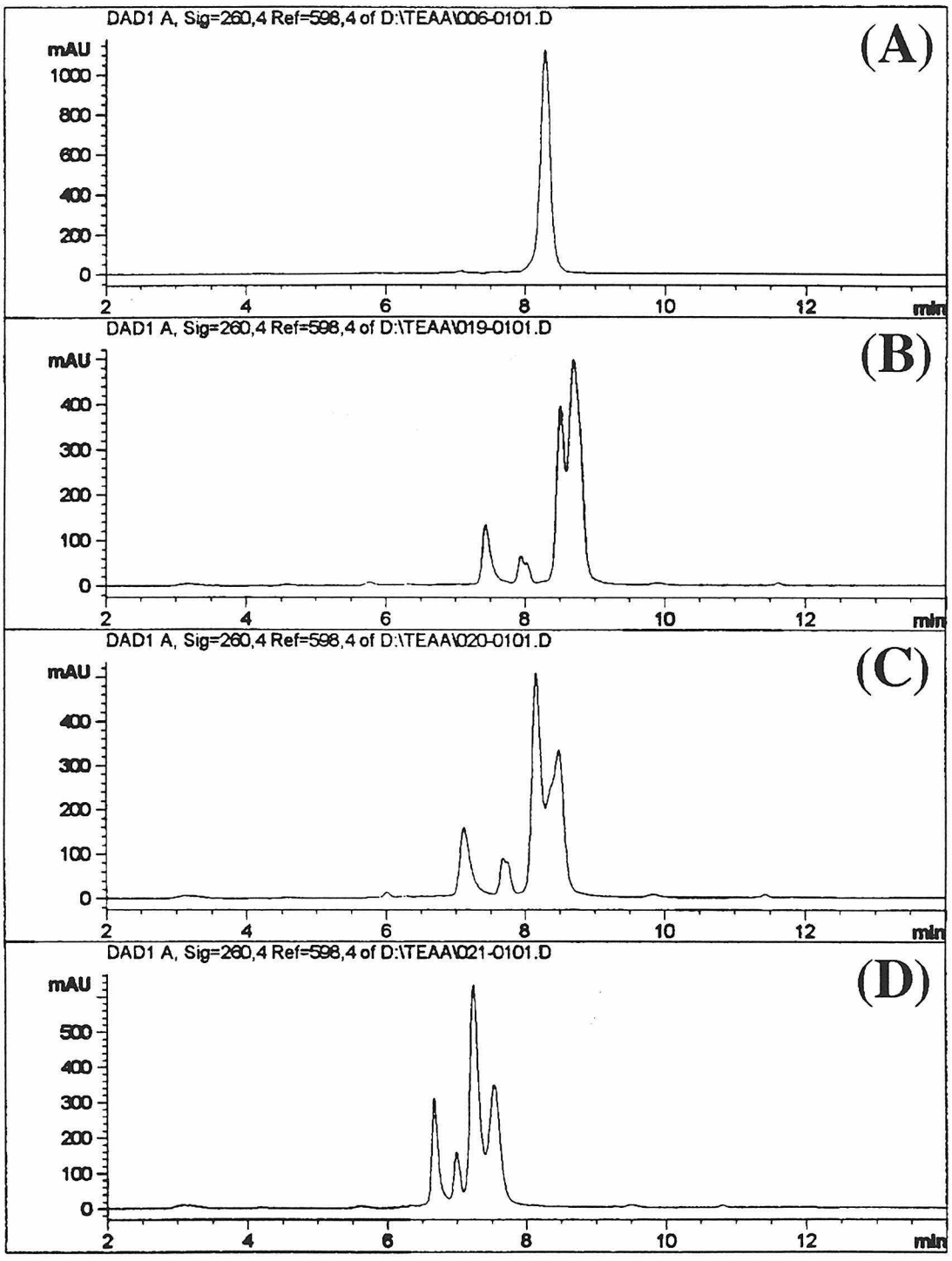
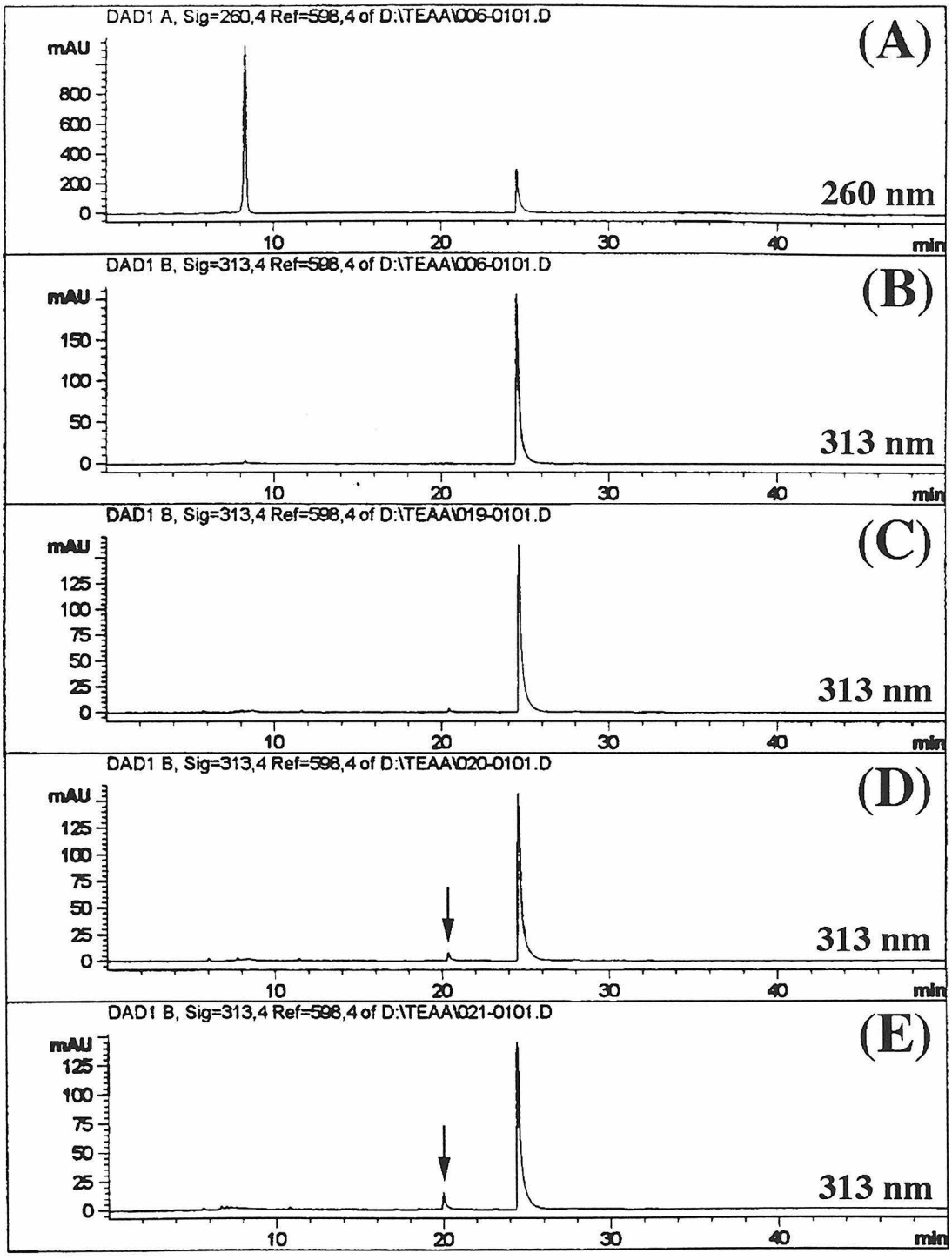

DAD1 A, Sig=260,4 Ref=598,4 of D:\TEAA\006-0101.D
(A)
mAU
1000
800
600
400
200
0
2
4
6
8
10
12
min
DAD1 A, Sig=260,4 Ref=598,4 of D:\TEAA\019-0101.D
(B)
mAU
400
300
200
100
0
2
4
6
8
10
12
min
DAD1 A, Sig=260,4 Ref=598,4 of D:\TEAA\020-0101.D
(C)
mAU
400
300
200
100
0
2
4
6
8
10
12
min
DAD1 A, Sig=260,4 Ref=598,4 of D:\TEAA\021-0101.D
(D)
mAU
500
400
300
200
100
0
2
4
6
8
10
12
min

Figure 5.17. HPLC Analysis of the Photolysis Products of $[Rh(bpy)_2(chrysi)]^{3+}$ Irradiated at 500 nm in the Presence of CC Mismatch-Containing DNA. Analytical chromatographic traces of metal complex photolysis products as time of irradiation at 500 nm is increased: (A) T=0, (B) 30 min, (C) 60 min, (D) 120 min. Chromatograms were constructed by monitoring the absorbance of eluted products at 260 nm, the absorbance maximum of DNA (Panel A) and 313 nm, an absorption maximum of the metal complex associated with its ancillary bpy ligands (Panels B-E). The intact metal complex (retention times of 24-25 min as assigned by absorption spectral measurement) shows very little reaction over the course of irradiation although a small amount of the novel photo-product (Figure 5.7B) with a retention time of approx. 20 min (indicated by the arrows in panels D and E) discussed previously is formed. Reaction and chromatography conditions are provided in the text.

Figure 5.17:


DAD1 A, Sig=260,4 Ref=598,4 of D:\TEAA\006-0101.D
(A)
mAU
800
600
400
200
0
260 nm
10
20
30
40
min
DAD1 B, Sig=313,4 Ref=598,4 of D:\TEAA\006-0101.D
(B)
mAU
150
100
50
0
313 nm
10
20
30
40
min
DAD1 B, Sig=313,4 Ref=598,4 of D:\TEAA\019-0101.D
(C)
mAU
125
100
75
50
25
0
313 nm
10
20
30
40
min
DAD1 B, Sig=313,4 Ref=598,4 of D:\TEAA\020-0101.D
(D)
mAU
125
100
75
50
25
0
313 nm
10
20
30
40
min
DAD1 B, Sig=313,4 Ref=598,4 of D:\TEAA\021-0101.D
(E)
mAU
125
100
75
50
25
0
313 nm
10
20
30
40
min

Samples were irradiated inside these boxes for increasing periods both under ambient laboratory lighting (≈1 m from diffused fluorescent tube lighting) and outside under "California sunlight" for a maximum period of 8 hr. As predicted, the rhodium complex cleaved the DNA mismatch specifically under both these irradiation conditions. Laboratory illumination was sufficient, at the maximal irradiation time, to cleave approx. 10% of the parent DNA strand. After 8 hr of sunlight exposure, the complex, which was in a 0.5 molar ratio to the concentration of DNA polymers in the sample, cleaved 96% of the DNA; the great majority of this cleavage had already taken place after only 2 hr of irradiation.

5.3.6: Other Photochemical Behaviors of Interest

In addition to the observation that $[Rh(bpy)_2(chrysi)]^{3+}$ cleaved DNA with visible light, the systematic variation of the wavelengths at which the metal complex was irradiated in the presence of DNA also led to the discovery of other novel photochemical behaviors. Although it was not possible to explore these behaviors comprehensively, they do emphasize the richness of the photochemical reactivity of $[Rh(bpy)_2(chrysi)]^{3+}$ with DNA and are presented here as fertile leads for further exploration.

5.3.6.1: Changes in Cleavage Specificity with Changes in Irradiation Wavelength

In addition to the observation that $[Rh(bpy)_2(chrysi)]^{3+}$ photocatalytically cleaved DNA next to its mismatch binding site when the wavelength of irradiation was shifted into the visible regime, comparison of the DNA cleavage patterns produced by the complex when the wavelength of irradiation was shifted indicated that the overall cleavage pattern of the complex also changed. This was an unexpected result but not an unprecedented one. Previously in this research group, such an observation of

altered specificity led to the discovery that $[Rh(phi)_2(bpy)]^{3+}$ and related compounds damaged guanine by long range electron transfer.[13]

Unlike $[Rh(phi)_2(bpy)]^{3+}$, however, in this case damage was not initially observed at guanine bases. Instead, when the irradiation wavelength was increased from the ultraviolet to the visible, $[Rh(bpy)_2(chrysi)]^{3+}$ was found to cause direct cleavage at cytosine bases which were separated from the proposed mismatch binding site of the molecule. Figure 5.18 includes a portion of two gels included in Chapter 4 exploring the sequence context of mispair recognition about the GG mismatch. Examining the gels from a somewhat different perspective, however, it is notable that when the irradiation wavelength is shifted from 313 nm (Figure 5.18, left) to 440 nm (5.18, right), damage at cytosine bases separated from the mismatch site (red arrows) is observed in every sequence context. This damage is independent of the extent of cleavage observed in the 313 nm irradiations. When samples analogous to those shown in Figure 5.18 were irradiated in sunlight, the change in specificity was even more dramatic (data not shown). These shifts in cleavage specificity were not restricted to cases where the metal complex bound at the GG mismatch; in the experiment described in Chapter 4 where a single CC mismatch was recognized in a 273 base pair restriction fragment, direct cleavage was observed both at the C base next to the mismatch, at a C base three bases away, and, if very closely examined, at C bases approx. 20 base pairs to either side of the mismatch site (data not shown). The efficiency of damage at these sites is quite low, however.

5.3.6.2: Oxygen Dependence of DNA Photocleavage

As part of the attempt to understand the possible reactivity mechanisms of $[Rh(bpy)_2(chrysi)]^{3+}$, experiments were performed to examine how DNA strand

Figure 5.18. Appearance of Direct Cytosine-Specific Strand Cleavage as a Result of Shifting Irradiation Wavelength from 313 nm to 440 nm. Abstracted portion of the GG sequence context gel included in Chapter 4. Irradiation and sample conditions are included in section **4.2.2**. Note the cytosine specific damage which is observed in the samples irradiated at 440 nm (red arrows). The analogous position in the samples irradiated at 313 nm (blue arrow) shows no cleavage. Instead, what is observed is damage at guanine (black arrow) which is consistent with the results reported in Chapter 3. A full description of the sequences and nomenclature above the gel lanes is included in Chapter 4. Briefly, the notation GG/GT, for example, indicates both the mismatch present in each hairpin, GG, and the two bases complementary to the bases W and Z.

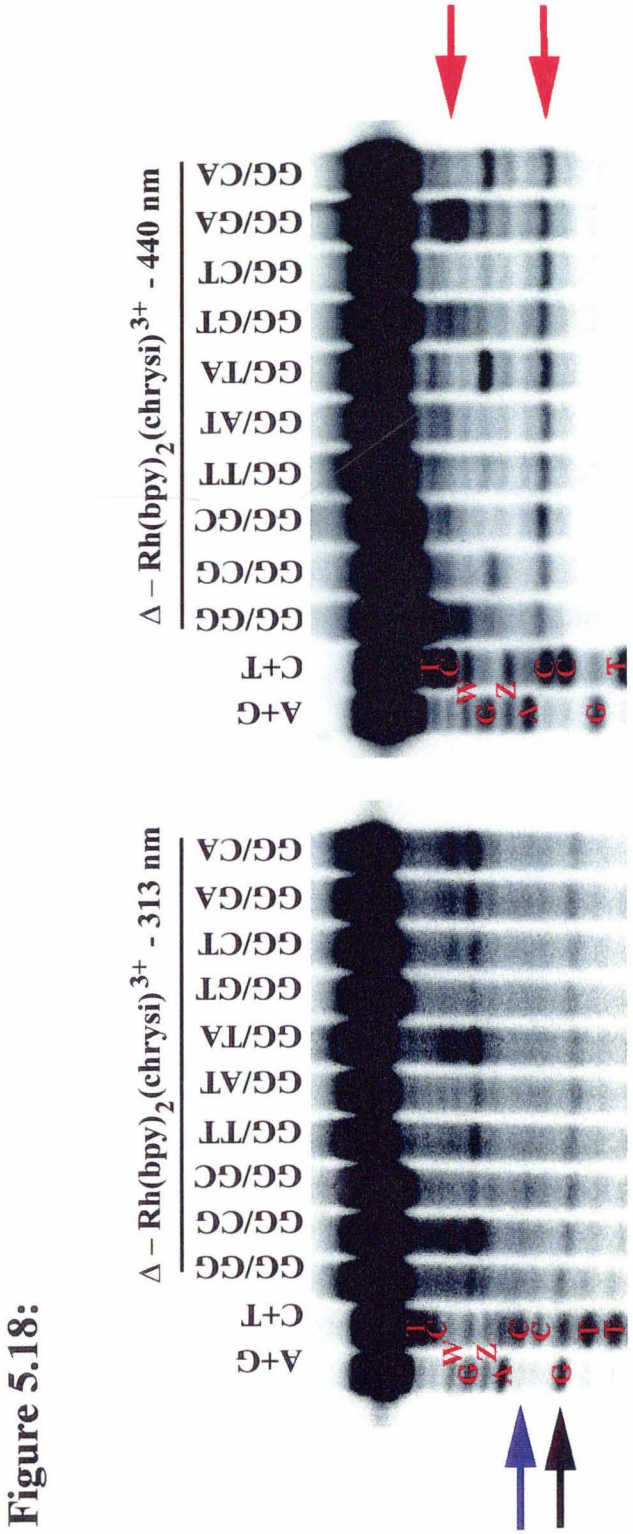

Δ – Rh(bpy)2(chrysi)3+ - 440 nm
Δ – Rh(bpy)2(chrysi)3+ - 313 nm
GG/CA
GG/GA
GG/CT
GG/GT
GG/TA
GG/AT
GG/TT
GG/GC
GG/CG
GG/GG
C+T
A+G

Figure 5.18:

cleavage depended on the presence of oxygen. In these experiments, samples were irradiated as prepared under ambient atmosphere or after being saturated with either argon or molecular oxygen. Since the potential also existed that $[Rh(bpy)_2(chrysi)]^{3+}$ photoreaction with DNA might produce lesions in DNA which did not lead to direct strand scission, samples were also prepared which were treated with hot piperidine after irradiation to convert any base sensitive modifications to strand breaks which could be characterized electrophoretically. The results of such an experiment are included as Figure 5.19.

In this and companion experiments, no reproducible dependence on oxygen was observed for direct strand scission at the primary cleavage site immediately to the 3' side of the base mismatch at any wavelength (red arrow in Figure 5.19). As this is the primary site where photocatalytic cleavage of DNA is observed, molecular oxygen can be ruled out as a central reactant mediating the direct photocatalytic cleavage of DNA by $[Rh(bpy)_2(chrysi)]^{3+}$. Independent of this negative result, however, a significant number of other DNA damage events were observed in these experiments which merit further discussion.

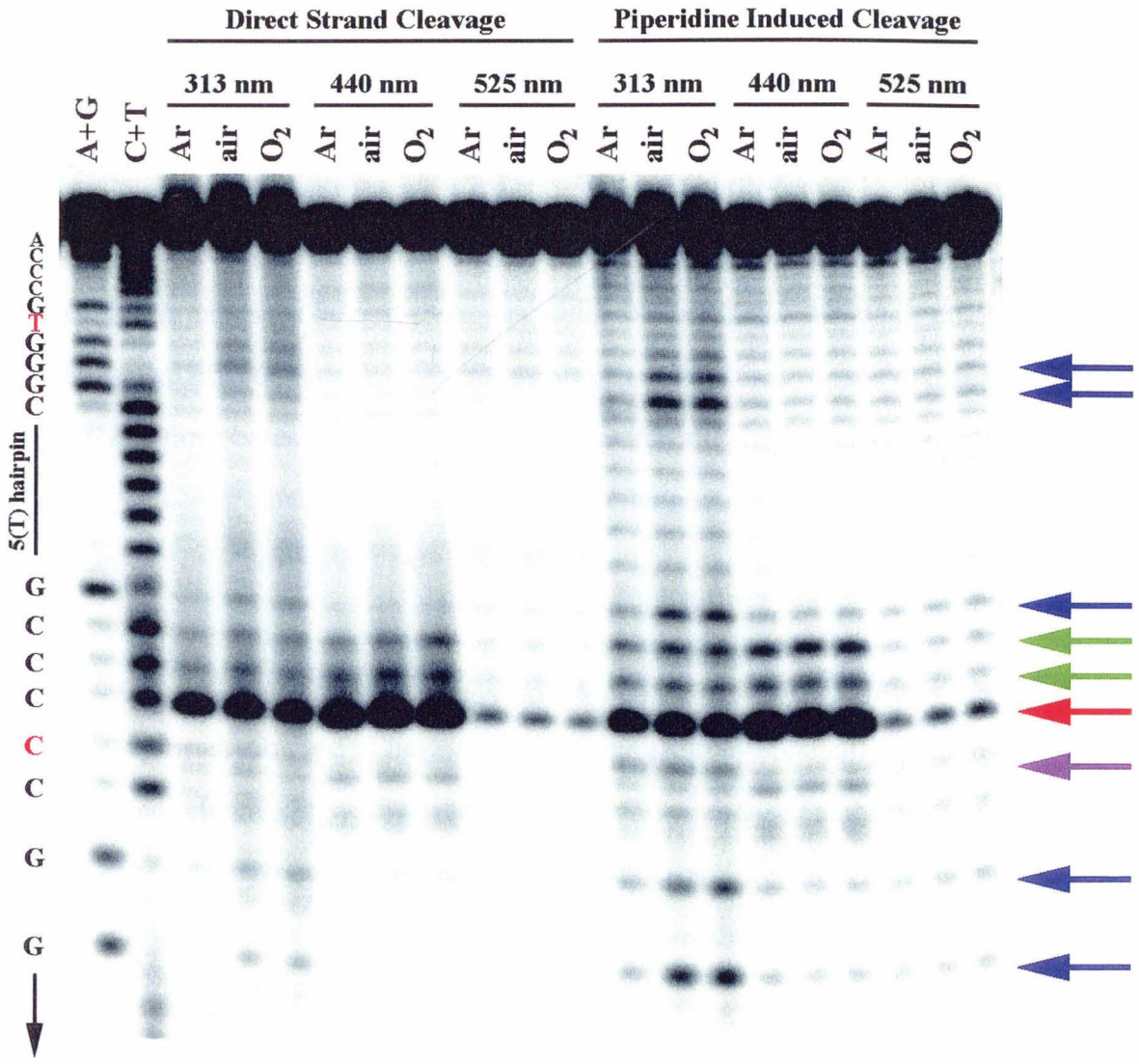
In addition to the cleavage at the expected site immediately 3' to the mismatch, irradiation of $[Rh(bpy)_2(chrysi)]^{3+}$ at 313 nm also produced damage at guanine sites at various sites in the hairpin duplex (blue arrows in Figure 5.19). Cleavage at these sites was significantly enhanced when the samples were post treated with piperidine and also exhibited a strong oxygen dependence. Direct cleavage at the guanine site three bases to the 5' side of the mismatch, for example, increased from a normalized value of 1 in argon, to 2.1 under atmospheric conditions, to 3.2 when purged with molecular oxygen (Figure 5.19). After piperidine treatment, the absolute dependence on oxygen remained the same although the cleavage intensity increased

Figure 5.19. Dependence of the Direct and Piperidine Induced Photocleavage of DNA by $[Rh(bpy)_2(chrysi)]^{3+}$ at 313 nm, 440 nm, and 525 nm on Oxygen. Sample and irradiation conditions are indicated above the gel lanes, more specific descriptions of the procedures are found in the text. Cleavage reactions were performed in the following hairpin oligonucleotide containing a CT mismatch (indicated in red in the sequence in the figure).

5'-CCTGGGC**C**CCCG $^{T}_{T}$ ^{T}
3'-GGACCCG**T**GGGC $_{T}^{T}$

Although only limited dependence on oxygen were observed in this experiment ruling it out as a central participant in photocatalytic DNA cleavage, several intriguing photochemical behaviors were observed. Piperidine sensitive, oxygen dependent cleavage is observed at guanine bases (blue arrows); this damage is similar to previously observed oxidative damage at these sites and likely occurs as a result of oxidative electron transfer. Direct cleavage one base 3' to the mismatch site (red arrow) is not oxygen dependent and only slightly enhanced by piperidine. Cleavage at other cytosine bases which are removed from the mismatch (green arrows), however, display a weak oxygen dependence but are also significantly enhanced by piperidine. It is also interesting to note that the shift in wavelength of irradiation from 313 nm to 440 nm also appears to change the nature of the cleavage products produced at the mismatched C base itself. The mobility of the products at these two wavelengths (purple arrow) are significantly different. No relevant cleavage was observed in light and dark control reactions performed under identical conditions.

Figure 5.19:


Direct Strand Cleavage
Piperidine Induced Cleavage
313 nm
440 nm
525 nm
313 nm
440 nm
525 nm
A+G
C+T
Ar
air
O2
5(T) hairpin
G
C
C
C
C
C
G
G

approximately 5 fold (Figure 5.19). This guanine damage was not observed at higher wavelengths consistent with the results obtained with this complex on other DNA systems (see section **3.2.5**). These results are analogous to previous work on guanine oxidation by rhodium bis(phi) complexes which displayed the same oxygen dependence. This is suggestive that, like $[Rh(phi)_2(bpy)]^{3+}$, this guanine damage is likely oxidative and also occurs as a result of electron transfer.[13]

In addition to damage at guanine bases, it is clear that $[Rh(bpy)_2(chrysi)]^{3+}$ also generates damage at cytosine bases (green arrows in Figure 5.19) and that this damage is enhanced by post-treatment with hot piperidine. Although small oxygen dependent effects were observed for direct cleavage at the cytosine sites removed by two and three bases to the 3' side of the mismatch at 313 nm and 440 nm, the fact that they were very small and also not preserved after post-treatment with piperidine made definitive conclusions difficult.

It should also be noted that damage to the mismatched C base (purple arrow in Figure 5.19) by irradiation at 313 nm and 440 nm with $[Rh(bpy)_2(chrysi)]^{3+}$ was also observed. Interestingly, the exact damage product produced at this base appears to differ between the two wavelengths. There are clear differences in mobility between the primary product produced at 313 nm, which comigrates with the sequencing band for the base, and the primary product observed at 440 nm, which migrates faster than the chemical sequencing product. This observation is consistent with the observations made by Turro and co-workers that photocleavage by $[Rh(phen)_2(phi)]^{3+}$ appeared to occur by two mechanisms which exhibited different pH dependences when the wavelength of irradiation was changed.[12] The formation of different cleavage products at different wavelengths by $[Rh(bpy)_2(chrysi)]^{3+}$ strongly supports

the existence of two unique cleavage pathways for mono-quinone diimine complexes of rhodium(III) with aromatic ancillary ligands.

5.3.7: Characterization of DNA Photocleavage Products

The observation that $[Rh(bpy)_2(chrysi)]^{3+}$ could react with DNA in ways beyond simply inducing direct strand scission at its site of binding led to interest in understanding the nucleic acid products which were produced by photolysis with the metal complex. Knowledge of the products of DNA photocleavage is critical in constructing reasonable mechanistic proposals for the course of reaction.

5.3.7.1: Free Base Release

It has been previously demonstrated that direct strand scission by $[Rh(phen)_2(phi)]^{3+}$ upon irradiation with UV light primarily produces nucleic acid fragments with phosphate termini with simultaneous release of the free base of the cleaved nucleoside.[7] These product determinations led to the mechanistic proposal that DNA cleavage occurred through radical formation at the C3' position of the deoxyribose sugar and subsequent breakdown through predominantly an oxygen independent pathway. A small amount of base propenoic acids was also observed which are associated with fragmentation reactions which are dependent on dioxygen.[7] These determinations were made by HPLC examination of DNA photocleavage reactions; under appropriate elution conditions, all the DNA base products can be readily separated and resolved from modified base products by reverse phase HPLC analysis.

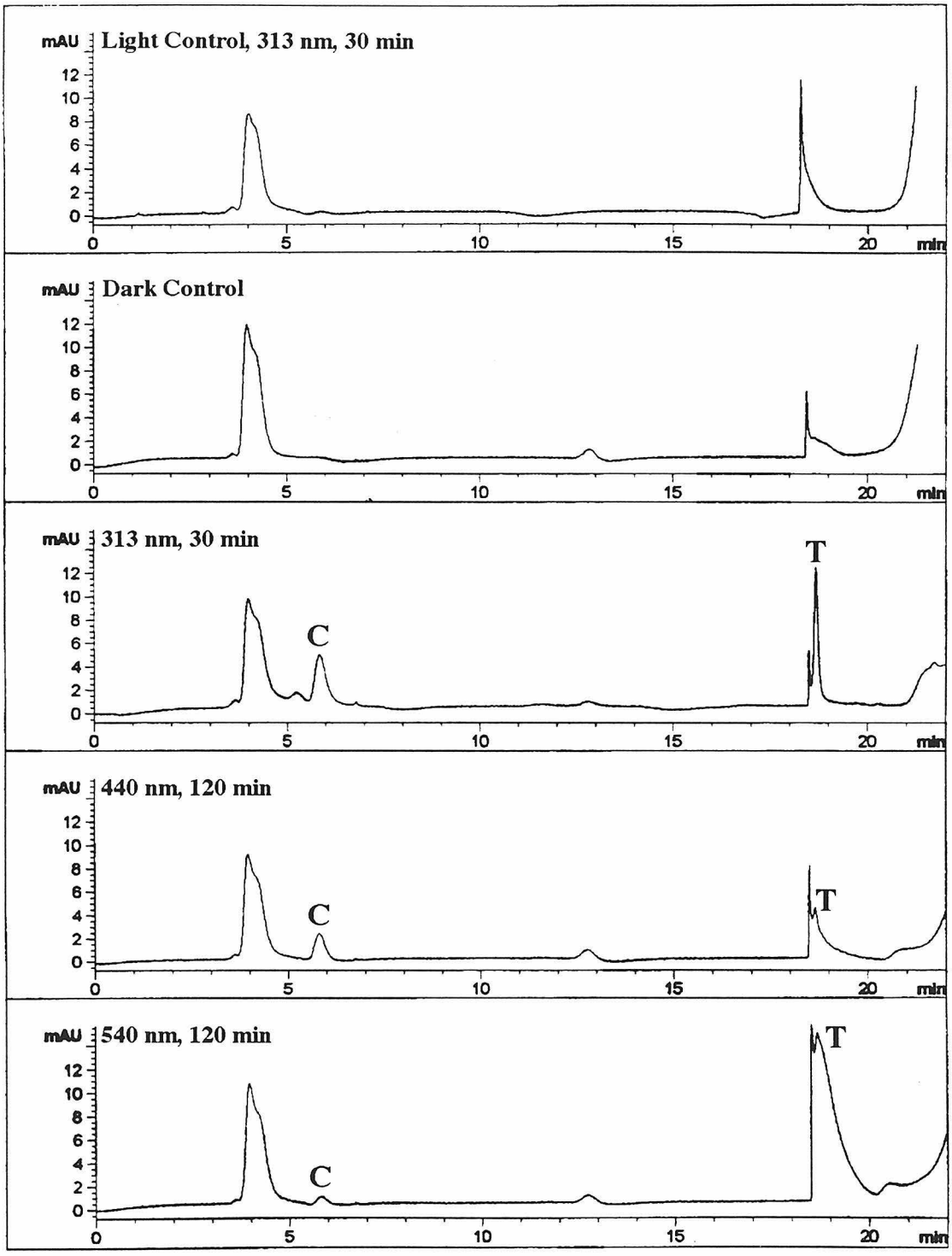
Analogous examination of the products of DNA photocleavage by $[Rh(bpy)_2(chrysi)]^{3+}$ indicated that its reactivity with DNA has many similarities with

the previously characterized $[Rh(phen)_2(phi)]^{3+}$. Like the phi complex, irradiation of $[Rh(bpy)_2(chrysi)]^{3+}$ bound to either calf thymus (properly paired DNA) or to mismatch-containing oligonucleotide hairpins produces free base products. An example of such an experiment is included as Figure 5.20. Upon irradiation, the free bases cytosine (retention time of approx. 6 min) and thymine (19 min) are clearly produced. Although adenine may be generated to some extent, its retention time (approx. 21.8 min assigned from commercial standards) makes it difficult to distinguish from the polymeric DNA products which begin to elute in the same region. No production of the guanine base (retention time of approx. 12.4 min from commercial standards) is observed in this experiment. This preferential formation of the free bases of C and T over guanine was observed in almost all experiments performed with this molecule. In contrast, identical irradiations performed with $[Rh(phen)_2(phi)]^{3+}$ did result in the production of free guanine. This preference for C and T could result either from a preferential reactivity or from binding specificity. When base release experiments were performed on CC mismatch-containing hairpins which placed specific bases at the site of cleavage (T to the 3' side of the mismatch in the hairpin CC/TT and C in the hairpin CC/GG), preferential release the corresponding base product was observed.

In addition to demonstrating the presence of free base products, the chromatograms of the $[Rh(bpy)_2(chrysi)]^{3+}$/DNA photolysis products produced at different wavelengths of irradiation suggest that base modification chemistry may be taking place over the course of DNA photoreaction. When the data presented in Figure 5.20 is examined more closely, it is possible to distinguish changes in the thymine base peak as the irradiation wavelength is changed from 313 nm to 540 nm. In the 313 nm chromatogram, the thymine peak is sharp and the absorption spectrum of the contained material is indistinguishable from that of the commercial standard

Figure 5.20. Free Base Release from Calf Thymus DNA after Photolysis with $[Rh(bpy)_2(chrysi)]^{3+}$ at 313 nm, 440 nm, and 540 nm. Identities of the free base products are indicated over the appropriate peaks and were established by comparison of their elution times and spectral characteristics to commercial standards. The artifactual peak at approx. 4 min, the small feature at 13 min, and the sharp peak eluting just before the thymine base peak present in the light and dark controls could be readily distinguished from the products of interest by their absorption spectra. Note that while the release of free thymine in the 313 nm irradiation produces a sharp chromatography peak, the analogous feature in the 540 nm irradiation is broad suggesting it is composed of more than one species with similar retention times.

Figure 5.20:


mAU
Light Control, 313 nm, 30 min
Dark Control
313 nm, 30 min
440 nm, 120 min
540 nm, 120 min
C
T
0
5
10
15
20
min

(Figure 5.21). In the 540 nm chromatogram, however, the peak has broadened considerably suggesting the possibility that the peak might be composed of more than one material with similar retention times. When the spectrum of this peak is compared to that of free thymine, an 8 to 10 nm blue shift is apparent (Figure 5.21). In later experiments, additional products whose HPLC mobilities were very similar to thymine were also observed whose absorbance maxima varied from 10 nm blue shifted to 5 nm red shifted from that of thymine (Figure 5.22).

Given the strong preference of $[Rh(bpy)_2(chrysi)]^{3+}$ for cleavage at cytosine (see Chapter 4), it was expected that a similar analysis of that free base peak might also produce evidence for modified base products. Surprisingly, no spectral inhomogeneity was observed over the course of many experimental trials utilizing both calf thymus DNA and mismatch hairpins with a cytosine base 3' to the mismatch site. This finding, coupled with the observation of piperidine sensitive damage at cytosine sites, led to the hypothesis that modified cytosines might not be released as free bases.

5.3.7.2: Nucleoside Analysis

In order to determine if any lesions were generated which were not released as free base products, the DNA products of photocleavage reactions were enzymatically digested to their individual nucleoside components for HPLC analysis. These methods have been applied previously to the identification of 8-oxoguanine bases produced in double stranded DNA by oxidative electron transfer.[13] The four different nucleosides are straightforward to resolve by reverse phase HPLC using either a methanol:water citric acid/ammonium acetate buffer system[9] or a simpler gradient procedure using acetonitrile/water containing 0.1% TFA.

Figure 5.21. Comparison of the Spectral Characteristics of Thymine Products Released from Calf Thymus DNA after Photolysis with $[Rh(bpy)_2(chrysi)]^{3+}$ at 313 nm and 525 nm. Note the blue shift in the absorbance maximum of the product produced *via* irradiation at 525 nm.

Figure 5.21:

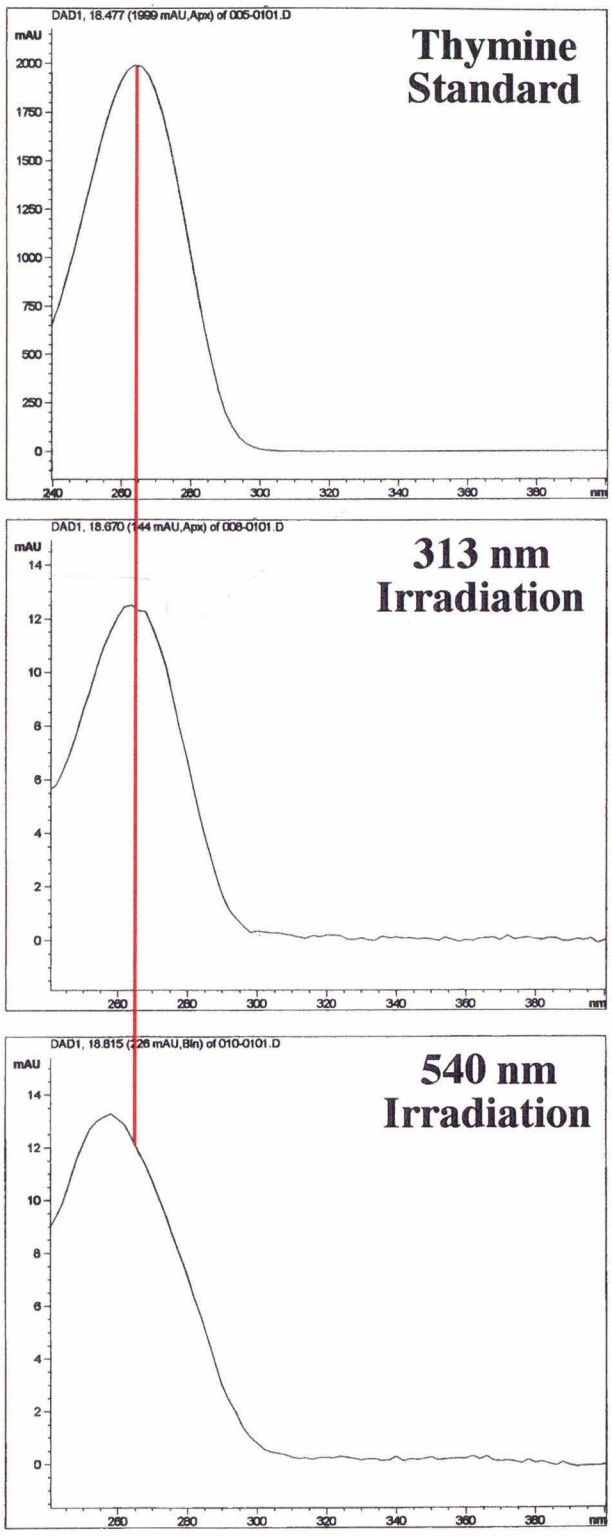
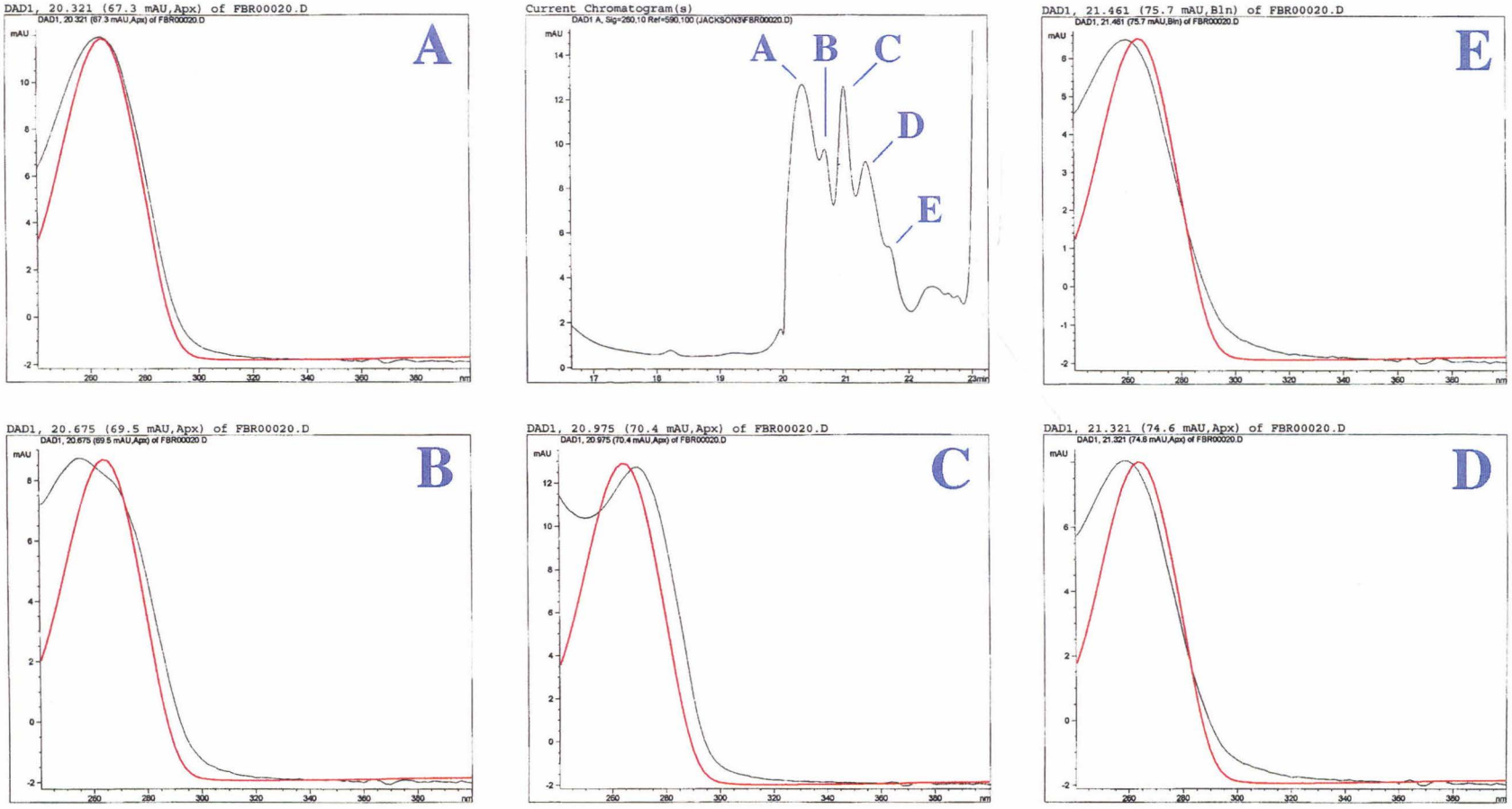

DAD1, 18.477 (1999 mAU,Apx) of 005-0101.D
mAU
Thymine Standard
DAD1, 18.670 (144 mAU,Apx) of 008-0101.D
313 nm Irradiation
DAD1, 18.815 (226 mAU,Bln) of 010-0101.D
540 nm Irradiation
nm

Figure 5.22. Varied Thymine-like Products Observed after Photolysis of $[Rh(bpy)_2(chrysi)]^{3+}$ with the CC Mismatch-Containing Hairpin CC/TT at 525 nm for 2 hr. When photolysis is performed on a larger scale than that included in Figure 5.20, additional reaction products with HPLC mobilities similar to the thymine free base are observed. The composite chromatographic peak observed in the thymine region (center top) can be resolved into at least five overlapping peaks. The absorption spectra of these peaks (panels A through E) correspond to the spectrum of thymine itself (red trace in each panel) to varying degrees. While peak A corresponds in both spectrum and expected retention time to the unmodified thymine base, the other materials have absorbance characteristics diverge considerably.

Figure 5.22:


DAD1, 20.321 (67.3 mAU,Apx) of FBR00020.D
A
Current Chromatogram(s)
A
B
C
D
E
DAD1, 21.461 (75.7 mAU,Bln) of FBR00020.D
E
DAD1, 20.675 (69.5 mAU,Apx) of FBR00020.D
B
DAD1, 20.975 (70.4 mAU,Apx) of FBR00020.D
C
DAD1, 21.321 (74.6 mAU,Apx) of FBR00020.D
D

An example chromatogram of the nucleoside products of a typical analysis is included as Figure 5.23. Under these HPLC conditions, utilizing the citric acid buffer system described above, the C (6.9 min), G (12.5 min), T (15.0 min), and A (27.4 min) nucleosides are cleanly separated. Unfortunately, however, the analysis of the photolysis products from 313 nm, 440 nm, and 525 nm irradiation of $[Rh(bpy)_2(chrysi)]^{3+}$ or $[Rh(phen)_2(phi)]^{3+}$ with both properly paired and mismatch-containing DNA did not reveal the significant production of any products readily discernable from these four standard nucleoside products. The single reproducibly observed novel peak appeared at approximately 17 min near the thymine nucleoside peak (Figure 5.24). This product, however, was generated in very small amounts given that under these conditions even just a stoichiometric reaction* between metal complex and the oligonucleotide would produce a peak between 30 and 100 times higher by conservative estimates (assuming comparable extinction coefficients for the product and the unmodified nucleosides). Although it is only a minor product of the reaction, the material has spectral features, including absorbance in the UV and a broad shoulder into the visible, suggestive of it being a modified nucleoside product (Figure 5.25).

5.4: Discussion

5.4.1: Photocatalytic DNA Cleavage by $[Rh(bpy)_2(chrysi)]^{3+}$ and $[Rh(phen)_2(phi)]^{3+}$

The results described here have demonstrated, clearly and unambiguously, that $[Rh(bpy)_2(chrysi)]^{3+}$ and $[Rh(phen)_2(phi)]^{3+}$ photocatalytically cleave DNA when

---

* Because equal molar amounts of the metal complex and hairpin oligonucleotides were combined for these reactions, a stoichiometric amount of reaction is the least which should be expected.

Figure 5.23. HPLC Chromatogram of a Representative Irradiation Sample Digested to its Individual Nucleoside Components. After enzymatic digestion and dephosphorylation, the individual nucleoside constituents of DNA can be readily resolved by HPLC using a methanol/water, citric acid/ammonium acetate buffer system as described in the text. Peaks corresponding to each nucleoside product are identified on the chromatogram as assigned by comparison to commerical standards.

Figure 5.23:

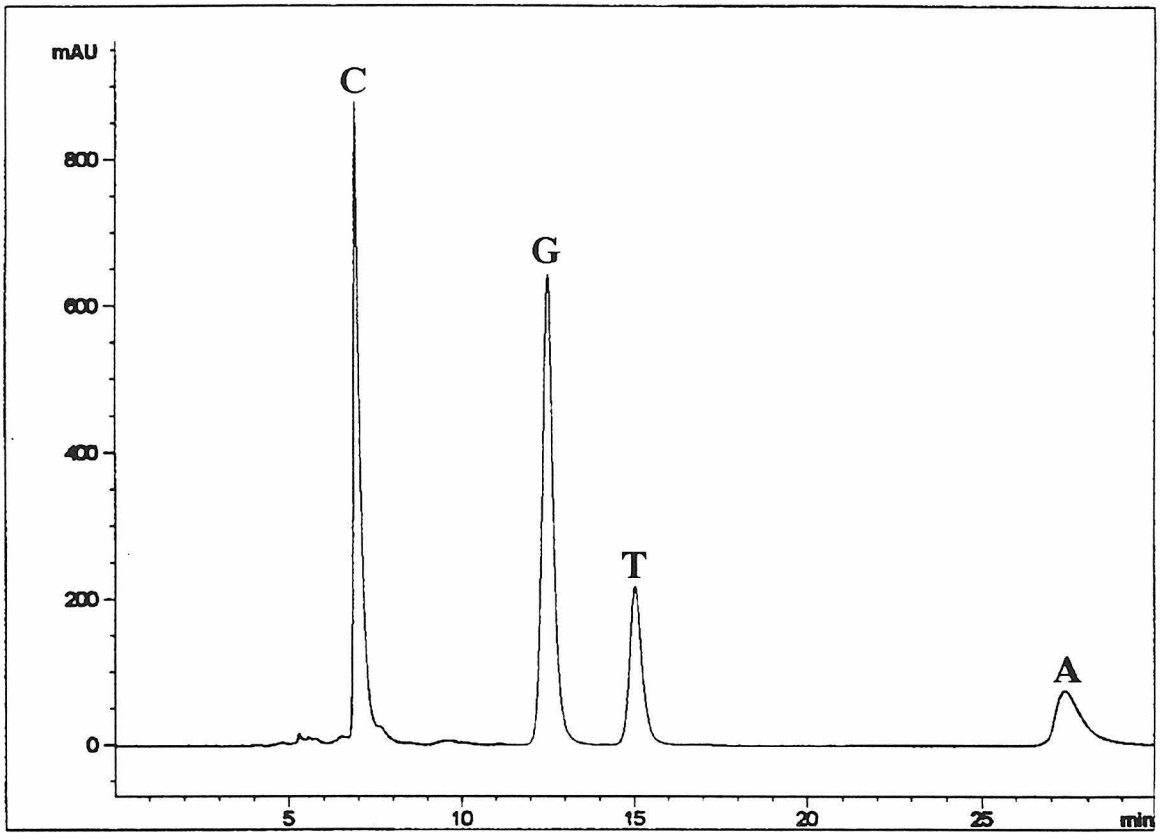


Figure 5.24. Comparison of the Nucleoside Digests of DNA Photocleavage of the CC Mismatch-Containing Hairpin CC/GG by $[Rh(bpy)_2(chrysi)]^{3+}$. The single reproducibly observed product other than the four standard DNA nucleosides is indicated by the arrow in the 440 nm irradiation trace (bottom panel).

Figure 5.24:

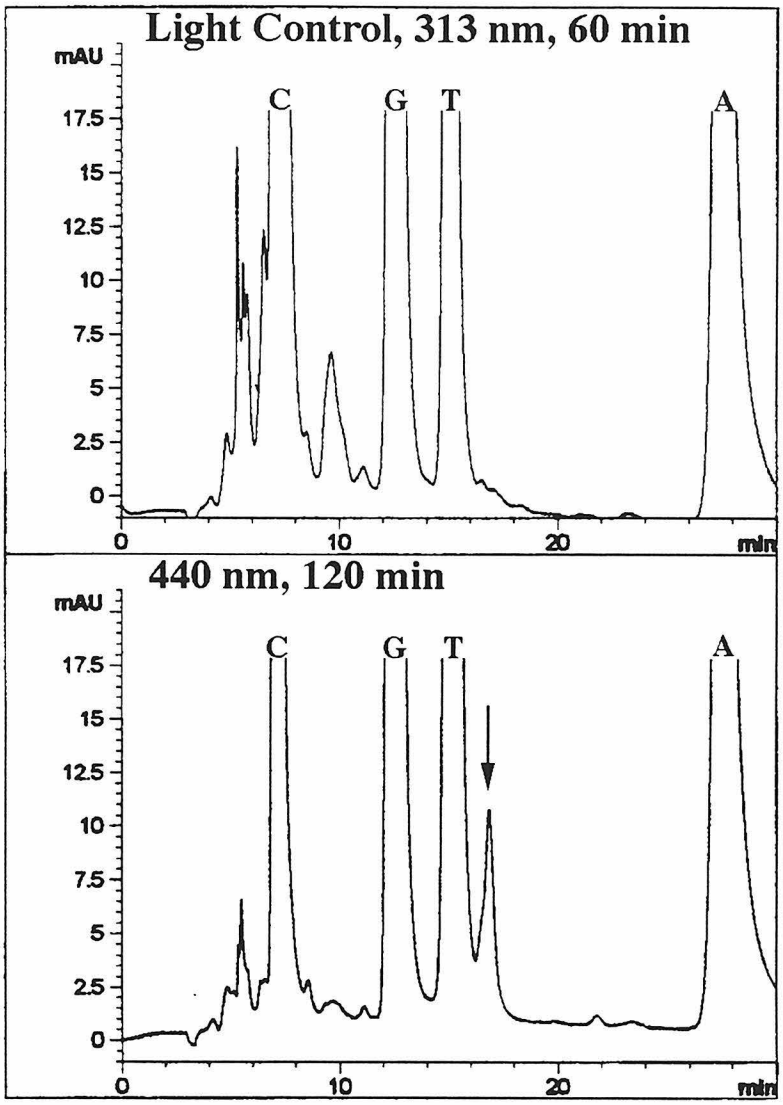
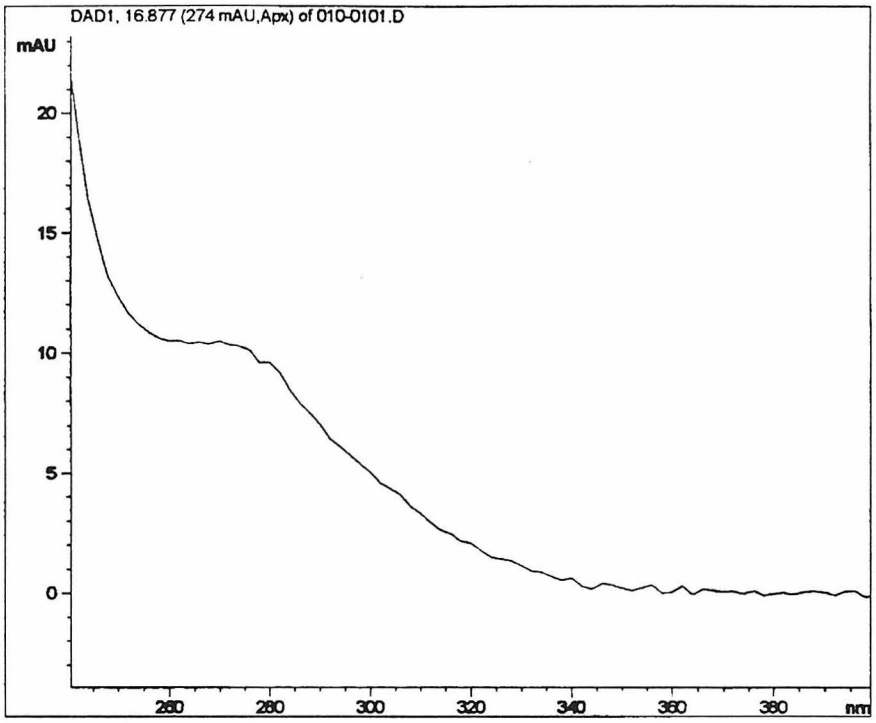

Light Control, 313 nm, 60 min
mAU
17.5
15
12.5
10
7.5
5
2.5
0
C
G
T
A
0
10
20
min
440 nm, 120 min
mAU
17.5
15
12.5
10
7.5
5
2.5
0
C
G
T
A
0
10
20
min

Figure 5.25. Absorption Spectrum Associated with the Peak Identified in Figure 5.24. Although lacking clear spectral features which would allow a hypothesis about its exact identity, this material does have absorbance in the UV region which is consistent with it being a modified base product.

Figure 5.25:


DAD1, 16.877 (274 mAU,Apx) of 010-0101.D
mAU
20
15
10
5
0
260
280
300
320
340
360
380
nm

irradiated with visible light. This photocatalytic cleavage is promoted by a wide range of irradiation wavelengths. As shown in Figure 5.26, the level of maximal photocleavage observed at a given wavelength is not directly related to the extinction coefficient of the metal complex at the wavelength of the incident radiation. The values plotted in Figure 5.26 are not, however, corrected for the variable power of the Hg/Xe arc lamp output from wavelength. When these values are normalized for the power of the lamp emission at each wavelength, the differences in photocatalytic cleavage are even more dramatic. These values, generated by dividing the maximal fraction cleaved by the corresponding spectral irradiance of the lamp at that wavelength (in $\mu W\ cm^{-2}\ nm^{-1}$ at 50 cm) and normalizing the results to one, are plotted in Figure 5.27 along with the original experimental cleavage fractions (also normalized to one). In this analysis the high level of photocatalytic cleavage obtained at 525 nm is highlighted further since the lamp output is at its minimum power between the wavelengths of 460-535 nm. Not surprisingly, examination of the components of photolysis reactions by HPLC confirmed that, in this region of low lamp power (500 nm) where the metal complex itself has a very small extinction coefficient, the rhodium complex is degraded to a very limited extent even over long periods of irradiation; what is remarkable is that under these conditions, DNA photocleavage chemistry occurs and can produce high levels of photocatalytic strand scission.

This fact, that a compound could promote efficient photo-induced DNA cleavage at wavelengths where it has only minimal absorbance (see Figure 5.26), has always been somewhat puzzling. The results described here suggest a possible explanation for this photochemical problem. The novel photoproduct identified in the rhodium complex and rhodium complex-DNA irradiations at 400 and 500 nm, in contrast to $[Rh(bpy)_2(chrysi)]^{3+}$, has strong absorbance features at 520 nm and 560 nm. As a

Figure 5.26. Saturation Photocleavage of DNA by Δ-$[Rh(bpy)_2(chrysi)]^{3+}$ at the CC/CC mismatch at Varied Wavelengths as Compared to the Metal-DNA Stoichiometry and the Absorption Spectrum of the Complex Bound to DNA. Levels of photocleavage from the experiment included as Figure 5.1 are indicated over their respective wavelengths by blue bars. Arrows indicate curves which did not reach a clear asymptotic level; the appended question mark indicates that the curvature of the plot was shallow enough that it was difficult to judge if its increase was slowing significantly by the last time point. The level of cleavage expected from the Rh:DNA ratio is indicated by the gray bar. The absorption spectrum of the complex bound to DNA (red line) is plotted to demonstrate the lack of correlation between absorbance characteristics and the maximal DNA photocleavage. Note that the data included in this graph have not been normalized for the variable power of the output of the Hg/Xe arc lamp as the wavelength selected is changed.

Figure 5.26:

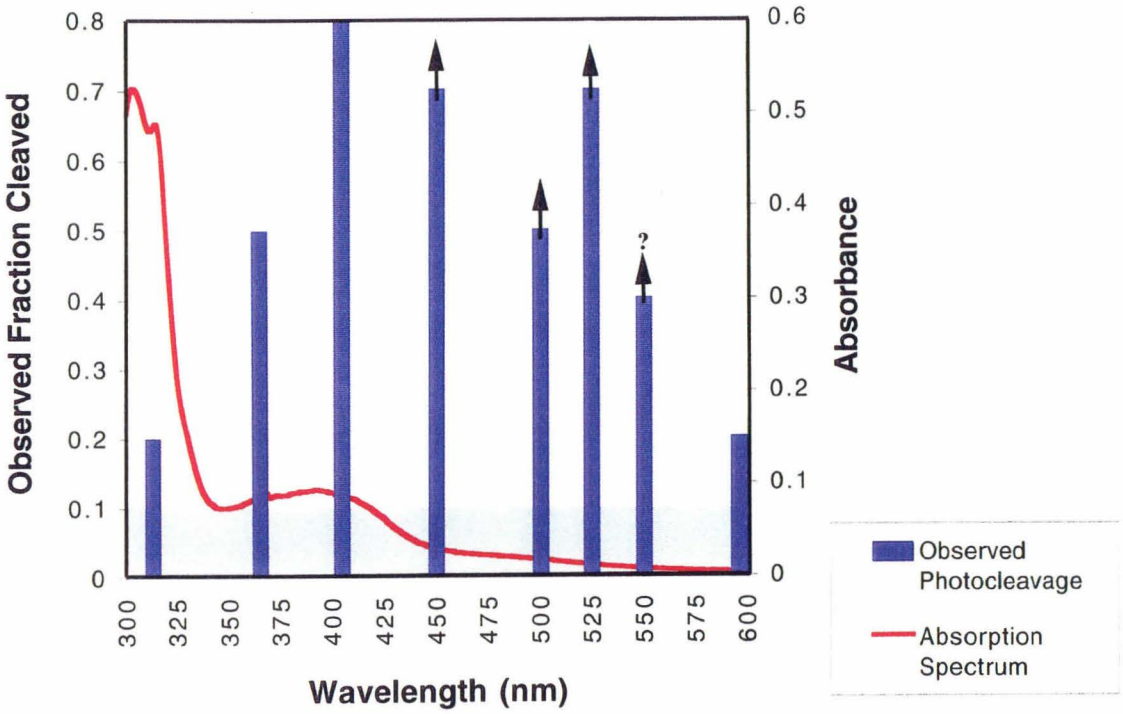
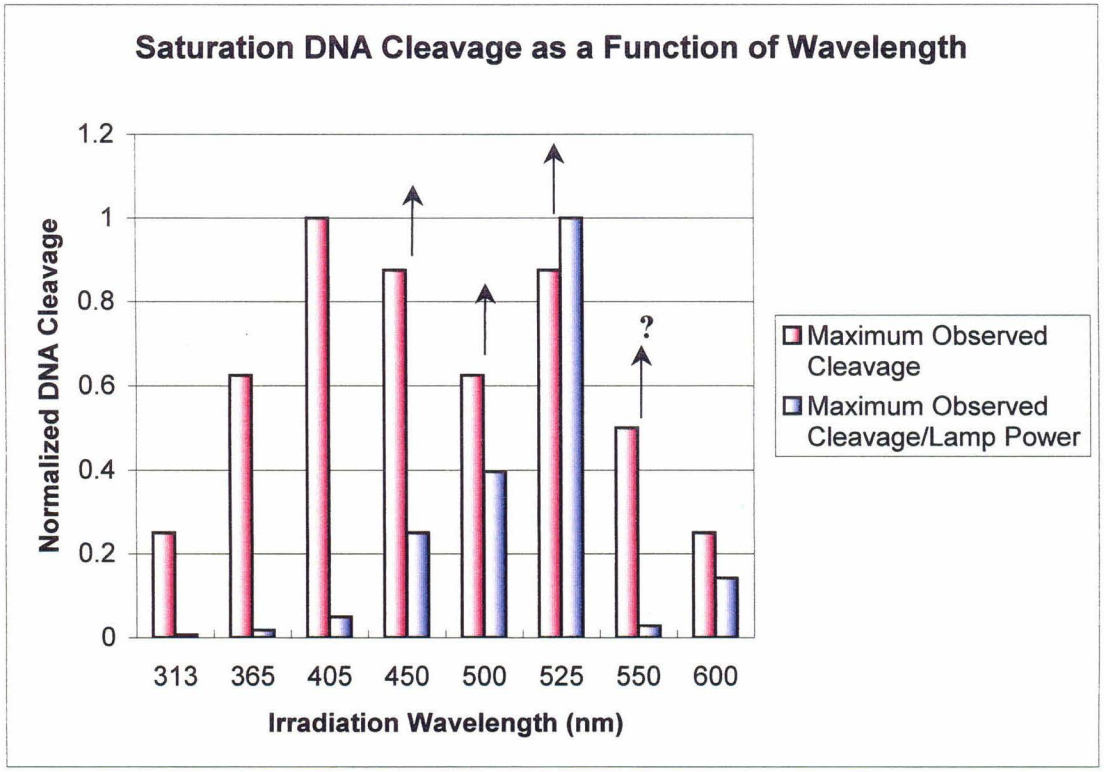

Observed Fraction Cleaved
0.8
0.7
0.6
0.5
0.4
0.3
0.2
0.1
0
0.6
0.5
0.4
0.3
0.2
0.1
0
Absorbance
300
325
350
375
400
425
450
475
500
525
550
575
600
Wavelength (nm)
?
Observed Photocleavage
Absorption Spectrum

Figure 5.27. Comparison of the Maximal Cleavage of DNA Observed After Photolysis with $[Rh(bpy)_2(chrysi)]^{3+}$ at Variable Wavelength – Normalized and Corrected for Lamp Power. Values included in Figure 5.26 were divided by the maximal spectral irradiance (in μW cm^{-2} nm^{-1} at 50 cm) of the Hg/Xe arc lamp in the 25 nm band passed by the Oriel monochrometer centered on the indicated irradiation wavelength. The resulting values were normalized and are plotted beside the observed fraction cleaved (also normalized to one). Note that the observed photocleavage per unit lamp power increases to a maximum in the 500-525 nm region. Since this is also the spectral region where the "true" maximal photocleavage could not be observed since cleavage had not reached an asymptotic limit by the conclusion of the experiment, the values indicated on the graph are artificially low.

Figure 5.27:


Saturation DNA Cleavage as a Function of Wavelength
Normalized DNA Cleavage
1.2
1
0.8
0.6
0.4
0.2
0
313
365
405
450
500
525
550
600
?
Irradiation Wavelength (nm)
Maximum Observed Cleavage
Maximum Observed Cleavage/Lamp Power

result, even in the absence of information about this compound's identity and structure, it is tempting to speculate that this product may be involved in DNA cleavage at these wavelengths. In this scenario, irradiation of the original metal complex at high wavelength (low energy) is sufficient to generate a small amount of this active species which then goes on to perform cleavage chemistry on the DNA photocatalytically.* This model is circumstantially supported by the fact that, even in the 500 nm samples analyzed by HPLC where the metal complex was quite stable over the course of photolysis, a small amount of this green-absorbing product is generated and persists through the entire irradiation. The identity of this species and its ability to promote DNA photocleavage is currently under investigation.

5.4.2: Differences in Photochemistry between Mono- and Bis-Quinone Diimine Complexes of Rhodium(III)

The work described here is not the first time that a quinone diimine complex of rhodium(III) has been demonstrated to perform chemistry photocatalytically on DNA. Recently, the compound $[Rh(phi)_2(bpy)]^{3+}$ has been shown to photocatalytically repair cyclobutyl thymine dimers by oxidative electron transfer through double stranded DNA. In this reaction, the dimer lesion is transiently oxidized by the rhodium complex, undergoes cyclo-reversion and then reoxidizes the complex *via* back electron transfer.[14] Significant chemical differences exist, however, between $[Rh(phi)_2(bpy)]^{3+}$ and the mono-quinone diimine complexes under consideration in this work.

---

* In addition, one might speculate that at the low energy, low photon flux conditions might also help minimize degradation of the active species. Because the oligonucleotide is a 29 base pair hairpin, any stoichiometrically modified material should make up åpprox. 3% of the reaction.

From the earliest studies done on rhodium(III) mono and bis(phi) complexes, differences in their photoreactivity have been recognized. Although both compounds were initially demonstrated to directly cleave DNA upon photo-activation with ultraviolet light, it was demonstrated that reactions with the two complexes produced somewhat different products and exhibited different oxygen dependencies.[7] Since that time, more dramatic differences in reactivity between the two classes of compounds have been observed. The bis(phi) complexes, when irradiated at higher wavelength (greater than or equal to 365 nm) have been shown to participate in oxidative reactions with DNA.[13] These reactions have been demonstrated to include both the thymine dimer repair[14] introduced above and also the formation of oxidative DNA damage at guanine sites *via* long range electron transfer.[13] Complexes with only a single phi ligand and two aromatic ancillary ligands, like $[Rh(phen)_2(phi)]^{3+}$, have proven to be significantly different from their bis(phi) counterparts. At 313 nm, these complexes exhibit a low level of DNA base oxidation alongside their primary, direct strand cleavage reactivity. Unlike the bis(phi) complexes, where direct strand scission gives way to predominantly oxidative base damage as the irradiation wavelength is increased, $[Rh(phen)_2(phi)]^{3+}$ continues to directly cleave DNA very efficiently into the visible region of the spectrum; as demonstrated in this work, this cleavage is also *photocatalytic*; guanine oxidation by electron transfer is not observed with $[Rh(phen)_2(phi)]^{3+}$ at these wavelengths. As discussed previously, DNA cleavage by all of the rhodium(III) phi complexes produce sharp cleavage bands suggesting that their reaction is not mediated by a diffusible species. The chrysi complexes described in this work behave essentially analogously to their phi analogs with $[Rh(chrysi)_2(phen)]^{3+}$ closely approximating $[Rh(phi)_2(bpy)]^{3+}$ and $[Rh(bpy)_2(chrysi)]^{3+}$ corresponding to $[Rh(phen)_2(phi)]^{3+}$.

5.4.3: Speculation on the Possible Mechanism of Photocatalysis

The experiments described in this chapter do not provide enough information to clearly propose an explanation for the photocatalytic behavior of these compounds. They do allow, however, a subset of possible explanations to be ruled out. One of the most common ways that such a photoactive molecule could catalytically damage DNA is the production of singlet oxygen. Upon electronic excitation, compounds which can intersystem cross to a triplet state have the potential to generate singlet oxygen if their triplet energy is high enough. Singlet oxygen is highly reactive and adds preferentially to guanine bases making them sensitive to subsequent alkali induced strand cleavage.[15] The behavior observed in these experiments is inconsistent with singlet oxygen generated reactivity in almost every respect. Rather than requiring piperidine, cleavage is generated directly and specificity is observed for C and T bases rather than guanine.

One could also envision another possible mechanism of photocatalytic DNA damage generated by reactivity similar to that displayed by $[Rh(phi)_2(bpy)]^{3+}$ in the repair of the thymine dimer. It is possible, for example, that irradiation with the rhodium complex could stimulate photocycloaddition reactions in the DNA. Although this reaction pathway cannot be definitively ruled out without comprehensive knowledge of the products of the photolysis reactions, it is difficult to envision how such reactions would lead to the high levels of direct strand scission observed in these experiments. One would also expect that such a reaction pathway would also produce a significant amount of a unique, dimeric nucleoside product readily distinguishable from monomeric nucleosides by chromatographic mobility and spectral characteristics; no such product was observed.

After elimination of both photoinduced cyclization chemistry and singlet oxygen as possible explanations for the photocatalytic cleavage of DNA by $[Rh(phen)_2(phi)]^{3+}$ and $[Rh(bpy)_2(chrysi)]^{3+}$, the most likely mechanisms must involve redox reactions between the metal complex and DNA. These reactions which could involve oxidation of the DNA sugar backbone or the pathways of oxidative or reductive damage to the DNA bases. Although $[Rh(phen)_2(phi)]^{3+}$ and $[Rh(bpy)_2(chrysi)]^{3+}$ have been shown to promote some oxidation of guanine bases in DNA (Figure 5.19), oxidative reactivity at base sites cannot explain the photocatalytic cleavage of interest. Photocatalysis is most efficient at wavelengths in the visible regime where no guanine oxidation is observed and is primarily observed at the pyrimidine bases C and T rather. Due to their high oxidation potentials relative to the purine bases, oxidative damage is not observed preferentially at pyrimidine sites in double stranded DNA.[16] Observation of any pyrimidine oxidation products requires very strong oxidants like $KMnO_4$ or OsO_4 and, in these cases, preference is observed for thymine rather than cytosine as seen in these experiments; these reactions also involve atom transfer reactions in addition to electron transfer. Furthermore, these oxidative reactivity pathways have generally been observed to require alkali post treatment to generate strand breaks from sites of base modification.[17]

The production of free base products and the observation that photocatalytic cleavage by $[Rh(phen)_2(phi)]^{3+}$ and $[Rh(bpy)_2(chrysi)]^{3+}$ is produced without post treatment of any kind suggests that these compounds, either directly or indirectly, must perform chemistry at the deoxyribose sugar in DNA.[15] Although the UV light-induced reaction of $[Rh(phen)_2(phi)]^{3+}$ with DNA has been shown to proceed through hydrogen atom abstraction from the deoxyribose leading to direct strand breaks at the site of binding, the mechanistic understanding of the reaction seemed to imply that ligand dissociation and photoaquation of the complex was required to generate strand

cleavage.[7,8] Given that DNA cleavage at visible wavelengths has been shown to proceed without complex consumption, if this cleavage process proceeds by hydrogen atom abstraction, it must do so by a different route. One example of a compound thought to perform photocatalytic hydrogen atom abstraction exists in the literature.[18] The metal complex $[Pt_2(P_2O_5H_2)_4]^{4-}$ ($P_2O_5H_2$ = "pop") has been shown to oxidize 1-phenylethanol to acetophenone with a maximum of 10^2 turnovers.[18] In the proposed catalytic scheme, $[Pt(pop)_4]^{4-}$ abstracts two hydrogen atoms in the course of oxidizing the substrate to the form $[Pt(pop)_4H_2]^{4-}$. The hydrogen atoms of this complex can be photodissociated to regenerate the active catalyst.[19] Such a "direct" photocatalytic cleavage mechanism is consistent with the observation of free base products over the course of photolysis of DNA with the two rhodium compounds. It does not, however, explain the presence of the putative modified base products observed in the experiments shown in Figure 5.20-5.22.

Although the proposal that photocatalytic DNA cleavage might be produced by catalytic hydrogen atom abstraction from the deoxyribose sugars cannot be conclusively ruled out, that a significant fraction of the products released from the photolysis of the complex with DNA have absorption characteristics consistent with base modification (Figure 5.20-5.22) suggests that the reaction pathway producing photocatalytic DNA cleavage must include a mechanism which can generate both base damage *and* the sugar modifications required for direct strand scission. Having eliminated DNA base oxidation on the basis of reactivity considerations, the single remaining candidate is reductive damage to DNA. Unlike the oxidative damage pathways discussed above, reductive damage to DNA is preferentially observed at the pyrimidines due to their more favorable reduction potentials (approx. -1.1 V/NHE).[20] This specificity for C and T is appealing since it is at those bases where the strongest strand cleavage proximal to a mismatch site was observed (see Figure 4.2). It was

also at cytosine bases where DNA cleavage appeared when the irradiation wavelength was changed from 313 nm to 440 nm (Figure 5.18).

Although these parallels are suggestive, in order to be completely consistent with the experimental results on these metal complex systems, such reductive lesions would have to lead subsequently to DNA strand breaks. It has been previously demonstrated that the *in situ* production of a pyrimidine radical in DNA by irradiation of a 5-bromouracil base can lead to abstraction of the H1' hydrogen atom of the base to the 5' of the radical site with subsequent DNA cleavage.[21] It has been further proposed that, based on the local DNA structure at a given radical site, abstraction of the H2' or H2" hydrogens might also be possible.[22] As a result, pathways have been characterized by which a radical localized on a pyrimidine base could result in the conversion of that lesion to a strand break. In this specific case, if a radical is generated on the mismatched base itself, it is possible that the added structural instability at the mismatch site could make other sites of reaction accessible as well.

In addition to the base preferences observed in the photocatalytic cleavage reaction, the notion of a reductive mechanism is also appealing for other reasons. The appearance of new cleavage bands when the irradiation wavelength is changed which are separated from the proposed site of metal complex binding implies a process which can occur over a long range. In the absence of any evidence that this reactivity is generated by a diffusible species, such an observation is highly suggestive of an electron transfer reaction.* Electrochemical examination of

---

* Highly preliminary EPR experiments have demonstrated that irradiation of $[Rh(bpy)_2(chrysi)]^{3+}$ with visible light also produces a radical species which is stable over very long periods of time (min to hr).[23] In the presence of DNA, other radical species are also observed. It is not

$[Rh(bpy)_2(chrysi)]^{3+}$ by cyclic voltammetry indicates that, although the electrochemical behavior of the compound was very complex, such a reaction pathway might be possible. In the CV included as Figure 5.28, performed in the presence of 0.1 M tetrabutylammonium tetrafluoroborate auxiliary electrolyte, there are two oxidations of the material at approx. 0.8 V and 1.0 V vs. SCE (see arrows in 5.28), or 1.1 V and 1.3 V vs. NHE. Although the higher potential oxidation is at least partially reversible, the small size and proximity of the lower potential transition makes it difficult to distinguish a return wave. Considering that photoactivation would further augment these values, this suggests that the potential exists for this compound to reductively damage DNA.*

Although limited enough in scope that any conclusions based on them should be viewed with great caution, the experiments characterizing the photolysis products of $[Rh(bpy)_2(chrysi)]^{3+}$ with DNA are also *not inconsistent* with this reductive hypothesis. It has been previously demonstrated in the field of radiation biology that reduction products of thymine have reaction pathways available which result in irreversible modification to the thymine base as a result of the formation of its radical anion. The primary irreversible pathway for this modification is protonation at carbon in the 6 position resulting in the formation of the 5,6-dihydrothymidine-5-yl

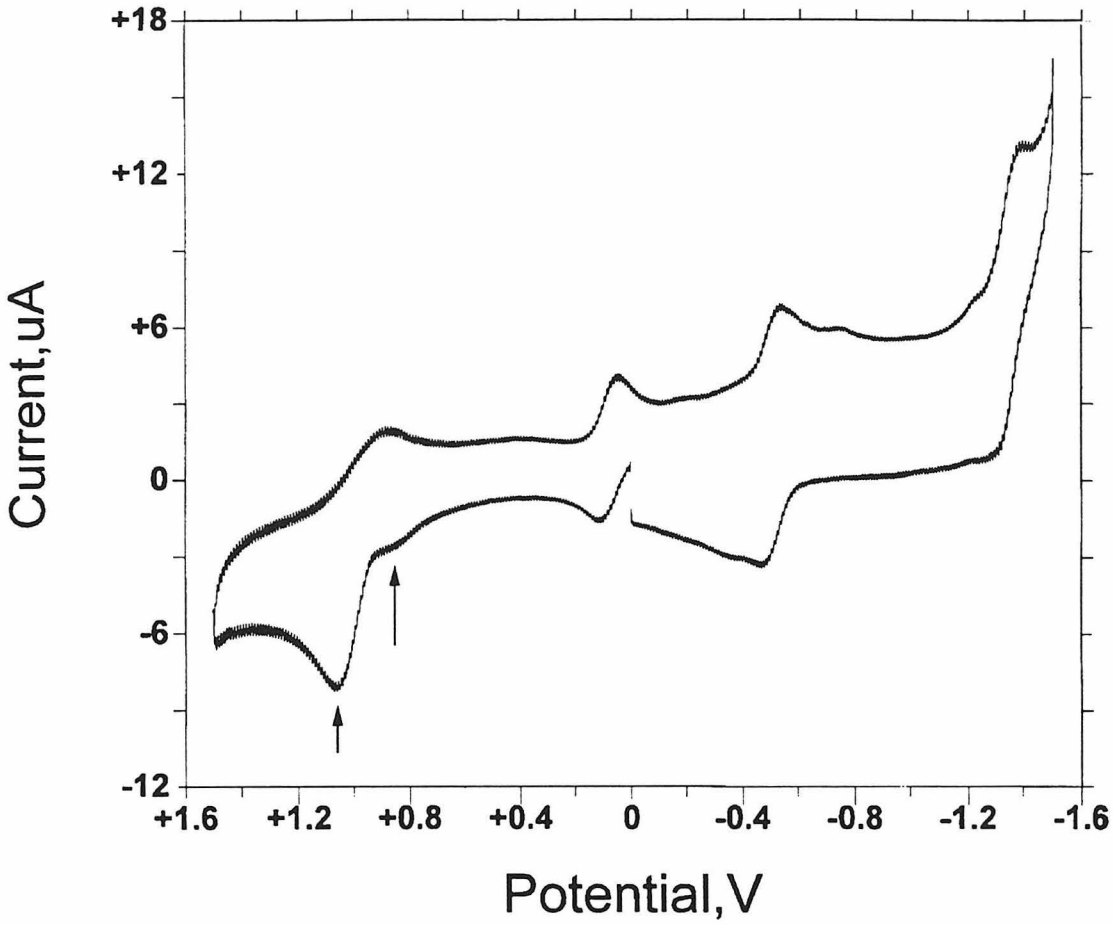
---

known at this time whether these species correspond to metal complex radicals, radicals of dissociated ligands, or some other species in solution.

* It is also relevant to note that such a reductive mechanism would provide an additional variable through which to explain the different intensities of photocleavage observed in the recognition experiments described in Chapter 4; if irradiation with visible light causes these complexes to preferentially photo-react with bases which are readily reduced, then the fact that cleavage intensity at the base 3' to the mismatch decreases in the order C>T>>G,A, which corresponds to the order of reduction potentials, may not be coincidental. Any preferential reactivity of this kind would represent another parameter which would be reflected in differential photocleavage efficiencies from binding site to binding site.

Figure 5.28. Cyclic Voltammogram of $[Rh(bpy)_2(chrysi)](PF_6)_3$. Complex oxidations of interest are indicated with arrows. Conditions and procedures are included in the text.

Figure 5.28:



radical.[24] It is possible that this radical is the only "final" product which results from electron capture by DNA.[24] Such irreversible products of the thymine base may correspond to the materials of varying spectral characteristics observed after photolysis of DNA with the metal complex with similar retention times to the thymine free base. Blue shifting of the absorption spectrum is consistent with reductive damage of the thymine base, specifically with saturation of the 5-6 olephinic moiety; the maximal absorbance of 5,6-dihydrothymidine, for example, occurs at 210 nm and falls off to virtually *no* absorbance intensity at 260 nm.[25] The radical anion of cytosine, however, behaves quite differently. Instead of reacting irreversibly at carbon, this radical has been demonstrated to protonate at either the N3 or O^2 site; this protonation event at a heteroatom protects the cytosine base from irreversible reaction at a carbon site.[24] The absence of any modified cytosine products is therefore not contradictory to this mechanistic hypothesis.

5.5: Conclusions

At its most unambiguous and simple level, the work described here has established that $[Rh(bpy)_2(chrysi)]^{3+}$ and, by extension, rhodium phi complexes like $[Rh(phen)_2(phi)]^{3+}$ have a much richer variety of photochemical reactions with DNA than has been previously appreciated. In addition to cleaving DNA with visible light, these compounds cleave the nucleic acid photocatalytically producing yields which can approach the complete cleavage of all the DNA in a reaction mixture. In addition, these experiments have demonstrated that these mono-quinone diimine complexes of rhodium(III) also have a very rich wavelength dependent photochemistry which is related, but not restricted, to their reactions with DNA. Both spectroscopic and direct analysis have shown that it is possible to generate photoproducts with novel spectroscopic characteristics, cleave DNA without

significant degradation of the metal complex, and produce changes in the specific sites and nature of DNA lesions produced just by varying the wavelength of light used for photolysis. Although the results from many of these studies are suggestive of possible chemical mechanisms to explain the photocatalytic cleavage of DNA, none of these suggestions can realistically be considered proven. As a result, although representing a significant contribution to the rapidly expanding body of knowledge about the photochemistry of these molecules, this work is also an open invitation to the further research required to bring closure to these interesting concerns.

5.6: Literature Cited

1) Pyle, A. M.; Chiang, M. Y.; Barton, J. K. *Inorg. Chem.* **1990**, *29*, 4487.

2) Chan, S.-F.; Chou, M.; Creutz, C.; Matsubara, T.; Sutin, N. *J. Am. Chem. Soc.* **1981**, *103*, 369.

3) Brown, G. M.; Chan, S.-F.; Creutz, C.; Schwartz, H. A.; Sutin, N. *J. Am. Chem. Soc.* **1979**, *101*, 7639.

4) Indelli, M. T.; Carioli, A.; Scandola, F. *J. Phys. Chem.* **1984**, *88*.

5) Ballardini, R.; Varani, G.; Balzani, V. *J. Am. Chem. Soc.* **1980**, *102*, 1719.

6) Frink, M. E.; Sprouse, S. D.; Goodwin, H. A.; Watts, R. J.; Ford, P. C. *Inorg. Chem.* **1988**, *27*, 1283.

7) Sitlani, A. *Sequence Specific Recognition and Photocleavage of DNA by Phenanthrenequinone Diimine Complexes of Rhodium(III)*. Ph.D. Thesis, Division of Chemistry, California Institute of Technology, 1995.

8) Sitlani, A.; Long, E. C.; Pyle, A. M.; Barton, J. K. *J. Am. Chem. Soc.* **1992**, *114*, 2303.

9) Ito, K.; Inoue, S.; Yamamoto, K.; Kawanishi, S. *J. Biol. Chem.* **1993**, *268*, 13221.

10) Pyle, A. M. *Phenanthrene Diimine Complexes of Ru(II) and Rh(III): Synthesis and Development of a New Class of Shape-Selective Probes for Nucleic Acid Structure*. Ph.D. Thesis, Department of Chemistry, Columbia University, 1989.

11) Erkkila, K. E.; Barton, J. K., unpublished results.

12) Turro, C.; Hall, D. B.; Chen, W.; Zuilhof, H.; Barton, J. K.; Turro, N. J. *J. Phys. Chem.* **1998**, *102*, 5708.

13) Hall, D. B. *Oxidative DNA Damage Through Long Range Electron Transfer*. Ph.D. Thesis, Division of Chemistry, California Institute of Technology, 1998.

14) Dandliker, P. J.; Holmlin, R. E.; Barton, J. K. *Science* **1997**, *275*, 1465.

15) Armitage, B. *Chem. Rev.* **1998**, *98*, 1171.

16) Sevilla, M. D.; Becker, D.; Yan, M.; Summerfield, S. R. *J. Phys. Chem.* **1991**, *95*, 3409.

17) Burrows, C. J.; Muller, J. G. *Chem. Rev.* **1998**, *98*, 1109.

18) Kalsbeck, W. A.; Gingell, D. M.; Malinsky, J. E.; Thorp, H. H. *Inorg. Chem.* **1994**, *33*, 3313.

19) Harvey, E. L.; Stiegman, A. E.; Vlcek, A. A.; Gray, H. B. *J. Am. Chem. Soc.* **1987**, *109*, 5233.

20) Steenken, S.; Telo, J. P.; Novais, H. M.; Candeias, L. P. *J. Am. Chem. Soc.* **1992**, *114*, 4701.

21) Sugiyama, H.; Tsutsumi, Y.; Saito, I. *J. Am. Chem. Soc.* **1990**, *112*, 6720.

22) Cullis, P. M.; Langman, S.; Podmore, I. D.; Symons, M. C. R. *J. Chem. Soc. Faraday Trans.* **1990**, *86*, 3267.

23) Schiemann, O.; Jackson, B. A.; Barton, J. K., unpublished results.

24) Steenken, S. *Free Rad. Res. Comms.* **1992**, *16*, 349.

25) Somers, B. (Glen Research Corporation), Personal Communication.

Chapter 6:

Conclusions and Perspectives

The research described in this thesis began with a deceptively simple and well defined goal: the molecular recognition of base mismatch sites in DNA *via* the binding of a small molecule. This goal has been achieved. Metallointercalators of rhodium(III) containing the sterically bulky intercalating ligand chrysenequinone diimine, in particular the complex $[Rh(bpy)_2(chrysi)]^{3+}$, have been shown to bind and photocleave at more than 80% of the single base pair mismatch sites which can exist in DNA. This level of general recognition is unprecedented for a small molecule and surpasses the generality of some proteins involved in mismatch recognition and repair. Beyond its generality, however, $[Rh(bpy)_2(chrysi)]^{3+}$ has also been shown to bind very tightly to a subset of mismatch sites. This tight binding to its target sites, when coupled with a very low binding constant for properly paired DNA, results in a very high specificity for some mismatch sites. It was this specificity which was exploited in the application of the molecule to the sequence specific detection of a single mismatch in a multi-kilobase plasmid DNA heteroduplex.

The success of this compound in the specific recognition of base mismatches is even more remarkable because the design strategy which formed the foundation of its construction is based on a very simple idea. The exploitation of destabilization and structural disorder at a site as a molecular recognition element is a novel approach for the design of a small binding molecule. As such, the work described here also stands as a much more general "proof of concept" indicating that this recognition strategy is an effective way to design compounds of both high binding affinity and specificity.

Like many programs of research, however, some of the discoveries made along the path to achieving the final objective have proven as exciting and profitable as the primary goal itself. Efforts directed toward the synthesis of chrysenequinone diimine intercalators resulted in the development of synthetic methods which have made

entirely new classes of molecules readily available for study which would have been synthetically cumbersome or inaccessible by earlier methodologies. The new compounds reported here represent only a small fraction of these novel methods' potential synthetic variety. As an auxiliary benefit, these condensation-based synthetic schemes have also provided far superior routes to many already characterized compounds. Methodology was also developed for the quantitative measurement of thermodynamic binding constants for small molecules which bind to and cleave nucleic acids. Such measurements, which are absolutely critical for the characterization of molecular recognition processes, make it possible to examine the binding of these DNA cleaving compounds without the convoluting influence of differences in cleavage efficiency from binding site to binding site. The discovery that rhodium(III) chrysi and phi complexes cleave DNA with visible light and do so photocatalytically has revealed an entirely new area of the photochemistry of these complexes and their reactivity with DNA. While a number of these peripheral discoveries could be fully characterized and now stand as finished tools to be applied by later researchers, not every tantalizing lead could be followed as it often seemed that every answered question raised compelling and exciting unanswered questions to replace it. It is these questions which ensure that there will never be a shortage of research problems associated with these molecules and their interactions and reactions with DNA for subsequent researchers to address.

Appendix 1:

Crystallographic Characterization of $[Rh(bpy)_2(chrysi)]Cl_3 \cdot 3CH_3CN \cdot 2H_2O$*

* The structure of this molecule was solved and the contents of this appendix prepared by Lawrence Henling of the Caltech X-Ray Crystallography Facility whose efforts and assistance are gratefully acknowledged.

Table A1.1: Crystal and Intensity Collection Data for Bis 2,2'-bipyidyl chrysenequinone diimine rhodium(III) chloride $\cdot 3CH_3CN \cdot 2H_2O$

Formula: $C_{44}H_{41}Cl_3N_9O_2Rh$	Formula weight: 937.13
Crystal color: Brown	Habit: Block
Crystal size: $0.13 \times 0.22 \times 0.33$ mm	$\rho_{calc} = 1.507$ g cm^{-3}
Crystal System: Triclinic	Space group: $P\bar{1}$ (#2)
$a = 9.079(3)$Å	$\alpha = 86.71(3)°$
$b = 10.970(3)$Å	$\beta = 89.21(3)°$
$c = 21.192(8)$Å	$\gamma = 78.58(3)°$
V = 2065.4(12)Å^3	$Z = 2$
Lattice parameters: 25 reflections,	$12° \leq \theta \leq 15°$
$\mu = 6.57$ cm^{-1} ($\mu T_{max} = 0.14$)	
CAD-4 diffractometer	ω scan
MoKα, $\lambda = 0.7107$Å	Graphite monochromator
2θ range: 3°–50°	$-10 \leq h \leq 10, -13 \leq k \leq 13, -25 \leq l \leq 25$
T = 85K	$F_{000} = 960$
Number of reflections measured: 15224	Number of independent reflections: 7250
Number with $F_o^2 > 0$: 7006	Number with $F_o^2 > 3\sigma(F_o^2)$: 6433
Standard reflections: 3 every 75 min	Variation: Within counting statistics
GOF_{merge} : 0.98 for 7250 multiples	R_{merge} : 0.017 for 6744 duplicates
Number used in refinement: 7250	Criterion: All reflections used

Final $R(F_o)$: 0.026 for 6433 reflections with $F_o^2 > 3\sigma(F_o^2)$

Final $R(F_o)$: 0.030 for 7006 reflections with $F_o^2 > 0$

Final weighted $R(F_o^2)$: 0.063 for 7250 reflections

Final goodness of fit: 1.81 for 728 parameters and 7250 reflections

$(\Delta/\sigma)_{max}$ in final least squares cycle: 0.02

$\Delta\rho_{max}$: 0.75 eÅ^{-3}, $\Delta\rho_{min}$: -0.56 eÅ^{-3} in final difference map

Table A1.2: Final Heavy Atom Parameters for
Bis 2,2'-bipyidyl chrysenequinone diimine rhodium(III) chloride
$\cdot 3CH_3CN \cdot 2H_2O$

x, y, z and U_{eq}

Atom	x	y	z	U_{eq}
Rh	0.07663(2)	0.44184(2)	0.23928(1)	0.00770(5)
Cl1	−0.25851(7)	0.75302(6)	0.28821(3)	0.0209(1)
Cl2	0.53452(6)	0.33062(6)	0.22957(3)	0.0176(1)
Cl3†	0.5929(7)	0.1022(5)	−0.0136(3)	0.0161(6)
Cl4†	0.8822(6)	0.0038(4)	0.0448(2)	0.0190(6)
O3†	0.574(2)	0.110(2)	−0.0273(7)	0.019(2)
O4†	0.884(2)	−0.007(1)	0.0646(5)	0.029(2)
O5	0.6054(3)	0.5090(2)	0.33744(10)	0.0317(5)
N1	0.1647(2)	0.5932(2)	0.21162(9)	0.0098(4)
N2	−0.0908(2)	0.5358(2)	0.18157(9)	0.0096(4)
N3	0.1590(2)	0.3416(2)	0.16400(9)	0.0095(4)
N4	−0.0208(2)	0.2915(2)	0.25483(9)	0.0098(4)
N5	0.0060(2)	0.5279(2)	0.31834(9)	0.0101(4)
N6	0.2385(2)	0.3640(2)	0.30089(9)	0.0097(4)
C1	0.2978(3)	0.6158(2)	0.23100(11)	0.0117(5)
C2	0.3548(3)	0.7153(2)	0.20522(12)	0.0143(5)
C3	0.2763(3)	0.7921(2)	0.15811(12)	0.0159(5)
C4	0.1377(3)	0.7711(2)	0.13955(12)	0.0149(5)
C5	0.0833(3)	0.6715(2)	0.16742(10)	0.0108(5)
C6	−0.0628(3)	0.6419(2)	0.15218(11)	0.0111(5)

Atom	x	y	z	U_{eq}
C7	−0.1682(3)	0.7167(2)	0.11262(11)	0.0137(5)
C8	−0.3045(3)	0.6814(2)	0.10290(11)	0.0150(6)
C9	−0.3309(3)	0.5727(2)	0.13316(11)	0.0142(7)
C10	−0.2226(3)	0.5022(2)	0.17246(11)	0.0129(5)
C11	0.2609(3)	0.3701(2)	0.12198(11)	0.0122(5)
C12	0.3054(3)	0.2992(2)	0.07087(11)	0.0152(6)
C13	0.2420(3)	0.1977(2)	0.06161(12)	0.0153(6)
C14	0.1385(3)	0.1667(2)	0.10520(11)	0.0137(5)
C15	0.1000(2)	0.2385(2)	0.15674(11)	0.0108(5)
C16	0.0014(3)	0.2089(2)	0.20861(11)	0.0113(5)
C17	−0.0634(3)	0.1043(2)	0.21292(12)	0.0158(5)
C18	−0.1491(3)	0.0832(2)	0.26550(12)	0.0173(6)
C19	−0.1716(3)	0.1685(2)	0.31169(12)	0.0155(6)
C20	−0.1070(3)	0.2716(2)	0.30493(11)	0.0129(6)
C21	0.0899(2)	0.4988(2)	0.36774(11)	0.0094(5)
C22	0.2211(2)	0.3945(2)	0.35905(11)	0.0096(5)
C23	0.3182(3)	0.3431(2)	0.41262(11)	0.0106(5)
C24	0.4187(3)	0.2236(2)	0.41186(11)	0.0118(5)
C25	0.4166(3)	0.1341(2)	0.36620(11)	0.0136(5)
C26	0.5167(3)	0.0229(2)	0.36809(12)	0.0154(5)

Atom	x	y	z	U_{eq}
C27	0.6262(3)	−0.0068(2)	0.41588(12)	0.0162(6)
C28	0.6279(3)	0.0733(2)	0.46244(12)	0.0169(6)
C29	0.5231(3)	0.1882(2)	0.46268(11)	0.0141(6)
C30	0.5147(3)	0.2662(2)	0.51387(12)	0.0161(6)
C31	0.4098(3)	0.3735(2)	0.51635(11)	0.0145(5)
C32	0.3090(3)	0.4155(2)	0.46545(11)	0.0116(5)
C33	0.1939(3)	0.5314(2)	0.47068(11)	0.0118(5)
C34	0.1928(3)	0.6080(2)	0.52137(11)	0.0137(5)
C35	0.0817(3)	0.7129(2)	0.52690(11)	0.0156(5)
C36	−0.0348(3)	0.7439(2)	0.48355(11)	0.0151(5)
C37	−0.0367(3)	0.6702(2)	0.43286(11)	0.0131(5)
C38	0.0785(3)	0.5664(2)	0.42539(11)	0.0114(5)
C39	0.4394(3)	0.0336(2)	0.20067(12)	0.0202(6)
C40	0.5725(3)	0.0270(3)	0.16099(14)	0.0263(7)
N7	0.3335(3)	0.0380(2)	0.23110(11)	0.0250(5)
C41	0.1485(4)	0.8547(3)	0.33137(15)	0.0344(8)
C42	0.1164(3)	0.9466(3)	0.37906(13)	0.0235(6)
N8	0.0915(3)	1.0190(2)	0.41597(12)	0.0338(6)
C43	0.2098(6)	0.6730(4)	−0.03079(23)	0.0623(14)
C44†	0.3227(6)	0.6071(5)	−0.00366(25)	0.0213(12)
C45†	0.1235(7)	0.5960(6)	−0.01880(29)	0.0301(15)
N9†	0.4280(5)	0.5483(4)	0.01874(24)	0.0315(12)
N10†	0.0355(7)	0.5347(5)	−0.00937(32)	0.0511(20)

[a] $U_{eq} = \frac{1}{3}\sum_i \sum_j [U_{ij}(a_i^* a_j^*)(\vec{a}_i \cdot \vec{a}_j)]$

† Population: 0.5

Table A1.3: Distances and Angles for

Bis 2,2'-bipyidyl chrysenequinone diimine rhodium(III) chloride

$\cdot 3CH_3CN \cdot 2H_2O$

	Distance(Å)		Distance(Å)
Rh –N1	2.035(2)	C8 –H8	0.91(3)
Rh –N2	2.039(2)	C9 –C10	1.381(3)
Rh –N3	2.039(2)	C9 –H9	0.93(3)
Rh –N4	2.030(2)	C10 –H10	0.94(3)
Rh –N5	2.006(2)	C11 –C12	1.379(3)
Rh –N6	2.005(2)	C11 –H11	0.93(2)
H6 ··· H25	1.96(4)	C12 –C13	1.375(3)
Cl3 ··· O3	0.338(16)	C12 –H12	0.93(3)
Cl4 ··· O4	0.427(15)	C13 –C14	1.385(3)
O4 –H4a	0.78(10)	C13 –H13	0.93(3)
O4 –H4b	0.73(12)	C14 –C15	1.383(3)
O5 –H5a	0.82(3)	C14 –H14	0.89(3)
O5 –H5b	0.88(4)	C15 –C16	1.470(3)
N1 –C1	1.355(3)	C16 –C17	1.387(3)
N1 –C5	1.355(3)	C17 –C18	1.385(4)
N2 –C6	1.356(3)	C17 –H17	0.92(3)
N2 –C10	1.340(3)	C18 –C19	1.378(4)
N3 –C11	1.344(3)	C18 –H18	0.95(3)
N3 –C15	1.362(3)	C19 –C20	1.373(3)
N4 –C16	1.358(3)	C19 –H19	0.88(3)
N4 –C20	1.344(3)	C20 –H20	0.94(2)
N5 –C21	1.291(3)	C21 –C22	1.497(3)
N5 –H5	0.85(3)	C21 –C38	1.457(3)
N6 –C22	1.295(3)	C22 –C23	1.463(3)
N6 –H6	0.86(3)	C23 –C24	1.443(3)
C1 –C2	1.380(3)	C23 –C32	1.401(3)
C1 –H1	0.95(2)	C24 –C25	1.420(3)
C2 –C3	1.378(4)	C24 –C29	1.429(3)
C2 –H2	0.96(3)	C25 –C26	1.369(3)
C3 –C4	1.389(4)	C25 –H25	0.93(2)
C3 –H3	0.91(3)	C26 –C27	1.408(4)
C4 –C5	1.386(3)	C26 –H26	0.95(3)
C4 –H4	0.89(3)	C27 –C28	1.361(4)
C5 –C6	1.470(3)	C27 –H27	0.94(3)
C6 –C7	1.387(3)	C28 –C29	1.422(3)
C7 –C8	1.389(3)	C28 –H28	0.94(3)
C7 –H7	0.89(2)	C29 –C30	1.412(3)
C8 –C9	1.383(3)	C30 –C31	1.363(4)

	Distance(Å)		Angle(°)
C30 –H30	1.00(3)	N1 –Rh –N2	80.0(1)
C31 –C32	1.420(3)	N1 –Rh –N3	94.9(1)
C31 –H31	0.91(3)	N1 –Rh –N4	172.4(1)
C32 –C33	1.486(3)	N1 –Rh –N5	87.7(1)
C33 –C34	1.400(3)	N1 –Rh –N6	97.1(1)
C33 –C38	1.411(3)	N2 –Rh –N3	87.7(1)
C34 –C35	1.381(3)	N2 –Rh –N4	94.2(1)
C34 –H34	0.90(3)	N2 –Rh –N5	97.1(1)
C35 –C36	1.388(4)	N2 –Rh –N6	174.5(1)
C35 –H35	0.96(3)	N3 –Rh –N4	79.9(1)
C36 –C37	1.383(3)	N3 –Rh –N5	174.8(1)
C36 –H36	0.95(3)	N3 –Rh –N6	97.2(1)
C37 –C38	1.400(3)	N4 –Rh –N5	97.9(1)
C37 –H37	0.95(3)	N4 –Rh –N6	89.2(1)
C39 –C40	1.455(4)	N5 –Rh –N6	78.0(1)
C39 –N7	1.145(4)	Rh –N1 –C1	125.5(2)
C40 –H40a	0.98(3)	Rh –N1 –C5	114.7(1)
C40 –H40b	0.99(3)	Rh –N2 –C6	115.0(1)
C40 –H40c	0.96(3)	Rh –N2 –C10	125.3(2)
C41 –C42	1.454(4)	Rh –N3 –C11	126.1(2)
C42 –N8	1.136(4)	Rh –N3 –C15	114.7(1)
C41 –H41a	0.98(3)	Rh –N4 –C16	115.2(1)
C41 –H41b	0.98(4)	Rh –N4 –C20	125.3(2)
C41 –H41c	0.94(3)	Rh –N5 –C21	117.2(2)
C43 –C44	1.257(7)	Rh –N5 –H5	116.3(21)
C43 –C45	1.275(8)	Rh –N6 –C22	117.6(2)
C43 –H43a	0.91(4)	Rh –N6 –H6	121.2(20)
C43 –H43b	0.82(5)	H4b –O4 –H4a	91(12)
C44 –N9	1.135(7)	H5b –O5 –H5a	111.3(32)
C45 –N10	1.150(9)	C5 –N1 –C1	119.6(2)
		C10 –N2 –C6	119.7(2)
		C15 –N3 –C11	119.2(2)
		C20 –N4 –C16	119.5(2)
		H5 –N5 –C21	125.2(21)
		H6 –N6 –C22	121.3(21)
		C2 –C1 –N1	121.3(2)
		H1 –C1 –N1	116.9(15)
		H1 –C1 –C2	121.7(15)

	Angle(°)		Angle(°)
C3 –C2 –C1	119.5(2)	H14 –C14 –C15	120.3(18)
H2 –C2 –C1	116.9(16)	C14 –C15 –N3	120.7(2)
H2 –C2 –C3	123.5(16)	C16 –C15 –N3	114.8(2)
C4 –C3 –C2	119.2(2)	C16 –C15 –C14	124.5(2)
H3 –C3 –C2	120.5(16)	C15 –C16 –N4	114.8(2)
H3 –C3 –C4	120.4(16)	C17 –C16 –N4	120.6(2)
C5 –C4 –C3	119.4(2)	C17 –C16 –C15	124.5(2)
H4 –C4 –C3	118.2(17)	C18 –C17 –C16	119.4(2)
H4 –C4 –C5	122.4(17)	H17 –C17 –C16	118.6(16)
C4 –C5 –N1	120.8(2)	H17 –C17 –C18	121.9(16)
C6 –C5 –N1	115.2(2)	C19 –C18 –C17	119.2(2)
C6 –C5 –C4	123.9(2)	H18 –C18 –C17	121.6(17)
C5 –C6 –N2	114.8(2)	H18 –C18 –C19	119.2(17)
C7 –C6 –N2	121.2(2)	C20 –C19 –C18	119.3(2)
C7 –C6 –C5	124.0(2)	H19 –C19 –C18	122.8(18)
C8 –C7 –C6	119.1(2)	H19 –C19 –C20	117.9(18)
H7 –C7 –C6	119.4(15)	C19 –C20 –N4	122.0(2)
H7 –C7 –C8	121.5(15)	H20 –C20 –N4	114.8(15)
C9 –C8 –C7	118.8(2)	H20 –C20 –C19	123.2(15)
H8 –C8 –C7	118.4(16)	C22 –C21 –N5	113.9(2)
H8 –C8 –C9	122.7(16)	C38 –C21 –N5	126.4(2)
C10 –C9 –C8	119.7(2)	C38 –C21 –C22	119.3(2)
H9 –C9 –C8	118.5(16)	C21 –C22 –N6	112.7(2)
H9 –C9 –C10	121.7(16)	C23 –C22 –N6	127.1(2)
C9 –C10 –N2	121.5(2)	C23 –C22 –C21	120.2(2)
H10 –C10 –N2	118.0(16)	C24 –C23 –C22	122.2(2)
H10 –C10 –C9	120.4(16)	C32 –C23 –C22	116.9(2)
C12 –C11 –N3	121.9(2)	C32 –C23 –C24	121.0(2)
H11 –C11 –N3	117.1(14)	C25 –C24 –C23	125.0(2)
H11 –C11 –C12	120.9(14)	C29 –C24 –C23	118.1(2)
C13 –C12 –C11	119.4(2)	C29 –C24 –C25	116.8(2)
H12 –C12 –C11	118.7(17)	C26 –C25 –C24	121.7(2)
H12 –C12 –C13	121.9(17)	H25 –C25 –C24	121.6(15)
C14 –C13 –C12	119.0(2)	H25 –C25 –C26	116.6(15)
H13 –C13 –C12	121.3(15)	C27 –C26 –C25	120.7(2)
H13 –C13 –C14	119.6(15)	H26 –C26 –C25	119.9(15)
C15 –C14 –C13	119.7(2)	H26 –C26 –C27	119.3(15)
H14 –C14 –C13	120.0(18)	C28 –C27 –C26	119.6(2)

			Angle(°)
H27	–C27	–C26	115.3(15)
H27	–C27	–C28	125.0(15)
C29	–C28	–C27	121.0(2)
H28	–C28	–C27	120.1(16)
H28	–C28	–C29	119.0(16)
C28	–C29	–C24	119.9(2)
C30	–C29	–C24	118.8(2)
C30	–C29	–C28	121.2(2)
C31	–C30	–C29	122.0(2)
H30	–C30	–C29	116.7(16)
H30	–C30	–C31	121.2(16)
C32	–C31	–C30	121.1(2)
H31	–C31	–C30	117.8(16)
H31	–C31	–C32	121.2(16)
C31	–C32	–C23	118.5(2)
C33	–C32	–C23	122.1(2)
C33	–C32	–C31	119.4(2)
C34	–C33	–C32	121.6(2)
C38	–C33	–C32	120.9(2)
C38	–C33	–C34	117.4(2)
C35	–C34	–C33	121.0(2)
H34	–C34	–C33	119.5(16)
H34	–C34	–C35	119.5(16)
C36	–C35	–C34	121.2(2)
H35	–C35	–C34	120.9(17)
H35	–C35	–C36	117.7(17)
C37	–C36	–C35	119.2(2)
H36	–C36	–C35	119.2(15)
H36	–C36	–C37	121.6(15)
C38	–C37	–C36	120.1(2)
H37	–C37	–C36	118.6(15)
H37	–C37	–C38	121.3(15)
C33	–C38	–C21	118.2(2)
C37	–C38	–C21	120.6(2)
C37	–C38	–C33	121.0(2)
N7	–C39	–C40	178.9(3)
H40a	–C40	–C39	108.3(19)
H40b	–C40	–C39	108.4(19)
H40c	–C40	–C39	105.4(20)
H40b	–C40	–H40a	107.2(26)
H40c	–C40	–H40a	113.5(27)
H40c	–C40	–H40b	113.8(27)
H41a	–C41	–C42	109.3(19)
H41b	–C41	–C42	113.8(23)
H41c	–C41	–C42	109.4(20)
H41b	–C41	–H41a	107.9(30)
H41c	–C41	–H41a	114.2(28)
H41c	–C41	–H41b	102.3(31)
N8	–C42	–C41	179.5(3)
C45	···C43	···C44	95.2(5)
H43a	–C43	–C44	112.1(25)
H43b	–C43	–C44	113.5(35)
H43a	–C43	–C45	123.2(25)
H43b	–C43	–C45	109.8(35)
H43b	–C43	–H43a	103.3(43)
N9	–C44	–C43	177.2(6)
N10	–C45	–C43	174.1(7)

Table A1.4: Final Refined Hydrogen Parameters (less four half atoms) for Bis 2,2'-bipyidyl chrysenequinone diimine rhodium(III) chloride ·3CH_3CN·2H_2O

x, y, z and U_{iso}

Atom	x	y	z	U_{iso}
H4a†	0.933(10)	−0.014(9)	0.034(5)	0.06(5)
H4b†	0.826(13)	0.040(11)	0.048(6)	0.12(6)
H5a	0.591(4)	0.465(3)	0.3088(16)	0.038(10)
H5b	0.624(4)	0.581(3)	0.3223(16)	0.045(11)
H5	−0.066(4)	0.591(3)	0.3142(15)	0.037(9)
H6	0.317(4)	0.313(3)	0.2889(14)	0.032(9)
H1	0.352(3)	0.558(2)	0.2615(12)	0.010(6)
H2	0.450(3)	0.726(2)	0.2210(12)	0.020(7)
H3	0.315(3)	0.855(2)	0.1390(12)	0.014(7)
H4	0.088(3)	0.822(2)	0.1089(13)	0.018(7)
H7	−0.148(3)	0.787(2)	0.0949(11)	0.003(6)
H8	−0.373(3)	0.732(2)	0.0771(12)	0.013(6)
H9	−0.423(3)	0.550(2)	0.1271(12)	0.018(7)
H10	−0.237(3)	0.426(2)	0.1917(12)	0.017(7)
H11	0.296(3)	0.443(2)	0.1274(10)	0.003(6)
H12	0.378(3)	0.322(2)	0.0435(13)	0.020(7)
H13	0.271(3)	0.147(2)	0.0279(12)	0.010(6)
H14	0.101(3)	0.099(3)	0.1010(13)	0.022(7)
H17	−0.046(3)	0.050(2)	0.1810(12)	0.012(6)
H18	−0.193(3)	0.011(3)	0.2704(13)	0.024(7)
H19	−0.226(3)	0.160(2)	0.3460(13)	0.023(7)
H20	−0.120(3)	0.334(2)	0.3341(11)	0.007(6)
H25	0.347(3)	0.148(2)	0.3334(12)	0.009(6)
H26	0.510(3)	−0.037(2)	0.3380(12)	0.011(6)
H27	0.690(3)	−0.084(2)	0.4136(11)	0.011(6)
H28	0.697(3)	0.052(2)	0.4959(13)	0.020(7)
H30	0.585(3)	0.237(2)	0.5495(13)	0.024(7)
H31	0.407(3)	0.418(2)	0.5513(12)	0.012(6)
H34	0.264(3)	0.588(2)	0.5509(12)	0.013(6)
H35	0.087(3)	0.770(3)	0.5590(13)	0.025(7)
H36	−0.110(3)	0.817(2)	0.4888(11)	0.011(6)
H37	−0.116(3)	0.693(2)	0.4029(12)	0.014(6)
H40a	0.546(3)	0.013(3)	0.1180(16)	0.038(9)
H40b	0.649(4)	−0.046(3)	0.1762(15)	0.040(9)
H40c	0.604(4)	0.106(3)	0.1646(15)	0.042(9)
H41a	0.214(4)	0.780(3)	0.3494(15)	0.041(9)
H41b	0.058(5)	0.830(4)	0.3150(18)	0.068(13)
H41c	0.188(4)	0.891(3)	0.2948(16)	0.044(10)
H43a	0.231(4)	0.699(3)	−0.0708(19)	0.058(12)
H43b	0.177(6)	0.738(5)	−0.0137(23)	0.096(18)

† Population: 0.5

Table A1.5: Anisotropic Displacement Parameters for

Bis 2,2'-bipyidyl chrysenequinone diimine rhodium(III) chloride

$\cdot 3CH_3CN \cdot 2H_2O$

Atom	U_{11}	U_{22}	U_{33}	U_{12}	U_{13}	U_{23}
Rh	0.0048(1)	0.0107(1)	0.0074(1)	−0.0010(1)	−0.0003(1)	−0.0007(1)
Cl1	0.0203(3)	0.0198(3)	0.0192(3)	0.0053(3)	−0.0041(3)	−0.0042(3)
Cl2	0.0105(3)	0.0195(3)	0.0230(3)	−0.0033(2)	0.0010(2)	−0.0022(2)
Cl3	0.0141(13)	0.0187(11)	0.0154(17)	−0.0025(8)	−0.0006(13)	−0.0013(11)
Cl4	0.0160(12)	0.0149(11)	0.0267(19)	−0.0048(8)	−0.0060(14)	0.0005(12)
O3	0.0118(43)	0.0293(42)	0.0168(69)	−0.0066(30)	−0.0050(36)	0.0004(37)
O4	0.0176(37)	0.0350(47)	0.0345(70)	−0.0060(28)	−0.0047(49)	0.0021(46)
O5	0.0423(13)	0.0339(13)	0.0207(11)	−0.0103(10)	−0.0033(9)	−0.0064(10)
N1	0.0088(10)	0.0107(10)	0.0095(10)	−0.0007(8)	0.0025(8)	−0.0030(8)
N2	0.0078(10)	0.0132(10)	0.0077(10)	−0.0012(8)	0.0014(8)	−0.0026(8)
N3	0.0066(9)	0.0113(10)	0.0101(10)	−0.0006(8)	−0.0021(8)	−0.0009(8)
N4	0.0068(9)	0.0122(10)	0.0095(10)	−0.0003(8)	−0.0033(8)	0.0016(8)
N5	0.0073(10)	0.0109(10)	0.0119(10)	−0.0013(8)	0.0004(8)	−0.0003(8)
N6	0.0080(10)	0.0102(10)	0.0111(10)	−0.0020(8)	0.0014(8)	−0.0014(8)
C1	0.0077(11)	0.0142(12)	0.0123(12)	0.0006(9)	−0.0015(9)	−0.0029(10)
C2	0.0097(12)	0.0169(13)	0.0173(13)	−0.0035(10)	0.0027(10)	−0.0065(10)
C3	0.0181(13)	0.0138(13)	0.0176(13)	−0.0075(10)	0.0036(10)	−0.0015(10)
C4	0.0167(13)	0.0138(13)	0.0133(13)	−0.0013(10)	−0.0006(10)	0.0013(10)
C5	0.0108(12)	0.0133(12)	0.0078(11)	−0.0005(9)	0.0012(9)	−0.0024(9)
C6	0.0106(12)	0.0124(12)	0.0099(12)	−0.0010(9)	0.0018(9)	−0.0023(9)
C7	0.0138(12)	0.0136(13)	0.0126(12)	−0.0006(10)	0.0001(10)	0.0010(10)
C8	0.0088(12)	0.0216(14)	0.0116(12)	0.0044(10)	−0.0026(10)	−0.0008(10)
C9	0.0060(12)	0.0227(14)	0.0138(12)	−0.0016(10)	−0.0016(9)	−0.0029(10)
C10	0.0117(12)	0.0165(13)	0.0114(12)	−0.0039(10)	0.0010(9)	−0.0060(10)
C11	0.0089(12)	0.0126(12)	0.0149(12)	−0.0021(10)	−0.0020(9)	0.0001(10)
C12	0.0100(12)	0.0213(14)	0.0129(13)	−0.0001(10)	0.0012(10)	−0.0008(10)
C13	0.0116(12)	0.0191(13)	0.0134(13)	0.0030(10)	−0.0012(10)	−0.0061(11)
C14	0.0129(12)	0.0128(13)	0.0158(13)	−0.0028(10)	−0.0033(10)	−0.0024(10)
C15	0.0067(11)	0.0121(12)	0.0129(12)	0.0002(9)	−0.0046(9)	−0.0008(9)
C16	0.0074(11)	0.0130(12)	0.0128(12)	−0.0006(9)	−0.0047(9)	0.0011(9)
C17	0.0133(12)	0.0158(13)	0.0193(13)	−0.0045(10)	−0.0018(10)	−0.0028(11)
C18	0.0138(13)	0.0176(14)	0.0216(14)	−0.0070(10)	−0.0050(10)	0.0045(11)
C19	0.0115(12)	0.0238(14)	0.0117(13)	−0.0062(10)	−0.0016(10)	0.0045(10)
C20	0.0095(12)	0.0197(13)	0.0087(12)	−0.0016(10)	−0.0021(9)	0.0011(10)
C21	0.0065(11)	0.0113(12)	0.0114(12)	−0.0049(9)	0.0015(9)	0.0011(9)
C22	0.0064(11)	0.0107(12)	0.0130(12)	−0.0047(9)	0.0012(9)	−0.0002(9)
C23	0.0065(11)	0.0148(12)	0.0108(12)	−0.0038(9)	0.0001(9)	0.0014(9)
C24	0.0076(11)	0.0161(12)	0.0122(12)	−0.0046(9)	0.0026(9)	0.0027(10)
C25	0.0104(12)	0.0175(13)	0.0132(12)	−0.0036(10)	−0.0013(10)	0.0004(10)

Atom	U_{11}	U_{22}	U_{33}	U_{12}	U_{13}	U_{23}
C26	0.0148(13)	0.0142(13)	0.0169(13)	−0.0021(10)	0.0035(10)	−0.0014(10)
C27	0.0131(13)	0.0144(13)	0.0193(14)	0.0006(10)	0.0033(10)	0.0027(10)
C28	0.0123(13)	0.0221(14)	0.0151(13)	−0.0020(10)	−0.0015(10)	0.0056(11)
C29	0.0092(12)	0.0178(13)	0.0156(13)	−0.0041(10)	0.0001(10)	0.0027(10)
C30	0.0125(12)	0.0220(14)	0.0138(13)	−0.0044(10)	−0.0029(10)	0.0040(10)
C31	0.0139(12)	0.0194(13)	0.0112(12)	−0.0054(10)	−0.0009(10)	−0.0021(10)
C32	0.0091(11)	0.0145(12)	0.0123(12)	−0.0058(9)	0.0011(9)	0.0014(9)
C33	0.0110(12)	0.0153(12)	0.0101(12)	−0.0058(9)	0.0014(9)	0.0012(9)
C34	0.0143(13)	0.0174(13)	0.0098(12)	−0.0047(10)	−0.0027(10)	0.0012(10)
C35	0.0196(13)	0.0173(13)	0.0114(12)	−0.0066(11)	0.0021(10)	−0.0031(10)
C36	0.0159(13)	0.0156(13)	0.0131(12)	−0.0017(11)	0.0034(10)	−0.0011(10)
C37	0.0119(12)	0.0160(13)	0.0115(12)	−0.0031(10)	−0.0010(10)	−0.0008(10)
C38	0.0089(11)	0.0136(12)	0.0123(12)	−0.0038(9)	0.0030(9)	−0.0021(9)
C39	0.0250(15)	0.0174(14)	0.0183(14)	−0.0032(11)	−0.0114(12)	−0.0021(11)
C40	0.0193(15)	0.0345(18)	0.0257(16)	−0.0050(13)	−0.0004(12)	−0.0081(13)
N7	0.0230(13)	0.0307(14)	0.0220(12)	−0.0059(10)	−0.0045(10)	−0.0042(10)
C41	0.0508(22)	0.0267(18)	0.0250(17)	−0.0063(16)	0.0098(15)	−0.0029(14)
C42	0.0216(14)	0.0244(15)	0.0226(15)	−0.0014(12)	−0.0014(11)	0.0032(12)
N8	0.0321(14)	0.0346(15)	0.0315(14)	0.0035(11)	−0.0074(11)	−0.0087(12)
C43	0.1082(40)	0.0316(22)	0.0484(27)	−0.0148(25)	−0.0107(26)	−0.0081(20)
C44	0.0256(31)	0.0166(27)	0.0243(29)	−0.0104(24)	−0.0081(25)	−0.0002(23)
C45	0.0273(34)	0.0224(32)	0.0371(36)	0.0059(27)	−0.0053(27)	−0.0090(26)
N9	0.0304(29)	0.0297(28)	0.0372(30)	−0.0153(23)	−0.0105(24)	0.0094(23)
N10	0.0408(42)	0.0389(42)	0.0641(45)	0.0135(29)	0.0044(32)	0.0019(32)

The form of the displacement factor is:

$$\exp -2\pi^2(U_{11}h^2a^{*^2} + U_{22}k^2b^{*^2} + U_{33}\ell^2c^{*^2} + 2U_{12}hka^*b^* + 2U_{13}h\ell a^*c^* + 2U_{23}k\ell b^*c^*)$$

Table A1.6: Distances and Angles Involving Hydrogen Bonding for Bis 2,2'-bipyidyl chrysenequinone diimine rhodium(III) chloride ·3CH_3CN·2H_2O

		Distance(Å)				Angle(°)
Cl1	···N5	3.128(2)	O5	···Cl1^{i}	···N5^{i}	70.5(1)
Cl1	···H5	2.28(3)	N6	···Cl2	···O5	80.7(1)
Cl1^{i}	···O5	3.276(2)	O3	···Cl3^{ii}	···O4^{ii}	95.6(4)
Cl1^{i}	···H5b	2.42(4)	O4	···Cl4^{iii}	···O3^{iii}	101.6(4)
Cl2	···O5	3.244(2)	Cl4	···O3	···Cl3^{ii}	98.1(4)
Cl2	···N6	3.034(2)	Cl4^{iii}	···O4	···Cl3	98.1(4)
Cl2	···H5a	2.42(3)	Cl2	···O5	···Cl1^{i}	116.4(1)
Cl2	···H6	2.36(3)	O4	–H4a	···Cl4^{iii}	165.5(95)
Cl3	···O4	3.129(15)	O4	–H4b	···Cl3	152.6(123)
Cl3	···H4b	2.46(12)	O5	–H5a	···Cl2	175.7(31)
Cl3^{ii}	···O3	3.103(16)	O5	–H5b	···Cl1^{i}	164.7(31)
Cl4	···O3	3.184(16)	N5	–H5	···Cl1	171.9(29)
Cl4^{iii}	···O4	3.124(15)	N6	–H6	···Cl2	135.5(26)
Cl4^{iii}	···H4a	2.36(10)	H4a	–O4	–H4b	91.(12)
O4	–H4a	0.78(10)	H5a	–O5	–H5b	111.(3)
O4	–H4b	0.73(12)				
O5	–H5a	0.82(3)				
O5	–H5b	0.88(4)				
N5	–H5	0.85(3)				
N6	–H6	0.86(3)				

Symmetry code $(i)\ 1+x,y,z\ \ (ii)\ 1-x,-y,-z\ \ (iii)\ 2-x,-y,-z$

Table A1.7: Observed and Calculated Structure Factors for Bis 2,2'-bipyidyl chrysenequinone diimine rhodium(III) chloride ·3CH_3CN·2H_2O

The columns contain, in order, ℓ, $10F_{obs}$, $10F_{calc}$ and $10\sigma F_{obs}$. A minus sign preceding F_{obs} indicates that F^2_{obs} is negative.

BAJ1 Bis 2-2'bipyridyl chrysenequinone diimine rhodium(III) chloride . 3 acetonitrile . 2 water

-10 1 1

1	267	264	7
2	315	327	7
3	317	313	7
4	316	321	7
5	412	426	7
6	269	260	7

-10 2 1

1	352	347	7
2	384	391	7
3	307	309	7

-9 1 1

1	313	309	6
2	181	162	7
3	343	338	6
4	105	108	9
5	233	224	7
6	242	238	7
7	321	324	7
8	432	430	7
9	168	165	7
10	306	302	7
11	398	384	7
12	407	400	7

-9 2 1

1	120	129	8
2	297	285	6
3	70	49	11
4	282	279	6
5	199	204	7
6	253	238	7
7	113	123	9
8	323	322	7
9	327	335	7
10	265	259	7
11	41	66	18

-9 3 1

1	354	375	7
2	312	315	7
3	31	35	20
4	118	127	9
5	169	182	7
6	105	101	9
7	71	64	12
8	187	199	7
9	360	373	7

-9 4 1

1	119	122	9
2	200	217	7
3	74	64	12
4	126	126	9
5	81	79	11
6	246	269	7
7	171	180	8

-8 1 1

1	99	83	8
2	252	251	6
3	525	521	7
4	396	380	6
5	393	382	6
6	250	260	6
7	458	463	6
8	89	93	9
9	422	424	6
10	93	82	9
11	281	279	6
12	173	169	7
13	299	292	7
14	67	71	12
15	184	164	7

-8 2 1

1	332	344	6
2	353	361	6
3	540	545	7
4	237	237	6
5	551	549	7
6	287	287	6
7	257	255	6
8	274	282	6
9	459	455	7
10	265	269	6
11	429	429	7
12	325	326	7
13	443	450	7
14	396	387	7
15	176	181	8

-8 3 1

1	174	194	7
2	278	289	6
3	357	367	6
4	279	264	6
5	377	374	6
6	469	470	7
7	346	344	6
8	520	517	7
9	153	161	7
10	194	181	7
11	276	274	7
12	595	592	8
13	35	60	19
14	334	338	7

-8 4 1

1	327	328	6
2	473	478	7
3	275	283	6
4	249	241	6
5	134	139	8
6	65	70	12
7	123	118	8
8	260	265	7
9	386	401	7
10	449	451	7
11	214	224	7
12	197	195	7

-8 5 1

1	373	383	7
2	611	614	8
3	125	109	8
4	333	340	7
5	125	118	8
6	54	59	14
7	170	182	7
8	399	410	7
9	129	118	8
10	418	421	7

-8 6 1

1	104	86	7
2	71	72	12
3	44	8	17
4	271	289	7
5	203	197	7
6	341	360	7
7	255	224	7

-7 1 1

1	454	457	6
2	89	75	8
3	437	441	6
4	163	146	6
5	670	657	7
6	100	90	8
7	300	293	6
8	137	112	7
9	422	413	6
10	68	19	10
11	107	102	8
12	114	102	8
13	37	18	17
14	-31	7	18
15	366	369	7
16	98	103	9
17	128	143	8
18	65	72	13

-7 2 1

1	127	118	7
2	504	507	6
3	633	619	7
4	59	43	11
5	217	213	6
6	347	344	6
7	422	413	6
8	114	99	7
9	95	75	8
10	162	172	7
11	81	42	10
12	150	156	7
13	-37	37	16
14	186	182	7
15	245	243	7
16	244	241	7
17	510	522	7

-7 3 1

1	429	429	6
2	151	141	6
3	339	325	6
4	227	221	6
5	619	620	7
6	291	294	6
7	89	93	9
8	177	173	6
9	106	110	8
10	-55	41	11
11	66	75	12
12	333	334	6
13	335	326	6
14	137	138	8
15	125	114	8
16	123	140	9
17	386	405	7

-7 4 1

1	175	176	6
2	147	134	7
3	466	470	6
4	237	231	6
5	304	296	6
6	200	206	6
7	541	529	7
8	76	59	10
9	508	518	7
10	76	51	11
11	608	609	7
12	318	320	7
13	239	236	7
14	206	219	7
15	239	233	7

-7 5 1

1	489	495	7
2	227	238	6
3	691	712	8
4	109	75	7
5	414	394	6
6	444	467	7
7	722	721	8
8	213	197	7
9	538	535	7
10	452	450	7
11	303	312	7
12	502	497	7
13	198	203	7
14	481	488	7

-7 6 1

1	386	382	6
2	313	323	6
3	350	344	6
4	218	212	7
5	209	192	7
6	200	203	7
7	65	57	12
8	409	408	7
9	164	169	7
10	613	612	8
11	214	216	7
12	402	398	7

-7 7 1

1	63	90	13
2	206	190	7
3	93	95	10
4	326	324	7
5	49	57	15
6	404	407	7
7	55	78	14
8	424	427	7
9	263	265	7

-7 8 1

1	231	233	7
2	445	434	7

-6 1 1

1	374	362	5
2	644	629	7
3	158	134	5
4	604	589	6
5	67	62	9
6	258	259	5
7	345	339	5
8	356	348	5
9	433	434	6
10	515	518	6
11	490	502	6
12	242	240	6
13	359	363	6
14	380	384	6
15	791	788	8
16	253	260	6
17	516	518	7
18	165	173	7
19	503	501	7
20	65	50	13

-6 2 1

1	533	530	6
2	639	624	7
3	757	735	8
4	557	548	6
5	811	811	8
6	422	403	6
7	776	771	8
8	108	90	7
9	623	610	7
10	137	132	7
11	42	33	14
12	376	378	6
13	207	197	6
14	154	144	7
15	657	670	6
16	200	209	7
17	294	293	6
18	322	330	7
19	400	408	7

-6 3 1

1	880	882	8
2	363	373	5
3	559	557	6
4	452	455	6
5	590	589	7
6	279	267	5
7	705	698	7
8	153	149	6
9	228	237	6
10	-38	11	14
11	173	177	6
12	70	58	10
13	118	110	8
14	451	446	7
15	639	641	8
16	192	193	7
17	35	28	19
18	334	330	7
19	403	416	7

-6 4 1

1	543	550	6
2	200	193	6
3	510	514	6
4	87	92	8
5	335	322	6
6	180	197	6
7	447	460	6
8	279	274	6
9	359	355	6
10	169	150	6
11	526	526	7
12	193	184	6
13	346	353	6
14	331	334	6
15	24	4	22
16	345	339	7
17	419	430	7
18	387	399	7

-6 5 1

1	388	399	6
2	357	348	6
3	47	38	13
4	277	276	6
5	398	397	6
6	541	551	7
7	189	191	6
8	25	6	20
9	438	436	6
10	316	312	6
11	292	301	6
12	508	499	7
13	359	356	6
14	149	148	8
15	204	214	7
16	183	193	7
17	-36	32	18

-6 6 1

1	332	335	6
2	88	76	9
3	518	523	7
4	265	273	6
5	38	44	16
6	148	168	5
7	411	424	6
8	256	253	6
9	29	65	20
10	171	172	7
11	148	144	7
12	172	165	7
13	54	60	14
14	181	187	7
15	139	135	8

-6 7 1

1	238	224	6
2	117	124	8
3	157	159	7
4	128	134	8
5	164	160	7
6	232	228	7
7	48	68	15
8	-15	18	27
9	108	121	9
10	216	216	7
11	-23	11	23
12	350	350	7
13	-36	32	18

-6 8 1

1	117	120	9
2	-37	20	17
3	170	168	7
4	305	296	7
5	-23	47	23
6	134	123	8
7	95	100	10
8	483	482	7
9	16	5	28
10	401	402	7

-6 9 1

1	7	7	35
2	352	353	7
3	-15	6	29
4	436	414	7

-5 1 1

1	253	233	4
2	618	600	6
3	295	271	5
4	359	364	5
5	484	465	6
6	385	356	5
7	614	601	6
8	306	306	5
9	-47	34	10
10	155	146	6
11	-40	11	12
12	114	116	7
13	295	286	6
14	-41	22	13
15	70	63	10
16	492	500	7
17	270	263	6
18	312	315	6

19	362	359	7
20	354	366	7
21	284	293	7

-5 2 1

1	119	104	6
2	422	418	5
3	135	107	5
4	313	308	5
5	228	214	5
6	561	548	6
7	399	388	5
8	251	233	5
9	164	159	6
10	334	333	5
11	319	318	5
12	194	197	6
13	28	46	18
14	128	118	7
15	600	606	7
16	435	428	6
17	187	192	7
18	312	303	6
19	222	219	7
20	401	407	7
21	224	237	7

-5 3 1

1	109	90	6
2	382	391	5
3	526	521	6
4	553	557	6
5	352	343	5
6	458	461	6
7	310	305	5
8	566	564	6
9	259	267	5
10	280	274	5
11	251	235	6
12	464	465	6
13	409	407	6
14	577	575	7
15	337	335	6
16	334	336	6
17	144	152	7
18	-38	5	16
19	304	301	7
20	125	126	9

-5 4 1

1	460	449	6
2	423	427	6
3	366	366	5
4	654	658	7
5	375	374	5
6	517	525	6
7	530	530	6
8	370	371	6
9	398	391	6
10	547	548	7
11	211	211	6
12	98	92	8
13	571	576	7
14	292	293	6
15	768	768	8
16	44	16	16
17	468	464	7
18	190	182	7
19	362	377	7
20	299	293	7

-5 5 1

1	415	424	4
2	487	492	6
3	629	646	7
4	299	296	5
5	412	426	6
6	154	149	6
7	544	550	6
8	126	128	7
9	190	192	6
10	475	463	6
11	477	470	6
12	445	451	6
13	380	377	6
14	393	399	6
15	425	413	7
16	545	548	7
17	464	452	7
18	206	204	7
19	298	315	7

-5 6 1

1	591	591	7
2	200	199	6
3	385	387	6
4	213	218	6
5	657	653	7
6	61	73	11
7	598	610	7
8	291	289	6
9	546	546	7
10	335	334	6
11	337	338	6
12	323	323	6
13	457	454	7
14	407	397	7
15	298	276	7
16	300	301	7
17	146	157	8

-5 7 1

1	445	460	6
2	-42	13	13
3	304	292	6
4	452	469	6
5	599	594	7
6	180	181	6
7	495	498	7
8	233	231	6
9	327	331	6
10	360	342	6
11	252	256	6
12	439	435	7
13	62	57	13
14	236	255	7
15	27	55	22
16	371	370	7

-5 8 1

1	356	360	6
2	201	203	7
3	350	345	6
4	239	237	6
5	68	77	11
6	-51	10	12
7	108	110	9
8	212	205	7
9	22	6	24
10	129	130	8
11	83	89	11
12	476	494	7
13	35	52	19

-5 9 1

1	21	40	24
2	287	283	7
3	177	175	7
4	252	243	7
5	-38	58	17
6	397	391	7
7	149	159	8
8	196	188	7
9	54	35	15
10	518	513	7

-5 10 1

1	65	74	13
2	376	369	7
3	-60	22	12
4	350	320	7

-4 1 1

1	559	563	6
2	594	611	6
3	173	179	4
4	703	688	7
5	689	660	7
6	1048	1016	9
7	209	183	4
8	1055	1050	9
9	213	208	5
10	909	911	8
11	-20	40	18
12	503	507	6
13	100	97	7
14	150	153	6
15	104	110	7
16	153	148	6
17	128	140	7
18	504	499	7
19	463	457	7
20	184	184	7
21	374	385	7
22	327	322	7
23	273	270	7

-4 2 1

1	790	768	7
2	239	267	4
3	31	14	12
4	1008	991	8
5	50	23	9
6	755	754	7
7	-28	28	13
8	569	574	6
9	106	115	6
10	451	456	6
11	232	229	5
12	178	178	5
13	98	109	7
14	84	85	8
15	201	200	6
16	484	484	6
17	405	405	6
18	158	139	7
19	308	299	6
20	212	215	7
21	560	556	7
22	109	111	9

-4 3 1

1	120	110	5
2	512	522	6
3	46	42	10
4	270	270	5
5	448	450	5
6	55	68	9
7	421	432	5
8	564	563	6
9	749	750	7
10	144	142	6
11	399	408	6
12	176	187	6
13	419	420	6
14	493	501	6
15	403	410	6
16	358	356	6
17	287	289	6
18	129	144	8
19	395	395	7
20	154	143	7
21	56	60	14
22	-50	25	14

-4 4 1

1	80	96	7
2	608	594	6
3	747	753	6
4	256	254	5
5	606	608	6
6	316	317	5
7	660	662	5
8	105	101	7
9	399	396	6
10	420	424	6
11	312	314	5
12	297	300	6
13	581	569	7
14	416	411	6
15	214	224	6
16	-30	23	18
17	459	459	7
18	164	155	7
19	244	259	7
20	97	92	10
21	188	190	7

-4 5 1

1	429	436	5
2	713	706	7
3	603	607	6
4	268	275	5
5	649	642	7
6	312	305	5
7	180	178	5
8	344	344	5
9	370	355	6
10	244	248	6
11	334	337	6
12	400	399	6
13	763	762	8
14	172	167	6
15	62	80	11
16	246	257	6
17	425	421	7
18	184	183	7
19	253	278	7
20	186	205	7

-4 6 1

1	185	188	6
2	114	139	7
3	66	50	9
4	270	261	5
5	135	143	6
6	288	281	5
7	466	456	6
8	286	287	6
9	105	95	8
10	62	84	11
11	265	250	6
12	31	52	18
13	5	12	32
14	30	39	19
15	576	578	7
16	240	247	7
17	509	514	7
18	8	24	33
19	521	518	7

-4 7 1

1	75	90	9
2	-38	7	14
3	164	161	6
4	66	80	10
5	360	360	6
6	184	191	6
7	505	515	6
8	165	159	6
9	298	289	6
10	234	235	6
11	363	355	6
12	6	42	33
13	491	484	7
14	161	157	7
15	396	397	7
16	92	67	10
17	320	310	7
18	101	90	10

-4 8 1

1	679	687	8
2	136	111	7
3	341	342	6
4	63	63	11
5	637	637	7
6	83	59	9
7	437	421	6
8	81	72	10
9	449	447	7
10	-32	22	18
11	442	436	7
12	188	189	7
13	51	18	15
14	247	252	7
15	73	58	12
16	162	173	8

-4 9 1

1	297	300	6
2	45	32	15
3	553	534	7
4	258	266	6
5	378	367	6
6	256	249	6
7	282	276	6
8	251	250	7
9	151	144	8
10	347	345	7
11	169	167	7
12	505	503	7
13	-30	38	20

-4 10 1

1	150	136	8
2	333	333	7
3	63	79	13
4	177	165	7
5	189	188	7
6	543	520	7
7	46	31	16
8	549	546	7
9	144	116	8
10	796	750	9

-3 1 1

1	304	289	4
2	268	243	4
3	477	454	5
4	234	227	4
5	77	76	6
6	437	436	5
7	264	247	4
8	372	370	5
9	378	379	5
10	314	298	5
11	458	457	5
12	738	739	7
13	119	103	6
14	158	153	6
15	145	158	6
16	100	98	8
17	72	78	6
18	261	255	6
19	191	194	6
20	265	258	4
21	-61	21	10
22	238	243	7
23	161	170	8

-3 2 1

1	186	180	4
2	123	124	5
3	167	181	4
4	1024	1002	8
5	298	302	4
6	499	495	5
7	345	358	5
8	493	484	5
9	577	583	6
10	451	455	5
11	394	398	5
12	359	353	5
13	320	325	3
14	323	319	5
15	361	367	6
16	242	234	6
17	580	585	7
18	296	281	6
19	-47	12	12
20	28	51	20
21	155	176	7
22	446	445	7
23	98	117	10

-3 3 1

1	953	966	7
2	482	519	5
3	130	77	5
4	733	724	6
5	1048	1043	9
6	983	988	8
7	55	61	8
8	362	369	5
9	210	219	5
10	423	434	5
11	59	59	6
12	621	620	7
13	190	181	5
14	727	736	7
15	139	131	6
16	642	634	7
17	453	456	6
18	462	474	6
19	342	337	6
20	289	284	6
21	560	557	7
22	327	331	7
23	270	276	7

-3 4 1

1	419	420	5
2	505	518	5
3	202	212	4

4	857	864	8
5	94	84	6
6	421	416	5
7	88	90	7
8	669	675	7
9	246	256	5
10	570	572	6
11	331	331	5
12	357	356	5
13	842	845	8
14	629	649	7
15	737	755	8
16	397	397	6
17	657	670	7
18	198	185	6
19	294	303	6
20	252	256	7
21	345	331	7
22	-45	26	15

-3 5 1

1	51	32	9
2	1123	1135	10
3	781	782	7
4	432	446	5
5	451	447	5
6	695	704	7
7	480	484	6
8	489	495	6
9	85	71	8
10	259	260	5
11	656	662	7
12	526	536	5
13	369	370	6
14	814	814	8
15	350	345	6
16	323	330	6
17	629	646	7
18	28	24	20
19	615	620	8
20	229	251	7
21	168	172	8

-3 6 1

1	516	525	6
2	530	548	6
3	411	420	5
4	341	363	5
5	373	387	5
6	197	199	5
7	575	584	6
8	442	443	6
9	127	126	6
10	27	44	18
11	205	198	6
12	325	336	6
13	315	307	6
14	179	192	6
15	303	312	6
16	149	176	7
17	530	545	7
18	274	256	7
19	456	469	7
20	396	396	7

-3 7 1

1	603	613	7
2	332	337	5
3	334	348	5
4	210	215	5
5	297	307	5
6	203	204	6
7	120	123	7
8	220	217	6
9	228	222	6
10	421	431	6
11	216	209	6
12	210	208	6
13	182	181	6
14	334	322	6
15	259	249	6
16	104	109	9
17	238	234	7
18	161	153	8
19	431	439	7

-3 8 1

1	384	392	6
2	117	151	7
3	554	561	7
4	184	190	6
5	329	327	6
6	242	241	6
7	431	430	6
8	330	328	6
9	174	167	6
10	145	153	7
11	426	426	6
12	244	240	6
13	400	406	7
14	103	121	9
15	365	363	7
16	230	242	7
17	32	33	21

-3 9 1

1	306	286	6
2	234	258	6
3	531	535	7
4	208	207	6
5	399	411	6
6	78	70	10
7	299	297	6
8	111	109	8
9	377	370	6
10	259	272	6
11	65	73	12
12	53	90	14
13	106	133	9
14	228	249	7
15	118	123	9

-3 10 1

1	510	497	7
2	77	96	11
3	446	428	7
4	81	93	10
5	285	287	6
6	207	210	7
7	168	165	7
8	189	186	7
9	-54	19	12
10	123	134	8
11	160	151	8
12	401	400	7

-3 11 1

1	233	246	7
2	233	237	7
3	238	227	7
4	195	187	7
5	303	295	7
6	329	332	7
7	72	67	12
8	448	432	7

-2 1 1

1	1118	1095	9
2	155	104	4
3	1239	1198	10
4	319	315	4
5	537	530	5
6	314	313	4
7	937	934	8
8	786	773	7
9	748	751	7
10	514	515	5
11	730	727	7
12	37	74	12
13	80	56	7
14	471	472	6
15	82	61	8
16	204	195	5
17	173	165	6
18	285	272	6
19	289	285	6
20	512	516	7
21	224	227	6
22	564	563	7
23	75	17	11
24	374	364	7

-2 2 1

1	1213	1205	9
2	269	261	4
3	97	113	5
4	536	544	4
5	467	453	5
6	595	596	6
7	583	569	6
8	1045	1061	9
9	230	223	4
10	1140	1137	10
11	80	80	7
12	718	731	7
13	218	213	5
14	467	477	6
15	80	83	8
16	464	466	6
17	277	267	6
18	398	381	6
19	49	39	13
20	288	290	6
21	58	42	13
22	226	233	7
23	183	187	7
24	191	187	7

-2 3 1

1	51	45	8
2	620	638	6
3	223	218	4
4	251	270	4
5	512	507	5
6	826	850	7
7	651	638	6
8	1054	1052	9
9	669	658	7
10	963	971	9
11	352	352	5
12	1034	1025	9
13	333	331	5
14	85	93	8
15	-56	14	9
16	268	264	6
17	195	198	6
18	167	169	6
19	214	219	6
20	511	521	7
21	153	164	7
22	216	224	7
23	190	188	7
24	139	143	8

-2 4 1

1	228	214	4
2	496	501	5
3	52	70	9
4	841	840	8
5	20	12	17
6	738	731	7
7	115	134	5
8	37	23	12
9	742	731	7
10	512	504	6
11	424	416	5
12	353	338	5
13	125	128	6
14	534	532	6
15	712	713	7
16	-45	9	12
17	143	148	7
18	134	132	7
19	384	389	6
20	232	245	6
21	338	355	7
22	379	382	7
23	190	170	7

-2 5 1

1	314	326	3
2	148	149	5
3	65	59	7
4	94	98	6
5	143	125	5
6	130	146	5
7	318	308	5
8	151	138	5
9	104	89	6
10	41	40	12
11	96	84	7
12	543	537	6
13	117	115	7
14	596	595	7
15	134	117	7
16	419	411	6
17	420	421	6
18	302	305	6
19	28	42	20
20	343	332	6
21	79	105	11
22	233	238	7

-2 6 1

1	161	163	5
2	-39	9	11
3	146	147	5
4	411	434	5
5	362	369	5
6	147	159	5
7	70	51	8
8	704	712	7
9	31	22	15
10	-21	10	19
11	497	496	6
12	407	400	6
13	285	275	6
14	483	478	6
15	266	254	6
16	516	526	7
17	201	199	6
18	300	305	6
19	427	431	7
20	-43	41	15
21	120	93	9

-2 7 1

1	42	48	12
2	615	635	7
3	573	571	6
4	438	440	6
5	116	127	6
6	579	584	6
7	423	425	6
8	755	739	8
9	522	532	6
10	-33	27	15
11	589	592	7
12	318	316	6
13	200	187	6
14	112	130	8
15	383	390	6
16	178	170	7
17	400	399	7
18	-67	34	9
19	245	252	7
20	146	147	8

-2 8 1

1	353	343	6
2	475	474	6
3	159	161	6
4	653	662	7
5	447	443	6
6	-35	36	14
7	171	175	6
8	188	192	6
9	497	486	6
10	-31	29	16
11	294	284	6
12	42	14	15
13	638	629	7
14	145	140	7
15	755	757	8
16	122	112	8
17	559	558	7
18	71	90	12
19	529	512	7

-2 9 1

1	647	640	7
2	95	61	8
3	795	793	8
4	236	229	6
5	499	506	6
6	363	355	6
7	482	469	6
8	248	241	6
9	442	440	6
10	253	246	6
11	493	479	7
12	349	357	6
13	622	613	8
14	272	273	7
15	524	520	7
16	268	281	7
17	340	339	7

-2 10 1

1	828	797	9
2	345	345	6
3	716	694	8
4	157	152	7
5	541	526	7
6	166	148	7
7	477	465	7
8	136	132	8
9	486	472	7
10	136	132	8
11	162	154	7
12	327	305	7
13	153	152	8
14	308	303	7

-2 11 1

1	205	185	7
2	60	63	13
3	252	251	7
4	50	5	15
5	429	419	7
6	216	210	7
7	185	172	7
8	246	234	7
9	-52	16	13
10	281	275	7
11	47	27	16

-2 12 1

1	72	87	12
2	52	83	15
3	92	88	11
4	-28	32	22

-1 1 1

1	446	404	4
2	413	427	4
3	1243	1252	10
4	1137	1108	7
5	2291	2254	19
6	654	622	6
7	402	410	4
8	252	265	4
9	938	925	8
10	525	519	5
11	78	100	6
12	187	195	5
13	694	702	7
14	198	200	5
15	438	444	6
16	58	39	10
17	153	153	6
18	285	285	6
19	366	365	6
20	67	50	11
21	328	337	6
22	108	95	9
23	333	332	7
24	294	273	7
25	294	280	7

-1 2 1

1	383	394	4
2	893	899	8
3	732	733	6
4	1366	1366	12
5	1615	1622	14
6	1284	1269	11
7	1615	1606	14
8	741	707	7
9	950	920	8
10	19	28	17
11	44	57	10
12	230	233	5
13	323	335	5
14	376	370	5
15	507	514	6
16	439	429	6
17	554	551	6
18	469	470	6
19	443	442	6
20	655	678	7
21	382	377	6
22	693	698	8
23	288	277	7
24	491	482	7

-1 3 1

1	272	272	4
2	127	146	4
3	163	131	4
4	1026	1007	9
5	1152	1154	10
6	113	77	5
7	1101	1089	10
8	133	123	5
9	1292	1278	11
10	1230	1215	11
11	205	209	5
12	340	347	5
13	686	700	7
14	473	481	6
15	172	179	6
16	477	483	6
17	283	273	6
18	641	632	7
19	43	46	14
20	601	602	7
21	255	256	6
22	553	555	7
23	46	0	16
24	419	425	7

-1 4 l

1	278	299	4
2	881	889	8
3	456	487	5
4	753	786	7
5	421	446	5
6	728	732	7
7	629	655	6
8	719	738	7
9	671	690	7
10	678	691	7
11	624	625	6
12	737	740	7
13	199	211	5
14	588	594	6
15	195	189	6
16	196	191	6
17	167	173	6
18	115	107	7
19	194	202	6
20	495	497	7
21	-36	21	17
22	395	391	7
23	291	292	7
24	544	559	8

-1 5 l

1	274	241	4
2	518	531	5
3	759	765	7
4	667	700	6
5	415	423	5
6	688	710	7
7	65	14	8
8	137	158	5
9	94	101	6
10	503	498	6
11	129	126	6
12	494	500	6
13	-8	47	27
14	289	284	5
15	280	292	6
16	114	99	7
17	123	113	7
18	185	186	6
19	574	580	7
20	355	382	6
21	384	374	7
22	222	236	7
23	356	354	7

-1 6 l

1	416	436	5
2	793	824	7
3	23	19	15
4	345	353	5
5	111	113	6
6	352	355	5
7	152	164	5
8	575	580	6
9	130	131	6
10	333	340	5
11	416	424	6
12	410	406	6
13	410	416	6
14	339	332	6
15	431	424	6
16	140	134	7
17	179	176	6
18	297	300	6
19	260	265	6
20	98	107	9
21	214	210	7
22	184	189	7

-1 7 l

1	380	389	5
2	343	358	5
3	416	431	5
4	484	487	6
5	489	502	6
6	555	562	6
7	123	148	6
8	35	27	14
9	642	640	7
10	353	343	6
11	495	500	6
12	665	674	7
13	248	245	6
14	282	275	6
15	-8	20	29
16	304	318	6
17	396	404	6
18	-8	56	22
19	-41	51	15
20	-27	37	21
21	246	245	7

-1 8 l

1	132	136	6
2	599	597	7
3	110	112	7
4	285	286	5
5	589	603	7
6	462	462	6
7	66	72	10
8	284	293	6
9	-19	20	22
10	167	164	6
11	421	418	6
12	121	118	7
13	220	224	6
14	216	205	6
15	325	342	6
16	98	92	9
17	181	204	7
18	-43	62	15
19	245	237	7

-1 9 l

1	344	340	6
2	467	461	6
3	494	488	6
4	259	258	6
5	128	120	7
6	163	161	6
7	47	67	13
8	-25	4	19
9	214	208	6
10	169	158	7
11	354	356	6
12	33	22	18
13	475	462	7
14	225	219	7
15	350	348	7
16	60	73	13
17	414	410	7
18	78	105	12

-1 10 l

1	250	249	6
2	18	39	23
3	86	91	9
4	101	125	8
5	180	186	6
6	98	98	9
7	23	50	21
8	91	80	9
9	360	351	6
10	60	77	13
11	343	327	6
12	148	163	8
13	576	563	7
14	74	60	12
15	612	597	8

-1 11 l

1	242	229	6
2	-42	6	15
3	260	254	6
4	83	97	10
5	128	114	8
6	304	300	6
7	591	567	7
8	97	99	9
9	283	262	7
10	27	57	22
11	380	348	7
12	50	27	15

-1 12 l

1	576	550	8
2	86	82	11
3	317	304	7
4	142	154	8
5	481	458	7
6	138	123	8
7	208	198	7
8	-48	40	15

0 0 l

2	1108	1153	9
3	776	816	6
4	1205	1185	10
5	477	446	4
6	49	11	9
7	216	234	4
8	520	515	5
9	539	536	5
10	419	423	5
11	707	721	7
12	288	287	4
13	699	701	7
14	163	162	5
15	671	685	7
16	120	117	6
17	836	844	8
18	229	228	6
19	-23	0	20
20	174	180	6
21	381	375	6
22	154	168	7
23	484	483	7
24	76	39	11
25	305	302	7

0 1 l

-24	84	65	11
-23	146	131	8
-22	113	102	8
-21	594	590	7
-20	369	381	6
-19	200	192	6
-18	432	432	6
-17	477	485	6
-16	436	439	6
-15	121	129	6
-14	579	586	6
-13	340	340	5
-12	957	971	9
-11	45	1	10
-10	582	608	6
-9	423	408	5
-8	985	1005	9
-7	99	84	5
-6	607	633	5
-5	937	935	8
-4	859	863	7
-3	404	385	4
-2	782	751	7
-1	828	820	7
0	1357	1402	11
1	472	499	4
2	1203	1206	10
3	960	951	8
4	760	783	6
5	744	739	6
6	574	577	5
7	516	514	5
8	150	143	4
9	965	977	8
10	288	259	4
11	735	748	7
12	81	67	6
13	711	717	7
14	95	87	7
15	778	781	8
16	58	24	10
17	672	676	7
18	112	100	7
19	754	760	8
20	173	164	6
21	179	174	7
22	-36	54	17
23	134	142	8
24	167	180	7
25	125	138	9

0 2 l

-24	270	270	7
-23	170	168	7
-22	22	3	23
-21	298	285	6
-20	188	200	6
-19	188	185	6
-18	814	817	8
-17	67	21	10
-16	659	658	7
-15	87	83	7
-14	906	921	8
-13	324	324	5
-12	681	705	7
-11	97	71	6
-10	950	971	8
-9	256	237	4
-8	243	246	4
-7	199	177	4
-6	483	484	5
-5	611	606	6
-4	228	219	3
-3	949	942	8
-2	88	92	6
-1	296	315	3
0	436	435	4

1 112 89 5
2 443 479 4
3 95 122 5
4 742 709 6
5 1721 1700 14
6 123 122 4
7 814 840 7
8 510 491 5
9 1158 1143 10
10 273 266 4
11 401 410 5
12 27 49 14
13 534 539 6
14 -53 12 8
15 247 246 5
16 87 87 8
17 465 471 6
18 438 439 6
19 237 238 6
20 466 467 6
21 313 318 6
22 507 519 7
23 201 200 7
24 146 141 8
25 129 137 9

0 3 l

-24	426	437	7
-23	171	173	7
-22	258	262	7
-21	34	53	18
-20	478	475	7
-19	69	48	10
-18	470	470	6
-17	-25	19	18
-16	793	806	8
-15	272	264	5
-14	519	527	6
-13	89	94	7
-12	368	380	5
-11	286	286	5
-10	48	45	9
-9	192	183	4
-8	528	528	5
-7	547	563	5
-6	699	697	6
-5	755	766	7
-4	139	106	4
-3	1269	1289	11
-2	354	370	4
-1	1003	1021	7
0	539	559	5

1 718 750 6
2 252 241 4
3 283 298 4
4 185 202 4
5 223 239 4
6 287 270 4
7 716 707 7
8 348 330 4
9 990 940 9
10 241 226 4
11 219 199 4
12 32 50 13
13 134 136 5
14 -16 7 21
15 87 84 7
16 393 387 6
17 55 42 11
18 284 285 6
19 409 398 6
20 399 404 6
21 234 237 6
22 358 356 6
23 265 248 7
24 468 467 7

0 4 l

-23	144	131	8
-22	431	421	7
-21	112	109	9
-20	308	314	6
-19	93	75	9
-18	326	316	6
-17	33	55	16
-16	365	355	6
-15	322	327	5
-14	362	349	5
-13	425	439	6
-12	79	85	8
-11	71	98	8
-10	213	200	5
-9	871	865	8
-8	37	8	11
-7	552	566	6
-6	281	282	4
-5	553	562	5
-4	133	121	4
-3	78	82	6
-2	146	152	4
-1	179	173	4
0	545	567	5
1	187	184	4
2	208	207	4
3	101	91	5
4	108	106	5
5	216	224	4
6	79	72	6
7	521	535	5
8	698	690	7
9	196	182	4
10	128	131	5
11	138	156	5
12	40	57	12
13	155	171	5
14	375	367	5
15	297	295	5
16	328	320	6
17	328	323	6
18	256	252	6
19	149	151	7
20	173	150	7
21	538	546	7
22	363	369	7
23	111	105	9
24	155	162	8

0 5 l

-22	355	367	7
-21	310	307	7
-20	-28	11	20
-19	209	208	7
-18	86	51	9
-17	269	256	6
-16	147	147	7
-15	312	302	6
-14	478	474	6
-13	463	462	6
-12	378	389	5
-11	1054	1050	10
-10	77	94	8
-9	396	399	5
-8	338	327	5

-7	466	466	5
-6	126	127	5
-5	608	601	6
-4	497	507	5
-3	777	789	7
-2	273	270	4
-1	-46	12	9
0	184	190	4
1	190	197	4
2	87	104	4
3	268	273	4
4	348	355	4
5	461	490	5
6	659	673	6
7	514	526	5
8	260	268	4
9	585	603	5
10	456	466	5
11	337	345	5
12	121	143	6
13	375	377	5
14	173	179	6
15	289	274	5
16	130	109	7
17	78	70	9
18	296	300	6
19	270	267	6
20	368	372	6
21	-61	0	10
22	236	241	7
23	86	97	11

0 6 l

-21	287	273	7
-20	311	308	7
-19	420	421	7
-18	56	42	13
-17	211	199	6
-16	174	171	6
-15	81	51	9
-14	547	551	7
-13	273	276	6
-12	528	533	6
-11	412	415	6
-10	111	106	7
-9	549	545	6
-8	348	347	5
-7	494	485	6
-6	-27	12	14
-5	283	279	5
-4	758	749	7
-3	827	825	8
-2	167	173	5
-1	43	2	10
0	52	66	9
1	300	319	4
2	279	296	4
3	506	515	5
4	753	760	7
5	548	572	6
6	353	351	5
7	838	839	8
8	690	705	7
9	385	401	5
10	10	53	25
11	554	558	6
12	290	292	5
13	85	102	8
14	252	251	6
15	257	273	6
16	320	310	6
17	51	14	13
18	433	434	6
19	204	203	7
20	555	564	7
21	201	188	7
22	408	384	7

0 7 l

-20	212	215	7
-19	149	152	8
-18	100	109	9
-17	269	267	6
-16	21	31	23
-15	72	60	10
-14	-17	40	23
-13	-12	39	26
-12	191	200	6
-11	259	263	6
-10	44	91	13
-9	566	575	6
-8	198	185	5
-7	644	646	7
-6	299	302	5
-5	674	689	7
-4	485	489	6
-3	457	473	6
-2	36	11	13
-1	621	647	6
0	367	378	5
1	496	513	6
2	326	330	5
3	640	643	7
4	484	480	6
5	664	669	7
6	846	848	8
7	33	3	14
8	408	406	5
9	23	35	18
10	532	545	6
11	301	306	5
12	486	487	6
13	-32	9	16
14	597	583	7
15	343	341	6
16	589	582	7
17	232	212	6
18	629	642	8
19	237	229	7
20	397	393	7
21	225	236	7

0 8 l

-18	26	0	23
-17	-46	7	14
-16	119	129	8
-15	141	143	8
-14	482	486	7
-13	282	277	6
-12	141	145	7
-11	255	254	6
-10	132	134	7
-9	378	385	6
-8	169	167	6
-7	649	662	7
-6	470	470	6
-5	500	508	6
-4	261	269	5
-3	650	652	7
-2	324	328	5
-1	186	191	5
0	181	197	5
1	72	64	8
2	517	520	6
3	99	86	7
4	610	631	7
5	86	65	8
6	957	964	9
7	115	87	7
8	513	513	6
9	629	626	7
10	724	727	8
11	158	166	6

12	586	573	7
13	528	538	7
14	361	354	6
15	198	203	6
16	331	332	6
17	366	380	6
18	130	131	8
19	331	329	7
20	113	121	9

0 9 l

-16	73	77	12
-15	398	398	7
-14	85	90	10
-13	138	118	8
-12	543	545	7
-11	483	474	7
-10	176	168	7
-9	38	11	15
-8	362	356	6
-7	60	58	11
-6	320	322	6
-5	179	184	6
-4	307	297	6
-3	68	67	10
-2	225	222	6
-1	164	169	6
0	604	596	7
1	476	468	6
2	488	488	6
3	295	288	3
4	559	554	7
5	885	882	9
6	766	758	8
7	306	304	6
8	62	32	11
9	296	295	6
10	698	682	8
11	477	471	6
12	180	185	6
13	381	370	6
14	169	176	7
15	428	410	7
16	33	11	19
17	285	275	7
18	126	121	9

0 10 l

-14	261	252	7
-13	102	109	10
-12	489	485	7
-11	156	144	7
-10	254	235	6
-9	129	134	8
-8	504	489	7
-7	254	248	6
-6	670	658	8
-5	301	294	6
-4	482	469	7
-3	158	166	7
-2	620	602	7
-1	459	454	6
0	252	244	6
1	165	161	6
2	561	547	7
3	432	431	6
4	38	34	15
5	129	120	7
6	192	208	6
7	23	20	21
8	-45	12	13
9	269	266	6
10	-21	25	23
11	397	388	6
12	66	75	12
13	488	485	7

14	-51	28	13
15	438	425	7
16	146	143	8

0 11 l

-11	68	22	13
-10	377	373	7
-9	182	165	7
-8	313	296	7
-7	229	221	7
-6	346	316	7
-5	347	339	6
-4	528	506	7
-3	326	310	6
-2	161	164	7
-1	152	155	7
0	227	218	6
1	304	298	6
2	145	144	7
3	352	330	6
4	225	224	6
5	63	72	12
6	24	11	22
7	169	174	7
8	110	106	9
9	298	284	7
10	323	325	7
11	427	416	7
12	133	126	8
13	535	500	7

0 12 l

-7	45	41	17
-6	96	88	10
-5	179	166	7
-4	78	80	11
-3	314	300	7
-2	114	93	9
-1	430	407	7
0	99	90	9
1	493	486	7
2	77	57	11
3	498	483	7
4	-38	2	17
5	276	263	7
6	-37	45	17
7	414	402	7
8	29	53	22
9	181	174	7

1 -12 l

0	128	123	8
1	661	620	8
2	78	70	11
3	482	476	7
4	40	60	18
5	450	435	7

1 -11 l

0	35	39	18
1	138	134	8
2	303	308	6
3	387	391	7
4	121	133	5
5	91	80	10
6	204	197	7
7	-29	8	20
8	-49	58	14
9	-55	12	12
10	256	245	7

1 -10 l

0	130	139	7

1	69	98	10
2	227	233	6
3	-10	39	29
4	37	66	16
5	103	101	8
6	-34	20	17
7	252	256	6
8	222	213	7
9	130	130	8
10	373	362	7
11	142	132	8
12	425	430	7
13	296	268	7

1 -9 l

0	536	535	6
1	336	336	6
2	576	562	7
3	40	32	14
4	527	525	7
5	157	146	6
6	85	99	9
7	104	95	8
8	24	67	21
9	278	287	6
10	219	225	6
11	32	25	19
12	281	288	6
13	288	290	7
14	124	118	8
15	138	160	8
16	-34	45	19

1 -8 l

0	399	406	6
1	447	452	6
2	463	463	6
3	172	180	6
4	375	369	6
5	163	159	6
6	167	162	3
7	94	83	8
8	91	76	8
9	230	221	6
10	93	51	8
11	80	25	9
12	773	767	8
13	45	36	15
14	101	103	9
15	335	318	6
16	627	617	8
17	250	241	7
18	222	223	7

1 -7 l

0	588	589	6
1	32	39	14
2	141	148	6
3	118	118	6
4	982	981	9
5	111	127	6
6	906	906	9
7	609	605	7
8	626	632	7
9	570	565	7
10	208	202	6
11	547	543	7
12	499	494	6
13	166	148	6
14	584	579	7
15	309	314	6
16	60	56	12
17	479	470	7
18	72	66	12
19	506	500	7

1 -6 l

0	297	310	5
1	404	408	5
2	815	836	8
3	707	740	7
4	389	402	5
5	555	546	6
6	848	865	8
7	843	850	8
8	709	715	7
9	650	654	7
10	488	489	6
11	191	186	6
12	170	161	6
13	443	435	6
14	49	25	13
15	292	293	6
16	47	59	14
17	344	348	6
18	280	287	6
19	469	463	7
20	139	128	8
21	517	499	7

1 -5 l

0	411	451	5
1	660	674	6
2	607	617	6
3	197	206	4
4	752	745	7
5	824	835	8
6	80	88	7
7	581	579	6
8	192	190	3
9	803	801	8
10	109	110	6
11	854	843	8
12	211	199	5
13	359	366	6
14	406	408	6
15	258	270	6
16	247	250	6
17	498	499	7
18	391	388	6
19	607	596	7
20	318	316	7
21	462	453	7
22	270	244	7

1 -4 l

0	120	99	5
1	99	107	5
2	78	56	6
3	656	673	6
4	640	651	6
5	594	611	6
6	414	430	5
7	1011	1015	9
8	475	487	5
9	732	742	7
10	173	194	5
11	482	488	6
12	588	588	6
13	157	155	6
14	489	487	6
15	182	179	6
16	205	211	6
17	187	191	6
18	182	182	6
19	212	222	6
20	309	314	6
21	131	138	8
22	253	245	7
23	46	6	17

1 -3 1

0	605	623	6
1	113	114	5
2	867	886	8
3	64	4	7
4	325	325	4
5	1043	1057	9
6	523	538	5
7	336	357	4
8	237	247	4
9	806	803	7
10	-37	24	10
11	247	253	5
12	128	131	6
13	347	339	5
14	-27	32	16
15	-52	41	10
16	244	240	6
17	70	77	10
18	134	138	7
19	-28	16	18
20	229	227	6
21	48	0	15
22	477	464	7
23	414	412	7

1 -2 1

0	403	411	4
1	344	341	4
2	946	941	8
3	1050	1042	9
4	659	667	6
5	37	18	11
6	637	637	6
7	32	6	12
8	717	698	7
9	675	656	6
10	96	59	6
11	606	590	6
12	356	358	5
13	80	93	7
14	455	461	6
15	35	5	14
16	564	556	6
17	67	28	10
18	377	366	6
19	79	80	9
20	395	386	6
21	259	249	6
22	209	204	7
23	-15	32	28
24	306	299	7

1 -1 1

0	714	703	5
1	799	809	7
2	614	624	5
3	596	565	5
4	810	786	7
5	237	230	4
6	518	497	5
7	107	94	5
8	541	536	5
9	122	126	5
10	524	516	5
11	18	6	17
12	683	686	7
13	416	403	5
14	535	543	6
15	123	105	6
16	520	510	6
17	225	238	6
18	456	465	6
19	300	305	6

20	109	103	8
21	111	91	8
22	56	50	13
23	-29	30	20
24	118	114	9

1 0 1

-25	289	278	7
-24	197	211	7
-23	128	125	8
-22	-50	4	13
-21	333	335	6
-20	290	307	6
-19	88	68	8
-18	69	31	10
-17	326	330	5
-16	342	336	5
-15	427	419	5
-14	70	53	8
-13	259	264	5
-12	69	39	7
-11	759	754	7
-10	60	40	8
-9	249	254	4
-8	367	350	4
-7	495	490	5
-6	327	329	4
-5	62	63	7
-4	380	356	4
-3	294	266	3
-2	955	907	8
-1	847	832	7
0	1237	1217	11
1	407	380	4
2	1162	1119	9
3	216	184	4
4	930	914	8
5	87	87	6
6	1249	1227	11
7	674	689	6
8	401	408	4
9	438	441	5
10	836	829	8
11	96	93	6
12	798	783	7
13	144	128	5
14	785	782	8
15	424	403	5
16	459	463	6
17	78	90	9
18	340	330	6
19	106	75	8
20	80	7	5
21	297	284	6
22	422	423	7
23	35	5	19
24	231	229	7
25	354	357	7

1 1 1

-24	35	16	19
-23	693	694	8
-22	73	38	11
-21	59	65	12
-20	174	172	6
-19	466	458	6
-18	120	100	7
-17	565	555	7
-16	87	6	8
-15	739	739	7
-14	109	89	6
-13	61	10	8
-12	40	19	11
-11	169	165	4
-10	239	229	4
-9	90	95	6

-8	300	300	4
-7	-11	53	22
-6	667	659	6
-5	411	412	4
-4	547	523	5
-3	11	10	24
-2	1226	1204	10
-1	242	216	4
0	1606	1622	12
1	358	336	4
2	211	190	4
3	533	529	5
4	424	395	4
5	367	373	4
6	614	625	6
7	505	505	5
8	528	541	5
9	59	43	8
10	235	233	4
11	496	480	5
12	703	706	7
13	723	720	7
14	218	216	5
15	609	614	6
16	564	572	6
17	883	876	9
18	383	384	6
19	212	204	6
20	57	16	12
21	667	669	8
22	260	255	6
23	606	593	8
24	170	154	7
25	520	519	7

1 2 1

-24	153	145	8
-23	340	337	7
-22	256	259	6
-21	271	265	6
-20	56	54	12
-19	229	234	6
-18	160	157	6
-17	409	413	6
-16	260	257	5
-15	107	100	7
-14	71	63	8
-13	140	146	5
-12	490	496	5
-11	225	200	4
-10	15	16	19
-9	316	302	4
-8	293	304	4
-7	377	381	4
-6	907	909	8
-5	546	549	5
-4	375	385	4
-3	284	278	3
-2	948	946	8
-1	117	116	5
0	1118	1145	9
1	236	226	3
2	246	246	3
3	640	653	5
4	184	197	4
5	536	529	4
6	522	533	5
7	201	181	4
8	344	357	4
9	562	559	6
10	824	816	7
11	1070	1068	9
12	87	83	6
13	633	643	6
14	644	650	7
15	706	719	7
16	404	410	6

17	614	614	7
18	171	180	6
19	577	581	7
20	38	36	16
21	308	304	6
22	165	168	7
23	415	410	7
24	92	97	10
25	412	412	7

1 3 1

-24	66	21	13
-23	338	341	7
-22	292	305	7
-21	265	265	6
-20	275	282	6
-19	397	379	6
-18	862	850	9
-17	145	148	6
-16	520	527	6
-15	424	427	6
-14	478	476	6
-13	185	190	5
-12	396	414	5
-11	381	392	5
-10	666	686	6
-9	655	675	6
-8	471	505	5
-7	334	337	4
-6	562	568	5
-5	145	145	4
-4	273	291	4
-3	29	71	13
-2	1335	1359	11
-1	307	297	4
0	439	474	4
1	170	183	4
2	1268	1292	11
3	1462	1488	12
4	60	18	8
5	552	573	5
6	153	170	4
7	1326	1346	11
8	630	633	6
9	849	853	8
10	227	176	4
11	901	912	8
12	145	146	5
13	757	784	7
14	67	48	9
15	453	469	6
16	214	220	5
17	521	534	6
18	319	326	6
19	249	249	6
20	253	254	6
21	201	193	7
22	300	300	6
23	187	184	7
24	342	328	7

1 4 1

-23	68	53	13
-22	136	125	8
-21	176	185	7
-20	371	358	6
-19	357	362	6
-18	776	781	8
-17	439	438	6
-16	955	951	9
-15	45	29	13
-14	946	953	9
-13	337	333	5
-12	112	137	6
-11	125	123	6
-10	839	842	8

-9	261	266	4
-8	685	704	7
-7	269	271	4
-6	527	547	5
-5	196	223	4
-4	560	570	5
-3	833	855	7
-2	212	227	4
-1	1078	1114	9
0	664	688	6
1	1431	1487	12
2	268	259	4
3	483	506	5
4	1025	1034	9
5	434	473	5
6	140	117	5
7	794	802	7
8	493	470	5
9	255	283	4
10	26	0	14
11	326	354	5
12	308	317	5
13	242	252	5
14	321	318	5
15	400	400	6
16	401	412	6
17	201	207	6
18	437	438	6
19	174	179	6
20	508	493	7
21	316	319	6
22	516	514	7
23	198	201	7
24	469	463	7

1 5 1

-22	231	223	4
-21	53	58	14
-20	177	180	7
-19	91	99	9
-18	488	482	7
-17	312	319	6
-16	531	528	7
-15	49	80	12
-14	615	608	7
-13	91	108	8
-12	459	458	6
-11	674	672	7
-10	658	655	7
-9	580	590	6
-8	470	470	5
-7	841	866	8
-6	288	309	4
-5	669	707	6
-4	570	571	6
-3	778	798	7
-2	771	776	7
-1	1440	1457	12
0	127	135	5
1	762	793	7
2	415	429	5
3	895	940	8
4	119	137	5
5	425	444	5
6	39	65	11
7	622	625	6
8	371	388	5
9	427	436	5
10	510	531	6
11	553	565	6
12	294	308	5
13	343	338	5
14	342	347	5
15	223	228	6
16	415	417	6
17	117	123	7
18	459	458	6

19	347	339	6
20	399	406	6
21	182	196	7
22	373	367	7
23	125	128	9

1 6 1

-21	102	119	10
-20	229	225	7
-19	292	291	6
-18	125	128	8
-17	359	355	6
-16	245	235	6
-15	238	229	6
-14	591	585	7
-13	471	463	6
-12	346	335	6
-11	609	610	7
-10	598	607	6
-9	962	974	9
-8	228	218	5
-7	619	623	6
-6	375	387	5
-5	721	737	7
-4	93	60	6
-3	431	455	5
-2	218	209	4
-1	269	292	4
0	271	286	4
1	860	863	8
2	742	775	7
3	410	414	5
4	661	677	6
5	543	542	6
6	942	968	9
7	194	193	5
8	478	496	6
9	531	529	6
10	517	535	6
11	86	90	7
12	294	296	5
13	258	268	5
14	309	302	6
15	162	177	6
16	-61	22	9
17	-42	7	13
18	353	363	6
19	175	208	7
20	197	189	7
21	36	65	18
22	378	389	7

1 7 1

-20	300	285	7
-19	443	437	7
-18	141	122	8
-17	438	433	7
-16	98	105	9
-15	351	354	6
-14	243	249	6
-13	382	377	6
-12	-49	14	11
-11	574	566	7
-10	83	105	8
-9	300	292	5
-8	273	268	5
-7	405	411	5
-6	194	187	5
-5	75	67	8
-4	469	462	6
-3	239	249	5
-2	291	319	5
-1	357	328	5
0	297	320	5
1	282	287	5
2	83	114	7

3	716	728	7
4	477	490	6
5	668	678	7
6	381	383	5
7	512	519	6
8	494	487	6
9	175	176	3
10	345	353	5
11	119	113	7
12	-46	25	11
13	175	171	6
14	241	252	6
15	86	75	9
16	-36	3	15
17	378	403	6
18	270	298	6
19	88	89	10
20	374	383	7
21	216	203	7

1 8 1

-18	60	28	13
-17	128	140	8
-16	90	97	10
-15	144	153	7
-14	-31	9	18
-13	49	48	13
-12	276	283	6
-11	89	96	8
-10	381	373	6
-9	408	399	6
-8	541	542	6
-7	137	145	6
-6	58	53	10
-5	440	445	6
-4	394	388	6
-3	268	270	5
-2	57	63	10
-1	218	224	5
0	276	287	5
1	250	261	5
2	302	304	5
3	309	308	5
4	185	191	5
5	142	144	6
6	685	684	7
7	-40	36	12
8	505	503	6
9	139	149	6
10	119	108	7
11	127	136	7
12	339	339	6
13	64	70	11
14	344	335	6
15	287	299	6
16	308	311	6
17	282	285	6
18	331	311	7
19	376	392	7
20	163	131	8

1 9 1

-17	114	99	9
-16	47	66	16
-15	71	19	12
-14	161	125	7
-13	472	467	7
-12	103	87	9
-11	411	421	6
-10	502	501	7
-9	251	250	6
-8	148	166	7
-7	291	293	6
-6	550	546	7
-5	213	208	6
-4	29	22	17
-3	239	249	6
-2	139	133	6
-1	-37	16	14
0	-44	14	12
1	202	196	6
2	10	19	27
3	302	302	5
4	384	375	6
5	53	78	12
6	-50	15	11
7	458	462	6
8	-57	33	9
9	123	131	7
10	584	576	7
11	61	54	11
12	509	497	7
13	155	169	7
14	368	355	6
15	68	86	12
16	439	415	7
17	105	102	9
18	271	262	7
19	230	251	7

1 10 1

-14	292	303	7
-13	586	581	8
-12	300	296	7
-11	218	200	7
-10	117	109	8
-9	259	269	6
-8	99	121	9
-7	38	64	16
-6	155	146	7
-5	128	140	7
-4	167	166	6
-3	-34	23	15
-2	309	294	6
-1	-33	6	15
0	450	431	6
1	352	335	6
2	204	205	6
3	161	154	6
4	558	548	7
5	88	35	9
6	331	328	6
7	169	173	6
8	388	379	6
9	99	116	8
10	361	365	6
11	-29	24	19
12	496	483	7
13	239	239	7
14	208	190	7
15	133	130	8
16	301	299	7
17	303	293	7

1 11 1

-12	265	245	7
-11	126	104	9
-10	82	74	11
-9	17	33	27
-8	250	259	7
-7	-50	30	13
-6	348	337	6
-5	151	153	7
-4	421	413	7
-3	45	67	15
-2	542	522	7
-1	39	39	16
0	571	559	7
1	216	217	6
2	504	487	7
3	186	182	7
4	517	504	7
5	101	118	9
6	277	270	6
7	110	113	8
8	235	247	7
9	224	212	7
10	323	320	7
11	463	441	7
12	-37	11	17
13	315	292	7
14	89	96	11

1 12 1

-8	461	454	7
-7	64	64	13
-6	434	428	7
-5	98	100	10
-4	536	505	7
-3	-56	18	12
-2	355	349	7
-1	157	135	7
0	282	269	7
1	-65	34	10
2	321	309	7
3	351	351	7
4	139	130	8
5	203	186	7
6	142	146	8
7	302	291	7
8	73	73	12
9	474	447	7
10	44	32	17

2 -12 1

0	258	257	7
1	115	113	9

2 -11 1

0	53	30	14
1	126	94	8
2	304	290	7
3	507	469	7
4	167	171	7
5	392	375	7
6	218	223	7
7	544	523	7
8	96	105	10

2 -10 1

0	151	144	7
1	513	519	7
2	131	124	8
3	120	110	8
4	205	209	7
5	152	152	7
6	172	178	7
7	59	51	8
8	210	208	7
9	259	252	7
10	323	314	7
11	86	82	11
12	458	454	7

2 -9 1

0	465	454	6
1	294	291	6
2	624	634	7
3	324	321	6
4	593	591	7
5	117	102	7
6	125	107	7
7	282	263	6
8	428	434	6
9	34	42	18
10	546	537	7
11	127	123	8
12	689	681	8
13	184	193	7
14	253	230	7
15	30	57	22

2 -8 1

0	670	677	7
1	358	352	6
2	848	844	8
3	132	107	7
4	669	667	7
5	107	90	7
6	372	371	6
7	185	194	6
8	80	73	9
9	-33	11	16
10	428	432	6
11	9	28	30
12	94	96	9
13	290	292	6
14	367	361	7
15	-50	12	13
16	263	276	7
17	278	257	7

2 -7 1

0	526	529	6
1	241	241	5
2	476	487	6
3	25	58	17
4	401	403	6
5	47	58	12
6	371	366	6
7	260	262	5
8	88	93	8
9	427	429	6
10	658	660	7
11	136	125	7
12	181	183	6
13	185	169	6
14	264	255	6
15	418	416	7
16	230	223	7
17	442	414	7
18	338	325	7
19	304	294	7

2 -6 1

0	215	231	5
1	402	406	5
2	241	249	5
3	286	290	5
4	588	583	6
5	375	385	5
6	560	561	6
7	487	493	6
8	203	201	5
9	403	398	6
10	74	65	9
11	277	280	6
12	518	517	6
13	314	312	6
14	434	433	6
15	189	187	6
16	127	136	8
17	188	187	7
18	83	86	10
19	199	201	7
20	262	253	7

2 -5 1

0	27	10	14
1	321	327	5
2	253	265	4
3	272	283	4
4	431	448	5
5	149	157	5
6	490	501	6
7	171	189	5
8	380	370	5
9	112	104	6
10	378	367	5
11	167	179	6
12	246	246	5
13	43	41	13
14	273	266	6
15	374	364	6
16	140	152	7
17	42	69	15
18	-38	55	16
19	470	468	7
20	55	53	14
21	249	236	7

2 -4 1

0	42	13	10
1	690	677	6
2	998	1019	9
3	82	80	6
4	300	332	4
5	164	174	4
6	705	710	7
7	420	429	5
8	557	549	6
9	331	331	5
10	96	62	7
11	273	259	5
12	114	86	6
13	434	437	6
14	170	165	6
15	230	206	6
16	99	92	8
17	498	498	7
18	371	386	6
19	566	563	7
20	27	72	21
21	396	379	7
22	227	224	7

2 -3 1

0	148	164	4
1	339	345	4
2	-27	30	13
3	337	353	4
4	533	538	5
5	917	915	8
6	381	359	5
7	375	381	5
8	668	641	6
9	439	446	5
10	95	46	6
11	623	639	6
12	117	82	6
13	533	525	6
14	194	180	5
15	719	725	7
16	70	43	10
17	498	499	6
18	54	54	12
19	444	450	6
20	414	405	7
21	326	326	6
22	337	344	7
23	131	114	8

2 -2 1

0	332	315	3
1	109	119	5
2	1468	1428	11
3	1391	1375	12
4	309	285	4
5	1313	1304	11
6	35	34	12
7	1670	1654	14
8	332	327	4
9	563	591	6
10	294	287	5
11	605	632	6
12	311	309	5
13	617	629	6
14	237	233	5
15	339	327	5
16	256	255	5
17	248	250	6
18	479	466	6
19	93	105	9
20	354	351	6
21	46	0	15
22	607	605	8
23	200	190	7
24	386	381	7

2 -1 1

0	96	78	5
1	2211	2120	15
2	726	695	5
3	2551	2514	23
4	297	293	4
5	1264	1265	11
6	1016	999	9
7	932	914	8
8	564	567	6
9	651	640	6
10	763	756	7
11	189	152	5
12	710	700	7
13	213	202	5
14	609	623	6
15	122	110	6
16	613	614	7
17	152	148	6
18	527	530	7
19	-21	0	21
20	345	348	6
21	155	158	7
22	336	333	6
23	-45	36	15
24	209	204	7

2 0 1

-24	365	356	7
-23	331	326	7
-22	485	478	7
-21	188	190	7
-20	440	432	6
-19	96	82	8
-18	93	101	8
-17	169	169	6
-16	170	180	6
-15	429	422	6
-14	198	184	5
-13	462	484	5
-12	114	97	6
-11	1108	1104	10
-10	158	145	4
-9	971	970	9
-8	63	32	8
-7	1376	1386	12
-6	491	478	5
-5	606	616	6
-4	199	183	4
-3	678	657	6
-2	490	483	5

-1	279	239	3					0	407	409	4						7	670	673	7	-4	86	82	8
0	540	516	5		2	2	1	1	83	99	6	-22	167	178	8		8	166	155	5	-3	406	422	6
1	1267	1216	11					2	-31	17	12	-21	148	153	8		9	745	751	7	-2	238	242	5
2	183	156	3	-24	174	158	8	3	513	510	5	-20	57	49	13		10	230	220	5	-1	264	272	5
3	117	71	4	-23	937	921	10	4	152	158	4	-19	-38	38	16		11	450	456	6	0	96	101	7
4	1390	1321	10	-22	123	51	8	5	142	137	4	-18	354	350	4		12	714	725	7	1	535	541	6
5	1421	1368	12	-21	429	423	7	6	118	129	5	-17	62	44	11		13	31	18	16	2	675	694	7
6	80	17	6	-20	329	334	6	7	87	96	6	-16	380	374	6		14	243	246	6	3	374	389	5
7	261	243	4	-19	656	656	7	8	370	374	4	-15	421	413	6		15	587	585	7	4	353	366	5
8	1007	1012	9	-18	98	61	8	9	344	348	4	-14	403	408	6		16	342	345	6	5	715	727	7
9	125	130	5	-17	619	622	7	10	207	213	4	-13	252	237	5		17	456	448	6	6	735	745	7
10	638	654	6	-16	241	237	3	11	416	413	5	-12	263	249	5		18	318	313	6	7	582	589	7
11	338	311	5	-15	442	448	6	12	186	209	5	-11	255	260	5		19	636	646	8	8	620	623	7
12	973	967	9	-14	204	206	5	13	660	669	7	-10	485	481	6		20	499	492	7	9	338	343	6
13	42	49	11	-13	371	375	5	14	124	141	6	-9	174	183	5		21	355	368	7	10	247	238	6
14	667	657	7	-12	150	168	5	15	388	380	5	-8	91	78	6		22	330	324	7	11	58	54	11
15	165	163	5	-11	286	301	5	16	167	168	6	-7	-42	18	9						12	475	477	6
16	673	676	7	-10	445	455	5	17	664	669	7	-6	200	202	4			2	7	1	13	208	210	6
17	65	31	10	-9	68	67	7	18	364	360	6	-5	212	222	4						14	405	407	6
18	425	420	6	-8	96	117	6	19	370	365	6	-4	817	810	7	-20	223	225	7		15	-20	34	23
19	-10	3	27	-7	64	50	7	20	250	259	6	-3	394	405	5	-19	68	74	12		16	456	448	7
20	361	363	6	-6	1087	1097	9	21	116	96	8	-2	642	627	6	-18	247	249	7		17	374	388	6
21	236	232	6	-5	73	41	7	22	100	87	9	-1	994	990	9	-17	300	300	6		18	321	310	7
22	323	325	6	-4	647	599	6	23	249	246	7	0	665	676	6	-16	223	211	6		19	220	208	7
23	28	15	21	-3	2022	1976	17	24	21	34	25	1	835	843	8	-15	131	112	7		20	436	417	7
24	170	182	8	-2	3236	3179	30					2	281	304	4	-14	131	118	7					
				-1	1169	1142	10		2	4	1	3	207	218	4	-13	503	500	6			2	9	1
	2	1	1	0	856	874	7					4	370	390	5	-12	87	74	8					
				1	125	113	4	-23	32	54	21	5	286	309	4	-11	310	314	6	-17	455	442	7
-24	364	360	7	2	643	653	6	-22	75	84	11	6	206	223	4	-10	399	409	6	-16	210	206	7
-23	262	260	7	3	149	131	4	-21	-34	34	18	7	739	717	7	-9	299	311	5	-15	349	324	7
-22	117	102	8	4	439	439	4	-20	415	405	7	8	898	900	8	-8	291	294	5	-14	206	215	7
-21	574	575	7	5	697	697	6	-19	76	86	10	9	268	284	5	-7	549	554	6	-13	273	275	6
-20	21	29	22	6	75	57	7	-18	426	420	6	10	125	131	6	-6	294	293	5	-12	153	171	7
-19	322	320	6	7	348	345	4	-17	341	340	6	11	194	190	5	-5	462	473	6	-11	568	570	7
-18	226	226	6	8	188	183	4	-16	625	619	7	12	404	416	5	-4	529	545	6	-10	138	129	7
-17	668	664	7	9	305	290	4	-15	157	134	6	13	303	296	5	-3	124	147	6	-9	629	628	7
-16	48	25	12	10	270	262	4	-14	555	547	6	14	4	6	31	-2	182	202	5	-8	202	200	6
-15	744	744	7	11	329	333	5	-13	81	61	8	15	132	134	6	-1	328	358	5	-7	599	602	7
-14	205	201	5	12	337	329	5	-12	661	664	7	16	-20	35	21	0	101	101	6	-6	386	391	6
-13	611	633	6	13	361	344	5	-11	147	134	5	17	687	683	7	1	189	196	5	-5	605	601	7
-12	433	430	5	14	187	189	5	-10	216	228	5	18	222	218	6	2	86	80	7	-4	230	228	6
-11	742	749	7	15	774	780	8	-9	102	96	6	19	391	386	6	3	703	726	7	-3	354	358	6
-10	245	231	4	16	526	522	6	-8	618	617	6	20	39	41	17	4	649	653	7	-2	314	303	6
-9	1002	1019	9	17	42	25	14	-7	677	664	6	21	441	445	7	5	528	546	6	-1	386	390	6
-8	295	293	4	18	149	160	6	-6	509	504	5	22	218	200	7	6	62	67	9	0	520	527	6
-7	123	89	5	19	288	275	6	-5	400	397	5	23	465	464	7	7	945	957	9	1	379	384	6
-6	50	55	10	20	39	15	15	-4	637	609	6					8	477	491	6	2	408	411	6
-5	773	757	7	21	390	399	6	-3	328	310	4		2	6	1	9	702	713	7	3	539	543	6
-4	1492	1458	13	22	80	57	10	-2	1038	1040	9					10	517	535	6	4	572	580	7
-3	139	151	4	23	240	234	7	-1	224	228	4	-21	174	185	8	11	445	454	6	5	-41	24	13
-2	778	752	6	24	230	230	7	0	813	821	7	-20	355	351	7	12	391	402	6	6	230	228	6
-1	712	674	6					1	52	62	8	-19	-41	22	15	13	545	558	7	7	13	10	25
0	214	190	3		2	3	1	2	-10	24	21	-18	263	261	6	14	365	350	6	8	325	320	6
1	351	317	4					3	267	268	4	-17	15	23	26	15	-39	48	14	9	428	436	6
2	994	947	8	-23	636	626	8	4	234	244	4	-16	393	400	6	16	416	427	6	10	131	121	7
3	334	321	3	-22	251	253	7	5	616	631	6	-15	225	233	6	17	151	160	7	11	-11	12	27
4	251	260	4	-21	287	292	6	6	382	391	5	-14	97	99	8	18	353	362	6	12	390	379	6
5	67	62	7	-20	185	180	7	7	574	578	6	-13	163	162	6	19	102	115	9	13	258	256	6
6	1142	1154	10	-19	698	706	8	8	490	485	5	-12	253	250	5	20	280	275	7	14	373	371	6
7	383	386	4	-18	333	333	6	9	153	172	5	-11	253	244	5	21	-50	3	14	15	291	288	6
8	827	840	7	-17	351	352	6	10	314	333	5	-10	218	218	5					16	499	493	7
9	97	106	6	-16	365	361	6	11	328	323	5	-9	252	245	5		2	8	1	17	256	251	7
10	898	898	8	-15	314	321	5	12	195	199	5	-8	477	478	6					18	386	369	7
11	-23	25	15	-14	637	627	7	13	247	262	5	-7	382	384	5	-18	382	373	7	19	248	250	7
12	972	955	9	-13	169	171	5	14	514	511	6	-6	366	393	5	-17	265	252	7				
13	272	272	5	-12	489	502	6	15	498	505	6	-5	190	214	5	-16	485	477	7		2	10	1
14	343	336	5	-11	66	43	8	16	169	174	6	-4	356	381	5	-15	240	237	6				
15	415	427	6	-10	33	59	12	17	222	215	6	-3	327	350	5	-14	353	361	6	-14	83	45	11
16	409	416	6	-9	543	500	6	18	136	154	7	-2	706	735	7	-13	62	56	12	-13	601	592	8
17	242	232	6	-8	404	417	5	19	177	171	6	-1	399	408	5	-12	444	437	6	-12	420	418	7
18	226	236	6	-7	397	407	5	20	121	113	8	0	485	517	5	-11	197	194	6	-11	416	399	7
19	543	540	7	-6	996	977	9	21	313	310	6	1	365	376	5	-10	238	234	6	-10	387	386	7
20	301	307	6	-5	266	251	4	22	45	37	16	2	362	380	5	-9	605	614	7	-9	377	366	6
21	243	246	6	-4	1293	1309	11	23	330	320	7	3	468	485	5	-8	276	282	6	-8	373	367	6
22	63	53	12	-3	904	866	8	24	226	222	7	4	503	512	5	-7	234	246	6	-7	295	292	6
23	592	594	7	-2	448	451	4					5	883	887	8	-6	195	198	6	-6	174	171	6
24	63	61	13	-1	985	962	8		2	5	1	6	277	285	5	-5	627	629	7	-5	528	515	7

-4	358	349	6	0	57	71	15	11	297	295	6	20	122	124	8	20	240	229	6	-5	731	731	7
-3	172	161	6	1	226	221	7	12	258	262	6	21	360	355	7	21	39	38	17	-4	768	745	6
-2	103	93	8	2	325	317	7	13	-36	16	16					22	213	206	7	-3	549	530	5
-1	8	24	29	3	154	150	8	14	323	314	6		3 -3 1			23	241	252	7	-2	568	550	5
0	244	241	6					15	78	96	11									-1	595	586	5
1	-20	21	21		3 -11 1			16	351	340	7	0	482	487	4		3 0 1			0	52	49	8
2	443	430	6					17	212	210	7	1	260	256	4					1	734	710	6
3	143	140	7	0	92	110	10	18	350	369	7	2	829	810	6	-24	325	327	7	2	360	359	4
4	407	399	6	1	96	91	10					3	626	616	5	-23	166	173	8	3	729	693	6
5	320	319	6	2	112	105	9		3 -6 1			4	420	423	5	-22	465	471	7	4	257	238	4
6	223	219	6	3	210	216	7					5	135	121	5	-21	151	152	7	5	672	672	6
7	379	373	6	4	135	123	8	0	492	509	6	6	579	585	6	-20	281	280	6	6	381	376	4
8	229	232	6	5	143	136	8	1	354	373	5	7	319	316	5	-19	179	179	6	7	172	175	4
9	176	187	7					2	549	584	6	8	110	92	6	-18	237	229	6	8	316	321	4
10	464	449	7		3 -10 1			3	305	305	5	9	432	430	5	-17	201	210	6	9	396	386	5
11	130	122	8					4	282	266	5	10	113	123	6	-16	197	194	6	10	633	632	6
12	518	517	7	0	157	142	7	5	406	398	6	11	134	145	6	-15	127	138	6	11	320	323	5
13	180	174	7	1	439	432	7	6	422	428	6	12	149	143	6	-14	656	653	7	12	961	965	9
14	360	338	7	2	257	260	6	7	154	158	6	13	268	258	5	-13	319	317	5	13	291	291	5
15	164	166	7	3	351	341	6	8	188	180	6	14	286	285	5	-12	441	417	5	14	985	979	9
16	243	230	7	4	169	166	7	9	191	186	6	15	200	212	6	-11	244	220	5	15	275	270	5
17	283	279	7	5	405	411	7	10	993	997	9	16	235	240	6	-10	419	408	5	16	975	978	9
				6	41	66	17	11	46	35	13	17	495	495	7	-9	488	473	5	17	144	125	6
	2 11 1			7	164	166	7	12	150	152	7	18	66	45	11	-8	221	209	4	18	270	265	6
				8	53	66	9	13	562	562	7	19	504	501	7	-7	636	620	6	19	145	140	7
-12	261	245	7	9	230	217	7	14	547	537	7	20	-20	26	24	-6	27	25	14	20	459	460	7
-11	256	227	7	10	56	66	14	15	484	487	7	21	435	426	7	-5	511	491	5	21	242	247	6
-10	378	378	7					16	352	342	6	22	224	226	7	-4	58	38	8	22	154	154	7
-9	98	94	9		3 -9 1			17	528	527	7					-3	698	671	6	23	242	249	7
-8	217	206	7					18	257	235	7		3 -2 1			-2	177	177	4	24	256	259	7
-7	357	358	7	0	111	128	8	19	462	440	7					-1	408	390	4				
-6	259	235	6	1	556	579	7					0	280	279	4	0	166	165	4		3 2 1		
-5	62	76	12	2	322	343	6		3 -5 1			1	235	233	4	1	571	564	5				
-4	126	124	8	3	180	177	6					2	198	166	4	2	92	76	5	-23	198	191	7
-3	125	122	8	4	157	166	7	0	235	250	5	3	393	381	4	3	601	575	6	-22	248	251	7
-2	330	313	6	5	218	213	6	1	295	275	5	4	487	454	5	4	330	311	4	-21	381	374	7
-1	233	233	6	6	-20	51	23	2	335	332	5	5	1232	1184	11	5	188	208	4	-20	372	370	6
0	398	397	6	7	57	70	13	3	209	204	5	6	71	57	7	6	777	735	6	-19	291	301	6
1	174	181	7	8	61	75	12	4	500	507	6	7	1048	1033	9	7	1155	1110	9	-18	162	169	6
2	78	73	10	9	179	172	7	5	461	481	6	8	178	173	5	8	332	318	4	-17	562	565	7
3	407	404	6	10	64	76	12	6	315	310	5	9	-12	21	21	9	66	9	7	-16	224	217	6
4	901	888	9	11	314	299	7	7	138	116	6	10	155	149	5	10	314	306	5	-15	303	315	5
5	123	122	8	12	340	317	7	8	502	500	6	11	125	141	6	11	43	32	11	-14	217	209	5
6	121	131	8	13	407	393	7	9	810	822	8	12	137	132	6	12	84	70	7	-13	777	768	8
7	215	210	7					10	429	433	6	13	418	419	6	13	325	318	5	-12	114	109	6
8	399	394	7		3 -8 1			11	376	374	6	14	135	136	6	14	449	448	6	-11	925	905	8
9	133	134	8					12	567	569	7	15	335	334	6	15	243	237	5	-10	129	123	5
10	267	263	7	0	133	136	7	13	328	331	6	16	-51	8	10	16	408	389	6	-9	1072	1083	9
11	62	81	13	1	454	471	6	14	40	40	15	17	464	447	6	17	233	229	6	-8	145	138	5
12	184	186	7	2	196	192	6	15	357	362	6	18	138	134	7	18	474	461	6	-7	395	420	5
13	110	104	9	3	229	228	6	16	-42	38	14	19	245	261	6	19	50	54	13	-6	535	509	5
14	199	199	7	4	57	68	11	17	413	425	7	20	133	141	8	20	453	455	7	-5	513	526	5
				5	457	449	6	18	-47	10	14	21	370	371	7	21	44	25	16	-4	334	313	4
	2 12 1			6	188	193	6	19	306	300	7	22	68	37	12	22	568	572	7	-3	796	775	6
				7	324	313	6	20	93	118	10	23	119	128	9	23	51	24	15	-2	214	211	4
-8	475	478	7	8	265	274	6									24	561	566	8	-1	614	608	5
-7	125	120	9	9	497	493	7		3 -4 1				3 -1 1							0	550	552	5
-6	218	211	7	10	746	746	8										3 1 1			1	390	403	4
-5	152	164	8	11	432	425	7	0	856	864	8	0	843	804	5					2	130	133	5
-4	468	463	7	12	430	409	7	1	712	718	7	1	89	67	6	-24	349	342	7	3	387	388	4
-3	180	157	7	13	390	379	7	2	414	428	5	2	407	406	4	-23	173	177	7	4	1329	1301	10
-2	353	359	7	14	394	378	7	3	1052	1040	9	3	1412	1349	12	-22	378	378	7	5	436	421	3
-1	227	219	7	15	264	248	7	4	142	89	5	4	183	172	4	-21	196	208	7	6	562	572	5
0	470	461	7	16	409	392	7	5	392	388	5	5	1437	1409	11	-20	109	98	8	7	525	530	5
1	320	316	7					6	343	357	5	6	440	416	5	-19	65	39	11	8	1098	1110	10
2	254	242	7		3 -7 1			7	513	537	6	7	1042	1020	8	-18	-24	9	19	9	48	53	9
3	61	55	13					8	630	629	7	8	123	109	5	-17	281	271	6	10	955	963	9
4	103	97	9	0	453	448	6	9	64	67	9	9	391	421	5	-16	342	332	6	11	181	158	5
5	-45	30	14	1	525	516	6	10	298	301	5	10	104	116	6	-15	317	306	5	12	969	973	9
6	-67	24	10	2	535	543	6	11	116	115	6	11	764	758	7	-14	333	329	5	13	301	282	5
7	102	121	9	3	403	416	6	12	155	160	6	12	100	79	6	-13	106	107	6	14	953	963	9
8	38	8	18	4	585	594	7	13	176	184	6	13	228	224	5	-12	67	65	8	15	119	66	6
9	97	89	10	5	181	167	6	14	183	184	6	14	71	43	9	-11	815	801	8	16	426	436	6
10	78	58	12	6	295	291	6	15	125	127	7	15	611	613	7	-10	343	331	5	17	168	151	6
11	87	74	11	7	490	497	6	16	-48	38	12	16	377	375	6	-9	409	424	5	18	154	146	6
				8	636	633	7	17	352	362	6	17	107	110	7	-8	318	285	4	19	611	613	7
	2 13 1			9	118	97	7	18	-62	12	10	18	170	161	6	-7	368	396	4	20	295	300	6
				10	602	600	7	19	312	313	6	19	170	176	7	-6	-39	37	10	21	406	383	7

22	86	89	10	-1	226	224	4	-20	440	441	7	13	33	57	16	8	55	59	12
23	453	445	7	0	1155	1174	9	-19	323	316	7	14	148	152	7	9	476	478	6
24	21	19	26	1	339	327	3	-18	499	497	7	15	160	157	7	10	42	57	14
				2	1144	1137	9	-17	90	88	9	16	249	253	6	11	255	234	6
3	3	1		3	134	114	5	-16	715	721	8	17	380	385	6	12	-37	9	15
				4	815	845	6	-15	251	259	6	18	312	324	6	13	509	522	7
-23	15	35	29	5	321	328	4	-14	274	288	6	19	243	242	7	14	259	252	6
-22	60	38	13	6	217	201	4	-13	220	228	6	20	254	242	7	15	151	181	7
-21	465	463	7	7	174	180	4	-12	439	435	6	21	350	335	7	16	306	300	7
-20	91	62	9	8	349	353	5	-11	272	271	5					17	176	181	7
-19	497	502	7	9	618	634	6	-10	396	396	6	3	8	1		18	504	487	7
-18	111	79	8	10	178	177	5	-9	343	347	5								
-17	809	812	8	11	457	471	5	-8	154	160	6	-18	147	159	8	3	10	1	
-16	192	174	6	12	731	718	7	-7	69	58	8	-17	241	231	7				
-15	505	510	6	13	843	856	8	-6	439	447	5	-16	277	279	7	-14	68	84	13
-14	62	79	10	14	435	430	6	-5	665	686	7	-15	157	144	7	-13	20	19	25
-13	458	474	6	15	535	535	6	-4	125	132	5	-14	141	146	7	-12	200	200	7
-12	192	190	5	16	155	149	6	-3	389	391	5	-13	138	129	7	-11	414	411	7
-11	689	694	7	17	330	337	6	-2	521	514	6	-12	367	365	6	-10	80	48	10
-10	93	100	6	18	188	182	6	-1	757	761	7	-11	105	86	8	-9	346	353	6
-9	546	538	6	19	260	256	6	0	94	73	6	-10	467	455	6	-8	26	33	21
-8	491	482	5	20	-49	28	13	1	505	513	6	-9	285	278	6	-7	321	323	6
-7	1207	1166	10	21	276	278	4	2	467	477	5	-8	243	238	6	-6	81	98	6
-6	397	407	5	22	83	93	11	3	64	110	8	-7	320	313	6	-5	402	405	6
-5	75	99	7	23	264	255	7	4	80	53	7	-6	196	203	6	-4	84	90	9
-4	1139	1126	10					5	624	624	6	-5	244	250	5	-3	126	110	7
-3	150	148	4	3	5	1		6	475	460	6	-4	23	47	19	-2	-43	1	13
-2	1228	1214	11					7	341	340	5	-3	38	60	14	-1	360	357	6
-1	793	784	7	-22	135	140	9	8	427	433	5	-2	197	198	5	0	168	154	6
0	631	661	6	-21	176	167	7	9	488	493	6	-1	411	417	6	1	574	576	7
1	712	700	6	-20	436	428	7	10	145	141	6	0	35	52	14	2	127	133	7
2	1309	1290	10	-19	201	195	7	11	398	385	6	1	34	35	14	3	291	289	6
3	69	37	7	-18	377	381	6	12	172	176	6	2	35	49	14	4	180	174	6
4	546	558	5	-17	344	357	6	13	147	156	6	3	195	184	5	5	403	398	6
5	286	292	4	-16	450	437	6	14	84	106	9	4	163	168	6	6	429	436	6
6	345	377	4	-15	101	112	8	15	119	124	7	5	263	264	5	7	339	339	6
7	46	59	9	-14	564	558	7	16	-20	33	22	6	295	302	5	8	202	195	6
8	175	195	4	-13	45	43	13	17	243	243	6	7	344	342	6	9	343	330	6
9	488	475	5	-12	771	789	8	18	303	302	6	8	246	249	5	10	211	208	6
10	681	693	7	-11	258	262	5	19	285	288	6	9	206	205	6	11	145	159	7
11	210	206	5	-10	602	601	6	20	271	273	7	10	281	282	6	12	138	134	8
12	218	211	5	-9	302	304	5	21	354	363	7	11	76	102	9	13	27	16	21
13	348	355	5	-8	730	732	7	22	433	425	7	12	115	125	7	14	284	277	7
14	331	338	5	-7	183	178	5					13	312	313	6	15	-16	7	27
15	409	419	6	-6	253	279	5	3	7	1		14	66	102	11	16	575	549	8
16	572	564	7	-5	256	256	4					15	344	323	6				
17	97	97	8	-4	896	906	8	-19	141	146	8	16	398	408	6	3	11	1	
18	42	47	14	-3	407	402	5	-18	447	428	7	17	326	336	6				
19	548	550	7	-2	538	539	6	-17	80	81	11	18	96	95	10	-11	442	432	7
20	191	191	7	-1	233	231	4	-16	294	291	6	19	353	344	7	-10	47	41	16
21	585	577	7	0	656	652	6	-15	109	114	8	20	331	333	7	-9	396	381	7
22	54	35	14	1	585	583	6	-14	164	161	7					-8	138	137	8
23	520	501	7	2	463	479	5	-13	384	380	6	3	9	1		-7	560	576	7
24	196	191	7	3	670	688	6	-12	107	107	8					-6	70	68	11
				4	229	215	4	-11	244	250	6	-16	120	118	9	-5	612	617	7
3	4	1		5	810	825	7	-10	34	2	16	-15	210	205	7	-4	169	173	7
				6	681	666	7	-9	118	127	7	-14	215	207	7	-3	437	438	7
-22	85	88	11	7	1043	1058	9	-8	179	190	6	-13	350	338	6	-2	51	82	14
-21	185	193	7	8	476	460	5	-7	492	490	6	-12	206	213	7	-1	298	288	6
-20	42	27	16	9	532	531	6	-6	64	64	9	-11	280	273	6	0	194	200	7
-19	411	407	6	10	71	86	8	-5	399	401	5	-10	589	582	7	1	126	125	8
-18	91	98	9	11	530	545	6	-4	346	349	5	-9	482	477	7	2	449	444	7
-17	451	448	6	12	68	78	9	-3	854	855	8	-8	70	59	10	3	365	346	6
-16	63	61	11	13	400	399	6	-2	127	113	6	-7	-11	36	27	4	270	258	6
-15	461	450	6	14	225	232	5	-1	317	320	5	-6	143	151	7	5	-41	6	15
-14	420	411	6	15	173	165	6	0	402	423	5	-5	86	93	9	6	208	215	7
-13	349	359	5	16	55	60	12	1	366	382	5	-4	133	145	7	7	109	110	9
-12	305	318	5	17	185	190	6	2	234	246	5	-3	99	98	8	8	588	574	7
-11	225	238	5	18	37	27	16	3	186	190	5	-2	176	196	6	9	94	69	9
-10	345	364	5	19	222	237	6	4	123	115	6	-1	197	193	6	10	639	635	8
-9	272	270	5	20	80	112	10	5	448	451	6	0	17	57	23	11	-47	20	14
-8	676	684	7	21	94	116	10	6	31	33	15	1	416	415	6	12	280	266	7
-7	895	867	8	22	149	155	8	7	404	397	5	2	141	152	6	13	82	96	11
-6	956	961	9	23	310	301	7	8	329	345	5	3	463	462	6	14	360	341	7
-5	85	72	6					9	640	635	7	4	66	79	10				
-4	894	888	8	3	6	1		10	421	434	6	5	667	668	7	3	12	1	
-3	329	332	4					11	418	423	6	6	22	5	20				
-2	1636	1641	14	-21	55	52	15	12	427	419	6	7	624	625	7	-8	172	180	8

-7	336	344	7																
-6	136	136	8																
-5	286	304	7																
-4	254	264	7																
-3	98	117	10																
-2	697	691	8																
-1	180	176	7																
0	343	353	7																
1	219	223	7																
2	593	569	7																
3	135	130	8																
4	478	458	7																
5	50	9	15																
6	641	604	8																
7	276	264	7																
8	449	438	7																
9	47	56	16																
10	532	512	7																
4	-10	1																	
0	293	290	7																
1	314	308	7																
2	325	338	7																
3	546	533	7																
4	44	65	16																
5	484	468	7																
6	102	82	10																
7	538	514	7																
4	-9	1																	
0	148	156	7																
1	604	594	7																
2	-17	0	25																
3	501	492	7																
4	84	83	10																
5	531	526	7																
6	62	4	13																
7	306	301	7																
8	59	5	13																
9	184	159	7																
10	11	51	31																
11	341	348	7																
4	-8	1																	
0	79	85	9																
1	317	319	6																
2	342	351	6																
3	471	454	6																
4	105	114	8																
5	91	91	9																
6	207	210	4																
7	195	196	7																
8	135	152	8																
9	62	93	12																
10	265	263	6																
11	296	302	7																
12	299	289	7																
13	210	212	7																
14	280	279	7																
4	-7	1																	
0	31	6	17																
1	351	365	6																
2	311	310	6																
3	75	64	9																
4	203	203	6																
5	124	139	7																
6	296	293	6																
7	124	127	7																
8	479	478	6																
9	-14	7	26																
10	677	684	8																
11	387	393	6																
12	352	371	6																

13	101	99	9
14	316	317	7
15	106	115	9
16	179	177	7

4 -6 1

0	290	299	5
1	127	123	6
2	112	118	7
3	308	318	5
4	237	244	5
5	334	329	6
6	50	28	12
7	118	111	7
8	376	374	6
9	425	419	6
10	31	18	17
11	59	80	12
12	428	438	6
13	142	122	7
14	212	211	7
15	105	105	9
16	285	286	7
17	108	143	9
18	-46	15	15

4 -5 1

0	461	453	6
1	466	492	6
2	292	283	5
3	298	314	5
4	342	333	5
5	608	617	7
6	450	452	6
7	338	334	5
8	546	547	6
9	320	322	6
10	405	406	6
11	112	126	7
12	442	431	6
13	72	35	10
14	399	403	6
15	305	300	6
16	482	493	7
17	282	301	7
18	365	350	7
19	263	256	7

4 -4 1

0	393	399	5
1	47	59	10
2	450	446	5
3	48	10	10
4	198	204	5
5	235	248	5
6	260	270	5
7	80	75	8
8	327	324	5
9	197	198	5
10	596	594	7
11	568	562	7
12	337	331	6
13	-22	0	20
14	515	528	7
15	41	22	15
16	497	518	7
17	246	238	6
18	461	470	7
19	262	259	7
20	426	422	7

4 -3 1

0	763	770	7
1	216	203	4
2	993	993	8
3	104	88	6
4	754	756	7
5	275	249	5
6	912	904	8
7	147	139	5
8	1105	1115	10
9	538	540	6
10	592	600	6
11	102	114	7
12	425	432	6
13	214	211	6
14	267	266	6
15	300	287	6
16	98	61	8
17	455	465	7
18	332	362	6
19	508	511	7
20	181	183	7
21	585	606	8

4 -2 1

0	1314	1307	11
1	623	625	6
2	840	825	8
3	653	623	6
4	654	653	6
5	513	502	6
6	1297	1260	10
7	1121	1081	9
8	193	169	5
9	424	424	5
10	334	341	5
11	708	706	7
12	250	236	5
13	322	327	5
14	116	123	7
15	362	347	6
16	529	555	7
17	516	534	7
18	37	15	17
19	532	529	7
20	193	188	7
21	499	496	7
22	31	30	21

4 -1 1

0	261	263	4
1	584	577	4
2	203	194	4
3	658	633	6
4	277	255	4
5	824	797	8
6	725	679	7
7	751	729	7
8	391	377	5
9	772	792	7
10	355	356	5
11	443	440	6
12	98	88	7
13	466	476	6
14	134	147	6
15	417	422	6
16	82	86	9
17	395	408	6
18	271	273	6
19	417	425	6
20	205	210	7
21	278	275	7
22	152	143	8

4 0 1

-23	90	67	11
-22	269	268	7
-21	267	278	7
-20	393	385	7
-19	7	29	32
-18	537	533	7
-17	48	47	13
-16	596	597	7
-15	354	351	6
-14	738	744	8
-13	401	396	6
-12	937	955	9
-11	492	499	6
-10	569	585	6
-9	304	290	5
-8	534	540	4
-7	753	729	7
-6	239	249	4
-5	174	183	4
-4	32	39	12
-3	615	607	6
-2	199	195	4
-1	556	557	5
0	531	515	5
1	1015	991	9
2	208	210	4
3	749	726	7
4	516	496	5
5	1152	1097	10
6	161	156	4
7	763	763	7
8	301	289	5
9	579	588	6
10	139	137	5
11	861	860	8
12	333	330	5
13	356	357	5
14	173	175	6
15	281	287	6
16	563	563	7
17	-5	14	31
18	326	328	6
19	133	134	7
20	277	274	6
21	105	87	9
22	368	360	7
23	147	134	8

4 1 1

-23	118	89	9
-22	581	574	8
-21	186	170	7
-20	595	580	7
-19	103	106	8
-18	351	349	6
-17	168	162	6
-16	708	706	8
-15	99	113	8
-14	337	337	5
-13	622	610	7
-12	333	332	5
-11	618	604	6
-10	147	132	5
-9	462	461	5
-8	135	136	5
-7	216	213	4
-6	267	253	4
-5	563	572	6
-4	410	412	5
-3	399	387	5
-2	113	95	5
-1	697	702	6
0	941	941	8
1	444	437	5
2	580	543	6
3	779	778	7
4	428	413	5
5	844	793	8
6	312	292	4
7	523	496	4
8	129	139	5
9	142	153	5
10	211	191	5
11	119	118	6
12	275	279	5
13	175	182	5
14	478	471	6
15	37	46	15
16	564	571	7
17	-35	4	15
18	365	369	6
19	24	41	21
20	363	366	6
21	-37	2	17
22	311	295	4
23	22	11	25

4 2 1

-23	140	143	8
-22	526	530	7
-21	129	136	8
-20	355	358	6
-19	-6	31	33
-18	-28	29	18
-17	210	224	6
-16	251	247	6
-15	220	218	6
-14	137	155	6
-13	702	694	7
-12	269	257	5
-11	758	744	7
-10	168	146	5
-9	843	834	8
-8	141	130	5
-7	698	696	7
-6	82	73	6
-5	570	562	6
-4	455	430	5
-3	894	871	8
-2	813	778	7
-1	387	386	4
0	302	307	4
1	182	198	4
2	192	179	4
3	333	323	4
4	317	290	4
5	399	374	5
6	255	248	4
7	182	162	4
8	289	296	5
9	35	26	12
10	208	210	5
11	307	320	5
12	342	340	5
13	152	164	6
14	511	521	6
15	53	71	11
16	436	438	6
17	254	254	6
18	410	414	6
19	-43	29	14
20	418	433	7
21	88	95	10
22	377	385	7
23	111	112	9

4 3 1

-22	94	97	10
-21	192	189	7
-20	42	43	16
-19	347	355	6
-18	171	176	7
-17	322	330	6
-16	-27	2	18
-15	486	490	6
-14	260	271	5
-13	454	457	6
-12	65	51	9
-11	941	928	9
-10	118	87	6
-9	196	171	5
-8	373	362	5
-7	250	238	4
-6	198	195	4
-5	591	576	6
-4	452	440	5
-3	866	835	7
-2	178	185	4
-1	363	360	4
0	689	663	6
1	164	173	4
2	278	267	4
3	77	77	6
4	634	634	5
5	69	77	7
6	345	357	5
7	461	467	4
8	373	382	5
9	394	384	5
10	523	524	6
11	308	316	5
12	359	360	5
13	100	89	7
14	636	630	7
15	599	610	7
16	139	134	7
17	258	262	6
18	91	87	9
19	349	348	6
20	133	126	8
21	-56	1	12
22	268	274	7
23	147	138	8

4 4 1

-22	13	41	30
-21	389	383	7
-20	95	88	10
-19	198	188	7
-18	48	57	14
-17	207	193	6
-16	75	60	10
-15	143	145	7
-14	199	216	6
-13	416	415	6
-12	154	157	6
-11	143	122	6
-10	231	237	5
-9	234	229	5
-8	493	489	6
-7	683	678	7
-6	776	739	7
-5	575	550	6
-4	1084	1042	10
-3	679	662	7
-2	469	488	5
-1	313	305	4
0	403	388	3
1	648	656	6
2	864	854	7
3	91	46	6
4	684	668	7
5	136	85	5
6	262	275	4
7	317	321	5
8	309	308	5
9	190	190	5
10	421	425	5
11	464	466	6
12	-36	5	13
13	286	283	5
14	1048	1048	10
15	78	60	9
16	255	260	6
17	197	178	6
18	209	197	6
19	310	315	6
20	-72	16	8
21	108	112	9
22	415	429	7
23	169	160	8

4 5 1

-21	372	365	7
-20	119	101	9
-19	345	347	7
-18	142	132	8
-17	227	217	6
-16	26	7	20
-15	353	362	6
-14	289	281	6
-13	138	134	7
-12	192	185	6
-11	477	472	6
-10	374	366	5
-9	179	165	5
-8	525	520	6
-7	257	249	5
-6	512	525	6
-5	187	200	5
-4	1002	1004	8
-3	791	808	7
-2	468	499	5
-1	542	539	6
0	523	531	6
1	147	172	5
2	389	405	5
3	22	24	16
4	274	280	5
5	-7	12	25
6	459	474	5
7	140	143	5
8	434	450	5
9	61	74	9
10	574	572	6
11	466	450	6
12	711	719	7
13	571	566	7
14	334	333	6
15	571	572	7
16	366	366	6
17	571	567	7
18	365	351	6
19	401	398	7
20	176	166	7
21	444	442	7
22	130	145	5

4 6 1

-20	117	115	9
-19	380	385	7
-18	209	198	7
-17	412	423	7
-16	251	243	6
-15	92	81	9
-14	293	285	6
-13	277	277	6
-12	132	129	7
-11	137	154	6
-10	307	306	5
-9	395	407	6
-8	339	343	5
-7	32	40	15
-6	328	332	5
-5	223	228	5
-4	865	871	8
-3	54	54	10
-2	663	672	7
-1	446	451	5

0	547	553	6
1	115	111	6
2	90	121	7
3	276	280	5
4	532	544	6
5	638	643	7
6	453	465	6
7	390	383	5
8	588	602	6
9	628	618	7
10	306	316	5
11	669	668	7
12	584	584	7
13	871	856	9
14	271	264	6
15	416	405	6
16	366	368	6
17	100	76	9
18	200	185	7
19	548	538	7
20	206	189	7
21	361	357	7

4 7 1

-19	200	182	7
-18	390	389	7
-17	499	491	7
-16	363	371	7
-15	435	431	7
-14	353	350	6
-13	300	289	6
-12	266	273	6
-11	361	371	6
-10	165	150	6
-9	429	432	6
-8	-32	16	15
-7	63	64	10
-6	662	657	7
-5	186	180	5
-4	501	517	6
-3	301	300	5
-2	566	572	6
-1	227	228	5
0	852	868	8
1	493	502	6
2	551	560	6
3	354	359	5
4	257	272	5
5	700	694	7
6	680	677	7
7	550	559	6
8	65	80	10
9	518	513	6
10	226	226	6
11	800	798	8
12	157	147	6
13	341	336	6
14	92	90	9
15	541	534	7
16	105	97	9
17	534	547	7
18	280	285	7
19	285	278	7
20	300	274	7

4 8 1

-17	143	128	8
-16	485	465	7
-15	229	223	7
-14	527	521	7
-13	90	95	9
-12	336	346	6
-11	164	184	7
-10	324	304	6
-9	129	121	7
-8	592	577	7
-7	320	311	6
-6	487	476	6
-5	632	626	7
-4	338	347	6
-3	397	414	6
-2	532	525	6
-1	477	479	6
0	352	345	5
1	403	410	6
2	245	250	5
3	502	505	6
4	324	333	5
5	528	537	6
6	26	25	18
7	83	86	8
8	235	231	6
9	484	483	6
10	527	529	7
11	-13	39	25
12	451	438	6
13	278	256	6
14	322	323	6
15	311	305	6
16	197	193	7
17	440	442	7
18	334	330	7
19	372	370	7

4 9 1

-16	293	272	7
-15	147	162	8
-14	305	293	7
-13	345	340	7
-12	526	530	7
-11	307	301	6
-10	477	468	7
-9	579	585	7
-8	292	274	6
-7	699	704	8
-6	132	123	7
-5	191	175	6
-4	172	167	6
-3	308	305	6
-2	74	66	9
-1	157	148	6
0	125	127	7
1	276	281	6
2	120	117	7
3	565	566	7
4	246	235	6
5	382	387	6
6	219	209	6
7	242	241	6
8	221	222	6
9	45	32	14
10	-55	11	10
11	542	539	7
12	-15	68	26
13	232	235	6
14	174	175	7
15	353	363	7
16	285	294	7
17	297	301	7
18	212	206	7

4 10 1

-13	196	174	7
-12	229	233	7
-11	471	479	7
-10	438	453	7
-9	406	418	7
-8	90	121	10
-7	410	413	6
-6	57	85	13
-5	318	324	6
-4	257	253	6
-3	154	152	7
-2	-31	5	17
-1	376	361	6
0	377	356	6
1	196	181	6
2	110	80	8
3	560	559	7
4	442	435	6
5	468	468	6
6	483	473	7
7	436	438	6
8	229	228	6
9	-35	26	17
10	265	270	6
11	-51	17	12
12	-8	45	32
13	130	150	8
14	96	104	10
15	-44	18	15
16	156	155	8

4 11 1

-11	317	310	7
-10	38	40	18
-9	282	276	7
-8	136	143	8
-7	471	489	7
-6	145	137	8
-5	250	248	7
-4	114	109	8
-3	272	274	6
-2	402	396	7
-1	227	235	6
0	267	275	6
1	511	509	7
2	298	296	6
3	155	161	7
4	68	79	12
5	296	296	6
6	56	72	13
7	260	252	6
8	473	465	7
9	158	157	7
10	238	219	7
11	193	217	7
12	-47	24	14
13	217	230	7

4 12 1

-7	196	210	7
-6	97	95	10
-5	251	248	7
-4	37	60	18
-3	-15	65	28
-2	-31	43	20
-1	221	226	7
0	342	352	7
1	35	54	19
2	257	263	7
3	307	308	7
4	47	74	15
5	47	63	16
6	218	203	7
7	242	249	7
8	455	435	7
9	33	32	20

5 -10 1

0	261	254	7
1	57	65	14
2	240	240	7

5 -9 1

0	186	180	7
1	206	222	7
2	294	302	7
3	190	188	7
4	151	160	8
5	375	360	7
6	236	224	7
7	461	458	7
8	141	127	8

5 -8 1

0	329	335	6
1	313	310	6
2	287	279	6
3	526	524	7
4	305	296	6
5	537	534	7
6	102	92	9
7	453	470	7
8	116	112	9
9	570	562	7
10	26	85	22
11	316	323	7
12	35	36	20

5 -7 1

0	602	614	7
1	426	426	6
2	241	237	6
3	300	306	6
4	130	146	7
5	269	270	6
6	70	78	11
7	440	448	7
8	199	190	7
9	357	366	6
10	344	339	6
11	461	470	7
12	440	453	7
13	224	219	7
14	232	255	7

5 -6 1

0	120	115	7
1	522	525	6
2	139	143	7
3	312	308	6
4	290	290	6
5	178	176	6
6	388	381	6
7	88	57	9
8	470	462	6
9	455	463	6
10	554	552	7
11	436	440	7
12	452	458	7
13	399	399	7
14	551	582	7
15	50	18	15
16	102	128	10

5 -5 1

0	241	237	5
1	737	744	8
2	656	655	7
3	102	82	7
4	326	328	6
5	329	329	6
6	650	656	5
7	149	153	6
8	295	285	6
9	350	347	6
10	134	132	7
11	306	303	6
12	405	413	6
13	77	78	10
14	230	246	7
15	-71	1	9
16	237	249	7
17	78	85	11
18	214	218	7

5 -4 1

0	720	742	7
1	162	152	5
2	324	325	5
3	550	545	6
4	333	321	5
5	-12	17	24
6	114	115	7
7	230	236	5
8	406	401	6
9	576	577	7
10	120	91	7
11	333	322	6
12	174	158	6
13	198	193	6
14	332	333	6
15	276	282	6
16	288	294	6
17	326	347	7
18	399	413	7
19	68	91	13

5 -3 1

0	68	4	8
1	103	85	6
2	495	477	6
3	337	348	5
4	200	189	5
5	162	155	5
6	315	296	5
7	182	185	5
8	561	569	6
9	198	205	6
10	665	660	7
11	189	192	6
12	149	141	6
13	39	49	15
14	245	234	6
15	137	150	7
16	236	248	6
17	90	128	10
18	364	376	7
19	51	72	15
20	236	240	7

5 -2 1

0	345	335	5
1	385	377	5
2	344	333	5
3	111	105	6
4	516	499	6
5	714	709	7
6	805	786	8
7	337	330	5
8	748	746	7
9	411	410	6
10	207	198	5
11	181	180	6
12	266	257	6
13	21	23	21
14	153	142	6
15	166	174	6
16	331	343	6
17	225	219	6
18	157	157	7
19	330	339	7
20	-5	3	35
21	354	381	7

5 -1 1

0	597	572	6
1	252	238	4
2	744	721	7
3	208	205	5
4	650	631	7
5	209	198	5
6	438	437	5
7	215	206	5
8	250	240	5
9	314	308	5
10	22	35	19
11	229	239	5
12	58	67	11
13	301	300	6
14	267	275	6
15	373	365	6
16	78	68	10
17	455	459	7
18	220	223	6
19	526	524	7
20	113	101	9
21	413	405	7

5 0 1

-22	11	0	32
-21	363	373	7
-20	-42	26	15
-19	133	128	8
-18	235	229	6
-17	45	48	14
-16	298	290	6
-15	126	96	7
-14	175	161	6
-13	175	172	6
-12	191	181	6
-11	102	93	7
-10	709	697	7
-9	192	204	5
-8	319	318	5
-7	107	87	6
-6	857	850	8
-5	118	98	5
-4	181	126	5
-3	516	505	6
-2	431	438	5
-1	194	175	4
0	725	701	5
1	158	143	5
2	560	551	6
3	269	263	4
4	522	496	6
5	413	391	5
6	571	568	6
7	464	462	5
8	373	358	5
9	267	274	5
10	97	110	7
11	594	603	5
12	74	79	9
13	690	695	7
14	103	107	8
15	886	882	9
16	80	34	9
17	838	843	9
18	230	227	6
19	533	541	7
20	56	26	14
21	457	451	7
22	274	259	7

5 1 1

-22	186	189	7
-21	-61	16	11

-20	217	231	7	11	369	366	5	-5	689	692	7	-17	235	239	7	19	194	192	7
-19	229	227	7	12	523	522	6	-4	109	108	6	-16	221	214	7				
-18	462	464	7	13	137	143	6	-3	486	490	6	-15	242	237	6		5 8 1		
-17	71	77	10	14	57	41	11	-2	644	646	5	-14	250	249	6				
-16	287	275	6	15	130	116	7	-1	388	385	5	-13	205	209	6	-16	253	251	7
-15	144	127	7	16	56	50	12	0	335	331	5	-12	170	156	6	-15	143	131	8
-14	701	711	6	17	227	224	6	1	7	41	25	-11	33	41	16	-14	316	326	7
-13	118	101	7	18	307	304	6	2	994	995	8	-10	424	412	6	-13	154	149	7
-12	786	783	8	19	253	249	6	3	35	34	12	-9	58	24	11	-12	441	442	7
-11	112	103	7	20	583	585	7	4	687	675	5	-8	167	152	6	-11	62	68	12
-10	735	733	6	21	29	50	21	5	133	121	5	-7	130	122	6	-10	130	138	7
-9	18	23	20	22	740	733	8	6	842	832	7	-6	238	229	5	-9	192	188	6
-8	1026	1008	9					7	53	12	10	-5	151	145	6	-8	303	293	6
-7	410	390	5		5 3 1			8	728	731	6	-4	691	690	7	-7	68	61	10
-6	455	455	5					9	120	105	6	-3	368	371	5	-6	239	251	6
-5	226	216	5	-21	-29	37	21	10	543	528	6	-2	764	771	6	-5	224	224	6
-4	202	211	5	-20	298	279	7	11	73	30	9	-1	37	35	13	-4	276	275	6
-3	198	160	4	-19	98	117	9	12	827	825	8	0	101	101	7	-3	25	42	19
-2	168	171	5	-18	327	318	6	13	142	116	6	1	404	417	5	-2	377	375	6
-1	94	68	6	-17	309	310	6	14	508	498	6	2	640	653	5	-1	386	397	6
0	89	81	6	-16	196	182	6	15	204	209	6	3	19	9	19	0	444	427	6
1	665	678	6	-15	44	3	14	16	84	83	9	4	22	26	18	1	45	21	13
2	273	257	4	-14	207	225	6	17	604	603	7	5	32	53	15	2	-72	11	7
3	912	909	8	-13	587	587	7	18	180	178	7	6	204	202	5	3	447	453	6
4	372	358	5	-12	281	280	5	19	134	123	8	7	293	303	5	4	-33	29	15
5	986	939	9	-11	550	554	6	20	33	48	19	8	197	184	5	5	115	136	7
6	469	441	5	-10	357	349	5	21	-59	17	11	9	336	335	5	6	544	544	7
7	606	609	6	-9	831	838	8	22	222	226	7	10	394	385	6	7	52	56	12
8	42	26	12	-8	39	41	12					11	499	511	6	8	553	557	7
9	953	943	7	-7	943	957	7		5 5 1			12	722	707	8	9	65	68	10
10	225	221	5	-6	336	324	5					13	610	609	7	10	476	481	6
11	229	230	5	-5	900	888	7	-20	68	49	13	14	290	276	6	11	143	144	7
12	88	98	8	-4	177	169	5	-19	519	517	7	15	457	459	6	12	284	289	6
13	594	607	7	-3	600	597	5	-18	104	106	9	16	-28	64	19	13	188	180	7
14	121	127	7	-2	88	69	6	-17	354	343	6	17	170	170	7	14	246	250	6
15	528	527	7	-1	776	778	7	-16	109	116	8	18	126	142	8	15	217	217	7
16	242	233	6	0	589	576	6	-15	423	431	6	19	298	304	7	16	48	61	15
17	505	511	7	1	738	742	7	-14	75	40	10	20	-12	63	30	17	364	352	7
18	484	489	7	2	187	170	5	-13	531	521	7					18	-36	17	18
19	156	154	7	3	955	955	9	-12	67	66	10		5 7 1						
20	417	419	7	4	383	367	5	-11	227	222	6						5 9 1		
21	87	46	10	5	774	750	7	-10	429	430	6	-18	187	201	7				
22	464	458	7	6	674	649	7	-9	606	607	7	-17	143	155	8	-15	111	109	9
				7	95	78	6	-8	140	148	6	-16	329	341	7	-14	283	290	7
	5 2 1			8	344	343	5	-7	99	93	7	-15	-39	0	16	-13	82	86	11
				9	316	307	5	-6	532	524	6	-14	546	550	7	-12	116	132	9
-21	162	161	8	10	767	777	8	-5	225	228	5	-13	-57	4	11	-11	79	105	11
-20	339	349	7	11	210	188	5	-4	884	887	8	-12	166	164	7	-10	246	260	6
-19	98	115	9	12	682	668	7	-3	289	274	5	-11	258	255	6	-9	137	149	7
-18	382	372	6	13	191	193	6	-2	474	488	6	-10	391	379	6	-8	140	150	7
-17	86	79	9	14	868	863	9	-1	380	386	5	-9	206	211	3	-7	111	116	8
-16	570	568	7	15	90	106	8	0	794	811	6	-8	368	372	6	-6	349	348	6
-15	65	29	10	16	342	330	6	1	109	114	6	-7	366	366	6	-5	506	519	7
-14	235	235	3	17	-16	30	25	2	405	407	5	-6	403	402	6	-4	212	199	6
-13	183	174	6	18	263	276	6	3	268	275	5	-5	167	171	6	-3	40	18	15
-12	551	553	5	19	56	64	13	4	544	556	5	-4	582	581	7	-2	594	590	7
-11	117	101	6	20	233	226	7	5	274	267	5	-3	82	83	8	-1	153	138	6
-10	582	580	6	21	106	120	9	6	243	260	5	-2	354	348	5	0	564	571	7
-9	505	490	6	22	275	273	7	7	166	155	5	-1	-24	21	17	1	172	160	6
-8	528	519	6					8	631	626	7	0	171	187	6	2	344	340	6
-7	225	214	5		5 4 1			9	237	237	5	1	-27	15	16	3	482	478	6
-6	575	566	5					10	471	461	6	2	404	414	6	4	99	101	8
-5	496	480	6	-21	189	174	7	11	84	87	8	3	27	41	17	5	175	184	6
-4	205	190	5	-20	213	216	7	12	289	279	6	4	343	327	5	6	-24	47	19
-3	795	777	7	-19	430	418	7	13	23	25	20	5	-40	11	13	7	171	177	6
-2	153	147	5	-18	170	168	7	14	731	727	8	6	183	174	6	8	-53	41	11
-1	922	926	8	-17	195	172	7	15	96	86	8	7	227	232	6	9	184	197	6
0	51	17	9	-16	196	184	6	16	-59	10	10	8	294	297	6	10	259	263	6
1	857	884	8	-15	508	499	7	17	388	393	6	9	304	306	6	11	396	392	6
2	331	318	5	-14	57	47	11	18	-33	32	18	10	173	181	6	12	-41	25	15
3	423	447	5	-13	744	738	8	19	295	287	7	11	376	376	6	13	290	280	6
4	154	125	5	-12	167	166	6	20	71	89	12	12	359	356	6	14	63	41	13
5	1330	1257	12	-11	965	961	9	21	380	377	7	13	237	224	6	15	406	396	7
6	609	569	6	-10	77	58	8					14	144	134	7	16	105	101	9
7	695	688	7	-9	836	838	8		5 6 1			15	32	18	19	17	414	404	7
8	220	209	5	-8	178	169	5					16	306	304	6				
9	231	239	5	-7	566	577	5	-19	459	436	7	17	194	194	7		5 10 1		
10	72	46	8	-6	277	276	5	-18	9	28	32	18	266	255	7				

-12	401	408	7								
-11	60	45	13								
-10	287	274	7								
-9	147	146	8								
-8	500	507	7								
-7	344	355	6								
-6	337	338	6								
-5	210	225	7								
-4	449	442	7								
-3	396	394	6								
-2	403	404	6								
-1	159	163	7								
0	400	419	6								
1	217	206	6								
2	380	386	6								
3	650	658	7								
4	81	94	10								
5	653	646	8								
6	285	273	6								
7	342	335	6								
8	161	171	7								
9	356	345	6								
10	200	208	7								
11	400	391	7								
12	-13	17	29								
13	338	313	7								
14	289	294	7								
15	439	435	7								
	5 11 1										
-9	247	227	7								
-8	-33	19	19								
-7	217	227	7								
-6	206	213	7								
-5	248	249	7								
-4	-31	13	19								
-3	393	396	7								
-2	124	111	8								
-1	432	427	7								
0	89	53	10								
1	571	576	7								
2	184	177	7								
3	637	633	8								
4	235	238	7								
5	637	618	8								
6	167	146	7								
7	656	639	8								
8	318	317	7								
9	290	261	7								
10	301	294	7								
11	479	462	7								
12	360	333	7								
	5 12 1										
-5	279	245	7								
-4	100	102	10								
-3	233	215	7								
-2	142	133	8								
-1	550	534	7								
0	124	130	9								
1	423	433	7								
2	177	187	7								
3	258	250	7								
4	320	305	7								
5	388	380	7								
6	351	323	7								
7	191	197	7								
	6 -9 1										
0	400	404	7								
1	257	253	7								
2	299	293	7								
	6 -8 1										

0	47	56	15
1	45	46	16
2	78	83	11
3	207	189	7
4	148	144	8
5	405	392	7
6	211	202	7
7	495	507	7
8	8	55	34

6 -7 1

0	63	64	12
1	218	216	6
2	104	102	9
3	176	179	7
4	351	365	6
5	362	357	6
6	223	223	7
7	179	169	7
8	219	236	7
9	343	361	7
10	-37	20	17
11	168	174	8

6 -6 1

0	469	483	6
1	402	405	6
2	385	397	6
3	194	189	6
4	133	146	7
5	166	164	7
6	209	223	6
7	212	207	6
8	67	66	12
9	231	243	7
10	98	120	9
11	212	203	7
12	-41	2	16
13	438	457	7
14	214	228	7

6 -5 1

0	128	135	7
1	306	296	6
2	-42	1	13
3	214	204	6
4	-16	41	24
5	219	223	6
6	19	13	23
7	32	20	17
8	336	335	6
9	392	392	6
10	57	34	13
11	602	614	7
12	275	287	6
13	379	379	7
14	192	216	7
15	267	255	7
16	289	275	7

6 -4 1

0	233	238	6
1	469	456	6
2	292	288	6
3	492	498	6
4	200	192	6
5	217	225	6
6	538	527	7
7	715	705	8
8	130	121	7
9	662	669	7
10	384	370	6
11	609	633	7
12	423	442	6
13	296	289	6
14	408	411	7
15	91	98	10
16	42	23	17
17	38	53	19

6 -3 1

0	421	415	6
1	496	506	6
2	724	726	7
3	978	962	9
4	71	27	9
5	283	276	5
6	804	802	6
7	165	138	6
8	718	721	8
9	101	83	8
10	662	656	7
11	170	162	6
12	568	571	7
13	296	308	6
14	374	375	6
15	218	224	7
16	485	496	7
17	443	450	7
18	216	221	7

6 -2 1

0	643	641	7
1	171	171	5
2	376	365	5
3	300	292	5
4	402	394	6
5	319	312	5
6	427	426	6
7	194	176	6
8	744	753	8
9	622	606	7
10	699	696	7
11	681	674	7
12	404	381	6
13	214	213	6
14	481	470	7
15	338	333	6
16	271	269	6
17	189	199	7
18	424	423	7
19	210	209	7

6 -1 1

0	547	538	6
1	172	131	5
2	920	911	9
3	401	400	5
4	352	345	5
5	205	190	5
6	447	449	6
7	353	357	5
8	609	605	7
9	144	117	6
10	655	651	7
11	255	247	6
12	465	452	6
13	445	441	6
14	63	29	11
15	403	428	6
16	356	371	6
17	307	298	6
18	-58	8	11
19	467	502	7
20	-51	17	14

6 0 1

-20	195	168	7
-19	343	340	7
-18	372	371	7
-17	557	566	7
-16	336	335	6
-15	389	409	6
-14	266	271	6
-13	398	390	6
-12	329	333	6
-11	131	134	7
-10	467	469	6
-9	200	206	6
-8	351	343	5
-7	292	280	5
-6	452	448	6
-5	52	5	10
-4	75	47	8
-3	567	554	6
-2	362	359	5
-1	61	9	9
0	766	765	7
1	191	186	5
2	388	381	5
3	241	233	5
4	660	652	7
5	603	609	6
6	28	21	16
7	58	49	10
8	114	110	7
9	102	96	7
10	164	165	6
11	96	70	8
12	205	198	6
13	125	105	7
14	186	196	6
15	689	705	8
16	105	96	8
17	457	465	7
18	62	79	13
19	524	529	7
20	-41	20	16

6 1 1

-20	238	240	7
-19	91	87	10
-18	263	273	7
-17	135	128	8
-16	404	422	6
-15	40	55	15
-14	387	396	6
-13	60	43	11
-12	509	515	6
-11	135	134	6
-10	594	585	7
-9	46	7	12
-8	762	758	8
-7	359	355	5
-6	580	562	6
-5	150	147	5
-4	422	424	5
-3	162	165	5
-2	470	462	6
-1	262	254	5
0	247	242	5
1	214	199	5
2	533	512	6
3	194	183	5
4	91	61	7
5	74	30	8
6	262	251	5
7	660	646	7
8	284	278	5
9	159	160	6
10	175	177	6
11	63	69	10
12	-35	24	15
13	59	67	11
14	275	268	6
15	459	465	6
16	-45	19	13
17	511	522	7
18	24	20	23
19	491	494	7
20	-24	10	23
21	244	233	7

6 2 1

-20	259	260	4
-19	36	56	18
-18	290	286	7
-17	279	283	6
-16	379	380	6
-15	295	292	6
-14	588	591	7
-13	299	299	6
-12	520	512	6
-11	92	97	8
-10	542	530	6
-9	486	482	6
-8	365	354	5
-7	116	102	6
-6	206	201	5
-5	260	240	5
-4	266	250	5
-3	84	72	7
-2	259	244	5
-1	260	249	5
0	272	256	5
1	491	488	6
2	326	324	5
3	579	554	6
4	301	279	5
5	710	694	7
6	183	169	5
7	600	577	6
8	88	94	7
9	617	608	7
10	148	136	6
11	145	134	6
12	114	112	7
13	28	6	18
14	156	157	6
15	260	255	6
16	84	97	9
17	276	289	6
18	-38	25	16
19	138	147	8
20	215	202	7
21	247	225	7

6 3 1

-20	211	211	7
-19	141	149	8
-18	395	396	7
-17	23	29	23
-16	170	161	7
-15	124	122	8
-14	208	189	6
-13	88	86	9
-12	403	392	6
-11	301	307	6
-10	220	211	6
-9	26	1	18
-8	372	366	6
-7	317	309	5
-6	49	41	11
-5	179	160	5
-4	402	397	5
-3	393	395	5
-2	236	241	5
-1	482	479	6
0	308	302	5
1	440	450	5
2	61	61	9
3	938	926	9
4	74	18	8
5	744	722	7
6	193	197	5
7	721	707	7
8	49	66	11
9	247	241	5
10	16	14	23
11	249	258	6
12	136	140	7
13	27	17	18
14	153	156	7
15	221	234	6
16	98	104	9
17	455	458	7
18	355	348	7
19	312	319	7
20	454	452	7
21	119	112	9

6 4 1

-19	60	81	14
-18	171	181	7
-17	80	91	11
-16	90	98	10
-15	115	118	8
-14	280	288	6
-13	126	114	7
-12	450	447	6
-11	347	352	6
-10	223	221	6
-9	667	666	7
-8	108	101	7
-7	594	586	7
-6	401	398	6
-5	577	584	6
-4	84	85	8
-3	477	465	6
-2	360	356	5
-1	810	809	8
0	143	135	6
1	352	350	5
2	61	55	9
3	514	503	6
4	-34	6	13
5	607	607	7
6	234	232	5
7	251	263	5
8	339	338	5
9	306	314	5
10	309	314	6
11	455	458	6
12	507	499	6
13	170	169	6
14	429	425	6
15	420	432	6
16	521	523	7
17	230	224	6
18	561	542	7
19	91	78	10
20	431	427	7

6 5 1

-19	149	162	8
-18	104	93	9
-17	156	163	8
-16	92	81	10
-15	171	165	7
-14	126	105	8
-13	415	426	6
-12	301	306	6
-11	471	480	6
-10	337	341	6
-9	104	97	8
-8	82	83	9
-7	352	350	6
-6	446	442	6
-5	44	37	12
-4	653	659	5
-3	453	453	4
-2	234	238	5
-1	523	514	6
0	58	56	10
1	437	446	6
2	351	357	5
3	433	427	6
4	491	498	6
5	506	495	6
6	367	380	5
7	450	441	6
8	495	489	6
9	514	517	6
10	590	589	7
11	53	29	12
12	1008	1002	10
13	764	758	8
14	496	495	7
15	169	169	7
16	498	496	7
17	25	11	22
18	130	130	8
19	62	60	13
20	283	275	7

6 6 1

-18	-36	48	18
-17	223	222	7
-16	256	261	7
-15	482	474	7
-14	84	42	10
-13	296	291	6
-12	421	404	6
-11	216	196	6
-10	73	16	10
-9	880	882	9
-8	589	592	7
-7	79	78	9
-6	283	287	6
-5	463	472	6
-4	196	202	6
-3	211	217	5
-2	273	277	5
-1	265	272	5
0	200	212	5
1	488	484	6
2	490	490	6
3	534	535	6
4	672	670	7
5	468	472	6
6	495	494	6
7	268	267	6
8	855	838	8
9	312	302	6
10	62	48	11
11	342	340	6
12	957	955	9
13	140	130	7
14	408	400	6
15	245	240	6
16	370	370	7
17	429	414	7
18	-13	51	30
19	321	313	7

6 7 1

-16	67	71	13
-15	314	315	7
-14	161	158	7
-13	568	563	7
-12	235	213	6
-11	248	236	6
-10	345	363	6

-9	335	343	6	-2	360	367	6	1	131	114	9	12	372	388	6	9	179	178	6	6	264	261	5
-8	153	141	7	-1	157	148	7					13	144	135	8	10	713	714	8	7	488	480	6
-7	322	327	6	0	558	569	7		7 -7 1			14	240	264	7	11	101	80	8	8	120	105	7
-6	703	708	8	1	419	406	6					15	-18	52	26	12	315	313	6	9	653	643	7
-5	852	849	8	2	43	1	14	0	320	319	7	16	170	183	8	13	218	238	6	10	90	73	8
-4	819	821	8	3	312	308	6	1	-29	2	20					14	475	474	7	11	495	481	6
-3	341	353	6	4	513	515	7	2	293	299	7		7 -2 1			15	242	234	6	12	69	2	10
-2	616	622	5	5	453	454	6	3	138	123	8					16	247	249	7	13	617	608	7
-1	184	190	6	6	65	75	11	4	506	519	5	0	331	328	6	17	245	248	7	14	82	63	10
0	249	256	6	7	361	361	6	5	501	485	7	1	354	358	6	18	195	196	7	15	704	701	8
1	-28	2	17	8	11	21	29	6	169	174	8	2	121	91	7					16	228	224	7
2	249	242	6	9	433	425	7	7	278	285	7	3	415	399	6		7 1 1			17	458	455	7
3	179	178	6	10	174	166	7					4	465	456	6					18	105	109	9
4	343	341	6	11	266	278	6		7 -6 1			5	225	231	6	-18	244	242	7	19	543	524	7
5	43	40	14	12	132	127	8					6	454	455	6	-17	426	427	4				
6	342	341	6	13	276	276	7	0	120	101	8	7	734	732	8	-16	38	49	18		7 3 1		
7	33	34	16	14	117	116	9	1	382	376	6	8	187	176	6	-15	517	519	7				
8	291	292	6	15	349	358	7	2	342	353	6	9	137	131	7	-14	230	231	6	-18	318	295	7
9	231	226	6					3	607	605	7	10	231	249	6	-13	179	169	7	-17	152	162	8
10	468	465	6		6 10 1			4	220	220	7	11	80	77	10	-12	173	183	6	-16	541	537	7
11	389	384	6					5	445	458	7	12	304	310	6	-11	394	381	6	-15	94	96	9
12	208	210	6	-11	297	273	7	6	235	242	7	13	-36	20	17	-10	331	317	6	-14	608	601	7
13	222	223	6	-10	106	107	9	7	536	547	7	14	312	322	6	-9	104	86	8	-13	176	173	7
14	142	132	7	-9	148	116	8	8	45	7	16	15	176	192	7	-8	544	533	7	-12	378	378	6
15	438	439	7	-8	204	221	7	9	209	208	7	16	410	409	7	-7	457	444	6	-11	61	23	11
16	-43	25	15	-7	297	304	7	10	41	10	18	17	-46	32	15	-6	311	299	6	-10	638	644	7
17	148	158	8	-6	293	283	7	11	126	127	9					-5	179	177	6	-9	149	146	6
18	267	262	7	-5	281	278	6						7 -1 1			-4	615	614	7	-8	755	747	8
				-4	444	440	7		7 -5 1							-3	60	8	10	-7	33	4	16
	6 8 1			-3	300	317	6					0	318	312	5	-2	611	615	7	-6	648	631	7
				-2	400	409	7	0	100	80	8	1	60	52	10	-1	73	32	9	-5	357	349	6
-15	462	458	7	-1	277	274	6	1	426	436	6	2	161	155	6	0	907	914	9	-4	464	451	6
-14	208	187	7	0	164	187	7	2	84	61	9	3	120	125	7	1	142	129	6	-3	334	347	5
-13	84	70	10	1	228	234	6	3	124	120	8	4	129	102	7	2	1016	1014	9	-2	205	196	5
-12	414	425	7	2	346	352	6	4	34	0	18	5	140	128	6	3	85	70	8	-1	442	446	6
-11	352	356	6	3	406	418	7	5	368	354	6	6	103	104	8	4	729	719	7	0	152	152	6
-10	475	481	7	4	83	104	10	6	59	45	13	7	224	231	6	5	147	148	6	1	604	607	7
-9	185	169	7	5	117	119	8	7	167	168	7	8	419	423	6	6	432	411	6	2	347	349	5
-8	352	349	6	6	186	185	7	8	-47	7	13	9	323	324	6	7	82	85	9	3	962	963	9
-7	304	294	6	7	306	284	6	9	292	282	7	10	675	667	7	8	369	345	6	4	66	54	10
-6	608	614	7	8	-53	2	12	10	189	177	7	11	96	96	8	9	128	126	7	5	431	423	6
-5	317	319	6	9	111	106	9	11	37	47	18	12	651	644	7	10	457	449	6	6	64	50	10
-4	825	853	8	10	69	82	12	12	224	241	7	13	124	123	8	11	110	92	8	7	917	903	9
-3	164	160	6	11	287	294	7	13	36	54	19	14	545	537	7	12	149	117	7	8	359	367	6
-2	607	618	7	12	143	149	8					15	130	152	8	13	478	484	7	9	471	451	6
-1	183	184	6	13	311	303	7		7 -4 1			16	579	583	7	14	75	44	11	10	247	240	6
0	57	69	11									17	102	110	9	15	360	349	6	11	265	260	6
1	341	350	6		6 11 1			0	199	205	6	18	432	461	7	16	211	208	7	12	43	23	14
2	174	161	6					1	299	301	6					17	454	441	7	13	434	422	6
3	474	475	6	-7	93	102	10	2	168	154	6		7 0 1			18	60	65	13	14	100	70	9
4	0	21	36	-6	254	249	7	3	357	349	6					19	324	311	7	15	305	300	6
5	150	137	7	-5	216	216	7	4	410	405	6	-18	258	257	7					16	44	2	16
6	420	422	6	-4	135	149	8	5	68	12	11	-17	665	663	8		7 2 1			17	407	410	7
7	282	280	6	-3	192	215	7	6	297	306	6	-16	54	66	14					18	284	282	7
8	193	191	6	-2	148	143	8	7	307	301	6	-15	429	438	7	-18	133	151	8	19	54	41	15
9	391	402	6	-1	-29	8	20	8	424	425	6	-14	138	143	7	-17	555	539	7				
10	334	321	6	0	149	155	8	9	337	338	6	-13	367	378	6	-16	478	490	7		7 4 1		
11	344	336	6	1	326	331	7	10	111	113	8	-12	200	201	6	-15	168	164	7				
12	465	464	7	2	26	35	22	11	577	610	7	-11	293	284	6	-14	151	134	7	-18	404	411	7
13	456	462	7	3	195	204	7	12	369	370	7	-10	143	133	7	-13	88	69	9	-17	90	85	10
14	285	279	7	4	103	87	9	13	404	418	7	-9	528	521	7	-12	486	489	7	-16	415	405	7
15	66	108	12	5	284	280	7	14	198	219	7	-8	161	158	6	-11	91	70	9	-15	49	55	15
16	173	184	7	6	175	164	7	15	130	132	9	-7	751	736	8	-10	467	449	6	-14	567	569	5
17	81	94	11	7	-71	21	9					-6	264	261	6	-9	133	127	7	-13	43	54	16
				8	72	31	12		7 -3 1			-5	267	252	5	-8	1089	1082	10	-12	508	516	5
	6 9 1			9	547	525	7					-4	287	269	5	-7	77	17	9	-11	528	525	7
				10	-20	19	26	0	124	116	7	-3	289	283	5	-6	730	722	8	-10	170	176	6
-13	143	158	8					1	173	174	6	-2	275	273	5	-5	80	70	8	-9	184	194	6
-12	473	473	7		6 12 1			2	96	79	8	-1	85	77	8	-4	629	627	7	-8	109	101	7
-11	247	260	7					3	216	213	6	0	266	273	5	-3	148	134	6	-7	-32	6	16
-10	177	165	7	0	33	58	21	4	233	218	6	1	495	495	6	-2	827	825	8	-6	87	91	8
-9	-56	38	12	1	203	212	7	5	529	512	7	2	480	480	6	-1	360	362	5	-5	308	295	6
-8	480	493	7	2	48	33	16	6	704	711	8	3	308	304	5	0	697	703	7	-4	84	75	8
-7	132	123	8	3	320	311	7	7	283	270	6	4	543	539	6	1	382	379	5	-3	651	661	7
-6	458	507	7					8	301	303	6	5	278	271	5	2	511	511	6	-2	81	20	8
-5	171	177	7		7 -8 1			9	430	425	6	6	431	432	6	3	401	394	6	-1	855	860	8
-4	407	417	6					10	440	474	7	7	117	113	7	4	445	445	6	0	455	457	6
-3	226	219	6	0	420	418	7	11	250	247	6	8	408	404	6	5	734	714	7	1	689	701	7

2	342	334	5	2	193	190	6	11	149	141	7	5	213	241	7	11	9	16	31
3	744	739	8	3	90	74	8	12	450	435	7					12	115	127	9
4	305	288	5	4	102	91	8	13	99	108	9		8	-5	1	13	69	55	12
5	549	552	6	5	411	413	6	14	289	282	7					14	303	306	7
6	153	157	6	6	418	421	6	15	100	95	10	0	309	307	7	15	288	308	7
7	231	224	6	7	71	43	10					1	403	409	7				
8	31	42	17	8	64	3	11		7	9	1	2	413	392	7		8	0	1
9	347	353	6	9	94	86	8					3	528	534	7				
10	245	240	6	10	437	426	4	-11	476	470	7	4	336	330	7	-16	250	259	7
11	175	178	6	11	131	130	7	-10	73	16	12	5	372	378	7	-15	315	324	7
12	186	172	6	12	191	186	7	-9	273	260	7	6	302	284	7	-14	152	170	8
13	187	185	6	13	432	436	7	-8	157	154	8	7	376	366	7	-13	397	403	7
14	131	114	8	14	-35	7	17	-7	394	383	7	8	293	297	7	-12	336	331	6
15	272	282	6	15	74	57	11	-6	564	557	7	9	396	399	7	-11	423	437	7
16	208	203	7	16	109	144	9	-5	353	365	6					-10	290	278	6
17	334	325	7	17	106	123	9	-4	396	398	7		8	-4	1	-9	433	436	6
18	388	390	7					-3	431	429	7					-8	318	300	6
19	27	19	23		7	7	1	-2	550	543	7	0	767	787	8	-7	547	531	7
								-1	213	219	7	1	496	499	7	-6	410	404	6
	7	5	1	-15	400	418	7	0	22	41	23	2	439	440	7	-5	581	571	7
				-14	230	226	7	1	138	131	7	3	506	517	7	-4	358	347	6
-17	188	179	7	-13	244	229	7	2	421	421	7	4	261	243	6	-3	619	617	7
-16	-62	0	11	-12	114	120	9	3	117	151	8	5	374	382	7	-2	424	419	6
-15	321	305	7	-11	489	499	7	4	404	408	6	6	116	102	8	-1	219	218	6
-14	292	308	6	-10	175	189	7	5	65	43	12	7	499	504	7	0	276	282	6
-13	294	305	6	-9	222	231	6	6	602	604	7	8	103	122	9	1	201	199	6
-12	413	416	6	-8	-38	13	15	7	185	193	7	9	440	460	7	2	66	18	10
-11	520	502	7	-7	365	376	6	8	396	398	7	10	69	69	12	3	142	131	7
-10	25	40	20	-6	368	371	6	9	357	357	7	11	467	484	7	4	282	276	6
-9	589	577	7	-5	250	253	6	10	585	574	7					5	139	107	7
-8	184	191	6	-4	145	138	7	11	300	291	7		8	-3	1	6	198	182	6
-7	371	366	6	-3	472	472	6	12	481	469	7					7	138	119	7
-6	315	309	6	-2	525	534	7	13	222	211	7	0	447	451	6	8	458	455	6
-5	179	173	6	-1	75	72	9					1	398	404	6	9	265	259	6
-4	66	61	10	0	321	314	6		7	10	1	2	177	168	7	10	221	207	6
-3	70	38	10	1	155	144	6					3	627	629	7	11	32	47	19
-2	71	55	9	2	219	210	6	-8	254	270	7	4	149	153	7	12	451	455	7
-1	380	375	6	3	85	80	9	-7	52	23	15	5	382	381	6	13	183	180	7
0	-25	20	18	4	188	172	6	-6	391	409	7	6	378	384	6	14	174	180	7
1	490	488	6	5	71	67	10	-5	143	163	8	7	462	460	7	15	123	143	9
2	59	29	11	6	307	308	6	-4	366	370	7	8	416	421	7	16	279	281	7
3	575	565	7	7	530	539	7	-3	139	152	8	9	569	557	7				
4	83	69	9	8	402	403	6	-2	490	491	7	10	440	463	7		8	1	1
5	138	128	6	9	245	239	6	-1	58	64	13	11	384	379	7				
6	36	21	15	10	228	222	6	0	222	207	7	12	310	334	7	-16	49	52	16
7	159	156	6	11	70	64	11	1	263	279	7	13	273	271	7	-15	242	233	7
8	397	397	6	12	264	260	6	2	327	319	7					-14	39	52	17
9	-57	5	9	13	347	340	7	3	234	223	7		8	-2	1	-13	347	350	7
10	134	134	7	14	48	73	15	4	492	495	7					-12	450	456	7
11	240	241	6	15	75	91	11	5	313	304	7	0	380	390	6	-11	286	274	6
12	433	420	6	16	103	113	10	6	507	515	7	1	163	155	7	-10	391	386	6
13	73	80	11					7	394	396	7	2	70	60	10	-9	386	382	6
14	465	462	7		7	8	1	8	392	367	7	3	80	53	9	-8	241	233	6
15	191	189	7					9	321	302	7	4	559	564	7	-7	171	166	6
16	565	564	7	-13	162	162	8	10	311	313	7	5	578	580	7	-6	308	304	6
17	89	93	10	-12	108	108	9	11	299	298	7	6	148	146	7	-5	286	295	6
18	533	534	7	-11	271	290	7					7	555	554	7	-4	465	453	6
				-10	-45	16	14		7	11	1	8	453	444	7	-3	182	188	6
	7	6	1	-9	223	213	7					9	339	338	6	-2	217	212	6
				-8	239	245	6	-4	413	412	5	10	161	164	7	-1	160	154	6
-16	89	88	6	-7	28	65	20	-3	124	123	9	11	311	311	7	0	393	402	6
-15	253	253	7	-6	207	219	6	-2	457	436	7	12	438	434	7	1	159	146	6
-14	69	74	12	-5	551	568	7	-1	115	101	9	13	134	140	8	2	166	164	6
-13	548	562	7	-4	481	487	7	0	245	235	7	14	101	95	10	3	157	166	6
-12	90	85	10	-3	177	188	7	1	211	231	7					4	193	182	6
-11	528	521	7	-2	35	25	17	2	415	390	7		8	-1	1	5	176	167	6
-10	414	426	6	-1	358	359	6	3	281	277	7					6	484	475	6
-9	459	455	4	0	308	291	6	4	214	217	7	0	694	681	8	7	83	21	9
-8	125	142	7	1	349	351	6	5	300	308	7	1	499	482	6	8	546	538	7
-7	332	334	6	2	262	259	6	6	44	47	17	2	458	445	6	9	235	233	6
-6	117	121	7	3	257	254	6					3	132	114	7	10	684	697	8
-5	54	72	12	4	180	174	6		8	-6	1	4	186	192	6	11	111	108	8
-4	53	34	12	5	164	171	7					5	356	356	6	12	123	109	8
-3	145	141	6	6	316	299	6	0	223	225	7	6	526	523	7	13	163	186	7
-2	289	287	6	7	89	93	9	1	72	84	12	7	57	13	12	14	354	363	7
-1	182	172	6	8	270	271	6	2	94	114	10	8	313	314	6	15	57	85	14
0	236	228	6	9	119	119	8	3	-21	1	25	9	230	233	6	16	242	228	7
1	91	79	8	10	590	584	7	4	433	429	7	10	200	184	7				

	8	2	1																
-16	89	89	11																
-15	107	118	9																
-14	135	135	8																
-13	104	114	9																
-12	151	161	7																
-11	169	160	7																
-10	-41	10	14																
-9	159	161	7																
-8	360	354	6																
-7	368	363	6																
-6	318	324	6																
-5	112	112	7																
-4	345	335	6																
-3	184	187	6																
-2	757	753	8																
-1	90	69	8																
0	281	274	6																
1	223	222	6																
2	557	556	7																
3	120	109	7																
4	474	476	6																
5	202	194	6																
6	394	390	6																
7	22	19	21																
8	417	411	6																
9	133	130	7																
10	412	418	6																
11	-46	26	13																
12	37	30	17																
13	355	360	6																
14	173	191	7																
15	255	253	7																
16	156	172	8																
17	306	302	7																
	8	3	1																
-16	217	245	7																
-15	47	50	16																
-14	170	172	7																
-13	154	168	7																
-12	58	68	13																
-11	114	111	8																
-10	85	81	10																
-9	217	210	6																
-8	446	443	6																
-7	123	105	7																
-6	399	396	6																
-5	181	174	6																
-4	825	829	8																
-3	241	232	6																
-2	387	381	6																
-1	82	84	9																
0	623	637	7																
1	68	62	10																
2	317	317	6																
3	147	163	6																
4	380	373	6																
5	173	165	6																
6	262	265	6																
7	235	236	6																
8	221	215	6																
9	205	218	6																
10	111	108	8																
11	417	409	6																
12	57	70	13																
13	494	478	7																
14	148	149	8																
15	520	518	7																
16	178	182	7																
17	508	499	7																
	8	4	1																
-15	64	49	13																
-14	398	399	4																

-13	58	61	13	-4	173	162	7					3	462	453	7	-8	114	96	8	9	301	292	6
-12	316	312	6	-3	611	612	7	-8	420	426	7	4	227	223	7	-7	452	458	7	10	126	127	8
-11	117	120	8	-2	261	259	6	-7	231	226	7	5	449	455	7	-6	338	343	6	11	193	194	7
-10	251	250	6	-1	608	615	7	-6	374	361	7	6	177	162	7	-5	526	528	7	12	139	139	8
-9	202	187	6	0	70	36	10	-5	246	266	7	7	513	511	7	-4	457	461	7	13	381	389	7
-8	234	235	6	1	573	578	7	-4	196	185	7	8	134	134	8	-3	42	28	15				
-7	191	182	6	2	74	61	10	-3	201	186	7	9	467	462	7	-2	545	554	7		9 5 1		
-6	40	0	15	3	523	532	7	-2	339	334	7	10	168	171	7	-1	331	341	6				
-5	63	18	11	4	67	48	11	-1	77	63	11	11	382	397	7	0	261	263	6	-12	254	258	7
-4	66	61	10	5	408	411	6	0	359	384	7	12	135	145	8	1	-9	48	30	-11	35	57	20
-3	88	89	9	6	305	311	6	1	152	169	8					2	306	311	6	-10	450	476	7
-2	320	317	6	7	94	94	9	2	279	278	7		9 0 1			3	43	51	15	-9	97	98	10
-1	65	40	10	8	262	271	6	3	155	163	7					4	551	568	7	-8	392	399	7
0	181	179	6	9	247	245	6	4	300	305	7	-13	217	228	7	5	49	7	14	-7	99	105	9
1	204	217	6	10	207	197	7	5	112	116	9	-12	74	68	12	6	641	642	8	-6	308	312	6
2	552	537	7	11	132	139	8	6	117	117	9	-11	319	328	7	7	170	167	7	-5	-28	47	20
3	536	540	7	12	327	316	7	7	39	70	18	-10	202	200	7	8	664	667	8	-4	323	329	6
4	222	222	6	13	147	139	8	8	401	423	7	-9	525	540	7	9	193	198	7	-3	25	58	22
5	269	261	6	14	284	280	7	9	307	309	7	-8	109	105	9	10	321	317	7	-2	-43	5	14
6	381	389	6	15	188	196	7	10	224	212	7	-7	351	353	6	11	323	337	7	-1	135	124	8
7	409	401	6									-6	189	184	7	12	453	442	7	0	358	376	6
8	309	312	6		8 7 1				8 10 1			-5	625	627	7	13	247	249	7	1	327	359	6
9	450	446	6									-4	101	38	9	14	174	190	8	2	235	245	6
10	224	232	6	-12	400	408	7	-4	202	215	7	-3	495	485	7					3	179	186	7
11	499	490	5	-11	377	353	7	-3	205	224	7	-2	304	308	6		9 3 1			4	33	12	19
12	96	67	9	-10	258	264	7	-2	24	59	24	-1	505	507	7					5	321	327	6
13	589	580	7	-9	482	486	7	-1	46	51	16	0	79	58	10	-13	331	336	7	6	62	47	12
14	76	62	11	-8	105	107	9	0	260	258	7	1	692	695	8	-12	167	166	4	7	330	331	6
15	743	729	8	-7	453	454	7	1	130	156	8	2	159	148	7	-11	52	35	15	8	83	66	10
16	51	24	15	-6	145	148	7	2	105	99	9	3	240	241	6	-10	382	394	7	9	257	239	7
				-5	375	376	4	3	166	163	8	4	345	348	6	-9	273	277	7	10	82	81	11
	8 5 1			-4	200	196	7	4	205	214	7	5	818	826	9	-8	144	141	8	11	303	284	7
				-3	559	574	5	5	31	18	21	6	373	359	6	-7	177	177	7	12	36	26	19
-15	209	224	7	-2	55	2	13	6	224	220	7	7	479	471	7	-6	399	400	6	13	134	150	8
-14	506	498	7	-1	509	517	7					8	243	239	7	-5	77	70	10				
-13	101	94	9	0	343	347	6		9 -4 1			9	279	289	7	-4	477	495	7		9 6 1		
-12	379	379	7	1	309	313	6					10	267	287	7	-3	197	205	7				
-11	40	54	17	2	374	375	6	0	341	347	7	11	350	351	7	-2	586	605	7	-10	329	338	7
-10	522	513	7	3	389	400	6	1	419	412	7	12	320	328	7	-1	341	347	6	-9	-41	7	16
-9	114	98	8	4	394	387	6	2	323	335	7	13	70	81	13	0	441	438	6	-8	149	157	8
-8	266	259	6	5	204	206	7	3	289	295	7					1	126	124	8	-7	22	19	24
-7	47	17	14	6	341	345	6	4	358	361	7		9 1 1			2	391	388	6	-6	119	115	8
-6	373	375	6	7	308	310	6	5	426	436	7					3	108	87	8	-5	290	299	7
-5	45	18	14	8	307	303	6	6	158	156	8	-13	264	267	7	4	564	554	7	-4	32	45	20
-4	51	40	13	9	165	169	7					-12	145	130	8	5	73	55	11	-3	364	380	7
-3	260	252	6	10	730	727	8		9 -3 1			-11	644	640	8	6	430	437	7	-2	546	552	7
-2	296	286	6	11	508	507	7					-10	127	122	8	7	351	360	6	-1	355	360	6
-1	81	66	9	12	255	252	7	0	178	166	7	-9	417	409	7	8	299	299	6	0	105	106	9
0	488	490	6	13	126	115	9	1	119	127	8	-8	89	76	10	9	64	57	12	1	516	538	7
1	899	916	9	14	378	352	7	2	258	258	7	-7	761	752	8	10	219	208	7	2	272	262	6
2	134	104	7					3	305	311	7	-6	322	323	6	11	365	369	7	3	392	402	7
3	701	710	8		8 8 1			4	132	122	8	-5	653	644	8	12	64	77	13	4	62	61	12
4	120	105	7					5	-24	5	23	-4	89	71	9	13	214	213	7	5	204	193	7
5	587	580	7	-10	190	211	7	6	322	337	7	-3	657	670	8	14	255	260	5	6	117	123	8
6	206	193	6	-9	237	211	7	7	164	182	8	-2	249	242	6					7	170	167	7
7	386	379	6	-8	79	100	11	8	92	94	10	-1	561	565	7		9 4 1			8	176	180	7
8	143	143	7	-7	499	507	7	9	273	291	7	0	291	303	6					9	268	245	7
9	266	261	6	-6	182	170	7					1	440	440	6	-12	339	323	7	10	59	62	14
10	136	148	8	-5	234	231	7		9 -2 1			2	333	329	6	-11	92	83	10	11	194	190	7
11	313	312	6	-4	247	246	7					3	125	120	8	-10	594	589	8	12	116	100	9
12	201	207	7	-3	260	265	6	0	385	364	7	4	394	394	6	-9	-50	6	13				
13	356	363	7	-2	385	391	7	1	414	413	7	5	158	123	7	-8	449	449	7		9 7 1		
14	418	419	7	-1	231	229	6	2	71	73	11	6	590	602	7	-7	142	142	8				
15	351	344	7	0	408	406	7	3	102	106	9	7	78	77	11	-6	221	208	7	-9	207	206	7
16	366	379	7	1	268	264	6	4	123	109	8	8	510	519	7	-5	117	109	8	-8	182	176	7
				2	471	460	7	5	244	226	7	9	-40	24	16	-4	293	303	6	-7	137	128	8
	8 6 1			3	264	263	6	6	70	81	12	10	655	654	8	-3	221	225	6	-6	106	101	9
				4	158	147	7	7	339	357	7	11	75	82	11	-2	295	303	6	-5	171	170	7
-14	388	379	7	5	199	199	7	8	13	54	29	12	538	538	7	-1	255	269	6	-4	165	159	7
-13	-27	38	22	6	605	602	7	9	388	394	7	13	86	85	11	0	59	54	12	-3	313	298	7
-12	492	489	7	7	413	413	7	10	207	215	7					1	76	82	10	-2	140	143	8
-11	478	474	7	8	-47	23	14	11	312	330	7		9 2 1			2	72	83	11	-1	205	213	7
-10	78	52	11	9	99	89	9									3	166	180	7	0	339	318	7
-9	456	464	7	10	666	668	8		9 -1 1			-13	299	290	7	4	153	148	7	1	548	551	7
-8	490	503	7	11	65	57	13					-12	205	186	7	5	168	175	7	2	173	172	7
-7	521	523	7	12	158	150	8	0	94	82	9	-11	275	262	7	6	64	2	12	3	139	142	8
-6	209	198	6					1	71	58	11	-10	34	19	19	7	86	39	10	4	409	417	7
-5	467	460	7		8 9 1			2	42	45	16	-9	648	666	8	8	250	242	6	5	197	190	7

6	47	38	16
7	141	154	8
8	134	123	8
9	399	381	7
10	25	32	23

9 8 1

-6	113	104	9
-5	417	425	7
-4	183	171	7
-3	260	258	7
-2	187	191	7
-1	462	474	7
0	-23	20	23
1	336	333	7
2	25	21	23
3	566	582	7
4	286	285	7
5	358	375	7
6	61	55	13
7	225	213	7
8	210	229	7

9 9 1

-2	261	256	7
-1	299	312	7
0	201	216	7
1	442	446	7
2	298	292	7
3	122	126	9
4	359	378	7

10 -2 1

0	352	347	4
1	408	398	7
2	168	160	8
3	174	172	8

10 -1 1

0	24	3	24
1	402	409	7
2	151	154	8
3	215	192	7
4	56	64	14
5	159	167	8
6	141	133	8

10 0 1

-8	69	66	13
-7	98	103	10
-6	17	0	28
-5	174	179	7
-4	151	127	8
-3	372	379	7
-2	43	5	17
-1	290	307	7
0	117	117	9
1	78	75	11
2	487	505	7
3	260	262	7
4	148	140	8

10 2 1

5	320	330	7
6	234	225	7
7	366	369	7
8	58	33	14

10 1 1

-8	74	70	12
-7	50	29	15
-6	46	35	16
-5	337	348	7
-4	211	209	7
-3	91	51	10
-2	201	198	7
-1	798	831	9
0	235	233	7
1	149	147	8
2	25	18	22
3	489	489	7
4	225	234	7
5	178	185	7
6	72	90	12
7	526	537	7
8	286	283	7
9	250	262	7

10 2 1

-9	291	290	7
-8	125	123	9
-7	279	280	7
-6	94	84	10
-5	441	438	7

-4	100	102	9
-3	254	247	7
-2	121	96	8
-1	445	454	7
0	98	96	9
1	191	189	7
2	298	313	7
3	39	7	17
4	88	105	10
5	397	401	7
6	258	258	7
7	140	157	8
8	187	208	7
9	108	105	9

10 3 1

-8	52	16	15
-7	505	514	7
-6	90	80	10
-5	168	158	7
-4	101	83	9
-3	141	134	8
-2	67	34	12
-1	123	134	8
0	127	120	8
1	167	164	7
2	110	113	9
3	197	197	7
4	486	504	7
5	93	70	10
6	466	484	7
7	261	261	7

8	539	558	7
9	230	246	7

10 4 1

-8	284	283	7
-7	247	252	7
-6	196	197	7
-5	315	306	7
-4	535	539	7
-3	259	252	7
-2	249	259	7
-1	267	246	7
0	201	192	7
1	225	220	7
2	399	404	7
3	118	103	9
4	687	707	8
5	58	62	14
6	569	569	7
7	230	234	7
8	473	471	7
9	-7	49	35

10 5 1

-7	248	246	7
-6	670	660	8
-5	104	97	10
-4	497	494	7
-3	107	85	9
-2	616	632	8
-1	51	48	15

0	456	467	7
1	165	167	7
2	464	482	7
3	36	65	19
4	453	456	7
5	311	333	7
6	237	246	7
7	160	178	8
8	185	190	7

10 6 1

-5	32	0	21
-4	584	588	8
-3	188	178	7
-2	219	225	7
-1	167	174	8
0	373	383	7
1	240	246	7
2	321	324	7
3	312	334	7
4	218	223	7
5	353	346	7
6	169	186	8

10 7 1

-1	550	562	8
0	148	148	8
1	486	491	7
2	55	61	15
3	375	387	7

0	ATOM	MSD	COSA	COSB	COSC	B11	B22	B33	B12	B13	B23
0	Rh					0.001185	0.001837	0.000328	-0.000418	-0.000059	-0.000120
		0.00473	0.9791	0.0198	0.1023						
		0.00744	-0.0800	0.0925	0.9941						
		0.01094	0.1869	0.9955	-0.0368						
0	Cl1					0.005063	0.003390	0.000848	0.002203	-0.000869	-0.000722
		0.01227	0.6358	-0.6244	0.0653						
		0.01700	0.2286	0.3488	0.9419						
		0.03342	0.7373	0.6989	-0.3296						
0	Cl2					0.002605	0.003340	0.001016	-0.001349	0.000217	-0.000386
		0.01023	0.9940	0.1212	-0.0679						
		0.01924	0.0924	0.9707	0.2725						
		0.02331	0.0584	-0.2073	0.9598						
0	Cl3					0.003514	0.003197	0.000679	-0.001019	-0.000135	-0.000220
		0.01386	-0.9114	0.0150	-0.3609						
		0.01554	0.3101	-0.1762	-0.9270						
		0.01904	-0.2706	-0.9842	0.1022						
0	Cl4					0.003994	0.002556	0.001176	-0.001963	-0.001254	0.000086
		0.01225	0.8518	0.6080	0.3075						
		0.01524	-0.3562	0.7873	-0.2831						
		0.02945	0.3842	-0.1027	-0.9084						
0	O3					0.002931	0.005013	0.000740	-0.002729	-0.001038	0.000061
		0.00800	0.8805	0.1898	0.4860						
		0.01909	0.4657	0.2459	-0.8543						
		0.02972	-0.0880	0.9505	0.1844						
0	O4					0.004393	0.005994	0.001521	-0.002475	-0.000988	0.000359
		0.01621	0.9702	0.1073	0.2346						
		0.03174	-0.2220	-0.7225	0.6439						
		0.03919	0.0973	-0.6830	-0.7283						
0	O5					0.010543	0.005806	0.000911	-0.004275	-0.000686	-0.001119
		0.01746	0.2288	0.3975	0.9264						
		0.03463	-0.2675	-0.9061	0.3605						
		0.04295	-0.9360	0.1446	0.1087						
0	N1					0.002190	0.001840	0.000421	-0.000297	0.000519	-0.000526
		0.00570	-0.5721	0.3920	0.6577						
		0.01110	-0.8169	-0.5810	-0.4215						
		0.01256	0.0734	-0.7133	0.6243						
0	N2					0.001950	0.002258	0.000340	-0.000513	0.000302	-0.000449
		0.00593	-0.5640	0.2259	0.7607						
		0.00903	-0.8060	-0.1905	-0.6030						
		0.01391	-0.1798	-0.9553	0.2401						
0	N3					0.001640	0.001940	0.000444	-0.000266	-0.000449	-0.000161
		0.00557	-0.8832	0.0256	-0.4221						
		0.01037	0.2082	-0.5816	-0.7749						
		0.01240	-0.4202	-0.8131	0.4705						
0	N4					0.001684	0.002083	0.000421	-0.000120	-0.000684	0.000278
		0.00432	0.7595	-0.1804	0.5469						
		0.01136	0.6410	0.3642	-0.7048						

```
          0.01359   0.1112 0.9137 0.4518
0     N5                                0.001814  0.001866  0.000525 -0.000526  0.000087 -0.000048
          0.00723   0.9680-0.0380-0.0897
          0.01093   0.1723 0.8978-0.3882
          0.01221   0.1826 0.4388 0.9172
0     N6                                0.001990  0.001751  0.000491 -0.000822  0.000288 -0.000235
          0.00745  -0.9289-0.0595 0.3416
          0.00993  -0.2397-0.9513-0.3579
          0.01185  -0.2822 0.3023-0.8691
0     C1                                0.001928  0.002435  0.000543  0.000262 -0.000316 -0.000496
          0.00702   0.9059-0.1988 0.1655
          0.01085   0.0592 0.5254 0.8782
          0.01727   0.4194 0.8273-0.4487
0     C2                                0.002409  0.002888  0.000762 -0.001457  0.000561 -0.001122
          0.00881  -0.9234 0.0262 0.3177
          0.01164  -0.3696-0.7768-0.6342
          0.02243   0.1033-0.6292 0.7049
0     C3                                0.004520  0.002365  0.000778 -0.003088  0.000758 -0.000260
          0.00979  -0.6424-0.8374 0.2000
          0.01575  -0.3226 0.4763 0.7946
          0.02229  -0.6952 0.2679-0.5733
0     C4                                0.004157  0.002360  0.000586 -0.000517 -0.000119  0.000219
          0.01141  -0.1860 0.6157-0.6869
          0.01522   0.3921-0.5341-0.7041
          0.01807   0.9009 0.5794 0.1799
0     C5                                0.002695  0.002285  0.000342 -0.000221  0.000261 -0.000425
          0.00658   0.3146-0.3029-0.8881
          0.01104   0.7995-0.2257 0.4437
          0.01487   0.5116 0.9259-0.1204
0     C6                                0.002646  0.002122  0.000437 -0.000397  0.000368 -0.000401
          0.00773   0.5143-0.3538-0.7384
          0.01208   0.7373-0.0400 0.6469
          0.01350   0.4381 0.9345-0.1904
0     C7                                0.003446  0.002321  0.000558 -0.000233  0.000022  0.000177
          0.01106  -0.3293 0.6085-0.6126
          0.01304   0.6441-0.2036-0.6951
          0.01702   0.6904 0.7670 0.3763
0     C8                                0.002191  0.003706  0.000510  0.001808 -0.000535 -0.000142
          0.00586  -0.8183 0.2761-0.3470
          0.01226   0.2657-0.2053-0.9369
          0.02686  -0.5096-0.9389 0.0416
0     C9                                0.001500  0.003884  0.000610 -0.000646 -0.000329 -0.000507
          0.00567   0.9698 0.0561 0.2061
          0.01353  -0.1566 0.2410 0.9596
          0.02359   0.1872 0.9689-0.1914
0     C10                               0.002924  0.002826  0.000502 -0.001603  0.000214 -0.001047
          0.00775   0.1149 0.5665 0.8552
          0.01129   0.9909 0.1905-0.1207
          0.01954  -0.0697 0.8018-0.5040
```

```
0    C11                                0.002216  0.002154  0.000659 -0.000878 -0.000416  0.000017
         0.00829   0.9543 0.0725 0.2803
         0.01251   0.1851 0.9731-0.1741
         0.01566  -0.2347 0.2188 0.9440
0    C12                                0.002503  0.003641  0.000569 -0.000031  0.000251 -0.000146
         0.00933  -0.8911 0.1404 0.3239
         0.01328  -0.2880 0.0802-0.9419
         0.02288   0.3508 0.9868 0.0886
0    C13                                0.002894  0.003275  0.000589  0.001236 -0.000247 -0.001065
         0.00854  -0.6166 0.5173 0.4680
         0.01143  -0.6041-0.1518-0.8051
         0.02597  -0.5049-0.8423 0.3644
0    C14                                0.003218  0.002190  0.000698 -0.001162 -0.000696 -0.000413
         0.00973  -0.7344-0.5492-0.5716
         0.01301   0.4365-0.7911 0.0453
         0.01840  -0.5197-0.2693 0.8193
0    C15                                0.001667  0.002067  0.000570  0.000087 -0.000958 -0.000136
         0.00423  -0.8536 0.0829-0.4499
         0.01218  -0.0552-0.9024-0.4628
         0.01600  -0.5181-0.4227 0.7639
0    C16                                0.001856  0.002226  0.000564 -0.000247 -0.000986  0.000188
         0.00462  -0.8197 0.1085-0.4968
         0.01368  -0.4001-0.9643 0.1004
         0.01561  -0.4098 0.2414 0.8621
0    C17                                0.003317  0.002701  0.000849 -0.001868 -0.000375 -0.000483
         0.01105  -0.8566-0.5760-0.3415
         0.01614   0.4741-0.7563-0.1931
         0.02022   0.2036 0.3102-0.9198
0    C18                                0.003435  0.003019  0.000951 -0.002887 -0.001046  0.000775
         0.01014  -0.9348-0.4955-0.1911
         0.01409   0.1436-0.7078 0.6034
         0.02766   0.3248-0.5035-0.7742
0    C19                                0.002869  0.004071  0.000517 -0.002573 -0.000331  0.000782
         0.00989  -0.0068-0.3305 0.9215
         0.01020   0.9950 0.2869 0.0586
         0.02638  -0.0998 0.8991 0.3838
0    C20                                0.002355  0.003379  0.000383 -0.000655 -0.000434  0.000185
         0.00690  -0.6021 0.0748-0.7695
         0.01110  -0.7744-0.0640 0.6195
         0.02055  -0.1944-0.9951-0.1553
0    C21                                0.001618  0.001935  0.000504 -0.002017  0.000322  0.000184
         0.00359  -0.8876-0.5218 0.2634
         0.01138  -0.4507 0.4335-0.6912
         0.01320   0.0950-0.7347-0.6730
0    C22                                0.001594  0.001830  0.000572 -0.001946  0.000243 -0.000033
         0.00395  -0.9194-0.5358 0.1231
         0.01175   0.3671-0.8390-0.0354
         0.01319  -0.1411-0.0944-0.9918
0    C23                                0.001615  0.002535  0.000477 -0.001582  0.000026  0.000235
```

```
          0.00560  -0.9816-0.3125 0.1278
          0.01020  -0.1813 0.2988-0.9042
          0.01584   0.0606-0.9017-0.4076
0     C24                                0.001906  0.002764  0.000538 -0.001913  0.000546  0.000463
          0.00461   0.8519 0.3857-0.4497
          0.01255   0.5211-0.3372 0.7066
          0.01838   0.0525 0.8588 0.5463
0     C25                                0.002581  0.002995  0.000580 -0.001493 -0.000277  0.000066
          0.00963   0.9539 0.1719 0.3114
          0.01321  -0.2946-0.3008 0.9037
          0.01791  -0.0581 0.9381 0.2939
0     C26                                0.003692  0.002426  0.000745 -0.000873  0.000725 -0.000240
          0.01202   0.7186-0.2722-0.5648
          0.01455   0.3097 0.9488-0.2352
          0.01964  -0.6226-0.1603-0.7910
0     C27                                0.003260  0.002472  0.000852  0.000241  0.000692  0.000467
          0.01087   0.7616-0.4782-0.1153
          0.01331   0.4276 0.6750-0.6335
          0.02455   0.4869 0.5619 0.7651
0     C28                                0.003058  0.003784  0.000667 -0.000839 -0.000318  0.000969
          0.01053   0.5648-0.3470 0.6601
          0.01349   0.8122 0.3270-0.5367
          0.02678   0.1461 0.8790 0.5256
0     C29                                0.002283  0.003051  0.000688 -0.001710  0.000017  0.000465
          0.00836  -0.9788-0.3059 0.1496
          0.01333   0.2046-0.5089 0.7727
          0.02070  -0.0034-0.8047-0.6169
0     C30                                0.003119  0.003773  0.000608 -0.001828 -0.000605  0.000692
          0.01010  -0.6773 0.1176-0.6834
          0.01359  -0.7324-0.4637 0.5691
          0.02473   0.0706-0.8781-0.4574
0     C31                                0.003458  0.003326  0.000495 -0.002243 -0.000188 -0.000358
          0.01016   0.4911 0.3172 0.8596
          0.01345   0.8438 0.2824-0.5046
          0.01986  -0.2165 0.9053-0.0804
0     C32                                0.002272  0.002485  0.000544 -0.002381  0.000226  0.000245
          0.00597   0.8711 0.5267-0.2999
          0.01249   0.4353-0.1634 0.8539
          0.01636  -0.2274 0.8342 0.4253
0     C33                                0.002746  0.002614  0.000445 -0.002409  0.000289  0.000201
          0.00692   0.7217 0.4879-0.5654
          0.01165  -0.6100-0.2027-0.7998
          0.01672   0.3272-0.8490-0.2016
0     C34                                0.003574  0.002973  0.000430 -0.001956 -0.000563  0.000201
          0.00853   0.3948-0.0290 0.9101
          0.01372   0.8385 0.6058-0.2720
          0.01870  -0.3755 0.7951 0.3126
0     C35                                0.004881  0.002964  0.000504 -0.002735  0.000445 -0.000540
          0.01046  -0.0727 0.2991 0.9600
```

```
          0.01461   0.6817 0.8283-0.1379
          0.02181   0.7280-0.4738 0.2439
0     C36                                 0.003975  0.002667  0.000577 -0.000696  0.000722 -0.000192
          0.01067  -0.5361 0.1294 0.8139
          0.01542   0.1523-0.8671 0.3232
          0.01916  -0.8303-0.4810-0.4829
0     C37                                 0.002971  0.002736  0.000508 -0.001262 -0.000202 -0.000131
          0.01066   0.6603 0.1402 0.7593
          0.01263   0.7507 0.1153-0.6502
          0.01598   0.0192 0.9834 0.0264
0     C38                                 0.002222  0.002337  0.000541 -0.001560  0.000633 -0.000372
          0.00688   0.8895 0.2048-0.4414
          0.01188   0.2915 0.7754 0.6595
          0.01536  -0.3519 0.5974-0.6085
0     C39                                 0.006224  0.002972  0.000805 -0.001324 -0.002396 -0.000373
          0.00916   0.5941 0.2586 0.8064
          0.01739  -0.1019 0.9497-0.0494
          0.03398   0.7979 0.1769-0.5894
0     C40                                 0.004822  0.005906  0.001134 -0.002052 -0.000092 -0.001407
          0.01900  -0.9677-0.1936-0.2650
          0.02209   0.2180-0.4547-0.8573
          0.03783   0.1263 0.8693-0.4414
0     N7                                  0.005737  0.005265  0.000972 -0.002440 -0.000948 -0.000726
          0.01680  -0.6552-0.2930-0.7540
          0.02665  -0.7272 0.2515 0.5669
          0.03167  -0.2048-0.9224 0.3318
0     C41                                 0.012660  0.004578  0.001103 -0.002613  0.002058 -0.000507
          0.02149   0.2950-0.1826-0.9314
          0.02686  -0.1091-0.9711 0.1672
          0.05485  -0.9492-0.1537-0.3232
0     C42                                 0.005373  0.004171  0.000995 -0.000571 -0.000295  0.000548
          0.01771   0.4863-0.5127 0.5854
          0.02321   0.7815 0.1498-0.6123
          0.02934   0.3907 0.8454 0.5314
0     N8                                  0.008009  0.005918  0.001389  0.001450 -0.001550 -0.001504
          0.02435   0.7416-0.2232 0.5429
          0.02568  -0.1297 0.6903 0.7084
          0.05131   0.6582 0.6883-0.4511
0     C43                                 0.026958  0.005417  0.002136 -0.006127 -0.002244 -0.001415
          0.02740   0.1598 0.9432 0.3845
          0.04884   0.1309-0.3194 0.9073
          0.11059   0.9784 0.0910-0.1701
0     C44                                 0.006375  0.002835  0.001072 -0.004292 -0.001698 -0.000033
          0.01032   0.6330 0.8246 0.3486
          0.01959  -0.3390 0.5254-0.6907
          0.03386  -0.6960 0.2096 0.6336
0     C45                                 0.006797  0.003834  0.001638  0.002418 -0.001118 -0.001561
          0.01507   0.4773-0.7579-0.1685
          0.02827  -0.6606-0.3855-0.7268
```

```
         0.04690  -0.5795-0.5263 0.6659
0    N9                                   0.007579  0.005083  0.001640 -0.006304 -0.002197  0.001641
         0.01841  -0.7462-0.7959 0.0305
         0.02385  -0.4990 0.3698-0.7018
         0.05220  -0.4407 0.4794 0.7117
0    N10                                  0.010157  0.006670  0.002829  0.005580  0.000931  0.000337
         0.02197  -0.6194 0.6467 0.0178
         0.05757   0.5080 0.4768-0.7414
         0.07383   0.5985 0.5954 0.6708
```

Appendix 2:

Determination of Site-Specific Binding Constants of Molecules that Bind to and Cleave Nucleic Acids*

* Adapted from Jackson, B.A., Hastings, C.A., Hudson, B.P., Johann, T.W., and Barton, J.K. *Manuscript in Preparation.*

A2.1: Introduction

In the design of molecular agents for the specific recognition of sites on nucleic acids, the first step in assessing a new molecule is the determination of the molecule's preferred binding sites. After these sites have been identified, however, quantitative information is required to comprehensively understand the characteristics of binding at different nucleic acid sites. Measurement of thermodynamic association constants provides an excellent way to explore the factors which govern binding and their effects on the nucleic acid and binding ligand.[1] In addition to providing energetic information and the ability to make arguments about the contributions of different intermolecular interactions at different binding sites, the comparison of binding constants is the most certain way to relate the strength of binding at different sequences of the nucleic acid.

Numerous methods have been described for the measurement of association constants of protein and small molecule ligands with bulk DNA.[2] The studies, which have utilized techniques including absorbance,[3,4] circular dichroism, fluorescence,[3,5] fluorescence depolarization,[6] equilibrium dialysis,[7] and calorimetry,[8] encounter difficulty with very weak and very strong binding ligands. More recently, several laboratories have begun to develop more general methods based on fluorescence quenching,[9] electrochemical analysis,[10,11] or degradation of unbound ligand.[12]

From the perspective or work in the Barton group, these methods have two shortcomings. Because of the bulk nature of their assays, they do not permit the determination of association constants of a molecule for discrete sites on an oligonucleotide. Additionally, the spectroscopic titration methods employed measure overall changes in the electronic properties of the ligand and cannot distinguish between specific and non-specific binding modes both of which might perturb the

observed absorbance or fluorescence. Footprinting techniques based on DNase I[13,14] and chemical cleavage[15] provide a method to examine binding at single sites; however, we are interested in measuring site-specific association constants for nucleic acid binding molecules that are capable of effecting strand scission. Such molecules, which include metallo-bleomycin,[16] the enediyne antibiotics,[17,18] and synthetic metal complexes[19] such as the aromatic diimine complexes of rhodium(III) of interest to our laboratory,[20,21] directly identify their binding positions by induced strand scission. Because the ability of these molecules to cleave DNA is almost always restricted to certain binding modes, the use of an internal cleavage assay eliminates any complicating signal from other binding modes. This is particularly relevant when only the modes that promote strand scission are of interest.

The binding of small molecule ligands to nucleic acids has been the subject of theoretical study. However, the practical problems of designing experiments which allow association constants of ligands at discrete high-affinity sites to be derived from cleavage data of oligonucleotides containing additional lower-affinity sites have not been addressed.[22-24] We have approached this problem by modeling the binding behavior of such molecules; we demonstrate that judicious selection of experimental conditions allows the accurate measurement of three types of association constants using a cleavage titration assay: (1) the association constant of a DNA cleaving ligand for a single, high-affinity site in a longer polymer; (2) the average, per-base non-specific association constant of a DNA cleaving ligand for an oligonucleotide which contains no high-affinity sites; and (3) the association constant at one high-affinity site relative to a known association constant of another high-affinity site. The application of our experimental approaches to the measurement of the association constants of 1-Δ-$[Rh(MGP)_2(phi)]^{5+}$ at two different DNA sites is described.

A2.2: Computational Methods

All mathematical operations and graphic simulations were performed using Mathematica 3.0 (Wolfram Research, Inc.) on a Power Macintosh 7200/120.

A2.2.1: Simulation of Ligand Binding at One High-Affinity Binding Site in the Presence of Multiple Low-Affinity Sites

The following mathematical description was adopted to describe the binding behavior of a ligand on an oligonucleotide containing one high-affinity site and an additional number of low-affinity binding sites (Figure A2.1a):

$[L]_{Total}$ = Total Ligand Concentration
$[L]_{Free}$ = Concentration of Unbound Ligand
$[L \cdot DNA]_i$ = Concentration of Ligand-DNA Complex at a Single Site i
$[DNA]_{Total}$ = Total Concentration of Oligonucleotides
$[DNA]_{Free,i}$ = Concentration of Oligonucleotides Unoccupied at Site i

The association constant at a given site i can then be described as:

(1) $$K_{b,i} = \frac{[L \cdot DNA]_i}{[L]_{Free}[DNA]_{Free,i}}$$

which can be solved and generalized for an oligonucleotide of s possible binding sites:

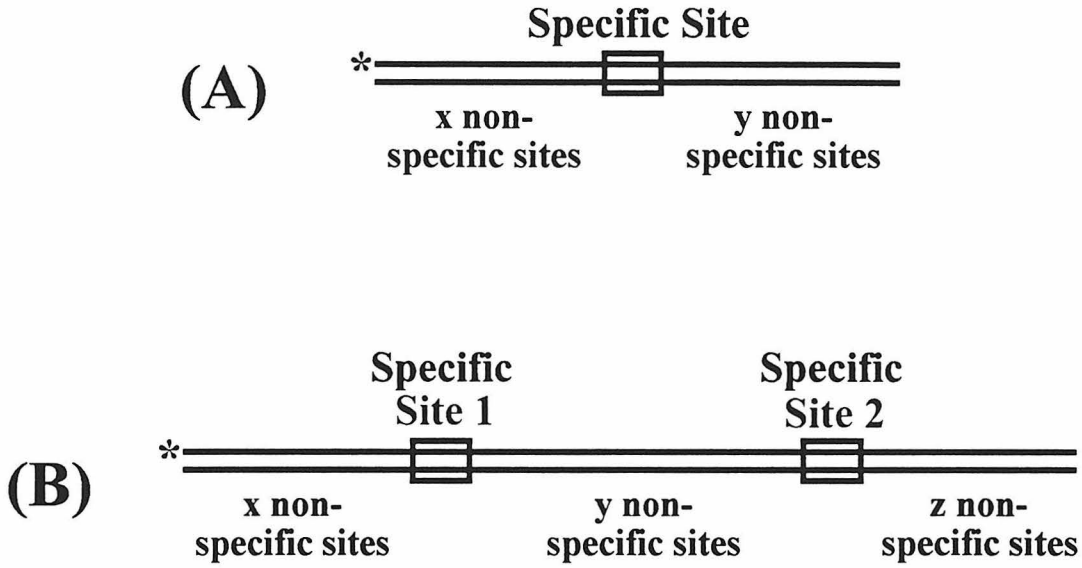
(2) $$[L \cdot DNA]_i = \frac{K_{b,i}[L]_{Free}[DNA]_{Total}}{(1 + K_{b,i}[L]_{Free})}$$

(3) $$[L]_{Total} = [L]_{Free} + \sum_{i=1}^{s}[L \cdot DNA]_i$$

(4) $$[L]_{Total} = [L]_{Free} + \sum_{i=1}^{s}\frac{K_{b,i}[L]_{Free}[DNA]_{Total}}{(1 + K_{b,i}[L]_{Free})}$$

Figure A2.1. (A) Diagram of site positioning for simulation of ligand binding at one high-affinity site surrounded by other low-affinity sites. (B) Diagram of site positioning for simulation of ligand binding at two high-affinity sites surrounded by other low-affinity sites.

Figure A2.1:


(A)
Specific Site
*
x non-
specific sites
y non-
specific sites
(B)
Specific
Site 1
Specific
Site 2
*
x non-
specific sites
y non-
specific sites
z non-
specific sites

If one assumes that the association constant at all low-affinity sites is the same, Equation 4 may be expressed as:

$$[L]_{Total} = [L]_{Free} + \frac{K_{b,H}[L]_{Free}[DNA]_{Total}}{(1 + K_{b,H}[L]_{Free})} + \frac{n \cdot K_{b,L}[L]_{Free}[DNA]_{Total}}{(1 + K_{b,L}[L]_{Free})} \quad (5)$$

where $K_{b,H}$ refers to the binding constant at the single high-affinity binding site and $K_{b,L}$ refers to the analogous value for the n low-affinity sites on the oligonucleotide. Such an expression is cubic in $[L]_{free}$ and can be represented as follows:

$$[L]_{Free}^{3} + \left[(1+n)[DNA]_{Total} - [L]_{Total} + \frac{1}{K_{b,H}} + \frac{1}{K_{b,L}}\right] \cdot [L]_{Free}^{2}$$
$$+ \left[K_{b,H}[DNA]_{Total} + n \cdot K_{b,L}[DNA]_{Total} - K_{b,L}[L]_{Total} - K_{b,H}[L]_{Total} + 1\right] \cdot [L]_{Free} \quad (6)$$
$$- \frac{[L]_{Total}}{K_{b,H}K_{b,L}} = 0$$

This expression can be solved for $[L]_{free}$ by first reducing the equation to a simpler cubic expression and then performing a trigonometric substitution.[25] This mathematical procedure yields a lengthy expression for the free ligand concentration under any set of conditions:

$$[L]_{Free} = \frac{-(K_{b,H} - K_{b,L} - K_{b,H}K_{b,L}[L]_{Total} + K_{b,H}K_{b,L}[DNA]_{Total} + K_{b,H}K_{b,L}[L]_{Total}[DNA]_{Total}}{3 \cdot K_{b,H}K_{b,L}} +$$

$$\left(2\sqrt{\frac{-3 \cdot X}{K_{b,H}K_{b,L}} + \frac{Y^2}{K_{b,H}^{\ 2}K_{b,L}^{\ 2}}}\right) \bullet \quad (7)$$

$$Cos\left(\left(ArcCos\left[\frac{\frac{-27 \cdot [L]_{Total}}{K_{b,H}K_{b,L}} - \frac{(9 \cdot X \cdot Y)}{K_{b,H}^{\ 2}K_{b,L}^{\ 2}} + \frac{Y^3}{K_{b,H}^{\ 3}K_{b,L}^{\ 3}}}{\left(2 \bullet \left(\frac{X}{K_{b,H}K_{b,L}} - \frac{Y^2}{K_{b,H}^{\ 2}K_{b,L}^{\ 2}}\right) \bullet \sqrt{\frac{X}{K_{b,H}K_{b,L}} + \frac{Y^2}{K_{b,H}^{\ 2}K_{b,L}^{\ 2}}}\right)}\right]\right) / 3\right)$$

Where:

$$X = (1 - K_{b,H}[L]_{Total} - K_{b,L}[L]_{Total} + K_{b,H}[DNA]_{Total} + K_{b,L} \cdot n \cdot [DNA]_{Total})$$

$$Y = (K_{b,H} + K_{b,L} - K_{b,H}K_{b,L}[L]_{Total} + K_{b,H}K_{b,L}[DNA]_{Total} + K_{b,H}K_{b,L} \cdot n \cdot [DNA]_{Total}$$

Substitution of that expression into equation 1 permits the calculation of the ligand-DNA complex concentration at both the high-affinity binding site ($[L \bullet DNA]_H$) and a given low-affinity site ($[L \bullet DNA]_L$) taking into account all multiple binding equilibria among the populations of sites.

(8) $$[L \cdot DNA]_H = \frac{K_{b,H}[L]_{Free}[DNA]_{Total}}{(1 + K_{b,H}[L]_{Free})}$$

(9) $$[L \cdot DNA]_L = \frac{K_{b,L}[L]_{Free}[DNA]_{Total}}{(1 + K_{b,L}[L]_{Free})}$$

When DNA binding ligands cleave DNA, however, the experimental observable is not the binding of the ligand itself but the population of end-labeled nucleic acid oligomers whose length is consistent with binding and cleavage at a given site (similar to reference 26). In most cases only a fraction, γ, of all bound complexes will afford cleavage products. As a result, the cleavage at a given site i, expressed as a fraction of the total DNA in the sample, is described as:

(10) $$FC_i = \left(\gamma \bullet \frac{[L \cdot DNA]_i}{[DNA]_{Total}} \right)$$

Of further concern, when binding occurs at multiple sites on a DNA oligomer, cleavage events between the high-affinity site of interest and the end-label will reduce the observed cleavage fraction at the high-affinity site and therefore apparently reduce the experimentally derived fraction of the high-affinity site which is bound by

ligand. This effect was modeled by reducing the observed cleavage fraction at a given site by the probability of at least one other cleavage event at any of the x low-affinity sites between it and the end-label. For the high-affinity site of the oligonucleotide shown in Figure A2.1a, the resulting, corrected cleavage expression is as follows:

$$\text{Corrected FC} = \left(\left(1-\left(\gamma \bullet \frac{[L \cdot DNA]_L}{[DNA]_{Total}}\right)\right)^x\right)\left(\gamma \bullet \frac{[L \cdot DNA]_H}{[DNA]_{Total}}\right) \tag{11}$$

A2.2.2: Simulation of Ligand Partitioning between Two High-Affinity Binding Sites in the Presence of Multiple Low-Affinity Sites

Beginning from equation 4 above, a similar model was constructed for a polymer containing two high-affinity binding sites and n low-affinity sites:

$$[L]_{Total} = [L]_{Free} + \frac{K_{b,S1}[L]_{Free}[DNA]_{Total}}{(1+K_{b,S1}[L]_{Free})} + \frac{K_{b,S2}[L]_{Free}[DNA]_{Total}}{(1+K_{b,S2}[L]_{Free})} + \frac{n \cdot K_{b,L}[L]_{Free}[DNA]_{Total}}{(1+K_{b,L}[L]_{Free}} \tag{12}$$

where $K_{b,S1}$ and $K_{b,S2}$ are the binding constants at the two high-affinity sites and $K_{b,L}$ is the analogous value for the n low-affinity sites. After multiplying and collecting terms, the resulting equation is quartic in $[L]_{free}$:

$$[L]_{Free}{}^4 + \left[(2+n)[DNA]_{Total} - [L]_{Total} + \frac{1}{K_{b,S1}} + \frac{1}{K_{b,S2}} + \frac{1}{K_{b,L}}\right]\cdot[L]_{Free}{}^3$$

$$+\left[\begin{array}{c} \frac{1}{K_{b,S1}K_{b,S2}} + \frac{1}{K_{b,L}K_{b,S2}} + \frac{1}{K_{b,S1}K_{b,L}} + \\ [DNA]_{Total}\left(\frac{1}{K_{b,S2}} + \frac{1}{K_{b,S1}} + \frac{2}{K_{b,L}} + \frac{n}{K_{b,S2}} + \frac{n}{K_{b,S1}}\right) \\ -[L]_{Total}\left(\frac{1}{K_{b,L}} + \frac{1}{K_{b,S1}} + \frac{1}{K_{b,S2}}\right) \end{array}\right]\cdot[L]_{Free}{}^2$$

(13)

$$+\left[\begin{array}{l} \left[\frac{1}{K_{b,S1}K_{b,S2}K_{b,L}} + ([DNA]_{Total} - [L]_{Total})\right] \\ \left[(\frac{1}{K_{b,S2}K_{b,L}} + \frac{1}{K_{b,S1}K_{b,L}} + \frac{1}{K_{b,S1}K_{b,S2}}\right] \end{array}\right]\cdot[L]_{Free}$$

$$-\frac{[L]_{Total}}{K_{b,S1}K_{b,S2}K_{b,L}} = 0$$

It can be solved for $[L]_{free}$, however, by conversion to its resultant cubic equation and the application of other standard mathematical techniques[25] to yield a lengthy real root:

$$[L]_{Free} = -\frac{a}{4} + \frac{1}{2}\sqrt{X + Y\cos Z} + \frac{1}{2}\sqrt{6X - Y\cos Z + \frac{(-a^3 + 4ab - 8c)}{4\sqrt{3X + Y\cos Z}}} \quad (14)$$

Where:

$$X = \frac{1}{3}\left(\frac{a^2}{4} - \frac{2b}{3}\right)$$

$$Y = \frac{2}{3}\sqrt{b^2 - 3(ac - 4d)}$$

$$Z = \frac{1}{3}ArcCos\left[\frac{-2b^3 + 9b(ac - 4d) + 27(-c^2 - a^2d + 4bd)}{2\sqrt{b^2 - 3(ac - 4d)}\cdot(-b^2 + 3(ac - 4d))}\right]$$

And, secondly:

$$a = \frac{K_{b,S1} + K_{b,S2} + \frac{K_{b,S1}K_{b,S2}}{K_{b,L}} + 2 \cdot K_{b,S1}K_{b,S2}[DNA]_{Total} + n \cdot K_{b,S1}K_{b,S2}[DNA]_{Total} - K_{b,S1}K_{b,S2}[L]_{Total}}{K_{b,S1}K_{b,S2}}$$

$$b = \frac{K_{b,L}(1 + (K_{b,S1} + K_{b,S2})([DNA]_{Total}(n+1) - [L]_{Total})) + K_{b,S1}(1 + K_{b,S2}(2[DNA]_{Total} - [L]_{Total})) + K_{b,S2}}{K_{b,L}K_{b,S1}K_{b,S2}}$$

$$c = \frac{1 + [DNA]_{Total}(K_{b,S1} + K_{b,S2} + K_{b,L} \cdot n) - [L]_{Total}(K_{b,S1} + K_{b,S2} + K_{b,L})}{K_{b,L}K_{b,S1}K_{b,S2}}$$

$$d = \frac{-[L]_{Total}}{(K_{b,L}K_{b,S1}K_{b,S2})}$$

This root was then substituted into equation 1 and adjusted to model the experimentally observed strand cleavage at each site using the cleavage efficiency parameter. With two high-affinity sites, the correction for multiple cleavage events on the same oligonucleotide (Figure A2.1b) is more complex. The cleavage at the high-affinity site closer to the end-label (Site 1) was adjusted for possible cleavage at the x low-affinity sites separating it from the end-label, and the cleavage at the high-affinity site farther from the end-label (Site 2) was corrected for cleavage at the x+y low-affinity sites (see Figure A2.1b) between it and the label and for cleavage at Site 1, resulting in the following corrected cleavage fractions:

(15) $$\text{Corrected FC}_{\text{Site 1}} = \left(\left(1 - \left(\gamma \bullet \frac{[L \cdot DNA]_L}{[DNA]_{Total}}\right)\right)^x\right)\left(\gamma \bullet \frac{[L \cdot DNA]_{S1}}{[DNA]_{Total}}\right)$$

(16) $$\text{Corrected FC}_{\text{Site 2}} = \left(\left(1 - \left(\gamma \bullet \frac{[L \cdot DNA]_L}{[DNA]_{Total}}\right)\right)^{(x+y)}\right)\left(1 - \left(\gamma \bullet \frac{[L \cdot DNA]_{S1}}{[DNA]_{Total}}\right)\right) \bullet \left(\gamma \bullet \frac{[L \cdot DNA]_{S2}}{[DNA]_{Total}}\right)$$

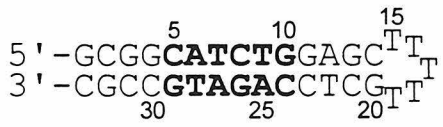
A2.3: Experimental Methods

A2.3.1: General Procedures

1-[Rh(MGP)$_2$(phi)]Cl$_5$ was prepared and its enantiomers were resolved as described.[27] Concentrations of stock solutions in deionized water were determined using an ε_{358nm} of 19,400 cm^{-1} M^{-1}. All oligonucleotides were prepared on an ABI 392 DNA/RNA Synthesizer by standard phosphoramidite chemistry and purified by reverse phase HPLC. Concentrations were estimated using per base extinction coefficients (in cm^{-1} M^{-1}) for A, 8600; G, 9700; C, 6800; and T, 8400. Oligonucleotides were 5' end-labeled with γ-^{32}P ATP (Dupont-NEN) and T4 polynucleotide kinase (New England Biolabs). Photocleavage reactions were performed using an Oriel Hg/Xe arc lamp equipped with a monochromator and a 300 nm cutoff filter. All photocleavage reactions were performed in 10 mM sodium cacodylate, 40 mM NaCl, pH 7.0 at ambient temperatures.

A2.3.2: Direct Measurement of Single Sequence-Specific Association Constants

Association constants of 1-Δ-[Rh(MGP)$_2$(phi)]$^{5+}$ were determined at two of its known high-affinity binding sites, 5'-CATCTG-3' and 5'-TATCTA-3'. To minimize the number of low-affinity sites on the oligonucleotides employed while ensuring they would remain annealed at the nanomolar concentrations required for these experiments, measurements were made on short 5'-^{32}P end-labeled hairpin oligonucleotides whose sequences (recognition site boldfaced) were as follows:





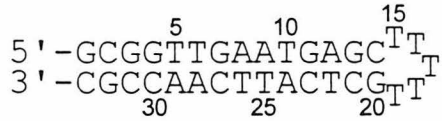
DNA samples were prepared at concentrations from 1 x 10^{-9} M to 1 x 10^{-4} M with a constant metallointercalator:DNA ratio of 1:10. The samples were incubated for 4 to 20 min and irradiated for 5 min at 313 nm. Formamide loading dye was added to each sample and a portion was assayed by 20% denaturing PAGE and visualized by Phosphorimagery (Molecular Dynamics, Inc.). Cleavage at C_8 (the central C in the recognition site) was quantitated using ImageQuant software and expressed as a fraction of the radioactivity in the uncleaved parent band. The data were fit using the following simple binding model to extract the specific association constant for each site:

$$\text{Cleavage Fraction} = \frac{[Rh \cdot DNA]}{[DNA]_T} \bullet \gamma \tag{17}$$

$$[Rh \cdot DNA] = \frac{(K_b([DNA]_T + [Rh]_T) + 1) - \sqrt{((K_b([DNA]_T + [Rh]_T) + 1)^2 - 4 \cdot K_b^2 [Rh]_T [DNA]_T}}{2 \cdot K_b}$$

A2.3.3: Measurement of the Average Non-Specific Association Constant of a DNA Binding Ligand

Quantitative photocleavage titration was performed as described above for the determination of specific binding constants, except a hairpin oligonucleotide containing no high-affinity binding sites was used. The sequence is as follows:



In addition, the metallointercalator:DNA ratio was increased to 1:2 to provide more observable signal in the experiment. Cleavage intensity over all cleaved products was quantitated by phosphorimagery and expressed as a fraction of the uncleaved parent DNA band. The cleavage fractions were corrected for light damage in the absence of the rhodium complex and fit as described above yielding an average non-specific binding isotherm. In order to account for the possibility of intercalation between any of the base pairs of the hairpin as well as in the hairpin itself, the site concentration was set to be 14 times the duplex concentration. This included the 13 possible intercalation sites in the duplex and an additional site for binding in the hairpin which has been observed for other rhodium phi complexes.

A2.3.4: Measurement of Two Sequence Specific Association Constants Relative to One Another

To measure the relative difference in affinity between the 5'-CATCTG-3' and 5'-TATCTA-3' sites, a longer oligonucleotide,

```
          5         10        15        20        25
5'-GCGGTATCTAGAGCGCATCTGGGCG-3
3'-CGCCATAGATCTCGCGTAGACCCGC-5
```

containing both sites of interest separated by a minimal number of low-affinity sites was prepared and annealed to its complement. Photocleavage experiments similar to those described for the hairpin oligonucleotides were performed at DNA duplex concentrations of 1 μM and 0.1 μM and metallointercalator:DNA ratios of 1:10, 1:20, 1:30, and 1:40. The cleavage intensity at both sites (C_8 and C_{19}) was quantitated by Phosphorimagery. Before comparison of band intensities, the integrated density in each band was corrected by subtraction of the quantitated damage at a nearby base which did not undergo site-specific cleavage (C_8 corrected with A_6, C_{19} corrected with G_{14}).

A2.3.5: Measurement of the Observed Cleavage Efficiency for a DNA Cleaving Ligand

To assess the DNA photocleavage efficiency of the complex at the two sites of interest, a set of samples (10 μM in DNA duplex, 1 μM 1-Δ-$[Rh(MGP)_2(phi)]^{5+}$) was prepared using the previously described hairpin oligonucleotides. Individual samples were irradiated at 313 nm for 1, 2, 5, 7, 9, 14, and 20 min. After PAGE, the fraction of DNA cleaved was determined by quantitating the cleavage band on the 5' strand of the hairpin. The resulting fractions were plotted as a function of irradiation time to determine the upper limit of observable cleavage. The cleavage efficiency was estimated by comparing the maximum observed cleavage fraction to the theoretical maximum of 10% under these concentration conditions.

A2.4: Results and Discussion

A2.4.1: Simulation of Ligand Binding at One High-Affinity Binding Site in the Presence of Multiple Low-Affinity Sites

Because of the need to separate ligand binding sites from the ends of oligonucleotides used in association constant measurements, it is not possible to measure the sequence-specific association constant of a DNA binding ligand in the absence of other low-affinity binding sites. As a result, experiments must be conducted under conditions which minimize the errors caused by the presence of additional lower-affinity sites. Mathematical models were constructed which facilitated such experimental design. Once estimates were made for the numerical components of the model, i.e., the association constants and the number and distribution of low-affinity binding sites, binding surfaces were constructed which show the fraction of high-affinity sites occupied over a range of DNA and ligand concentrations. An example surface where

$K_{b,H} = 10^8\ M^{-1}$, $K_{b,L} = 10^6\ M^{-1}$, n=20 and x=10 is shown in Figure A2.2. To emphasize the relationship between the number of binding ligands available per high-affinity DNA site and the distribution of ligand between the high-affinity site, low-affinity sites, and solution, the fraction of the high-affinity site bound by ligand is plotted against the concentration of oligonucleotides and the ratio between ligand and DNA concentration. As expected, binding gradually increases both with increasing ratio and increasing DNA concentration to saturate the high-affinity binding site. Similar plots were constructed for individual low-affinity sites that reflect their lower K_b (data not shown).

By estimating the strand cleavage efficiency of the DNA cleaving ligand (in this case 10% or 0.1), an analogous surface was constructed which illustrates the observed cleavage fraction at the high-affinity site under varied experimental conditions (Figure A2.3). Inspection of this surface shows that, at high ligand to DNA ratios, the observed cleavage fraction decreases above a limiting concentration, in contrast to the saturating binding behavior shown in Figure A2.2.* In order to quantify the discrepancy between the observed cleavage data and the underlying binding behavior, an additional surface was constructed which compares the observed cleavage at the high-affinity site as modeled here to that derived from a similar experiment in which there are no low-affinity sites on the polymer. This was accomplished by performing calculations as previously described with the number of low-affinity sites, n, set to zero and by plotting the ratio of the derived surface to the surface shown in Figure A2.3. The results of this calculation are shown in Figure A2.4.

---

* We have observed this effect experimentally (data not shown).

Figure A2.2. Simulation of Ligand Binding at One High-Affinity Binding Site in the Presence of Multiple Low-Affinity Sites: Surface illustrating the fraction of specific, high-affinity DNA binding sites occupied as a function of site concentration and the ligand:binding site ratio. Conditions for this surface are $K_{b,H} = 10^8\ M^{-1}$, $K_{b,L} = 10^6\ M^{-1}$, and n, the total number of low-affinity binding sites = 20.

Figure A2.2:

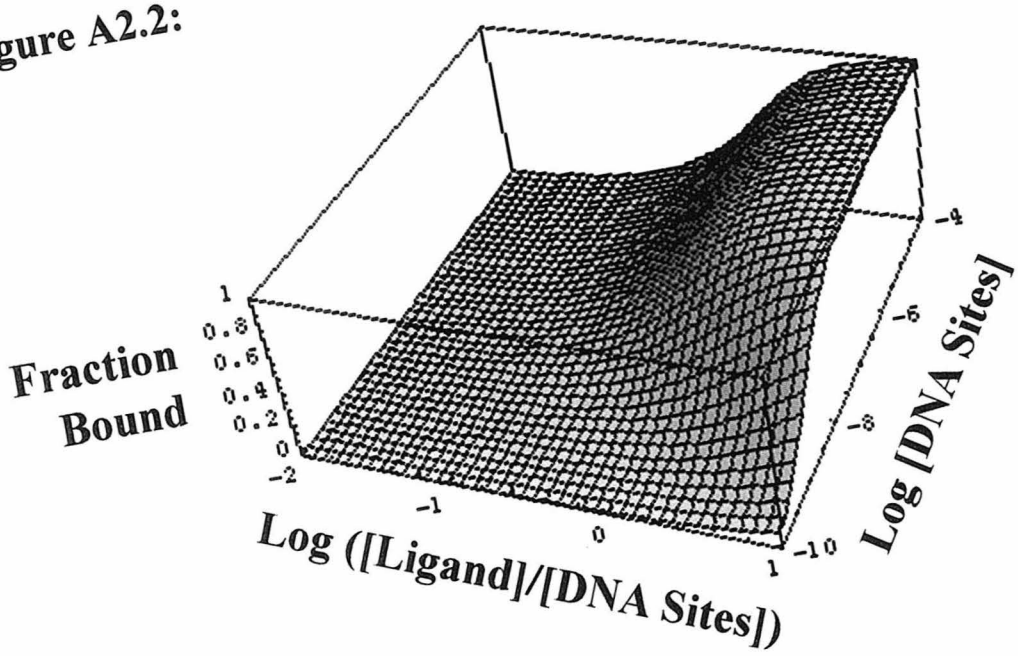

Fraction Bound
1
0.8
0.6
0.4
0.2
0
-2
-1
0
1
Log ([Ligand]/[DNA Sites])
-4
-6
-8
-10
Log [DNA Sites]

Figure A2.3. Simulation of Ligand Binding and Strand Cleavage at One High-Affinity Binding Site in the Presence of Multiple Low-Affinity Sites: Surface illustrating the observed specific-site cleavage product of an end-labeled DNA strand by a DNA binding and cleaving ligand as a function of site concentration and the ligand:binding site ratio. Conditions are as described for the analagous binding surface in Figure 2 with the addition that γ, the strand cleavage efficiency, = 0.1 and x, the number of low-affinity sites between the high-affinity site and the end-label, = 10. Note the decrease in observed specific site cleavage products at high ligand:DNA ratios.

Figure A2.3:

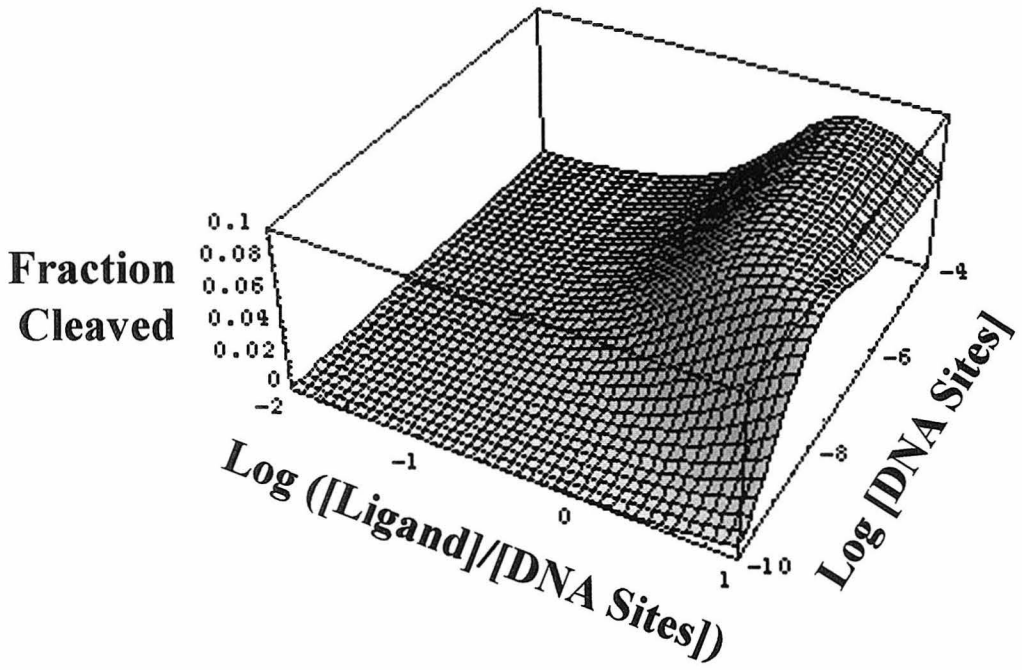
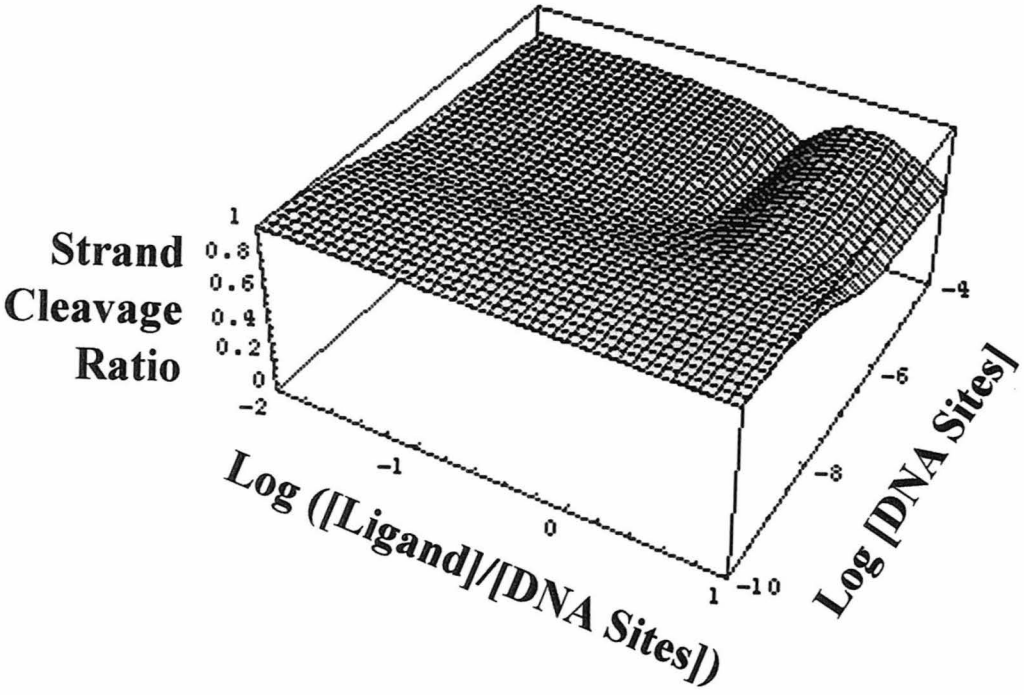

Fraction Cleaved
0.1
0.08
0.06
0.04
0.02
0
-2
-1
0
1
Log ([Ligand]/[DNA Sites])
-4
-6
-8
-10
Log [DNA Sites]

Figure A2.4. Simulation of Ligand Binding and Strand Cleavage at One High-Affinity Binding Site in the Presence of Multiple Low-Affinity Sites: Surface showing the ratio between observed specific site cleavage products with and without the effect of low-affinity binding sites. Regions of this surface where the ratio approaches one minimize the distortion in observed cleavage data from both binding competition with low-affinity sites and multiple cleavage events on the same DNA polymer.

Figure A2.4:


Strand Cleavage Ratio
1
0.8
0.6
0.4
0.2
0
-2
-1
0
1
Log ([Ligand]/[DNA Sites])
-10
-8
-6
-4
Log [DNA Sites]

This surface clearly shows that, at high ligand:DNA ratios and high concentration, multiple cleavage events cause a significant reduction in the observed cleavage. There is an additional region, however, closer to a 1:1 ligand:DNA ratio where there is also a significant deviation between the data derived from the model which accounts for the effects of the low-affinity sites and the model that neglects them. This region, whose existence is not obvious from inspection of Figure A2.3, presumably results from competition between the high-affinity site and the low-affinity sites for available binding ligand which is exacerbated as the high-affinity site becomes saturated.

Because of the number of parameters and calculational complexity associated with these models, they are not a practical method for the treatment of experimental data. Using these equations requires knowledge of the non-specific association constant, the number and position of low-affinity sites, and the cleavage efficiency, any of which might not be readily accessible in the early characterization of a new DNA cleaving ligand. Accordingly, an experimental approach which allows a relatively accurate measurement of the association constant by fitting the data using a simplified single-binding-site model would be of substantial value. Two experimental considerations make this possible. Measurement of association constants on the shortest possible oligonucleotides minimizes the number of low-affinity sites which compete for available ligand and undergo cleavage events which reduce the observed cleavage at the high-affinity site. We have achieved this objective using hairpin oligonucleotides with a 10-12 base pair double-stranded region. Additionally, conducting experiments under metal-limiting conditions minimizes errors caused by saturation effects at the high-affinity site as well as by cleavage at low-affinity sites. We have found it practical to routinely conduct

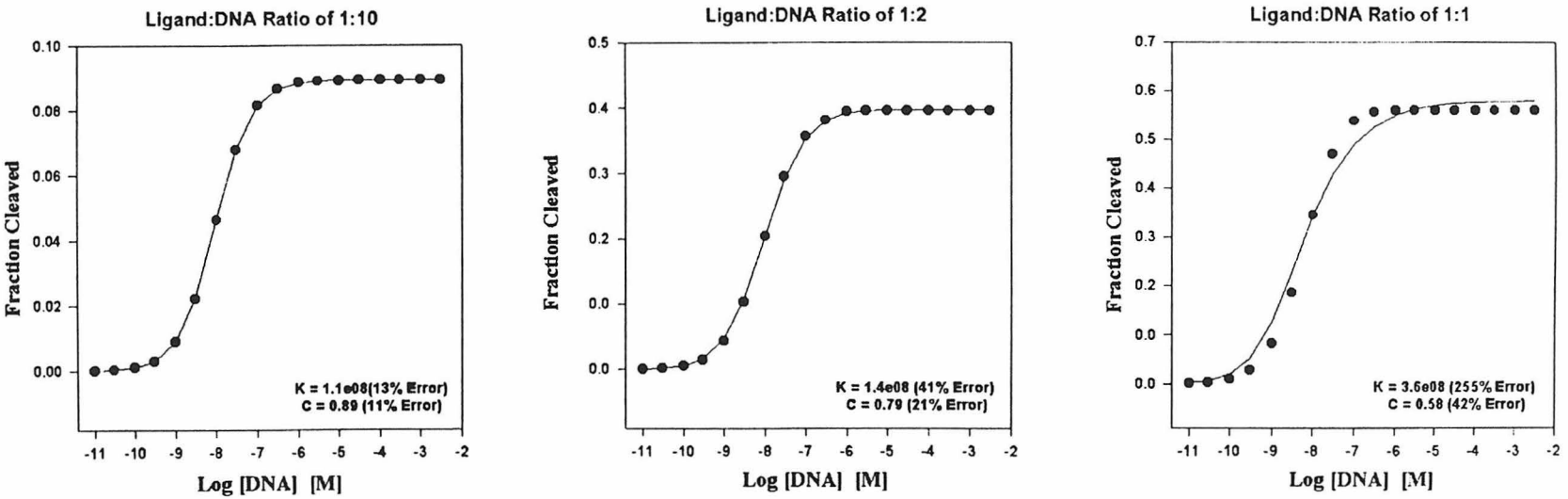
association constant measurements of the photocleaving metallointercalators studied in our laboratory at ligand:DNA ratios as low as 1:10.

To assess the systemic error introduced by neglecting the effects of the low-affinity sites in deriving association constants from cleavage data, simulated data extracted from a cleavage surface similar to Figure A2.3 (all variables identical except the γ = 1, which emphasizes the effects of multiple cleavage events) was fit to a simple one-site binding equation. When the ligand:DNA ratio was 1:10, the derived association constant differed from the input value by only 13%. Data taken at higher ligand:DNA ratios had more systemic error; the derived value at a 1:2 ligand to DNA ratio differed from the input value by 41% and, as expected, higher ligand to DNA ratios yielded even poorer results. Errors in the derived cleavage efficiency parameter also increased with an increasing ligand to DNA ratio, but not as dramatically as the errors in the association constants. Sample data derived from our theoretical models is included in Figure A2.5 and emphasize that cleavage data which contains significant intrinsic error can afford isotherms which appear normal. It is important to note that the systemic error is highly dependent on the value of γ, the strand cleavage efficiency. At high cleavage efficiencies, multiple cleavage events are more common and measurement error increases.

The effects of other deviations from ideality in the system described in Figures A2.2 though A2.5 were explored using these models. The presence of additional, low-affinity binding sites on either side of the high-affinity site resulted in increased errors in association constants derived from fitted cleavage data provided by our model. Additionally, as the value of the non-specific association constant approached the value of the specific association constant, the effects of the low-affinity sites were maximized, effectively placing a lower limit of approximately 10:1 on the ratio

Figure A2.5. Simulation of Ligand Binding and Strand Cleavage at One High-Affinity Binding Site in the Presence of Multiple Low-Affinity Sites: Examples of simulated strand cleavage data (single high-affinity binding site, $K_{b,H} = 10^8\ M^{-1}$, $K_{b,L} = 10^6\ M^{-1}$, n = 20, x=10, γ=1) fit to a simple two parameter binding equation as described in text. The association constants extracted from each fit are indicated on each graph. Note that higher ligand:DNA ratios yield fitted association constants that diverge more and more from the inputted $10^8\ M^{-1}$ value for this simulation. In addition, it is important to recognize that even well shaped isotherms might contain significant intrinsic error.

Figure A2.5:


Ligand:DNA Ratio of 1:10
Fraction Cleaved
0.10
0.08
0.06
0.04
0.02
0.00
K = 1.1e08(13% Error)
C = 0.89 (11% Error)
-11 -10 -9 -8 -7 -6 -5 -4 -3 -2
Log [DNA] [M]
Ligand:DNA Ratio of 1:2
Fraction Cleaved
0.5
0.4
0.3
0.2
0.0
0.0
K = 1.4e08 (41% Error)
C = 0.79 (21% Error)
-11 -10 -9 -8 -7 -6 -5 -4 -3 -2
Log [DNA] [M]
Ligand:DNA Ratio of 1:1
Fraction Cleaved
0.7
0.6
0.5
0.4
0.3
0.2
0.0
0.0
K = 3.6e08 (255% Error)
C = 0.58 (42% Error)
-11 -10 -9 -8 -7 -6 -5 -4 -3 -2
Log [DNA] [M]

between the specific and non-specific association constants which permits application of this approach.

A2.4.2: Simulation of Non-Specific Ligand Binding at Multiple Low-Affinity Sites

Although it is not possible to accurately measure an association constant at a high-affinity site as the ratio between the specific and non-specific association constants decreases, it is possible to obtain an estimate of the non-specific association constant of a nucleic acid binding ligand. We have modeled the behavior of a system in which all available sites have the same association constant using the equations described above by setting the association constant, $K_{b,H}$, of the high-affinity site equal to the association constant, $K_{b,L}$, of the n low-affinity sites, resulting in a description of a system with n+1 equivalent sites.

In the absence of the high-affinity site, the simple model described above accurately describes the behavior of the system if the binding sites on the oligonucleotide are considered to act independently, i.e., ignoring nearest neighbor effects, etc. However, as was discussed in the previous model, multiple cleavage events on the same oligonucleotide can introduce errors into the measured cleavage fractions at sites remote from the end-label. While such errors could be rendered moot by deriving the fraction of sites occupied by ligand at the sites nearest the label, it is desirable to obtain a binding isotherm which represents the average of the non-specific association constants at a variety of sites. Accordingly, the systemic error introduced by multiple cleavage events on the same oligonucleotide was modeled by adjusting the observed cleavage at each site (moving away from the end-label) by the probability of cleavage at sites between it and the radioactive tag. This results in a series of equations describing the cleavage fraction at each site as follows:

$$\text{FC Site}_1 = \left(\gamma \bullet \frac{[L \cdot DNA]_{S1}}{[DNA]_{Total}}\right)$$

(16)

$$\text{FC Site}_2 = \left(\gamma \bullet \frac{[L \cdot DNA]_{S2}}{[DNA]_{Total}}\right)\left(1 - \left(\gamma \bullet \frac{[L \cdot DNA]_{S1}}{[DNA]_{Total}}\right)\right)$$

$$\text{FC Site}_3 = \left(\gamma \bullet \frac{[L \cdot DNA]_{S2}}{[DNA]_{Total}}\right)\left(1 - \left(\gamma \bullet \frac{[L \cdot DNA]_{S1}}{[DNA]_{Total}}\right)\right)^2$$

et cetera

where $[L \bullet DNA]_{S1}$ is the concentration of the DNA bound complex at the site closest to the end label, $[L \bullet DNA]_{S2}$ is the concentration of complex bound at the next site down the oligonucleotide, etc. The FC Site_i values refer to the observed cleavage fractions at each of these sites after multiple cleavage events have been considered. Because the association constants, and therefore the occupancy fractions, at each site are the same, the sum of the cleavage fractions across the whole oligonucleotide can be described as:

(17)

$$\text{Total Cleavage} = \left(\gamma \bullet \frac{[L \cdot DNA]_{Sx}}{[DNA]_{Total}}\right)\sum_{i=0}^{n-1}\left(1 - \left(\gamma \bullet \frac{[L \cdot DNA]_{Sx}}{[DNA]_{Total}}\right)\right)^i$$

where i is the number of sites on the oligonucleotide and $[L \bullet DNA]_{Sx}$ refers to the concentration of bound DNA complex at any of these i identical sites. Cleavage data were derived as a function of DNA concentration and ligand:DNA ratio and represented on surfaces as described in the previous section (data not shown). In order to facilitate selection of conditions for these experiments, a ratio surface comparing the observed cleavage with and without the effects of multiple cleavage

was constructed. An example surface for an oligonucleotide containing 11 sites each with a 1 x 10^6 M^{-1} association constant is included as Figure A2.6. As before, the cleavage efficiency was set to 0.1. As expected, low ligand to DNA ratios minimize the deviation between the observed cleavage fractions and the underlying binding behavior. The requirement for low ligand:DNA ratios here is less strict, however, because binding competition has been made irrelevant by measurement of strand cleavage at all sites on the oligonucleotide.

Data extracted from the simulation described were fit to a one-binding-site model to assess the degree of systemic error that would be observed in a non-specific association constant measurement. At a 1:10 ratio of ligand to DNA polymers, the derived association constant differed by only 0.4% from the input value. As expected, greater differences between the input value and the derived value occurred at higher ligand:DNA ratios.*

A2.4.3: Simulation of Ligand Partitioning between Two High-Affinity Binding Sites in the Presence of Multiple Low-Affinity Sites

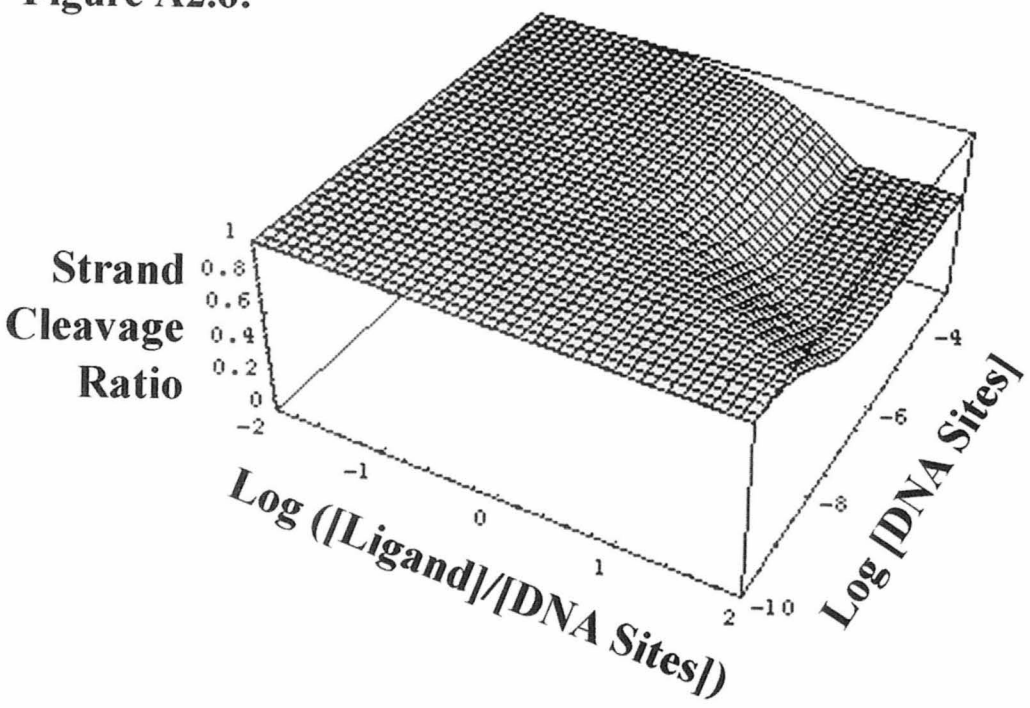
A method which would allow the determination of the relative association constants of a nucleic acid binding and cleaving ligand at two different high-affinity sites is also of significant experimental interest because of the labor intensive nature of DNA cleavage titrations. Relative association constant measurements could provide an accurate and simple means of examining the binding of a ligand to sites which are

---

* To further generalize this work, an additional simulation was conducted using the two site model described in the next section. A polymer was constructed with five sites of three types (K_b = 1 x 10^6 for three sites, 1.2 x 10^6 for one, and 1.3 x 10^6 for one). When the simulated total cleavage at all five sites was fit to the one-binding-site model, the derived value of the non-specific association constant was 1.10 x 10^6, identical to the weighted average of the K_b's of the five sites.

Figure A2.6. Simulation of Non-Specific Ligand Binding and Strand Cleavage at Multiple Low-Affinity Sites on a DNA Polymer: Surface showing the ratio of total cleavage products over an entire 11 base pair DNA polymer with and without the effect of multiple cleavage events. In this case, all sites have a $K_b = 10^6\ M^{-1}$ and γ=0.1. Note that observed total cleavage only deviates from the theoretical value at high ligand:DNA ratios.

Figure A2.6:


Strand Cleavage Ratio
1
0.8
0.6
0.4
0.2
0
-2
-1
0
1
2
Log ([Ligand]/[DNA Sites])
-10
-8
-6
-4
Log [DNA Sites]

subtly different, and the results of such experiments can be valuable in determining the factors that lead to high sequence specificity. Because of the need to separate the high-affinity sites of interest from each other and the ends of oligonucleotides used in these experiments, however, systemic errors may occur if experimental conditions are chosen injudiciously. Accordingly, a set of models was constructed which allowed the possible systemic error under a variety of experimental conditions to be assessed.

Estimates were made for the association constants, the cleavage efficiencies, and the position of the high-affinity sites on the end-labeled strand and binding surfaces were constructed for both of the high-affinity sites and a given low-affinity site. After correction for the possibility of multiple cleavage events on the same oligonucleotide, derived strand cleavage surfaces were constructed. These surfaces are similar to those shown in the previous sections and are not shown. In order to select experimental conditions under which the observed ratio of cleavage products accurately reflects the underlying ratio of association constants, we considered the surface shown in Figure A2.7 which describes the ratio of observed cleavage products at the two sites of interest as a function of DNA concentration and ligand:DNA ratio. This surface describes a case where $K_{b,L} = 1 \times 10^6\ M^{-1}$, $K_{b,S1} = 1 \times 10^8\ M^{-1}$ (see Figure A2.1b for position identification,) and $K_{b,S2} = 7 \times 10^7\ M^{-1}$. In this experiment, six low-affinity sites were placed between each high-affinity site and the ends of the oligonucleotide (x and z in Figure A2.1b) and ten sites were placed between them. The cleavage efficiency at all sites was set to 0.1. As expected, these experiments must also be run at low ratios of ligand:DNA in order to minimize binding competition and produce accurate comparisons between binding sites. *It is important to note this model assumes that the cleavage efficiency at the two high-affinity sites is equal.* The validity of this assumption is a function of the DNA

cleaving ligand under study and the differences between the sites, and should be verified experimentally.

Additional simulations show that good agreement between the ratio of observed cleavage at the two sites and ratio of their underlying association constants is a function of difference between the K_b's of the high-affinity sites. As the ratio between the two high-affinity association constants increases, the close agreement between the cleavage ratio and the association constant ratio breaks down. To demonstrate this, an example calculation with all variables identical to the calculation shown in Figure A2.7, except $K_{b,S2} = 1 \times 10^7\ M^{-1}$, is included as Figure A2.8. With the two association constants now tenfold apart, agreement between the observed cleavage fraction and the actual relationship between the two thermodynamic parameters breaks down.

A2.4.4: Measurement of Single Sequence-Specific Association Constants of 1-Δ-$Rh(MGP)_2(phi)^{5+}$

Examples of binding isotherm gels for both the 5'-CATCTG-3' and the 5'-TATCTA-3' hairpins are included in Figure A2.9. Binding isotherms constructed from the normalized data by these and other trials are included in Figure A2.10. The association constants derived by fitting these data to the one-site binding equation are as follows: 5'-CATCTG-3', 9.5 (3) x $10^6\ M^{-1}$; 5'-TATCTA-3', 1.8 (0.6) x $10^7\ M^{-1}$. Errors were estimated by comparison of fitted data from independent trials. The error bars of this experiment demonstrate that independent measurement of association constants is not an optimal method for comparing ligand binding sites of similar affinity.

Figure A2.7. Simulation of Ligand Partitioning between Two High-Affinity Binding Sites in the Presence of Multiple Low-Affinity Sites: Surface illustrating the variation of the ratio in observed strand cleavage between two high-affinity sites as a function of DNA concentration and the ligand:DNA ratio. In this case, $K_{b,L} = 1 \times 10^6\ M^{-1}$, $K_{b,S1} = 1 \times 10^8\ M^{-1}$, $K_{b,S2} = 7 \times 10^7\ M^{-1}$, γ=0.1, x=z=6, and y=10. See Figure 1b for site positioning and variable information. Areas of this surface where the ratio approaches 1.43 (the ratio of the association constants inputted in the simulation) indicate experimental conditions where binding competition and multiple cleavage events do not convolute the observed data.

Figure A2.7:

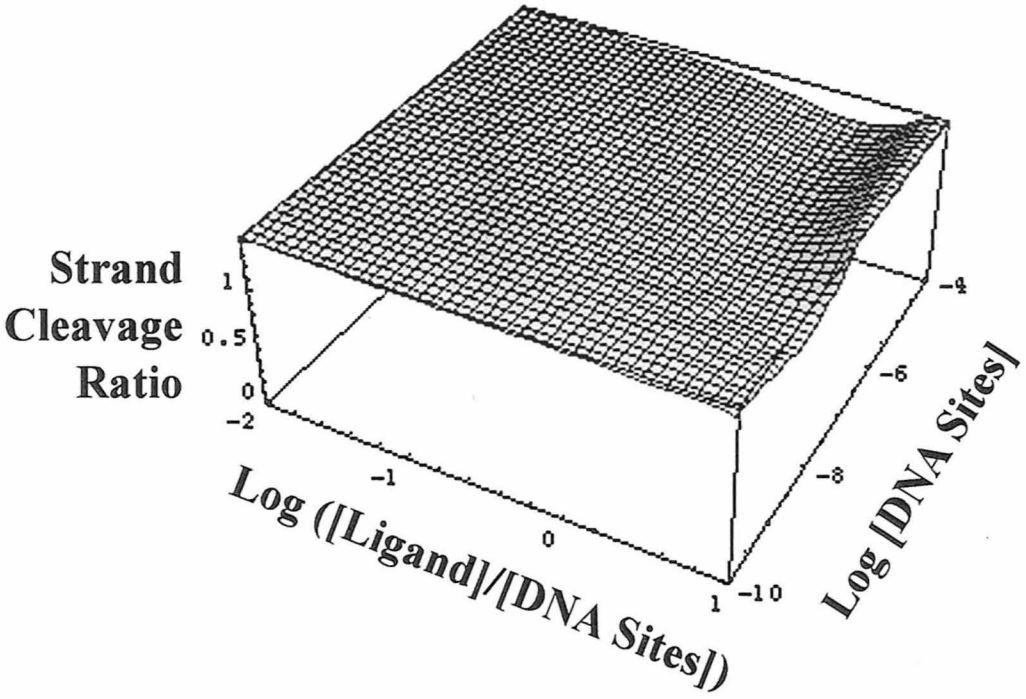

Strand
Cleavage
Ratio
1
0.5
0
-2
-1
0
1
Log ([Ligand]/[DNA Sites])
-4
-6
-8
-10
Log [DNA Sites]

Figure A2.8. Simulation of Ligand Partitioning between Two High-Affinity Binding Sites in the Presence of Multiple Low-Affinity Sites: Surface identical to that shown in Figure 7 except, in this case, $K_{b,S2} = 1 \times 10^7\ M^{-1}$. With the two high-affinity association constants more different in magnitude, much larger areas of deviation exist where the ratio of oberved cleavage differs from the theoretical value of 10.

Figure A2.8:

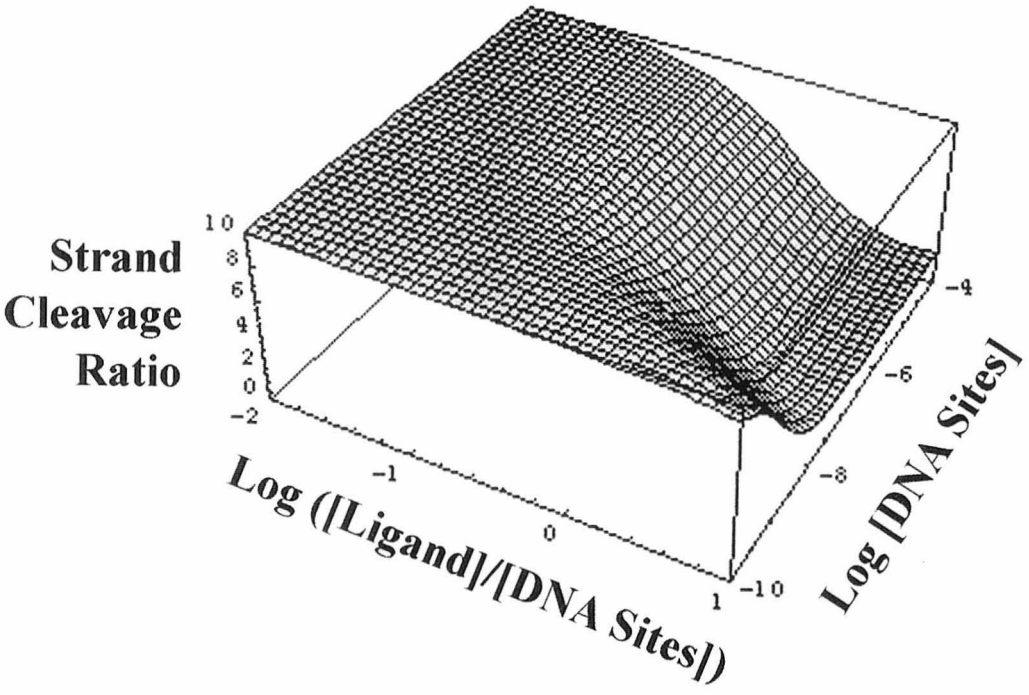

Strand Cleavage Ratio
10
8
6
4
2
0
-2
-1
0
1
Log ([Ligand]/[DNA Sites])
-10
-8
-6
-4
Log [DNA Sites]

Figure A2.9. Quantitative photocleavage titration for 1-Δ-[Rh(MGP)$_2$(phi)]$^{5+}$ at 5'-CATCTG-3' (left) and 5'-TATCTA-3' (right). Lanes labeled A+G and C+T are standard Maxam-Gilbert sequencing reactions. DC refers to samples of DNA (3 x 10^{-9} M) and metal complex (1 x 10^{-5} M) incubated without irradiation, LC to samples of DNA (3 x 10^{-9} M) irradiated without metal complex. Binding experiments were performed from 1 x 10^{-9} M to 1 x 10^{-4} M DNA with the metal complex held at a constant Rh:DNA ratio of 1:10. Increasing concentrations indicated by the bar above the experimental lanes. Reactions were performed in 10 mM sodium cacodylate, 40 mM NaCl, pH 7.0 at ambient temperatures. Sample preparation, irradiation and treatment are described in the Experimental Section.

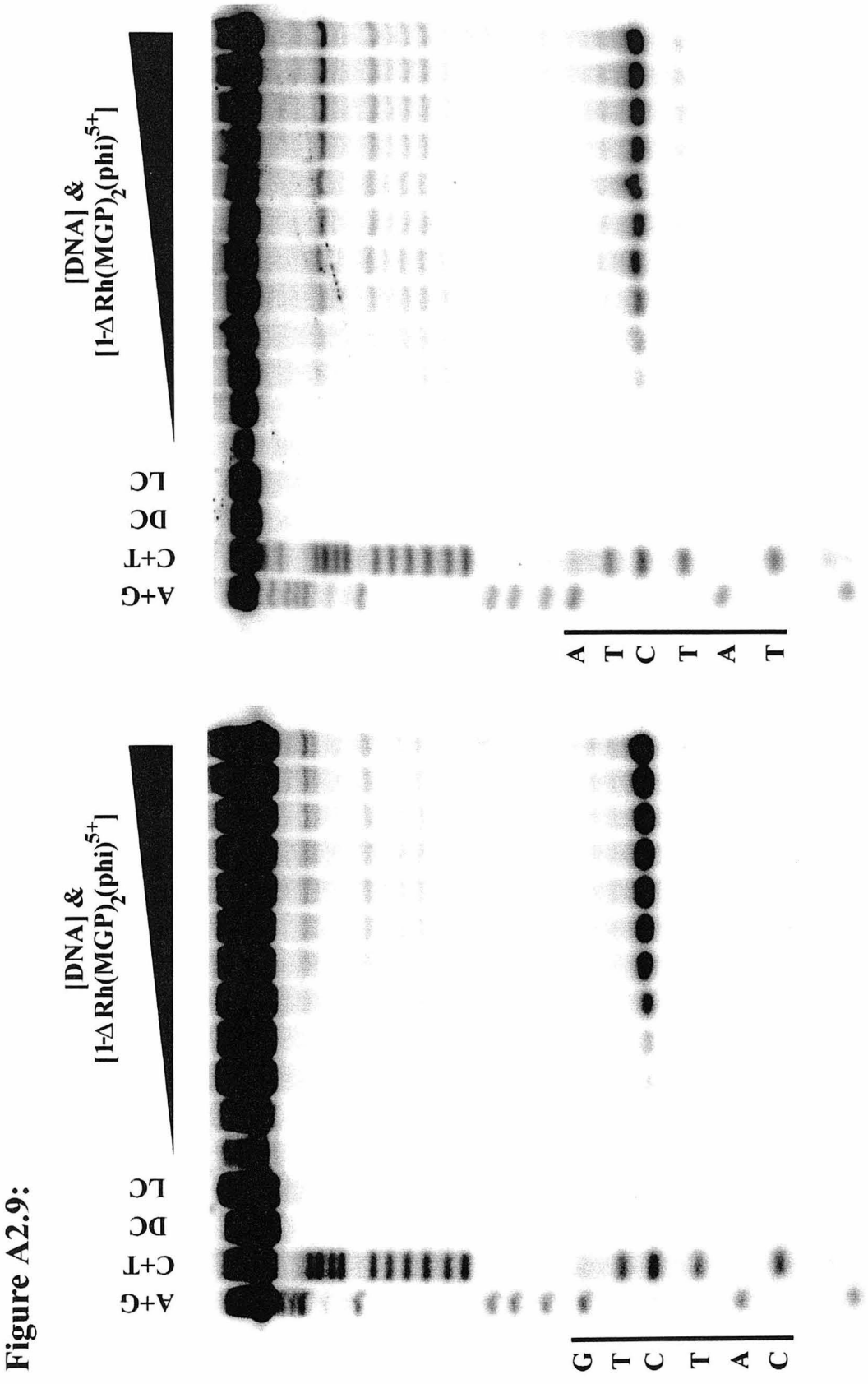
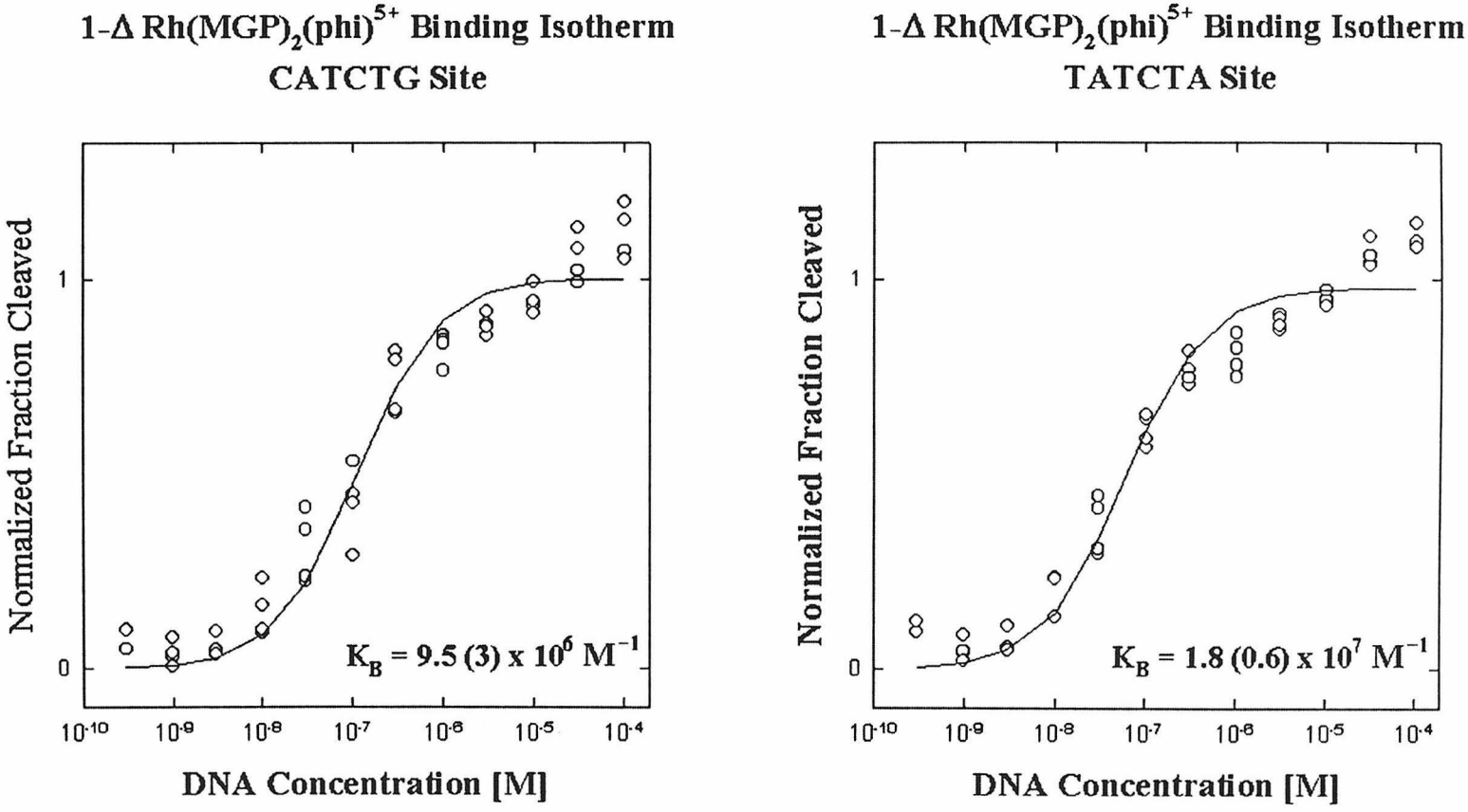

[DNA] &
[1-Δ Rh(MGP)2(phi)5+]
A+G
C+T
DC
LC
G T C T A C
[DNA] &
[1-Δ Rh(MGP)2(phi)5+]
A+G
C+T
DC
LC
A T C T A T

Figure A2.9:

Figure A2.10. Binding Isotherms derived from photocleavage titration of 1-Δ-$[Rh(MGP)_2(phi)]^{5+}$ at 5'-CATCTG-3' (left) and 5'-TATCTA-3' (right) data shown in Figure 10. Gel results were quantitated as described previously, normalized and the fraction bound was fit to a simple one site binding equation as described in the text.

Figure A2.10:


1-Δ Rh(MGP)2(phi)5+ Binding Isotherm
CATCTG Site
Normalized Fraction Cleaved
1
0
KB = 9.5 (3) x 10^6 M^-1
10^-10 10^-9 10^-8 10^-7 10^-6 10^-5 10^-4
DNA Concentration [M]
1-Δ Rh(MGP)2(phi)5+ Binding Isotherm
TATCTA Site
Normalized Fraction Cleaved
1
0
KB = 1.8 (0.6) x 10^7 M^-1
10^-10 10^-9 10^-8 10^-7 10^-6 10^-5 10^-4
DNA Concentration [M]

A2.4.5: Relative Association Constant Measurements for 1-Δ-[Rh(MGP)$_2$(phi)]$^{5+}$

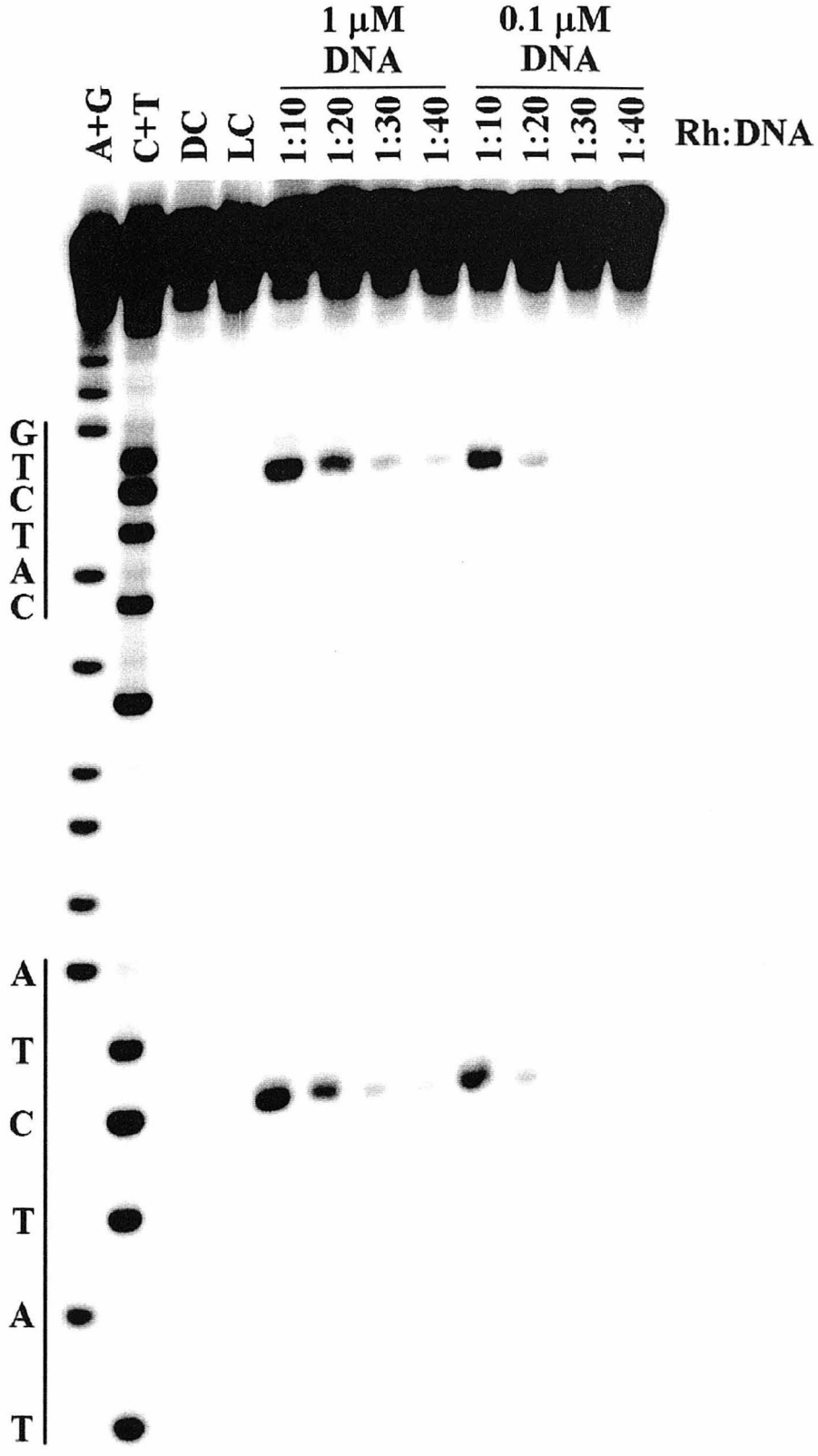
As discussed previously, comparison of cleavage intensity at sites on the same oligonucleotide is a more accurate method than independent measurement of absolute association constants for determining the ratio between K_b's at two sites of similar affinity. Figure A2.11 shows data resulting from such an experiment. These measurements were performed using low metallointercalator:DNA ratios as suggested by the mathematical models. Quantitation of the resulting gel electrophoresis experiments demonstrates that the most reliable results are obtained at the lowest practical ratios of ligand to DNA. At a 1:10 metallointercalator:DNA ratio (0.1 μM DNA) the ratio between the cleavage at the 5'-CATCTG-3' and 5'-TATCTA-3' sites was 0.94. As the ratio of metallointercalator to DNA was reduced, the cleavage ratio also declined, leveling off at approximately 0.80 at a metallointercalator:DNA ratio of 1:40. The average 5'-TATCTA-3':5'-CATCTG-3' ratio derived from multiple experiments performed with metallointercalator:DNA ratios of 1:30 and 1:40 is 0.80 (0.11). Before deriving the underlying ratio of association constants, however, the observed cleavage ratio must be corrected for the possibility of variation in the DNA photocleavage efficiencies at the two sites.

A2.4.6: Measurement of the Observed Photocleavage Efficiency, γ, of 1-Δ-[Rh(MGP)$_2$(phi)]$^{5+}$

To measure the photocleavage efficiency of the metal complex at the two sites of interest, the irradiation time was varied in a series of experiments performed at high concentrations of DNA (10 μM hairpin containing one site of interest) and metal (1 μM). Under these conditions, our estimates of the association constants suggest that the ligand is completely bound to its target sites. We anticipated that the observed photocleavage would increase with irradiation time until all of the available metal

Figure A2.11. Autoradiogram of a denaturing 20% PAGE gel showing photocleavage of a 5'-^{32}P endlabeled oligonucleotide, 5'-GCGG**TATCTA**GAGCG**CATCTG**GGCG-3', containing both 5'-CATCTG-3' and 5'-TATCTA-3' recognition sites by 1-Δ $Rh(MGP)_2(phi)^{5+}$. Lanes labeled A+G and C+T are standard Maxam-Gilbert sequencing reactions. DC refers to a DNA sample (0.1 μM) incubated with metal complex but not irradiated; LC to a DNA sample irradiated in the absence of metallointercalator. Sample conditions in experimental lanes are indicated above them. Sample preparation, irradiation, and data treatment are indicated in the text.

Figure A2.11:


1 μM DNA
0.1 μM DNA
A+G
C+T
DC
LC
1:10
1:20
1:30
1:40
1:10
1:20
1:30
1:40
Rh:DNA
G
T
C
T
A
C
A
T
C
T
A
T

complex had been consumed either through DNA cleavage or other degradation pathways. Samples were assayed by 20% denaturing PAGE and cleavage was quantitated at C_8 as described above. Plots of cleavage fraction versus time (Figure A2.12) reveal that γ is less that 100% for both sites and differs significantly between them – 5'-CATCTG-3', γ = 77%; 5'-TATCTA-3' γ = 57%.

Examination of the gels shown in Figure A2.9 reveals that the difference in apparent photocleavage efficiency results from an asymmetric distribution of cleavage between strands of the DNA polymer. Cleavage at the 5'-CATCTG-3' site is primarily restricted to one strand of the DNA, whereas at the 5'-TATCTA-3' site cleavage events are more evenly distributed between the two strands. Because these experiments were performed using hairpin oligonucleotides, this behavior may be readily observed in the form of an additional cleavage band near the top of the 5'-TATCTA-3' gel. Although the same cleavage band may be observed on the 5'-CATCTG-3' gel, it is much less intense. When adjusted for the difference in photocleavage efficiency, the relative association constant measurement described above affords a ratio of association constants for 5'-TATCTA-3':5'-CATCTG-3' of 1.1 (0.2) which is in agreement with the value [0.9 (0.1)] determined from the individual binding isotherms.

A2.4.7: Measurement of the Non-Specific Association Constant of 1-Δ-$[Rh(MGP)_2(phi)]^{5+}$

An example gel and binding isotherm for the titration of 1-Δ-$[Rh(MGP)_2(phi)]^{5+}$ with a non-specific hairpin oligonucleotide is included as Figure A2.13. The association constant derived from the data using a one-site binding equation, correcting the site concentration for the possibility of binding at any of the intercalation sites along the

Figure A2.12. Determinination of the Photocleavage Efficiency for $Rh(MGP)_2(phi)^{5+}$ at 5'-CATCTG-3' and 5'-TATCTA-3' binding sites. Plot of fraction DNA cleaved as a function of irradiation time on hairpins containing one of the two sites of interest. Sample preparation and data treatment as described in the text. The fraction of observed cleavage is less than the 0.1 theoretical maximum based on the Rh:DNA ratio in the samples corresponding to cleavage efficiencies of 77% at 5'-CATCTG-3' and 57% at 5'-TATCTA-3'.

Figure A2.12:

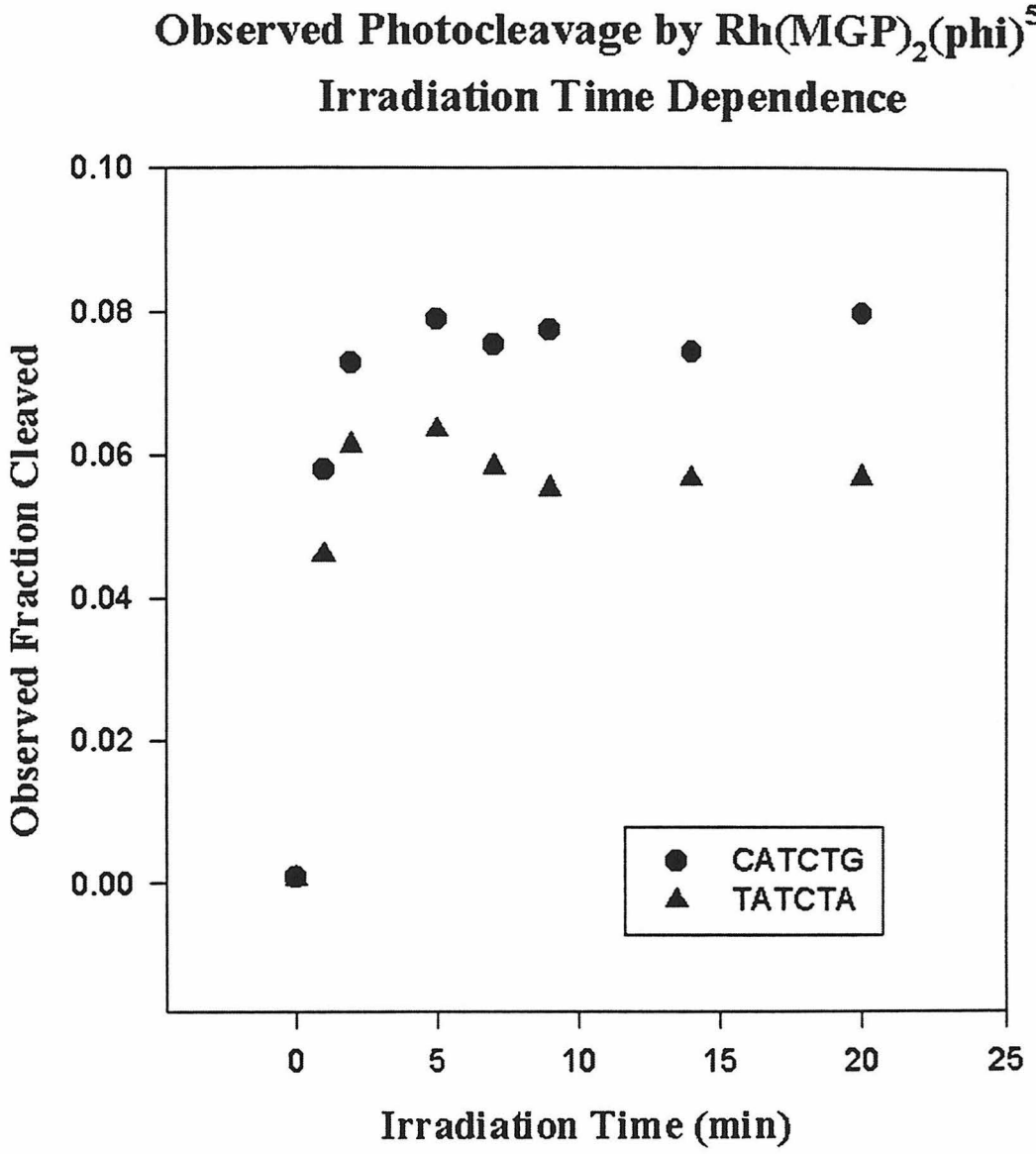
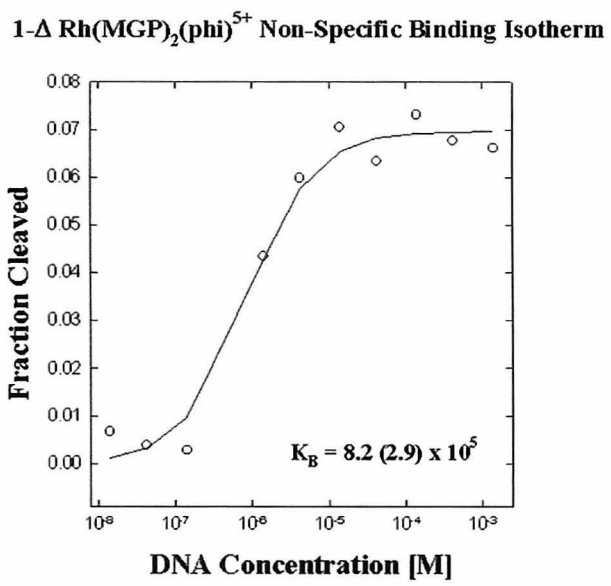
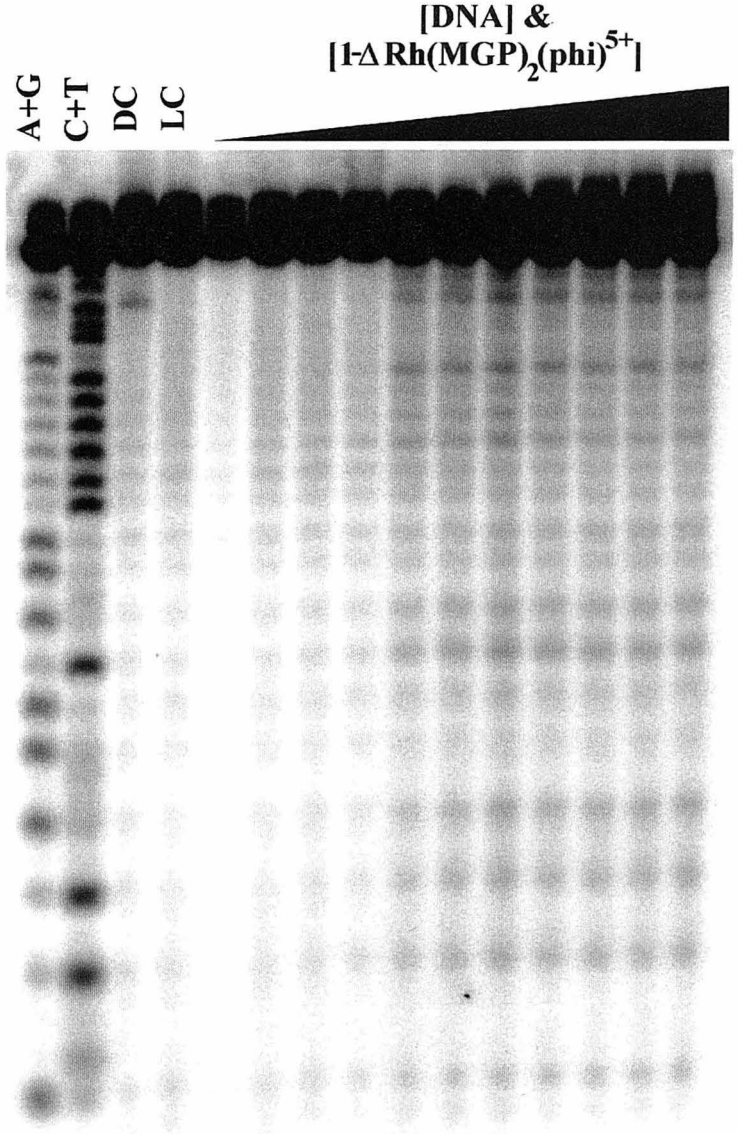

Observed Photocleavage by Rh(MGP)2(phi)5+:
Irradiation Time Dependence
Observed Fraction Cleaved
0.10
0.08
0.06
0.04
0.02
0.00
0
5
10
15
20
25
Irradiation Time (min)
CATCTG
TATCTA

Figure A2.13. (Left) Quantitative photocleavage titration of 1-Δ $Rh(MGP)_2(phi)^{5+}$ on a hairpin oligonucleotide containing no high-affinity binding sites. Lanes labeled A+G and C+T are standard Maxam-Gilbert sequencing reactions. DC refers to samples of DNA (3×10^{-9} M) and metal complex (1×10^{-5} M) incubated without irradiation, LC to samples of DNA (3×10^{-9} M) irradiated without metal complex. Binding experiments were performed from 1×10^{-9} M to 1×10^{-4} M hairpin DNA with the metal complex held at a constant Rh:DNA ratio of 1:2. Increasing concentrations indicated by the bar above the experimental lanes. Sample preparation and irradiation are described in the Experimental Section. (Right) Binding isotherm derived from the gel data at the left by integrating the intensity of all cleavage products as a fraction of uncleaved DNA in the parent band. Data were fit to the binding equation in the caption to Figure 10 using 14 times the DNA duplex concentration as the concentration of possible low-affinity binding sites.

Figure A2.13:


1-Δ Rh(MGP)2(phi)5+ Non-Specific Binding Isotherm
Fraction Cleaved
0.08
0.07
0.06
0.05
0.04
0.03
0.02
0.01
0.00
K_B = 8.2 (2.9) x 10^5
10^-8
10^-7
10^-6
10^-5
10^-4
10^-3
DNA Concentration [M]


[DNA] &
[1-Δ Rh(MGP)2(phi)5+]
A+G
C+T
DC
LC

duplex, was 8.2 (2.9) x 10^5 M^{-1}. This corresponds to a specificity ratio (K_H/K_L) of 22.

A2.5: Conclusions

When measuring the association constants of molecules that bind to and cleave DNA with sequence specificity, it is important to consider how the processes of competitive binding between high and low-affinity sites and multiple cleavage events on a single oligonucleotide affect observed binding isotherms. Depending on the specific values of the association constants and strand cleavage efficiencies of the molecule of interest, a given set of experimental conditions may produce a well-fit isotherm that does not accurately describe binding at the site under consideration. Our results recommend two general courses of action to minimize the effect of these competing processes. Experiments should be performed using the shortest practical segments of DNA in order to reduce the number of competing binding sites. Additionally, measurements should be made at the lowest possible ratio of ligand to DNA in order to minimize saturation effects at the high-affinity site which exacerbates the effects of competition between the low-affinity sites and the high-affinity site for available ligand.

Further considerations in experimental design were derived from measurements of the specific association constants of 1-Δ-$[Rh(MGP)_2(phi)]^{5+}$ at two high-affinity sites. The variation in data from experiment to experiment indicated that a quantitative comparison of binding affinities between closely related sites would be difficult. Accordingly, a more accurate method based on direct comparison of cleavage fractions at the two sites of interest on a single oligonucleotide was modeled and tested experimentally. After correction for differences in cleavage efficiency between

the sites of interest, a relative value of the two association constants was obtained which was in agreement with that derived from independent measurement.

Using the experimental approaches described here, measurement of single-site association constants for nucleic acid cleaving ligands is relatively straightforward. Strand scission by the nucleic acid binding ligands allows direct access to sequence specific binding information without the need for exogenous reagents or enzymes. Furthermore, the use of a DNA cleavage assay disregards the contribution of binding modes which do not lead to strand scission. The utility of these methods in studying the changes in affinity that result from single-base changes in the preferred sites of a nucleic acid binding ligand has been demonstrated for the metallointercalator 1-Δ-$[Rh(MGP)_2(phi)]^{5+}$.

A2.6: Literature Cited

1) Lohman, T. M.; Mascotti, D. P. *Meth. Enz.* **1992**, *212*, 400-424.

2) Winzor, D. J.; Sayer, W. H. *Quantitative Characterization of Ligand Binding*; Wiley-Liss: New York, 1995.

3) Chaires, J. B.; Satyanarayana, S.; Suh, D.; Fokt, I.; Przewloka, T.; Priebe, W. *Biochemistry* **1996**, *35*, 2047-2053.

4) Takusagawa, F.; Wen, L.; Chu, W.; Li, Q.; Takusagawa, K. T.; Carlson, R. G.; Weaver, R. F. *Biochemistry* **1996**, *35*, 13240-13249.

5) Roche, C. J.; Berkowitz, D.; Sulikowski, G. A.; Danishefsky, S. J.; Crothers, D. M. *Biochemistry* **1994**, *33*, 936-942.

6) Wang, Y.; Killian, J.; Hamasaki, K.; Rando, R. R. *Biochemistry* **1996**, *35*, 12338-12346.

7) Pyle, A. M.; Rehmann, J. P.; Meshoyrer, R.; Kumar, C. V.; Turro, N. J.; Barton, J. K. *J. Am. Chem. Soc.* **1989**, *111*, 3051-3058.

8) Rentzeperis, D.; Marky, L. A.; Dwyer, T. J.; Geierstanger, B. H.; Pelton, J. G.; Wemmer, D. E. *Biochemistry* **1995**, *34*, 2937-2945.

9) Kalsbeck, W. A.; Thorp, H. H. *J. Am. Chem. Soc.* **1993**, *115*, 7146-7151.

10) Welch, T. W.; Thorp, H. H. *J. Phys. Chem.* **1996**, *100*, 13829-13836.

11) Carter, M. T.; Rodriguez, M.; Bard, A. J. *J. Am. Chem. Soc.* **1989**, *111*, 8901-8911.

12) Ding, L.; Bernadou, J.; Meunier, B. *Bioconj. Chem.* **1991**, *2*, 201-206.

13) Goodisman, J.; Dabrowiak, J. C. in *Advances in DNA Sequence Specific Agents.* Hurley, L. H., Ed.; Jai Press: Greenwich, CN, 1992; Vol. 1, pp 25-49.

14) Ward, B.; Rehfuss, R.; Goodisman, J.; Dabrowiak, J. C. *Biochemistry* **1988**, *27*, 1198-1205.

15) Guo, D. Q.; Gupta, R.; Lown, J. W. *Anti-Cancer Drug Des.* **1993**, *8*, 369-397.

16) Absalon, M. J.; Kozarich, J. W.; Stubbe, J. *Biochemistry* **1995**, *34*, 2065-2075.

17) Xu, Y.-j.; Zhen, Y.-s.; Goldberg, I. H. *Biochemistry* **1994**, *33*, 5947-5954.

18) Sugiura, Y.; Matsumoto, T. *Biochemistry* **1993**, *32*, 5548-5553.

19) Hiort, C.; Goodisman, J.; Dabrowiak, J. C. *Biochemistry* **1996**, *35*, 12354-12362.

20) Johann, T. W.; Barton, J. K. *Phil. Trans. Royal Soc. A.* **1996**, *354*, 299-324.

21) Dupureur, C. M.; Barton, J. K.; in *Comprehensive Supramolecular Chemistry.* Lehn, J.-M., Ed.; Pergamon Press: Tarrytown, NY, 1996; Vol. 5, pp 295-315.

22) Stigter, D.; Dill, K. A. *Biophys. J.* **1996**, *71*, 2064-2074.

23) Correia, J. J.; Chaires, J. B. *Meth. Enz.* **1994**, *240*, 593-614.

24) Saroff, H. A. *Biopolymers* **1995**, *36*, 121-134.

25) Beyer, W. H. *CRC Standard Mathematical Tables*; 26th ed.; CRC Press, Inc.: Boca Raton, FL, 1981.

26) Karlovsky, P. *Biochem. Biophys. Res. Comm.* **1986**, *138*, 778-782.

27) Terbrueggen, R. H.; Johann, T. W.; Barton, J. K. *Inorg. Chem.* **1998**, *37*, 6874-6883.